LA-10070-PR
Progress Report

UC-28
Issued: April 1984

Progress at LAMPF

January—December 1983
Clinton P. Anderson Meson Physics Facility

Editor

John C. Allred

Scientific Editorial Board

Olin B. van Dyck
Richard L. Hutson
M. Stanley Livingston
Mario E. Schillaci

Production Staff

Kit Ruminer
Beverly H. Talley

LA--10070-PR

DE84 011027

ABSTRACT

Progress at LAMPF is the annual progress report of the MP Division of the Los Alamos National Laboratory. The report includes brief reports on research done at LAMPF by researchers from other institutions and Los Alamos divisions.

Los Alamos National Laboratory
Los Alamos, New Mexico 87545

PROMISES vs ACHIEVEMENTS

This year marks the fifteenth anniversary of the publication of a paper in Science Journal [Science J. 5A, No. 1, 39 (1969)] in which I documented our hopes for the construction and operation of LAMPF. It is interesting to compare what we promised more than 15 years ago with what we actually achieved. A forthcoming paper will make this comparison in some detail, but a simple table shows many of the salient points.

The following table does not show how our research program has evolved compared to initial predictions, or how LAMPF has served the national scientific and academic communities. Here too, we need make no apologies.

As the realization that basic science and derivative technologies are absolutely vital to our Nation's well being continues to invade our civilization's consciousness, the scientific community's obligations toward its credibility and responsibilities become even more important. Making worthwhile promises that can be kept and then keeping them are two ways we can achieve those goals.

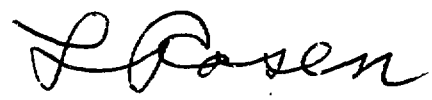

Louis Rosen
Director, LAMPF

LAMPF PROMISES vs ACHIEVEMENTS

Parameter	Promised	Achieved
• Energy	Variable up to 800 MeV	Variable up to 800 MeV
• Intensity	1 mA	>1 mA
• Extraction efficiency	>99%	>99.8%
• Energy spread at $\frac{1}{2}$ max	0.5%	0.15%
• Duty factor	>5%	>9%
• rf power sources	Computer-controlled rf power sources, modulators, and switch gear	Computer-controlled reliable and stable rf power >80% beam availability
• Accelerator structures	High-efficiency accelerator structures	At 1 mA, 30% of rf power is converted to beam power
• H^+ and H^- beams	Simultaneous beams	Simultaneous dual-beam operation and energy variability 20-nA average 90% polarized H^-
• Secondary beams	Six beam lines	12 experimental ports plus 6 neutron lines at WNR
• Practical applications	National defense Isotope production Radiation damage Radiobiology	WNR Isotope production Pion therapy (successfully initiated, now in abeyance)

CONTENTS

Experimental Areas

Primary beam lines in experimental areas:

Line A	—	Main Beam Line for Pion and Muon Channels
Line B	—	Neutron and Proton Beams and Nuclear Chemistry Facility
Line C	—	High-Resolution Proton Spectrometer
Line D	—	Weapons Neutron Research Facility

Experimental beam lines:

Area A:

BSA	—	Beam Stop A
EPICS	—	Energetic Pion Channel and Spectrometer
LEP	—	Low-Energy Pion Channel
P^3	—	High-Energy Pion Channel
SMC	—	Stopped Muon Channel
TTA	—	Thin Target Area

Area B (AB or Nucleon Physics Facility):

BR	—	Neutrons and Protons
EPB	—	External Proton Beam
LB-NC	—	Line B, Nuclear Chemistry

Area C:

CCH	—	Area C Control and Counting House
HRS	—	High-Resolution Proton Spectrometer

Area A-East:

Biomedical Pion and Muon Channel

TA-5	—	Target A-5
ISORAD	—	Isotope Production and Radiation Effects Facility

Neutrino Area

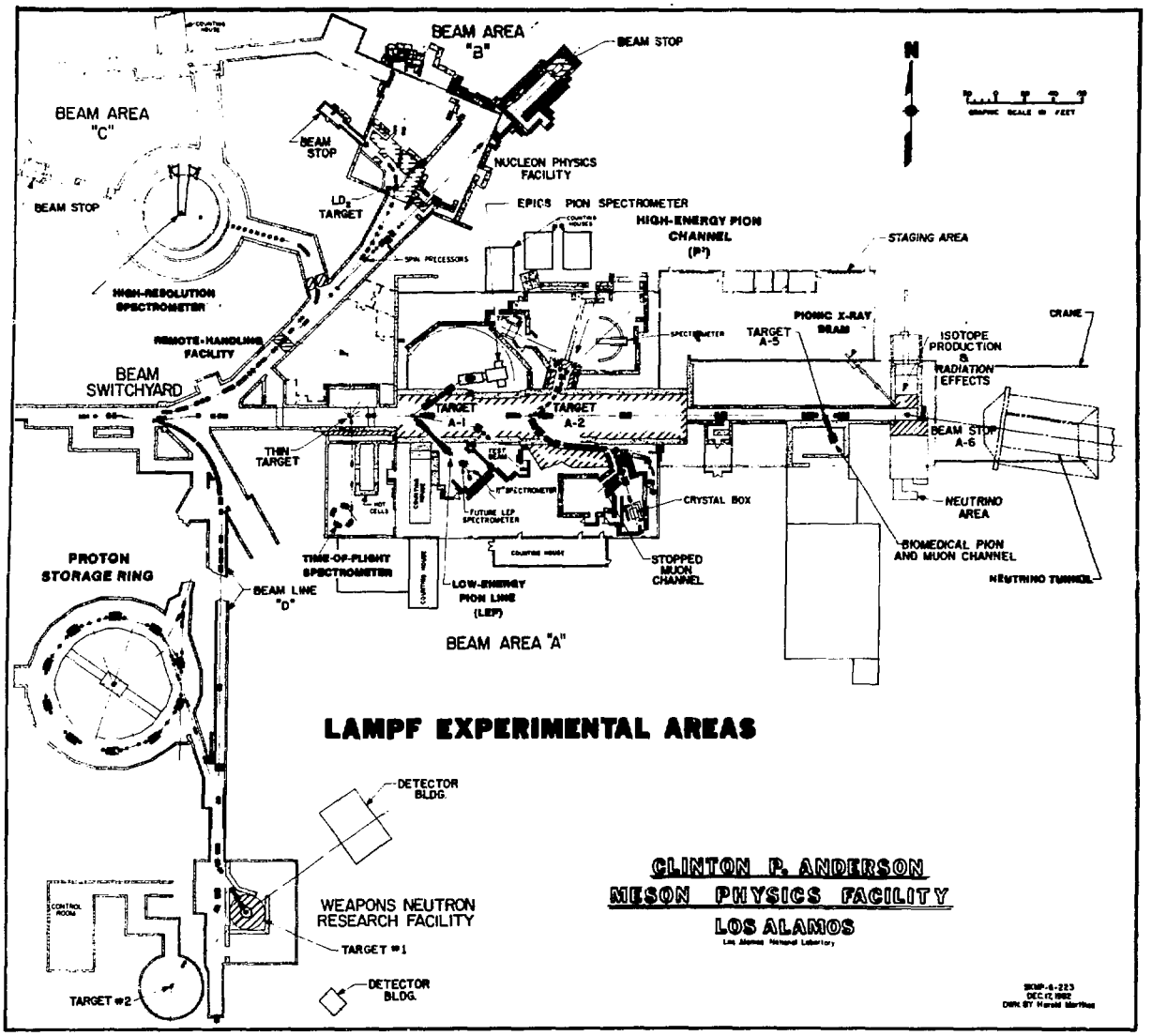
BEAM AREA "B"
BEAM STOP
BEAM AREA "C"
BEAM STOP
BEAM STOP
NUCLEON PHYSICS FACILITY
LD2 TARGET
EPICS PION SPECTROMETER
HIGH-ENERGY PION CHANNEL (P3)
STAGING AREA
HIGH-RESOLUTION SPECTROMETER
REMOTE-HANDLING FACILITY
BEAM SWITCHYARD
PIONIC X-RAY BEAM
TARGET A-5
CRANE
ISOTOPE PRODUCTION & RADIATION EFFECTS
TARGET A-1
TARGET A-2
BEAM STOP A-6
THIN TARGET
CRYSTAL BOX
NEUTRINO AREA
BIOMEDICAL PION AND MUON CHANNEL
PROTON STORAGE RING
TIME-OF-FLIGHT SPECTROMETER
BEAM LINE "D"
LOW-ENERGY PION LINE (LEP)
STOPPED MUON CHANNEL
NEUTRINO TUNNEL
BEAM AREA "A"
LAMPF EXPERIMENTAL AREAS
DETECTOR BLDG.
WEAPONS NEUTRON RESEARCH FACILITY
TARGET #1
TARGET #2
DETECTOR BLDG.
CLINTON P. ANDERSON
MESON PHYSICS FACILITY
LOS ALAMOS
Los Alamos National Laboratory

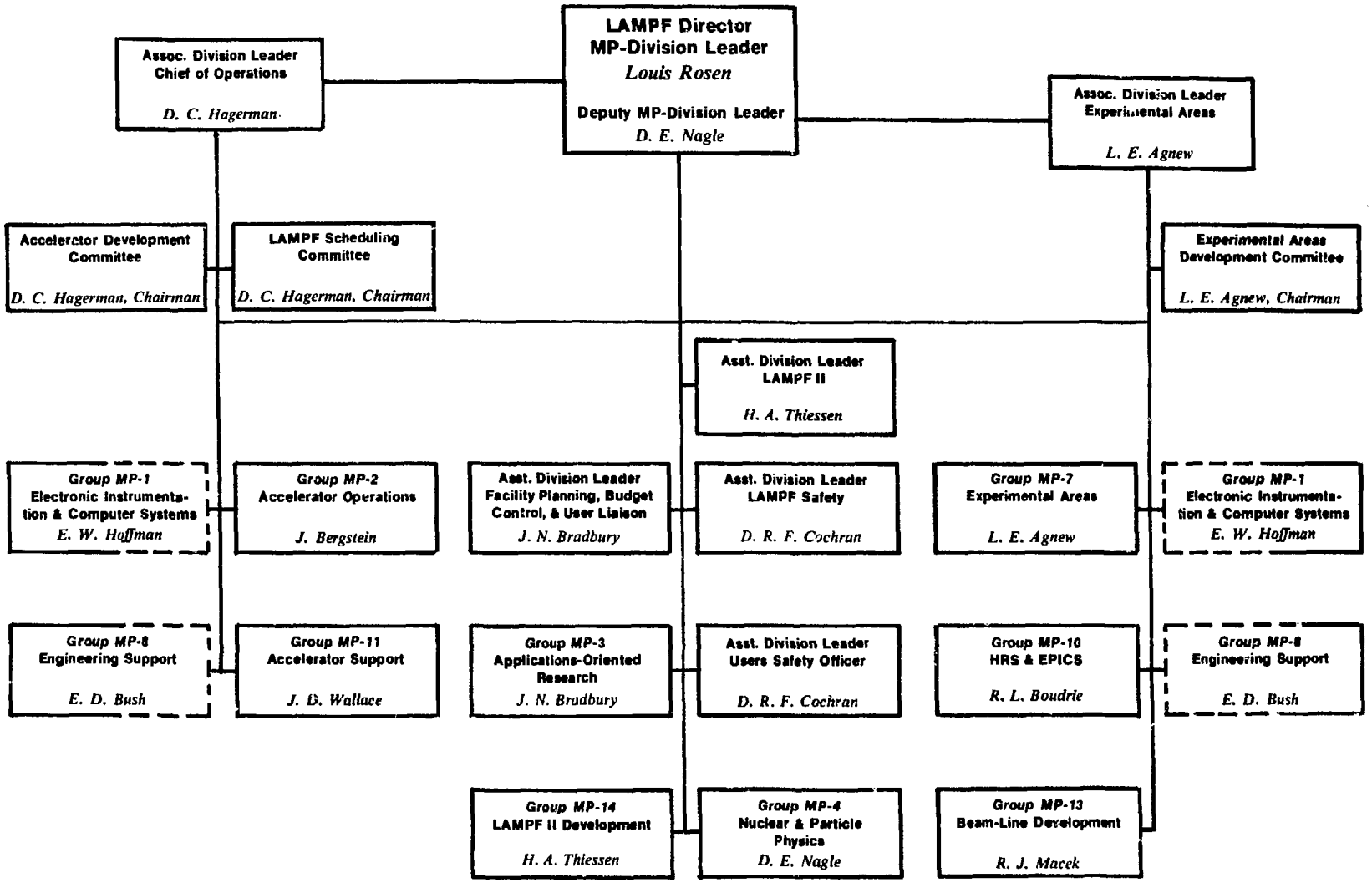

LAMPF ORGANIZATION

December 1983

PROGRESS AT LAMPF

JANUARY — DECEMBER 1983

CLINTON P. ANDERSON MESON PHYSICS FACILITY

I. LAMPF NEWS

• At its March 1983 meeting, the Board of Directors of the LAMPF Users Group, Inc., established a new award, the Louis Rosen Prize. This prize, consisting of $1000 and a certificate, is awarded annually for the outstanding Ph.D. thesis based on LAMPF research. Judging is done by the Board of Directors. Theses should be submitted to the Users Group Office at LAMPF by August 31 for consideration. To be eligible, a thesis must have been completed since the previous August. Announcement of the winner of the prize is made at the annual Users Meeting in November.

• At the Users Meeting of November 7, 1983, Chairman George Igo announced the award of the first Louis Rosen Prize to Stephen A. Wood for his thesis entitled "An Experimental Study of Inclusive Pion Double-Charge-Exchange Reactions in the Delta-Resonance Region."

• On February 7, 1983, at the end of a production run, the LAMPF accelerator was tested for maximum proton beam current. An average current of 1.2 mA, 20% above design, was produced for several hours.

On behalf of the LAMPF Users Group, Inc., Director Andy Bacher presents to Stephen Wood the Louis Rosen Prize. Left to right: Rosen, Wood, Bacher.

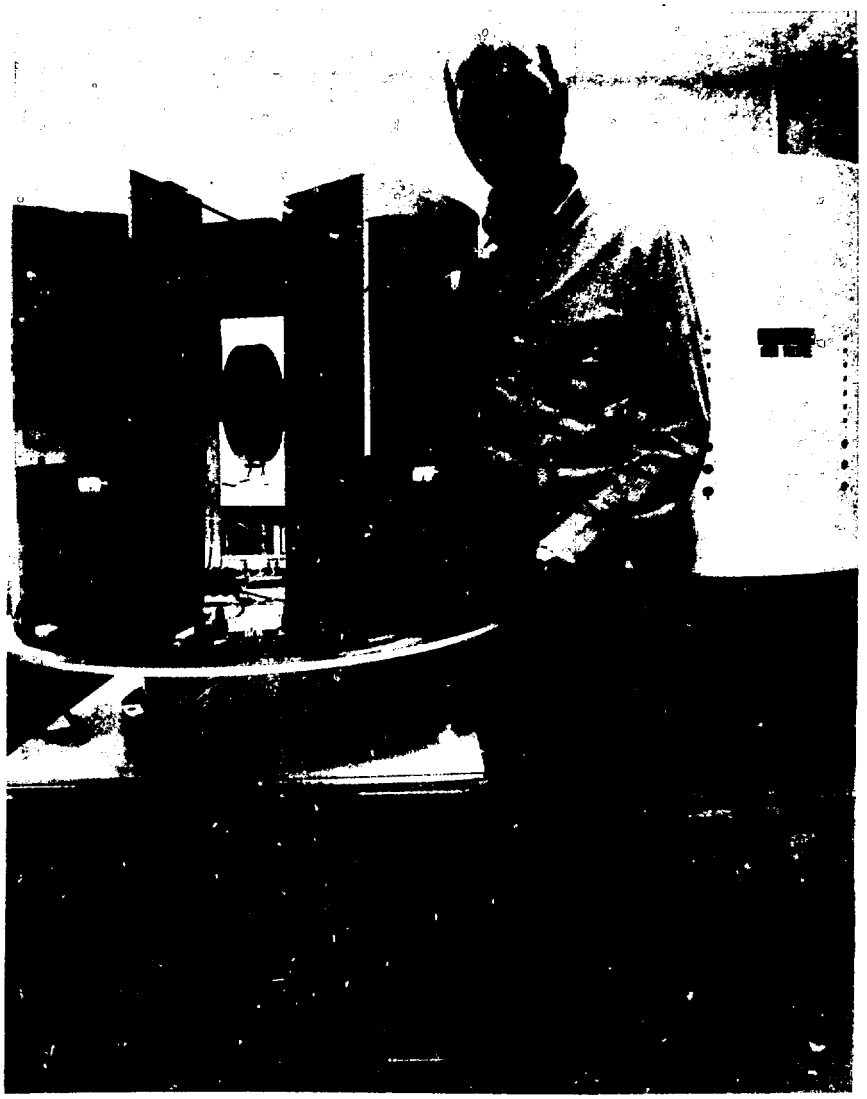

George J. Krausse, MP-4, with the prototype H^- beam modulator he designed and built. The beam modulator will shape the beam pulse for injection into the PSR. Extended-life tests were performed successfully in December 1983; the slew rate of the modulator is 500 kV/μs.

• With the Proton Storage Ring (PSR) coming on line in 1985, major necessary modifications of the LAMPF accelerator are proceeding. (1) An H^- beam modulator prototype that will shape the beam pulse for injection into the PSR (see photograph above) has been designed, built, and tested; (2) a new high-intensity H^- ion source has been designed and a prototype built; and (3) components are being built for a new injector and for a reconfigured switchyard.

During summer/fall of 1983 a collaboration (Japan, UCLA, University of Minnesota, Los Alamos) worked at the HRS making nucleon-nucleon measurements in the Coulomb-nuclear interference region at forward-scattering angles. Polarized beam struck polarized $\vec{p}$ and $\vec{d}$ targets cooled to 25-50 mK by a dilution $^3He/^4He$ refrigerator furnished by KEK. Shown in the photograph, left to right, are George Igo (UCLA), Hiromi Hasai (Hiroshima University), Akira Masaike (KEK), Steven Greene (Los Alamos), and Yuji Ohashi (Nagoya University).

LAMPF Satellite? **Jerry Davis, MP-11, displaying the 805-MHz intermediate driver amplifier he designed. This amplifier, with an output power of 1 kW, drives a vacuum-tube amplifier which in turn drives the klystrons of the side-coupled-cavity linac.**

• On August 5, 1983 a serious electrical accident occurred at LAMPF. Three technicians from MP-8 began what they thought was routine maintenance of a portion of the power supply to the klystron test stand at the Engineering Test Laboratory.

Through an unexpected sequence of circumstances — things that "could not happen" — a key interlock was unknowingly by-passed and a hand-held grounding hook contacted an energized 4160-V, 60-Hz power bus. The resulting fireball caused burns to all three persons exposed; the person holding the grounding hook was painfully burned. Injuries were fortunately much less serious than they might have been.

Of greater interest than the actual details are the boundary conditions. The person closest to the accident was a senior, skilled technician, who believed (as did his supervisors) that he understood the hazards and how to manage them. All three persons involved believed, without doubt, that the circuit in question was de-energized. The mechanical and key interlocks were in

place and were functioning properly, but the system was by-passed. It is now clear that none of the people involved realized the seriousness of the risks associated with the operation.

The hazards at LAMPF are many — electrical, chemical, cryogenic, radiation and radioactive materials, pressurized and evacuated systems, and magnets — practically every hazard that can be imagined. Experimental areas can be especially hazardous because conditions are constantly changing. Even for a single experiment, in a matter of weeks an experimental area may undergo a drastic rearrangement.

An accident such as the one of August 5 must remind all of us that safety is always paramount. The safety record at LAMPF is outstanding because all the people here, Users and lab employees alike, work at safety. Safety requires continuous vigilance; it is not a matter of good luck.

- The radiation monitoring system at the entrance to the LAMPF site paid an unexpected dividend. A truck carrying construction steel from Mexico independently wandered onto the LAMPF site and triggered our radiation alarm system. Sure enough, the entire load of steel was sufficiently radioactive to set off a search in the United States and Mexico for other steel from the same mill. Once again LAMPF served the national interest in an unexpected way.

II. MEETINGS

LAMPF Users Group, Inc.

Seventeenth Annual LAMPF Users Group Meeting

The LAMPF Users Seventeenth Annual Meeting was held in Los Alamos on November 7-8, 1983, with 222 attendees. Chairman George Igo (UCLA) presided at the first session, which opened with a welcoming address by Warren F. Miller, Associate Director of Los Alamos National Laboratory. The session continued with a LAMPF Status Report presented by Louis Rosen, Director of LAMPF, and a report on LAMPF operations by Andrew A. Browman.

During the second portion of the morning session, George Igo gave the Annual Users Group Report, followed by a presentation of the election results. Robert Redwine (MIT) is the Chairman-Elect of the Board of Directors, and new members are Peter D. Barnes (Carnegie-Mellon University), Barry Preedom (University of South Carolina), and John D. Walecka (Stanford University). Members whose terms continue in 1984 are Charles Glashausser, Chairman, and George Igo, Past-Chairman. A presentation was given by Charles Bowman (Los Alamos) on Proton Storage Ring Research.

The afternoon session was conducted by incoming Chairman Charles Glashausser (Rutgers University). The following talks were given during this session:

"*New Approach to Polarized-Proton Scattering Based on Dirac Dynamics*," Steven J. Wallace (University of Maryland),

"*Progress Report—LAMPF II*," Henry A. Thiessen (Los Alamos), and

"*Muon Neutrino Physics Before the PSR*," Gerard Stephenson (Los Alamos).

The afternoon session concluded with a panel discussion on the present LAMPF II concept in the context of nuclear and particle physics needs of the 1990s.

Talks given during the Tuesday morning session, presided over by Igo, were

"*Energy and Angular Dependence of the Tensor Polarization T20 in π Elastic Scattering*," Willi Grüebler (ETH),

"*Tensor Polarization in Pion-Deuteron Elastic Scattering*," Roy Holt (Argonne),

"*Simple Features of (pπ⁻) Reactions Near Threshold*," Steven Vigdor (Indiana University),

"pp *and* np *Phase Shifts up to 800 MeV*," Catherine Lechanoine-LeLuc (University of Geneve), and

"*Status of Exp. 225, A Study of Neutrino-Electron Elastic Scattering*," Herbert Chen (University of California, Irvine).

Working group meetings were held the rest of the day.

Visitors Center

During this report period, 572 research guests worked on LAMPF-related activities or participated in experiments at LAMPF; of these, 126 were foreign visitors. A total of 656 check-ins and 625 check-outs were processed by the Visitors Center.

• MEMBERSHIP

Non-Los Alamos National Laboratory	706
Los Alamos National Laboratory	171
TOTAL	877

• INSTITUTIONAL DISTRIBUTION

Membership by Institutions

Los Alamos National Laboratory	171
National or Government Laboratories	96
U.S. Universities	364
Industry	41
Foreign	162
Hospitals	30
Nonaffiliated	13
TOTAL	877

Number of Institutions

National or Government Laboratories	19
U.S. Universities	108
Industry	30
Foreign	82
Hospitals	25
Nonaffiliated	7
TOTAL	271

• REGIONAL BREAKDOWN

East (Pennsylvania, New Jersey, Delaware, Washington DC, Massachusetts, New York, Connecticut, Vermont, Rhode Island, New Hampshire, Maine)	132
Midwest (Ohio, Missouri, Kansas, Indiana, Wisconsin, Michigan, Illinois, North Dakota, South Dakota, Nebraska, Iowa, Minnesota)	102
South (Maryland, Virginia, Tennessee, Arkansas, West Virginia, Kentucky, North Carolina, South Carolina, Alabama, Mississippi, Louisiana, Georgia, Florida)	71
Southwest, Mountain (Montana, Idaho, Utah, Wyoming, Arizona, Colorado, New Mexico, Oklahoma, Texas) (excluding Los Alamos)	128
West (Alaska, Hawaii, Nevada, Washington, Oregon, California)	110
Foreign	163
Los Alamos National Laboratory	171
TOTAL	877

1984 WORKING GROUP CHAIRMEN

High-Resolution Spectrometer (HRS)
M. Gazzaly
University of Minnesota

Neutrino Facilities
Thomas A. Romanowski
Ohio State University

Stopped-Muon Channel (SMC)
Fesseha Mariam
Los Alamos National Laboratory

Nuclear Chemistry
Yoshitaki Ohkubo
Los Alamos National Laboratory

Energetic Pion Channel and Spectrometer (EPICS)
William Cottingame
New Mexico State University/
Los Alamos National Laboratory

High-Energy Pion (P^3) Channel
Jon Engelage
University of California,
Los Angeles

Nucleon Physics Laboratory (NPL)/ Polarized Facilities
Tarlochan Bhatia
Texas A&M University/
Los Alamos National Laboratory

Computer Facilities
James F. Amann
Los Alamos National Laboratory

Solid-State Physics and Materials Science
Walter F. Sommer
Los Alamos National Laboratory

Muon-Spin Rotation (μSR)
Art Denison
University of Wyoming

Low-Energy Pion (LEP) Channel
Michael J. Leitch
Los Alamos National Laboratory

LAMPF PROGRAM ADVISORY COMMITTEE (PAC)

The PAC consists of about 25 members appointed for staggered 3-year terms. Members advise the Director of LAMPF on the priorities they deem appropriate for the commitment of beam time and the allocation of resources for the development of experimental facilities. The PAC meets twice each year for 1 week during which time all new proposals that have been submitted at least 2 months before the meeting date are considered. Old proposals, and the priorities accorded to them, may also be reviewed.

Terms Expiring 1983

Richard Arndt
Virginia Polytechnic Inst. and State University

Robert Redwine
Massachusetts Institute of Technology

S. Peter Rosen
Los Alamos National Laboratory

Dieter Kurath
Argonne National Laboratory

Louis Remsberg
Brookhaven National Laboratory

Stephen J. Wallace
University of Maryland

Terms Expiring 1984

Franz L. Gross
College of William & Mary

Leonard S. Kisslinger
Carnegie-Mellon University

Darragh Nagle
Los Alamos National Laboratory

Barry Holstein
University of Massachusetts

June L. Matthews
Massachusetts Institute of Technology

Bruce VerWest
Arco Oil and Gas Company

Sheldon B. Kaufman
Argonne National Laboratory

Daniel W. Miller
Indiana University

Robert Lee Walker
Tesuque, New Mexico

Terms Expiring 1985

David Axen
TRIUMF

Frieder Lenz
SIN

Victor E. Viola, Jr.
Indiana University

Barry Barish
California Institute of Technology

Harold M. Spinka, Jr.
Argonne National Laboratory

Larry Zamick
Rutgers University

Dietrich Dehnhard
University of Minnesota

1984 TECHNICAL ADVISORY PANEL (TAP) OF THE LAMPF USERS GROUP, INC.

The TAP provides technical recommendations to the Board of Directors and LAMPF management about the development of experimental facilities and experiment support activities. The TAP has 12 members, appointed by the Board of Directors, serving 3-year staggered terms. The Chairman of the Board of Directors serves as TAP chairman. The TAP membership and term expiration dates are listed below.

1984	Billy E. Bonner Los Alamos National Laboratory	1985	Christopher L. Morris Los Alamos National Laboratory
1984	Thomas J. Bowles Los Alamos National Laboratory	1986	Michael A. Oothoudt Los Alamos National Laboratory
1986	George R. Burleson New Mexico State University	1984	Barry Preedom University of South Carolina
1984	Gerald Dugan Fermi National Accelerator Laboratory	1985	Thomas A. Romanowski Ohio State University
1985	Donald Geesaman Argonne National Laboratory	1986	Gary Sanders Los Alamos National Laboratory
1985	Kazuo Gotow Virginia Polytechnic Institute and State University	1986	Charles A. Whitten University of California, Los Angeles Los Angeles

SCIENCE POLICY ADVISORY COMMITTEE (SPAC)

A Science Policy Advisory Committee was formed during 1983 to advise the Board of Directors on the long-term development of research and facilities at LAMPF. The first charge to the SPAC was the examination of the LAMPF II concept and justification in the context of nuclear and particle physics needs of the 1990s.

Barry C. Barish California Institute of Technology	Frederick Reines University of California, Irvine
Leonard S. Kisslinger Carnegie-Mellon University	S. Peter Rosen Los Alamos National Laboratory
Alan D. Krisch University of Michigan	Lee C. Teng Fermi National Accelerator Laboratory
Malcolm MacFarlane Indiana University	Akihiko Yokosawa Argonne National Laboratory
Sydney Meshkov National Bureau of Standards	John D. Walecka Stanford University

1984 BOARD OF DIRECTORS OF THE LAMPF USERS GROUP, INC.

The Board of Directors consists of seven members elected by the LAMPF Users Group, Inc., whose interests they represent and promote. They concern themselves with LAMPF programs, policies, future plans, and especially with how users are treated at LAMPF. Users should address problems and suggestions to individual Board members.

The Board also nominates new members to the Program Advisory Committee (PAC).

The 1983 membership and term expiration dates are listed below.

1985 Charles Glashausser (Chairman)
Rutgers University

1986 Robert Redwine (Chairman-Elect)
Massachusetts Institute of Technology

1984 George Igo (Past-Chairman)
University of California, Los Angeles

James Bradbury (Secretary/Treasurer)
Los Alamos National Laboratory

1984 Andrew D. Bacher
Indiana University

1985 Peter D. Barnes
Carnegie-Mellon University

1985 Barry Preedom
University of South Carolina

1985 John D. Walecka
Stanford University

BOARD OF DIRECTORS

The LAMPF Users Group Board of Directors (BOD) met on March 6-7, July 20-21, and November 8, 1983. All meetings were chaired by George Igo; selected topics of discussion are provided below.

The 1983 Annual Users Meeting was very successful. There were 222 registrants, of whom 119 were from outside the Laboratory. The panel discussion about LAMPF II, involving the BOD, the Science Policy Advisory Committee (SPAC), and the attending users, received favorable comments for being stimulating and informative. A summary of the discussion is provided in these proceedings.

Sixty-one new proposals were received for review by the Program Advisory Committee (PAC) at the January 1984 meeting. The breakdown by channel is: EPICS - 15, HRS - 10, NPL - 7, LEP - 12, P^3 - 11, SMC - 3, Neutrino - 1, Radiation Effects - 1, and Nuclear Chemistry - 1. Because of the proposal load, the Low-Energy Pion Channel (LEP) and High-Energy Pion Channel (P^3) PAC subcommittees will be augmented by one member (either from the Laboratory or from another subcommittee) for the January meeting.

Those PAC members whose terms nominally expire in 1983 have been asked, as usual, to serve in January and also to serve at the summer meeting in 1984, as there was no meeting in the summer of 1983. The summer 1984 meeting will thus be the "overlap" meeting. New PAC members will be recommended by the BOD at their next meeting.

Four new members were appointed to the Technical Advisory Panel from the lists provided by the LUGI working groups. The appointees are Michael Oothoudt, Computer Facilities; Gary Sanders, Stopped-Muon Channel (SMC); George Burleson, Energetic Pion Channel and Spectrometer (EPICS); and Charles Whitten, High-Resolution Spectrometer (HRS).

The Board agreed to employ Users Group funds to establish and support a new award, the Louis Rosen Prize. This prize, consisting of $1000 and a certificate, is to be awarded annually for the outstanding Ph.D. thesis based on LAMPF research. The judging is to be done by the Board of Directors. For consideration, theses should be submitted to the Users Group Office at LAMPF by August 31; announcement of the winner will be made at the Users Meeting in November. To be eligible, a thesis must have been completed since the previous August.

The criteria for thesis evaluation were discussed. In addition to intellectual content, quality of presentation, and significance of results, the level of the contributions to the work by the student is obviously important. Contributions to the experiment design, data analysis, and data interpretation are to be assessed by requiring explanatory letters from both student and advisor.

The BOD selected Stephen A. Wood as the recipient of the Louis Rosen Prize for 1983. The title of the thesis is "An Experimental Study of Inclusive Pion Double-Charge-Exchange Reactions in the Delta Resonance Region."

MP Division has purchased a 10- by 55-ft trailer to be equipped as a Users lounge. The trailer will be located to the east of the Data-Acquisition Center and will arrive about December 1, 1983. The lounge will contain space for a library, kitchen, and computer terminal as well as a large open area; some landscaping in the vicinity is planned. Users representatives will be asked to consider furnishings for the lounge and arrange for their purchase with User funds available for this purpose.

George Igo announced the formation of a Science Policy Advisory Committee (SPAC) whose role is to advise on the long-term development of research and facilities at LAMPF. The following persons participated in an organizational meeting on July 26, 1983.

Barry Barish	Caltech
Leonard Kisslinger	Carnegie-Mellon University
Alan Krisch	University of Michigan
Sydney Meshkov	National Bureau of Standards
Fredrick Reines	University of California/Irvine
Peter Rosen	Los Alamos National Laboratory
Dirk Walecka	Stanford University
Akihiko Yokosawa	Argonne National Laboratory

The first charge to the SPAC is to examine the present LAMPF II concept and physics justification in the context of nuclear and particle physics needs of the 1990s. The committee is to advise the LUGI-BOD on

- specific strengths and weaknesses in the LAMPF II concept and justification,
- the highest priority experimental programs and facilities to be developed at LAMPF II, and
- the best strategies for advancing the case and developing support for LAMPF II in the nuclear and particle physics communities.

The SPAC met on October 22, 1983 at UCLA. Preliminary reports were presented on four topics important to the LAMPF II concept: accelerator design (Alan Krisch), experimental facilities (Akihiko Yokosawa), and physics justification and community support (Barry Barish). George Igo will assemble the written reports and send them, together with a summary of the panel discussion during the Annual Users Meeting, to the Users. This is a crucial period for LAMPF II because the concept and justification must become firm very soon in order to produce a proposal by the end of 1984. Strong support of physicists in both nuclear and particle physics must be garnered and maintained. Consequently the BOD feels that the SPAC should be requested to continue to provide input to the LAMPF II plan. A nuclear physics subcommittee of the SPAC will be organized by C. Glashausser to define more precisely the potential of LAMPF II in this area.

Following a suggestion by Louis Rosen, plans are being made to hold a comprehensive workshop in May of 1984 on the interface between particle and nuclear physics. To members of the SPAC, Alan Krisch and Malcolm MacFarlane, have agreed to head an organizing committee for this workshop. A one-half-day session of invited papers on the interface region will be held at the spring APS meeting.

To bolster the case for LAMPF II, it is important to publicize the achievements of existing meson factories and their impact on the development of nuclear physics. Members of LUGI are encouraged to give presentations at universities and an article should be prepared for *Physics Today*. A semitechnical brochure on LAMPF accomplishments could also be prepared for widespread distribution.

The Annual Users Meeting in 1984 will be held on October 29-30 (November 6 is election day). The next BOD meeting will be on February 17, 1984 at LAMPF.

TECHNICAL ADVISORY PANEL

The Technical Advisory Panel (TAP) met on July 29 and November 6, 1983. Some excerpts of the minutes are presented below. After noting that the budgetary position of LAMPF appears reasonable for FY 1984, Louis Rosen made some general comments about the LAMPF neutrino program. The proposed neutrino program using the Proton Storage Ring (PSR) is in abeyance at this time, primarily because the neutron scattering and defense programs have first priority on PSR beam and it is not clear that an adequate amount of current will be available for the neutrino program. However, as neutrino physics is an important component of LAMPF research, experiments are being conducted at the beam stop and Line E. At Line E, neutrino cross sections will be measured using a 5-ton liquid scintillator detector (Exp. 764). LAMPF will provide up to $200 thousand to prepare Line E, which is expected to be ready to receive beam in January 1984. If approved by PAC, a modular detector may be constructed, which might eventually be used at LAMPF II.

Louis Rosen commented that for long-term survival, LAMPF needs a major upgrade. He feels that the Laboratory top management will support such a project, as it clearly will provide important opportunities for performing high-quality research and for extending the base for education of young scientists. Interested members of the scientific community must make the DOE and Congress aware that they need and will use a LAMPF II. In addition to the in-house work of Los Alamos in terms of proposal preparation, there must be a well-established effort by external users to define and support LAMPF II.

Richard Boudrie reported that the new Low-Energy Pion Channel (LEP) spectrometer project is proceeding very well. The spectrometer will be useful for pion-inelastic scattering in the 20- to 80-MeV range and will provide <0.1% resolution with large acceptance. The pole pieces and yoke are presently being machined at a cost much less than anticipated; the vacuum can has been cast and vacuum tests will soon be performed. It is expected that the poles, yoke, and vacuum can will be assembled and doweled at the machine-shop facility by late September. One coil has been fabricated and the second coil is expected by October.

A conceptual design and drawing have been completed for the scattering chamber and target mechanism. Comments are being solicited from potential users and engineers. Studies have been made regarding the relative merits of the vertical drift (VDC) and MP-10 drift chambers for the focal plane. Tests of the MP-10-style chambers at a 45° angle of incidence for the incoming particle will be made at the end of cycle 38 to evaluate their performance. The project is on schedule and within the budget of $350 thousand. A working system ready to accept beam is expected by April 1984.

Helmut Baer reviewed the development history and current performance characteristics of the π^0 spectrometer. Highlights of the research program include the studies of isobaric analogs to determine the isovector component of the optical potential, and the studies of giant resonances with $(\pi^{\pm},\pi^0)$ reactions. Of particular significance is the presence of the nuclear monopole signal.

The π^0 spectrometer is capable of obtaining a resolution of 2-MeV FWHM, although 4 MeV is more typical. To make a significant improvement in resolution, the γ-ray energy resolution must be improved. If the photon resolution were 5% FWHM at 100 MeV, the π^0 energy resolution could be improved to approximately 0.5 MeV FWHM. Monte Carlo design studies are being performed to determine the advantages of replacing the lead-glass photon detectors with either NaI or BGO modular arrays. Such an improvement might cost about $1 million. If the modification project is deemed worthwhile, the group will prepare a detailed proposal for evaluation by the TAP.

LAMPF may be able to acquire a new polarized ion source with 1 to 2 orders of magnitude higher intensity than the present source at a cost of several million dollars and several man-years of effort. Perhaps Accelerator Improvements Project (AIP) funds (estimated to be about $1 million per year after FY 1984) could be used. It is necessary, however, to evaluate the physics justification for such a source, and a workshop will be convened for that purpose in November.

Billy Bonner discussed his investigation of new polarized ion source possibilities for LAMPF. The National Laboratory for High-Energy Physics in Japan (KEK) has developed an optically pumped source with demonstrated output of 10-25 μA and an anticipated output of about 60 μA. An atomic beam ion source (Gruebler, SIN) has produced 6 μA with projections (perhaps optimistic) of 100 μA. A 20-μA source would provide an increase in intensity by a factor of 50-100 over the present LAMPF source.

Lewis Agnew reported on experimental-area development projects. The A-2 target cell was rebuilt during the 1983 shutdown. Production currents up to 900 μA have been achieved on Line A. Replacement of the A-1 target cell is planned for the 1984 spring shutdown. Both the LEP and time-of-flight-isochronous (TOFI) spectrometers are making reasonable progress: first use of the LEP spectrometer is planned for next summer. The polarized-target program at the High-Resolution Spectrometer (HRS) was successful; plans for the 1984 continuation of this program are being reviewed. Design work for the HRS focal-plane shielding is complete, but installation in 1984 will be in conflict with the polarized-target setup. The shielding will be deferred until 1985 if the polarized-target program is scheduled for 1984.

Planned modifications to the beam-stop area were presented by Walter Sommer. The major design considerations and goals are to provide:

- improved environment for beam-line diagnostics,
- improved shielding and elimination of cracks to reduce leakage of activated gas,
- new facility for proton- and neutron-radiation-effects studies that allows multiple bulk samples and control of irradiation parameters,
- improved facility for high-speed and ultra-high-speed isotope transport and identification,
- access for additional experiment initiatives in nuclear and solid-state physics,
- remote handling and shielded transport of radioactive material, and
- one-day repair/replacement of components or experimental hardware.

Design of the new facility is nearing completion and accelerator improvement funds are available for the project. Material procurement and fabrication have been initiated, and a schedule calling for completion in the spring of 1985 has been established.

A status report on the Long-Range Planning Committee for LAMPF Computing Needs was presented by Martha Hoehn. The committee met for 3 days, October 24-26, 1983.

The committee generally discussed topics in two areas: data acquistion and data analysis. A few notable points in each section were presented to the TAP.

Five topics were discussed for data acquisition: (1) front-end processing, (2) hardware standards, (3) buffer processors, (4) data-acquisition program Q, and (5) networks in the experimental area. These are briefly summarized below.

1. *Front-end processing.* The committee heard a presentation by James Amann summarizing the status of the committee looking into this topic. The microprogrammable branch driver (MBD) does not satisfy all the needs of the users, but there is no obvious candidate for a replacement. It appears that auxiliary crate controllers may solve some problems for some applications. A new high-speed flexible electronics system, FASTBUS, looks like a promising technology to pursue, and the committee recommended that Group MP-1 should do that.

2. *Hardware standards.* The committee felt that we should be moving toward 32-bit VAX-class machines for data acquisition, primarily to solve the 16-bit address space problem with PDP-11s. The committee also felt that LAMPF should begin upgrading tape units to 6250/1600 bpi.
3. *Buffer processors.* Michael Oothoudt presented to the committee a simple idea for taking advantage of the processing capabilities of the new machines without adding overhead from peripherals. The basic idea is to attach multiple processors to a central unit. As an event comes in, it is sent to the first processor, the second event to the second, and so on. Thus, the analysis of events would be carried on in parallel and increase the computing capacity of the central unit.
4. *Data-acquisition system Q.* The committee identified a few Q projects that should be completed, for example, VAX data acquisition and documentation of internals of Q. However, they felt that the Q programmers should not spend time adding "bells and whistles" to Q but should direct their efforts in more productive areas such as FASTBUS and buffer processors.
5. *Networks.* Networks to the experimental area are long overdue and should be implemented with a high priority.

Three topics were discussed under data analysis: (1) Data-Analysis Center (DAC) functions, (2) problems, and (3) external networks. Each of these areas is discussed below.

1. *DAC functions.* The committee discussed at some length the functions that the DAC can serve and those that should be addressed elsewhere. Specifically, the DAC should provide interactive graphics capabilities, should be able to handle tapes effectively, and should serve as a convenient computing tool for the LAMPF community. However, it should be recognized that the DAC cannot necessarily satisfy all the needs of the users and that LAMPF should be willing to use other resources at this Laboratory, namely the Central Computing Facility (CCF).
2. *Problems.* Two main problem areas were identified:
   (1) unacceptable interactive response time on the current systems, and
   (2) inadequate disk space.
   These problems are being addressed.
3. *External networks.* The committee recognized a need to provide convenient communications with other locations. Specifically, MP-1 should investigate implementation of a network system such as Telenet and should provide a convenient method to dial out of the DAC. This communication enhancement can, for example, facilitate distribution of drafts of papers.

The TAP members had several comments and questions concerning this presentation. These questions are listed here.

- Did the committee consider small (personal) computers as a standard for data acquisition?
- Has parallel processing been considered for the DAC?
- Has the committee properly considered options for the long term—specifically, writing data acquisition systems in portable languages?
- Has the committee considered other standard operating systems, such as UNIX?

These points will be brought up at the Long-Range Planning Committee meeting before the final report is prepared.

III. RESEARCH

Nuclear and Particle Physics

Transverse Spin Dependence of the Proton-Proton Total Cross Section (Exps. 504/505, EPB)

(Rice Univ., Univ. of Houston, Institute "Ruđer Bošković," Univ. of Bonn, Los Alamos)

Spokesman: G. C. Phillips (Rice Univ.)

Participants: W. P. Madigan, D. A. Bell, J. A. Buchanan, M. M. Calkin, J. M. Clement, M. D. Corcoran, K. A. Johns, J. D. Lesikar, H. E. Miettinen, G. S. Mutchler, C. J. Naudet, G. P. Pepin, G. C. Phillips, J. B. Roberts, S. E. Turpin, A. D. Hancock, B. W. Mayes, L. S. Pinsky, K. K. Sekharan, M. Furic, V. Valkovic, W. von Witsch, J. C. Allred, B. E. Bonner, and C. Hollas

Final analysis of the total-cross-section difference data $\Delta\sigma_t = \sigma(\uparrow\downarrow) - \sigma(\uparrow\uparrow)$ for proton-proton scattering with the protons in transverse spin states has been completed. The measurements were made for 12 incident proton energies from 300 to 800 MeV. The experiment was performed during the period from June to November 1980, using the LAMPF variable-energy polarized proton beam and the Rice University polarized proton target. The detectors were precision ionization chambers.

The measurements were made by holding the spin orientation of the target constant and reversing the spin orientation of the beam every minute. Thus a measurement of $\Delta\sigma_t$ is made every 2 min. The target polarity was reversed every hour, and in this way 60-80 values of $\Delta\sigma_t$ were obtained for each target polarity. As a result of the current- and position-dependent responses of the ionization chambers, the $\Delta\sigma_t$ values were systematically dependent on the changes of beam position and current, which we found were correlated with the beam spin reversals.

These dependences were removed by regressions against the mensured changes in vertical position, horizontal position, and beam current. The remaining small systematic dependences were adequately randomized by the target polarity reversals to produce nearly complete cancellation on averaging the positive- and negative-target polarity data. This procedure was applied to the data from each of the six transmission chambers (each subtending a different solid angle). Coulomb-nuclear interference corrections were applied at each solid angle, and an extrapolation to zero solid angle was made.

The results are tabulated in Table I. The total error is the pure statistical error added in quadrature with the systematic errors in the target polarization, beam polarization, and the target constant, which is the reciprocal of the target density and target length. The last column lists the Coulomb-nuclear interference corrections.

Figure 1 is a plot of $\Delta\sigma_t$ (mb) vs T(MeV), the kinetic energy of the incident proton. All the published data[1-5] in this energy range are plotted. The four experimental groups used a variety of techniques: Rice University at LAMPF (this experiment) used ionization chambers; Rice University at ZGS[1] and Bugg et al.,[2] scintillators; Bystricky et al.,[3] Gray-encoded scintillators with a frozen spin target; and Ditzler et al.,[4] scintillators with a frozen-spin target. The Rice data indicate a sharper structure at T 562 MeV than that previously observed.

These results were reported at the 1983 meeting of the Division of Particles and Fields, Blacksburg, Virginia. A Ph.D. thesis based on this work is in preparation.

REFERENCES

1. J. D. Lesikar, Ph.D. thesis, 1981.

2. D. V. Bugg et al., TRIUMF Annual Report, June 1983.

3. J. Bystricky et al., preliminary results of $\Delta\sigma_t$ at Saclay, Commissariat a L'Energie Atomique note CEA N 2276, ISSN 0750 6678, 1980 1981.

4. W. R. Ditzler et al., Phys. Rev. D 27, 680 (1983).

5. R. A. Arndt et al., Phys. Rev. D 28, 97 (1983).

Table I. Summary of Results from LAMPF Exp. 504, a Measurement of the Total Cross-Section Difference ($\Delta\sigma$) for Transversely Polarized Protons. The energies quoted are the laboratory beam energies at the center of the target. The $\Delta\sigma$'s are final values, corrected for Coulomb-Nuclear Interference (CNI). The total error is the pure statistical error added in quadrature with the systematic errors in the target polarization, beam polarization, and target constant C (the reciprocal of the product of the target density and target length). The CNI corrections are tabulated in the last column.

			Errors (mb)					
Energy (MeV)	Momentum (GeV/c)	$\Delta\sigma$(mb)	Total	Statistical	Target Polarization	C	Beam Polarization	CNI
304	0.81	-0.2976	1.0010	0.5486	0.8302	0.1011	0.0404	1.7236
436	1.00	5.8415	0.7296	0.3051	0.6132	0.2334	0.0934	1.1729
485	1.07	8.3381	0.9669	0.2816	0.8375	0.3646	0.1459	1.0452
519	1.12	8.6139	1.1843	0.2106	1.0950	0.3705	0.1482	1.2042
536	1.14	10.4697	0.8767	0.2056	0.6888	0.4661	0.1864	1.1486
571	1.18	12.2696	1.4226	0.2079	1.2698	0.5634	0.2254	1.0014
587	1.20	9.8386	1.2944	0.6410	1.0153	0.4489	0.1796	0.8607
620	1.24	7.8671	0.4935	0.0778	0.3079	0.3507	0.1403	0.8522
637	1.27	7.1526	1.0763	0.2184	0.9954	0.3216	0.1286	0.7207
689	1.33	5.6256	0.5337	0.1191	0.4498	0.2427	0.0971	0.7712
741	1.39	5.6360	0.3122	0.1006	0.1299	0.2464	0.0986	0.7072
791	1.45	5.8884	1.0627	0.1231	1.0177	0.2604	0.1041	0.6809

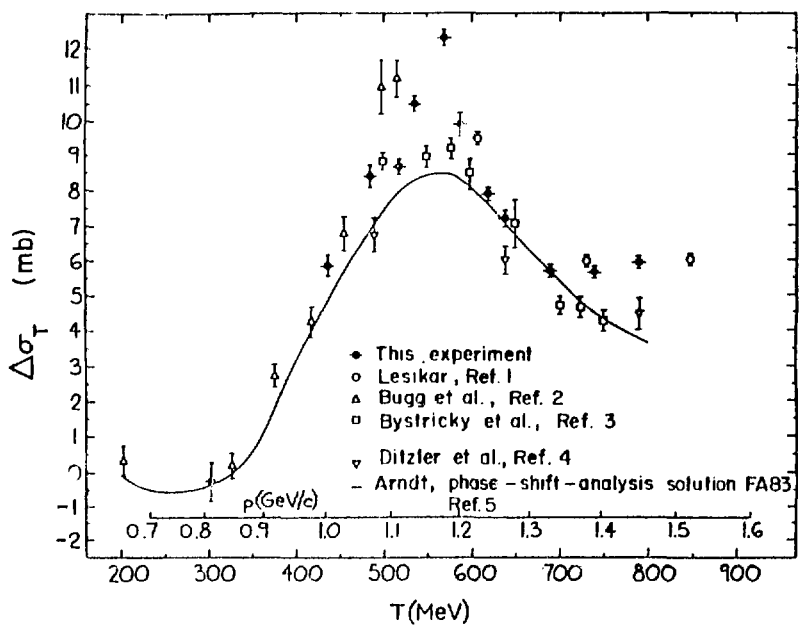

Fig. 1.

Plot of $\Delta\sigma_T$ (mb) vs T(Mev), the kinetic energy of the incident proton. Error bars show statistical errors only.

Measurements of the Spin-Rotation Parameters for $\vec{p}d \rightarrow \vec{p}d$ Elastic Scattering at 496, 647, and 800 MeV

(Exp. 635, EPB)

(Los Alamos, UCLA, Univ. of Texas at Austin, Rice Univ.)

Spokesmen: B. E. Bonner (Los Alamos) and G. J. Igo (UCLA)

This collaboration has completed $\vec{p}d \rightarrow \vec{p}d$ elastic-scattering experiments at 500, 650, and 800 MeV[1-3] at the EPB area. These experiments used a polarized proton beam and an unpolarized liquid-deuterium target, and measure the outgoing proton polarization in the "Janus" polarimeter, which incorporates a carbon analyzer (efficiency ~10%). A two-arm counter system is used to obtain a clean two-body trigger.

A publication is in progress on the 1981 measurements of D_{NN}, D_{SS}, D_{LS}, P, and A_N at 500 and 800 MeV[1] (D is the polarization memory parameter). In 1982 we re-measured the above parameters with a faster data-acquisition system, thereby obtaining smaller statistical errors in addition to measuring D_{SL} and D_{LL} at 500 and 800 MeV. The measurement of L in the final state required a bending magnet to precess the outgoing proton spin direction sideways (S) in order that it be observable; the magnet also serves as an analyzer for momentum.

In August 1983 we measured D_{NN}, D_{SS}, D_{LS}, D_{SL}, D_{LL}, P, and A at 650 MeV for the four-momentum transfer range $-t = 0.4$-1.18 $(GeV/c)^2$ (30-60° lab).

All the data taken since September 1982 have been analyzed and a compilation has been submitted to Physical Review C. The EPB experiments complement HRS experiments at smaller angles.

REFERENCES

1. A. Rahbar, Ph.D. thesis, University of California at Los Angeles, 1982, *unpublished*.

2. Sun Tsu hsun et al., submitted to Phys. Rev. C.

3. Sun Tsu-hsun et al., in Proc. of the 10th Int. Conf. on Few Body Problems, Karlsruhe, Germany (1983), p. 233.

Studies of the Spin Dependence of $p \uparrow p \rightarrow \pi X$ (Exp. 336, EPB)

(Rice Univ., Univ. of Houston, Los Alamos)

Spokesmen: G. S. Mutchler (Rice Univ.) and L. S. Pinsky (Univ. of Houston)

Participants: S. D. Baker, J. A. Buchanan, J. M. Clement, M. D. Corcoran, I. M. Duck, M. Furic, G. P. Pepin, G. C. Phillips, E. A. Umland, A. D. Hancock, E. V. Hungerford, B. W. Mayes, Y. Xue, J. C. Allred, T. M. Williams, M. W. McNaughton, and C. Hwang

Analysis of the $pp \rightarrow pp\pi^0$ data from Phase II of this experiment has been completed. In Phase II the spin-dependent cross section $d^5\sigma/dp_1 d\Omega_1 d\Omega_2$ for the reactions $p \uparrow p \rightarrow p\pi^+ n$ and $pp\pi^0$ were measured at EPB at 500 and 647 MeV, along with some repeated measurements at 800 MeV. This was a kinematically complete experiment using a liquid-hydrogen target and a polarized beam. The angles θ_1 and ϕ_1 and momentum p_1 of the proton were measured in a magnetic spectrometer, in coincidence with the angles θ_2 and ϕ_2 of the pion (second proton) in a time-of-flight arm. The data were taken during the summer of 1982.

Of the 17 angle pairs measured in Phase II, 14 have good statistics for the reaction $pp \rightarrow pp\pi^0$. There are six angle pairs at 800 MeV and four each at 500 and 647 MeV. The asymmetries and fifth-order differential cross section $d^5\sigma/dp_1 d\Omega_1 d\Omega_2$ are plotted against p_1, the momentum of the proton in arm 1 in Figs. 1-3. The data appear as dots; errors are small on the scale of the figures.

The solid lines are the predictions of Dubach et al.,[1] who have provided us with their nucleon-nucleon computer code, which incorporates a relativistic, unitary, three-body pion-exchange model. Since the system had a solid-angle acceptance of 9 × 10 sr or more in each arm, it was necessary to average the theoretical predictions over the actual geometry used. The theoretical curves shown in the figures thus have been averaged over the system acceptance using a Monte Carlo program.

Comparison of the data with theory shows excellent agreement at 800 MeV. At lower energies the general shape of the asymmetries is reproduced, but the cross

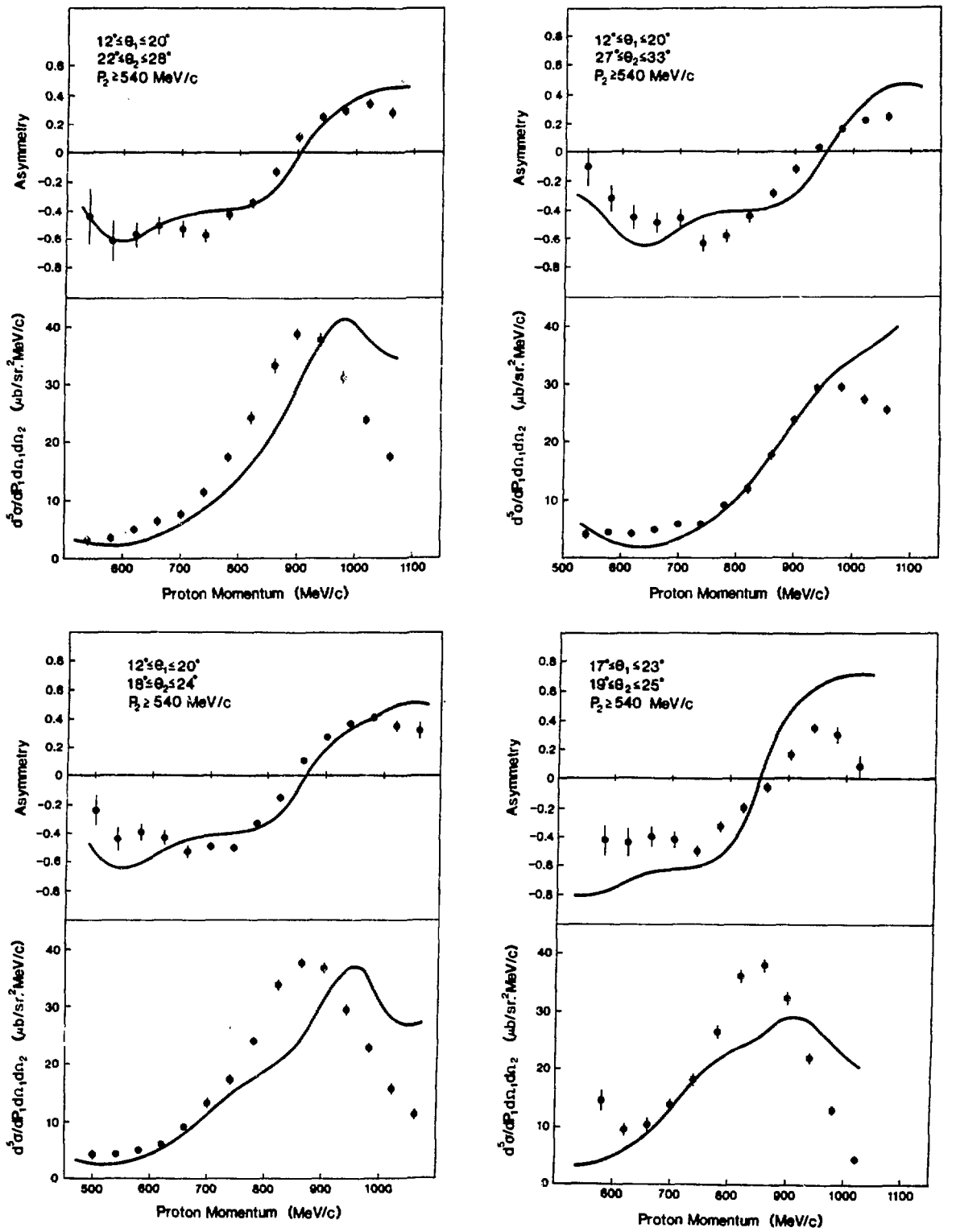

Fig. 1.
Cross sections and asymmetries $p \uparrow p \rightarrow pp\pi^0$ at 800 MeV.

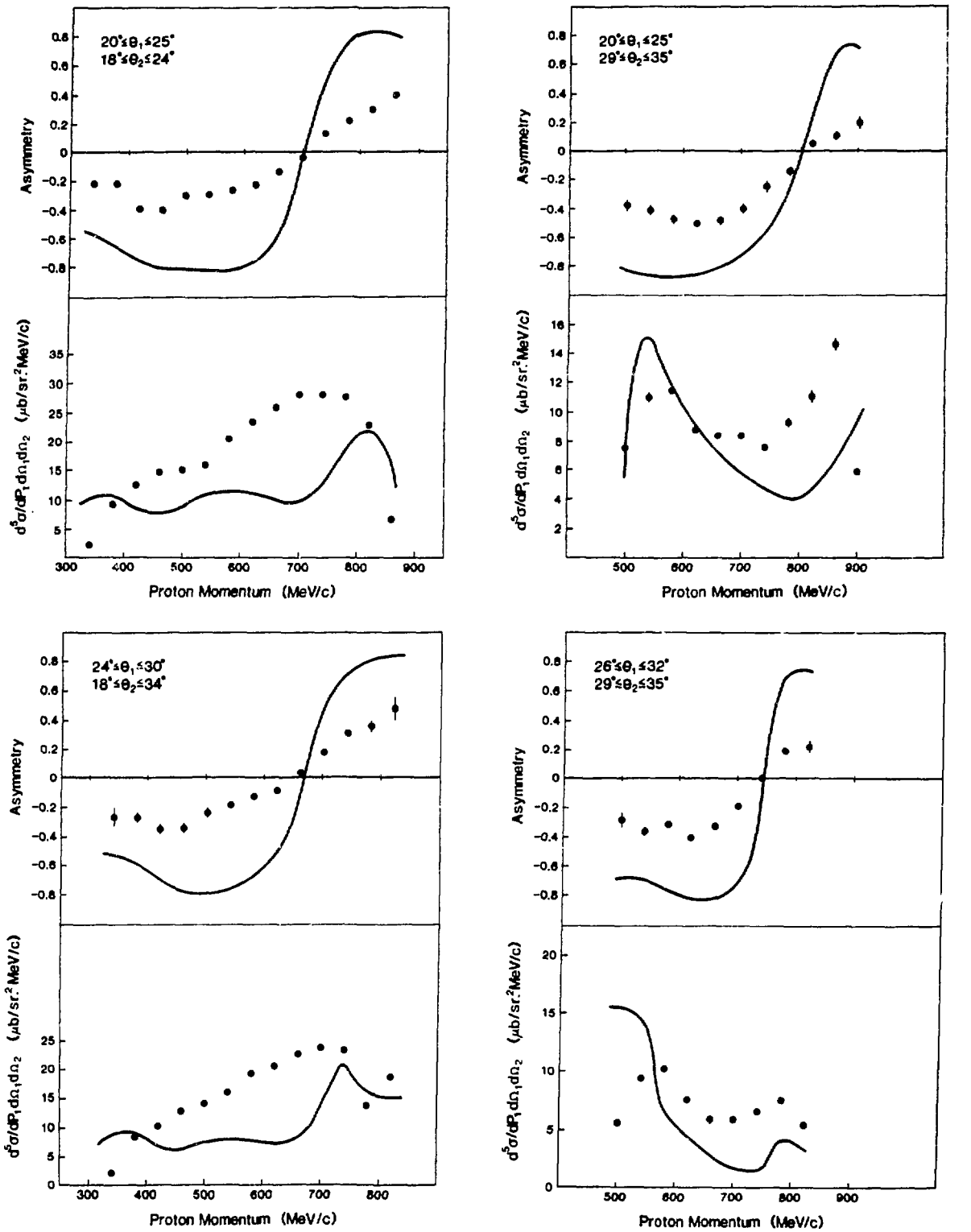

Fig. 2.
Cross sections and asymmetries $p \uparrow p \rightarrow pp\pi^0$ at 647 MeV.

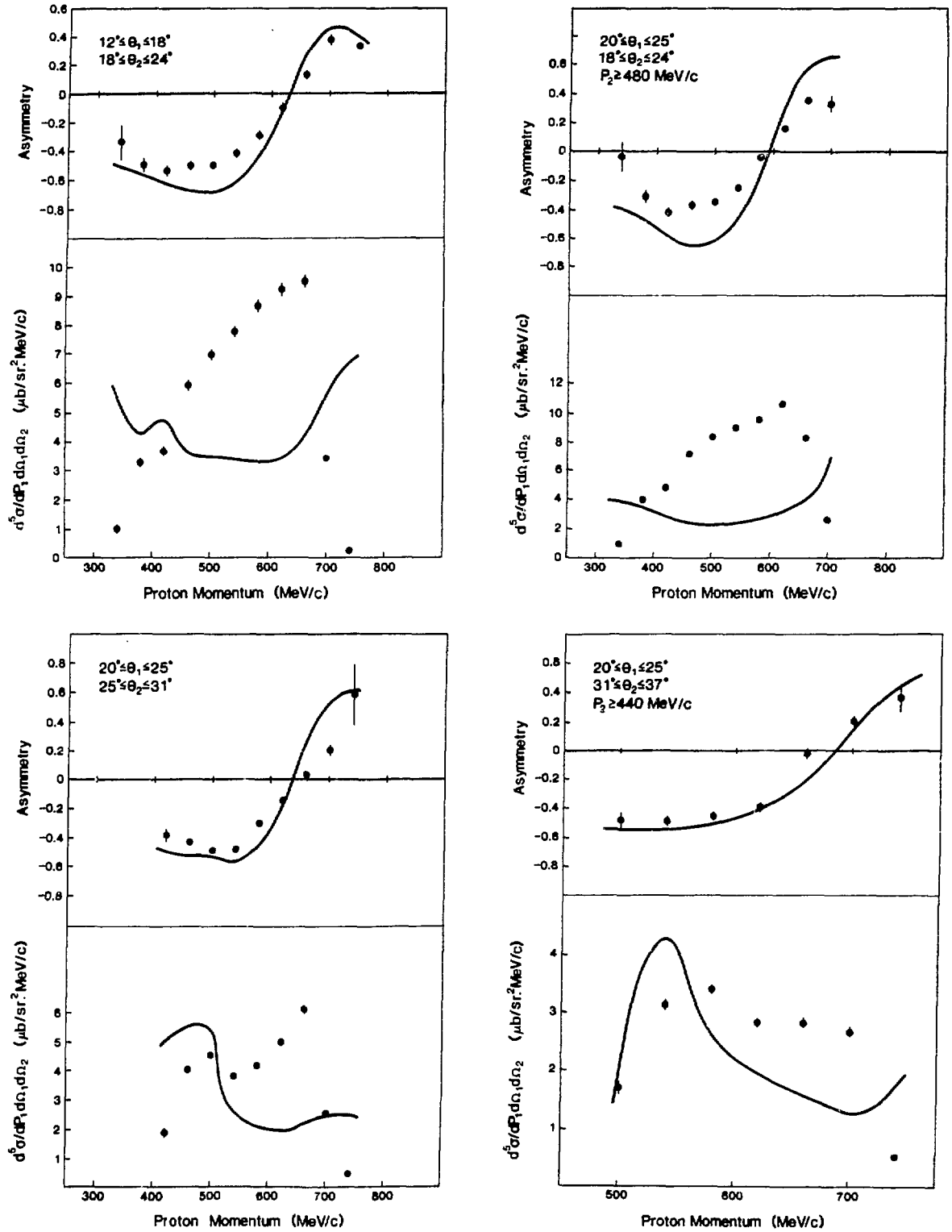

Fig. 3.
Cross sections and asymmetries $p \uparrow p \rightarrow pp\pi^0$ at 500 MeV.

sections are underestimated, with the discrepancy getting worse at the lower energy.

Preliminary results of this work were presented in April at the American Physical Society meetings in Baltimore.

REFERENCE

1. J. Dubach, W. M. Kloet, A. Cass, and R. R. Silbar, Phys. Lett. **106B**, 29 (1981), and J. Phys. C (Nucl. Phys.) **8**, 475 (1982); and W. M. Kloet and R. R. Silbar, "Nucleus-Nucleon Dynamics at Medium Energies" (I and II), Nucl. Phys. A **338**, 231 (1980).

Measurement of Parity Violation in the *pp* and *p*-Nucleus Total Cross Sections at 800 MeV (Exp. 792, EPB)

(Los Alamos, Univ. of Illinois, Princeton Univ., Univ. of Maryland)

Spokesman: V. Yuan (Los Alamos)

Participants: J. D. Bowman, R. Carlini, D. MacArthur, R. E. Mischke, D. E. Nagle, H. Frauenfelder, R. W. Harper, A. B. McDonald, and R. L. Talaga

The goal of Exp. 792 is to measure the contribution of the weak force to nucleon-nucleon scattering at 800 MeV. Although the scattering is dominated by strong and electromagnetic interactions, the weak interaction may be identified by the signature of parity violation.

In the experiment, longitudinally polarized protons are scattered from an unpolarized target; parity violation manifests itself as a small helicity dependence in the total cross section. A longitudinal asymmetry can be defined as $A_L = (\sigma_+ - \sigma_-)/(\sigma_+ + \sigma_-)$, where $\sigma_+(\sigma_-)$ is the total cross section for positive- (negative-) helicity protons on the target.

Experiment 792 was active for two run periods during the second half of 1983: a 1-week run in August, which served as a tuneup to test several important improvements to the experiment, was followed by a 2-week-long data run in November with a liquid-hydrogen target. In the November run a statistical sensitivity in A_L of 1.5×10^{-7} was achieved.

This experiment is one of a series to measure the contribution of the weak force to nucleon-nucleon scattering as a function of energy. At 15 and 45 MeV, the experiments[1-3] yield $A_L = -(1.7 \pm 0.8) \times 10^{-7}$ and $A_L = -(3.2 \pm 1.1) \times 10^{-7}$, respectively, in good agreement with theoretical predictions based on a meson-exchange model[4-6] and a hybrid quark model.[7] In contrast, for 6-GeV/c protons on a water target, a value of $A_L = (2.65 \pm 0.60) \times 10^{-6}$ has been reported.[8] This value is larger than the meson-exchange prediction by more than an order of magnitude.[9] It is in agreement, however, with recent calculations that treat wave-function renormalization[10] and the parity-violating effects of the quark constituents of nucleons.[11]

The basic experimental layout is shown in Fig. 1. The experiment uses the LAMPF polarized proton beam at an intermediate energy of 800 MeV, with polarization reversed at a rate of 30 Hz at the injector. Two low-noise ion chambers[12] determine the cross section by measuring the transmission of the polarized beam incident on the target. By analyzing the signal for a component correlated with the 30-Hz polarization-reversal frequency, we can determine the magnitude of any helicity dependence of the total cross section. Auxiliary detectors monitor 30-Hz changes in beam properties that may

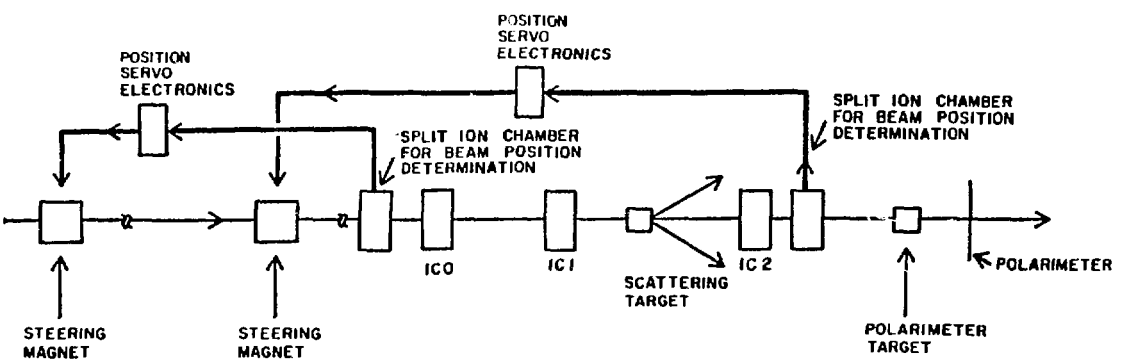

Fig. 1.
Schematic of experimental apparatus.

Table I. Results for November 1983 Run.

	Data	A_7	Chi-Squared	Number of Runs
Normal	Raw	$(-1.9 \pm 1.7) \times 10^{-7}$	79.5	74
	Corrected	$(0.3 \pm 2.1) \times 10^{-7}$	64.4	74
Reverse	Raw	$(-7.2 \pm 1.6) \times 10^{-7}$	200.0	83
	Corrected	$(-2.1 \pm 1.9) \times 10^{-7}$	85.6	83

Combined Result $\left(\frac{NN-RR}{2}\right)$: $A_L = (1.2 \pm 1.4) \times 10^{-7}$.

mimic a true parity-violation signal. The beam properties monitored include intensity modulation, position motion, residual transverse polarization, and a phase-space distribution of residual transverse polarization across the profile of the beam.

In August 1983 we implemented and tested two important improvements to the experiment. The first was to supplement our split-foil position monitors with new position/size detectors of multiwire design. Not only did we obtain pulse-by-pulse information on beam size for the first time, but we were able to calculate beam position in a way that takes the beam spot size into account. The second improvement was to use the EPB precessor to provide longitudinal polarization in EPB. In the November data run that followed, this change greatly improved the compatibility of Exp. 792 with other experiments running concurrently in Line C.

Following the successful conclusion of the August tests, an extensive data run on hydrogen was undertaken in November. In this run, a third important improvement was introduced: a rotating stripper wheel that gave a better measurement of our sensitivity to intensity modulation. With proper synchronization of the rotating wheel, the effects of intensity changes correlated to the polarization reversal could, for the first time, be examined directly.

Sufficient LH_2 data were taken in the November run to reach a statistical error limit of 1.5×10^{-7} in A_L for hydrogen. As had been done in the past, equal amounts of data were taken in both the "normal" and "reverse" configurations of the polarized source. By using the dual source configurations, we can measure and remove systematic contributions not included in the corrections that are applied for systematics of known origin.

Obtaining final results for the November run is under way, but awaits completion of a careful determination of systematic corrections. However, an initial estimate of the asymmetry has been made, based on a rough calculation of the systematic corrections.

Table I shows the results for "normal" and "reverse"; the combined value is $A_L = (1.2 \pm 1.4) \times 10^{-7}$. Such a value is consistent with predictions for 800 MeV based on the meson-exchange[9] and hybrid quark[7] models. It disagrees, however, with the large value predicted by the wave-function-effect analysis of Nardulli et al.[13] We point out that all errors quoted are based only on statistical uncertainties and do not include any nonstatistical contributions.

Systematic corrections used in the calculation of A_L are listed in Table II. The nonstatistical uncertainties in the determination of systematic corrections are estimated to be 10-15% as large as those corrections.

Table II. Systematic Contributions to A_L.

Quantity	Source	Contribution to A_L
Intensity	Normal	-3.7×10^{-7}
	Reverse	-7.0×10^{-7}
Position	Normal	1.6×10^{-7}
	Reverse	1.3×10^{-7}
Polarization		$\leq 9 \times 10^{-8}$

REFERENCES

1. D. E. Nagle et al., in *High Energy Physics with Polarized Beams and Targets*, G. H. Thomas, Ed., AIP Conf. Proc. 51, 224 (1978).
2. R. Balzer et al., Phys. Rev. Lett. 44, 699 (1980).
3. M. Simonius, in *High Energy Physics with Polarized Beams and Targets*, C. Joseph and J. Soffer, Eds., Experientia, Suppl. No. 38 (International Symposium, Lausanne, 1980), p. 355.
4. V. R. Brown, E. M. Henley, and F. R. Krejs, Phys. Rev. C 9, 935 (1974).
5. M. Simonius, Nucl. Phys. A 220, 269 (1974).
6. B. Desplanques, J. F. Donoghue, and B. R. Holstein, Ann. Phys. 124, 449 (1980).
7. L. S. Kisslinger and G. A. Miller, Phys. Rev. C 27, 1602 (1983).
8. N. Lockyer et al., Phys. Rev. Lett. 45, 1821 (1980).
9. E. M. Henley and F. R. Krejs, Phys. Rev. D 11, 605 (1975).
10. G. Nardulli and G. Preparata, Phys. Lett. 117B, 445 (1982).
11. T. Goldman and D. Preston, Nucl. Phys. B 217, 61 (1983).
12. J. D. Bowman et al., Nucl. Instrum. Methods 216, 399 (1983).
13. G. Nardulli, E. Scrimeri, and J. Soffer, Centre de Physique Théorique, CRNS, Marseille, France, preprint CPT-82, p. 1420 (to be published in Z. Phys. Chem.).

Inelastic Pion Scattering from ^{17}O and ^{18}O (Exp. 369, EPICS)

(Univ. of Minnesota)

Spokesman: D. Dehnhard (Univ. of Minnesota)

The analysis of data taken during Exp. 369 has been completed and a manuscript is being prepared for publication. The π^+ and π^- scattering cross sections were measured on ^{17}O, using version I of the EPICS cooled-gas target. Because the gas was made up of $\simeq$50% ^{17}O, 25% ^{18}O, and 25% ^{16}O, extensive ^{18}O runs were made for background subtraction. Here, we report on some of the results of the analysis of the ^{17}O and ^{18}O data.

Octupole transitions in ^{17}O had been studied before by inelastic electron scattering[1,2] and the strength had followed approximately the rules of a weak-coupling model assuming a

$$\left[{}^{16}O(3^-) \times 1d^n_{5/2}\right]_{J^\pi = (\frac{1}{2})^- \ldots (^{11}/_2)^-}$$

multiplet.

In this work the angular distributions (Fig. 1) for the 4.55-MeV $[(\frac{3}{2})^-]$, 3.85-MeV $[(\frac{5}{2})^-]$, 5.69-MeV $[(\frac{7}{2})^-]$, 5.22-MeV $[(\frac{9}{2})^-]$, and 7.76-MeV $[(^{11}/_2)^-]$ states in ^{17}O closely resemble those of the 3^- states in ^{16}O (6.13 MeV) and ^{18}O (5.09 MeV), even though the transitions in ^{17}O can proceed by other than the total angular momentum transfer $J = 3$, as in ^{16}O and ^{18}O. For example, the $(\frac{7}{2})^-$ state can be reached by $J = 1$, 2, 3, 4, 5, and 6. Nevertheless, judging by the similarity of all angular distributions, the contributions with $J \neq 3$ appear to be not very important for these states in ^{17}O. An exception might be the $(\frac{3}{2})^-$ state, for which $J = 1$ is predicted to be quite important, but the data are not sufficiently good to extract the relative contributions from $J = 1$ and 3. [No cross sections could be extracted for the very weakly excited $(\frac{1}{2})^-$ state.]

If we compare the relative cross section for these transitions with the prediction of the simpie version of the $[3^- \times 1d^n_{5/2}]$ model (that is, without proper antisymmetrization), we find that the octupole strength is not split among the states according to this model. For instance, for the $(^{11}/_2)^-$state we observe only about 50% of the predicted strength (Table I).

To analyze the data in the distorted-wave impulse approximation (DWIA), calculations were done with the code ARPIN.[3] Microscopic transition densitites from three different models were used. Here, we report the results that were obtained using the large-space shell-model

Table I. Renormalization factor $R^\pm = \sigma^\pm_{exp}/\sigma^\pm_{DWIA}$ at $\theta_{c.m.} = 44°$ for Octupole Transitions in ^{17}O and ^{16}O Calculated Without ($\delta = 0$) and With ($\delta = 0.6$) Polarization Charges.

			($\delta = 0$)		($\delta = 0.6$)	
	J_f	E_x (MeV)	R^+	R^-	R^+	R^-
	$(^{11}/_2)^-$	7.76	3.5	8.0	1.0	1.2
	$(\frac{9}{2})^-$	5.22	6.0	12.0	1.1	1.0
^{17}O	$(\frac{7}{2})^-$	5.69	10.0	9.0	1.2	1.0
	$(\frac{5}{2})^-$	3.84	3.5	2.5	0.8	0.8
	$(\frac{3}{2})^-$	4.55	5.0	4.5	1.1	0.9
^{16}O	3^-	6.13	4.0	4.0	1.0	1.0

calculations.* Both the $1p \rightarrow 2s1d$ and $2s1d \rightarrow 1f2p$ excitation amplitudes are included for the transitions to low-lying negative-parity states in ^{17}O and ^{18}O. The DWIA curves for ^{17}O (π,π'), with these transition densities and without any effective charge enhancements, are shown in Fig. 1 as broken lines.

For all states, the predicted cross sections are significantly smaller than the data because these transitions are collectively enhanced. The ratios of experimental and theoretical cross sections, $R^{\pm} = \sigma^{\pm}_{exp}/\sigma^{\pm}_{DWIA}$, are given in Table I, columns 2 and 3. Clearly, there is no systematic behavior in R. Next, the $\{LSJ\} = \{303\}$ parts of the neutron and proton transition densities ρ_n and ρ_p were multiplied by enhancement factors E_n and E_p, respectively—that is, $\rho_n' = E_n\rho_n$ and $\rho_p' = E_p\rho_p$. (Here, L, S, and J are, respectively, the transferred orbital, spin, and total angular momenta.) This calculation has been done in Ref. 3 for the $\{202\}$ parts of the $L = 2$ transitions in the p shell. For the $(^{11}/_2)^-$ state, we found that $E_n = 4.7$ and $E_p = 1.7$ are needed to fit the data. For the other states, very different factors were necessary, which makes this approach quite unattractive. Similar erratic behavior in the enhancement factor was found for the $[3^- \times 1d^n_{5/2}]$ model, even when the wave functions were properly antisymmetrized.

A consistent description of the data was obtained by enhancing only the isoscalar, spin-independent part of the transition density. Use of $\delta_n = \delta_p = 0.6$, or equivalently $\delta_0 = 1.2$ and $\delta_1 = 0$, resulted in the absolute cross sections, shown as solid lines in Fig. 1. The ratios are now strikingly close to 1. The same isoscalar enhancement factor $(1 + \delta_0) = 2.2$ gave a good fit to the pion data for ^{16}O $(3^-, 6.13$ MeV).

We have used the same parameters for the DWIA analysis as in Ref. 4. The oscillator parameter, $b = 1.63$ fm, is smaller than the value ($b = 1.76 - 1.78$ fm) needed to fit the ground-state densities of ^{17}O (Refs. 1 and 3). Using $b = 1.76$ fm results in smaller polarization changes slightly larger π^+/π^- asymmetries, and a slight shift of the angular distribution toward smaller angles—that is, the fit to the pion data is not as good as with $b = 1.63$ fm. It is worth mentioning that $b = 1.63$ fm and $\delta_p = \delta_n = 0.6$ give good agreement (just as $b = 1.76$ and $\delta_p = \delta_n = 0.35$ do) between the large-space shell-model calculations and the experimental $B(E3)$ values. An exception is the value for the $(\frac{7}{2})^-$ state, for which the (e,e') data[1] are suspect.

*The large-space shell-model calculations used in this experiment are from D. J. Millener, private communication.

Cross sections for $^{18}O(\pi,\pi')$ were extracted for the first three 2^+ (1.98-, 3.92-, and 5.26-MeV) states, the 1^- (4.45-MeV) state, and the 3^- (5.10-MeV) state. In the previous ^{18}O experiment,[5] cross sections for the second and third 2^+ states could not be extracted because of poor energy resolution. Figure 2 shows the π^+ and π^- data for the three lowest 2^+ states. The ratio $R = \sigma(\pi^-)/\sigma(\pi^+) = 2.1$ for the 2^+ (1.98-MeV) state is consistent with that previously measured for this transition by Iversen et al.[5] For the second 2^+ (3.92-MeV) state, the π^+ and π^- cross sections are more nearly equal, $R = 1.27$. The third 2^+ (5.26-MeV) state is somewhat surprising in that the cross section is much larger than most models predict for ^{18}O wave functions and there is a large π^+ enhancement, $R = 0.2$.

The π^+ and π^- cross sections for the 3^- state at 5.10 MeV are essentially equal. The dashed curves are DWIA calculations using the transition densities of the full $1\hbar\omega$ shell-model calculations of Millener. The predicted cross sections are too small, and the π^+/π^- asymmetry is not observed in the data. The data can be reproduced by enhancing the isoscalar $J(LS) = 3(30)$ amplitude by a factor of 2 and completely omitting the isovector amplitude. This implies a very large neutron polarization change, which indicates a lack of understanding of the neutron components in the wave function of ^{18}O.

The data obtained for the 1^- state at 4.45 MeV were initially very surprising. The π^+ and π^- angular distributions are very similar, with the π^+ being slightly larger than the π^-. The angular-distribution shapes are completely out of phase with calculations using simple single particle-hole transition densities, such as $1p_{1/2} \rightarrow 2s_{1/2}$ or $1p_{3/2} \rightarrow 1d_{5/2}$. The DWIA calculations, using one-body density-matrix elements (from shell-model calculations) as transition densities,[4] produce angular-distribution shapes closer to that of the data. The magnitudes for both π^+ and π^- are more than an order of magnitude smaller than the data [Fig. 3(a) and (b)].

The two calculations use the full $1\hbar\omega$ shell-model calculation of Millener (solid curve) and the *p-sd* calculations of Brown.* The addition of the *sd-fp* components in the full $1\hbar\omega$ calculation decreased the large ratio $\sigma(\pi^+)/\sigma(\pi^-)$, but it is still much larger than experimentally observed. It should be noted that a calculation using an ^{16}O shell-model calculation that included core polarization in pertubation theory produces agreement with the data for both the ^{18}O, 1^- (4.45-MeV) and ^{16}O, 1^- (7.12-MeV) states.

*B. A. Brown, private communication.

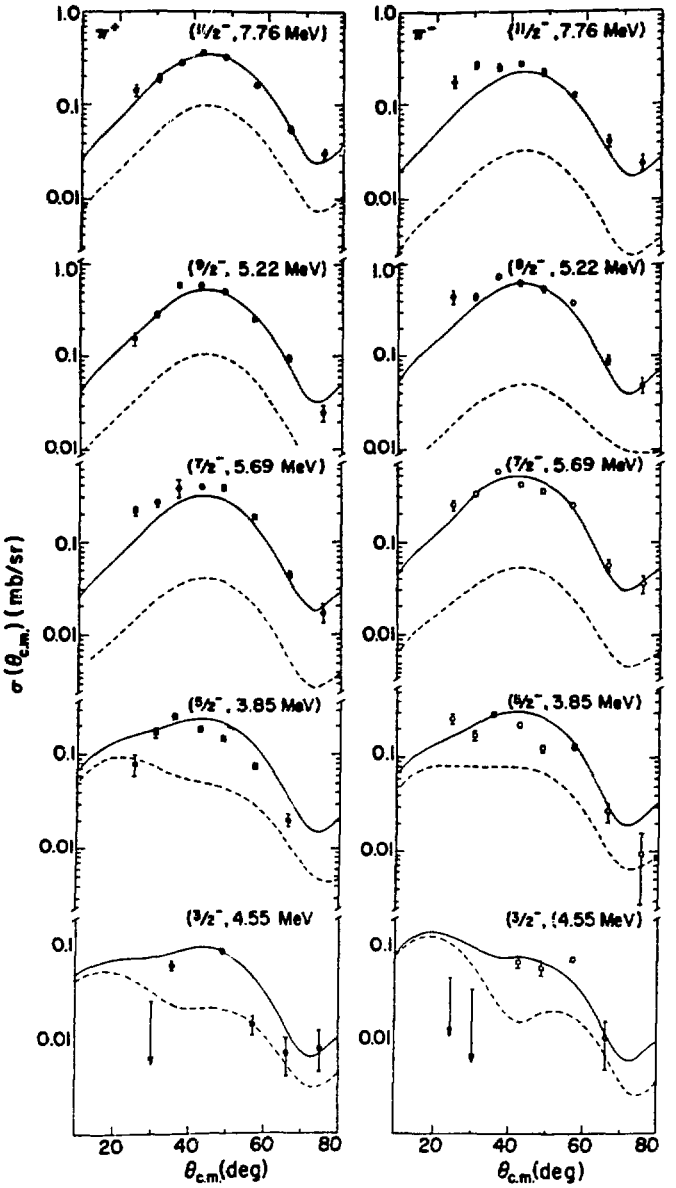

Fig. 1.
Angular distributions for states in ^{17}O. The curves are DWIA calculations with (solid-line) and without (broken-line) effective charge enhancements.

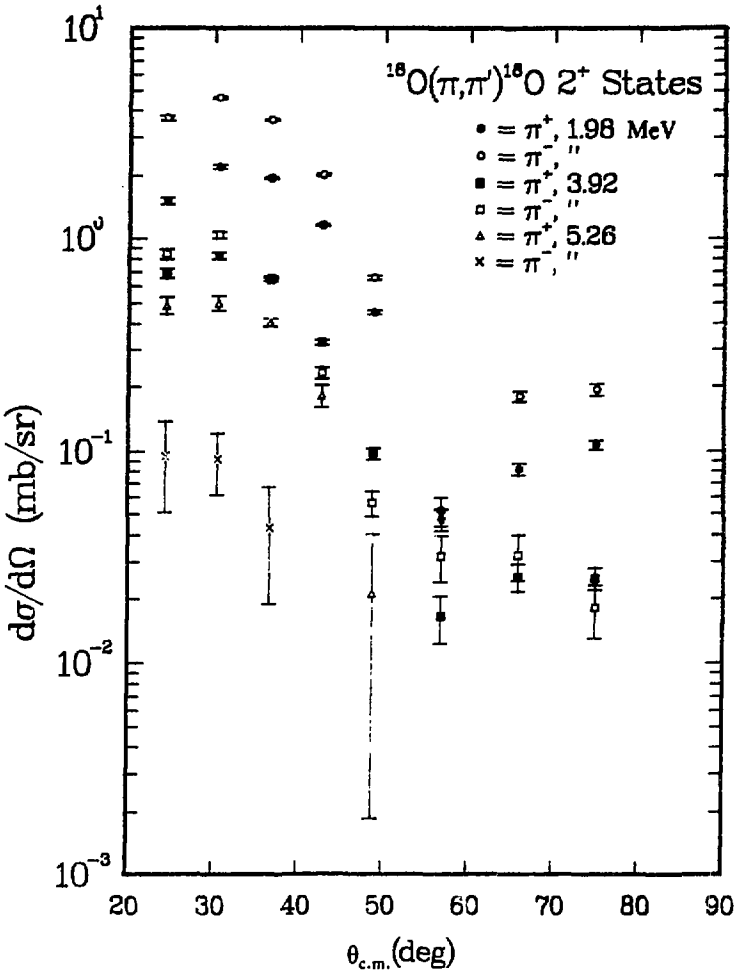

Fig. 2.
Angular distributions for the three lowest 2$^+$ states in ^{18}O.

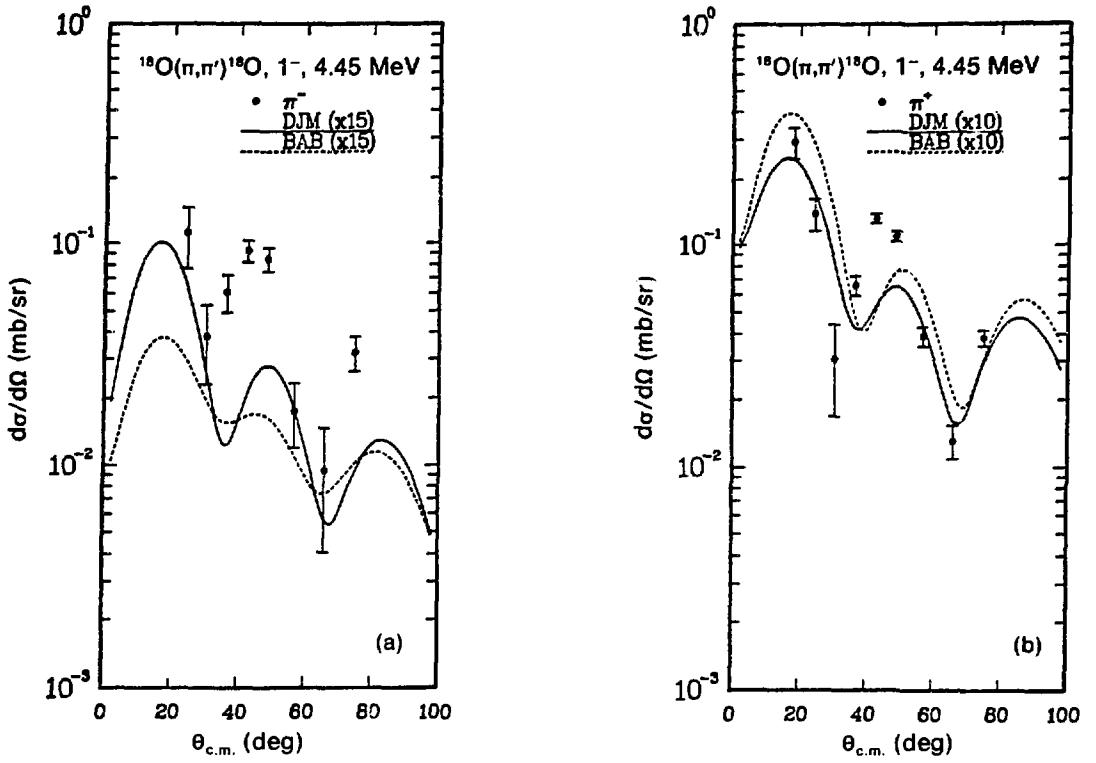

Fig. 3(a) and (b).
Angular distributions for the 1^- state in ^{18}O for (a)π^- and (b) π^+ scattering. The curves are described in the text.

REFERENCES

1. J. C. Kim et al., Phys. Lett. 57B, 341 (1975), and Nucl. Phys. A 297, 301 (1978).

2. J. Kelly et al., Bull. Am. Phys. Soc. 25, 575 (1980).

3. T.-S. H. Lee and D. Kurath, Phys. Rev. C 21, 293 (1980).

4. T.-S. H. Lee and R. D. Lawson, Phys. Rev. C 21, 679 (1980).

5. S. Iverson et al., Phys. Rev. Lett. 40, 227 (1978).

Excitation of 8^- States in ^{54}Fe (Exp. 565, EPICS)

(Argonne National Lab.; Univ. of Birmingham, United Kingdom; Indiana Univ.; New Mexico State Univ; Los Alamos; Univ. of Massachusetts; Montana State Univ.; Northwestern Univ.; Oregon State Univ.)

Spokesman: B. Zeidman (Argonne National Lab.)

We have investigated the excitation of 8^- states in ^{54}Fe with 162-MeV pions at EPICS. At large momentum transfer, such high-spin particle-hole (stretched) states are selectively excited in pion inelastic scattering.[1] By combining the analysis of the pion data and previously published electron data, isoscalar and isovector transition strengths were extracted for each 8^- state.

The selectivity of pion inelastic scattering for isoscalar spin-flip strength is particularly valuable because no other probe shares this selectivity. This fact makes pion scattering a natural complement to 180° electron scattering, which selectively excites isovector spin-flip states.

With the ^{54}Fe results obtained in this work, it is clear that in high-spin particle-hole states much less isoscalar spin-flip strength has been identified than isovector spin-flip strength. This phenomenon persists from *p*-shell nuclei, at least up to the middle of the *f-p* shell. It is already well known that the isovector spin-flip strength to such high-spin states is only 30-50% of simple single-particle estimates.[2] This amount of quenching also has been observed for Gamow-Teller resonances ($L=0$, isovector spin-flip excitations),* where it has been interpreted as evidence for non-nucleonic degrees of freedom, and in particular isobar-hole states.[4] Since non-nucleonic degrees of freedom contribute only weakly to isoscalar excitations, the large unexplained relative quenching of the isoscalar strength compared to the isovector strength implies that the nuclear-structure input must be examined more critically for both modes of the nuclear response.

The experiment was carried out on the EPICS channel and spectrometer system. A large (10- by 20-cm) isotopically enriched (>97%, ^{54}Fe, 151-mg/cm^2) target was used. Spectra with π^+ were accumulated in 10° steps from 40 to 100°; π^- spectra were accumulated at 70, 80, and 90°. Short runs were taken at 5° intervals to establish the elastic-scattering yields. The channel and spectrometer were used in the conventional fashion. In addition to the 8^- states at 8.31, 8.95, 9.97, 10.68, and 13.26 MeV identified in electron scattering, two new 8^- states at 9.80 ± 0.05 and 11.65 ± 0.05 MeV excitation were observed.

The inelastic yields to the different 8^- states differ greatly for π^+ and π^-. This difference is the result of interference of isoscalar and isovector amplitudes, since for a transition with a pure isospin structure (either pure $\Delta T=0$ or pure $\Delta T=1$) the π^+ and π^- yields must be equal, as they are for the 13.26-MeV $T=2$ state. By combining the pion data with the electron inelastic-scattering results,[5] it is possible to separate the isospin amplitudes for each state. The experimental cross sections and $B(M8)$ satisfy the following relations for each state i:

$$\sigma^i_{\pi^-}(\theta) = [Z^i_0 M^{\pi^-}_0(\theta) + Z^i_1 M^{\pi^-}_1(\theta)]^2 ,$$

$$\sigma^i_{\pi^+}(\theta) = [Z^i_0 M^{\pi^-}_0(\theta) - Z^i_1 M^{\pi^-}_1(\theta)]^2 ,$$

$$B^i(M8)_e = (Z^i_0 M^e_0 + Z^i_1 M^e_1)^2 .$$

In these equations, M^π_0 (M^π_1) is the square root of the cross section for exciting an isoscalar (isovector) transition to a pure one-particle one-hole state in a closed-shell nucleus by π^- inelastic scattering. The M^e_0 and M^e_1 are similar amplitudes $[B(M8)]^{1/2}$ for electron inelastic scattering. The coefficients Z_0 and Z_1 contain the nuclear-structure amplitudes of isoscalar and isovector excitation of each state. The reaction dynamics is contained in the M factors, which can be obtained from distorted-wave impulse approximation (DWIA) calculations. Based on the free-nucleon properties,

$$M^{\pi^-}_0 \approx 2M^{\pi^-}_1 ,$$

$$M^e_0 = \left(\frac{\mu_n + \mu_p}{\mu_n - \mu_p}\right) M^e_1 = -0.187\ M^e_1 ,$$

where μ_n and μ_p are the neutron and proton magnetic moments, respectively.

For electron scattering, the absolute values of M^e_0 and M^e_1 can be obtained from DWIA. However, the uncertainties in the reaction dynamics make the DWIA calculation of the absolute values of M^π_0 and M^π_1 more

*See, for example, Ref. 3 and references therein.

uncertain. To avoid this uncertainty, M_1^π can be obtained for the $T = 2$ state, since Z_1 is determined by the electron-scattering data. Then, only the ratio M_0^π/M_1^π need be extracted from the DWIA calculations.

This procedure renders the results insensitive to the exact choice of the radial form factor or the pion optical potential. Because the ratio of isoscalar to isovector cross sections is determined essentially by an isospin Clebsch-Gordan coefficient, it is not expected to be sensitive to the reaction dynamics. This is particularly true for high-spin states where the transition density is surface localized. Recent calculations indicate that although medium corrections may modify the ratio of M_0^π/M_1^π for low-spin states, they have little effect for high-spin states, thereby supporting the procedure used here. It should also be noted that in the few cases where the isoscalar pion results have been checked with proton inelastic scattering, the results have agreed very well,[2] although there are considerable uncertainties in the reaction dynamics in the proton case.[6]

The structure coefficients Z_0 and Z_1 for each 8^- state are tabulated in Table I. For comparison, the coefficients obtained in a $[(f_{7/2}^{-3}) \times g_{9/2}]_{8^-}$ calculation are also given. In this model space, the structure coefficients satisfy a sum rule — that is,

$$\sum_i (Z_0^i)^2 = \frac{7}{8}$$

and

$$\sum_i (Z_1^i) = \frac{7}{8} .$$

The isovector strength can be further subdivided into strength in $T = 2$ states,

Table I. Isospin Amplitudes for ^{54}Fe 8^- States.

Experiment			Theory[a]		
Excitation Energy	Z_0	Z_1	Excitation Energy	Z_0	Z_1
8.31	$0.12 \pm {0.02 \atop 0.04}$	0.24 ± 0.02	8.31	0.336	0.444
8.95	0.02 ± 0.04	0.20 ± 0.04			
9.80	$0.16 \pm {0.02 \atop 0.04}$	0.04 ± 0.04	9.58	0.226	0.193
9.97	0.08 ± 0.04	-0.20 ± 0.02	10.37	0.312	−0.349
			10.80	0.204	0.202
10.68	$0.20 \pm {0.04 \atop 0.02}$	-0.14 ± 0.04	11.014	0.432	−0.192
11.65	$0.12 \pm {0.03 \atop 0.06}$	0.04 ± 0.08	11.57	0.353	0.125
			11.98	0.380	0.064
13.26	0	0.44 ± 0.02	13.26	0	0.601
$\sum_i Z^2$	0.102	0.354		0.759	0.815
$1p$-$3h$ sum rule	0.875	0.875			
Fraction of $1p$-$3h$ sum	12%	40%			

[a]Only the eight states with the largest expected cross sections in pion or electron inelastic scattering are listed.

$$\sum_i (Z_1^i)^2 = \frac{3}{8}$$

and $T = 1$ states,

$$\sum_i (Z_1^i)^2 = \frac{4}{8} .$$

The sum of the experimental isoscalar strength is only 12% of this limit, and the sum of the isovector strength is only 40% of this extreme three-hole one-particle calculation.

It is significant that the quenching of the particle-hole strengths is similar to the values obtained in other nuclei for high-spin particle-hole states. The ratio of the summed isoscalar strength to the summed isovector strength for all cases of stretched particle-hole states, where information on the isoscalar strength exists, exhibits a consistent trend in which the isoscalar strength is more strongly quenched than the isovector strength. (A stretched state is one that has the maximum angular momentum available for a $1\hbar\omega$ excitation—that is, 4^- in the $0p$ shell, 6^- in the $1s$-$0d$ shell, and 8^- in the $0f$-$1p$ shell.) The present data therefore give a clear indication that the strong quenching of isoscalar spin-flip strength is a rather general phenomenon.

In summary, data for pion inelastic scattering to 8^- levels in ^{54}Fe have been presented. By combining these data with previous electron-scattering data, isoscalar and isovector transition amplitudes were extracted for each 8^- state. Only 12% of the simple one-particle three-hole strength was observed for the isoscalar excitations, and only 40% of the one-particle three-hole strength was observed for the isovector excitations. This stronger quenching of the isoscalar spin-flip strength compared to the isovector strength appears to be a general feature for high-spin particle-hole states; the present case represents the heaviest nucleus where such an isospin decomposition has been done thus far.

REFERENCES

1. C. Olmer, B. Zeidman, D. F. Geesaman, T.-S. H. Lee, R. E. Segel, L. W. Swenson, R. L. Boudrie, G. S. Blanpied, H. A. Thiessen, C. L. Morris, and R. E. Anderson, Phys. Rev. Lett. 43, 612 (1979).

2. R. A. Lindgren, W. J. Gerace, A. D. Bacher, W. G. Love, and F. Petrovich, Phys. Rev. Lett. 42, 1524 (1979).

3. C. Goodman, Nucl. Phys. A 374, 241c (1982).

4. M. Ericson, A. Figureau, and C. Thevenot, Phys. Lett. 45B, 19 (1973); E. Oset and M. Rho, Phys. Rev. Lett. 42, 47 (1979); A. Bohr and B. Mottelson, Phys. Lett. 100B, 10 (1981); and R. D. Lawson, Phys. Lett. 125B, 255 (1983).

5. R. A. Lindgren, J. B. Flanz, R. S. Hicks, B. Parker, G. A. Peterson, R. D. Lawson, W. Teeters, C. F. Williamson, S. Kowalski, and X. K. Maruyama, Phys. Rev. Lett. 46, 706 (1981).

6. C. Olmer et al., to be published in Phys. Rev. C.

Inelastic Pion Scattering from ^{24}Mg and ^{26}Mg: The New Year's Experiment (Exp. 573, EPICS)

(Univ. of South Carolina, Univ. of Texas, Univ. of Pennsylvania, Los Alamos, Drexel Univ., Univ. of Massachusetts)

Spokesman: G. Blanpied (Univ. of South Carolina)

This experiment first ran at EPICS during New Year's Day 1983, using about one-half of the allotted time. The second half is scheduled for New Year's, 1984.

In the first run, π^+ and π^- data were taken on ^{26}Mg at three energies. Angles were chosen to provide steps of momentum transfer $\ell \sim qR$, where R was determined by the ratio $A^{1/3}$ for ^{28}Si and compared with π^+ data on ^{28}Si (Refs. 1-3). Data were obtained at scattering angles corresponding to $qR \sim 2$, 3, 4, and 6 at 116 and 292 MeV, and $qR \sim 2$-8 at 180 MeV, where $R \sim 3.3$ fm. Inelastic spectra up to an excitation of more than 20 MeV were acquired with a resolution of better than 250 keV at most angles. The normalization was done relative to $\pi^{\pm}p$ scattering. Of interest is the comparison of the relative π^-/π^+ strengths for the excitation of $J^\pi = 2^+$, 3^-, and 4^+ collective states to shell-model predictions.

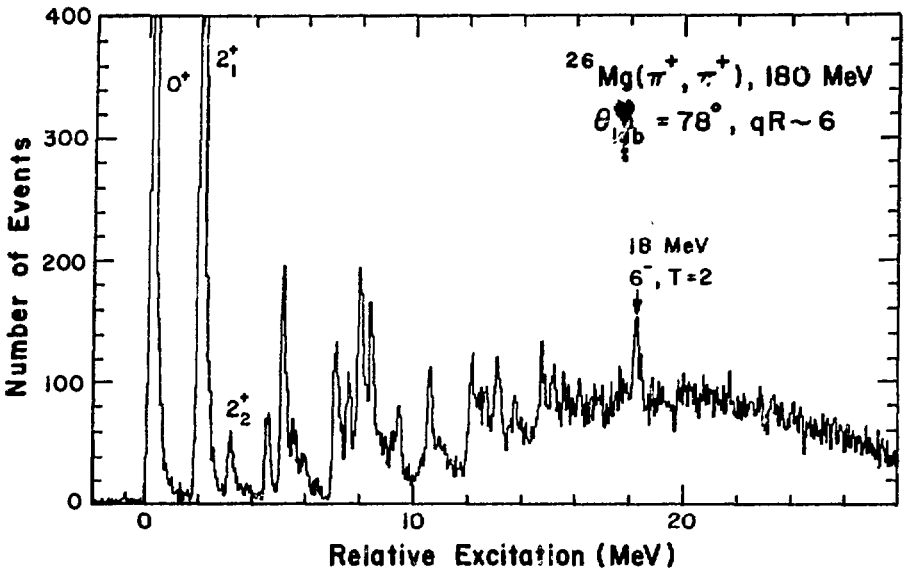

Fig. 1.
Spectrum of π^+ scattering from ^{26}Mg at a laboratory angle of 78° where the momentum transfer is relatively large.

Seen in the π^+ spectrum (Fig. 1), obtained at an angle corresponding to $qR \sim 6$, is the $(6^-, T=2)$ state at 18 MeV. This state also has been seen in 180° electron scattering[4] at Bates and with (p,p') at the Indiana University Cyclotron Facility (IUCF).* The π^+ and π^- cross sections are approximately equal, as expected for a pure isovector transition, and are equal to 11 μb/sr at the peak. The same cross section for the $(T=1, 6^-)$ state in ^{28}Si excited by 162-MeV pions was observed to be 24 μb/sr (Ref. 2).

*D. F. Geesaman et al., Ref. 5, and private communication.

REFERENCES

1. B. M. Preedom et al., Nucl. Phys. A 236, 385 (1979).

2. C. Olmer et al., Phys. Rev. Lett. 43, 612 (1979).

3. B. Zeidman et al., Phys. Rev. Lett. 40, 1539 (1978).

4. R. A. Lindgren et al., Bull. Am. Phys. Soc. 27, 697 (1982); and Long Don Pham, University of Massachusetts B.S. thesis, May 1983, unpublished.

5. D. F. Geesaman et al., Bull. Am. Phys. Soc. 27, 697 (1982).

Isovector Properties of Collective States and the Interacting Boson Approximation Model (Exp. 671, EPICS)

(Northwestern Univ.)

Spokesmen: A. Saha and K. K. Seth (Northwestern Univ.)

Isovector (or, equivalently, proton-neutron) properties of nuclear states provide extremely sensitive tests of nuclear-structure models.[1,2] For heavy nuclei, one model, which has gained increasing attention in recent years, is the Interacting Boson Approximation (IBA) model.[3] In the latest version of this model, called the IBA-2 model,[4] the active part of the nucleus (outside a supposedly inert core) is described in terms of a small number of mutually interacting proton and neutron bosons that can be either in the *s* or *d* state. This model can make explicit predictions regarding the isovector properties of nuclear transitions. Here we report on the first successful experiment specifically designed to test these predictions.

We have measured differential cross sections for elastic and inelastic scattering of 180-MeV π^+ and π^- from enriched targets (≥95%) of ^{104,106,108,110}Pd at the EPICS facility. As illustrated in Fig. 1, the energy resolution obtained was ≃165 keV. To extract M_n and M_p from our data, we have made distorted-wave impulse approximation (DWIA) calculations with the coordinate-space computer code DWPI[5] using a Kisslinger-type optical potential and collective form factors. As is well known, the proton transition matrix element M_p is related to β_p as

$$B(E\ell\uparrow) \equiv M_p^2 \equiv (3ZR^\ell/4\pi)^2\,\beta_p^2 \quad .$$

The M_n is defined in exactly the same manner in terms of N and β_n. We note that our values of M_p for the 2_1^+ states agree well within errors (≤5%) with those from lifetime measurements.[6] For the 3_1^- states, no other direct results for M_n are available for comparison.

In the IBA-2 model the neutron and proton quadrupole transition matrix elements are defined[7] as

$$Q_p = \alpha_p A_p + \beta_p B_p$$

and

$$Q_n = \alpha_n A_n + \beta_n B_n \quad .$$

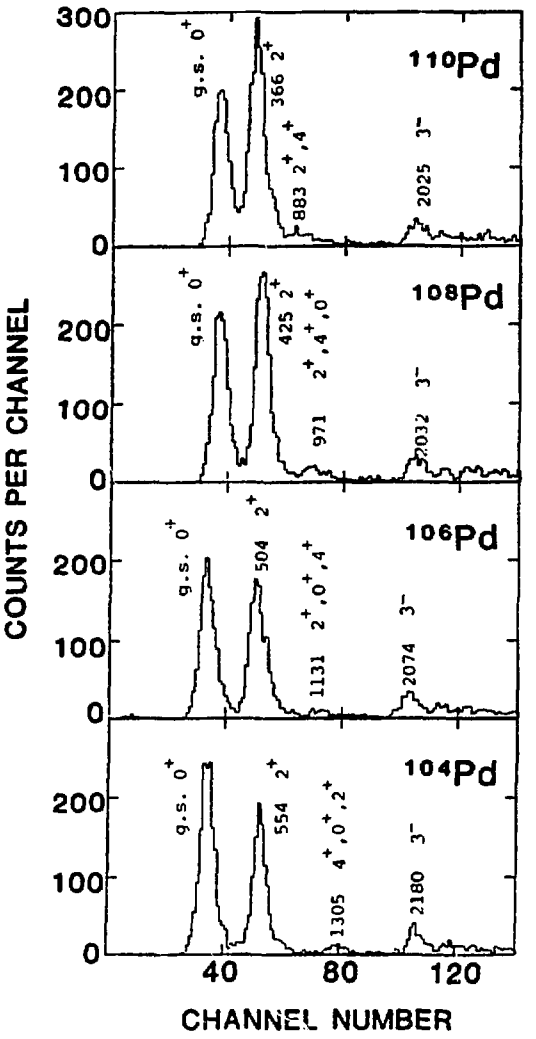

Fig. 1.
Excitation-energy spectra for the reaction Pd(π,π′) at $\theta_{lab} = 42.5°$.

The nuclear-structure information is contained in the reduced boson proton-neutron transition matrix elements, $A_{p,n}$ and $B_{p,n}$, for the *d*-boson nonconserving and *d*-boson conserving parts, respectively. The $\alpha_{p,n}$ and $\beta_{p,n}$ are the corresponding values of the quadrupole operators.

We relate our experimental results to the IBA-2 model at two different levels, with or without core polarization. Further, we can treat $\alpha_{n,p}$ and $\beta_{n,p}$ as adjustable parameters, as was done in Ref. 7, or we can use the values calculated in a generalized seniority scheme using

a surface delta interaction.[8] These calculations for palladium give the following results.

	^{104}Pd	^{106}Pd	^{108}Pd	^{110}Pd
	(fm^2)			
α_n	18.5	16.6	15.6	14.8
β_n	−8.2	−8.2	−3.7	2.4
α_p	14.7	15.1	15.3	15.6
β_p	−4.3	−3.9	−2.6	−3.3

In all these comparisons we take A_i and B_i from Ref. 7.

We first consider the IBA-2 model without core polarization. If we follow the phenomenological procedure, using $\chi_p \equiv \alpha_p/\beta_p$ and $\chi_n = \alpha_n/\beta_n$, as optimized in Ref. 7, and setting $M_n = eQ_n$ and $M_p = eQ_p$ for the 2_1^+ states, we obtain the average values $\langle\alpha_n\rangle = 21.2$ fm^2 and $\langle\alpha_p\rangle = 38.8$ fm^2. These lead to a constant $M_p \approx 86$ e-fm^2 and to the rapidly changing M_n/M_p, shown by the thin solid curve in Fig. 2. Neither of these results is in agreement with the data. Further, the M_p for the 2_2^+ states are predicted to be ≈2.5 times larger than the experimental results. If we use the calculated values of α and β, we obtain even poorer agreement with the data. We obtain M_n, which are ≈75 (±8)% of the experimental results; M_p, which are ≈41 (±4)%; and M_n/M_p, which are a uniform factor of ~2 larger than the experimental results (thin dashed curve in Fig. 2). The M_p for the 2_2^+ states fare better, being only ≈21 (±5)% smaller than the experimental values.

From the above results, we conclude that irrespective of what approach is adopted toward α's and β's, we must compensate for the truncation of the valence boson space by including core polarization. As in the shell model, one can do this by introducing "effective" charges e_p and e_n for proton and neutron bosons and note that for a self-conjugate core (here $N = Z = 50$),

$$M_p = e_p Q_p + e_n Q_n \ ,$$

$$M_n = e_n Q_p + e_p Q_n \ .$$

For a given nucleus, once Q_p and Q_n are known, e_p and e_n are determined uniquely by fitting the measured values of M_n and M_p. We first use χ's, as empirically optimized in Ref. 7, and $\langle\alpha_n\rangle = 16.4$ ... .5.2 fm^2 (which are averages of the calculated results) to obtain Q_p and Q_n for each isotope. Comparison with M_p and M_n then leads to a set of e_p and e_n that is essentially the same (within ≈±5%) for all isotopes: $\langle e_p\rangle = 1.13e$, $\langle e_n\rangle = 0.49e$. The results for M_p and M_n/M_p obtained by using these effective charges are shown in Table I and by the thick solid curve in Fig. 2. The fit to the data is quite good. The same effective charges (Table I) predict M_p for the 2_2^+ states, which are in fair agreement with the data. In addition, they lead to very distinctive predictions for M_n/M_p that should be tested in future experiments.

Unfortunately, if we use α's and β's, as obtained from the microscopic calculations referred to earlier, the results are much poorer. Individual e_n are fairly constant ($e_n = 0.46e \rightarrow 0.50e$), but e_p show an unacceptable amount of variation ($e_p = 1.02e \rightarrow 1.35e$) in going from ^{104}Pd to ^{110}Pd. Equivalently, we note that if we use the average values, $\langle e_n\rangle = 0.48e$ and $\langle e_p\rangle = 1.17e$, we fail to reproduce the trend of M_p and M_n individually,

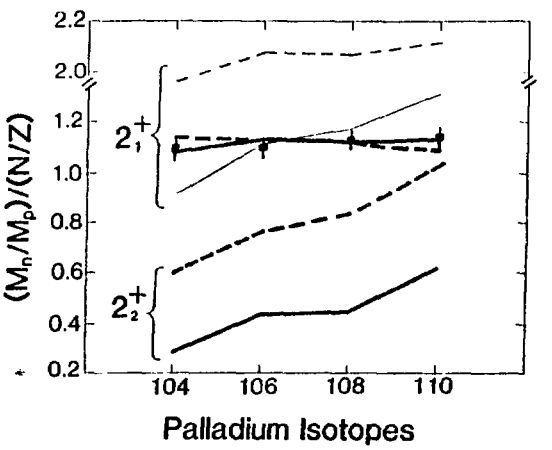

Fig. 2.
The $(M_n/M_p)/(N/Z)$ for the 2^+ states in palladium isotopes. The curves refer to IBA-2 calculations described in the text.

Without core polarization: thin solid line for empirically adjusted $\langle\alpha\rangle$, $\langle\beta\rangle$; thin dashed line for microscopically calculated α, β.

With core polarization: thick solid line for empirically adjusted $\langle\alpha\rangle$, $\langle\beta\rangle$ and $\langle e_p\rangle = 1.12e$, $\langle e_n\rangle = 0.49e$; thick dashed line for microscopically calculated α, β and $\langle e_p\rangle = 1.17e$, $\langle e_n\rangle = 0.48e$.

Table I. Summary of Results for Excitation of 2^+ States in Palladium Isotopes.[a]

		Experimental Results					Model Predictions			
		Ref. 6	(π,π')				IBA-2			
J^π	A	M_p	M_p	M_n	M_n/M_p	N/Z	M_n[b]	M_p[b]	M_n[c]	M_p[c]
2_1^+	104	74(2)	77(2)	106(3)	1.38(5)	1.26	108	79	119	83
	106	83(3)	83(2)	118(3)	1.43(5)	1.30	125	85	126	86
	108	88(3)	89(2)	136(3)	1.52(5)	1.35	135	89	129	87
	110	94(3)	98(2)	156(4)	1.59(6)	1.39	150	95	136	90
2_2^+	104	16(1)					6	17	13	17
	106	13(1)					10	18	19	19
	108	13(1)					9	15	21	18
	110	11(1)					14	16	30	21
3_1^-	104		365(9)	542(14)	1.49(5)	1.26				
	106		360(9)	533(13)	1.48(5)	1.30				
	108		334(8)	539(13)	1.61(6)	1.35				
	110		315(8)	523(13)	1.66(6)	1.39				

[a] $M_{p,n}$, in units of e-fm^2 for 2^+, and e-fm^3 for 3^-.
[b] Average $\langle e_p \rangle = 1.13e$, $\langle e_n \rangle = 0.49e$, and empirical α's and β's.
[c] Average $\langle e_p \rangle = 1.17e$, $\langle e_n \rangle = 0.48e$, and calculated α's and β's.

although M_n/M_p agree with the data (thick dashed curve in Fig. 2). For the 2_2^+ states, the predicted M_p differ from the experimental ones by 43 ($\pm$23)% and the predicted M_n/M_p differ by a factor of 2 from those with empirically adjusted α's and β's.

Because of the limited success obtained above with the IBA-2 model without empirically adjusted parameters, it is instructive to examine what other simple phenomenological models predict. In the hydrodynamical model, nuclei in the palladium region are well described as vibrational nuclei, with

$$E(\lambda) = \hbar^{-2} \langle C_\lambda / B_\lambda \rangle^{1/2} ,$$

$$M_p^2 = \hbar^{-2}(\lambda + 1/2)\,|(3/4\pi) Z e R_0^\lambda|^2 / (B_\lambda C_\lambda) p^{1/2}$$

By analogy, M_n is defined in terms of N, R_n, and $(B_\lambda, C_\lambda)_n$. The parameters B_λ (related to the mass transport associated with the vibration), C_λ (related to the effective surface tension or restoring force), and R, in principle, can vary from nucleus to nucleus and between neutron and proton fluids, but generally are considered constant in a small region of N and Z. Thus, this model predicts M_p = constant for a series of isotopes and $M_n/M_p = N/Z$. As seen in Table I, the experimental M_p increased by ~25% from ^{104}Pd to ^{110}Pd. Also, the experimentally observed ratios of M_n/M_p for the 2_1^+ and 3_1^- states are, respectively, ~12 and ~18% higher than N/Z (see Table I). Better agreement with the experimental results can be obtained by treating B_λ, C_λ, and R as adjustable parameters. For example, we can obtain excellent fits to the measured M_p by simply varying C_2 with neutron number. Similarly, the experimental M_n/M_p for both 2_1^+ and 3_1^- can be fitted perfectly by assuming either that the effective-radius parameters R_n and R_p are different, or that $(B_\lambda, C_\lambda)_p$ and $(B_\lambda, C_\lambda)_n$ are different.

We can summarize our results as follows. The IBA-2 model without core polarization is clearly unsuccessful in explaining the experimental results. By including core-polarization effects, using effective charges, the IBA-2 model can provide a good description of the data if one allows empirical adjustment of its parameters. However,

at this level, it is worthwhile to remember that other, even simpler models, also can explain the experimental results, provided that their parameters are also adjusted from isotope to isotope. Our first attempts to calculate some of the IBA-2 parameters on a microscopic basis have so far been unsuccessful. Clearly more theoretical work is required. At the experimental front, measurement of M_n/M_p for other quadrupole transitions, particularly 0_1^+ to 2_2^+, would help narrow the range of alternative explanations.

REFERENCES

1. A. Saha et al., Phys. Lett. 114B, 419 (1982), and references therein.

2. S. G. Iversen et al., Phys. Rev. Lett. 40, 17 (1978); and S. G. Iversen et al., Phys. Lett. 82B, 51 (1979).

3. A. Arima and F. Iachello, Phys. Rev. Lett. 35, 1069 (1975); and F. Iachello, in "Interacting Bosons in Nuclear Physics" (Plenum Press, New York, 1979), p. 1.

4. T. Otsuka, A. Arima, F. Iachello, and I. Talmi, Phys. Lett. 76B, 139 (1978); and T. Otsuka, A. Arima, and F. Iachello, Nucl. Phys. A 309, 1 (1978).

5. R. A. Eisenstein and G. A. Miller, Comput. Phys. Commun. 11, 95 (1976).

6. Nuclear Data sheets, 18, 125 (1976); 30, 305 (1980); B7, 33 (1972); and 22, 135 (1977).

7. P. Van Isacker and G. Puddu, Nucl. Phys. A 238, 125 (1980).

8. O. Scholten, Michigan State University preprint #MSUCL-416 (1983).

Studies of Giant Resonances in ^{208}Pb with Inelastic Pion Scattering (Exp. 672, EPICS)

(Los Alamos, Univ. of Minnesota)

Spokesmen: T. A. Carey and J. M. Moss (Los Alamos) and S. Seestrom-Morris (Univ. of Minnesota)

To broaden our base for investigating the high-lying nuclear response, we have used 162-MeV inelastic pion scattering to study giant resonances in ^{208}Pb at excitations <40 MeV.

Pions cause isovector transitions relative to isoscalar ones much more strongly than do either 200- or 800-MeV protons, so (π,π') should be better for exciting the isovector giant quadrupole resonance. Comparisons of π^+ and π^- scattering are also a powerful tool for identifying the isospin character of specific transitions. Furthermore, in view of the intrinsic energy dependences of Coulomb excitation, we expect that this mechanism will be much weaker in the excitation of giant resonances with 162-MeV pions than is the case with 800-MeV protons. In general, then, (π,π') should nicely complement our (p,p') studies and be most helpful in unraveling the specific natures of the observed resonances.

High-precision data were acquired in November 1982 at LAMPF. Replay of these data is now complete and several avenues of theoretical analysis currently are being pursued. Both π^+ and π^- spectra exhibit a definite resonance at $E_x \simeq 21$ MeV. Analysis thus far suggests that its quantum numbers are $J^\pi,T = 1^-,0$, but conclusive assignments await ongoing considerations of Coulomb excitation and the underlying continuum. Still, we may have the first strong evidence for a surface-compressional mode as opposed to the volume-compressional mode associated with the isoscalar giant monopole resonance.

To date the most extensive analysis has concentrated on the lower lying isoscalar giant quadrupole resonance (ISGQR) and 3_1^- states because they have been thoroughly studied with other probes and because the extraction of precise absolute yields for them is less hindered by underlying backgrounds. These excitations are believed to involve strongly collective, isoscalar transitions. The generally successful pure collective model predicts $R = \alpha(\pi^-)/\alpha(\pi^+) \simeq N/Z = 1.5$ for such states in ^{208}Pb. Surprisingly, we find that our data give $R = 1.8 \pm 0.1$ for the 3_1^-, whereas for the ISGQR $R = 3.0 \pm 0.5$.

The data for ISGQR transitions, shown in Fig. 1, indicate an even more serious discrepancy than that recently reported for the ISGQR from an independent ^{118}Sn(π,π') experiment.[1] Also, a preliminary analysis of our data for the isoscalar high-energy octupole resonance gives $R = 3.3 \pm 1$. These results could imply the presence

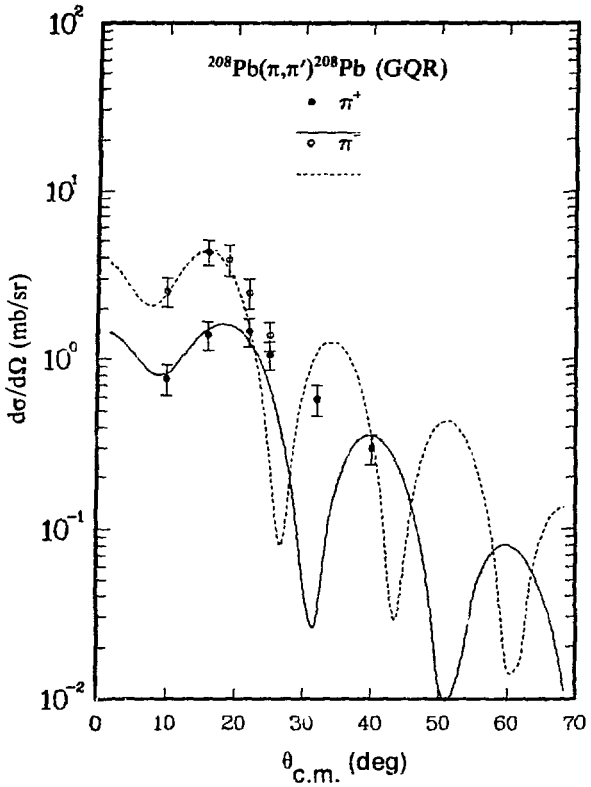

Fig. 1.
The π^+ and π^- angular distributions and collective-model calculations for the giant quadrupole resonance in ^{208}Pb.

of substantial isovector contributions to these purportedly isoscalar transitions, but the rather systematic nature of the disagreement between experiment and theory for more than one giant resonance in more than one nucleus may also be indicative of a breakdown in the standard collective model. Further analysis is in progress.

REFERENCE

1. J. L. Ullman et al., Phys. Rev. Lett. 51, 1038 (1983).

Measurements of Large-Angle Pion-Nucleus Scattering
(Exp. 681, EPICS)

(New Mexico State Univ., Univ. of Texas, Univ. of Minnesota, Los Alamos)
Spokesman: G. Burleson (New Mexico State Univ.)

The motivation for this experiment was to explore possible systematics of pion-nucleus scattering in the large-angle region, where the behavior is poorly known from an experimental point of view and poorly understood from a theoretical point of view. In general, there are many models of pion-nucleus scattering that give a good description of elastic and inelastic scattering over the angular range for which data are abundant (to ~100°) but that diverge drastically for large angles. For a realistic description of pion-nucleus scattering, a fair amount of data is required in the backward hemisphere to constrain the calculations. The results of this first experiment on large-angle pion-nucleus scattering at LAMPF have begun to reveal some of these features.

The experimental configuration is as follows. Basically, a circular magnet is placed at the EPICS pivot point, which is displaced laterally from its normal position. The incident pion enters parallel to a line through the center of the magnet, effectively bends through the arc of a circle, and is incident upon the scattering target at the center of the magnet. A pion scattered at a large angle is bent so as to enter the spectrometer when it is positioned within its normal operating angular range. With this design, the effective solid angle of the spectrometer should be independent of the scattering angle.

Wire-orbit measurements of the magnet were made in place before the experiment began. No indication of azimuthal asymmetry was found over the angular region of the scattered pion. During the experiment, the yield of pions scattered from protons tracked the pion-proton cross section calculated from the phase shifts of Rowe et al.[1] to within ±5% over the full range of scattering angles, 115-180°, confirming the design characteristics of the system.

Some of the preliminary results are shown in Figs. 1-4. All data points were normalized to pion-proton scattering

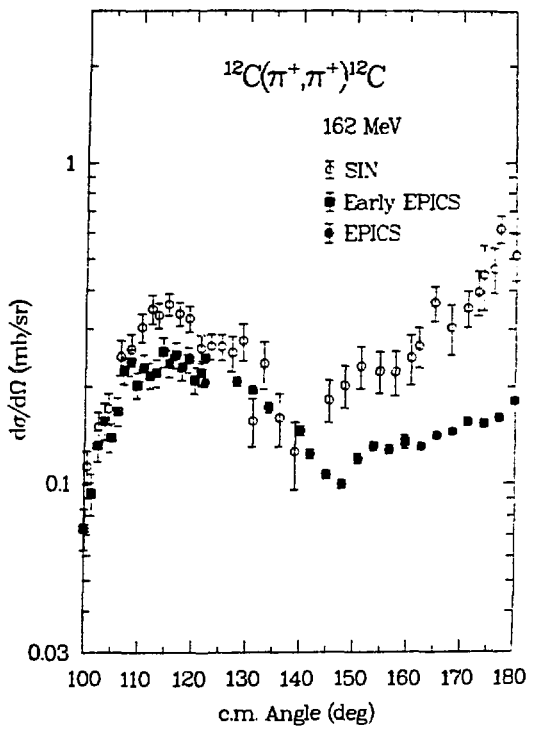

Fig. 1.
Preliminary results for the π^+-^{12}C angular distribution at 162 MeV, compared with previous data (Ref. 2).

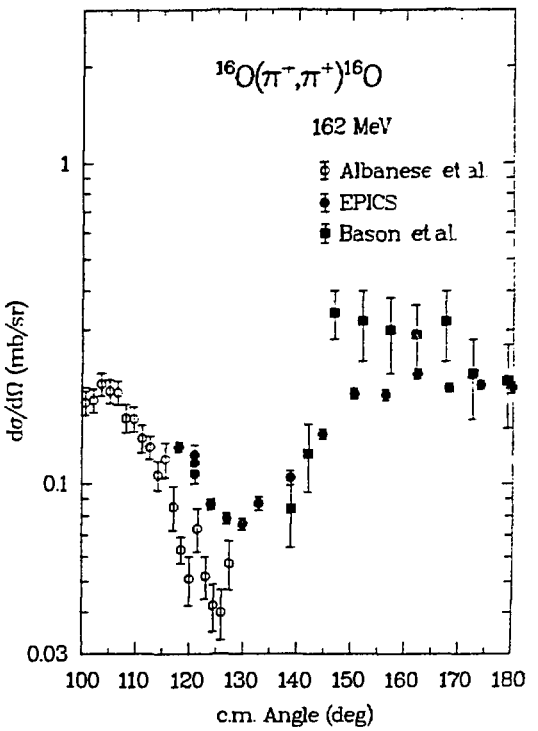

Fig. 2.
Preliminary results for the π^+-^{16}O angular distribution at 162 MeV, compared with previous data (Ref. 3).

measured under spectrometer conditions identical in angle and magnetic-field settings with those used for the pion-nucleus scattering measurements. The experimental differential cross sections for π^+-^{12}C scattering at 162 MeV are shown in Fig. 1. The agreement with previous EPICS data is good, but there is a disagreement with the previous SIN backward data[2] in that the SIN results show a fairly strong backward peaking, whereas the new results do not, and in that there is a difference in absolute value of about a factor of 2.

The results for π^+-^{16}O scattering at 162 MeV are shown in Fig. 2, with previous data from SIN[3] and CERN.[4] The agreement with the CERN results is satisfactory, considering the large error bars, but there is again a disagreement with some previous results from SIN, this time with data taken with the "normal" spectrometer setup.

An excitation function for π^+-deuteron scattering at 176° is shown in Fig. 3 and compared with previous data[5-7] at 180°. There is disagreement with the absolute values of some of the previously measured cross sections, but the new data points join smoothly onto the recent data from KEK.[7] An excitation function for π^+-^{12}C scattering is shown in Fig. 4, with a prediction of the optical model of Cottingame and Holtkamp.[8] It is interesting that this model, which has had good success in predicting pion-nucleus cross sections at angles up to ~100°, makes a fairly good prediction of the structure observed between 130 and 170 MeV, even though it misses the magnitude of the cross sections.

Further studies of these results are in progress.

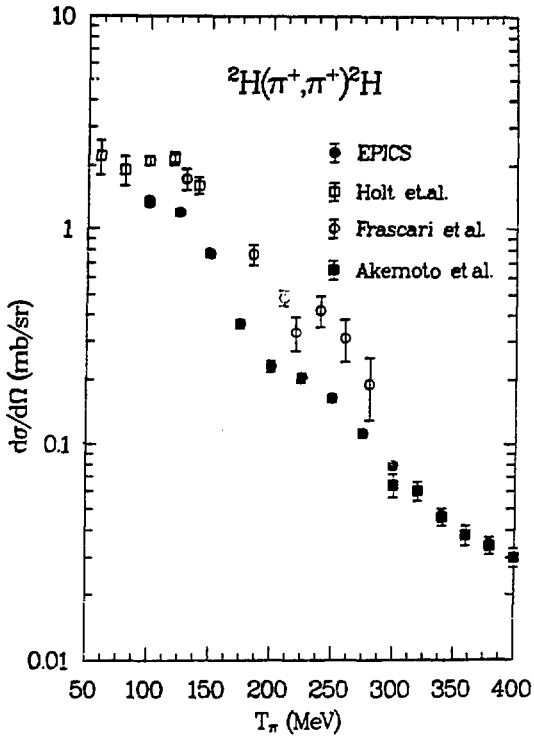

Fig. 3.
Preliminary results for the π^+-deuteron excitation function at 176°, compared with previous data (Refs. 5-7) at 180°.

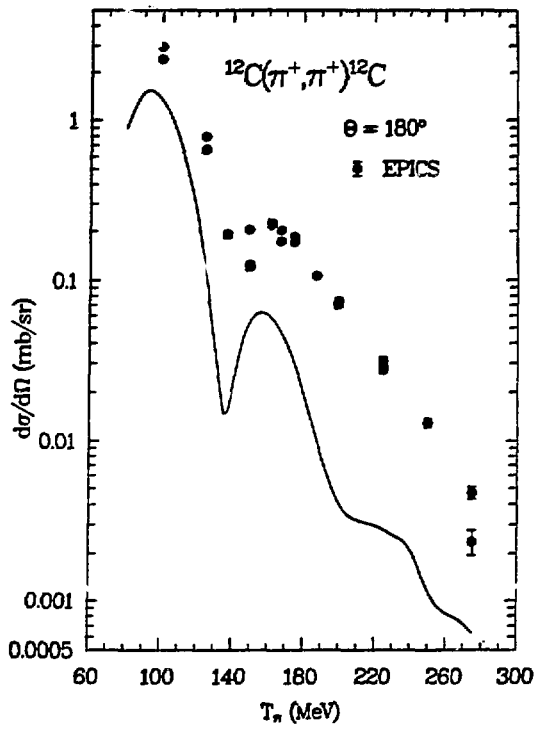

Fig. 4.
Preliminary results for the π^+-^{12}C excitation function at 180°, compared with the prediction of the model of Cottingame and Holtkamp (Ref. 8).

REFERENCES

1. G. Rowe, M. Saloman, and R. H. Landau, Phys. Rev. C **18**, 584 (1978).
2. B. Chabloz et al., Phys. Lett. **81B**, 143 (1979).
3. J. P. Albanese et al., Nucl. Phys. A **350**, 301 (1980).
4. E. Bason et al., contribution to the Ninth Int. Conf. on High-Energy Physics and Nuclear Structure, Versailles, France, 1981.
5. R. J. Holt et al., Phys. Rev. Lett. **43**, 1229 (1979).
6. R. Frascaria et al., Phys. Lett. **91B**, 345 (1980).
7. M. Akemoto et al., Phys. Rev. Lett. **50**, 400 (1983).
8. W. B. Cottingame and D. B. Holtkamp, Phys. Rev. Lett. **45**, 1828 (1980).

π^+/π^- on ^{15}N

(Exp. 703, EPICS)

(Univ. of Minnesota, Los Alamos, Univ. of Texas)

Spokespersons: D. B. Holtkamp (Los Alamos) and S. J. Seestrom-Morris (Univ. of Minnesota)

Experiment 703 ran during January 1983, measuring π^+ and π^- cross sections for excitation of states in ^{15}N. Replay of the data is complete, as is the peak stripping for states below about 8-MeV excitation energy. Calculation of the absolute normalization of the data is currently under way.

Figure 1 shows spectra of π^+ and π^- scattering at $T_\pi = 164$ MeV near the maximum in the angular distribution for $M4$ transitions. Arrows indicate those groups that have been identified as due to $M4$ transitions, $(\frac{3}{2})^+$ states; π^+/π^- asymmetries have been observed for some of these transitions, for example,

$$\frac{\sigma(\pi^+)}{\sigma(\pi^-)} > 3 \text{ for } 10.6 \text{ MeV},$$

$$\frac{\sigma(\pi^+)}{\sigma(\pi^-)} \simeq 5 \text{ for } 12.5 \text{ MeV}.$$

Although the $M4$ transitions were the primary goal of this experiment, interesting data also were obtained on the low-lying excited states. One example is the transition from the $(\frac{1}{2})^-$ ground state to the $(\frac{3}{2})^-$ state at 6.32 MeV. In the extreme shell model, the ^{15}N ground state can be described as a single proton hole in the $1p_{1/2}$ shell and the $(\frac{3}{2})^-$ state as a single proton hole in the $1p_{3/2}$ shell. In this model the transition from $(\frac{1}{2})^- \rightarrow (\frac{3}{2})^-$ would be a pure proton $p_{3/2} \rightarrow p_{1/2}$ single-particle transition. Such a transition would yield a ratio of $R = \sigma(\pi^+)/\sigma(\pi^-) = 9$.

The preliminary data of Exp. 703 for this transition show a significantly smaller value of $R = 1.5$. This difference probably is due to contributions of collective electric quadrupole components. To try to account for this, distorted-wave impulse approximation (DWIA) calculations were performed using a combination of a pure proton $p_{3/2} \rightarrow p_{1/2}pn$ component and a $J(LS) = 2(20)$ component scaled by neutron and proton polarization changes $(1 + \delta_n)$ and $(1 + \delta_p)$. The data and resulting calculations are displayed in Fig. 2. These values of $\delta_p = 0.3$ and $\delta_n = 1.0$ and an additional renormalization of the DWIA amplitude by 1.13 produce electromagnetic properties in agreement with those measured using other probes.

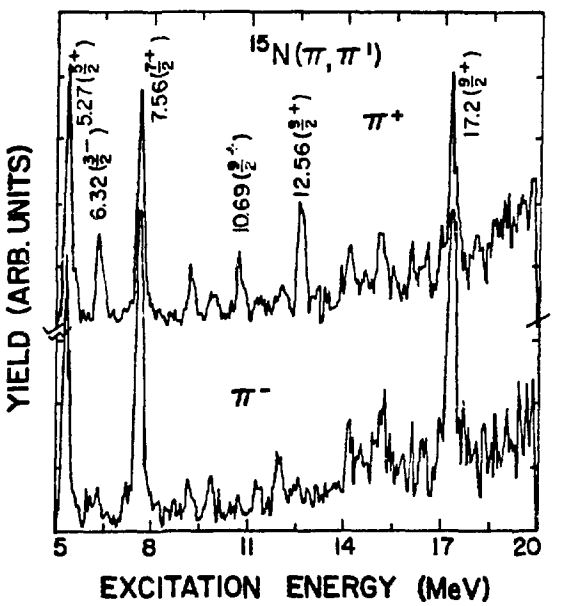

Fig. 1.

The π^+ and π^- spectra for ^{15}N at a scattering angle where the momentum transfer for $M4$ transitions is maximum. States labeled have been identified as $M4$ transitions.

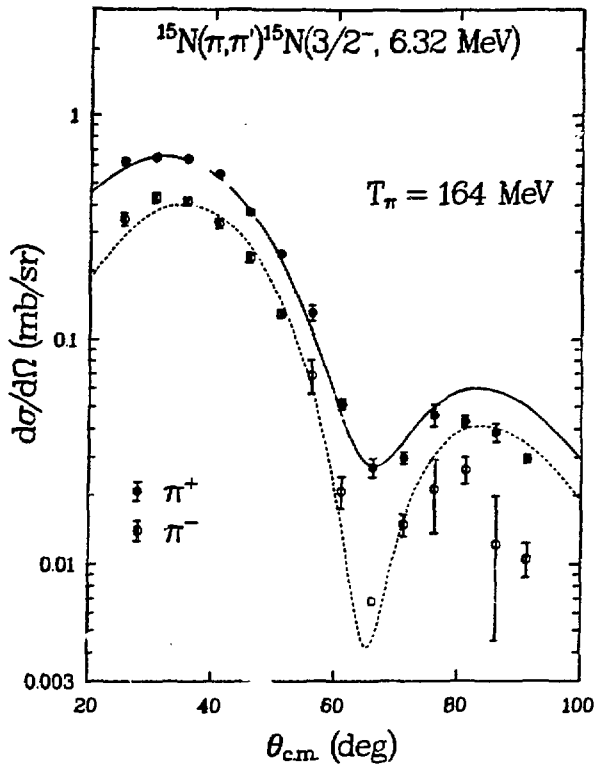

Fig. 2.
The π^+ and π^- angular distributions for the $(\frac{3}{2})^-$ state at 6.32 MeV in ^{15}N. The curves are DWIA calculations described in the text.

Energy Dependence of Pion Double-Charge-Exchange Angular Distributions for the Reaction $^{16}O(\pi^+,\pi^-)^{16}Ne$ (g.s.)

(Exp. 749, EPICS)

(Univ. of Texas, Los Alamos, New Mexico State Univ., Univ. of Pennsylvania)
Spokesmen: L. C. Bland and H. T. Fortune (Univ. of Pennsylvania)

Experiment 749 is one of a series of EPICS experiments, including Exps. 310, 448, 577, and 701, that have investigated the features of nonanalog pion double-charge-exchange (DCX) transitions between ground states of $T=0$ and $T=2$ nuclei. The previous experiments have measured $\theta=5°$ excitation functions, $T_\pi = 164$-MeV angular distributions, and the mass dependence of nonanalog DCX. The observed systematics included the following.

(1) Forward-angle excitation functions show a peaked energy dependence.
(2) The peaks all have similar widths.
(3) Angular distributions at $T_\pi = 164$ MeV are consistent with being diffractive.
(4) The target-mass dependence of $\theta=5°$ cross sections at $T_\pi = 164$ MeV is approximately $A^{-4/3}$.

The proposal for Exp. 749 suggested that these features are consistent with a single-step process leading to $\Delta(3,3)$ components of the residual nuclear wave function. The explanation included the following.

(1) The rapid energy dependence results from the intermediate Δ propagator.
(2) The shape of the angular distributions follows from the surface domination of the single-step process.
(3) The single step should lead to an $A^{-4/3}$ mass dependence.
(4) The deduced size of the Δ-component admixture in ^{16}Ne (g.s.) is reasonable.

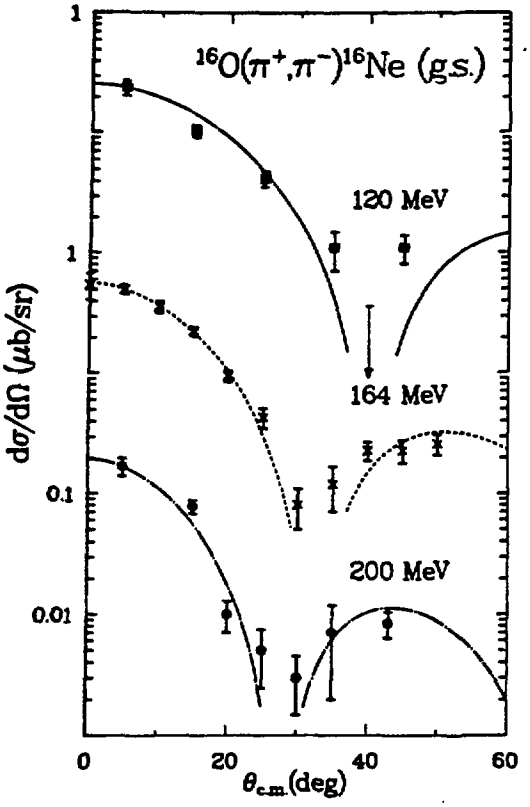

Fig. 1.
Comparison of angular distributions at three energies for the DCX reaction $^{16}O(\pi^+,\pi^-)^{16}Ne$ (g.s.). The curves are described in the text.

Experiment 749 was designed to investigate the energy dependence of the $^{16}O(\pi^+,\pi^-)^{16}Ne$ (g.s.) angular distributions to see if they changed in a diffractive manner. The experiment was run during cycle 39 (replay and analysis are continuing). Some on-line results for the two angular distributions obtained are displayed in Fig. 1 along with the previously measured (Exp. 577) angular distribution for $^{16}O(\pi^+,\pi^-)^{16}Ne$ (g.s.) at $T_\pi = 164$ MeV. The curves presented are damped Bessel functions,

$$\sigma = N J_0^2(qR)\, e^{-qd} \quad ,$$

where the radius $R = 3.3$ fm and damping length $d = 1.2$ fm are independent of energy. The quantity N is an energy-dependent normalization factor. The results appear consistent with a diffractive process.

Isospin Dependence of Nonanalog Pion Double Charge Exchange
(Exp. 780, EPICS)

(Univ. of Texas, Los Alamos, New Mexico State Univ., and Univ. of Pennsylvania)
Spokesmen: R. Gilman (Univ. of Pennsylvania) and P. A. Seidl (Univ. of Texas)

Experiment 780, which was run during cycle 38, is the most recent in a series of experiments that have investigated the features of nonanalog pion double-charge-exchange (DCX) reactions. Previous experiments, including Exps. 310, 448, 577, and 701, have measured $\theta = 5°$ excitation functions, $T_\pi = 164$-MeV angular distributions, the mass dependence of nonanalog DCX, and recently in Exp. 749 (this Progress Report, above), the energy dependence of the angular distributions. All of these measurements were made for transitions between J^π, $T = 0^+,0$ and J^π, $T = 0^+,2$ ground states.

These experiments had determined that the target-mass dependence of $\theta = 5°$ cross sections for nonanalog transitions is approximately $A^{-4/3}$. Experiment 780 proposed to measure transitions between $T = 1$ and $T = 3$ nuclei to investigate possible effects of isospin dependence or nuclear structure on the size of the cross section. Data obtained include

(1) a $\theta = 5°$ excitation function for the reaction $^{18}O(\pi^-,\pi^+)^{18}C$ ground state (g.s.);
(2) a $T_{\pi^-} = 164$-MeV angular distribution for the reaction $^{18}O(\pi^-,\pi^+)^{18}C$ (g.s.);
(3) a $\theta = 5°$, $T_{\pi^-} = 164$-MeV cross section obtained for the reaction $^{14}C(\pi^-,\pi^+)^{14}Be$ (g.s.); and
(4) a $\theta = 5°$, $T_{\pi^-} = 164$-MeV cross section obtained for the reaction $^{58}Ni(\pi^-,\pi^+)^{58}Fe$ (g.s.).

Figure 1 compares the ^{18}O angular distribution to a fit with earlier measurements (Exp. 577) of the $^{16}O(\pi^+,\pi^-)^{16}Ne$ (g.s.) reaction; Fig. 2 compares the ^{18}O excitation function to a fit to earlier measurements (Exps. 310/448/577) of the same reaction. The energy and the angular dependence of nonanalog DCX are obviously similar in the two cases. Figure 3 compares $\theta = 5°$, $T_\pi = 164$-MeV, on-line cross sections for the $T = 1$ to $T = 3$ transitions of Exp. 780 with an $A^{-4/3}$ fit to the $T = 0$ to $T = 2$ cross sections. There is an enhancement of the $T = 1$ to $T = 3$ transitions of about 30% over the fit to the $T = 0$ to $T = 2$ transitions. Thus, we may have evidence for an isospin dependence or nuclear-structure effects in the nonanalog reaction mechanism.

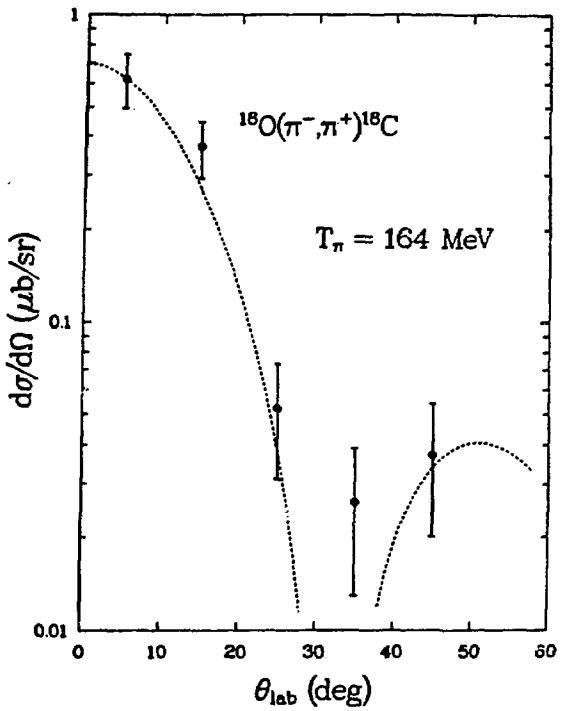

Fig. 1.
Comparison of on-line angular distribution for the reaction $^{18}O(\pi^-,\pi^+)^{18}C$ (g.s.) with a fit to the previously measured angular distribution of $^{16}O(\pi^+,\pi^-)^{16}Ne$ (g.s.). The fit has been renormalized to the value of the $\theta = 5°$ point.

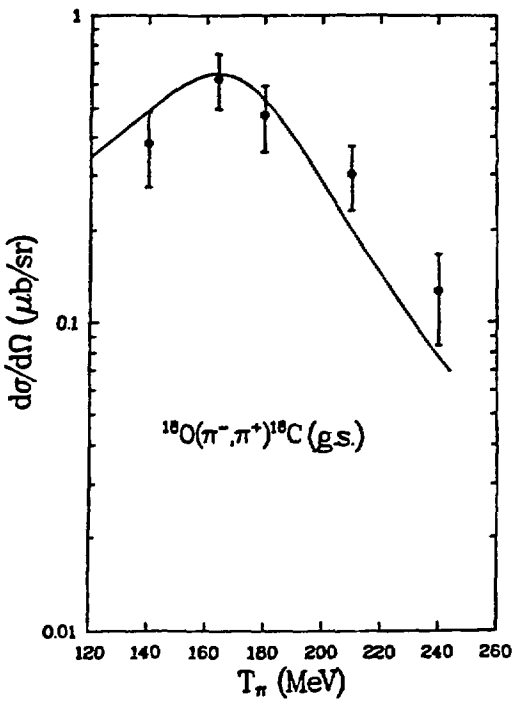

Fig. 2.
Comparison of on-line excitation function for the reaction $^{18}O(\pi^-,\pi^+)^{18}C$ (g.s.) with a Breit-Wigner fit to the previously measured excitation function for $^{16}O(\pi^+,\pi^-)^{16}Ne$ (g.s.). The fit has been renormalized by 30%.

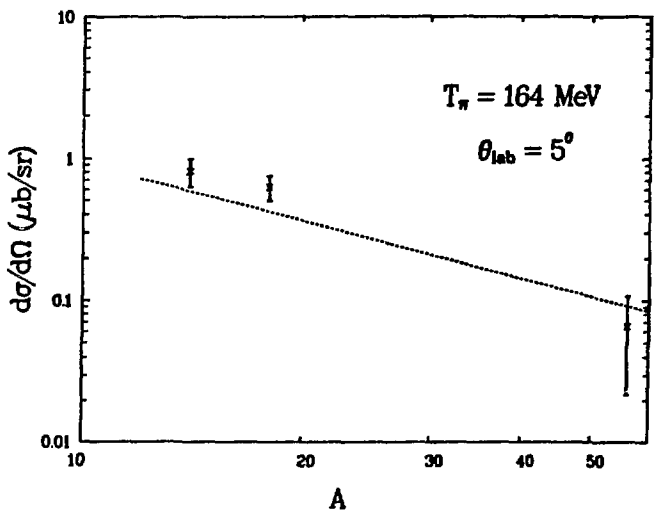

Fig. 3.
Comparison of on-line $\theta = 5°$, T_π = 164-MeV data from Exp. 780 with best-fit $A^{-4/3}$ curve for $T = 0$ to $T = 2$ transitions.

Inelastic Scattering from ^{12}C at Intermediate Energies
(Exps. 432 and 531, HRS)

(Rutgers Univ., Los Alamos, Univ. of Minnesota, Saclay, Univ. of Texas, UCLA, Univ. of Pittsburgh)

Spokesmen: C. Glashausser (Rutgers Univ.) and J. Moss (Los Alamos)

Analysis of the data from Exps. 432/531 is in the final stages, and some results have already been published. We present here a brief summary of the current status of this work.

Differential cross-section and analyzing-power angular distributions spanning the momentum transfer range from 0.3 to 2.4 fm^{-1} have been obtained for elastic and inelastic (up to an excitation energy of 21 MeV) proton scattering from ^{12}C at 398, 597, and 698 MeV. Analysis of the data has been performed using the recently improved version of the nucleon-nucleon t matrix of Love and Franey. This analysis has yielded several interesting results, both for the energy dependence of various components of the interaction and in the identification of the 2^- strength in the high-excitation region (18-20 MeV) of ^{12}C (Ref. 1).

Carbon-12 is a nucleus well suited to the study of systematic effects as it provides a full complement of well-resolved states excited by all possible combinations of spin transfer ($\Delta S = 0,1$) and isospin transfer ($\Delta T = 0,1$). Microscopic wave functions for these levels, such as those derived by Cohen and Kurath and Millener, have been tested extensively in inelastic electron scattering, which also establishes oscillator parameters for bound-state orbitals.

Cross-section and analyzing-power data for the 4.44- and 12.71-MeV states are shown in Fig. 1 at a variety of incident energies. Typical data for the states at 15.11, 16.11, and 16.58 MeV are shown in Fig. 2. The most striking feature of the data is the energy independence of the cross section (both the absolute magnitude and the angular distribution) for all classes of transitions except isoscalar states of natural parity. The solid curves in the figures show the results of distorted-wave impulse approximation (DWIA) calculations. Renormalization factors required to bring the calculations into agreement with the data are included and are listed in Table I. These factors necessarily include some arbitrariness because of imperfect fits.

The analysis shows that there is considerable room for improvement in the DWIA description of the energy dependence of the cross sections and analyzing powers. Whereas the shapes of the angular distributions for the cross sections are generally adequately predicted at 400 MeV and above, the angular distributions for $A_y(A_N)$, with the exception of the 12.71-MeV state, are not. In addition, normalization factors required to match theory and experiment show substantial variation with energy. The origin of these problems is not clear. Certainly, the wave functions may be partly responsible. A detailed examination of the effect of coupled-channels corrections and of changes in the optical potentials and single components in the NN force is currently under way. Furthermore, it will be useful to determine whether density-dependent forces or relativistic theories yield significant improvements.

Analysis of the 18- to 20-MeV region of excitation for the beam energies mentioned previously has yielded interesting results. States at 18.30 and 19.40 MeV of excitation with widths of 380 ± 30 and 480 ± 40 keV

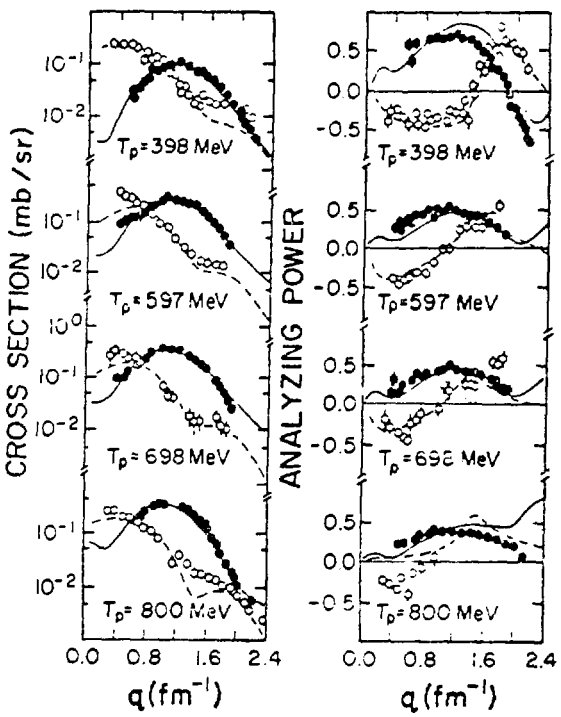

Fig. 1.
Cross-section and analyzing-power data for the 4.44- (solid circles) and 12.71- (open circles) MeV states at a variety of incident energies. Solid and dashed curves are DWIA calculations for these states.

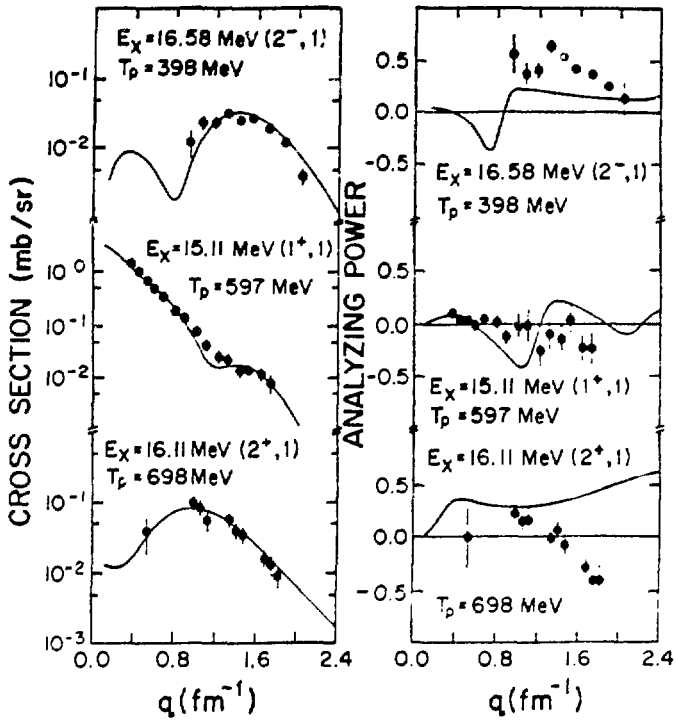

Fig. 2.
Cross-section and analyzing-power data for the states at 15.11, 16.11, and 16.58 MeV at a variety of incident energies. Solid curves are DWIA calculations.

Table I. Renormalization Factors. The theoretical cross sections were multiplied by the factors shown below to achieve the best fit to the experimental cross sections. See text for additional factors for the 16.11-MeV state.

			(p, p')				
E_x (MeV)	J^π; T	(e, e')	200 MeV	398 MeV	597 MeV	698 MeV	800 MeV
4.44	2^+, 0	2.0	1.0	2.0	2.68	3.0	2.65
12.71	1^+, 0	---	0.3	1.0	1.40	1.30	1.15
15.11	1^+, 1	1.0	1.0	1.0	1.44	1.15	1.38
16.11	2^+, 1	1.0	0.60	0.78	1.32	0.90	1.15
16.58	2^-, 1	0.67	0.20	0.30	0.50	0.58	0.38

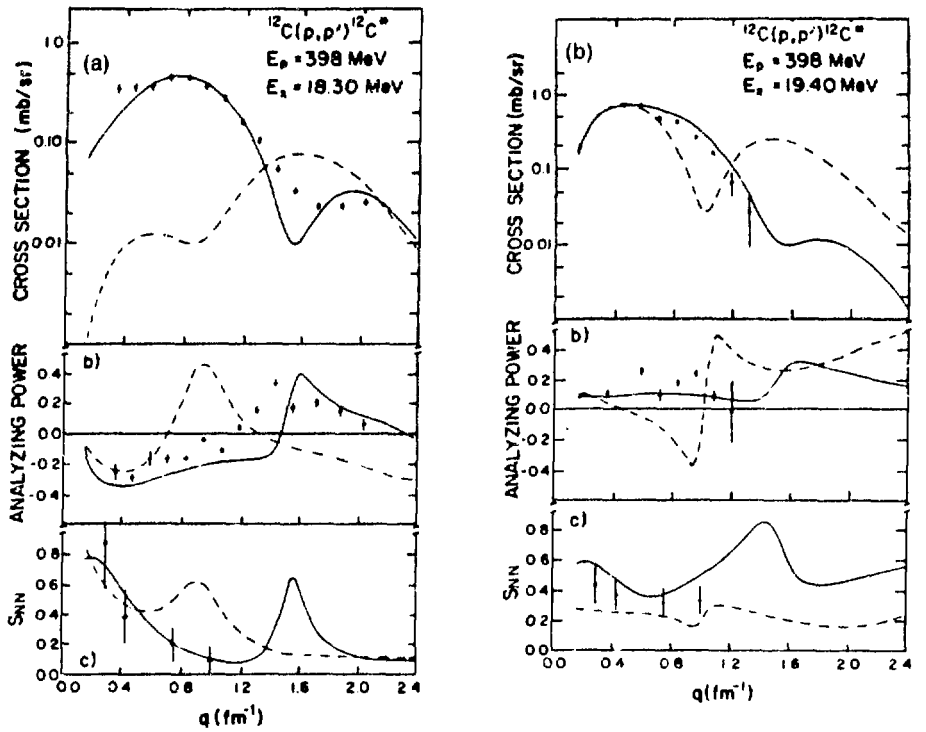

Fig. 3(a) and (b).

Cross-section, analyzing-power, and spin-flip data for the 2^-,0 and 2^-,1 states at (a) 18.30 and (b) 19.40 MeV. Solid curves are renormalized DWIA calculations for 2^-,0(2) and 2^-,1(2) configurations, as discussed in the text. Dashed curves are 2^-,0(1) and 1^-,1 configurations for the 18.30- and 19.40-MeV states, respectively.

have been identified. Angular distributions of cross sections, analyzing powers, and spin-flip probabilities are shown in Fig. 3. Analysis of the data in the DWIA, using the Love-Franey t matrix and transition densities of Millener, have permitted identification of these two states to be 2^-,0 and 2^-,1, respectively. In particular, the state at 18.30 MeV is very well described by the second transition density predicted by Millener. This state is dominated by the $(1d_{5/2}, 1p_{3/2}^{-1})$ configuration, whereas the remaining states, such as the third shown as the dotted line in the figure, are dominated by the $(2s_{2/1}, 1p_{3/2}^{-1})$ configuration. A renormalization factor of about 0.7 is required at all energies to bring the calculations into agreement with the data. The 19.40-MeV state is best described by the second $(2^-,1)$ transition density of Millener. Renormalization by factors of 0.33 is required to bring the calculations into agreement with the data. In general, 1^-,0 and 1^-,1 transitions may be ruled out because of poor agreement with the data. The results of this work substantiate and verify previous ambiguous assignments of spin, parity, and isospin in this region.

REFERENCE

1. K. W. Jones et al., Phys. Lett. 128B, 281 (1983).

Proton Scattering from ^{20}Ne and ^{22}Ne at 0.8 GeV (Exp. 475, HRS)

(Univ. of South Carolina, Univ. of Texas, Drexel Univ.)
Spokesman: G. Blanpied (Univ. of South Carolina)

In several recent publications,[1-6] coupled-channel analyses of ~1-GeV proton inelastic scattering from *s-d* shell nuclei and heavy rare-earth nuclei have been shown to be generally successful, provided deformation and multistep processes are properly treated. These collective rotational-model calculations provide an excellent description of the data for the lowest 0^+, 2^+, and 4^+ states in ^{24,26}Mg and ^{20}Ne (Refs. 6 and 7). The results of the first half of this experiment confirmed the large hexadecapole deformation of ^{20}Ne. Data on the negative-parity rotational bands in ^{20}Ne also were explained in the coupled-channels framework.

These results motivated the measurement of (*p,p'*) inelastic scattering from ^{22}Ne. The experiment consisted of scattering 0.8-GeV protons from a ^{22}Ne gas target enriched to 99%. Angular distributions were obtained using the high-resolution spectrometer (HRS). Data were acquired for ^{20}Ne and ^{14}N using a gas target of identical geometry and were compared to the data from the previous run. The absolute cross section is obtained relative to a solid melamine target and a ^{208}Pb foil. The resulting angular distributions are given in Fig. 1.

Coupled-channel calculations using a deformed optical potential have been performed using the code ECIS,[8] in which the 0^+, 2^+, and 4^+ states, and a 6^+ state that is not available, are treated as members of the ground-state rotational band and are coupled with deformation up to β_6. The results are given in Fig. 1, using $\beta_2 = +0.42$, $\beta_4 = +0.10$, and $\beta_6 = 0.0 \pm 0.05$. This range for β_6 is larger than that observed for other 6^+ states in this mass region, although in general the 6^+ data are poorly explained. This range in β_6 has no effect on the 0^+ and 2^+ angular distributions, although the results for the 4^+ are small, as seen in Fig. 1. The values for the multipole moments of

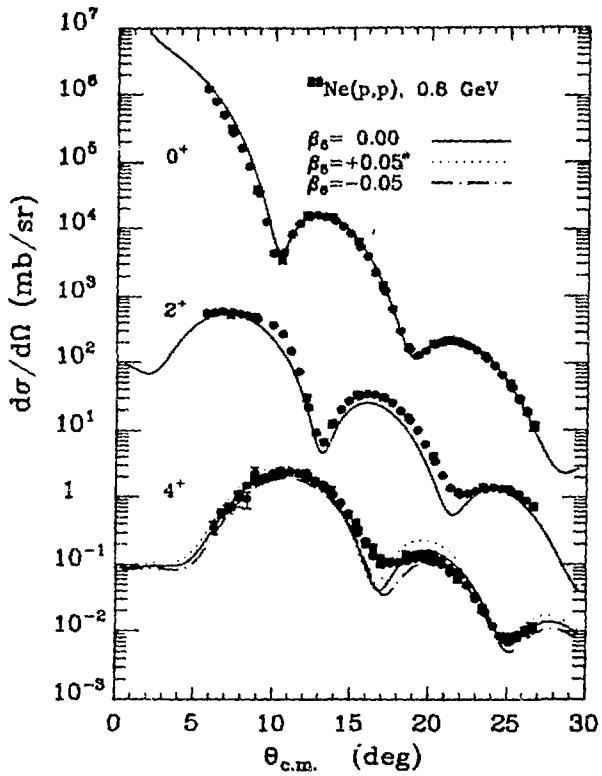

Fig. 1.
Angular distributions of ^{22}Ne (*p,p*) at 0.8 GeV for the 0^+, 2^+, and 4^+ members of the ground-state rotational band. The curves result from coupled-channel calculations, as discussed in the text.

Table I. Deformation Moments of Some Neon and Magnesium Isotopes.

	Matter $M(E2)$ (eb)	Charge $B(E2)$ (eb)	Neutron $M_N(E2)$ (eb)	Matter $M(E4)$ (eb^2)
^{20}Ne	0.164	0.171(11)	0.155	+0.0253
^{22}Ne	0.132	0.151(3)	0.135	+0.0109
^{24}Mg	0.187	0.207(2)	0.162	+0.0073
^{26}Mg	0.152	0.174(4)	0.150	-0.0025
^{22}Ne/^{20}Ne	0.80	0.88	0.87	Difference = 0.0144
^{26}Mg/^{24}Mg	0.81	0.84	0.93	Difference = 0.0098

the matter distribution, the known $B(E2)$ charge moments, the inferred neutron moments $|M_N(E2)|$, and the matter $M(E4)$ are given in Table I for ^{20,22}Ne and ^{24,26}Mg. In both elements, the $M(E2)$ and $M(E4)$ deformations decrease when adding a neutron pair to the $N=Z$ isotope. The inferred neutron deformations are essentially equal to that of the protons in the cases studied. Calculations are under way for other excited states in ^{20}Ne and ^{22}Ne.

REFERENCES

1. L. Ray et al., Phys. Rev. Lett. 40, 1547 (1978).
2. G. S. Blanpied et al., Phys. Rev. C 23, 2599 (1981).
3. G. S. Blanpied et al., Phys Rev. C 20, 1490 (1979).
4. L. Ray, G. S. Blanpied, and W. R. Coker, Phys. Rev. C 20, 1236 (1979).
5. M. Barlett et al., Phys. Rev. C 22, 1168 (1980).
6. G. S. Blanpied et al., Phys. Rev. C 25, 422 (1982).
7. G. S. Blanpied et al., submitted to Phys. Rev. C.
8. J. Raynal, International Atomic Energy Agency report IAEA-SWR-918, 281 (1972).

Measurement of Spin-Dependent Observables for $\vec{p}d \rightarrow \vec{p}d$ Elastic Scattering at 500, 650, and 800 MeV

(Exp. 540, HRS)

(UCLA, Los Alamos)

Spokesmen: G. J. Igo and M. Bleszynski (UCLA)

An extensive program for measuring the spin-dependent observables in $\vec{p}d \rightarrow \vec{p}d$ elastic scattering at intermediate energies continues at LAMPF at the HRS and EPB experimental areas.

A UCLA-Los Alamos collaboration is measuring the complete set of proton spin-transfer observables for $\vec{p}d \rightarrow \vec{p}d$ elastic scattering at 500, 650, and 800 MeV at the HRS using the focal plane polarimeter (FPP). In September 1982. we measured D_{NN}, D_{SS}, D_{SL}, D_{LL}, D_{LS}, P, and A_y at 800 MeV over the four-momentum transfer range $-t = 0.006 - 0.46$ (GeV/c)^2 (3-28° lab). These data have been analyzed and are being prepared for publication.

As an example, the preliminary results for D_{LL} and A_y are shown in Figs. 1 and 2. As seen, the multiple-scattering calculation[1,2] is not in good agreement with the data. The multiple-scattering calculation includes noneikonal and several kinematic corrections and has the nucleon-nucleon (NN) amplitudes and the deuteron wave function as input. Energy dependence in the NN amplitudes has been included. Further work with this calculation is in progress.

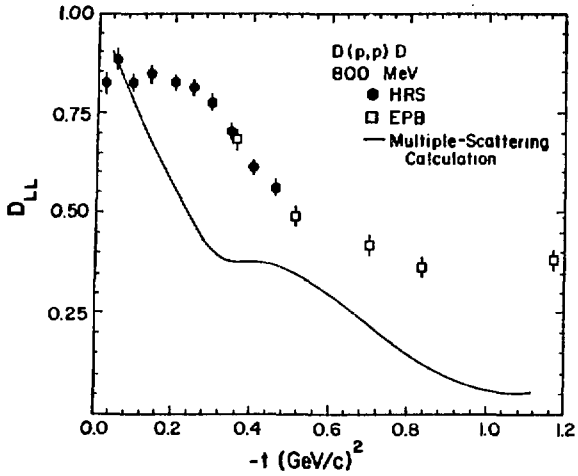

Fig. 1.
Spin-transfer parameter D_{LL} at 800 MeV for the $D(\vec{p},\vec{p})D$ reaction compared to multiple-scattering calculation.

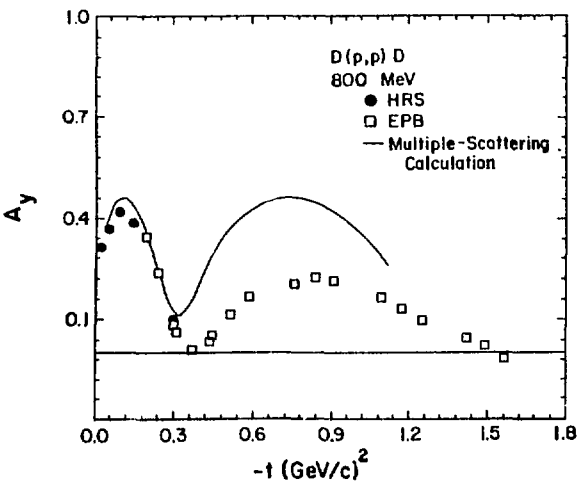

Fig. 2.
Asymmetry parameter A_y at 800 MeV for the $D(\vec{p},p)D$ reaction compared to multiple-scattering calculation.

In November 1983, the same experiment was done at 500 MeV, again using an unpolarized liquid-deuterium target. A proposal has been submitted to measure the same spin-transfer parameters at the HRS with a 650-MeV incident proton beam over the same four-momentum transfer range.

REFERENCES

1. G. Alberi, M. Bleszynski, and T. Jaroszewicz, Ann. Phys. 142, 299 (1982).

2. M. Bleszynski, Phys. Lett. 92B, 91 (1980).

Measurement of the Depolarization Parameters in Proton-Nucleus Scattering to Very High Excitation Energies (Exp. 626, HRS)

(Rutgers Univ., Los Alamos, Univ. of Texas at Austin)
Spokesmen: J. A. McGill and C. Glashausser (Rutgers Univ.)

During cycle 35 (1982), data were taken for the inclusive reaction $^{12}C(p,p')X$ for $D_{NN'}$, $D_{LL'}$, $D_{SS'}$, and $D_{SL'}$ at laboratory angles of 5, 11, 15, and 20°. The momentum of the outgoing protons extended from the quasi-elastic peak to ~600 MeV/c at each angle. Interpretation of these data, however, awaited the corresponding data for the reactions $^1H(p,p')X$ and $^2H(p,p')X$.

In cycle 39 (1983), the data for hydrogen and deuterium were taken at comparable lab angles and momenta. The experiment ran for approximately 120 h. Normally polarized beam was delivered in the usual slow-reversal mode, but both longitudinal and sideways polarizations came during the rapid-reversal mode of the polarized source. The RR mode precludes a regular quench measurement of the beam polarization, so that P_B cannot be monitored when longitudinal polarized beam is delivered. The experiment therefore ran with orthogonal spin directions, precessed about 40° from sideways and longitudinal directions, respectively. This provided some sideways component to the beam polarization for both spin directions, which was monitored with the Line C polarimeter. The arrangement was a first for the HRS.

With the exception of a few minor problems in the double-flask cryogenic target (another first), the run went smoothly. The data are in the process of being analyzed now.

Work for this experiment was supported by the National Science Foundation, the USDOE, and the Robert A. Welch Foundation.

Inclusive (p,p') Cross Sections and Analyzing Powers for ^1H and ^{12}C in the Delta Region (Exp. 642, HRS)

(Rutgers Univ. and Univ. of Texas at Austin)
Spokesmen: G. W. Hoffmann (Univ. of Texas) and J. A. McGill (Rutgers Univ.)

The delta isobar plays an important role as an intermediate state in pion-nucleus scattering to low-lying excited states; it has also been suggested that excitation of the isobar leads to quenching of Gamow-Teller and $M1$ transition strengths observed in (p,n) and (p,p') reactions. Yet, the region of nuclear excitation around 300 MeV, where the direct excitation of the delta resonance can be seen as a (decaying) final state, has been little explored thus far in intermediate-energy proton scattering.

Thus, to examine the spin structure of the $NN \rightarrow N\Delta$ interaction and to investigate deviations from quasi-free scattering, we have carried out experiments using the HRS in which the inclusive (p,p') cross sections and analyzing power were measured for $^1H(p,p'X)$ and $^{12}C(p,p'X)$. An 800-MeV proton beam was scattered from either a 267-mg/cm^2 liquid-hydrogen target or a 174-mg/cm^2 ^{12}C foil. Cross sections and analyzing powers were measured between 5 and 20°. At each angle, the HRS fields were changed by 20-30 MeV/c to search for detailed structure in the delta region. In the figures presented here, each point represents a single spectrometer setting, corresponding to a momentum acceptance of ± 1%. The cross-section data were normalized to the $^1H(p,p)$ elastic data of Barlett et al.[1]

Figure 1 shows the hydrogen cross sections at 5, 11, and 15° plotted vs the laboratory momentum of the outgoing proton. The cross sections agree with our earlier work,[2] but show the structure, particularly near pion threshold, in greater detail. The solid lines in the figure are the result of a calculation carried out with the code by VerWest,[3] which uses a Born approximation treatment of NN scattering and includes π and ρ exchange.

The analyzing powers in Fig. 1 fall from a maximum value of about 0.3 at threshold to small values with little structure at low outgoing momenta. When the product of σ and A_y is formed, an interesting feature is observed — a clear peak, which crosses zero at the maximum of the

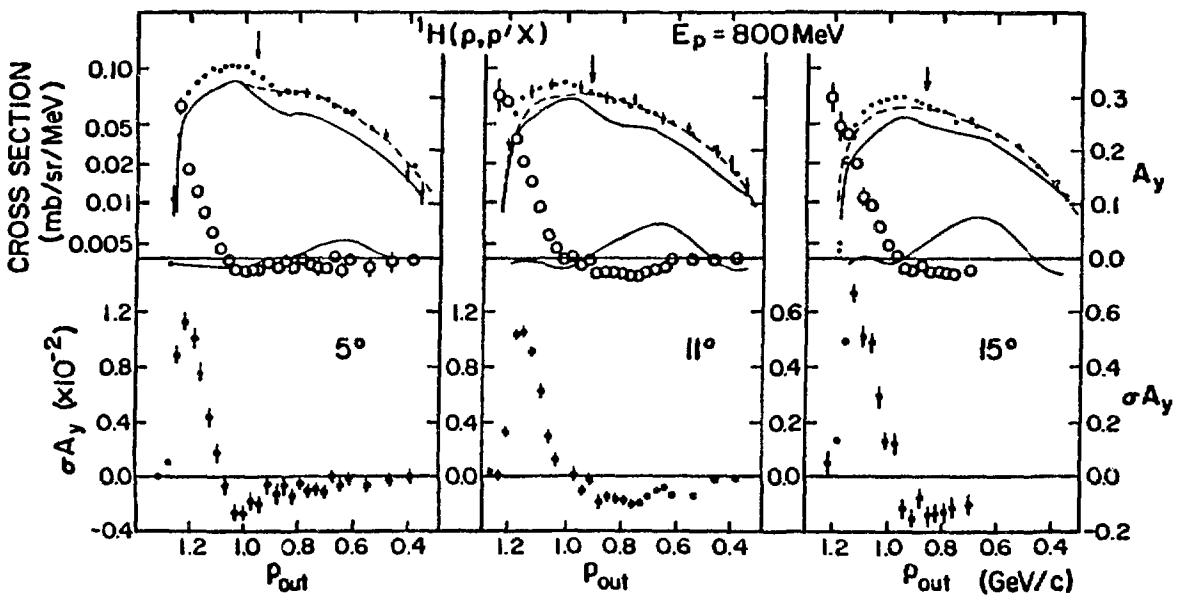

Fig. 1.
Differential cross sections, analyzing powers, and the products σA_y for inclusive (p,p') scattering from ^1H at lab angles of 5, 11, and 15°. The abscissa is the laboratory momentum of the outgoing proton. The solid curves are from a Born calculation of σ and A_y (Ref. 3). The dashed curves are the phase space available to a nucleon in the $NN \rightarrow NN\pi$ reaction. The arrows correspond to an excitation energy of 300 MeV.

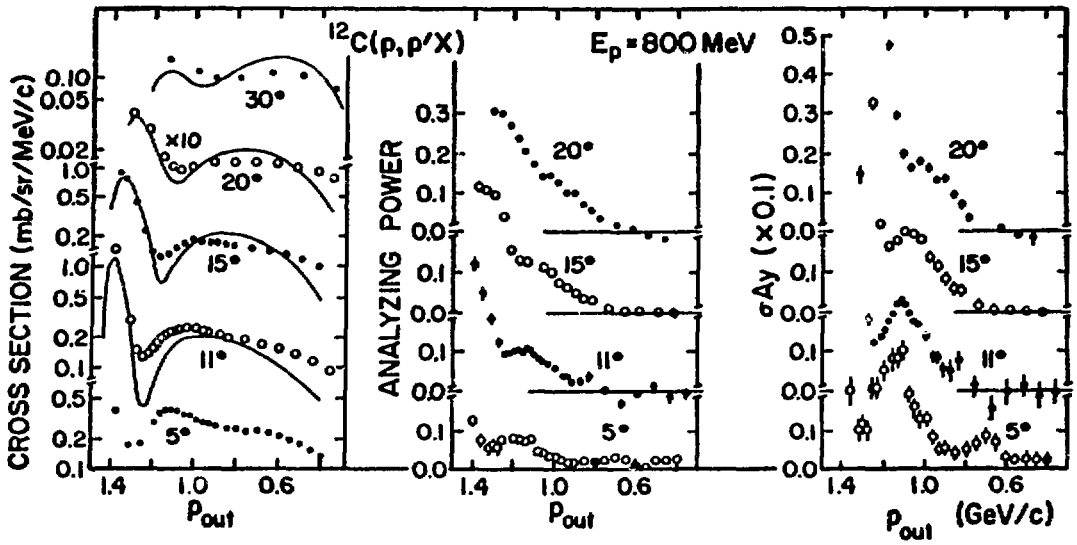

Fig. 2.
Differential cross sections, analyzing powers, and the products σA_y for inclusive (p,p') scattering from ^{12}C at lab angles of 5, 11, 15, and 20°. The curves for σ are taken from Ref. 6.

cross section. In fact, the σA_y spectrum resembles the logarithmic derivative of the cross section with respect to outgoing proton momentum; such a relation is surprisingly simple for an inclusive reaction. (Note that the product σA_y eliminates processes with zero analyzing powers and so can be a sensitive indicator of weak processes.) An attempt to predict A_y with the VerWest model fails badly, as shown in Fig. 1. A unitary-model calculation recently has been shown to be more successful in predicting spin-observables for exclusive final states; it is currently being adapted for application to these inclusive data.[4]

Examples of corresponding data for ^{12}C are shown in Fig. 2. Even with the greater accuracy of these measurements, they are strikingly similar to those for ^1H, as in the earlier work.[2] The cross sections for ^{12}C are about 7 times larger than for ^1H; the value of σA_y at the maximum in ^{12}C is 3 times larger.

It is important to note that the peak in the σA_y data for ^{12}C moves with angle approximately according to ^1H, not ^{12}C, kinematics, even though it is shifted down by about 50 MeV/c from the ^1H peak position. A smaller shift would be expected from binding-energy effects. We also note that at 5° the peak in the cross section is shifted by ~100 MeV/c to higher outgoing momenta. Fermi broadening can be expected to lower the threshold and wash out the structure of the nucleon-nucleon spectrum. Also, a peaking of the nucleon-nucleon cross section at some energy away from the incident beam energy can cause such a "Fermi shift" (as has been suggested[5] for the quasi-free $pp \rightarrow d\pi^+$ reaction), but the pion-production cross sections involved here are relatively flat above 750 MeV.

The solid curves in Fig. 2 have been calculated in a plane wave impulse approximation using an isobar-doorway model by Alexander et al.[6] The curves are arbitrarily normalized in the region of the quasi-elastic peak. Some of the discrepancies between the data and these curves, particularly at low outgoing momentum, can be attributed to the absence of distortions in the calculation. It would be useful to have a more detailed calculation of the theoretical expectations, including distortions. No calculations at all are available for the analyzing power in ^{12}C, partly because the pp data are themselves not explained.

In summary, we have reported the measurement of cross sections and analyzing powers for inclusive (p,p') reactions on ^1H and ^{12}C at 800 MeV. The cross sections, but not the analyzing powers, for ^1H can be reasonably explained in the Born-approximation model of VerWest. The data for ^{12}C are qualitatively similar to those for ^1H. A narrow peak is observed in the σA_y spectrum for both nuclei; even in ^{12}C, it moves with ^1H kinematics. Nevertheless, there are differences in detail, notably energy shifts, between the data for ^1H and ^{12}C.

This work was supported by the National Science Foundation, the USDOE, and the Robert A. Welch Foundation.

REFERENCES

1. M. L. Barlett et al., Phys. Rev. C 27, 682 (1983).

2. J. A. McGill et al., Phys. Rev. C (to be published).

3. B. J. VerWest, Phys. Lett. 3B, 61 (1979).

4. W. M. Kloet and R. R. Silbar, Nucl. Phys. A 338, 231 (1980); and J. Dubach, W. M. Kloet, A. Cass, and R. R. Silbar, Phys. Lett. 106B, 29 (1981).

5. H. Toki, to be published in Phys. Lett. B.

6. Y. Alexander, J. W. VanOrden, E. F. Redish, and S. J. Wallace, Phys. Rev. Lett. 44, 1579 (1980).

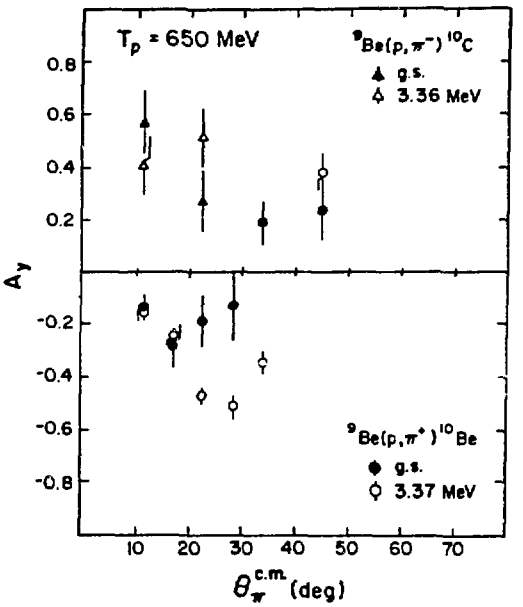

Fig. 1.
Analyzing power as a function of scattering angle in the center-of-mass system for both ^{9}Be(p,π^+) and ^{9}B(p,π^-) going to the ground state and first excited state.

The ^{9}Be($\vec{p},\pi^+$)^{10}Be and ^{9}Be($\vec{p},\pi^-$)^{10}C Reactions at 650 MeV
(Exp. 649, HRS)

(Los Alamos, Univ. of California, Univ. of Minnesota, Univ. of South Carolina, Univ. of Texas at Austin)
Spokesman: Bo Höistad (Univ. of Texas at Austin)

Tentative results from the differential cross section as well as the analyzing power for the ^{9}Be($\vec{p},\pi^+$)^{10}Be and ^{9}Be($\vec{p},\pi^-$)^{10}C reactions are now available at 650 MeV. The angular distribution of the analyzing power A_y is presented in Fig. 1. The ($\vec{p},\pi^+$) data from 10 to 30° were obtained in April 1981 and the rest of the data are from a run between December 28, 1983 and January 3, 1984. In addition, this experiment will receive beam time January 12-16, 1984, during which time more ($\vec{p},\pi^-$) data will be collected.

From the present data, the salient features of A_y appear clearly. The $A_y(\pi^+)$ is negative out to ~35°, where it becomes positive. This trend is the same as observed previously for the ^{3,4}He($\vec{p},\pi^+$)^{4,5}He reactions at 800 MeV.[1] Also, there is an indication of nuclear-structure dependence in the detailed shape of A_y.

The present data represent the first measurement of $A_y(\pi^-)$ far above the energy threshold. We note with interest that $A_y(\pi^-)$ has opposite sign compared to $A_y(\pi^+)$ in the observed angular range. In fact, this general behavior was predicted from a "pion knockout model" and was used as an argument to measure $A_y(\pi^-)$ as a test of this reaction model.

A diagram of the model is shown in Fig. 2. In this process, a virtual pion is emitted from the target nucleus and knocked out by the incident proton. Since the upper vertex in the diagram corresponds to $\vec{p}\pi^+$ scattering for the ($\vec{p},\pi^+$) and $\vec{p}\pi^-$ scattering for the (p,π^-) reaction, we can use A_y data from elastic πN scattering to predict $A_y(\pi^\pm)$ for ^{9}Be. A procedure for how this can be done is given in Ref. 1. If the large momentum transfer involved in the (p,π) reaction is assumed to be equally shared between the two lower vertices in Fig. 2, and if the captured proton is assumed to be on its mass shell (that is, the emitted pion is off shell), we get a shape of A_y for

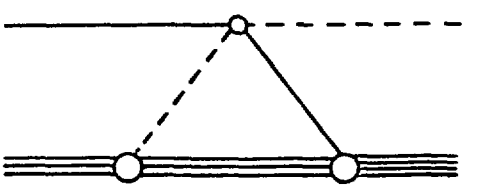

Fig. 2.
Diagram for pion knockout in the (p,π) reaction.

^{9}Be(p,π^{+})^{10}Be that is in qualitative agreement with the experimental data. Moreover, A_y for ^{9}Be($\vec{p},\pi^{-}$)^{10}C is positive up to ~45°, which is consistent with the two data points available.

A further analysis will be performed when the data from the run in the middle of January 1984 can be included.

REFERENCE

1. B. Höistad et al., Phys. Rev. C 29, to be published.

Measurement of Spin Excitations in the ^{48}Ca($\vec{p},\vec{p}'$)^{48}Ca and ^{90}Zr($\vec{p},\vec{p}'$)^{90}Zr Reactions (Exp. 660, HRS)

(Rutgers Univ., Los Alamos, Arizona State Univ., Northwestern Univ., Tokyo Institute of Technology)
Spokesman: C. Glashausser (Rutgers Univ.)

The $M1$ transition in ^{48}Ca is an excellent test case for the study of magnetic dipole transitions because of the expected simple shell structure and the small fragmentation of the observed $M1$ strength. A strong $M1$ state was first observed at an excitation energy of 10.23 MeV in inelastic electron scattering[1]; the analog of this state has been observed in (p,n) measurements.[2] Previous (p,p') experiments with proton energies in the range of 45-200 MeV also have reported observation of this state, which is believed to be mostly a pure neutron $(\nu f_{7/2}^{-1}, f_{5/2})_{1^+}$ configuration. The experimentally observed strength for the 10.23-MeV transition is approximately 30% of the predicted theoretical value obtained from the pure independent-particle model with bare g factors.

We have measured the cross section $\sigma(\theta)$, the analyzing power $A_y(\theta)$, and the spin-flip probability $S_{NN}(\theta)$ for the 10.23-MeV state in the ^{48}Ca(p,p')^{48}Ca* reaction at 319 MeV. The data were taken at the HRS with a vertically polarized (N) proton beam. The polarization of the outgoing particles was measured with the focal plane polarimeter. An isotopically enriched ^{48}Ca (94.7%) target 100 mg/cm^2 thick was used; the total energy resolution was 120 keV. The data were taken at 3.5 and 5.0° laboratory angles.

Angular distributions for $\sigma(\theta)$, A_y, and S_{NN} are shown in Fig. 1. The shape of the σ angular distribution plotted vs momentum transfer q agrees well with the 200-MeV data[3]; the absolute cross section is about 10% higher. The curves represent distorted-wave impulse approximation (DWIA) predictions with the code DW81 for the $M1$ transition assuming a $(\nu f_{7/2}^{-1}, f_{5/2})_{1^+}$ transition; exchange was included exactly. The 325-MeV t matrix of Love and Franey was used; optical parameters were extrapolated from nearby energies. The σ angular distribution is well described by the DWIA calculation. The absolute cross section is about 28% of the DWIA prediction, which is consistent with the quenching observed in the (e,e') results of Ref. 1 and the previous (p,p') results at 200 MeV of Ref. 3.

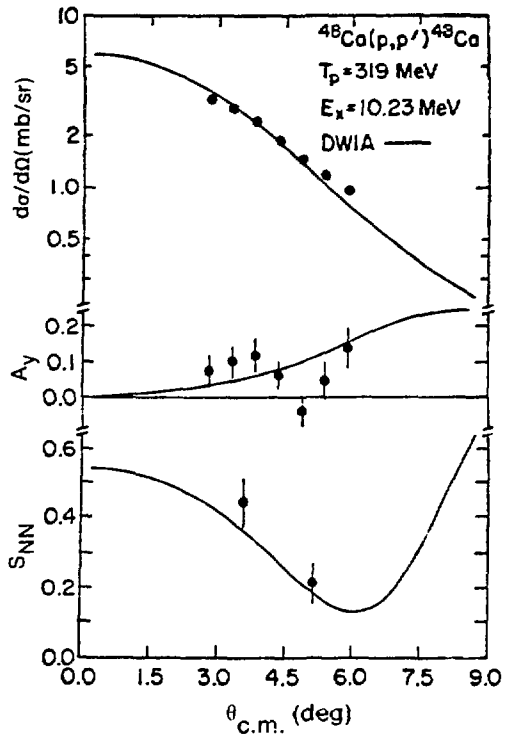

Fig. 1.
Measured values of $\sigma(\theta)$, A_y, and S_{NN} for the 10.23-MeV $M1$ transition in ^{48}Ca(p,p')^{48}Ca* at 319 MeV. The solid curves correspond to DWIA calculations described in the text.

The values of A_y for the 10.23-MeV state shown in Fig. 1 are small and mostly positive, similar to those measured for the 15.11-MeV 1^+ state in ^{12}C at energies from 400 to 800 MeV. There is a hint of structure in the ^{48}Ca data that has not been observed in ^{12}C. The DWIA calculations for ^{48}Ca agree reasonably well with the data; there is no indication of structure. Note that the pure neutron transition assumed here has equal amplitudes of isovector and isoscalar components in the wave function.

A pure isoscalar transition yields a negative A_y of about −0.30 at these q values, both in data for the 12.71-MeV 1^+, $T = 0$ state between 400 and 800 MeV and in calculations for ^{12}C and ^{48}Ca at 319 MeV. The A_y for the pure neutron transition is very similar to the A_y for a pure $\Delta T = 1$ transition, however, because of the weakness of the $\Delta T = 0$ components in the effective interaction at these energies.

In the plane-wave impulse approximation using only central forces and excluding exchange effects in the reaction, an $L = 0$, 0^+ to 1^+ transition should yield an S_{NN} value of 2/3, independent of q. Distortion effects, noncentral forces, and exchange effects tend to produce structure in the angular distribution of S_{NN}. In contrast, transitions with $\Delta S = 0$ yield S_{NN} values close to zero. Our measured values of S_{NN} are 0.44 ± 0.08 at 3.5° and 0.20 ± 0.07 at 5.0° for the 10.23-MeV state; the angular distribution is in good agreement with the DWIA predictions.

In summary, our measurements at small q for the 10.23-MeV transition in ^{48}Ca show large values of S_{NN} and small values of A_y, in good agreement with the DWIA. The measured σ is about 28% of the single-particle DWIA prediction, consistent with previous work. The results support the usefulness of S_{NN} measurements in searching for $M1$ strength in heavy nuclei, as well as the validity of a DWIA description of such data.

To determine whether significant unnatural-parity strength exists at excitations above the $M1$ giant resonance in ^{90}Zr, we measured $\sigma(\theta)$, $A_y(\theta)$, and $S_{NN}(\theta)$ in the $^{90}Zr(p,p')^{90}Zr$ reaction at 319 MeV. As with back-angle electron-scattering cross sections, the spin-flip cross section σS_{NN} is a measure of $\Delta S = 1$ excitations, whereas σ data by themselves can seldom distinguish between $\Delta S = 0$ and $\Delta S = 1$. The data were taken at the HRS, as described above. A thick target (250 mg/cm^2) was required, so the energy resolution was 180 keV and the instrumental background was significant.

Shown in Fig. 2 are the spectra of S_{NN} and σS_{NN} at 3.5° without background subtraction; data at 5° are similar, but they extend only to 16 MeV. As expected, spin-flip cross sections are small at low-excitation energy in the region of isolated states; they rise to significant values around 8 MeV. Compared to the higher excitation energy region, however, the region around 9 MeV is in no way remarkable. Rather, spin excitations are observed up to at least 25 MeV where only natural-parity states previously have been seen.

If a simple background is drawn in the 9-MeV region, a value of 0.62 ± 0.20 is obtained for S_{NN}, but because of

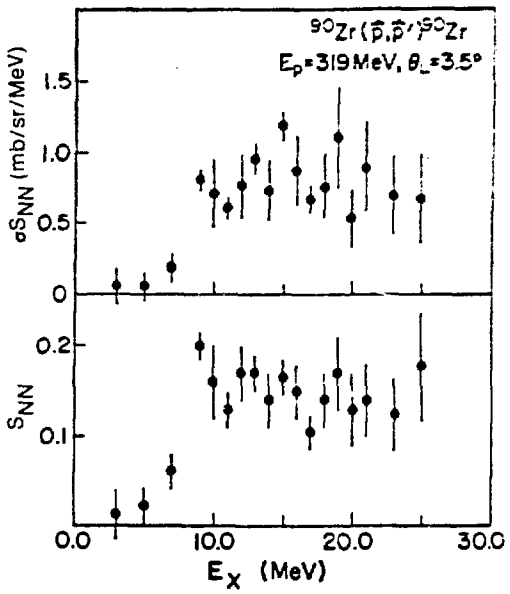

Fig. 2.
Spectra of S_{NN} and σS_{NN} for the $^{90}Zr(p,p')^{90}Zr^*$ reaction at 3.5°.

the uncertainty in the background, the systematic error in this value is large. To calibrate the value expected for a pure $M1$ transition, S_{NN} was measured for the $^{48}Ca(p,p')^{48}Ca^*$ reaction to the 10.23-MeV 1^+ state as described above. The value obtained, 0.44 ± 0.08 at 3.5°, is consistent with an $M1$ assignment for the 9-MeV bump in ^{90}Zr. The poor resolution of the present S_{NN} data does not permit isolation of individual $E1$ states.

We have closely examined many possible sources of error in obtaining the spectra of Fig. 2, but because of the uniform spreading of the spin-flip strength, it is difficult to be certain that all sources of error have been eliminated. Nevertheless, our results strongly suggest that the spin-flip cross section at 3.5° is approximately 0.8 mb/sr/MeV throughout the region from 8- to 25-MeV excitation.

Although no spin excitations previously have been observed above 10 MeV, it is important to note that no experiments really sensitive to such strength have been performed. The uniform spreading of the σS_{NN} strength is suggestive of the apparent quasi-free background observed in the (p,n) reaction; Osterfeld explains this as $\Delta S = 1$ excitations up to spin 3^+ even at 0°. It is interesting to observe that the S_{NN} predicted by Arndt's phase-shift solutions at 3.5° are 0.37 and 0.20 for free pp and pn scattering, respectively. Comparison with the S_{NN}

values in Fig. 2 shows that the nuclear response is not dramatically different from that of a Fermi gas, even though this is a region of high natural-parity collectivity. This result disagrees with the conclusions of Moss et al.[4] for ^{208}Pb at 400 MeV.

REFERENCES

1. W. Steffen et al., Phys. Lett. 95B, 23 (1980).

2. B. D. Anderson et al., Phys. Rev. Lett. 45, 699 (1980); and C. D. Goodman, Nucl. Phys. A 374, 241 (1982).

3. G. M. Crawley et al., Phys. Lett. 127B, 322 (1983).

4. J. M. Moss et al., Phys. Rev. Lett. 48, 789 (1982).

Giant Resonance Studies with Medium-Energy Protons
(Exp. 670, HRS)

(Los Alamos, Univ. of South Carolina)

Spokesmen: T. A. Carey and J. M. Moss (Los Alamos) and G. S. Adams (Univ. of South Carolina)

Our efforts in the development of unique small-angle scattering techniques for the exploration of $M1$ strength at the HRS have proved equally fruitful in searches for new giant resonances (GRs).

Starting with our discovery[1] of an isoscalar high-energy octupole resonance (ISHEOR) occurring systematically at $E_x \simeq 110A^{-1/3}$ in heavy nuclei, increased attention has been focused on the high-excitation spectrum of ^{208}Pb. In addition to the ISHEOR at $E_x \simeq 19$ MeV, theoretical calculations have predicted the existence of both isoscalar giant dipole resonances (ISGDRs) and isovector giant quadrupole resonances (IVGQRs) at about 22 MeV of excitation in ^{208}Pb. Since they are isospin partners of the well-known isovector giant dipole resonances (IVGDRs) and isoscalar giant quadrupole resonances (ISGQRs), an experimental determination of their existence and properties would place important general constraints on theoretical models of the nuclear response and of the residual interaction in nuclei. Previous investigations of this region have led to strongly conflicting interpretations; a group from Jülich using 172-MeV α particles favors the ISGDR at $E_x \simeq 21$ MeV, whereas a group from Orsay has claimed strong excitation of the IVGQR near $E_x \simeq 22$ MeV with 200-MeV protons.

In our opinion, both of these experiments suffered from low sensitivity because of large backgrounds and neither provided adequate evidence to support their respective conclusions. On the other hand, the small-angle system at the HRS is virtually free of instrumental background. Furthermore, we have previously shown[2] that in 800-MeV proton inelastic scattering the nuclear continuum is dominated by quasi-free scattering, and at small momentum transfers, Pauli-blocking suppresses it in such a way as to considerably enhance the signals of weakly excited GR.

Exploiting these two facts in a February 1983 run, we obtained GR data of the unparalleled quality illustrated in Fig. 1. At the larger scattering angles the previously observed ISGQR ($\Delta L = 2$) and ISHEOR ($\Delta L = 3$) are clearly evident, and as we move to very forward angles we see the definite appearance of other broad structures near 13 and 22 MeV of excitation in ^{208}Pb. The dominantly isoscalar character of 800-MeV protons, in conjunction with the angular distribution of the high-excitation bump as compared with that for the ISGQR, strongly suggests an isoscalar dipole ($\Delta L = 1$) assignment.

We have identified similar structures in comparable data for ^{144}Sm and ^{116}Sn, and together their excitation energies exhibit a target-mass dependence close to that predicted for the ISGDR. The peak near $E_x = 13$ MeV in ^{208}Pb that is strong at $\theta_{lab} = 1.8°$ and completely disappears by $\theta_{lab} = 2.5°$ might tentatively be identified with the isoscalar giant monopole ($\Delta L = 0$) resonance (ISGMR), but such extreme forward peaking could also be indicative of Coulomb excitation of the standard isovector dipole mode. Therefore, a considerable fraction of the concentrated strength seen near $E_x = 22$ MeV at the smallest angles may be due to Coulomb excitation of the IVGQR. Theoretical analysis of these possibilities employing microscopic transition densities in extensive inelastic-scattering calculations is in progress.

To further aid us in sorting out this region of the ^{208}Pb spectrum, we have also explored it with pion inelastic scattering, since (π,π') incorporates an isospin selectivity fundamentally different from that of (p,p').

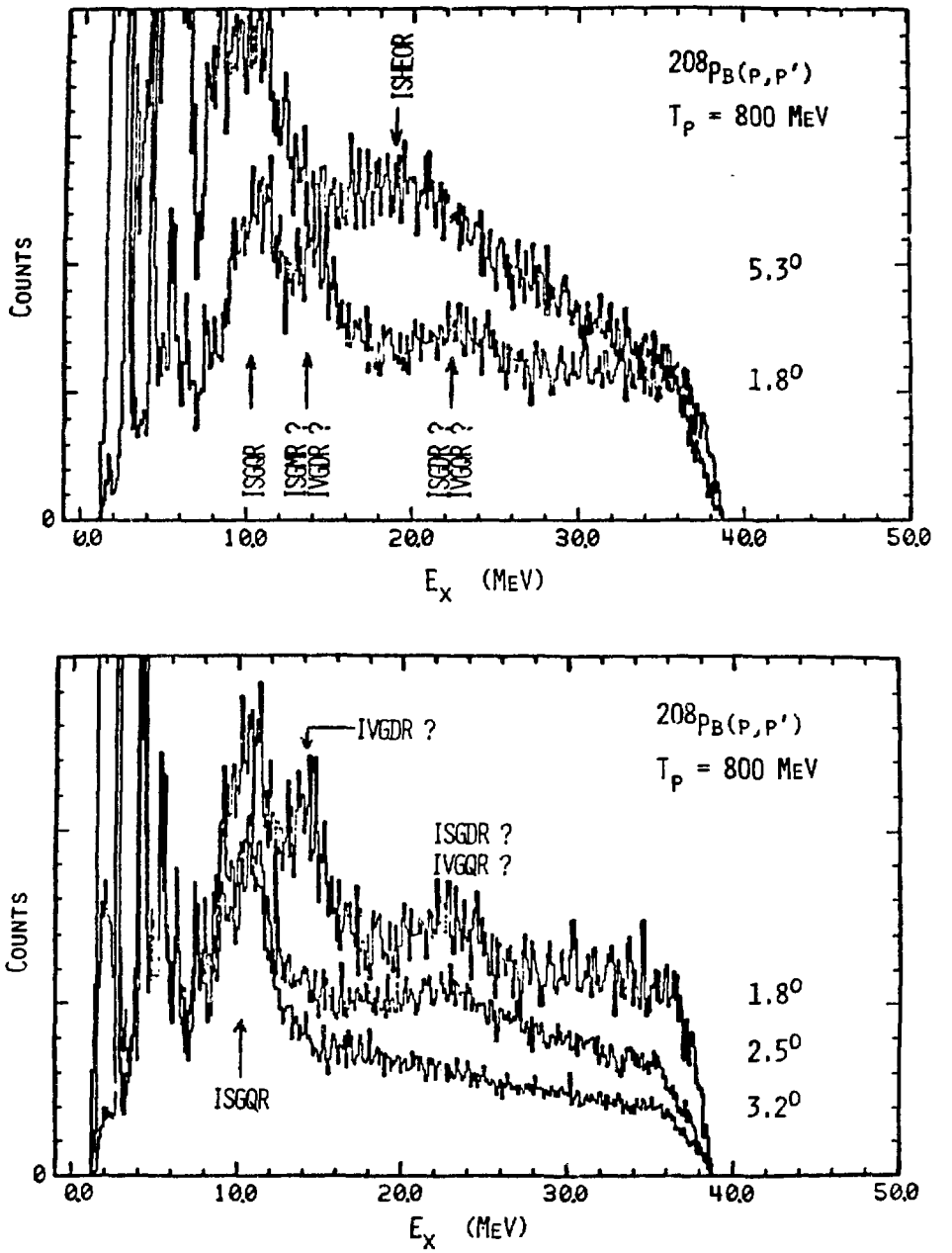

Fig. 1.

On-line excitation spectra for ^{208}Pb at various laboratory scattering angles. The relative normalizations between different angle bins were arbitrarily selected for display purposes only.

REFERENCES

1. T. A. Carey et al., Phys. Rev. Lett. 45, 239 (1980).

2. J. M. Moss et al., Phys. Rev. Lett. 48, 789 (1982).

Measurement of the Third-Order Spin-Dependent Observables for the $\vec{p}\vec{d} \rightarrow \vec{p}d$ at 800 MeV with a Polarized Deuterium Target (Exp. 685, HRS)

(UCLA; Los Alamos; KEK Lab.; Hiroshima Univ.; Kyoto Univ. of Education, Japan; Univ. of Minnesota)
Spokesmen: G. J. Igo and M. Bleszynski (UCLA)

A collaboration has measured some third-order spin-dependent observables for $\vec{p}\vec{d} \rightarrow \vec{p}d$ elastic scattering at 800 MeV at the HRS. This experiment uses a polarized proton beam and a polarized deuterium target while measuring the polarization of the scattered proton. During the period September-October 1983 we used an *N*-type (perpendicular to the scattering plane) polarized deuterium target. By using an *N*-type polarized target with all three independent proton beam spin directions, we plan to extract roughly 14 observables that have never been measured for the spin-1/2 on spin-1 system at 800 MeV. The analysis of these data has just started, so no results are available yet.

To completely determine the *pd* scattering amplitude, 23 independent observables must be measured.[1] During the next 2 years, we plan to complete the measurement of these third-order $\vec{p}\vec{d} \rightarrow \vec{p}d$ observables with *L*- and *S*-type polarized deuterium targets using a superconducting magnet. This should allow us to completely determine the *pd* scattering amplitude at 800 MeV for the four-momentum transfer range $-t = 0.03$-0.22 $(\text{GeV/c})^2$ (7-19° lab). As a result of this work, we also hope to better understand the multiple-scattering theory.

In these experiments with a polarized deuteron target, we use a horizontal dilution refrigerator,[2,3] thus pumping on the ^{3}He/^{4}He dilution phase. The propanediol-D8 target can be cooled to ~20 mK and can be polarized using microwaves (~69 GHz) to ~30% deuteron vector polarization (tensor polarization ~7%) in a 25-kOe magnetic field. Because of the low temperature attainable, we operate the polarized target in a spin-frozen mode using a holding magnetic field of 10 kOe and still have a deuteron spin-relaxation time > 100 h. A drawing of the experimental floor layout is shown in Fig. 1. After the scattering target, the HRS was used in its standard configuration with the focal-plane polarimeter. Wire chambers C1 and C2 and scintillators M1 through M8 make up the monitor telescope used to measure the target and beam polarizations.

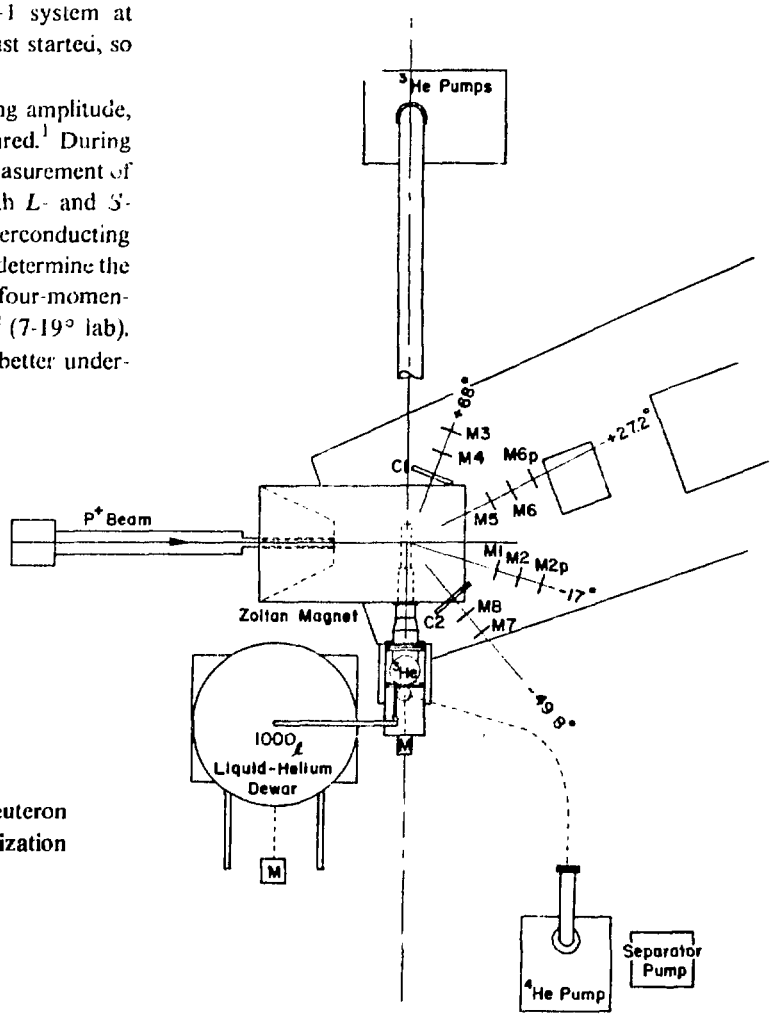

Fig. 1.
Experimental floor layout for polarized deuteron target, including layout of target polarization monitor.

We hope to measure the deuteron target polarization in three ways. The first technique involves measuring left/right (±22° c.m., near maximum of deuteron analyzing power) with the HRS. Using the proton analyzing power with the deuteron vector and tensor analyzing powers previously measured[4] allows one to extract the target and beam polarizations. The second method uses the monitor telescope. By monitoring the *pp* quasi-free scattering asymmetry from the deuterium target, we hope to determine both the target and beam polarizations. In addition to these scattering asymmetry measurements, a third method uses coils positioned around the target flask to obtain deuteron magnetic resonance (DMR) data, which determine the average target polarization throughout the target flask. This method should provide a relative measure of the target polarization. All three of these techniques are presently being pursued.

REFERENCES

1. G. Alberi, M. Bleszynski, T. Jaroszewicz, and S. Santos, Phys. Lett. 92B, 41 (1980).

2. S. Ishimoto et al., Nucl. Instrum. Methods 171, 269 (1980).

3. A. Masaike, "Polarized Target with Dilution Refrigerator," Argonne National Laboratory report ANL-HEP-PR-77-88.

4. M. Bleszynski et al., Phys. Lett. 87B, 198 (1979).

Neutron Transition Densities in ^{208}Pb (p,p') at 318 MeV

(Exp. 686, HRS)

(Univ. of Minnesota, Los Alamos, Univ. of Texas)

Spokesman: N. Hintz (Univ. of Minnesota)

The purpose of this experiment was to obtain high-resolution (ΔE = 35- to 45-keV) data on inelastic proton scattering to the low-lying "collective" states and the high-spin particle-hole states of ^{208}Pb. From these data we plan to extract neutron transition densities, making use of collective or microscopic models and proton densities from electron scattering.

In our earlier experiment (Exp. 347) at 800 MeV, the high-spin natural-parity states (10^+, 12^+) were poorly resolved, and the unnatural-parity states (12^-, 14^-) were not seen above background. However, at 318 MeV, because of improved resolution and the increased ratio of the spin-dependent to spin-independent parts of the *NN* force, the high-spin states are better (though not completely) resolved. In January 1983, data were obtained up to an excitation energy of $E^* \simeq 12$ MeV over an angular range of θ_L = 3-40°. A spectrum at θ_L = 28° is shown in Fig. 1.

The ground-state angular distribution is shown in Fig. 2. The absolute normalization is still tentative but is believed to be good to ±10%. The elastic angular distribution was fit with a 2PF phenomenological optical

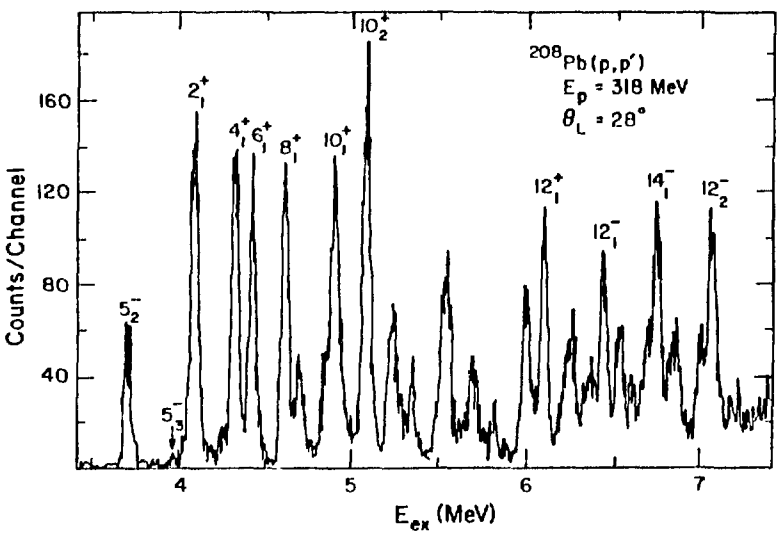

Fig. 1.
Spectrum for proton scattering from ^{208}Pb at an incident energy of 318 MeV.

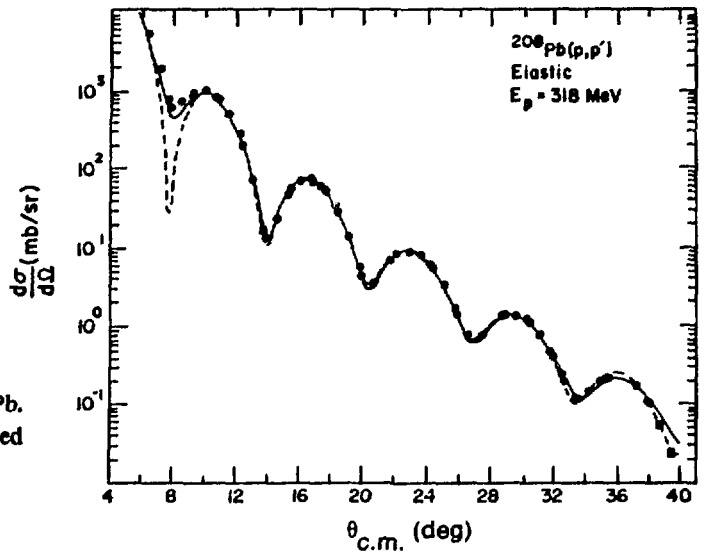

Fig. 2.
Elastic-scattering angular distribution for ^{208}Pb. The curves are with (solid line) and without (dashed line) a spin-orbit potential.

potential by searching with the program RELOM, both with and without a spin-orbit potential. The results are not completely satisfactory, even with the spin-orbit potential included, in contrast to the situation at 800 MeV where excellent fits were obtained both with and without spin orbit. We are now attempting, with folded [first-order Kerman-McManus-Thaler (KMT)] and with phenomenological optical potentials with repulsive real cores, to obtain a better representation of the elastic data for the inelastic analysis.

For the low-spin states, we have, as a first step, used collective form factors (vibrating potential model) to obtain deformation lengths δ_λ for comparison with those obtained at other energies. Figure 3 shows predictions (theory normalized to data to obtain β_λ) for the 3^- state (using the optical potential with a spin-orbit term) with the spin-orbit deformation β_s varied. The best fit is for β_c (central potential deformation) = β_s. However, as Fig. 4 shows, there is some indication that the fits improve for higher spin collective states ($J \geq 6$) with $\beta_s > \beta_c$. Our

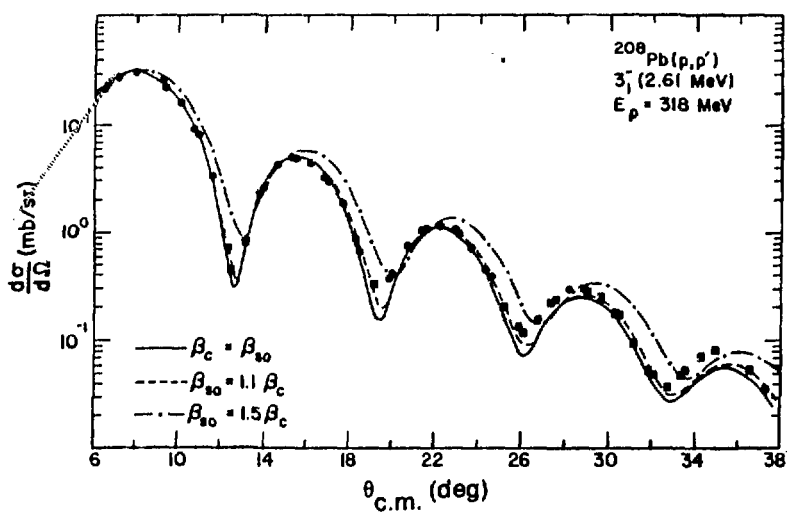

Fig. 3.
Angular distribution for the 3^- state in ^{208}Pb. The curves are described in the text.

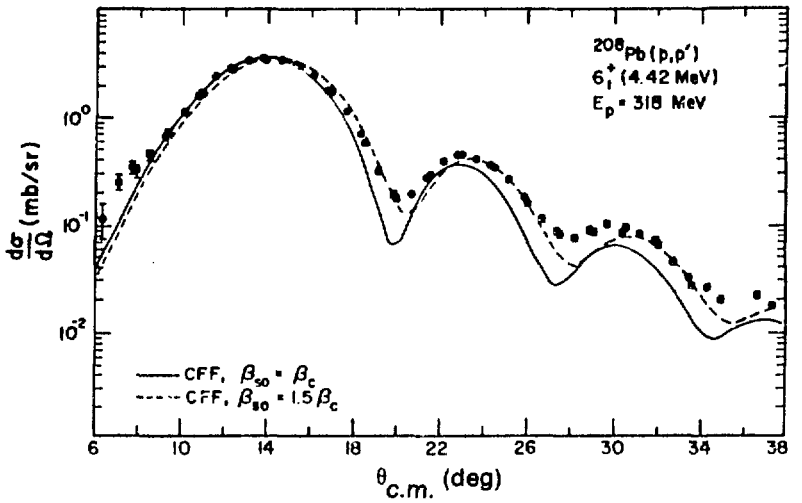

Fig. 4.
Angular distribution for the 6^+ state in ^{208}Pb. The curves are described in the text.

tentative fits are not of the same quality as the 800-MeV fits.[1]

Another purpose of this experiment was to examine high-spin "stretched configuration" states in ^{208}Pb. In Fig. 5 the angular distribution for the 14^- (6.74-MeV) state is shown. The calculation was done in the distorted-wave impulse approximation (DWIA) with bound-state Woods-Saxon wave functions ($r = 1.2$, $a = 0.65$) for a pure $\nu(i_{13/2}^{-1}, j_{15/2})$ configuration, using the free Love-Franey *NN* force to represent the interaction. The theoretical curve has been normalized to the data, with $\sigma_{EXP}/\sigma_{THEO} = 0.25$. However, as can be seen in Fig. 1, there is significant background under this peak, which leads to an uncertainty in σ_{EXP} well above that resulting from the absolute normalization alone.

REFERENCE

1. M. Gazzaly et al., Phys. Rev. C 25, 408 (1982).

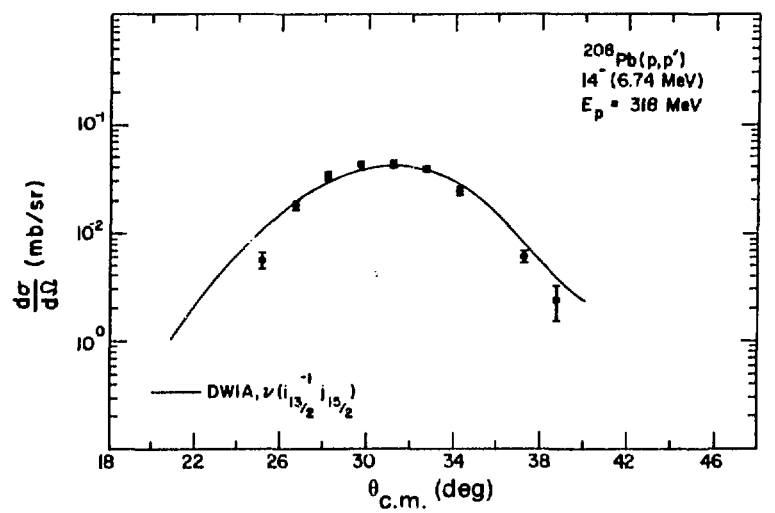

Fig. 5.
Angular distribution for the stretched 14^- state in ^{208}Pb. The curve is described in the text.

Measurement of A_{NN} for $\bar{p}p$ Elastic Scattering in the Coulomb-Nuclear Interference Region at 650 and 800 MeV

(Exp. 709, HRS)

(Univ. of Minnesota; UCLA; Los Alamos; KEK Lab.; Hiroshima Univ.; Kyoto Univ. of Education, Japan)

Spokesmen: M. Gazzaly (Univ. of Minnesota), G. Pauletta (UCLA), and N. Tanaka (Los Alamos)

The first of a series of experiments to measure the real parts of the forward, double spin-flip amplitudes at intermediate energies was completed in September 1983. Measurements were made at 650 and 800 MeV with an N-polarized proton beam and N-polarized frozen-spin target on HRS. The dilution refrigerator and polarized target expertise were provided by a team from KEK Laboratory, Hiroshima University, and Kyoto University of Education, Japan.

Whereas the imaginary parts of the forward, double spin-flip pp amplitudes at intermediate energies have been determined by measurements of the total pp cross sections (σ_{tot}, $\Delta\sigma_L$, $\Delta\sigma_T$) with polarized beam and target combinations,[1] we still rely on the semiphenomenological predictions of the forward dispersion relations[2] (FDRs) for our knowledge of the real parts. These predictions are used as constraints on current phase-shift analyses. The experimental determination of the real parts by measurements of A_{NN}, A_{LL}, A_{SS}, and A_{LS} in the Coulomb-nuclear interference region are therefore desirable, but have not yet been attempted because of experimental difficulties. At intermediate energies, the motivation for experimental data is enhanced by the observation of energy dependence in the imaginary parts.[2] This structure leads to similar structure in the FDR predictions of the real parts and to counterclockwise rotations of their Argand diagrams, which have been interpreted as evidence for the existence of dibaryon resonances.

Motivated by the interests outlined above, a series of experiments to determine the real parts of the forward pp double spin-flip amplitudes at 650 and 800 MeV has been initiated. Here we report on the first of these measurements, namely, that of A_{NN}.

To extend such measurements to small angles, one must be able to distinguish between scattering from the heavier target and cryostat components and scattering from hydrogen. Since the energy of the recoil proton is too small to allow detection, one must rely entirely on momentum resolution for the forward-scattered proton to separate out the hydrogen elastic-scattering component. The intrinsic momentum resolution of the HRS is more than adequate, so that the total experimental momentum resolution is determined by the combined thickness of the polarized target and the cryostat walls.

For our experiment, the outermost and thickest of the cryostat walls was modified so that the incident beam and the scattered protons passed through thin (0.2-mil) titanium windows and so that the effective target thickness was 0.5 cm. The polarizing field of 25 kG was provided by a C-type magnet (Zoltan) obtained from Lawrence Berkeley Laboratory. After the target polarization had been frozen, the field was reduced to 3 kG to minimize deflections of the incident and scattered protons in the field of Zoltan. Using calculations based on field maps, the scattering angle measured by the HRS was corrected for these deflections.

Spectrometer calculations were performed using a series of wire targets, and the beam position on target was determined by inserting a phosphor at the target position. The cryostat could be removed from the target position and replaced reproducibly by means of a system of synchronized servo-motors that moved the cryostat and associated liquid helium dewar in unison. The target position was checked by x-ray photographs. Upstream and downstream wire chambers were used to monitor beam profiles, which were typically 3 mm (horizontally) by 4 mm (vertically) FWHM. At larger angles, where momentum and angular resolution were not critical, the beam was wiggled $\sim\pm3$ mm about its central horizontal position, with a frequency of $\sim$60 Hz to reduce the incident beam density, permitting higher beam currents with acceptable target depolarization. A beam flux of $\sim2\times10^6$/s in a stationary spot of size given above produced an $\sim$5 h target polarization relaxation time.

Mean target polarizations were measured by NMR, but since the polarization in the target volume illuminated by the beam varied more rapidly than the average polarization, it was necessary to measure and monitor the relevant target polarization by other means. A polarimeter made up of two scintillation counter telescopes at $\pm18.5°$ and two conjugate recoil telescopes at $\sim\pm61.5°$ was used to monitor both beam and target polarization. Each of the recoil arms consisted of a multiwire proportional chamber (MWPC) and two scintillators. The scattering-angle information from the MWPCs was used to distinguish between elastic pp scattering and quasi-free pp scattering from bound protons in the nuclei of the target material and cryostat

windows. Since A_N is known to $\sim\pm 3\%$ for 800-MeV elastic scattering at 18.5°, the beam and target polarizations could be determined to this accuracy. The beam polarization also was obtained independently by the quench method.[3] The beam intensities were monitored by means of high-gain ion chambers filled with xenon and krypton gas, respectively, at 2-atm pressure.

Four independent measurements were made at each spectrometer angle: $Y(\uparrow\uparrow)$, $Y(\downarrow\uparrow)$, $Y(\uparrow\downarrow)$, and $Y(\downarrow\downarrow)$, where the first arrow in the parentheses refers to the direction of the beam polarization relative to the scattering plane, and the second arrow refers to that of the target. The target polarization was reversed once at each angle, whereas the beam polarization was reversed every 120 s in a repetitive cycle: up-quench-down-quench.... From the above measurements, four independent quantities were calculated:

$$\epsilon_1 = Y(\uparrow\uparrow) - Y(\downarrow\uparrow) - Y(\uparrow\downarrow) + Y(\downarrow\downarrow) = 4Y_0 P_b P_T A_{NN} ,$$

$$\epsilon_2 = Y(\uparrow\uparrow) + Y(\downarrow\uparrow) - Y(\uparrow\downarrow) - Y(\downarrow\downarrow) = 4Y_0 P_T A_N ,$$

$$\epsilon_3 = Y(\uparrow\uparrow) - Y(\downarrow\uparrow) + Y(\uparrow\downarrow) - Y(\downarrow\downarrow) = 4Y_0 P_B A_N ,$$

$$\epsilon_4 = Y(\uparrow\uparrow) + Y(\downarrow\uparrow) + Y(\uparrow\downarrow) + Y(\downarrow\downarrow) = 4Y_0 ,$$

where Y_0 is the spin-averaged yield, P_T is the target polarization, and P_B is the beam polarization. Since both the beam and target polarizations were determined independently as described above, values of A_{NN} and A_N could be extracted at each angle. A more sophisticated analysis that takes into account differences in the values of the beam and target polarizations as a function of the polarization direction is needed to eliminate spurious asymmetries; such an analysis is in progress.

REFERENCES

1. I. P. Auer, Nucl. Phys. A 335, 193 (1980); and D. Bugg, Nucl. Phys. A 374, 95 (1982).

2. W. Grein and P. Kroll, Nucl. Phys. B 136, 425 (1978).

3. M. A. McNaughton et al., Phys. Rev. C 23, 1128 (1981).

Development of 0° Capabilities at the HRS Facility (Exp. 768, HRS)

(Los Alamos, Univ. of Minnesota, Rutgers Univ.)

Spokesmen: J. B. McClelland and T. A. Carey, (Los Alamos) and S. Seestrom-Morris (Univ. of Minnesota)

A great deal of time and effort has been devoted in the past several years to obtaining very forward-angle inelastic proton spectra on medium to heavy nuclei at different medium-energy facilities. The thrust of this effort has been directed toward the identification of giant monopole and dipole excitation in these nuclei. The most successful measurements have been made at low energies (200-300 MeV) where the interaction causes a selectivity of spin-flip over non-spin-flip transitions, especially for low momentum transfer to the nucleus.

The ultimate goal of this experiment is to obtain high-quality spectra on medium to heavy nuclei in an effort to identify $M1$ strength systematically. The added selectivity of 0° measurements might disentangle the question of $M1$, $E1$, and $M2$ assignments.

We have recently run this experiment at 318 MeV on a variety of targets, and show here some preliminary on-line spectra taken during this run. This is the lowest energy at which 0° spectra have successfully been acquired at HRS. These spectra were taken without the use of either the active collimator system or focal-plane beam-pipe setup. The primary source of background was due to rescattering of particles from the exit flange of the spectrometer, provided that all other parameters had been optimized.

The quality of the preliminary spectra is good. The ^{12}C spectrum [Fig. 1(a)] is comparable to the best obtained at $T_p = 500$ MeV [Fig. 1(b)]. The 1^+ state in ^{48}Ca is clearly seen in Fig. 2, and the periodic structure seen in these spectra likely will be removed when calibrations are optimized. Evidence for increased Coulomb scattering because of the heavier mass target may be seen at low excitation in the ^{48}Ca spectrum.

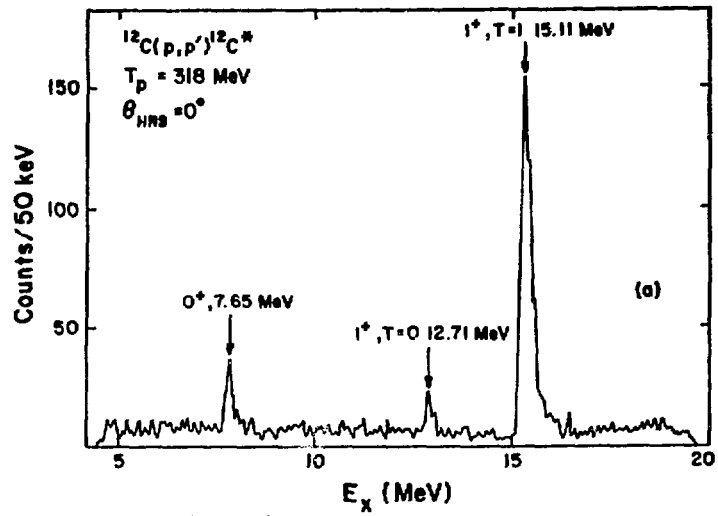

Fig. 1(a) and (b).
Spectra for ^{12}C at a 0° scattering angle for incident proton energies of (a) 318 MeV, and (b) 500 MeV.

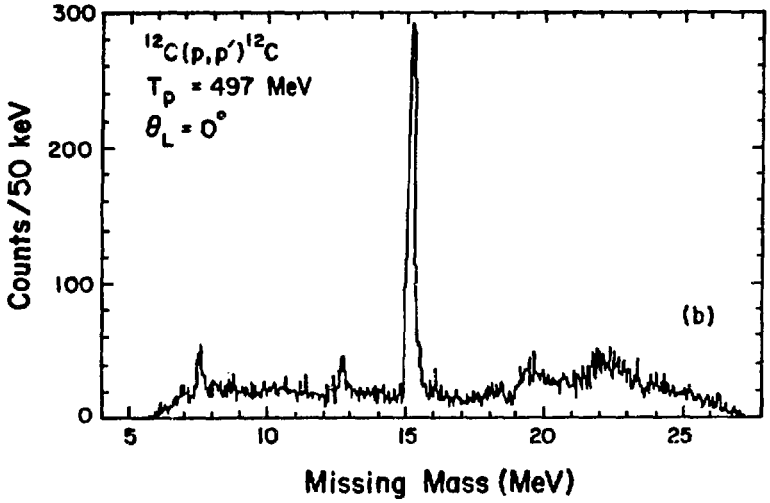

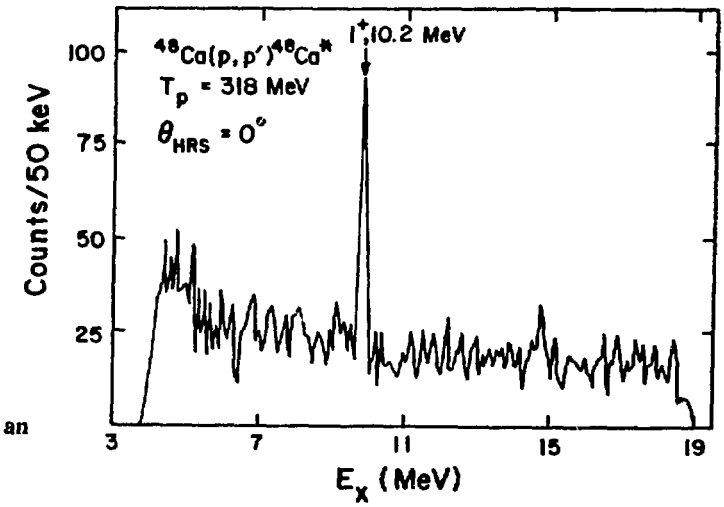

Fig. 2.
Spectrum for ^{48}Ca at a 0° scattering angle for an incident proton energy of 318 MeV.

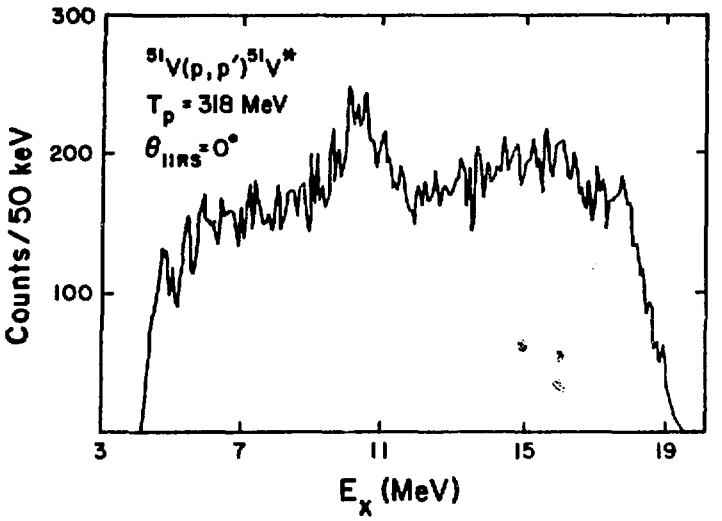

Fig. 3.
Spectrum for ^{51}V at a 0° scattering angle for an incident proton energy of 318 MeV.

Figure 3 shows a spectrum for ^{51}V at 0°. The quality of this spectrum is comparable to, if not better than, small-angle spectra taken at Orsay at 200 MeV. Furthermore, preliminary results show that the resonance is at about the same excitation energy as that seen at 200 MeV. Inadequate calibrations preclude any statement about fine structure in the resonance at this stage. Absolute normalization data have been taken, and it is hoped that absolute cross sections with reasonable error bars may be extracted from these data.

Measurement of A_{NN} for the $\vec{p}\vec{p} \rightarrow d\pi^+$ Reaction at 650 and 800 MeV (Exp. 790, HRS)

(UCLA; Univ. of Minnesota; Los Alamos; KEK Lab.; Hiroshima Univ.; Kyoto Univ. of Education, Japan)
Spokesmen: G. Pauletta (UCLA), M. Gazzaly (Univ. of Minnesota), and N. Tanaka (Los Alamos)

The $A_{NN}(\vec{p}\vec{p} \rightarrow d\pi^+)$ was measured at 650 and 800 MeV for laboratory angles of 2, 3.5, 5.5, and 7.5°. The aim of the experiment is to measure A_{NN}, A_{LL}, A_{SS}, and A_{LS} for this reaction at angles not previously accessible. When combined with measurements from previous experiments, complete angular distributions will be obtained. This can be integrated to obtain $\Delta\sigma_L(\vec{p}\vec{p} \rightarrow d\pi^+)$ and $\Delta\sigma_T(\vec{p}\vec{p} \rightarrow d\pi^+)$. The decomposition of the total cross sections $\Delta\sigma_L(\vec{p}\vec{p})$ and $\Delta\sigma_T(\vec{p}\vec{p})$ into their inelastic components will be obtained by further combination of these data with complete elastic $\vec{p}\vec{p}$ angular distributions (Exps. 583 and 709). The measurement of A_{LL} at 0 and 180° is of particular interest since it will provide the only measurements for the deuteron tensor polarization T_{20}. These data will contribute to our general understanding of the $I = 1$ nucleon-nucleon interaction and of the specific problem of the reaction mechanism involved in the $pp \rightarrow d\pi^+$ reaction.

This experiment was performed at the HRS using the same experimental setup as Exp. 709. Figure 1 presents a dot plot of energy loss vs time of flight. Since the deuteron momenta are greater than any proton momenta from the beam-target interactions, a clear deuteron group is observed in Fig. 1 along with a proton group caused by protons that scatter off the spectrometer magnet pole faces. Figure 2 presents a missing-mass spectrum for the deuterons. A clear peak is observed that corresponds to the $pp \rightarrow d\pi^+$ reaction. The data from this experiment are being analyzed.

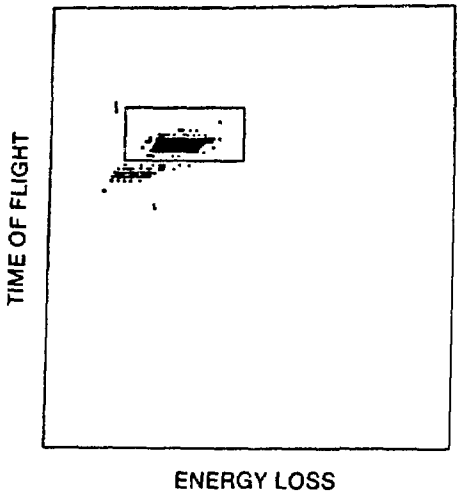

Fig. 1.
A dot plot of energy loss vs time of flight measured by the detector array at the focal plane of the HRS. Deuterons are designated by the box.

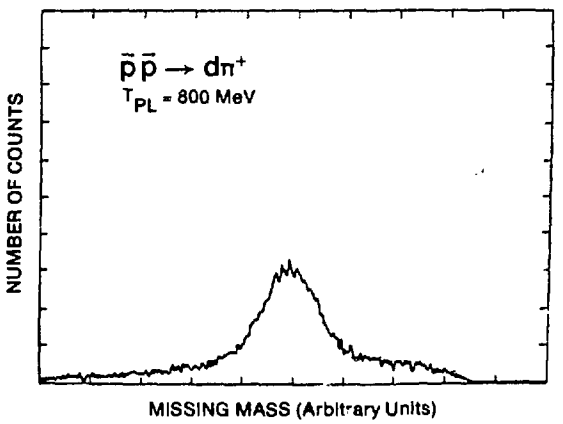

Fig. 2.
A deuteron missing-mass spectra measured at the HRS focal plane. A clear peak corresponding to the $pp \rightarrow d\pi^+$ reaction is observed.

Spin-Depolarization Measurements on the Oxygen Isotopes
(Exp. 643, HRS)

(MIT, Indiana Univ., UCLA, Lawrence Livermore Lab., Los Alamos)
Spokesmen: James J. Kelly (MIT) and M. V. Hynes and B. Aas (Los Alamos)

This experiment will use measurements of the spin-depolarization coefficients $D_{\alpha\beta}$ to enhance the study of the two-nucleon effective interaction in the nuclear medium and to improve the precision with which nuclear-structure comparisons can be made among the oxygen isotopes. Ultimately, we wish to obtain spin-rotation measurements for elastic scattering by $^{16\text{-}18}O$ and spin-depolarization measurements for as many inelastic excitations of all three isotopes as possible. Data taking has been completed for ^{16}O but has not yet begun for ^{17}O or ^{18}O.

The central data-analysis problem is to apply line-shape analysis techniques to many spectra simultaneously and to obtain the maximum statistical precision without introducing bias. Because we believe that the techniques currently available are inadequate, we have formulated the maximum-likelihood estimators for the observables of interest and are studying the application of these estimators to line-shape fitting. An extensive Monte Carlo simulation program for the HRS and focal-plane polarimeter has been written, but the optimal data-reduction strategy has not yet been decided. It is clear from the volume of magnetic tape requiring processing that a careful decision is advisable before replaying the data.

A preliminary analysis of the cross-section and analyzing-power data obtained with N-type beam has been performed. These data have been compared with impulse-approximation calculations. Qualitatively, the same systematics is observed at 500 MeV as was observed at 318 MeV, with a somewhat stronger enhancement of the interior states over the predictions.

Energy Dependence of the Two-Nucleon Effective Interaction

Exp. 718, HRS)

(MIT, Indiana Univ., UCLA, Lawrence Livermore Lab., Los Alamos)

Spokesmen: James J. Kelly (MIT) and M. V. Hynes (Los Alamos)

The two-nucleon effective interaction is modified in the nuclear medium by the local density in the vicinity of the interacting nucleons. These modifications have been most carefully studied for incident proton energies between 100 and 200 MeV.

The magnitude of these medium corrections is expected to decrease slowly with energy. To study this energy dependence, we have measured the cross section and analyzing power for the excitation of all narrow states of ^{16}O below 13-MeV inelasticity by 318-MeV protons. These data will be combined with comparable 135- and 180-MeV data taken at the Indiana University Cyclotron Facility (IUCF) and 500-MeV data taken at LAMPF (Exp. 643).

Approximately one-half of the data has been reduced, forming angular distributions with twice the expected final-step size. These data have been compared with impulse-approximation calculations based on the Love-Franey interaction, and with local density approximation calculations using a *G* matrix based on the Paris potential. The nuclear structure was specified by transition densities fitted to electron-scattering data.

To summarize the comparisons between theory and experiment, it is convenient to divide the states into two classes: (1) interior states whose transition densities peak in the high-density nuclear interior, and (2) surface states whose transition densities peak in the low-density nuclear surface. The predicted cross sections for surface states agree well with the data at the peak of the angular distributions. For interior states the predicted peak cross sections are about 30% below the data. The high momentum-transfer (q) predictions for all states are substantially below the data.

These results allow us to draw several conclusions about the 318-MeV effective interaction. First, the low-q amplitude is approximately correct for small density. Second, the strength of the dominant imaginary part of the isoscalar spin-independent central component is enhanced as the density increases. And third, the high-q interaction needs to be enhanced, but it is not yet clear whether this effect depends on density. These conclusions will be quantified using the modeling techniques briefly described below.

Direct Reaction Analysis with Linear Expansions

James J. Kelly (MIT)

A general modeling technique has been developed that can fit a variety of linear expansions to any set of direct reaction observables. This technique has been implemented for nucleon-nucleus scattering, but can be readily expanded to include electron scattering and pion scattering.

If we expand the scattering operator U in a linear basis such that

$$U = \sum_n a_n U_n \ ,$$

the distorted-wave matrix element for the reaction $A(\vec{a},\vec{b})B$ may be written

$$T = \sum_n a_n \langle \vec{k}_f \, {}^{J_B J_b}_{m_B m_b} \left| \, U_n \, \right| \, {}^{J_A J_a}_{m_A m_a} \vec{K}_i \rangle$$

$$= \sum_n a_n H^n_{m_B m_b m_A m_a}(\theta) \ ,$$

where the $(j_i m_i)$'s are the spins and spin projections of the particles involved, and $\sigma_{\alpha m m'}$ represent the Pauli spin operators for the projectile. It is convenient to construct the quadratic forms

$$X^{nn'}_{\alpha\beta}(\theta) = \sum H^n_{m_B m_b m_A m_a}(\theta) \, \sigma_{\alpha m_a m_a'} \, H^{n'}_{m_B m_b' m_A m_a'}(\theta) \, \sigma_{\beta m_b' m_b} \ .$$

The observables are then contractions of these quadratic forms (sum on six repeated indices):

$$\sigma_0(\theta) = \frac{\mu_a \mu_b}{(2\pi)^2} \frac{k_b}{k_a} I_0(\theta) ,$$

$$I_0(\theta) = \frac{1}{2} \sum_{nn'} a_n X^{nn'}_{oo}(\theta) a^*_{n'} ,$$

$$I_0 A_y = \frac{1}{2} \sum_{nn'} a_n X^{nn'}_{yo}(\theta) a^*_{n'} ,$$

$$I_0 P = \frac{1}{2} \sum_{nn'} a_n X^{nn'}_{oy}(\theta) a^*_{n'} ,$$

$$I_0 D_{\alpha\beta} = \frac{1}{2} \sum_{nn'} a_n X^{nn'}_{\alpha\beta}(\theta) a^*_{n'} .$$

A very simple search algorithm can minimize the total χ^2 for an arbitrary set of observables with respect to the expansion coefficients a_n. Several applications that have used this technique follow.

(1) Effective Interactions. We expand medium corrections to the effective interaction in the form

$$t_{eff} = t_{free} + \sum_{n=1}^{N} a_n t_n(q,\rho) .$$

For a given projectile energy, the effective interaction is common to all transitions excited. The maximum sensitivity to the density (ρ) and momentum transfer (q) dependence of the medium corrections is obtained in a simultaneous fit to the cross-section and analyzing-power data for many multipolarities We have performed this type of fit at several projectile energies using the 0^+_3, 1^- 2^+_1, 3^-_1, and 4^+_1 states of ^{16}O.

(2) Neutron Densities. For normal parity transitions whose spin and current contributions are negligible, the proton distribution can be fully specified by electron-scattering measurements. The neutron distribution ρ_n can then be fit to proton-scattering data using linear expansions of the form

$$\rho_n^{(r)} = \sum_n a_n f_n(r) ,$$

where $f_n(r)$ are any convenient complete set of radial functions. We have used both Fourier-Bessel expansions and polynomial-times-Gaussian expansions. The error envelope $S_{\rho n}(r)$ is obtained from the covariance matrix V_{ij} using

$$|S_{\rho n}(r)|^2 = \sum_{ij} f_i(r) V_{ij} f_i(r) .$$

Fits have been made for several states of ^{18}O and ^{88}Sr. Pseudodata studies also have been made.

(3) Longitudinal Spin Density. The 0^+ to 0^- transitions are driven by the longitudinal spin density, which can be expanded as above. The $^{16}O(p,p')$ 0^-, $T=0$ reaction has been studied at 135 MeV.

Study of Isobaric-Analog States in (π^+,π^0) Reactions (Exp. 412, LEP)

(Los Alamos, Tel Aviv Univ., Arizona State Univ.)
Spokesmen: H. W. Baer and J. D. Bowman (Los Alamos)

We completed[1] a series of measurements of 0° differential cross sections for isobaric-analog states (IASs) on nuclei ranging from ^{7}Li to ^{208}Pb. The measurements were performed with the π^0 spectrometer at the LEP channel at four energies between 100 and 300 MeV. The A dependence at each energy is shown in Fig. 1. These data showed that 0° IAS cross sections follow a remarkably regular pattern when plotted against $g(E)(N-Z)A^{-\alpha(E)}$.

Using the determined parameters $g(E)$ and $\alpha(E)$, it appears first that one can estimate a 0° IAS cross section on any nucleus in the periodic table to an average accuracy of 20% for beam energies between 100 and 300 MeV. Second, the regular pattern in the data established that the parameters g and α constitute a good meeting ground for comparisons between experiments and theories, particularly those theories that attempt to describe the general features of π-nucleus scattering. For example, the data show that α decreases from 1.35 at the resonance energy (165 MeV) to 1.10 at 295 MeV (Fig. 2). Generally, this reflects the changing nature of pion single-charge-exchange (SCX) scattering, going from approximately black-disk scattering at 165 MeV (a value of $\alpha = \frac{4}{3}$ is given in Ref. 2) to increased volume scattering at higher energies. A third consequence of these measurements is that it now becomes possible to recognize with some degree of confidence an "anomalous" 0° IAS cross section.

At resonance energies, deviations from the general trends are expected to arise primarily from unusual neutron-proton density distributions in the surface region; ^{90}Ar appears to be such a case.[1] Since it is generally believed that pion SCX to the IAS is one of the most sensitive tools available to study the relative neutron-to-proton density distributions ($\Delta\rho$) in nuclei, determining the systematic features is particularly desirable.

Figure 3 presents $\sigma_{IAS}(0°)$ as a function of incoming pion kinetic energy. For comparison we show in Fig. 3 the energy dependence of the free cross section $\sigma_{\pi^- p \to \pi^0 n}(0°)$. In general, the maximum of the 0° IAS cross section is observed on the (3,3) resonance energy. It drops quickly when below and slowly when above the resonance. These trends follow the shape of the free cross section but are less pronounced.

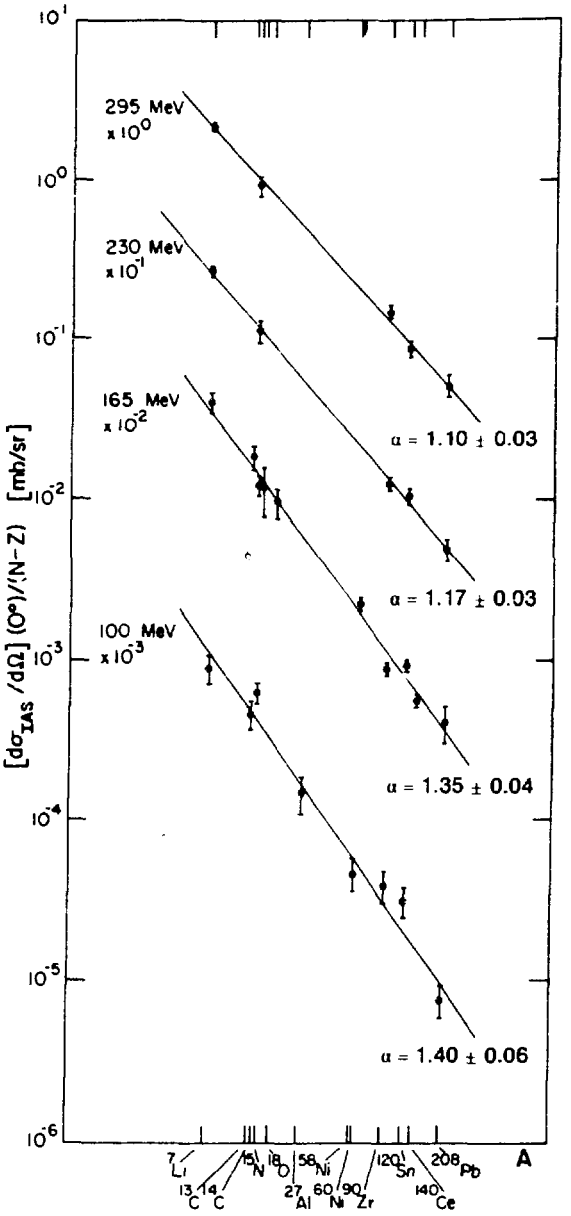

Fig. 1.
Measured (Ref. 1) $\sigma_{IAS}(0°)$. The straight lines represent $g(E)(N-Z)A^{-\alpha}$.

An anomalous behavior is observed for the ^{90}Zr nucleus where the cross section is monotonically increasing with the energy and does not reflect the (3,3) resonance as do the other nuclei. This effect might be related to the neutron-proton density difference at the surface. In general, the ratio of the number of neutrons to protons, evaluated as

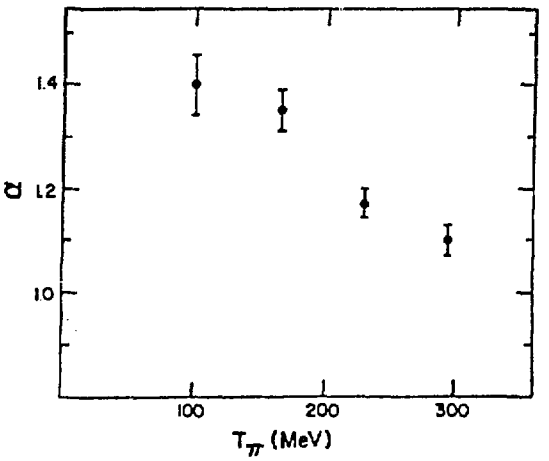

Fig. 2.
The energy dependence of the exponent α in the function $g(N-Z)A^{-\alpha}$ deduced from the measurements shown in Fig. 1.

$$\frac{\int_R^\infty \rho_n \, d\tau}{\int_R^\infty \rho_p \, d\tau}$$

with the use of density-matrix expansion or Hartree-Fock Skyrme III force densities,[3,4] exceeds the N/Z ratio in the surface region probed by the strongly absorbed pions; ^{90}Zr is an exception, as the calculated ratio is very close to N/Z. This means that for ^{90}Zr the SCX cross section near the (3,3) resonance is relatively suppressed because the interaction occurs near the surface, which has a comparatively low neutron density. At higher energies, with a larger penetration depth, the behavior is closer to that of an average nucleus. This interpretation agrees with the observation that the reduced cross section (see Fig. 1) of ^{90}Zr at 165 MeV is lower than the fitted line whereas that of ^{120}Sn (a nearby nucleus with a large "neutron halo") is higher.

We have proposed (Exp. 728) to extend the (π^+,π^0) IAS measurements into the 300- to 500-MeV region using the π^0 spectrometer at the P^3 pion channel. A major motivation is to see whether the remarkably regular patterns found for the 0° cross sections in the 100- to 300-MeV region continue at the higher energies. A second goal is to provide more evaluation of the dis-

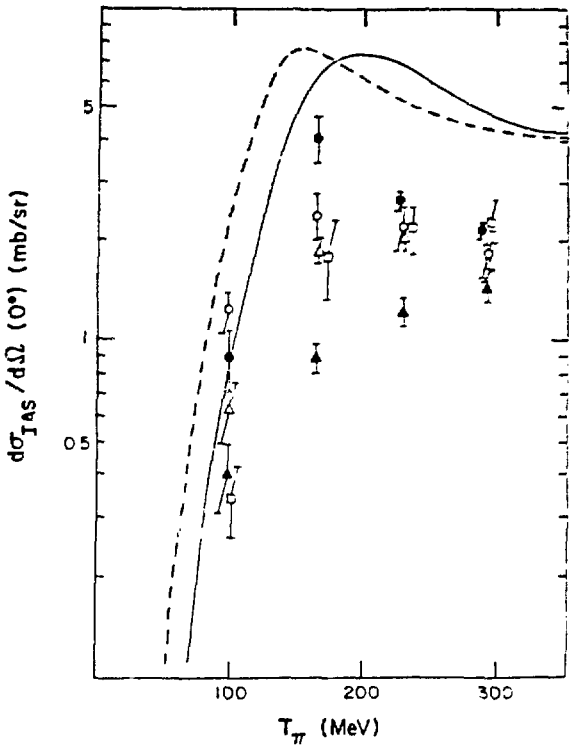

Fig. 3.
Excitation function of the 0° IAS cross sections (c.m. system) for ^{7}Li (solid circles), ^{14}C (open circles), ^{90}Zr (solid triangles), ^{120}Sn (open triangles), and ^{208}Pb (open squares). The solid line represents the c.m. cross section of the free charge-exchange reaction $\pi^+ + n \rightarrow \pi^0 + p$ plotted vs the laboratory kinetic energy; the dashed line, vs the c.m. kinetic energy.

torted-wave impulse approximation (DWIA) theory. If the DWIA theory is more accurate at higher energies, $\sigma_{IAS}(0°)$ should increase* in the 300- to 500-MeV interval. If this behavior is not observed, it will show unequivocally that a major ingredient is missing in the theoretical description.

If $\sigma_{IAS}(0°)$ continues to follow the shape of the free $\sigma(\pi N)$, the excitation functions for most nuclei should follow the shape shown in Fig. 4. The $\sigma(\pi N)$ curve was normalized to the 295-MeV data point.

It is our belief that the experimental determination of the systematics for IAS excitation as a function of E and

*See, for example, LAMPF proposal 728, where calculations performed with the code PIESDEX are presented.

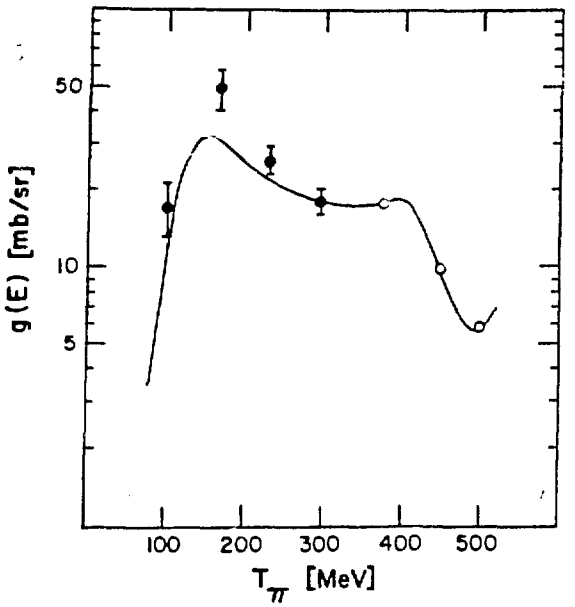

Fig. 4.
The deduced values of $g(E)$ obtained by fitting $g(E)(N-Z)A^{-\alpha}$ to the measured $\sigma_{IAS}(0°)$. The curve represents the shape of $\sigma(\pi^- p \rightarrow \pi^0 n)$ at 0°; it is normalized to the 295-MeV data point.

A constitutes a basic characterization of the π-nucleus interaction between 100 and 500 MeV. We have completed the first part of this study at the LEP and plan to perform the high-energy part of the study at P^3 in 1984.

REFERENCES

1. U. Sennhauser et al., Phys. Rev. Lett. 51, 1324 (1983).

2. M. B. Johnson, Phys. Rev. C 22, 192 (1980).

3. J. W. Negele and D. Vautherin, Phys. Rev. C 5, 1472 (1972).

4. M. Beiner et al., Nucl. Phys. A 238, 29 (1975).

Pion Elastic-Scattering and Single- and Double-Charge-Exchange Reactions on ^{14}C

(Exp. 523, LEP)

(Los Alamos, Univ. of Colorado, Arizona State Univ., Tel Aviv Univ.)

Spokesmen: H. W. Baer (Los Alamos) and J. L. Ullmann (Univ. of Colorado)

(Exp. 539, EPICS)

(Los Alamos, Univ. of Minnesota)

Spokesmen: H. W. Baer (Los Alamos) and D. B. Holtkamp (Univ. of Minnesota)

(Exp. 558, EPICS)

(Los Alamos, New Mexico State Univ., Univ. of Texas, Univ. of Minnesota)

Spokesmen: H. W. Baer (Los Alamos) and G. R. Burleson (New Mexico State Univ.)

This set of experiments is intended to provide complete data on a single nucleus for pion reactions that are related by isospin invariance: π^+ and π^- elastic scattering, (π^+,π^0) to the isobaric-analog state (IAS), and (π^+,π^-) to the double-isobaric-analog state (DIAS). Carbon-14 was chosen because it has the most favorable level separations among the $T \geq 1$ nuclei.

The measurements are being made at various energies between 35 and 300 MeV. These data should provide a good picture of the changing nature of the pion-nucleus interaction with energy. Specifically, comparisons will be made with theories that attempt to describe in a continuous manner the dynamical changes that occur in the pion nucleus interaction at energies below, on, and above the Δ resonance.

Elastic-scattering data now have been measured at 164 MeV (Exp. 539) and at 80 and 65 MeV.[1] The 164-MeV data are shown in Fig. 1. The difference in the angle of the first minimum between π^+ and π^- scattering is approximately 2.5°, indicating a slightly larger effective radius for neutrons than for protons in ^{14}C.

Forward-angle single-charge-exchange (SCX) cross sections have been measured at 35, 50, 65, 80, 100, 165, 230, and 295 MeV. The dramatic energy dependence in the forward-angle IAS cross sections is exhibited in Figs. 2 and 3. At energies between 100 and 300 MeV, the

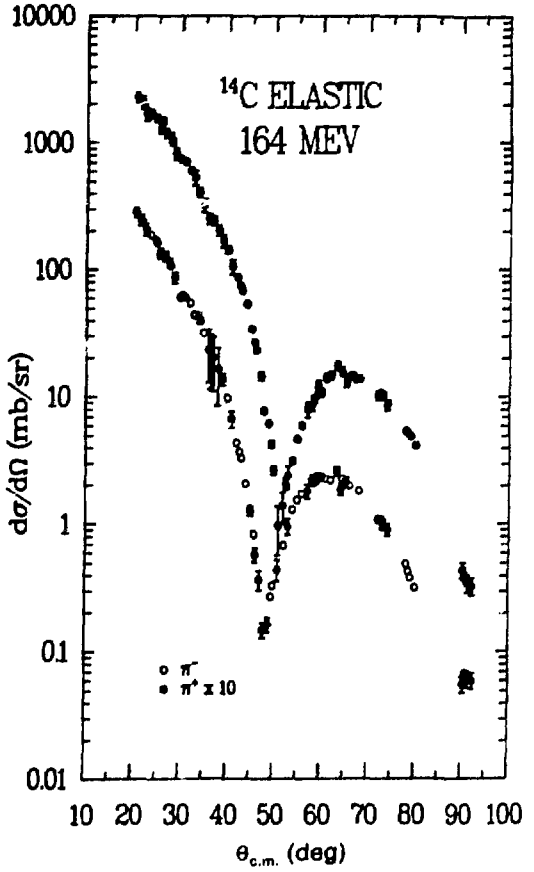

Fig. 1.
Elastic-scattering cross sections for π^+ and π^- on ^{14}C.

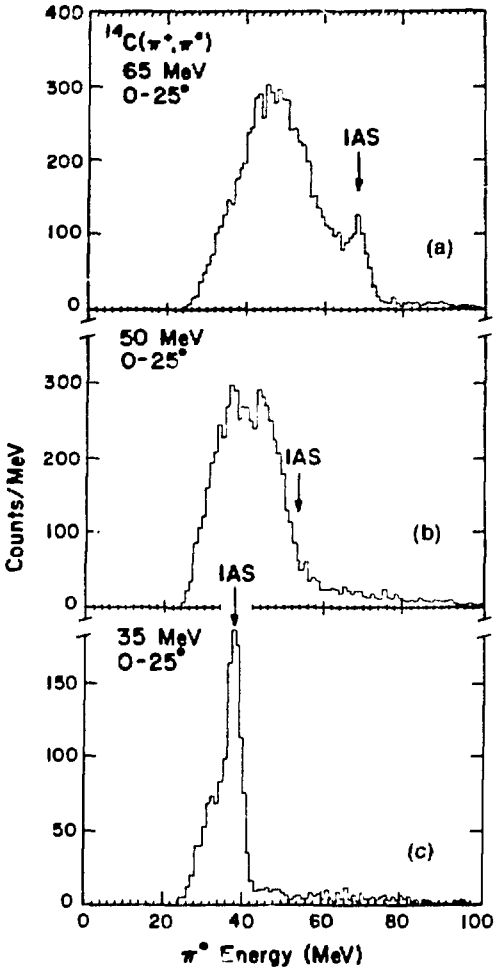

Fig. 3(a)-(c).
Measured spectra for the ^{14}C(π^+,π^0) reaction at low energies.

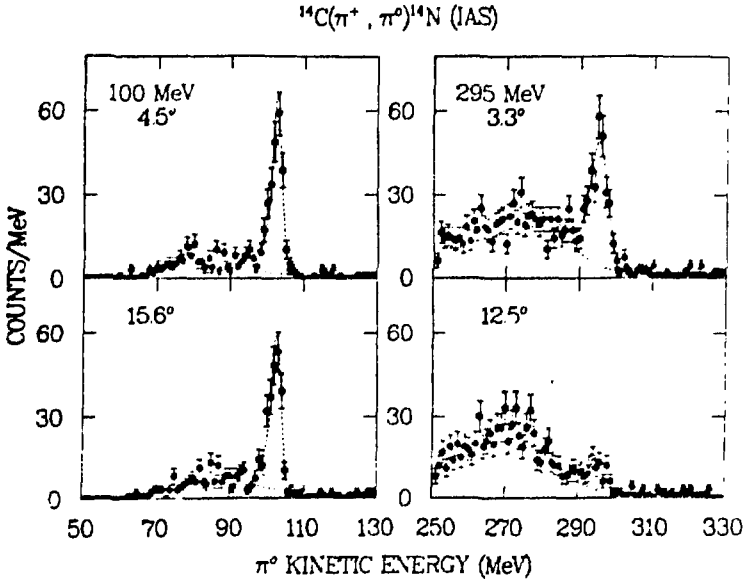

Fig. 2.
Measured π^0 spectra for the ^{14}C(π^+,π^0) reaction.

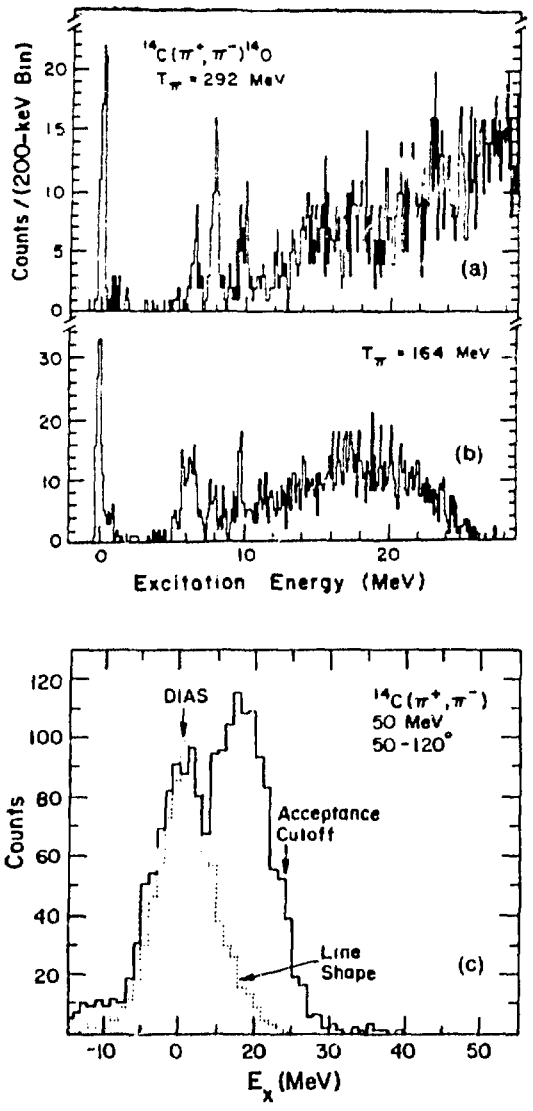

Fig. 4(a)-(c).
Measured spectra for the $^{14}C(\pi^+,\pi^-)$ reaction at (a) 292 MeV, EPICS; (b) 164 MeV, EPICS; and (c) 50 MeV, TRIUMF-TPC.

IAS is a prominent feature of forward-angle (π^+,π^0) reactions. At 50 MeV the IAS vanishes. An upper limit on the 0° cross section, based on the data of Fig. 3(b), is 5 μb/sr. At 35 MeV the IAS is again a prominent feature of the spectrum [Fig. 3(c)].

The deep minimum in the 0° cross section near 50 MeV would seem to be a direct reflection of the corresponding deep minimum in the $\pi^- p \rightarrow \pi^0 n$ reaction. However, calculations by Siciliano[2] have shown that sizable isovector-correlation (ρ^2) terms are required to obtain a deep minimum in the 0° cross section at 50 MeV for the $^{15}N(\pi^+,\pi^0)$ reaction. The ^{14}C data are being analyzed in the framework of the Johnson-Siciliano[3] theory and the Kauffman-Gibbs[4] multiple-scattering theory.

The first double-charge-exchange (DCX) cross sections for a DIAS transition at 50 MeV were measured in 1983 using the time-projection chamber (TPC) at the M9 channel at TRIUMF.* These measurements at a low energy were made possible by a large solid-angle detector (TPC) and a sufficient quantity (7 g) of ^{14}C packaged into suitable target cells. In Fig. 4 the spectrum measured with the TPC at 50 MeV is compared with spectra measured at EPICS at 165 and 292 MeV. The measured angular distributions at these energies are shown in Fig. 5. The high resolution in the EPICS data is attractive, but not necessary, to measure $^{14}C(\pi^+,\pi^-)^{14}O$ (DIAS) because the first excited state in ^{14}O is at 5.9 MeV.

EPICS, because of its long length, is not well suited to measure 50-MeV cross sections. It is interesting to see that the 50-MeV cross sections for angles $\theta \geq 50°$ are larger than the cross sections at 165 and 295 MeV for $\theta \geq 20°$.

This first measurement of DCX at low energy should put constraints on the very uncertain theoretical calculations. The main features that can be observed in the results follow.

- The shape of the angular distribution has some resemblance to the shape of elastic scattering, but the minimum at 70° is much shallower.
- The angular-distribution seems to increase at small angles, unlike SCX,[3] which has a minimum at 0°.

Optical-model calculations, using a modified version of the code PIESDEX, were done by E. Siciliano. The parameters were the same ones that gave good agreement with the 50-MeV SCX of ^{15}N (Ref. 3) and 50-MeV elastic scattering on ^{16}O. The results of the calculations with and without the isotensor Lorentz-Lorenz term are shown with the experimental data in Fig. 5(c).

The calculations have the right magnitude, but the shape has only a modest resemblance to the data. Clearly a better theoretical understanding and more data are desirable.

*Experiment TPC-DCX at TRIUMF, "Pion Double Charge Exchange at Low Energy," by a TRIUMF collaboration and H. W. Baer of Los Alamos as Spokesmen.

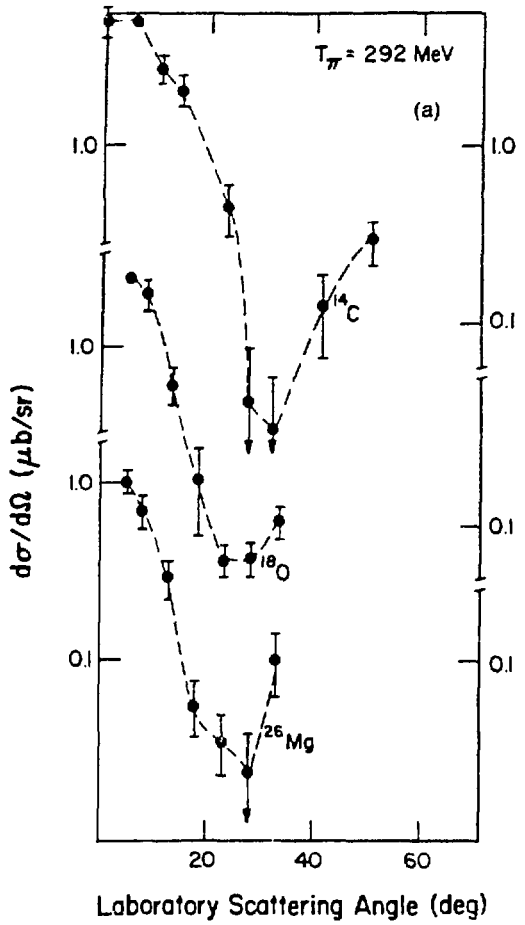

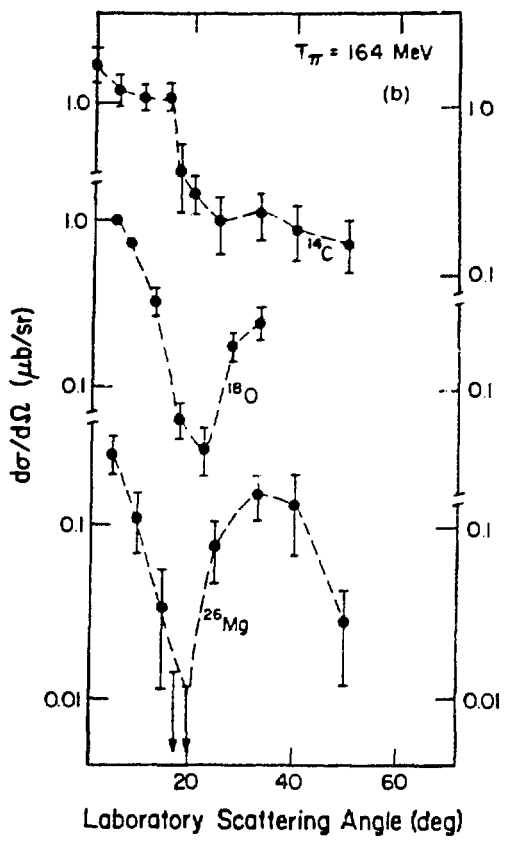

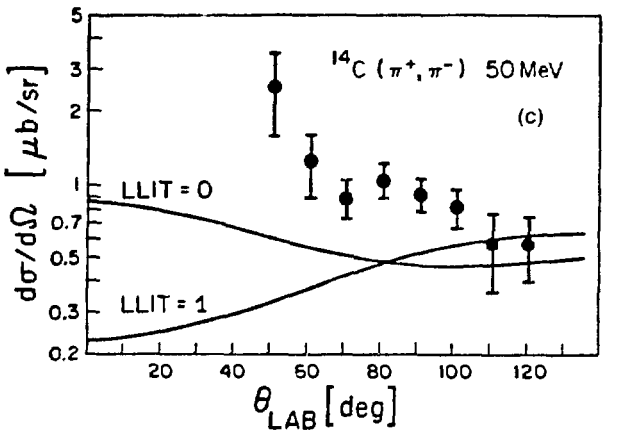

Fig. 5(a)-(c).
Differential cross sections for the reaction $^{14}C(\pi^+,\pi^-)$ at (a) 292 MeV, EPICS; (b) 164 MeV, EPICS; and (c) 50 MeV, TRIUMF-TPC.

REFERENCES

1. M. Blecher et al., Phys. Rev. C 28, 2033 (1983).

2. M. D. Cooper et al., submitted to Phys. Rev. Lett.

3. M. B. Johnson and E. R. Siciliano, Phys. Rev. C 27, 720 (1983).

4. W. Kaufmann and W. R. Gibbs, Los Alamos National Laboratory document LA-UR-83-736 (1983).

A Dependence of the Excitation Energy, Width, and Cross Section of the Isovector Monopole Resonance (Exp. 607, LEP)

(Los Alamos, Tel Aviv Univ., Arizona State Univ., SIN)
Spokesmen: J. D. Bowman and H. W. Baer (Los Alamos) and J. Alster (Tel Aviv Univ.)

We have used the (π^-,π^0) charge-exchange reaction at 165-MeV kinetic energy to study the $T+1$ component of the isovector monopole resonance (IVM). The nuclei ^{40}Ca, ^{60}Ni, ^{90}Zr, ^{120}Sn, ^{140}Ce, and ^{208}Pb were used as targets. We also observed the $T+1$ component of the giant dipole resonance (GDR) in the lighter targets. The (π^+,π^0) reaction cross sections showed the presence of the $T-1$ component of the IVM and GDR in ^{40}Ca, ^{60}Ni, and ^{90}Zr.

Pion charge exchange is well suited to the study of the isovector giant resonance, and particularly the IVM, for a number of reasons. The pion is spinless, and at forward angles the excitation of spin-flip states is strongly inhibited. The charge-exchange reactions proceed through the $T\cdot\tau$ piece of the π-nucleon t matrix; hence, charge-exchange reactions must excite isovector states. This is in contrast to inelastic hadron scattering, which strongly excites isoscalar states.

Giant resonances have large transition densities in the nuclear surface. Because 165-MeV π's are strongly absorbed, they couple efficiently to these surface-peaked transition densities. This point is crucial for monopole modes where the volume integral of the transition density vanishes. The excitation of a monopole mode by a weakly absorbed probe therefore is strongly suppressed at forward angles. The angular distributions produced by the strongly absorbed 165-MeV π's are sharply diffractive and allow a direct determination of the angular momentum of the final states. Finally, the Coulomb energy shifts the $T+1$ component of the IVM to a low excitation energy in the (π^-,π^0) daughter nucleus. The decay width of this state, therefore, is reduced.

Figure 1 shows plots of doubly differential cross sections for the (π^-,π^0) reaction vs the kinetic energy of the detected π^0's. Representative targets, ^{60}Ni and ^{140}Ce, are shown. The top spectra are for a scattering angle of 4.5° near the forward direction where the IVM cross section is largest; the middle spectra are for 15° where the IVM cross section is small and that of the GDR is largest; and the bottom spectra are for 33° where both the IVM and GDR have small cross sections. The dashed lines represent a smoothly interpolated background.

In Fig. 2 we plot the normalized cross section S in the monopole region of the spectra vs momentum transfer squared ($q = k_\pi \sin\theta$). The monopole-region cross sections were divided by the observed differential cross section

$$S = \frac{\int \frac{d^2\sigma}{d\Omega dT} dT \text{ (monopole region)}}{\int \frac{d^2\sigma}{d\Omega dT} dT \ (E_x < 70 \text{ MeV})} .$$

It is the excess of cross section above the linearly extrapolated background that we identify as caused by the IVM. The first minimum of the IVM angular distribution occurs where $qR = \pi/2$, where R is the π-absorption radius. This point is indicated on Fig. 2. The observed break points between the background and the forward-peaked IVM feature are near the $\pi/2$ point for each nucleus.

Angular distributions, excitation energies, and widths were extracted by fitting the doubly differential cross sections to a sum of IVM, GDR, and nonresonant background components. The background was smoothly interpolated under the resonances as a function of q^2 and T_{π^0}. The angular distribution for the IVM and GDR peaks in the ^{60}Ni(π^+,π^0) data is shown in Fig. 3. The solid lines are the angular distribution of Auerbach and Klein[1] normalized to the data.

In Fig. 4(a) we show the extracted maximum monopole and dipole cross sections compared to calculations of Auerbach and Klein for the different targets.

In Fig. 4(b) we show excitation energies and widths, again compared to the random-phase-approximation (RPA) theory of Auerbach and Klein. The agreement is remarkable.

We observed no hint of isovector quadrupole signal. For example, in the ^{60}Ni (π^-,π^0) data where we observe 70% of the IVM and GDR cross sections predicted by the RPA distorted-wave impulse approximation (DWIA) theory, we observe <25% (90% confidence level) of the isovector quadrupole predicted cross section.

Our conclusions are that the IVM is a systematic feature of nuclei from ^{40}Ca to ^{208}Pb. Its excitation energy and width are well reproduced by RPA calculations. Its cross section is large, indicating the collective nature of

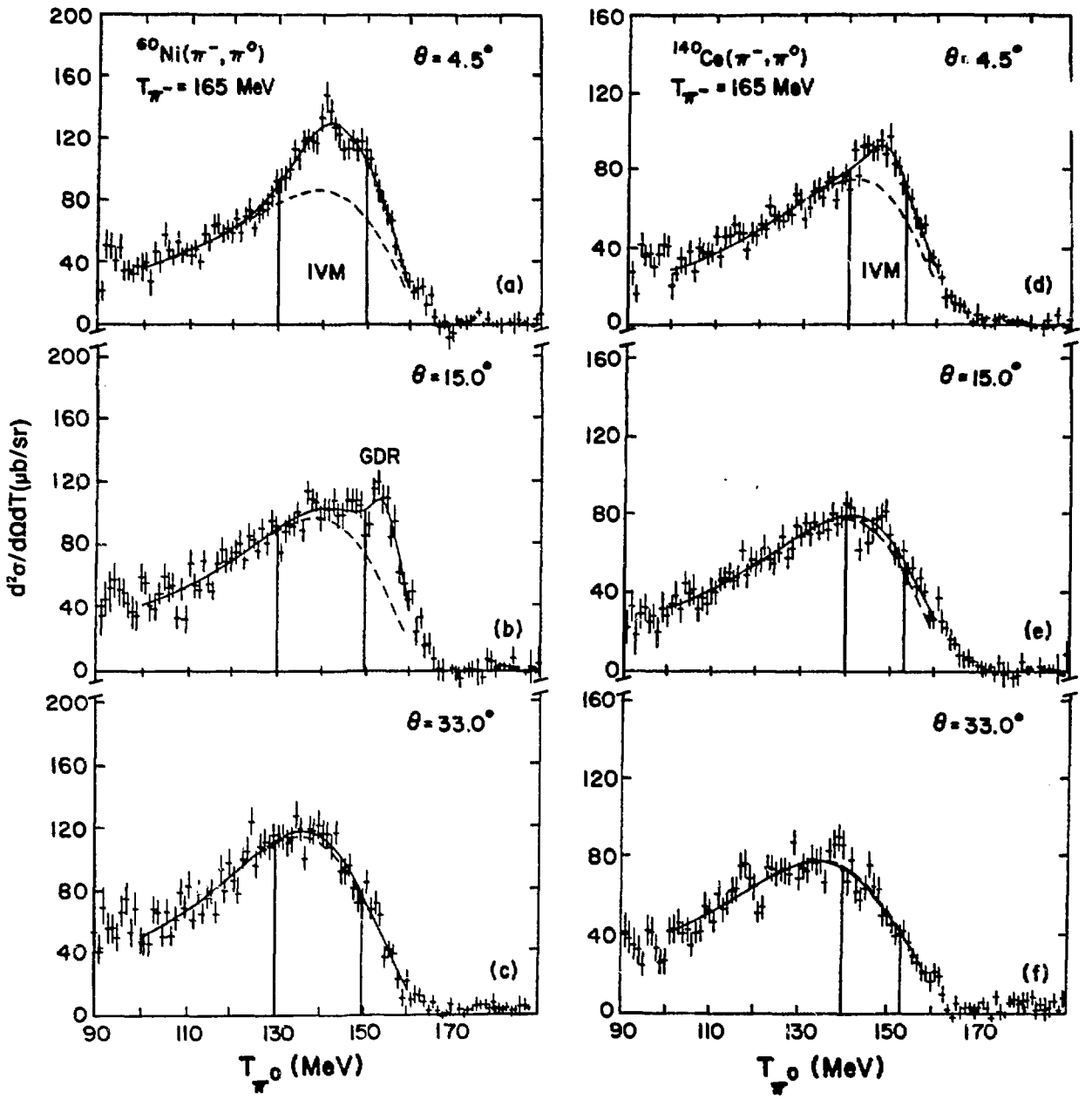

Fig. 1.
Doubly differential cross sections vs π^0 kinetic energy for $^{60}Ni(\pi^-,\pi^0)$ and $^{140}Ce(\pi^-,\pi^0)$ at laboratory angles of 4.5, 15.0, and 33.0°.

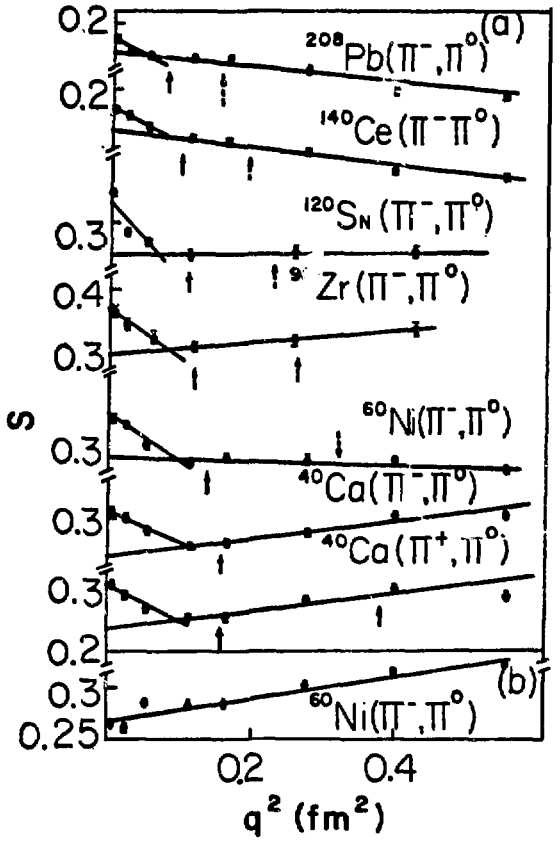

Fig. 2(a) and (b).
The ratio S plotted vs momentum-transfer squared. The region of integration is (a) centered on the expected IVM energy, and (b) centered above the IVM energy.

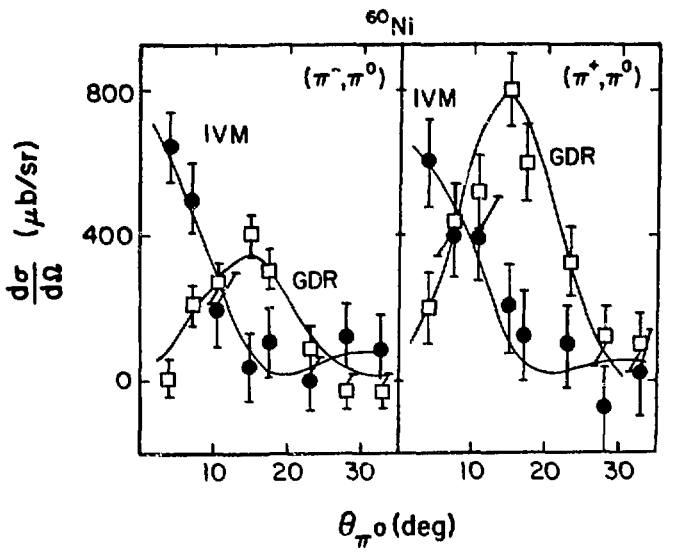

Fig. 3.
Angular distribution for the IVMs and GDRs in $^{60}Ni(\pi^{\pm},\pi^0)$.

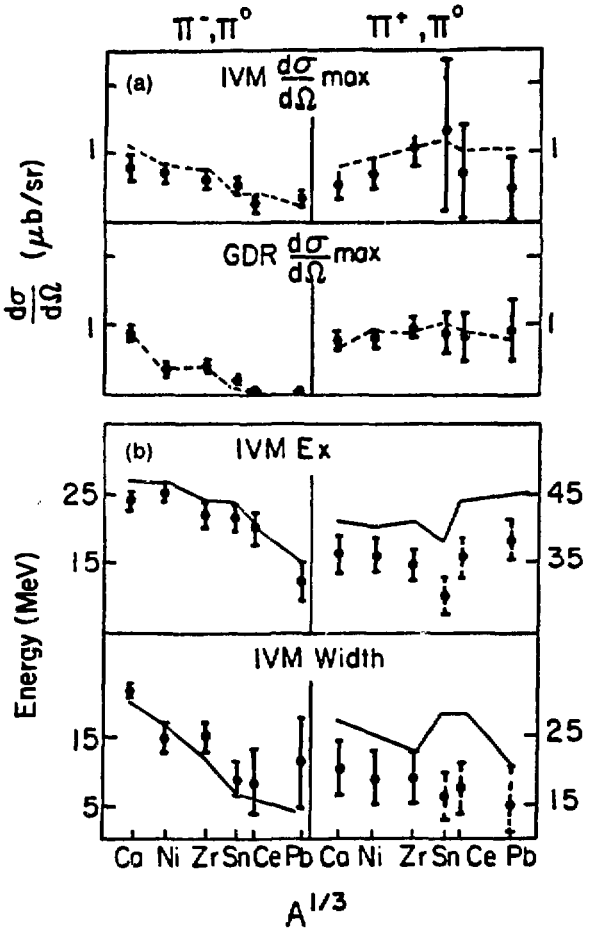

Fig. 4(a) and (b).
(a) Maximum cross section for the isovecto. monopole and giant dipole resonances in the $(\pi^{\pm},\pi^0)$ reactions, and (b) excitation energies and widths of the isovector monopole resonance in the $(\pi^{\pm},\pi^0)$ reaction. The (π^-,π^0) reaction excites the $T + 1$ component and the (π^+,π^0) excites the $T - 1$ component of each resonance.

the state, and is in qualitative agreement with RPA-DWIA theory. The IVM and GDR cross sections deviate from RPA-DWIA theory by the same ratio. The absence of the isovector quadrupole resonance poses an interesting problem.

REFERENCE

1. N. Auerbach, Proc. of the Conf. on Highly Excited States and Nuclear Structure (HESANS), 1983 Int. Symp., Orsay, France, September 5-8, 1983.

Study of the Mass and Energy Dependence of Low-Energy Pion Single Charge Exchange (Exp. 688, LEP)

(Los Alamos, Tel Aviv Univ., TRIUMF, Arizona State Univ.)

Spokemen: M. D. Cooper and M. J. Leitch (Los Alamos)

At low energies the free-nucleon charge-exchange angular distribution is strongly backward peaked with a deep forward minimum. Furthermore, phase-shift analyses predict that the 0° excitation function has a minimum around 50 MeV. These minima are the result of a near perfect cancellation of *s*- and *p*-wave π-nucleon amplitudes. If the nucleus is transparent, the nuclear single-charge-exchange (SCX) reaction to the isobaric-analog state (IAS) should show the same features. Of course, in nuclear matter these features will be distorted by effects such as absorption and Pauli blocking.

In this experiment we have measured forward-angle differential cross sections for $^{7}Li(\pi^{+},\pi^{0})$(IAS) at th 33.5-, 41.1-, 48.5-, and 58.8-MeV incident pion energy. Also, angular distributions for $^{39}K(\pi^{+},\pi^{0})$(IAS) and $^{48}Ca(\pi^{+},\pi^{0})$(IAS) were measured at 48-MeV incident pion energy. The experiment was performed at the LEP channel using the π^{0} spectrometer.[1]

Typical π^{0} spectra for incident pion beam energies of 33.5, 41.1, 48.7, and 58.8 MeV on the ^{7}Li target are shown in Fig. 1. The π^{0} energy resolution (FWHM) in these measurements was 3.0-3.5 MeV. In the analysis of the data, angle-dependent line shapes, together with kinematic constraints on the energies of states in residual nuclei and three-body thresholds, were used to separate the IAS peak from continuum charge exchange and background. The line shapes were obtained by Monte Carlo simulation of the beam, target, and spectrometer conditions.[1]

The decomposition of the spectra into background and the IAS peak for the $^{7}Li(\pi^{+},\pi^{0})$ measurement can be seen from the dashed lines in Fig. 1. The data were fitted by the maximum-likelihood method described in Ref. 2. The statistical and instrumental error in the extraction of the IAS area was 20-30%; the error caused by the unfolding of the IAS peak was typically 50% of the statistical error. The normalization procedure is described in detail in Ref. 3.

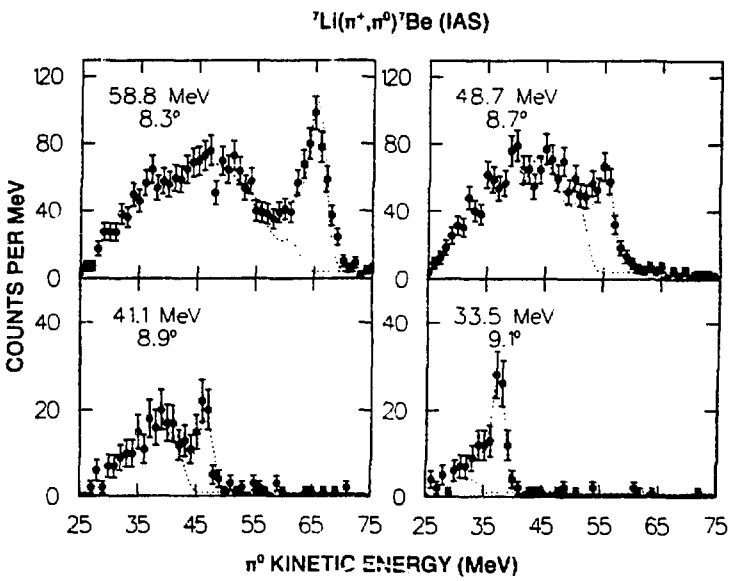

Fig. 1.
Measured π^{0} spectra for the $^{7}Li(\pi^{+},\pi^{0})$ (IAS) reaction at 33.5-, 41.1-, 48.7-, and 58.8-MeV incident pion energy. The dashed curves show the fits to the IAS and to the second excited state.

In Fig. 2 we show the measured cross sections for ^{7}Li, ^{39}K, and ^{48}Ca taken near 50-MeV incident pion beam energy, and for comparison we also include the ^{15}N(π^{+},π^{0}) (IAS) data of Cooper et al.[3] taken at 48-MeV pion energy. These data show that as we increase nuclear size, the shape of the angular distribution continues to reflect the forward-angle minimum and backward-angle peaking nature of the free-nucleon charge-exchange cross section. Also shown in Fig. 2 is the prediction of the PIESDEX code* for SCX on ^{15}N at 48 MeV. In this calculation, second-order terms representing isovector true pion absorption and the Lorentz-Lorenz effect are included in the optical potential; optical-model calculations without second-order terms are unable to reproduce the deep minimum at 0° seen for ^{15}N (Ref. 3).

*E. R. Siciliano and M. B. Johnson, private communication, 1983.

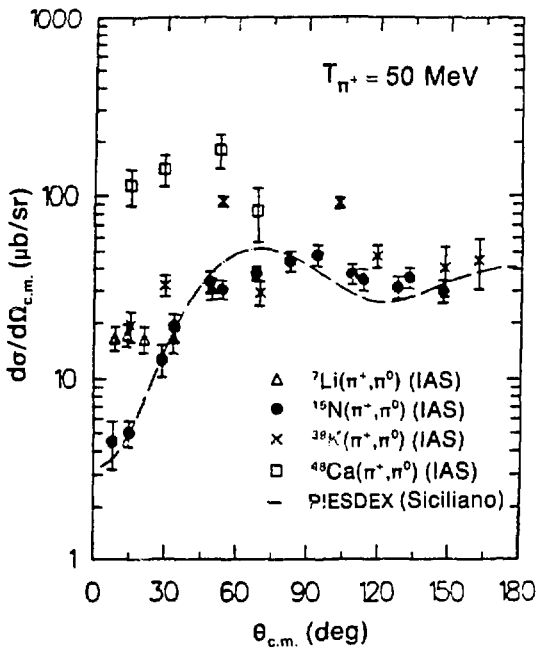

Fig. 2.
Angular distributions for the ^{7}Li(π^{+},π^{0}) (IAS), ^{15}N(π^{+},π^{0}) (IAS), ^{39}K(π^{+},π^{0}) (IAS), and ^{48}Ca(π^{+},π^{0}) (IAS) at incident pion energy near 50 MeV. The solid curve is an optical-model calculation that includes the second-order isovector terms described in the text.

For ^{7}Li data, the 0° cross sections were extrapolated by fitting the angular distributions with $A + B\theta^{2}$ functional form. This is based on expansion of angular distribution at small angles in terms of the Legendre polynomials. The measured 0° excitation function for ^{7}Li is shown in Fig. 3. The error bars are the combined error from the extrapolation to 0°, the uncertainty in the normalization, and the statistical fluctuations. The data points at 70 and 98 MeV were taken previously with the π^{0} spectrometer. To estimate the location of the minimum, we fit the four data points with a parabola (Fig. 3). The minimum of the parabola is at 42.3 ± 1 MeV. It is interesting to note that the minimum in ^{7}Li data obtained in this work is different by 3-8 MeV from predictions of different phase shifts for the minimum in a free πN excitation function. For comparison we show only the prediction of Rowe et al.[4] in Fig. 3.

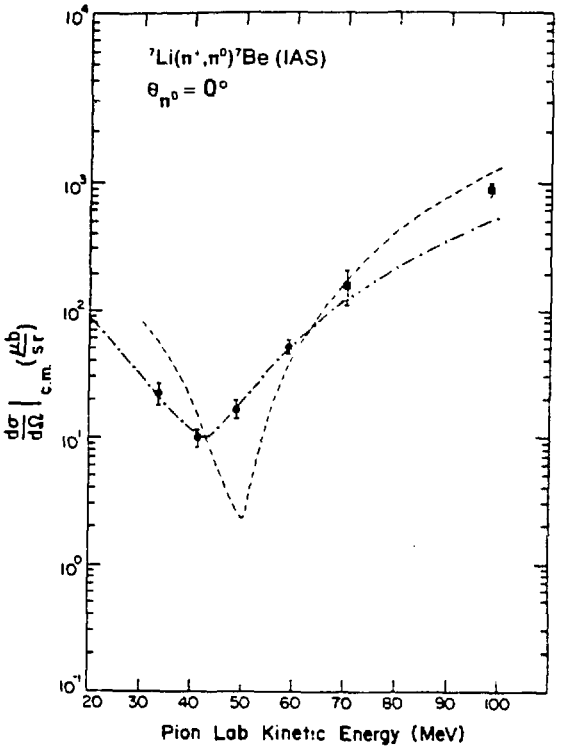

Fig. 3.
The ^{7}Li(π^{+},π^{0}) (IAS) excitation function. The dot-dashed curve is a least squares fit to the data. The dashed curve represents the free πN cross sections (Ref. 4).

The differences in forward-angle behavior among ^{7}Li, ^{15}N, ^{39}K, and ^{48}Ca indicate that π-nucleus charge exchange is sensitive to the medium effects. These medium effects cause changes in the delicate cancellation between π-nucleon s- and p-wave amplitudes that result in a shift in position of the minimum of the excitation function with increasing nuclear size (A), or alternatively in a change in the depth of the 0° minimum for different nuclei at a particular energy.

Presently there are very few low-energy SCX data, with the exception of several angular distributions near 50 MeV and one excitation function. To understand the effect of the second-order terms and establish the systematics of the A dependence and energy dependence of forward-angle SCX at low energies, a larger body of data is needed. Future experiments using the π^0 spectrometer are planned to study the mass and energy dependence of low-energy SCX.

REFERENCES

1. H. W. Baer et al., Nucl. Instrum. Methods **180**, 495 (1981).

2. M. D. Cooper et al., Phys. Rev. C 25, 438 (1982).

3. M. D. Cooper et al., "Angular Distribution for ^{15}N(π^+,π^0)^{15}O (g.s.) at T_π = 48 MeV," submitted to Phys. Rev. Lett

4. G. Rowe et al., Phys. Rev. C 18, 546 (1987).

Muon Decay Spectrum
(Exp. 455, P³-West)

Los Alamos; Univ. of Chicago; National Research Council, Canada)

Spokesmen: H. L. Anderson and W. Wayne Kinnison (Los Alamos)

The measurement of the positron spectrum of muon decay is one of the most fundamental experiments in particle physics because it is the best way to determine the attributes and magnitudes of the weak interaction. We are making a new measurement to improve the existing accuracy by a factor of 5. The spectrum can be calculated precisely from the accepted theory, based on a simple symmetry proposed by Feynman and Gell-Mann, in which the neutrinos are massless, with two rather than four components. The theory also is characterized by the fact that the only interactions entering are vector and axial-vector interactions, of equal magnitude and opposite sign, referred to as $V-A$. In this theory the currents are purely left-handed. All searches to date to find right-handed currents or massive neutrinos have been unsuccessful. (We discount the Russian experiment, which has reported a finite neutrino mass, because of doubts about the correctness of the result.)

The weak-interaction theory is beautiful in its simplicity, but we do not know whether that beauty is more than skin deep; that is the purpose of this experiment. We plan to measure the spectrum with high resolution and statistics 100 fold greater than previously obtained. We will compare the spectrum with its well-known theoretical value.

As part of the comparison of the spectrum to theory, the experiment first will attempt to improve the high-energy shape parameter ρ to a new level of precision, nearly ±0.0003. This will represent an improvement in the existing limits on this parameter by about a factor of 10. Beg et al.[1] have shown that such an improvement in ρ can place a constraint on possible left-right weak-interaction theories. In such theories, there are two charged intermediate-vector bosons, W_L and W_R, that couple to left- and right-handed currents, respectively. These bosons are not necessarily themselves eigenstates of the mass matrix. Instead, the mass eigenstates W_1 and W_2 may be expressed as Cabibbo-like mixtures of W_L and W_R,

$$W_1 = W_L \cos\zeta - W_R \sin\zeta \quad ,$$

$$W_2 = W_L \sin\zeta + W_R \cos\zeta \quad .$$

Thus, it is of interest to place limits on $\kappa \equiv [M(W_2)/M(W_1)]^2$, the mass-squared ratio, and ζ, the mixing angle. An improved measurement of ρ can reduce the allowable range of ζ almost independently of the value of κ. This is shown in Fig. 1, where the current limits on κ

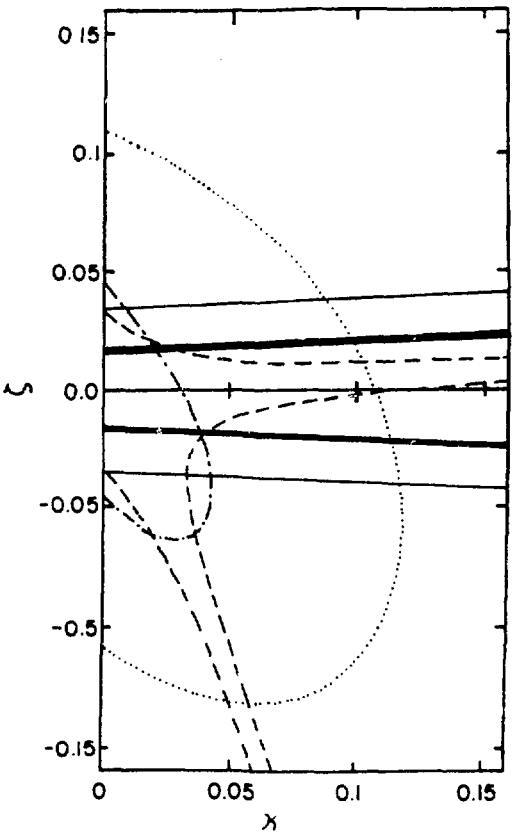

Fig. 1.
Experimental 90% confidence-limit contours on the mass-squared ratio, $\kappa \equiv [M(W_2)/M(W_1)]^2$, and mixing angle ζ for possible left-right symmetric weak-interaction theories. The two bold solid lines represent the constraint that would result from this experiment's improved 0.3-per-mil measurement of ρ. The current limits are from the recently improved measurement of the end-point spectrum ζP_μ (dot-dashed curve, Ref. 2); the previous measurement of ζP_μ (dotted curve, Ref. 3); the present value for the ρ parameter (solid curve, Ref. 4); and a comparison between Fermi and Gamow-Teller β polarization (dashed curve, Ref. 5). In all cases, the allowed regions are those that include the origin, $\zeta = \kappa = 0$.

and ζ are given.* As seen in the figure, these limits currently come predominantly from the recently improved measurement of ξ by Mark Strovink's group[2] at TRIUMF. The figure also shows how the limit on ζ will be improved by the proposed 0.3-per-mil measurement of ρ, which is the immediate goal of Exp. 455. Figure 2 shows a schematic view of the Exp. 455 apparatus. The major component of the detector is a time-projection chamber (TPC), which has a sensitive volume 52 cm in length and 122 cm in diameter. The TPC magnetic field is provided by an iron-enclosed solenoid that supplies a maximum field of 0.7 T, which is uniform to better than 0.6% over the entire TPC sensitive volume. Such a magnetic field will allow a precision measurement of the positron momentum absolutely.

*References 2-5. The dotted and solid curves in Fig. 1 represent world-average values, with primary contributions from Refs. 3 and 4, respectively.

The muons for the experiment, which are from a surface muon beam in P^3-West, are brought to rest in the TPC gas at the center of the chamber. An event trigger requires that a muon enter the TPC as determined by the 0.25-mm (10-mil) muon transmission scintillator at the TPC entrance during the LAMPF beam gate, and that this muon stop in the central 10 cm of the TPC gas, as determined by signals from the TPC sense wires. When a muon enters the chamber, the deflector/separator is used to turn off the beam. In this manner, the experiment looks at events that have one, and only one, muon in the chamber. The momentum of the decay positron is then measured by analysis of its helical track in the known magnetic field.

Figure 3 shows the three plane projections and a three-dimensional view of a typical event. In the figure the incoming muon is indicated by coordinates drawn with the letter *M*, and the helical trajectory of the decay positron is indicated by coordinates drawn with a small

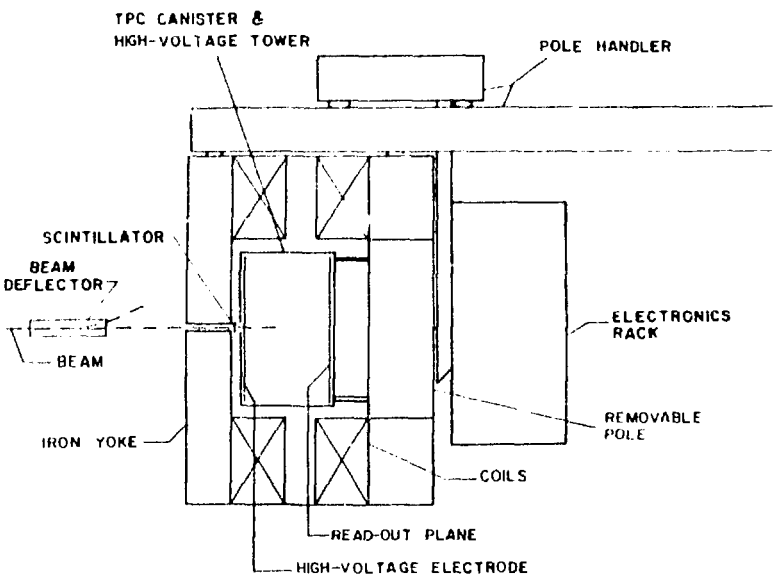

Fig. 2.

A pictorial view of the LAMPF Exp. 455 experimental apparatus. The detector consists of a 122-cm-diam by 52-cm-long TPC inside an iron-enclosed solenoid. This TPC drift region, which is filled with an 80-20 Ar-CH_4 gas mixture, is bounded on one end by a high-voltage electrode and on the other end by the read-out plane. The read-out plane consists of 21 modules, each of which has 15 sense wires spaced on 1-cm centers. Under each sense wire there are seventeen 0.8- by 0.8-cm pads spaced on 1-cm centers for determination of coordinate positions along the sense wires. The muons enter the TPC through a hole in the magnet pole after passing through a deflector/separator that is used to turn off the surface muon beam when a muon enters the TPC, as determined by a coincidence signal from the phototubes attached to the 0.25-mm- (10-mil-) thick scintillator covering the TPC entrance hole.

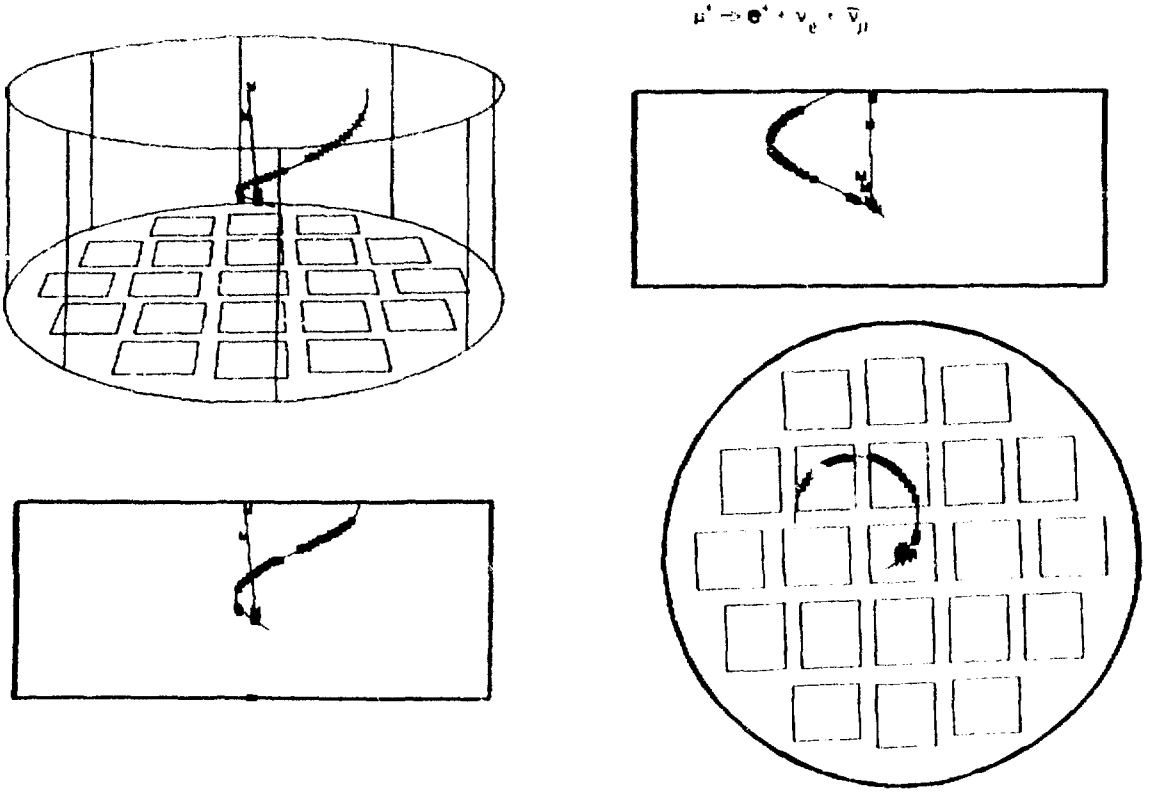

Fig. 3.

Three plane projections and a three-dimensional view of a typical muon decay event, as measured in the TPC apparatus. The entering muon coordinates, indicated by the letter *M*, are fitted to a straight line, as shown in three of the views. (No attempt is made to fit them to their actual helical track.) The decay positron coordinates, which are fitted with a helix, are indicated by square boxes.

box. To obtain the necessary experimental precision, about 10^8 such events will be analyzed. The experimental apparatus is designed to collect events at a rate of 1 per LAMPF macropulse (usually 120 per second).

In 1983, Exp. 455 had two data-collection runs. During the first run, the high-speed data-acquisition electronics was not in place and the resulting event rate was approximately 1 per second. About 4×10^5 events were collected during the 4-week running period and these data were analyzed to study the TPC resolutions and acceptance. It was found that the coordinate resolution along the drift direction was about 900 μm, more than a factor of 2 better than the proposed value of 2 mm, and that the resolution along the wire direction, uncorrected for known systematic errors, was about 600 μm. The resulting positron momentum resolution was 0.6% rms averaged over the Michel spectrum, which is only slightly worse than the proposed resolution of 0.5%. However, the combination of detector acceptance and software cuts resulted in only about 25% of all triggers being analyzed. Some of the rejected events will be recoverable by more sophisticated software algorithms, but mostly the acceptance is limited because of the length of detector. Ways of getting around this problem are currently under investigation.

The second data-collection run during 1983, of 1-week duration, was devoted to the development of the high-speed data-acquisition electronics. This new electronics, which consists primarily of three asynchronous, bit-slice computers in the read-out system, was installed and successfully tested during the run. It was found that a maximum event rate of about 50 per second could be

handled. This was somewhat below the 120-per-second goal, but the test run was limited by diagnostic codes that were in the bit-slice computers.

In the coming year, two large data-collection periods are planned and considerably more time will be spent optimizing the detector parameters, such as drift electric field voltage, gas mixtures, and magnetic field settings. We expect to achieve, or in some cases surpass, the design goals for the detector.

REFERENCES

1. M. A. B. Beg, R. V. Budny, R. Mohapatra, and A. Sirlin, Phys. Rev. Lett. 38, 1252 (1977).

2. J. Carr, G. Gidal, B. Gobbi, A. Jodidio, C. J. Oram, K. A. Shinsky, H. M. Steiner, D. P. Stoker, M. Strovink, and R. D. Tripp, Phys. Rev. Lett. 51, 627 (1983).

3. V. V. Akhmanov, I. I. Gurevick, Yu. P. Dobretsov, L. A. Makarina, A. P. Mishakova, B. A. Nikolskii, B. V. Sokolov, L. V. Surkova, and V. D. Shestakov, Yad. Fiz. 6, 316 (1977).

4. J. Peoples, Nevis Cyclotron report 147, 1966 (unpublished).

5. J. Van Klinken, K. Stam, W. Z. Venema, V. A. Wickers, and D. Atkinson, Phys. Rev. Lett. 50, 97 (1983).

Tensor Polarization in πd Scattering (Exp. 673, P^3)

(Argonne National Lab., Indiana Univ. Cyclotron Facility, Los Alamos, MIT)

Spokesman: R. J. Holt (Argonne)

Participants: W. S. Freeman, D. F. Geesaman, J. R. Specht, E. Ungricht, B. Zeidman, E. J. Stephenson, J. D. Moses, M. Farkhondeh, S. Gilad, and R. P. Redwine

The prospect of measuring the quadrupole form factor or D-state probability of the deuteron by observing the tensor polarization t_{20} in πd scattering led to an early interest in measuring t_{20} at backward angles.[1] During the past few years this interest has been spurred by questions regarding true pion absorption in nuclei and the possible existence of dibaryon resonance in the πd system.

In this experiment the angular dependence of t_{20}^{lab} for recoiling deuterons in πd elastic scattering was measured as a function of incident pion energy in the range 134-256 MeV. No evidence was found for rapid energy or angular dependences in t_{20}, contradicting recent publications[2] that claim the observation of dibaryon resonances in t_{20}. Our results agree most favorably with theoretical calculations in which the P_{11} πN amplitude has been removed altogether. This suggests that pion absorption has a small effect on t_{20} in the elastic channel.

The experimental apparatus used to measure t_{20} is illustrated in Fig. 1. Pions from the P^3-East channel at LAMPF were focused onto a liquid-deuterium target of 5 mm thickness. Scattered pions were detected in an array of three plastic scintillators, in coincidence with the

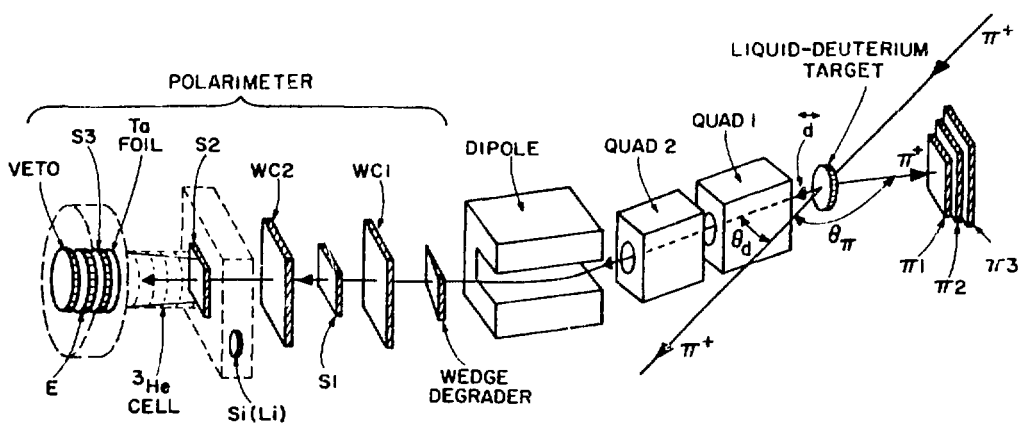

Fig. 1.
Apparatus to measure t_{20} in πd scattering (not to scale).

recoil deuterons that were focused onto the polarimeter with a QQD system.

The key feature for performing measurements of t_{20} in $\vec{d}$ scattering is the development of a high-efficiency deuteron tensor polarimeter. The polarimeter employs the ^{3}He$(d,p)^4$He reaction, which has a large cross section and tensor-analyzing power T_{20} at forward angles, and a large Q value, 18.4 MeV.

The polarimeter was calibrated in a separate experiment at the Berkeley 88-in cyclotron. The calibration of the polarimeter was determined as a function of incident deuteron energies, position, and angle of incidence on the polarimeter. The calibration was checked 2 years after the primary calibration by measuring the efficiency ϵ_0 again at the Los Alamos three-stage tandem Van de Graaff. We conclude from this test that the measurement of the efficiency ϵ_0 is reproducible to ~2%. The same polarimeter was used in previous measurements of the tensor polarization in πd scattering at 142 MeV[3] and in an ed scattering experiment.[4]

As shown in Fig. 2, our excitation function at $\theta^*_{c.m.} \approx 144°$ differs from recent data of Grüebler et al.[2] In that experiment the deuteron beam size, when the effects of second-order beam optics are taken into account, is comparable with the size of the polarimeter aperture (30 mm). This problem is not encountered in the present work because the deuteron beam size is 20 mm (FWHM) but the polarimeter aperture is 89 mm. Clearly, there are no dramatic energy or angular dependences

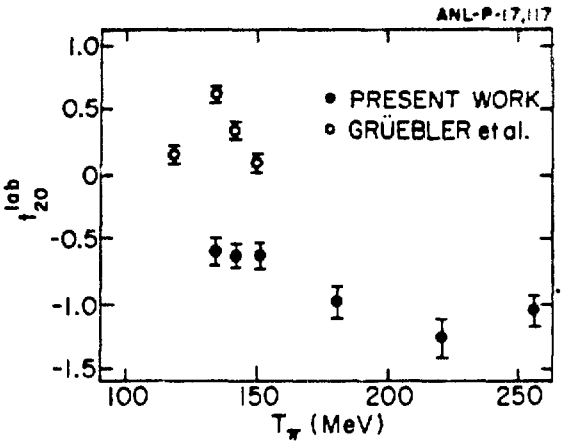

Fig. 2.
Excitation function at $\theta_d = 18°$ (solid dots) compared with the results of Grüebler et al. (Ref. 2) at $\theta_d = 15°$ (open circles). The angular acceptances are ±1.5 and ±2.5°, respectively.

observed in our work, so there is no apparent evidence for dibaryon-resonance effects.

Angular distributions at pion energies of 142, 180, 220, and 256 MeV are compared with recent theoretical predictions in Fig. 3. Presently, the theoretical calculations of the πd system have achieved a high level of sophistication. These calculations are typically three-body in nature and include both the absorptive channel

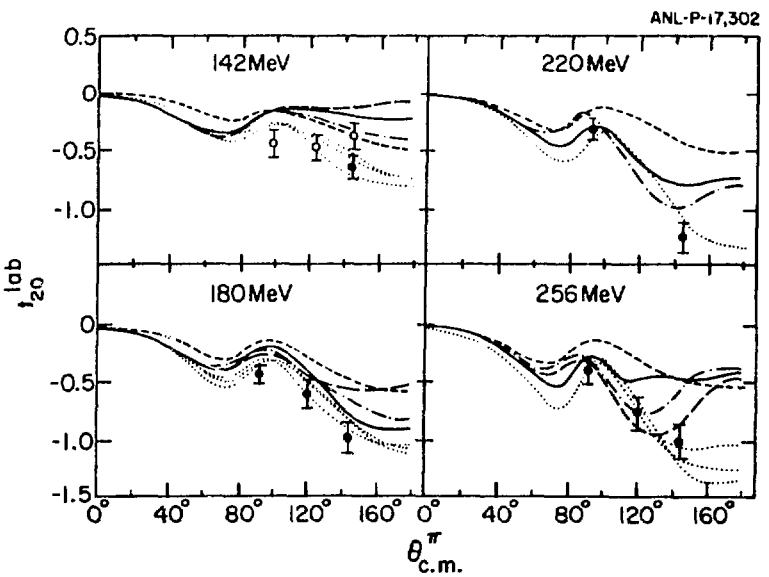

Fig. 3.
Angular distributions at pion energies of 142, 180, 220, and 256 MeV (open circles are from the previous experiment) (Ref. 3). The calculations are solid line, from Blankleider and Aman (Ref. 6); long-dashed line, from Betz and Lee (Ref. 7); short-dashed line, from Fayard, Lamot, and Mizutani (Ref. 8); and dot-dashed line, from Rinat and Starkand (Ref. 9), all including true pion absorption. The dotted lines are results without P_{11} amplitude, that is, without pion absorption.

$\pi d \rightarrow NN$ and pion scattering. All calculations without a P_{11} πN amplitude give very similar results (dotted curves in Fig. 3) and are remarkably close to the present experimental data.

Omitting the P_{11} channel has the effect of both removing pion absorption and P_{11} πN rescattering from the calculation. Although omitting the P_{11} channel from the calculation is a somewhat drastic measure, especially since absorption is removed, it may not be as unreasonable as it appears. Afnan and Blankleider[5] have shown that the dominant absorptive effects in $\pi d \rightarrow \pi d$ and $\pi d \rightarrow pp$ occur in different spin-isospin channels. Therefore, it seems possible that the absorption amplitudes can be adjusted to improve t_{20} without worsening the results for other observables. Since it appears that absorption affects the elastic amplitudes far less than previously predicted, the chance for constraining the deuteron quadrupole form factor has improved, but more theoretical and experimental work must be done.

We are grateful to S. J. St. Lorant for the loan of the ^{3}He gas and to N. Jarmie and R. Martinez for assistance during the calibration at the Los Alamos tandem. In addition, we thank K. Stephenson, J. S. Frank, and M. J. Leitch for their substantial part in developing the new polarimeter.

This research was supported by the USDOE and the National Science Foundation.

REFERENCES

1. W. R. Gibbs, Phys. Rev. C 3, 1127 (1971).

2. W. Gruebler, J. Ulbricht, V. König, P. A. Schmelzbach, K. Elsener, C. Schweizer, M. Merdzan, and A. Chisholm, Phys. Rev. Lett. 49, 444 (1982); and 5th Int. Symp. on High Energy Spin Particles, Brookhaven, New York (1982).

3. R. J. Holt, J. R. Specht, K. Stephenson, B. Zeidman, J. S. Frank, M. J. Leitch, J. D. Moses, F. J. Stephenson, and R. M. Laszewski, Phys. Rev. Lett. 47, 472 (1981).

4. M. E. Schulze, D. Beck, M. Farkhondeh, S. Gilad, S. Kowalski, R. P. Redwine, W. Turchinetz, R. J. Holt, J. R. Specht, K. Stephenson, B. Zeidman, R. M. Laszewski, F. J. Stephenson, J. D. Moses, M. J. Leitch, R. Goloskie, and D. P. Saylor, Tenth Int. Conf. on Few Body Problems in Physics, Karlsruhe, Germany, 1983.

5. I. R. Afnan and B. Blankleider, Phys. Lett. 93B, 367 (1980).

6. B. Blankleider and I. R. Afnan, Phys. Rev. C 24, 1572 (1981).

7. M. Betz and T. S. H. Lee, Phys. Rev. C 23, 375 (1981).

8. C. Fayard, G. H. Lamot, and T. Mizutani, Phys. Rev. Lett. 45, 524 (1980).

9. A. S. Rinat and Y. Starkand, Nucl. Phys. A 397, 381 (1983).

Pion-Induced Pion Production on the Deuteron (Exp. 783, P^3-West)

(Los Alamos, Univ. of Wyoming, Colorado College, MIT, Tel Aviv Univ.)

Participants: E. Piasetzky, P. A. M. Gram, D. W. MacArthur, G. A. Rebka, Jr., C. A. Bordner, S. Høibråten, E. R. Kinney, J. L. Matthews, S. A. Wood, D. Ashery, and J. Lichtenstadt

One way to characterize the study of pion-nucleus reaction mechanisms is to say that we are trying to find out how many nucleons it takes to scatter a pion. For example, pion quasi-free scattering appears to be almost entirely a single-scattering process, but even in this reaction the single scattering peak in the momentum spectrum is thought to exist only because multiply scattered pions tend to be absorbed. Thus, information about pion multiple scattering is difficult to extract from the rather extensive measurements of quasi-free scattering that have been performed.

Recent editions of *Progress at LAMPF*[1,2] have presented our observations of inclusive pion double charge exchange. In this reaction a pion must interact with at least two nucleons and then escape from the nucleus. Comparisons of the momentum spectra of double charge exchange with the low energy tail of quasi-free scattering are beginning to shed light on the contribution of multiple scattering to pion reactions.[3]

Another reaction in which the participation of more than one nucleon might be seen is in pion-induced pion production. Because the intermediate states that may contribute to $(\pi,2\pi)$ reactions are different from those that contribute to either quasi-free scattering or to double charge exchange, the balance between single and multiple scattering may be altered in an observable way.

Pion-induced pion production on the proton has been studied* systematically to obtain $\pi\pi$-scattering parameters, but there is virtually no information about this process in nuclei. The simplest system in which multiple-nucleon processes may occur is the deuteron. The reactions

*A bibliography of previous work is given in Ref. 4.

$\pi^- d \rightarrow \pi^+ \pi^- nn$

and

$\pi^+ d \rightarrow \pi^+ \pi^+ pp$

can be studied and compared with $\pi^- p \rightarrow \pi^+ \pi^- n$ to search for two-nucleon mechanisms.

One two-nucleon mechanism for $(\pi,2\pi)$ was proposed by Brown et al.[5] who predicted, based on the $SU(4)$ quark model, the existence of a strong $\Delta N \rightarrow \Delta\Delta$ transition in systems of two or more nucleons. Subsequent decay of the two Δ's contributes to the $(\pi,2\pi)$ reaction. The $\pi^- nn$ or the $\pi^+ pp$ component of the final state has $T = 2$. If the NN system is formed at low momentum, it is likely to be in a $^1S_0$ state with $T = 1$. The pion may then be attracted to it through the P_{11} interaction to form a state that may be considered an off shell ΔN.

In heavier nuclei these $T = 2$, ΔN states can be doorways to the formation of $T = 2$, $\Delta\Delta$ states. Since a ΔN state cannot decay by either the strong or the electromagnetic interaction, it may appear in the reactions studied here as a narrow resonance or even as a bound state. This subject was recently discussed by Garcilazo,[6] who showed that with certain parameterizations of the πN and NN interactions, the calculations predict the existence of a bound state. However, the uncertainties in our knowledge of these parameterizations, and in particular of the πN effective range, leave ample room to doubt its existence.

We report an experimental study of the $\pi^\pm d \rightarrow \pi^+ \pi^\pm NN$ reactions that was performed at the high energy pion channel (P^3). The doubly differential cross section $d^2\sigma/d\Omega dT$ for the production of pions with charge opposite to that of the incident beam was measured at uniformly distributed locations in baryocentric $\bar{T}$-cos $\bar{\theta}$ phase space. Double charge exchange is impossible on the deuteron, so this method unambiguously identifies pion production. Measurements were made with π^+ and π^- beams at an incident kinetic energy of 256 MeV and with a π^- beam at 331 MeV. The momentum spread of the beams was $\Delta p/p = 4\%$ FWHM and their intensities were approximately 2×10^8 π^-/s and 10^9 π^+/s.

Outgoing particles were detected by a 180° double-focusing magnetic spectrometer[3,7] (the "Little Yellow Spectrometer") with a solid angle of 15 msr and momentum acceptance of 9.5%. The detector system consisted of a multiwire proportional chamber between the two dipole magnets of the spectrometer, a pair of multiwire proportional chambers immediately behind the focal plane, a 1.6-mm-thick plastic scintillation detector, a fluorocarbon (FC 88) threshold Cerenkov counter, and last, an Aerogel ($n = 1.055$) Cerenkov counter.

A quadruple coincidence among signals from the three wire chamber delay lines and the scintillator defined an acceptable event. The last two wire chambers established the trajectory of a particle as it crossed the focal plane. For events that corresponded to an allowable trajectory, pulse heights from the scintillator and Cerenkov detectors and the time of flight through the second bending magnet discriminated against electrons or, when set for positive charge, positrons, protons, and other light nuclei. Corrections for pions decaying in the relatively short 3.5-m flight path and for muons that were recorded as good events were calculated with the Monte Carlo simulation DECAY TURTLE.[3]

A cylindrical target flask 2.5 cm in diameter, which was concentrically mounted on the axis of rotation of the spectrometer, contained liquid deuterium (99.83% deuterium) for observing pion production or liquid hydrogen for calibration. Background from the 50 μm Mylar walls was observed with the flask empty. The incident pion flux was measured with an ionization chamber as well as with a scattering monitor downstream from the spectrometer.

The measured pion-production cross sections were normalized to πp elastic scattering. At each incident energy, relative πp elastic cross sections were measured at several angles and the angular distribution was normalized to fit the "known cross sections" with a scale factor that calibrated the system as a whole. Below 300 MeV, known cross sections were derived from the phase-shift analysis of Carter, Bugg, and Carter[8] using the routine SCATPI.[9] Above this energy, they were interpolated directly from the measurements.[10] The interpolation procedure is described in detail in Ref. 4 and is the same procedure used to normalize the $\pi^- p \rightarrow \pi^+ \pi^- n$ cross sections of Ref. 1.

Figure 1 shows the doubly differential cross sections for the $\pi^- d \rightarrow \pi^+ \pi^- nn$ reaction at 256 and 331 MeV. At 256 MeV the measured cross sections for the $\pi^+ d \rightarrow \pi^+ \pi^+ pp$ reaction are equal to those for the $\pi^- d \rightarrow \pi^+ \pi^- nn$ reaction within the experimental uncertainties. To this accuracy the Coulomb force appears to have no influence on this reaction. The errors shown in the figure represent the combination of statistical uncertainty and those systematic uncertainties that depend on the outgoing momentum. Overall normalization is uncertain by a further 4%.

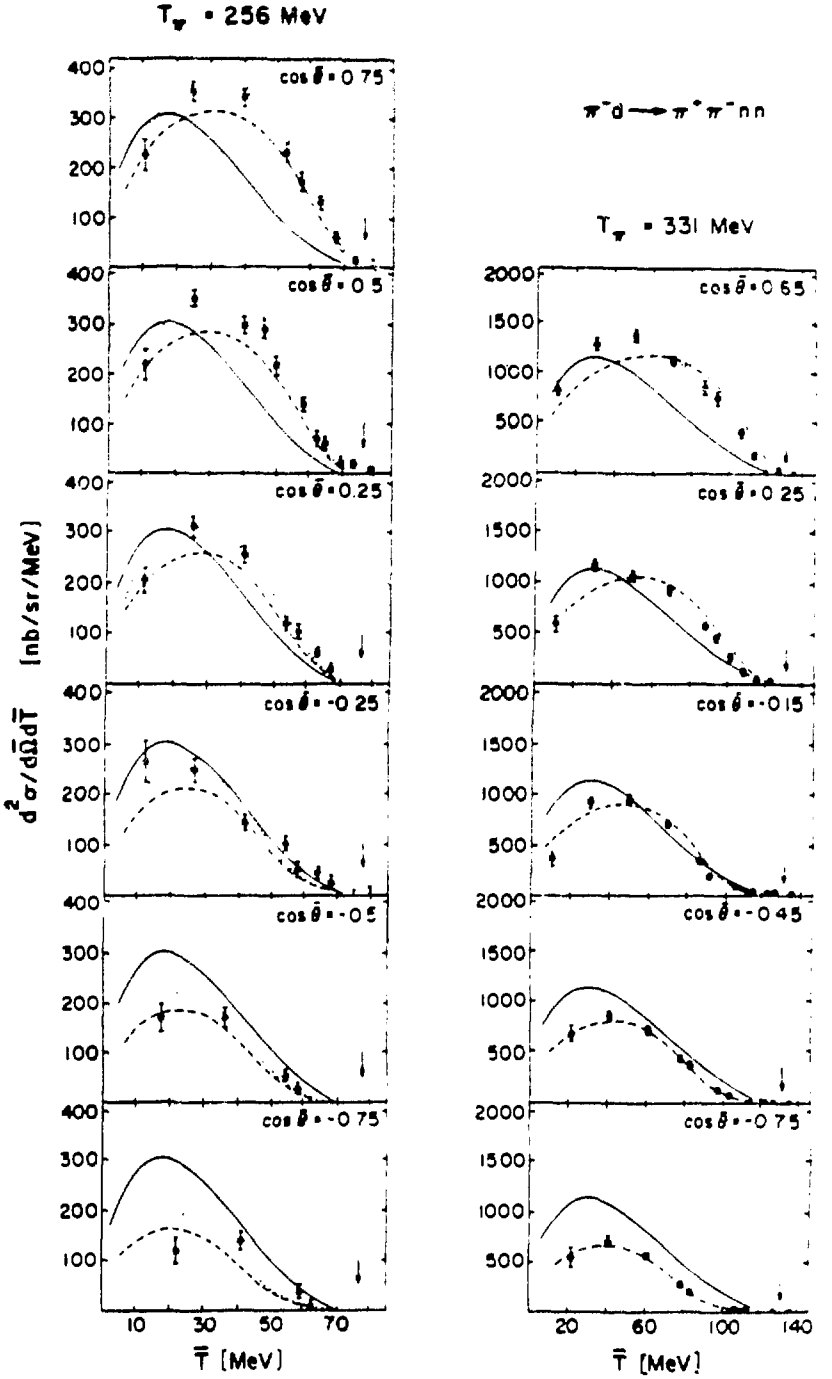

Fig. 1.

Doubly differential cross section for the $\pi^- d \rightarrow \pi^+ \pi^- nn$ reaction at 256 and 331 MeV. $\bar{T}$ and $\bar{\theta}$ are the outgoing π^+ kinetic energy and angle in the center-of-mass system. The arrows mark the energy corresponding to the two-body $\pi(\pi NN)$ production, with zero binding energy for the πNN system. The solid curves represent four-body phase space normalized to the data. The dashed and dotted lines are quasi-free calculations in plane-wave Born approximation (see text).

The solid curves in Fig. 1 represent the distribution of events in four-body phase space, normalized so that its integral over energy and angle will equal the integrated reaction cross section determined from the data. The dashed curves are the predictions of a simple calculation,[11] in plane-wave Born approximation, of quasi-free pion production on the one-nucleon using phenomenological on-shell amplitudes deduced from the $\pi p \rightarrow \pi^+\pi^- n$ data.[4]

The quasi-free calculation is in good agreement with the general features of the data, although some discrepancies do exist. At 256 MeV the quasi-free calculation reproduces the shape of the spectra very well, but the absolute value of the cross section is 20% below the measured result. The dotted curve in Fig. 1 is the quasi-free calculation normalized by the ratio of the measured and calculated integrated cross sections. At 331 MeV the integrated reaction cross section obtained from the quasi-free calculation is in agreement with that measured, within the experimental uncertainty, but a slight discrepancy exists between the measured and calculated shape of the spectra at forward angles. These effects could be attributed either to rescattering of the pion by the second nucleon or to the formation of πNN systems.

In pion production on protons, the average squared modulus of the matrix element[4,7] increases by a factor of 2 at forward angles and low outgoing pion energies, presumably because of the onset of significant contribution from a $\pi\Lambda$ intermediate state. Indeed, in an isobar-model analysis of $\pi p \rightarrow \pi\pi n$, the P_{33} partial wave first becomes important above 300 MeV.[7] One is tempted to speculate that a two-nucleon-reaction mechanism, either the $N\Lambda \rightarrow \Lambda\Lambda$ transition or a rescattering process, would become significant where the $\pi\Lambda$-state formation is most pronounced.

The measured doubly differential cross sections were integrated over the energy and angle of the produced pion to determine an integrated reaction cross section. To estimate the contribution from the unobserved kinematic range, we assumed the form of the cross section given by the plane-wave Born approximation and assigned a 25% uncertainty to the contribution from the extrapolated region. The integrated-reaction cross sections for $\pi d \rightarrow \pi^+\pi^- nn$ are 160 ± 10 μb at 256 MeV and 1000 ± 100 μb at 331 MeV. The corresponding cross sections for $\pi p \rightarrow \pi^+\pi^- n$ are 166 ± 6 μb and 1160 ± 50 μb at 256 and 331 MeV, respectively.[4]

In October 1983 we continued these measurements at an incident energy of 450 MeV, including a measurement of $\pi^- p \rightarrow \pi^+\pi^- n$, which had not previously been done, for comparison. These data are presently being analyzed.

We intend to extend these observations to the ^{3}He nucleus in the next series of experiments, studying $\pi^+ {}^3\text{He} \rightarrow \pi^-\pi^+ ppp$. The ^{3}He nucleus differs from the deuteron by the addition of a proton, but also and more importantly because it is a much denser structure. The density of ^{3}He approaches that of normal nuclear matter, and one expects that two nucleon effects will be stronger in ^{3}He than in deuterium. The second proton in ^{3}He does not contribute to the quasi-free part of the interaction, and the proton pair cannot contribute to the two-nucleon mechanism of pion production.

As for $\pi^+ d \rightarrow \pi^-\pi^+ pp$, the quasi-free pion production is only from the neutron, and the two-nucleon mechanism can only be attributed to the np pair. To first order, the quasi-free contribution in ^{3}He is expected to be equal to that in the deuteron, whereas the two-nucleon contributions are expected to be twice as large. The advantage of and interest in obtaining a larger and clearer signal for the two-body mechanism is obvious. Even if, disappointingly, no large two-nucleon contribution is found for pion production on ^{3}He, this result itself would be critical for possible application of the $(\pi,2\pi)$ reaction to nuclear-structure studies[5] in the future and for understanding the $N\Lambda \rightarrow \Delta\Delta$ process.

REFERENCES

1. Los Alamos National Laboratory report LA-9256-PR (March 1982), p. 55.

2. Los Alamos National Laboratory report LA-9709-PR (March 1983), p. 57.

3. S. A. Wood, Ph.D. thesis, Massachusetts Institute of Technology, 1983 (unpublished).

4. C. W. Bjork et al., Phys. Rev. Lett. 44, 62 (1980).

5. G. E. Brown, H. Toki, W. Weise, and A. Wirzba, Phys. Rev. Lett. 118B, 39 (1982).

6. H. Garcilazo, Phys. Rev. C 26, 2685 (1982).

7. A. T. Oyer, Los Alamos National Laboratory report LA-6599-T (1976); J. B. Walter, Los Alamos National Laboratory report LA-8377-T (1979); and D. Manley, Los Alamos National Laboratory report LA-9101-T (1981).

8. J. R. Carter, D. V. Bugg, and A. A. Carter, Nucl. Phys. B 58, 378 (1973).

9. J. B. Walter and G. A. Rebka, Jr., Los Alamos National Laboratory report LA-7731-MS (1979).

10. P. J. Bussey et al., Nucl. Phys. B 58, 363 (1973); H. R. Rugge and O. T. Vik, Phys. Rev. 129, 2300 (1963); and Philip M. Ogden et al., Phys. Rev. 137, B1115 (1965).

11. L.-C. Liu, R. S. Bhalerao, and E. Piasetzky, contribution to the Symp. on Delta-Nucleus Dynamics, Argonne, Illinois, 1983.

The Crystal Box Experiments (Exps. 400/445 and 726, SMC)

'Los Alamos, Univ. of Chicago, Stanford Univ., Temple Univ.)

Spokesmen: (Exps. 400/445) — C. M. Hoffman, J. D. Bowman, and H. S. Matis (Los Alamos); (Exp. 726) — V. L. Highland (Temple Univ.) and G. H. Sanders (Los Alamos)

Discussions of these experiments have been presented in the past several Progress Reports. The aim of these experiments is to search with unprecedented sensitivity for several rare decay modes of the muon and the pion. Experiments 400/445 are searching for the muon-number-violating decays $\mu^+ \rightarrow e^+e^+e^-$, $\mu^+ \rightarrow e^+\gamma$, and $\mu^+ \rightarrow e^+\gamma\gamma$, with branching ratios somewhat smaller than 10^{-11}. Experiment 726 will search for the charge-conjugation-violating decay $\pi^0 \rightarrow 3\gamma$ with a sensitivity to a branching ratio as low as 10^{-9}.

Experiments 400/445

A schematic of the apparatus is shown in Fig. 1. The detector consists of a modular array of 396 NaI(Tl) crystals that surround an array of plastic scintillation counters and a high-resolution drift chamber. Approximately 5×10^5 μ^+/s are stopped in a thin target located in the center of the apparatus. The major source of backgrounds is the random coincidence of e^+'s and γ's from the uncorrelated decays of several muons. These backgrounds are eliminated by requiring that the detected particles be in time coincidence and satisfy the conservation of energy and momentum. For the $\mu^+ \rightarrow e^+e^+e^-$ mode, there is the additional constraint that the three tracks must emerge from a common vertex. To reject the backgrounds to an adequate level, excellent resolutions in timing, energy, and position are required.

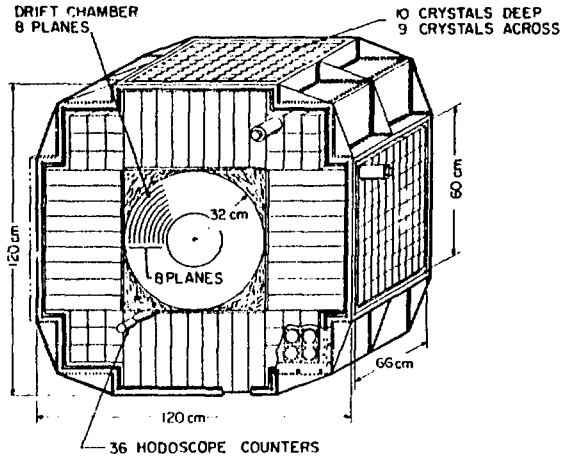

Fig. 1.
Schematic of the Crystal Box detector.

A short tuneup run was taken in January 1983, with two of the four NaI(Tl) quadrants instrumented. The purpose of this run was to measure trigger rates and check all parts of the system. Several problems were uncovered. The $\mu^+ \rightarrow e^+e^+e^-$ trigger rate was unacceptably high because of particles that trigger the scintillation counters but that deposit little or no energy in the sodium iodide; some of these are from low-energy particles present in the electromagnetic showers in the crystals. After analyzing data tapes, it was determined that the best way to eliminate these triggers is to require at least one discriminator from the crystals behind the scintillator fire. The electronics needed to implement this logic was constructed in the spring and summer and installed this fall; it performed according to expectations. The photon definition in the tune-up run also was found to be inadequate (a photon is defined as a quadrant with a sodium iodide discriminator firing but no scintillator firing). The major improvement needed here was the installation of separate leading-edge discriminators for the scintillators to provide the photon veto. Other changes involved minor improvements in how the corner crystals were apportioned between the two quadrants straddling the corner, and the removal of the most upstream and downstream rows from the photon definition.

The final major problem uncovered was the need for a more sophisticated system to detect pileup in the NaI(Tl). The system we had designed was not efficient enough at detecting low levels of pileup and also rejected many events that were, in fact, not piled up. A compact CAMAC-based sample-and-hold system was purchased and installed to solve this problem. It also was necessary to modify the circuits that clip the NaI(Tl) output pulses and to use higher quality delay lines to shorten the length of the pulse at the circuit that measures the pulse area (for the energy determination). All these improvements and modifications were installed by the fall of 1983.

As discussed in the last Progress Report, the method used to mount photomultiplier tubes on the first two quadrants led to several vacuum leaks in the hermetically sealed container housing the crystals. An alternative mounting scheme that subjects the container to much

smaller stresses was designed and has been used on all four quadrants. In the 5 months since this was done, no vacuum leaks have occurred and we believe the problem is solved.

During several test runs in the fall, the entire system was connected, timed, calibrated, and debugged. This included all the electronics and the on-line data-acquisition code. A nagging problem in the LSI-11-based system, which reads out the NaI(Tl) pulse height and timing information, was fixed with the aid of Jerry Potter, Group MP-1; this system now works flawlessly. We also installed a crystal calibration system that uses a xenon flash tube and fiber optics cables; this system is working quite well.

In addition to all the above hardware changes, substantial progress was made in our analysis programs. For example, the track reconstruction efficiency in the drift chamber has risen from 86 to 97%. This is due to a combination of improvements in the software and hardware.

During our last run in 1983, we took data for 5 days at a reduced muon rate of 2×10^5 μ^+/s, and we are now analyzing these data. A typical $\mu \rightarrow e\gamma$ candidate is shown in Fig. 2. At the end of this run, the drift chamber was removed, a small liquid-hydrogen target was inserted, and data were taken with incident π^-. Figure 3 shows a spectrum from π^0's produced in the reaction $\pi^- p \rightarrow \pi^0 n$ at rest. These data are used to help calibrate the apparatus.

Plans call for a 3-week data run in January 1984 and more runs next summer.

Experiment 726

During the aforementioned running with a π^- beam and a liquid-hydrogen target, a data tape was taken while triggering on $\pi^0 \rightarrow 3\gamma$. A study of this tape will be invaluable for designing the details of the trigger electronics.

Data taking for this experiment will take place after the muon data have been obtained.

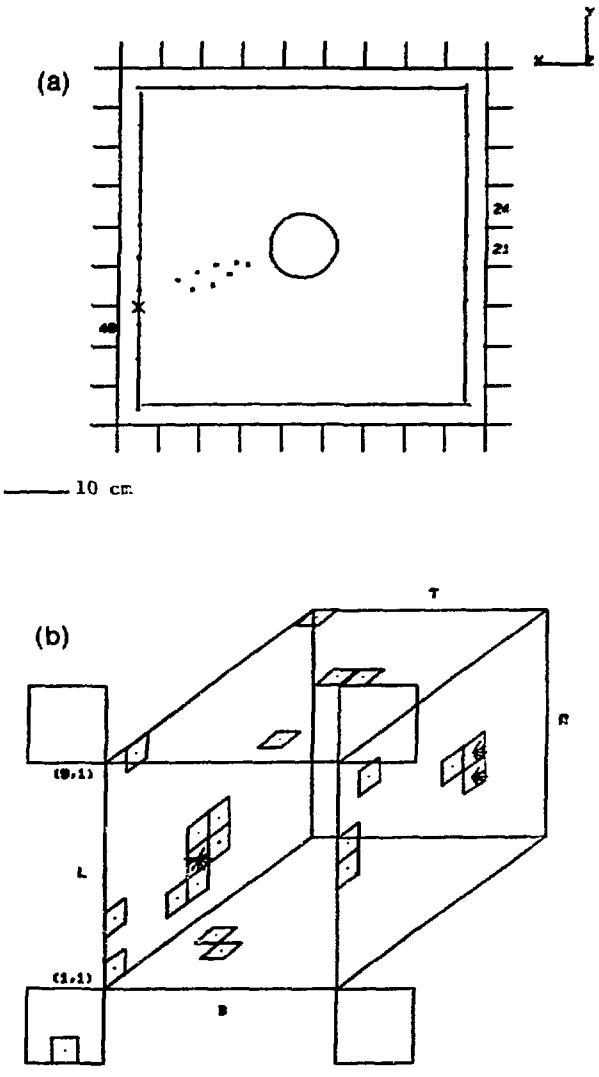

Fig. 2(a) and (b).
A typical $\mu \rightarrow e\gamma$ event: (a) view along beam line showing drift chamber wire hits, the struck scintillator, and the sodium iodide row sum energies; and (b) a three-dimensional view of the sodium iodide.

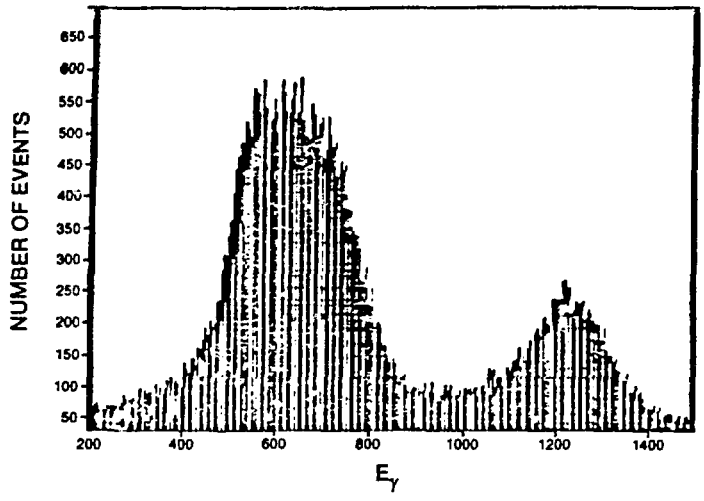

Fig. 3.
An on-line spectrum of single γ-ray energies from stopping π^- in hydrogen. The units for the abscissa are not MeV.

Deformation of Rare-Earth Nuclei and the Sternheimer Effect

(Exp. 698, SMC)

(Purdue Univ., Los Alamos, Princeton Univ.)

Spokesmen: R. M. Steffen (Purdue Univ.) and E. B. Shera (Los Alamos)

Participants: Y. Tanaka, W. Reuter, M. V. Hoehn, and J. D. Zumbro

Values of nuclear quadrupole moments Q_1 deduced from electronic-atom hyperfine measurements are rather uncertain even though measurements of optical hyperfine-splitting energies are very precise. The reason lies in the difficulty of exactly calculating the electrostatic gradient at the nucleus produced by the multielectron environment. In general, the nonspherical shape of the nuclear quadrupole field causes a nonspherical distribution of the core electrons (the Sternheimer effect) that in turn affects the electronic valence states.

In a muonic atom, however, the (single) muon is overwhelmingly responsible for the field gradient at the nucleus, allowing nuclear quadrupole moments to be precisely extracted from measurements of the hyperfine-splitting energies of muonic $3d$ and $4f$ states (that is, by observation of the muonic-M x rays).

We have measured the ground-state quadrupole moments of 11 odd-A nuclei in the region from $Z = 63$ to 77 by observing the hyperfine structure of their muonic-M x rays. The total errors of the present quadrupole moments, including the uncertainty arising from the model assumed for the radial quadrupole charge distribution within the nuclear volume, are less than 1%.

Our data for the odd-A nuclei demonstrate that, after the abrupt onset of deformation at $N = 90$, the deformation parameter β_2 varies smoothly with neutron number (see Fig. 1). Contrary to the rather scattered electronic-atom results (see Fig. 2), the present results indicate that the deformations of the odd-A nuclei are quite consistent with those of the adjacent even-A neighbors.

We expect that our precise new quadrupole-moment values will stimulate theoretical calculation of the ground-state deformation of odd-A nuclei. Correct prediction of the equilibrium deformation of the ground state is a central issue in gauging the success of mean-field theories of nuclear structure.

By comparing our muonic-atom quadrupole-moment values with electronic-atom values, we have computed experimental Sternheimer shielding factors for several electronic orbitals relevant to rare-earth atoms. We are thus led to the following conclusions.

1. The shielding factors have the same value for isotopes of the same element, even though the nuclear quadrupole moments may be quite different (by almost a factor of 3 for europium isotopes).
2. The $R(5d)$ shielding factors vary irregularly from −0.16(13) to −0.75(17), in serious disagreement with the theoretical estimate of $R(5d) = -0.25(5)$. Whereas the $R(4f)$ shielding factors for terbium, dysprosium, and erbium, and the $R(6p)$ shielding factors for europium and gadolinium, are close to

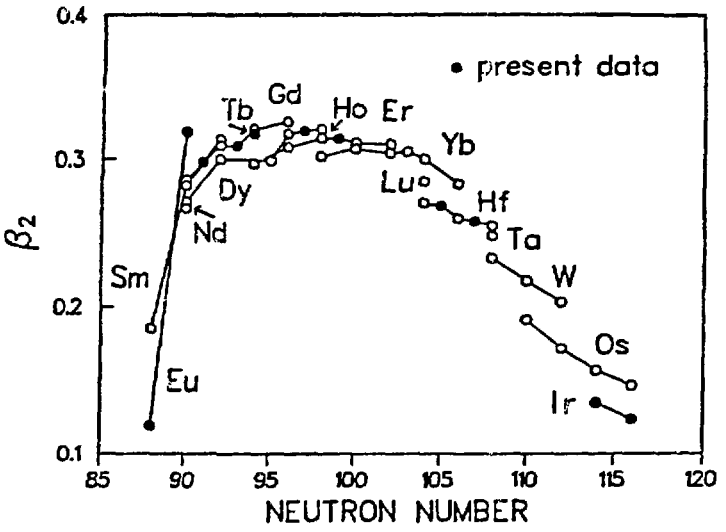

Fig. 1.

Systematics of the deformation parameter β_2 in the rare-earth region. The new muonic data for odd-A nuclei are shown as solid dots.

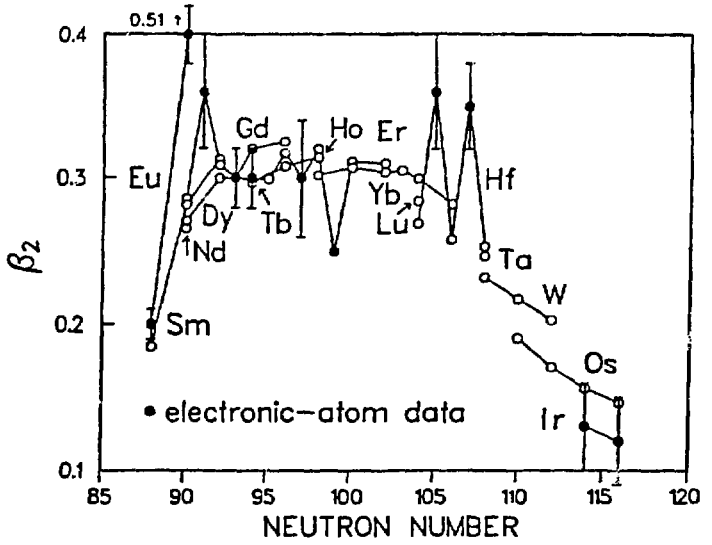

Fig. 2.

Similar to Fig. 1, except that the widely scattered optical data are shown for the odd-A nuclei.

the theoretical values, the $R(6p)$ value for dysprosium is several times smaller than the theoretical value. Clearly, the theory of the Sternheimer shielding effect in the $5d$ and $6p$ electronic valence states of rare-earth atoms must be reexamined.

Although our understanding of the electronic electrostatic gradients at the nucleus in rare-earth atoms is far from complete, it seems that no matter which effects contribute to the shielding phenomena, the same shielding factor is valid for all isotopes of a particular element regardless of the value of the nuclear quadrupole moment. Hence electronic-atom hyperfine measurements, which require only small amounts of target material, are well suited for determining accurate ratios of ground-state nuclear quadrupole moments of different isotopes of the same element. Furthermore, if the appropriate muonic-atom data are available for empirical calibration of the Sternheimer effect, the electronic-atom measurements can furnish absolute measurements of the quadrupole moments of otherwise inaccessible nuclei.

Further information concerning this work can be obtained from Phys. Lett. 108B, 8 (1982) and Phys. Rev. Lett. 51, 1633 (1983).

Formation of Muonium in the 2S State and Observation of the Lamb-Shift Transition (Exp. 724, SMC)

(Yale Univ., Univ. of Heidelberg, College of William and Mary, Los Alamos, Univ. of Mississippi)

Spokesmen: P. O. Egan and V. W. Hughes (Yale Univ.), and M. Gladisch (Univ. of Heidelberg)

Participants: A. Badertscher, S. Dhawan, P. O. Egan, V. W. Hughes, D. C. Lu, M. W. Ritter, K. A. Woodle, M. Gladisch, H. Orth, G. zu Putlitz, M. Eckhause, J. Kane, F. G. Mariam, and J. Reidy

Muonium (M) is an atom consisting of a positive muon and an electron and is an ideal system to test quantum electrodynamics (QED).[1] High-precision measurements of the hyperfine-structure interval $\Delta\nu$ and of the Zeeman effect in its ground state have provided very sensitive tests of QED, as well as precise values of the fine structure constant α and the ratio of the muon and proton magnetic moments.[2,3] In these experiments muonium was formed by stopping μ^+ in gaseous targets.

Another important QED test would be a precise measurement of the Lamb shift in muonium in the $n = 2$ state, since it would be free of the effects of proton structure that complicate the interpretation of the Lamb shift in hydrogen.[4] For this measurement muonium in the $2S$ state must be obtained in vacuum to avoid collisional quenching of $M(2S)$ atoms. Using a method similar to beam neutralization in proton beam foil spectroscopy,[5] we have shown that muonium in its ground state is formed by passing a μ^+ beam through a thin foil in vacuum.[6] From proton data[7] we expect that metastable $M(2S)$ atoms will be formed as well, and that $M(2S)/M(1S)$ will be about 0.1. Higher excited states will also be formed, but their formation probabilities are lower and most of these excited-state atoms will decay rapidly.

Here we report on further developments for producing muonium in vacuum, detecting $M(2S)$ by a static electric-field quenching method, and observing the Lamb-shift transition $2S \rightarrow 2P$ induced by an electric rf field of about 1140 MHz.

Our experiment was done at the SMC at LAMPF. Figure 1 shows a diagram of our apparatus.

Figure 2 is the energy-level diagram for muonium in its $n = 1$ and $n = 2$ states, including fine structure, Lamb shift, and hyperfine structure. The value of the Lamb-shift interval of $2S_{1/2}$ to $2P_{1/2}$ for muonium has been calculated from QED.[8] The $2S$ atomic state is metastable with the mean lifetime of 1/7 s for two-photon decay to the $1S$ state; however, the mean life of 2.2 μs for μ^+ decay determines the lifetime of $M(2S)$. Our first approach to observation of $M(2S)$ was to detect the static electric-field quenching of $M(2S)$.

We searched for $M(2S)$ by modulating the static electric field between on (600 V/cm) and off and by looking for a difference in the event rate due to Lyman-α photons emitted during the field-on phase. An event required a triple coincidence between an incoming muon, a delayed Lyman α photon in one of the four ultraviolet phototubes, and a further-delayed $M(1S)$ atom detected in the microchannel plate. The time gates were set to accept $M(2S)$ atoms with kinetic energies between 4 and 26 keV. The asymmetry between quenching field on and field off, defined with the events (E) normalized to the number of incoming muons,

$$A = \frac{(E/\mu)_{on} - (E/\mu)_{off}}{(E/\mu)_{on} + (E/\mu)_{off}},$$

was $A = (41.5 \pm 5.8)\%$.

The next step in establishing the formation of $M(2S)$ atoms was to search for the Lamb-shift transition $2S_{1/2}$,

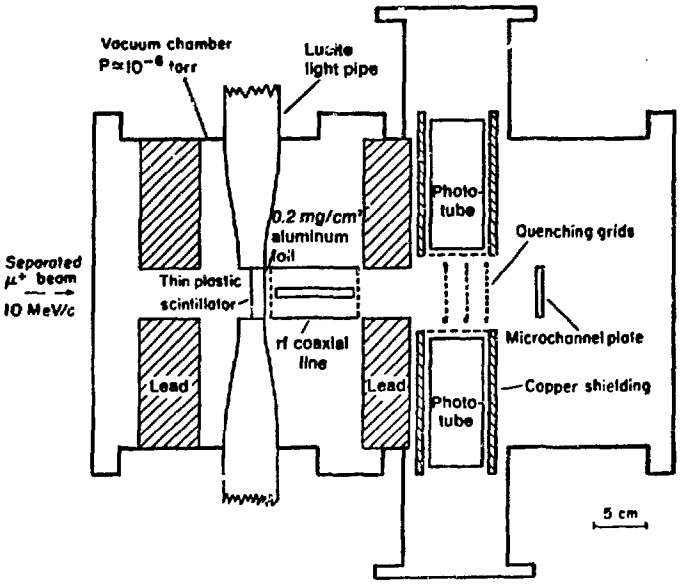

Fig. 1.
Diagram of the apparatus.

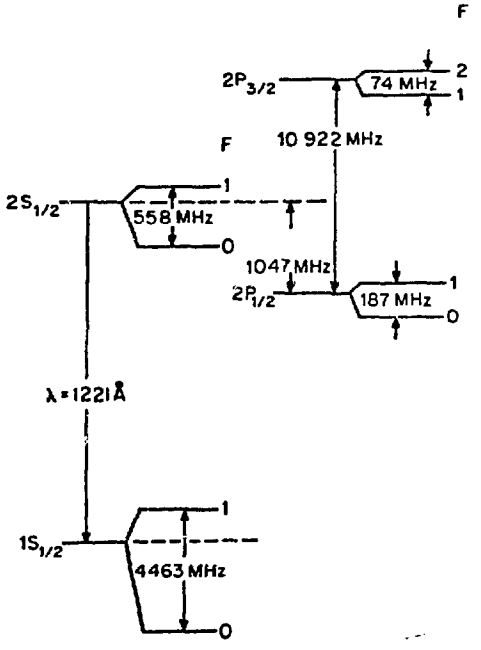

Fig. 2.
Energy-level diagram of the $n = 1$ and $n = 2$ states of muonium.

$F = 1 \rightarrow 2P_{1/2}, F = 1$ driven with an electric rf field. In Fig. 3 the solid curve shows the theoretical non-power-broadened resonance lines for two transitions between the hyperfine sublevels of the $2S_{1/2}$ and $2P_{1/2}$ states. The natural linewidth of 100 MHz (FWHM) is due to the

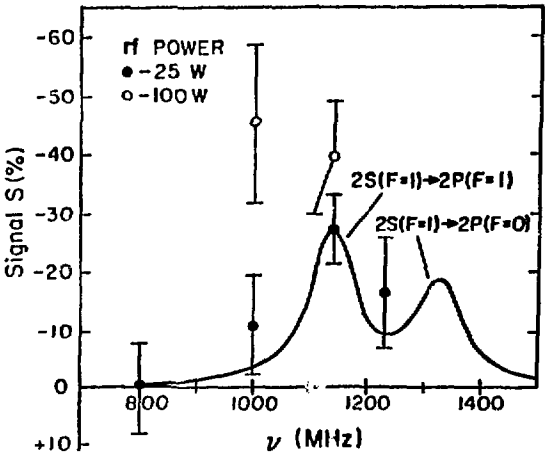

Fig. 3.
Muonium $2S_{1/2} = 2P_{1/2}$ resonance lines. The solid curve shows the theoretical non-power-broadened resonance line shape. The data points for 100- and 25-W rf input power are shown.

lifetime of the $2P_{1/2}$ state. Our rf interaction region (Fig. 1) consisted of a coaxial line. The experimental data are shown.

We conclude from our data that we have formed muonium in the $2S$ state with the expected rate and that we have observed the Lamb-shift transition. We are making measurements of the $2S_{1/2} \rightarrow 2P_{1/2}$ transitions to determine the Lamb shift and hfs intervals.

REFERENCES

1. V. W. Hughes and T. Kinoshita, in *Muon Physics I*, V. W. Hughes and C. S. Wu, Eds. (Academic Press, New York, 1977), p. 12.
2. F. G. Mariam et al., Phys. Rev. Lett. 49, 993 (1982).
3. J. R. Sapirstein et al., Phys. Rev. Lett. 51, 982 and 985 (1983).
4. S. R. Lundeen and F. M. Pipkin, Phys. Rev. Lett. 46, 232 (1981).
5. H. G. Berry, Rep. Prog. Phys. 40, 155 (1977).
6. P. R. Bolton et al., Phys. Rev. Lett. 47, 1441 (1981).
7. G. Gabrielse, Phys. Rev. A 23, 775 (1981).
8. D. A. Owen, Phys. Lett. 44B, 199 (1973).

$E2$ and $E4$ Moments in $^{233,234,235,238}U$ (Exp. 745, SMC)

(Princeton Univ., Los Alamos, Purdue Univ., Oak Ridge National Lab.)

Spokesmen: J. D. Zumbro (Princeton Univ.) and E. B. Shera (Los Alamos)

Participants: Y. Tanaka, C. E. Bemis, Jr., R. A. Naumann, M. V. Hoehn, W. R. Reuter, and R. M. Steffen

The rigid-rotor model postulates that the low-lying excited nuclear states arise from rotations of an intrinsically deformed ground state. With this model the quadrupole and hexadecapole moments of the low-lying states are related by well-known geometrical factors (Clebsch-Gordon coefficients). In a heavy, highly deformed nucleus like uranium it is possible to test the (adiabatic) rotational-model predictions by studying the interaction of the nucleus with a bound muon. This is possible because in heavy nuclei several excited nuclear states are mixed appreciably in the muonic $3d$ and $2p$ states. By simultaneously analyzing the muonic $2p \rightarrow 1s$ (K), $3d \rightarrow 2p$ (L), and $4f \rightarrow 3d$ (M) x-ray transitions, a large number of $E2$ matrix elements can be independently determined. We therefore are able, for the first time, to make a detailed electromagnetic test of a principal underlying assumption of the rotational model.

Figure 1 summarizes our results for ^{233}U. The upper section of the figure shows the $E2$ matrix elements that were independently determined; the lower part of the figure indicates that the measured matrix elements are consistent with an adiabatic intrinsic state at the level of a few per cent.

The present muonic-atom experiments on uranium also represent the first direct measurement of spectroscopic hexadecapole ($E4$) nuclear moments. The measurements are direct in the sense that the hyperfine splitting produced by the interaction of the nuclear $E4$ moment with the (readily computed) electric-field gradient at the nucleus is observed directly.

The muonic-atom method stands in contrast to previous methods that have employed strongly interacting probes and that have sometimes yielded inconsistent results, presumably from model dependence or interference from strong-interaction effects. Discrepancies between different types of experiments have suggested[1]

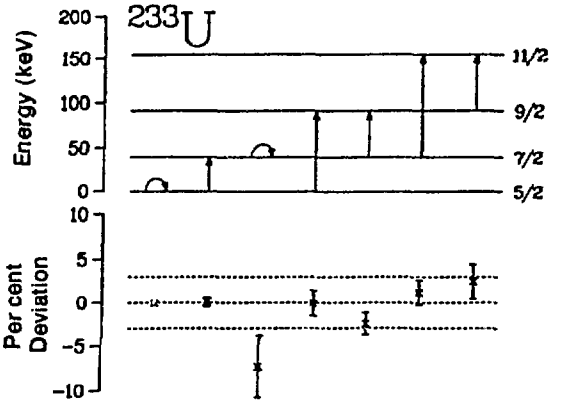

Fig. 1.
Results for $E2$ matrix elements in ^{233}U that were independently determined. The upper part of the figure indicates the $E2$ moments that were independently determined. A line between two levels indicates a dynamic $E2$ moment $|B(E2)|$, and the circular line closing on a level indicates a static $E2$ moment. In the lower part of the figure the deviation of each moment from the rotational-model value is shown; these deviations indicate that the measured matrix elements are consistent with an adiabatic intrinsic state at the level of a few per cent. The dashed lines are ± 3%.

that nuclear shapes depend somehow on the probe or reaction mechanism used to explore them.

The results of our muonic $E4$ measurements are shown in Fig. 2. These results, while more precise, are in reasonable agreement with the Coulomb excitation work of Bemis et al.[2] The hexadecapole moments have approximately the same value ($\sim$2.5 eb^2) for all four uranium isotopes that we have studied. This result is in agreement with equilibrium shapes of the uranium isotopes predicted by Brack et al.[3] using the Strutinsky shell-correction method with a Woods-Saxon potential. We are now using the Hartee-Fock deformed density-matrix-expansion theories from Negele and Rinker[4] to perform calculations for these nuclei.

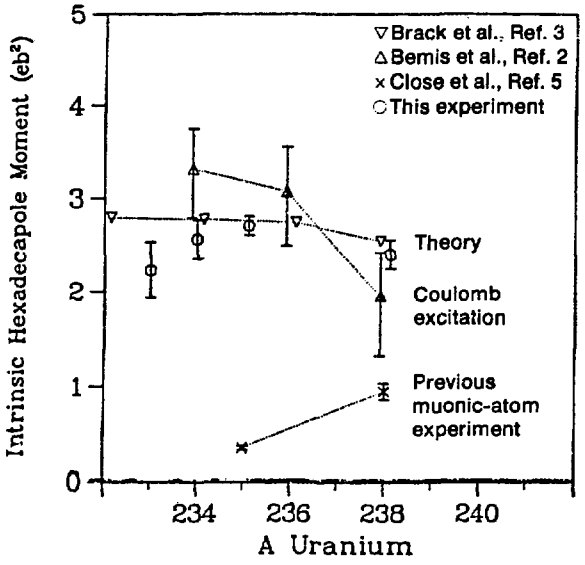

Fig. 2.
Intrinsic hexadecapole moment vs A for the uranium isotopes.

The early muonic-atom results of Close et al.[5] are in serious disagreement with the present results, with Coulomb excitation, and with theoretical calculations (see Fig. 2). The present work indicates that a carefully analyzed muonic-atom experiment produces results in agreement with other methods, thereby removing one piece of evidence for probe dependence of nuclear shapes.

REFERENCES

1. V. A. Madsen, V. R. Brown, and J. D. Anderson, Phys. Rev. Lett. 34, 1938 (1975); and V. A. Madsen et al., Phys. Rev. C 12, 1205 (1975).

2. C. E. Bemis, Jr., F. K. McGowan, J. L. C. Ford, Jr., W. T. Milner, P. H. Stelson, and R. L. Robinson, Phys. Rev. C 8, 1466 (1973).

3. M. Brack, T. Ledergerber, H. C. Pauli, and A. S. Jensen, Nucl. Phys. A 234, 185 (1974).

4. J. W. Negele and G. Rinker, Phys. Rev. C 15, 1499 (1977).

5. D. A. Close, J. J. Malanify, and J. P. Davidson, Phys. Rev. C 17, 1433 (1978).

Theory of Muon-Catalyzed *dt* Fusion: Resonant Mesomolecule Formation
(Biomed)

Spokesman: M. Leon (Los Alamos)

Muon catalysis of deuterium-tritium fusion has recently become a topic of widespread interest. On one hand, experiments probing this process under a variety of conditions are being performed at several muon facilities.[1,2] On the other, the sustained assault mounted by Ponomarev and his colleagues on many of the theoretical problems involved has made impressive progress in removing many of the gaps in our understanding.*

The most crucial and perhaps the most fascinating aspect of the muon-catalysis cycle is the role played by the resonant formation of the $dt\mu$ molecule.[5] This resonant formation occurs because of the existence of a very loosely bound $J=1$, $v=1$ excited state in the $dt\mu$ mesomolecule. The binding energy ($\simeq$0.64 eV) is small enough that the energy released in the $dt\mu$ formation from the $t\mu + d$ state can go into vibration and rotation of the resulting $dt\mu$-d (or $dt\mu$-t) molecule instead of into Auger emission. The resulting molecular-formation rates are at least two orders of magnitude larger than the nonresonant (Auger) rates.[5,6]

In developing the theory of resonant $dt\mu$ formation, we have generalized the calculation of Vinitsky et al.[6] (hereafter referred to as VP) to include the very important effects of the (1) orbital angular momentum carried into the reaction by the $t\mu$-D_2 (or DT) relative motion, and (2) initial D_2 (DT) angular momentum $K_i > 0$. We show as a result that, rather than a single resonance as in VP, the molecular formation reactions are dominated by a plethora of resonances, with a variety of initial and final molecular angular momenta. We also find that both the $v=2$ and $v=3$ vibrational levels of the final $dt\mu$-d molecule contribute significantly. Our final calculations for the molecular-formation rates as functions of temperature therefore include contributions from about 500 individual resonances.

The matrix element of the transition is written by VP as

$$T_{fi} = \int d\bar{R}\, d\bar{r}\, d\bar{\rho}\, \psi_f^*(\bar{r},\bar{R})\, \psi_f^*(\bar{\rho})\, H\psi_i(\bar{\rho})\psi_i(\bar{r},\bar{R}) \quad ,$$

where $\Psi(\bar{r},\bar{R})$ are the wave functions of the internal coordinates of the mesosystem $t\mu + d$ and where $\psi(\bar{\rho})$ are that of the motion of the mesosystem with respect to the spectator nucleus (see Fig. 1). The $t\mu + d$ collision time (at thermal energies) is estimated to be $\sim 10^{-15}$ s, which means that whereas the collision is sudden for the D_2 (DT) molecule, it is adiabatic for the electrons. Hence no electron excitation takes place during the "compound-molecule" formation. However, it is important that the next stage, deexcitation of the compound molecule by Auger emission, is much more probable than dissociation.

For the wave function $\psi_i(\bar{\rho})$, VP simply use the ground-state wave function of the target D_2 molecule (for $K_i = 0$ and vibrational $v_i = 0$):

$$\psi_i(\bar{\rho}) = \frac{y_0(\rho)}{\sqrt{4\pi}\,\rho}$$

An obvious generalization is to replace

$$1/\sqrt{4\pi} \qquad [\equiv Y_{00}(\hat{\rho})]$$

with

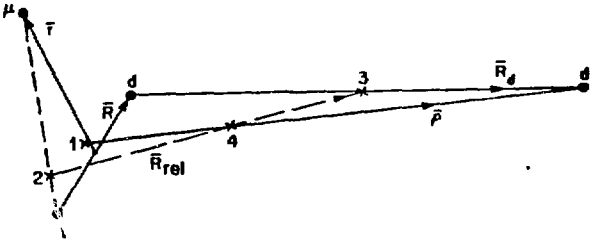

Fig. 1.
Vectors involved in the molecular-formation calculation: $\bar{r}$ goes from the midpoint of $\bar{R}$ to μ, $\bar{\rho}$ from the $dt\mu$ c.m. (marked 1) to the spectator d, and $\bar{R}_{rel}$ goes from the c.m. of the $t\mu$ (marked 2) to that of the D_2 (marked 3). The overall c.m. is marked 4.

*References 3 and 4. For a readily accessible review, see Bracci and Fiorentini, Ref. 4.

$Y_{K_i M_i}(\hat{\rho})$.

However, it is also necessary to include a factor to express the motion of the $t\mu$ atom and the D_2 molecule with respect to the overall center of mass (c.m.). This implies the factor $\exp(i\bar{p}\cdot\bar{R}_{tel})$, which introduces the dependence on the orbital angular momentum L; here $\bar{p}$ is the c.m. momentum (Fig. 1). Because of the small size of the $t\mu$ atom, interaction takes place when $r,R \ll \rho$. Then $\bar{R}_{tel} \simeq \eta\bar{\rho}$, where $\eta = 1/2$ for D_2, 3/5 for DT. Thus the VP expression is replaced by

$$\psi_i(\bar{\rho}) \simeq e^{i\eta\bar{p}\cdot\bar{\rho}}\, y_0(\rho)\, Y_{K_i M_i}(\hat{\rho})/\rho$$

$$= \sum_L (2L+1)\, i^L j_L(\eta p\rho)\, P_L(\cos\theta_{\bar{\rho}})$$

$$\times\, y_0(\rho)\, Y_{K_i M_i}(\hat{\rho})/\rho \quad . \qquad (1)$$

The interaction Hamiltonian is approximated by

$$H \simeq \frac{\bar{d}\cdot\rho}{\rho^3} = \left(\frac{4\pi d}{3\rho^2}\right) \sum_{m=-1}^{1} Y^*_{1m}(\hat{d})\, Y_{1m}(\hat{\rho}) \quad ,$$

where $\bar{d}$ is the dipole moment of the $dt\mu$ system.[6] The angular factors are now separated so that the angular integrals can be performed and the results expressed in terms of 3-J coefficients.[7] Taking the absolute square of T_{fi} and averaging over M_i and summing over M_f, we find the factor

$$F(K_i, K_f) = (2K_f+1)\sum_L (2L+1)\; J^2_{L\nu}$$

$$\times \left\{ (2L+3)\left[\begin{pmatrix} K_i & L+1 & K_f \\ 0 & 0 & 0 \end{pmatrix}\begin{pmatrix} L & 1 & L+1 \\ 0 & 0 & 0 \end{pmatrix}\right]^2 \right.$$

$$\left. + (2L-1)\left[\begin{pmatrix} K_i & L-1 & K_f \\ 0 & 0 & 0 \end{pmatrix}\begin{pmatrix} L & 1 & L-1 \\ 0 & 0 & 0 \end{pmatrix}\right]^2 \right\} . \qquad (2)$$

The

$$\begin{pmatrix} K_i & L\pm1 & K_f \\ 0 & 0 & 0 \end{pmatrix} \quad \text{etc.}$$

are 3-J coefficients,[7] and the second term in the $\{\,\}$ is absent for $L = 0$. (The ±1 arises from the $J = 1$ of the loosely bound $dt\mu$ state.) The factor

$$J_{L\nu} \equiv \int d\rho\, y_0(\rho)\, y_\nu(\rho)\, j_L(\eta p\rho)\rho^{-2}$$

replaces the vibrational matrix element I_ν of VP. Since the vibrational motion is of rather small amplitude around the equilibrium value $\rho_0 \simeq 1.4\, a_0$ (Ref. 8), for a rough approximation we can replace ρ with ρ_0 in the argument of the spherical Bessel function j_L, and therefore get

$$J_{L\nu} \simeq j_L(\eta p\rho_0) I_\nu ,$$

where, as in VP,

$$I_\nu \equiv \int d\rho\, y_0(\rho)\, y_\nu(\rho)\rho^{-2} \quad .$$

For $p \to 0$, only the S wave survives and $j_0 \to 1$; then for $K_i = 0$, only $K_f = 1$ is possible and $F \to I^2_\nu$. Thus

$$\bar{F}(K_i, K_f) \equiv \frac{F(K_i, K_f)}{I^2_\nu}$$

is precisely the factor that corrects the VP result for the incoming orbital angular momentum and $K_i > 0$. Orbital angular momentum $L > 0$ obviously allows a much greater variety of K_f values, not just $K_f = K_i \pm 1$, and therefore greatly increases the number of resonances contributing to molecular formation. For any fixed collision energy, however, the centrifugal barrier factor $j^2_L(\eta p\rho_0)$ will limit the number of partial waves contributing to the sum in Eq. (2).

The incoming $t\mu$ atom can be in the singlet ($S = 0$) or triplet ($S = 1$) spin state. Because the deuteron has spin 1,

the singlet $t\mu$ can only give the $S = 1$, $dt\mu$ mesomolecule, whereas triplet $t\mu$ can give rise to $S = 0$, 1, or 2. The $dt\mu$ hyperfine splittings have been calculated by Bakalov al.[9] For our purposes, we can ignore the energy splitting between the three hyperfine states formed from triplet $t\mu$; then the hyperfine shifts mean that the effective $dt\mu$ binding energy is decreased by 38 meV for singlet $t\mu$ and increased by 13 meV for triplet $t\mu$.

Consider collisions of singlet $t\mu$ with D_2 molecules. Angular momentum conservation requires that the $L = 0$ partial wave have $K_f = K_i \pm 1$; then the corresponding $v \leq 2$, K_f states have energies below the initial-state threshhold and hence cannot contribute to resonant mesomolecule formation. Thus only $v \geq 3$ formation can occur, which (it turns out) requires at least 0.27 eV in initial kinetic energy. Therefore $L = 0$ can contribute significantly to the molecular-formation rate $\lambda^0_{dt\mu-d}$ only at extremely high temperature (T).

In contrast, when $L > 0$ is permitted, K_f can be as large as $K_i + L + 1$, adding a significant amount of rotational energy and thus moving several $v = 2$ levels above threshhold. In this way, $K_i \rightarrow K_f$ transitions of $2 \rightarrow 4$, $3 \rightarrow 5$, ... (requiring $L = 1$), and $0 \rightarrow 3$, $1 \rightarrow 4$, ... (requiring $L = 2$), etc., produce resonances at energies of tens of milli-electron-volts or less. These terms are dominant not only because the resonant energies are extremely low, but also because I_2 is significantly larger than I_3 (Ref. 6).

These very low energy resonances produce a $\lambda^0_{dt\mu-d}$ that is very sensitive to the precise value of the $dt\mu$ excited-state binding energy. Changing this number by 10 meV, which is the present limit of accuracy of the calculation,[3] will drive several of the resonances below threshold or introduce new ones. The temperature dependence comes not only from the positions and strengths of the resonances, which determine the contribution of different parts of the Maxwell-Boltzmann distribution of initial $t\mu$ energies[6] (the $t\mu$ is assumed thermalized), but also from the Boltzmann factor for the initial molecular excitation.

The calculated temperature dependences of the four molecular-formation rates are shown in Fig. 2, including for $\lambda^0_{dt\mu-d}$ the effect of varying the $dt\mu$ binding energy. These results make use of the $\lambda_{dt\mu-d}$ value computed by VP for $L = 0$ and resonance energy 0.07 eV. For D_2 collisions of singlet $t\mu$ atoms, the $v = 2$ contribution is strongly dominant, as stated above; the extreme sensitivity to the $dt\mu$ excited-state binding energy seen in Fig. 2(b) and its qualitatively different behavior both come from the low-energy resonances (indicated schematically). For triplet $t\mu$, an additional 51 MeV of rotational excitation is needed for resonant formation with $v = 2$; this requires a larger increase in rotational angular momentum (for example, $2 \rightarrow 6$ rather than $2 \rightarrow 4$) and therefore larger L ($L = 3$ rather than $L = 1$),

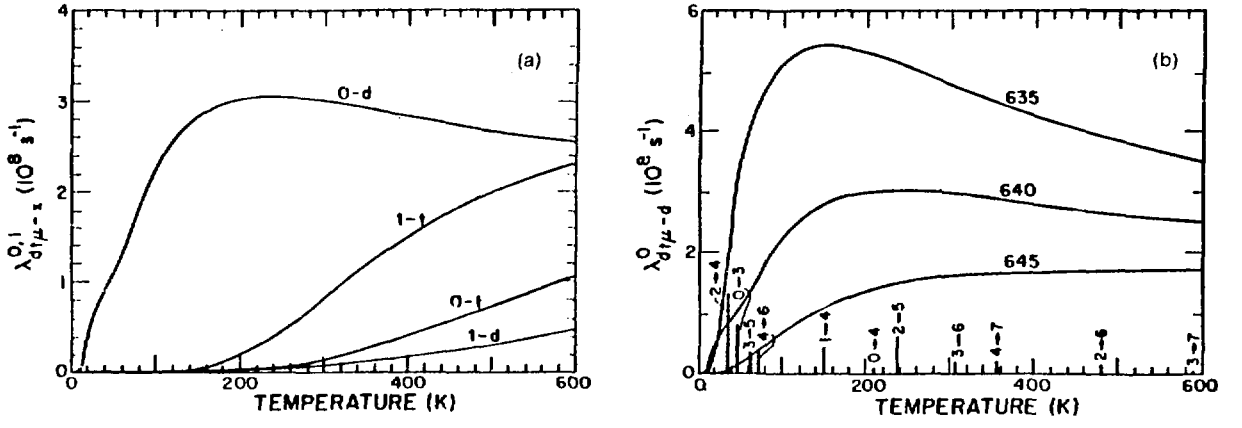

Fig. 2.

(a) The four molecular-formation rates, calculated for $dt\mu$ binding energy 640 meV; 0-d indicates $\lambda^0_{dt\mu-d}$, etc.

(b) The variation of $\lambda^0_{dt\mu-d}$ with binding energy, marked in milli-electron-volts. The variation with binding energy of the other three molecular-formation rates is rather small. For 640-meV binding energy, the positions and approximate strengths of the important low-energy resonances are shown as vertical bars, with the $K_i \rightarrow K_f$ values marked.

For *DT* collisions, the greater reduced mass lowers the vibrational levels so that the $v = 2$ contribution is completely negligible and only $v = 3$ is significant. Here the majority of important resonant contributions involve a reduction in rotational energy. For $dt\mu$-t, the vibrational energies and matrix elements are scaled from the $dt\mu$-d values of VP using harmonic oscillator behavior.

To make contact with experiment, we must consider how the four molecular formation rates contribute to the experimentally determined (normalized) muon-cycling rate λ_c. Introducing the effective (singlet or triplet) molecular-formation rates, which depend on the atomic concentrations C_d and C_t (see Refs. 1 and 10),

$$\lambda^{0,1}_{dt\mu} = \lambda^{0,1}_{dt\mu-d}\, C_d + \lambda^{0,1}_{dt\mu-t}\, C_t \quad ,$$

it can be seen that

$$\frac{1}{\lambda_c} = \frac{P_d}{\lambda_{dt} C_t} + \frac{3}{4}\,\frac{1}{\lambda_{10} + \lambda^1_{dt\mu}\, C_d} + \frac{\frac{1}{4} + \frac{3}{4}\,\chi}{\lambda^0_{dt\mu}\, C_d} \quad . \tag{3}$$

P_d is the probability for a ground-state $d\mu$ atom; because transfer to tritium can take place during the $d\mu$ deexcitation, this can be significantly less than C_d (Ref. 3). We use $P_d = C_d \exp(-\alpha C_t)$ to express this effect. Furthermore, λ_{dt} is the $d \rightarrow t$ ground-state transfer rate. The branching ratio χ is given by

$$\chi = \frac{\lambda_{10}}{(\lambda_{10} + \lambda^1_{dt\mu}\, C_d)} \quad ;$$

λ_{10} is the effective triplet-quenching rate, which has contributions from both d and t collisions

$$\lambda_{10} = \lambda^d_{10}\, C_d + \lambda^t_{10}\, C_t \quad .$$

The rate λ^t_{10} has been predicted to be very large: $9 \times 10^8\ s^{-1}$ (Ref. 11). If this is indeed the case, the second term of the right-hand side of Eq. (3) is always dominated by either the first or third term, and only the singlet molecular-formation rates can be easily extracted from experiment.

We show in Fig. 3 the data of Jones et al.[2] and two sets of calculated curves for $\lambda_c(T)$. Although parameters to give good agreement for $C_t = 10$, 20, and either 50 or 80% can readily be found (including increasing the rate given by VP by an overall factor β), we have not been able to fit all of the data simulaneously. Although our exploration of the six-dimensional parameter space certainly has not been exhaustive, we strongly suspect that this represents a real discrepancy. To pin down the source of this discrepancy, we urge the experimenters to

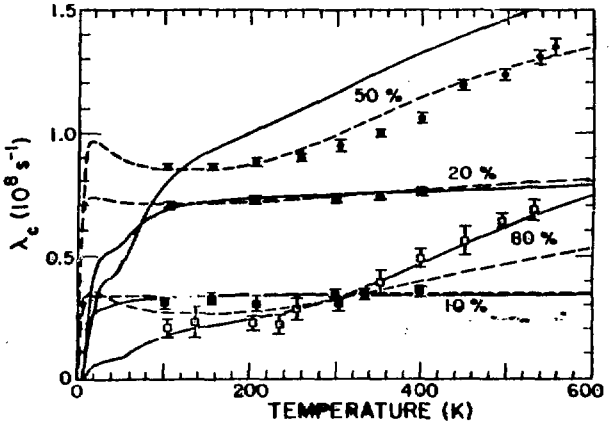

Fig. 3.
Theoretical and measured cycling rates λ_c for the C_t values marked. The curves were calculated using the following parameter values.

Solid curves:
Binding energy = 641 meV,
$\lambda_{dt} = 2.8 \times 10^8\ s^{-1}$,
$\alpha = 2.0$,
$\lambda^d_{10} = 5 \times 10^8\ s^{-1}$,
$\lambda^t_{10} = 0$, and
$\beta = 2.5$.

Dashed curves:
Binding energy = 628 meV,
$\lambda_{dt} = 2.6 \times 10^8\ s^{-1}$,
$\alpha = 3.3$,
$\lambda^d_{10} = 1.75 \times 10^5\ s^{-1}$,
$\lambda^t_{10} = 0$, and
$\beta = 1.6$.

measure as many of the various rates and parameters as possible.

REFERENCES

1. S. E. Jones et al., Phys. Rev. Lett. 51, 1757-1760 (1983).

2. Proceedings of the Third Int. Conf. on Emerging Nuclear Energy Systems, Helsinki, Finland, June 6-9, 1983, Atomkernenergie-Kerntechnik 43, No. 3 (1983).

3. L. I. Ponomarev, Proc. of the Third Int. Conf. on Emerging Nuclear Energy Systems, Helsinki, Finland, June 6-9, 1983, Atomkernenergie-Kerntechnik 43, No. 3 (1983); Proc. of the 10th European Conf. on Controlled Fusion and Plasma Physics (Moscow, 1981), Vol. II, p. 66; and S. I. Vinitsky and L. I. Ponomarev, Sov. J. Part. Nucl. 13, 557 (1982) [Fiz. Elem. Chastits At. Yadra 13, 1336 (1982)].

4. L. Bracci and G. Fiorentini, Phys. Rep. 86, 169 (1982).

5. S. S. Gershtein and L. I. Ponomarev, Phys. Lett. 72B, 80 (1977).

6. S. I. Vinitsky et al., Sov. Phys.-JETP 47, 444 (1978) [Zh. Eksp. Teor. Fiz. 74, 849 (1978)].

7. A. R. Edmonds, *Angular Momentum in Quantum Mechanics* (Princeton University Press, 1957).

8. D. Rapp, *Quantum Mechanics* (Holt, Rinehart, and Winston, New York, 1971).

9. D. D. Bakalov et al., Sov. Phys.-JETP 52, 820 (1980) [Zh. Eksp. Teor. Fiz. 79, 1629 (1980)].

10. S. S. Gershtein et al., Sov. Phys.-JETP 51, 1053 (1980) [Zh. Eksp. Teor. Fiz. 78, 2099 (1980)].

11. A. V. Matveenko and L. I. Ponomarev, Sov. Phys.-JETP 32, 871 (1971) [Zh. Eksp. Teor. Fiz. 59, 1593 (1970)].

Experimental Investigation of Muon-Catalyzed *dt* Fusion
(Exp.727, Biomed)

(Idaho National Engineering Lab., Los Alamos)
Spokesman: S. E. Jones (Idaho Engineering Lab.)

Because the dimensions of a muonic-hydrogen molecule are about 200 times smaller than those of an ordinary hydrogen molecule, negative muons stopped in a mixture of hydrogen isotopes can rapidly bring about fusion reactions. Muon-catalyzed fusion was first seen by Alvarez et al.[1] in 1957 but had been predicted even earlier by Frank and others.[2]

The recent revival of interest in the *dd* and *dt* reactions is mainly due to the discovery of a resonant molecular-formation process that precedes the fusion reactions.[3] For *dt*, this allows the formation of a loosely bound excited state of the $dt\mu$ mesomolecule, with the released energy going into vibration and rotation of the resulting large molecule (for which the $dt\mu$ is one nucleus) rather than electron emission (see Fig. 1). This resonant process is predicted to enhance the molecular-formation rate by two orders of magnitude and to induce a strong temperature dependence. In dense *dt* mixtures this opens the interesting possibility of a single negative muon catalyzing ~100 fusions.[4-6]

An experiment to measure the parameters governing muon-catalyzed fusion in deuterium-tritium mixtures is being carried out at the Biomed channel. The processes involved are shown schematically in Fig. 2. Of the rates defined there, only the transfer rate λ_{dt} and a lower limit on the molecular-formation rate $\lambda_{dt\mu}$ had been determined previously.[7] We have now measured λ_{dt}, $\lambda_{dt\mu}$ as a function of temperature in the range 100-540 K, the sticking probability ω_s, and the ^{3}He scavenging parameters (see below). (The fusion rate λ_f and the atomic capture rate λ_a are too fast to be measured.) Furthermore, we are also able to separate the two constituents[8] of $\lambda_{dt\mu}$:

$$\lambda_{dt\mu-d}: \quad t\mu + D_2 \rightarrow [(dt\mu)\, d\, 2e^-]^* \,, \qquad (1a)$$

$$\lambda_{dt\mu-t}: \quad t\mu + DT \rightarrow [(dt\mu)\, t\, 2e^-]^* \,. \qquad (1b)$$

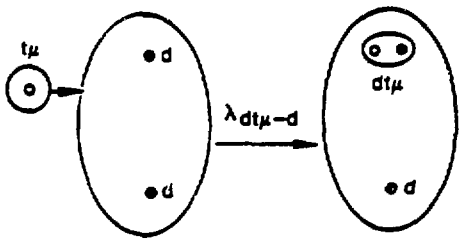

Fig. 1.
Resonant production of $dt\mu$ molecules.

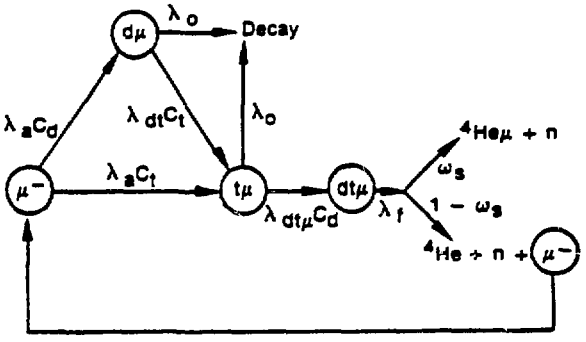

Fig. 2.
Muon catalysis in a mixture of deuterium and tritium.

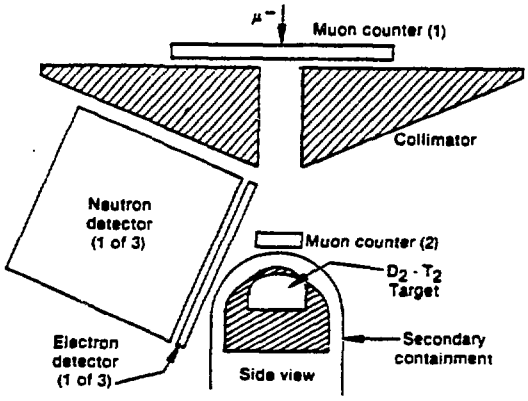

Fig. 3.
Layout of the experiment.

The apparatus is sketched in Fig. 3. The deuterium-tritium mixtures (0.45 and 0.60 of liquid-hydrogen density) are contained in gold-lined stainless steel vessels that can be heated or cooled.[9] Entering negative muons are registered by a scintillator telescope, the 14-MeV fusion neutrons by three liquid scintillators, and the muon-decay electrons by the combination of plastic scintillation counters plus the liquid scintillators. An accepted event requires, in sequence, (1) entry of a single muon, (2)

detection of one or more neutrons, and (3) detection of the muon-decay electron.

The times between neutron and e^- pulses following muon arrival are recorded. Neutron and γ events in the neutron detectors are distinguished by fast pulse-shape discrimination. These methods reduce background to acceptable levels. The neutron detector efficiencies are determined using the Los Alamos Van de Graaff accelerator as a 14-MeV neutron source in conjunction with Monte Carlo calculations that incorporate geometrical acceptance.[10] Overall neutron detection efficiency ϵ is $3.4 \pm 0.4\%$.

For any set of conditions there are two basic quantities to be determined: $\bar{n}$, the average number of neutrons produced per muon stopped in the gas, and λ_n, the rate associated with the time dependence of the appearance of the neutrons. The equations relating $\bar{n}$, λ_n, and the muon-cycling rate λ_c to the fundamental rates can easily be deduced from some simple considerations. Because λ_f and λ_a are very large,[5] the cycling time ($1/\lambda_c$) of the muon is simply the sum of the time spent waiting to transfer from d to t for that fraction captured in deuterium C_d, plus the time the $t\mu$ atom waits for molecular formation. Therefore,

$$\frac{1}{\lambda_c} = \frac{C_d}{\phi\lambda_{dt}\, C_t} + \frac{1}{\phi\lambda_{dt\mu}\, C_d} \quad . \tag{2}$$

(By convention, the fundamental rates are normalized to liquid-hydrogen density, hence the density factor ϕ, which is the ratio of the actual number density to liquid-hydrogen density.) Rate λ_n depends on all the processes that remove muons from the cycle; for small ^{3}He concentrations,

$$\lambda_n = \lambda_0 + \omega_s\lambda_c\left(\omega_{He} + \frac{C_d}{C_t}\frac{\lambda_{dHe}}{\lambda_{dt}} + \frac{\lambda_{tHe}}{C_d\lambda_{dt\mu}}\right) \quad , \tag{3}$$

where ω_{He} is the probability for initial capture on ^{3}He plus the probability of transferring to ^{3}He during the muonic-hydrogen cascade, and where λ_{dHe} and λ_{tHe} are the rates for transfer from the ground state of the muonic-hydrogen atoms. Finally, as indicated by reactions of Eq. (1), there are two components of $\lambda_{dt\mu}$:

$$\lambda_{dt\mu} = \lambda_{dt\mu-d}\, C_d + \lambda_{dt\mu-t}\, C_t \quad . \tag{4}$$

Our principal experimental results obtained so far are displayed in Figs. 4 and 5 and Table I; the error bars in

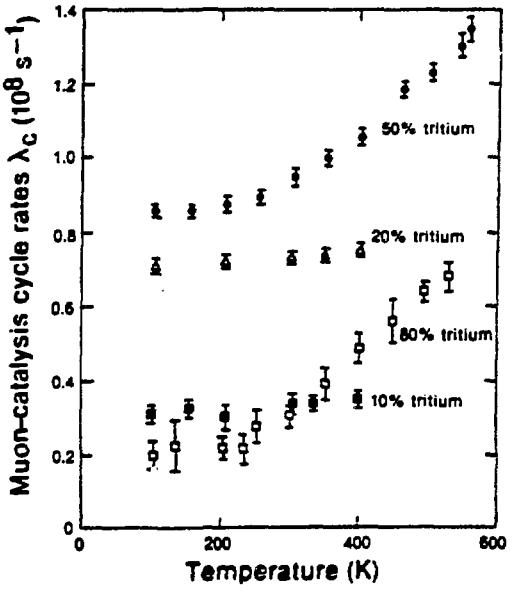

Fig. 4.
Muon-cycle rate λ_c normalized to liquid-hydrogen density as a function of temperature.

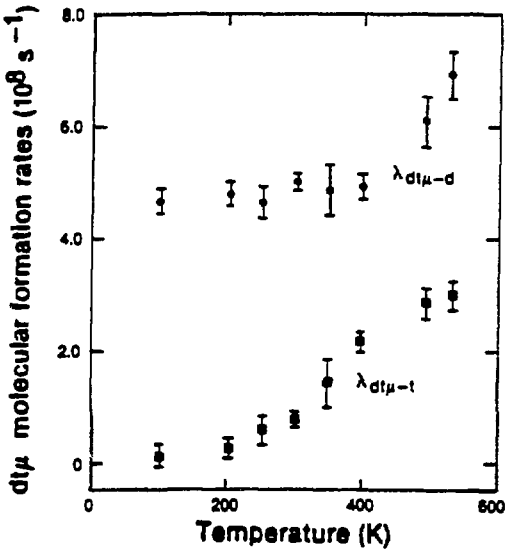

Fig. 5.
Mesomolecular formation rates as functions of temperature.

Table I. Parameters of Muon Catalysis in Deuterium-Tritium Mixtures.

Parameter	Theory	Reference	Previous Experiment[a]	This Experiment
λ_{dt}	$2 \times 10^8\ s^{-1}$	8	$(2.9 \pm 0.4) \times 10^8\ s^{-1}$	$(2.8 \pm 0.3) \times 10^8\ s^{-1}$
$\lambda_{dt\mu}$	$\sim 10^8$	5	$>10^8\ s^{-1}$	see Fig. 5
ω_s	0.86%	11	---	$(0.77 \pm 0.08)\%$
	0.91%	12		
ω_{He}	~ 1	14	---	1 ± 1
λ_{dHe}	$1.5 \times 10^8\ s^{-1}$	13	---	$(2 \pm 1) \times 10^8\ s^{-1}$
λ_{tHe}	$5.6 \times 10^8\ s^{-1}$	13	---	$(7 \pm 2) \times 10^8\ s^{-1}$
$\bar{n}$	$\sim 10^2$	5	---	90 ± 10

[a]Reference 7.

the figures are statistical, whereas the errors quoted in the table include systematic errors. Figure 4 shows the temperature dependence of λ_c for four concentration ratios. Whereas the low C_t data show no significant temperature dependence, in agreement with the experiment of Bystritsky et al.,[7] the temperature dependence for the higher tritium concentrations is quite striking. The low tritium concentration data are flat because the cycling time is dominated by the $d \rightarrow t$ transfer time $(1/C_t\lambda_{dt})$. The rate λ_{dt} (assumed to be independent of temperature) extracted from our data agrees very well with that reported in Ref. 7 (see Table I).

Once λ_{dt} is determined, $\lambda_{dt\mu}$ can be obtained using Eq. (2). From the concentration dependence of Eq. (4), the separate components of $\lambda_{dt\mu}$ are found (Fig. 5). Both of these components appear to be resonant. However, whereas $\lambda_{dt\mu-t}$ has the expected property of approaching zero as $T \rightarrow 0$, the $\lambda_{dt\mu-d}$ surprisingly appears to be constant in the temperature range 100-400 K.

The experiment also determines the sticking probability ω_s [see Eq. (3)]. The result for ω_s $(0.77 \pm 0.08)\%$ is in fair agreement with the two calculations.[11,12] (High-Z contamination of our target gas, which could produce an artificially large value of ω_s, was calculated to be less than 2 ppm and therefore negligible, but so far has not been measured.)

The final results concern the scavenging of muons by ^{3}He produced from tritium decay. The three contributions to this scavenging have been separated roughly by their λ_c and C_t dependence [see Eq. (3)]; the results are shown in Table I. The λ_{dHe} and λ_{tHe} values agree quite well with the calculations of Aristov et al.,[13] and the ω_{He} value is quite reasonable.[14]

In summary, this first investigation of muon-catalyzed fusion in high-density *dt* mixtures has produced a number of new results. Formation rates for $dt\mu$ molecules have been observed to be large and dependent on temperature, and quite different for the two molecular species involved (D_2 and DT). The measured sticking probability ω_s is consistent with calculation. The cycle rates and neutron yields demonstrate that a significant number of *dt* fusions per muon can be realized. Indeed, our measurements indicate that an average of 90 ± 10 fusions per muon will be produced in an equimolar deuterium-tritium mixture at $\phi = 1$ and 540 K.

REFERENCES

1. L. W. Alvarez et al., Phys. Rev. 105, 1127 (1957).
2. F. C. Frank, Nature 160, 525 (1947); A. D. Sakharov, Report of the Physics Institute, Academy of Sciences (1948); and Ya. B. Zeldovitch, Dokl. Akad. Nauk SSSR 95, 493 (1954).
3. E. A. Vesman, Sov. Phys.-JETP Lett. 5, 113 (1967).
4. S. S. Gershtein and L. I. Ponomarev, Phys. Lett. 72B, 80 (1977).
5. L. I. Ponomarev, Proc. of the 10th European Conf. on Controlled Fusion and Plasma Physics (Moscow, 1981), Vol. II, p. 66.
6. L. I. Ponomarev, Proc. of the 6th Int. Conf. on Atomic Physics, R. Danberg, Ed. (Plenum Press, New York, 1978), p. 182.
7. V. M. Bystritsky et al., Sov. Phys.-JETP 53, 877 (1981).
8. S. S. Gershtein et al., Sov. Phys.-JETP 51, 1053 (1980).
9. A. J. Caffrey, S. E. Jones, and K. D. Watts, Bull. Am. Phys. Soc. 28, 646 (1983).

10. N. R. Stanton, Ohio State Research Foundation report COO-1545-92 (1971); and A. J. Caffrey and S. E. Jones, to be published.

11. S. S. Gershtein et al., Sov. Phys.-JETP 53, 872 (1981).

12. L. Bracci and G. Fiorentini, Phys. Rep. 86, 169 (1982).

13. Yu. A. Aristov et al., Sov. J. Nucl. Phys. 33, 564 (1981).

14. J. S. Cohen, R. L. Martin, and W. R. Wadt, Phys. Rev. A 27, 1821 (1983).

Materials Science

Dilution Refrigerator for μSR Measurements (Exps. 499, 640, 771, SMC)

(Los Alamos, Rice Univ., Univ. of California at Riverside)

Spokesman: D. Wayne Cooke (Los Alamos)

The potential of muon spin rotation (μSR) as a condensed matter probe has been well established. Recent experiments have shown that such phenomena as fluctuation dynamics near spin-glass transition temperatures and muon motion in noble metals, for example, are amenable to study by muon-spin rotation and relaxation techniques. It is expected that potentially exciting physics occurs at temperatures below 4 K and that future μSR experiments will thus require cryogenic apparatus that can attain temperatures in the millikelvin region.

Accordingly, Group MP-3, assisted by Group P-10, has undertaken the task of designing and constructing a ^{3}He/^{4}He dilution refrigerator suitable for use in μSR studies. In addition to the temperature requirements, the refrigerator also must satisfy space requirements — namely, it must fit inside the existing μSR high-field Helmholtz coil.

Such a refrigerator has been designed and constructed, and initial testing has indicated the need for several modifications. During the past year these modifications have been made and tested, and include

- an improved method of mounting the refrigerator so that thermal isolation between the 1 K cold plate and 4 K heat shield is assured;
- the installation of a larger diameter heat shield to minimize risk of thermal shorts between the mixing chamber and heat shield;
- the construction and installation of a new counterflow heat exchanger that provides the proper pressure gradient between the still and mixing chamber; and
- an improved method of connecting the still and mixing chamber so that the thermal link between the two is minimized for temperatures below 1 K.

To date the minimum temperature attained by operating in a continuous mode has been 235 mK. It is expected that replacement of a faulty ^{4}He dewar will lower this temperature further to the design value of 50 mK. The present experimental effort is directed toward designing a suitable target chamber and devising a sample temperature control scheme in anticipation of performing μSR experiments with the dilution refrigerator.

Muon Longitudinal and Transverse Relaxation Studies in Systems with Random Exchange (Exp. 499, SMC)

(Rice Univ.; Los Alamos; UC, Riverside; Univ. of Leiden, The Netherlands)

Spokesmen: S. A. Dodds (Rice Univ.), R. H. Heffner (Los Alamos), and D. E. MacLaughlin (UC, Riverside)

Silver-Manganese Spin Glasses

Progress has been made in understanding the field dependence of zero- and longitudinal-field muon-spin relaxation (μSR) in *Ag*Mn spin-glass alloys at temperatures well below the freezing or "glass" temperature T_g (Ref. 1). These experiments provide a direct measurement of spin-glass dynamics, which is quite different in *Ag*Mn spin glasses than in their ordered counterparts (ferromagnets, antiferromagnets). In particular, the local spin correlations die off as $t^{-\nu}$; that is, the correlations possess "long-time tails." This is in contrast to the behavior of correlations in comparable nonrandom systems, which typically decay with an exponential time dependence.[2] Recent theories,[3] which use Langevin equations to represent the dynamics of the spin glass, also give this result, with $\nu \simeq \frac{1}{2}$, when applied to a mean-field model of the spin-glass state.

Our results may be summarized as follows.

1. Over a wide range of magnetic fields for $0.3 < T/T_g < 0.7$, and for several manganese concentrations, the positive-muon (μ^+) spin-lattice relaxation rate $\lambda_{\|}$ varies with effective applied field as $H^{\nu-1}$, with $\nu \simeq 0.54 \pm 0.05$. On general grounds we expect $\lambda_{\|} \propto J(\omega_\mu)$, where $J(\omega)$ is the noise spectrum of fluctuating fields produced at μ^+ sites by manganese spins and where ω_μ is the μ^+ Larmor frequency. Thus the field dependence of $\lambda_{\|}$ gives the functional form of $J(\omega)$, *if* the external field (1) dominates ω_μ, and (2) does not affect the functional form of $J(\omega)$ directly.

Static internal field distributions are known from μSR measurements in zero- and transverse-applied fields, so corrections can be made. Confirmation that the manganese-spin dynamics is indeed independent of applied field comes from ^{63}Cu and ^{109}Ag nuclear-magnetic-resonance experiments[4] in *Cu*Mn and *Ag*Mn alloys for $T \ll T_g$, which directly demonstrate the absence of a field

dependence of $J(\omega)$. Our data therefore provide the first experimental evidence that spin correlations decay algebraically and not exponentially in spin glasses below T_g. The observed value of ν is within experimental error of that obtained from dynamic theories.

2. For T near T_g we obtain $\nu \simeq 0.2$, which is not in agreement with the dynamic theories. Here, however, $J(\omega)$ may be directly affected by the applied field. The data are shown in Fig. 1.

3. A scaling law of the form

$$\lambda_{\parallel} = x^2 f(T/T_g, H/T_g)/T_g \ , \qquad (1)$$

where x is the manganese concentration and $f(u,v)$ is a dimensionless function, is obeyed. This form is expected for dilute spin glasses, where the dipolar coupling scales as x and spin-glass energies (and frequencies) scale as T_g (Ref. 5).

These results call for further theoretical work. It is important to know, for example, how much intrinsic field dependence of $J(\omega)$ is to be expected from current theory. The most fundamental question, perhaps, is whether power-law correlation decays can be obtained from more realistic models than have been studied up to the present time.

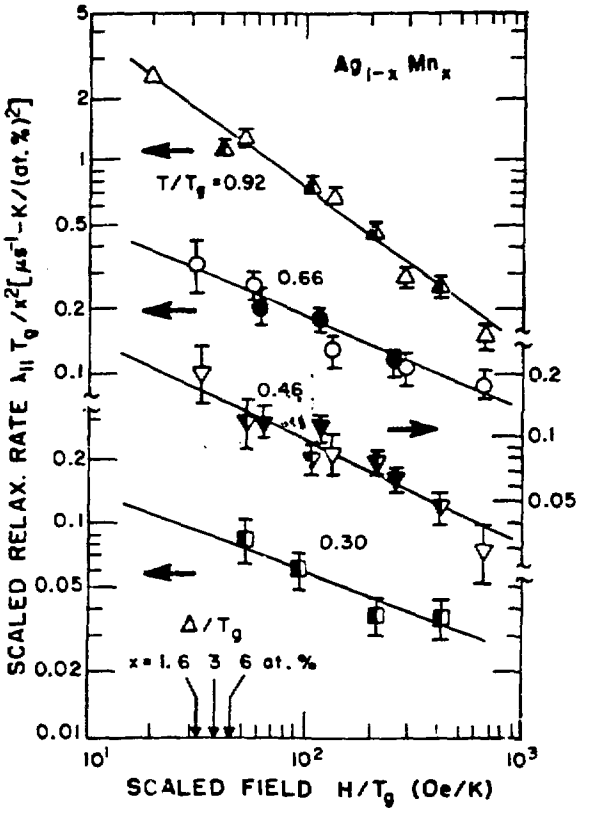

Fig. 1.
Scaled isotherms of μ^+ spin-lattice relaxation rate $\lambda_{\parallel}$ vs effective longitudinal field H for temperatures below T_g in $Ag_{1-x}Mn_x$ spin glasses.
Open symbols: $x = 0.016$,
Half-filled symbols: $x = 0.03$,
Filled symbols: $x = 0.06$.
Least squares fits to a power law are shown for each scaled temperature T/T_g. Scaled widths Δ/T_g of the μ^+ dipolar field distributions for the various manganese concentrations are shown by arrows on the horizontal axis.

Palladium Manganese

The $Pd_{1-x}Mn_x$ system has been widely studied, both as an example of a non-RKKY spin glass and as a dilute ferromagnet. A competition between direct antiferromagnetic couplings and long-range ferromagnetic couplings leads to a complicated phase diagram[6] with a ferromagnetic phase for $x \lesssim 3$ at.% and a spin-glass phase for $x \gtrsim 5$ at.%. In addition, manganese in palladium possesses a giant moment described by spin $S = \frac{5}{2}$ and effective g factor $g_{eff} \simeq 2.7$. Both the $x = 0.02$ ferromagnetic ($T_c = 5.8$ K) system and $x = 0.07$ spin-glass ($T_g = 5$ K) system have been studied using μSR as a microscopic probe of magnetic ordering and dynamics. Measurements were carried out in zero applied field and with both transverse- and longitudinal-applied fields. The data were analyzed using standard expressions[7] for the μSR linewidths. The data analysis and sample characterization are described in Ref. 8 for *Pd*Mn (2 at.%) and in Ref. 9 for *Pd*Mn (7 at.%).

Ferromagnetic *Pd*Mn (2 at.%)

It was determined that the transverse-field relaxation-rate data $\lambda_{\perp}$ were much larger than the longitudinal-field rates $\lambda_{\parallel}$ for nearly all temperatures and fields. Furthermore, measurements of muon diffusion in palladium with gadolinium impurities indicate a negligible

muon diffusion rate below about 100 K. Thus the $\lambda_\perp$ data reflect the distribution of quasi-static internal fields.

Walstedt and Walker (WW) have treated[10] the problem of local-field distributions at spin-probe sites in dilute magnetic alloys and find a Lorentzian line shape with a width $\lambda_\perp$ given by

$$\lambda_\perp/\lambda_{\perp 0} = \begin{cases} <|S_z|>_{th} & \text{(quasi-static limit)} \\ <S_z>_{th} & \text{(rapid limit)} \end{cases}, \quad (2)$$

where $\lambda_{\perp 0}$ denotes the dilute-limit dipolar coupling and the brackets refer to a thermal average of the Z component of spin S. This can be generalized in cases where the impurity spins possess randomly distributed values of $<S_z>_{th}$, as discussed in Ref. 8.

In Fig. 2 we compare our transverse-field relaxation rates $\lambda_\perp$ to the linewidth computed using the WW coupling scheme. The quantity $<S_z>_{th}$ is given by (1) a uniform mean-field model, and (2) the measured magnetization data of Star et al.[11] We used $g_{eff} = 2$ because the induced conduction-electron polarization cloud about the manganese spins is comparable to the average manganese-manganese spacing, thus giving rise to a uniform magnetization density that does not contribute greatly to the spread in local fields sensed by the muon. For $T \gtrsim 1.5\ T_c$ both the mean-field model and the magnetization data give excellent fits to $\lambda_\perp$. This is in contrast to the spin-glass *Pd*Mn (7 at.%) discussed below.

Below T_c, however, the homogeneous mean-field model overestimates both $\lambda_\perp$ (Fig. 2) and the zero-field inhomogeneous linewidth $a(T)$ (Fig. 3). These data therefore are compared to the infinite-range mean-field Ising model of Sherrington and Kirkpatrick (SK).[12] In spite of a great deal of theoretical work, this is the only model that explicitly accounts for the disorder in a random magnet. In the SK model, impurity spins ($S_i = \pm 1$) are coupled by random interactions with mean and variance given by J_0/N and J^2/N, respectively. Here N is the number of spins and $J_0 = k_B T_c$. Figures 2 and 3 show that the SK model yields a better description of both the zero- and transverse-field ferromagnetic linewidths than does the mean-field model. The "shortfall" in μSR linewidths in the ferromagnetic state is thus qualitatively explained in the SK model by including antiferromagnetic coupling ($J_0/J = 1.1$).

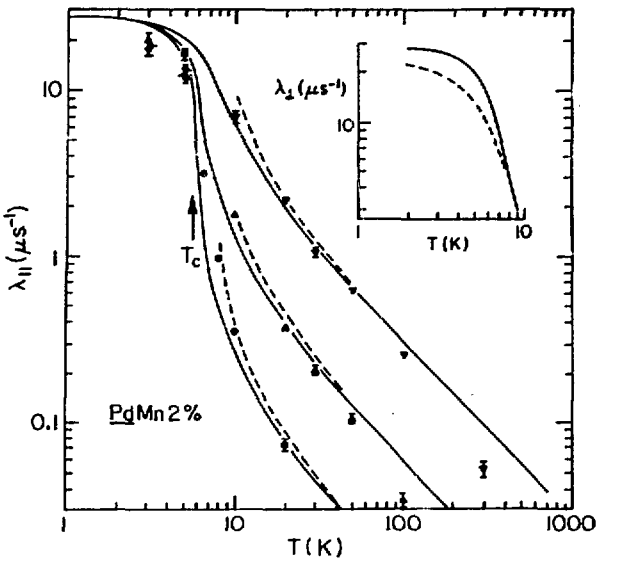

Fig. 2.
Temperature and field dependence of the transverse μ^+ relaxation rate $\lambda_\perp(H,T)$ in Pd + 2.0 at.% Mn.
Circles: $H = 200$ Oe,
Upright triangles: $H = 1$ kOe,
Inverted triangles: $H = 5$ kOe.
The dashed curves were obtained from susceptibility data. The solid curves are obtained from the uniform mean-field model. The inset shows the temperature dependence of $\lambda_\perp$ in the SK model with $H = 5$ kOe.
Dashed curve: $J_0 = 5.8$ K, $J_0/J = 1.1$,
Solid curve: $J_0 = 5.8$ K, $J = 0$.

The muon spin-lattice relaxation rate $\lambda_\parallel$ is shown in Fig. 4. The data show a sharp cusp in the zero-field $\lambda_\parallel$ at $T = T_c$ that is completely destroyed by a 5-kOe applied field. This cusp presumably is due to critical spin fluctuations; the broad temperature range is larger than usually observed in ordered ferromagnets, however. Similar results are seen in neutron-scattering data on ferromagnetic *Pd*Mn.

Raman-magnon scattering[13,8] can explain the order of magnitude of $\lambda_\parallel$ well below T_c, as shown in Fig. 4. This is in contrast to spin-glass *Ag*Mn where the observed $\lambda_\parallel$ at $T \sim T_g/2$ are almost two orders of magnitude larger than estimates obtained from simulated low-temperature magnon spectra. In ferromagnetic *Pd*Mn there appears to

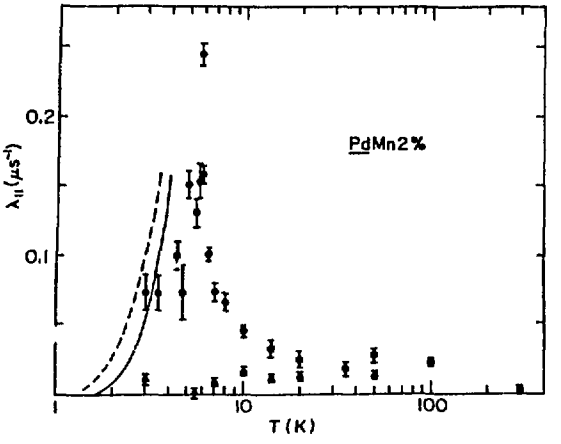

Fig. 3.
Temperature dependence of the zero-field μ^+ quasi-static field distribution width $a(T)$ (in frequency units) in Pd + 2.0 at.% Mn.
Solid curve:
SK model with $J_0 = 5.8$ K, $J_0/J = 1.1$,
Dashed curve:
SK model, $J_0 = 5.8$ K, $J_0/J = 1.5$,
Dash-dot curve:
Homogeneous mean-field model, $S = \frac{5}{2}$.

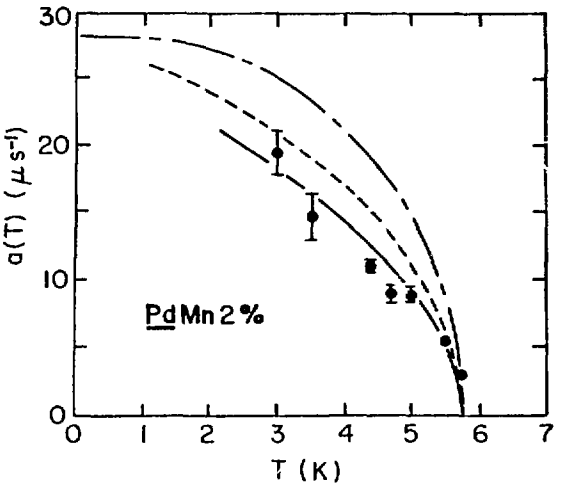

Fig. 4.
Temperature dependence of the μ^+ spin-lattice relaxation rate in Pd + 2.0 at.% at zero field (circles) and 5 kOe (triangles). The curves are predictions of the two-magnon (Ramon) scattering mechanism (see text).
Solid curve:
Anisotropy energy $\hbar\omega_A = 0.3\, k_B T_c$.
Dashed curve:
$\hbar\omega_A = 0.2\, k_B T_c$.

be no additional relaxation mechanism caused by the random nature of the spin system.

Spin-Glass *Pd*Mn (7 at.%)

The main goal of this is to measure the temperature and field dependence of both the quasi-static local-field distribution at the muon site and the muon's dynamic spin-lattice relaxation. Theories of linewidths and relaxation mechanisms in dilute alloys have been used to infer features of the impurity spin configuration. Comparisons with ferromagnetic *Pd*Mn (2 at.%), discussed above, are useful to show how the difference in magnetic ordering brought about by a change in concentration influences microscopic properties.

Figure 5 shows measured transverse-field exponential relaxation rates $\lambda_\perp$ for applied fields of 200 G, 1 kG, and 5 kG. Measured spin-lattice relaxation rates (discussed below) indicate that the nonsecular contribution to $\lambda_\perp$ is small. Thus the rates shown in Fig. 5 represent only the quasi-static field distribution in *Pd*Mn (7 at.%).

The observed paramagnetic susceptibility in a *Pd*Mn (5-at.%) sample is well described by a $g = 2$, $S = \frac{5}{2}$ Curie law for $T \gtrsim 3\ T_g$ and low field.[14] Using this Curie law for $\langle S_z \rangle_{th}$ in Eq. (2) gives the lines shown in Fig. 5. At low temperatures, we simulate the spin-glass state by assuming spins to be quasi-static and equally distributed among the $2S + 1$ M_S states in calculating the order parameter $\langle |S_z| \rangle_{th}$. Equation (2) then gives the high-field frozen-spin linewidth $(\lambda_\perp)_{frozen} = 57.1\ \mu s^{-1}$. A concentration of 7 at.% is not ordinarily considered to be in the dilute limit, so we have calculated a polycrystalline-averaged line shape numerically; the result differs in width from the WW result by no more than 7%.

The discrepancy in Fig. 5 between the $\lambda_\perp$ data and the WW prediction using a Curie law well above T_g is not understood. Similar data on the disordered ferromagnet *Pd*Mn (2 at.%) show very good agreement with the WW result. Since our numerical work indicates that the WW result should still be valid at this higher concentration, we conclude that the observed discrepancy is due to the spin-glass ordering and is present for T well above T_g. Transverse-field μSR results in spin-glass *Ag*Mn show an increase above the WW result, however, to at least 10 T_g.

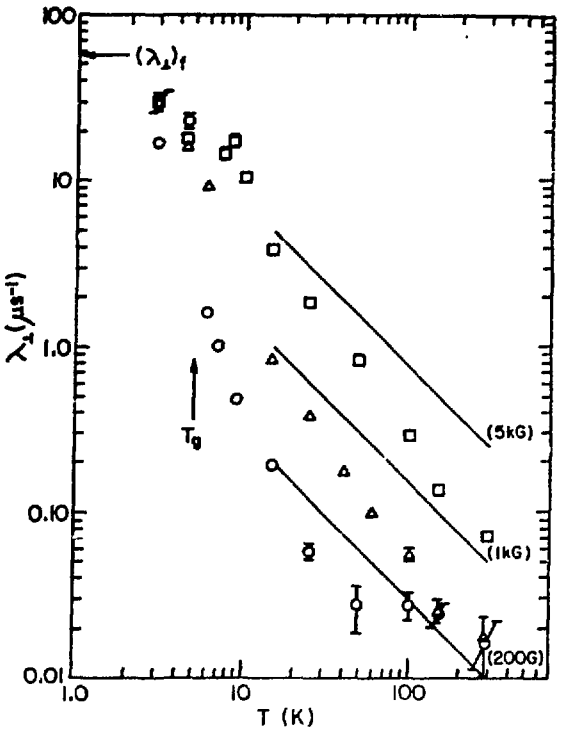

Fig. 5.
Temperature and field dependence of the transverse muon relaxation rate $\lambda_\perp$ in *Pd*Mn (7 at.%).
Circles: 200 G,
Triangles: 1 kG,
Squares: 5 kG.
The solid lines are from Eq. (2) using a Curie law for $<S_z>$; $(\lambda_\perp)_f$ is the frozen-spin rate.

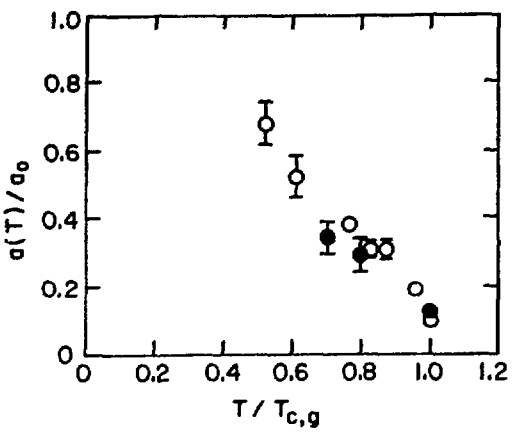

Fig. 6.
Reduced temperature dependence of the zero-field quasi-static field distribution width $a(T)$, normalized to the theoretical zero-field frozen rate a_0.
Open circles:
***Pd*Mn (2 at.%), $a_0 = 28\ \mu s^{-1}$, $T_c = 5.8$ K.**
Filled circles:
***Pd*Mn (7 at.%), $a_0 = 85\ \mu s^{-1}$, $T_g = 5$ K.**

The zero-field muon-relaxation function[7] allows a separation between the quasi-static field distribution of width $a(T)$ and relaxation from dynamic spin-lattice relaxation (rate $\lambda_\parallel$). In zero-applied field the WW result is no longer valid, however, because all three components of the local-field distribution contribute to the muon relaxation. Including this effect,[16] one obtains the zero-field frozen-spin linewidth $a_0 = 85\ \mu s^{-1}$ for *Pd*Mn (7 at.%). The temperature dependence of $a(T)$, normalized by a_0, shows a temperature dependence similar to ferromagnetic *Pd*Mn (2 at.%), as shown in Fig. 6. Thus the development of a static field distribution is independent of the character of the magnetic ordering.

Figure 7 presents measured muon-spin-lattice relaxation rates in zero and applied longitudinal fields above and below T_g. Above T_g the relaxation was fit to the "root exponential" form[7] appropriate for rapidly fluctuating (paramagnetic) spins in a dilute alloy. Fits of the data to a simple exponential form for $G_z(t)$ yield a similar χ^2 value, so that we have not explicitly demonstrated the root exponential form. Below T_g we expect that fluctuations will remain rapid, since this has been observed by μSR in spin-glass *Ag*Mn (Ref. 7). Thus a root exponential decay of the dynamical component of the relaxation function was used to fit the low-temperature data for $\lambda_\parallel$.

The peak in the zero-field spin-lattice relaxation rate at T_g is interpreted as being due to a change in the power spectrum of manganese spin fluctuations near the glass transition. Note that a relaxation mechanism is still effective near T_g in an applied field of 5 kG, whereas in ferromagnetic *Pd*Mn (2 at.%) an applied field of 5 kG completely suppresses the fluctuation-induced relaxation.

At temperatures well below T_g, spin-lattice relaxation presumably is due to spin wave-like excitations of the ground state.[17] Walker and Walstedt[18] have computed the spectrum of excitation frequencies numerically for a

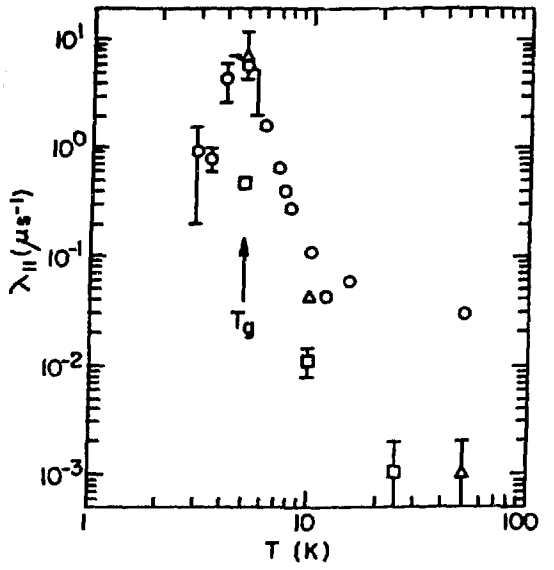

Fig. 7.
Temperature and field dependence of the muon-spin lattice relaxation rate in spin-glass *Pd*Mn (7 at.%).
Circles: Zero field,
Triangles 200 G,
Squares: 5 kG.
Fitting functions used are described in Ref. 7.

realistic model of a ground state of a *Cu*Mn spin glass. These excitations are localized (nonpropagating) modes of the linearized equations of motion. A similar calculation[19] for spin-glass *Pd*Mn (10 at.%) has shown a more complicated three-peak structure for the excitation spectrum, with the mean spectral weight at a frequency $\sim 5 \times 10^{12}\ s^{-1}$. Because these fluctuations are much too fast to cause depolarization through the dipolar interaction in the lifetime of the muon, the observed relaxation must be due to some other (other than WW) lower frequency component of the excitation spectrum.

Recent analytic theories of spin-wave excitations in spin glasses predict that small k magnons can propagate through the system with a dispersion relation linear in k (Ref. 20). Further evidence for propagating modes has been seen in recent computer simulations.[21] These excitations are at frequencies lower than the localized modes and may be responsible for the relaxation observed at low temperatures. Future zero-field μSR studies in spin glasses at lower temperatures may provide useful data on relaxation for comparison with these theories.

In conclusion, the transverse-field relaxation rate $\lambda_{\perp}$ in *Pd*Mn (7 at.%) is not proportional to the observed Curie law magnetization for temperatures as high as 100 K (20 T_g), where the onset of muon diffusion makes interpretation of $\lambda_{\perp}$ difficult. This result is especially surprising because $\lambda_{\perp}$ in ferromagnetic *Pd*Mn (2 at.%) is proportional to a Curie-Weiss magnetization over a wide temperature range, indicating that the observed reduction in $\lambda_{\perp}$ below the Curie law prediction may be a high-temperature precursor of the spin-glass phase. We know of no satisfactory explanation for this effect nor for the increase in $\lambda_{\perp}$ above the measured magnetization in spin-glass *Ag*Mn (1.6 at.%).

In zero field we observe the onset of a quasi-static field distribution below T_g with a similar temperature dependence to that observed in *Pd*Mn (2 at.%). Spin-lattice relaxation near T_g shows a strong cusp, indicating a change in the spectrum of manganese-spin fluctuations. These fluctuations continue to induce relaxation in a large applied field, in contrast to *Pd*Mn (2 at.%).

REFERENCES

1. D. E. MacLaughlin, L. C. Gupta, D. W. Cooke, R. H. Heffner, M. Leon, and M. E. Schillaci, Phys. Rev. Lett. 51, 927 (1983).

2. S.-K. Ma, *Modern Theory of Critical Phenomena* (Benjamin, Reading, Massachusetts, 1976), pp. 442-444.

3. H. Sompolinsky and A. Zippelius, Phys. Rev. Lett. 47, 359 (1981); Phys. Rev. B 25, 6860 (1982); and J. Phys. C 40, L1059 (1982).

4. H. Alloul, S. Murayama, and M. Chapellier, J. Magn. Magn. Mater. 31-34, 1353 (1983).

5. J. Souletie and R. Tournier, J. Phys. (Paris) Colloq. 32, C1-172 (1971).

6. H. A. Zweers and G. J. van den Berg, J. Phys. F 5, 555 (1975); and B. R. Coles, H. Jamieson, R. H. Taylor, and A. Tari, J. Phys. F 5, 565 (1975).

7. R. H. Heffner, M. Leon, M. E. Schillaci, D. E. MacLaughlin, and S. A. Dodds, J. Appl. Phys. 53, 2174 (1982).

8. S. A. Dodds, G. A. Gist, D. E. MacLaughlin, R. H. Heffner, M. Leon, M. E. Schillaci, G. J. Nieuwenhuys, and J. A. Mydosh, Phys. Rev. B 28, 6209 (1983).

9. R. H. Heffner, M. Leon, M. E. Schillaci, S. A. Dodds, G. A. Gist, D. E. MacLaughlin, J. A. Mydosh, and G. J. Nieuwenhuys, in Proc. of the 29th Magnetism and Magnetic Materials Conf., Pittsburgh, Pennsylvania, 1983, to be published in J. Appl. Phys.

10. R. E. Walstedt and L. R. Walker, Phys. Rev. B 9, 4587 (1974).

11. W. M. Star, S. Foner, and E. J. McNiff, Phys. Rev. B 12, 2690 (1975).

12. D. Sherrington and S. Kirkpatrick, Phys. Rev. Lett. 35, 1792 (1975); and S. Kirkpatrick and D. Sherrington, Phys. Rev. B 17, 4384 (1978).

13. E. A. Turov and M. P. Petrov, *Nuclear Magnetic Resonance in Ferro- and Antiferromagnets* (Halsted Press, New York, 1972), p. 93.

14. B. R. Coles, H. Jamieson, R. H. Taylor, and A. Tari, J. Phys. F 5, 565 (1975).

15. J. A. Brown, R. H. Heffner, T. A. Kitchens, M. Leon, C. E. Olsen, M. E. Schillaci, S. A. Dodds, and D. E. MacLaughlin, J. Appl. Phys. 52, 1766 (1981).

16. A. T. Fiory, Hyperfine Interactions 8, 777 (1981).

17. D. Beeman and P. Pincus, Phys. Rev. 166, 359 (1968); and A. H. Mitchell, J. Chem. Phys. 27, 17 (1957).

18. L. R. Walker and R. E. Walstedt, Phys. Rev. B 22, 3816 (1980).

19. W. Y. Ching, D. L. Huber, and B. H. Verbeek, J. Appl. Phys. 50, 1715 (1979).

20. B. I. Halperin and W. M. Saslow, Phys. Rev. B 16, 2154 (1977); W. M. Saslow, Phys. Rev. B 22, 1174 (1980); K. H. Fischer, Z. Phys. B 39, 37 (1980); and S. E. Barnes, J. Phys. F 11, L249 (1981).

21. D. L. Huber, W. Y. Ching, and M. Fibich, J. Phys. C 12, 3535 (1979).

Fusion Materials Neutron Irradiations (Exp. 545, Radiation Effects Facility)

(Los Alamos, Arizona State Univ.)
Spokesman: R. D. Brown (Los Alamos)

Toroids wound from strips of the soft magnetic alloys Mumetal (crystalline) and 2605S-3 (amorphous) were neutron irradiated at the LAMPF Radiation-Effects Facility. The initial magnetic permeability values for both materials decreased during irradiation. The permeability of the Mumetal decreased more rapidly than that for the amorphous alloy, resulting in the 2605S-3 having the higher permeability for neutron fluences exceeding about 3×10^{21} n/m^2. At the beginning of the irradiation the Mumetal had permeability of 23 000 and the 2605S-3 had permeability of 5000. Four months later, after irradiation to 2×10^{23} n/m^2, the permeability of the Mumetal approached unity, whereas that for the 2605S-3 was about 2000.

We have reported similar results for a comparative irradiation of Permalloy and the amorphous alloy 2605S-3 (Ref. 1). For both the crystalline Mumetal and the amorphous 2605S-3, the drop in permeability was very rapid initially, followed by a slow decrease that appeared to continue to the maximum fluence.

A quantitative analysis of the permeability decay curves was made using the direct spectrum analysis method,[2] which is capable of determining a good approximation of the spectrum of relaxation constants for a process involving first-order kinetics, without requiring initial assumptions as to the nature of the spectrum. Analysis of our data in terms of a relaxation fluence (analogous to a relaxation time) showed that both the Mumetal and the amorphous 2605S-3 alloy exhibited virtually identical spectra. Each spectrum consisted of two discrete peaks, one centered at a fluence of about 1×10^{21} n/m^2 and the second at a fluence of about 4×10^{22} n/m^2. The two widely separated peaks provide evidence for the permeability decay occurring in two stages, each associated with a particular mechanism.

Our interpretation of the data[3] assumes that the first stage is governed by short-range ordering because of excess point defects introduced during the irradiation, whereas the second stage is dependent on agglomerations of these point defects, such as dislocation loops and voids that pin the magnetic domain walls. The finding that the relaxation fluences are virtually identical for the crystalline Mumetal and the amorphous 2605S-3 was surprising. Although it was not totally unexpected that defect agglomerates could pin domain walls, the presence or absence of short-range ordering in amorphous alloys has been the subject of controversy.

Further work is planned to obtain more information on these stages observed during irradiation. The effects of the initial heat treatment on the permeability of several 2605 amorphous alloys will be studied. This alloy system may be suitable, because of its relative stability under irradiation, as a replacement for the present Mumetal toroids used upstream of the beam stop, where radiation damage results in a rapid decay in permeability, requiring frequent replacement.

REFERENCES

R. D. Brown, J. R. Cost, and J. T. Stanley, "Effects of Neutron Irradiation on Magnetic Permeability of Amorphous and Crystalline Magnetic Alloys," to be published in J. Appl. Phys., Suppl. Part 2 (March 1984).

2. J. R. Cost, J. Appl. Phys. 54, 2137 (1983).

3. R. D. Brown, J. R. Cost, and J. T. Stanley, "Irradiation-Induced Decay of Magnetic Permeability of Metglas 2605S-3 and Mumetal," submitted to J. Nucl. Mater.

Muon-Spin-Rotation (μSR) Studies of Dilute Magnetic Alloys (Exp. 571, SMC)

(Los Alamos, Rice Univ., Univ. of California at Riverside, Sandia National Lab.)

Spokesmen: S. A. Dodds (Rice Univ.) and R. H. Heffner and M. E. Schillaci (Los Alamos)

Experimental Program

Experiment 571 is designed to measure muon diffusion in fcc materials other than copper and aluminum. The resulting diffusion data will provide a basis for understanding the apparently anomalous motion of muons in copper, aluminum, and bcc materials. In addition, knowledge of muon mobility is needed to properly interpret data from the other muon-spin-rotation (μSR) experiments being undertaken by our group.

Our muon-diffusion measurements have exploited the impurity-doping technique first applied[1] to μSR at LAMPF. As noted in the previous report,[2] we have extensive data on the field and temperature dependence of the muon depolarization rate in silver, gold, and palladium doped with gadolinium, erbium, and manganese. We have extracted the muon-diffusion rate from these data with a model that treats the muon hopping, muon-impurity interaction, and impurity spin-flip time rather simply.[1,3] This model gives a reasonable account of the observed temperature dependence in the systems studied, but it is not able to account for the magnetic-field dependence of the depolarization rate, as shown by the dashed lines in Fig. 1.

Several features of the simple model have been examined to determine the cause of the problem. We have been able to show that the muon-impurity interaction is weak enough that "strong-collision" effects as seen in NMR[4] are unimportant here. We have also shown that the effective correlation time approximation used in our model yields the same results as a near-exact treatment of the combined muon hopping and impurity spin flipping, at least in the parameter region of interest.

Our next approach was to examine the effect of host or muon-induced electric fields on the impurity relaxation. The simplest case, an axial field gradient, improves the agreement between the model and the data considerably,[5] as shown by the solid lines in Fig. 1.

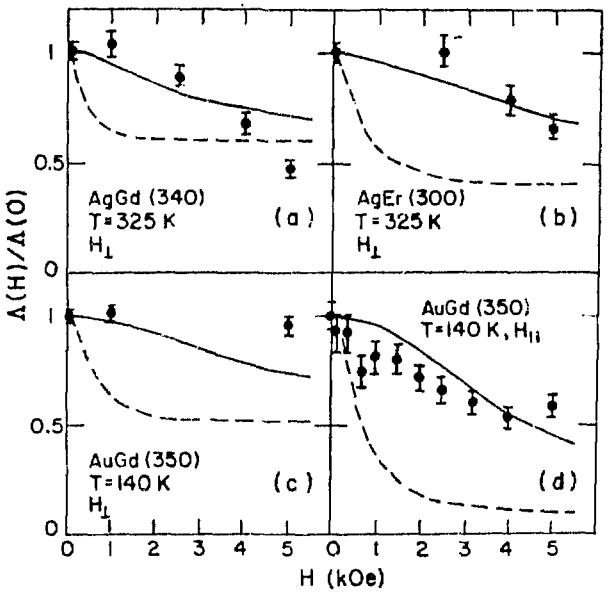

Fig. 1.
Magnetic-field dependence of muon depolarization rates for the alloys listed. Rare-earth concentrations are in parts per million (atomic). Data are shown for both transverse ($H_\perp$) and longitudinal ($H_\parallel$) applied fields. The curves are fits to the two models described in the text.

At the temperatures of interest, all of the crystal-field levels are populated, so the cubic fields of the host must be considered together with the axial field due to the muon. We have reformulated a theory[6] for spin dynamics of a multilevel system and have carried out numerical calculations for erbium [$J = (^{15}/_{2})$] in silver and gold. To the best of our knowledge, this is the first calculation that treats a high-spin system in an unsymmetric electric-field environment with arbitrary applied magnetic field. Preliminary results show that the muon-induced axial field has a profound effect on the erbium fluctuation rate that leads to an enhanced depolarization rate for the muon. Yet to be done is incorporating this model into our hopping model, so that muon diffusion and muon-ion interaction are treated together.

Theory: Calculaton of Muon Polarization Function

P. F. Meier (Univ. of Zürich) and M. E. Schillaci (Los Alamos)

The spin dynamics of a muon localized at an interstitial site interacting with nearest neighbor nuclear spins is being investigated. Kubo and Toyabe[7] studied the spin-relaxation process in zero or weak external magnetic field by approximating the influence of the surrounding nuclear spins by a random local field.

For a static muon in zero external field the muon polarization decreases from its initial value of unity, passes through a minimum, and smoothly reaches a value of one-third asymptotically with time. Recently, Celio and Meier[8,9] reported on exact numerical calculations for $N = 4$ nuclear spins with angular momentum $J = \frac{1}{2}$ and $J = 1$, and for $N = 6$ with $J = \frac{1}{2}$. Both dipolar and quadrupolar interactions with the muon were incuded. Their principal result is that the muon polarization function continues to oscillate with time, contrary to the smooth, asymptotic behavior predicted by the Kubo-Toyabe theory.

The critical limitations in these investigations are the time and memory required to diagonalize very large Hamiltonian matrices. Using a Cray-1 computer at Los Alamos, we were able to study $N = 4$ nuclear spins with $J = \frac{3}{2}$, which corresponds, for example, to a muon localized in a tetrahedral site in copper. Dipolar and quadrupolar interactions between the nuclei and the muon were included, and applied fields in transverse and longitudinal orientations, as well as zero field, were treated. Including isotope effects (for example, copper) and internuclear dipolar interactions had little effect on the results.

Recently, Holzschuh and Meier[10] gave an analyti... zero-field approximation for $J = \frac{3}{2}$ and $N = 4,6,8$ corresponding to tetrahedral, octahedral, and cubic arrangements, respectively. For $J = \frac{3}{2}$, $N = 4$, their solution is in good agreement with our exact numerical result. Also, they find that with increasing N the oscillations of the muon polarization function are reduced and the minimum is shifted to shorter times.

We have started numerical calculations for $N = 8$, $J = \frac{1}{2}$ and have begun preparations for $N = 6$, $J = 1$, corresponding to cubic and octahedral arrangements, respectively. The dimension of the state space is given by $2(2J + 1)^N$; consequently, we are nearing the 4×10^2 word capacity of our largest Cray-1. In some cases, group-theoretical reduction techniques can be applied to reduce the maximum dimension; however, for zero external field, the approximation scheme given in Ref. 10 is better suited for studying larger systems (for example, the effects of next-nearest neighbor nuclear spins).

REFERENCES

1. J. A. Brown, R. H. Heffner, R. L. Hutson, S. Kohn, M. Leon, C. E. Olson, M. E. Schillaci, S. A. Dodds, T. L. Estle, D. A. Vanderwater, P. M. Richards, and O. D. McMasters, Phys. Rev. Lett. 47, 261 (1981).

2. "Progress at LAMPF, January–December 1982," J. C. Allred, Ed., Los Alamos National Laboratory report LA-9709-PR (March 1983), p. 70.

3. M. E. Schillaci, R. L. Hutson, R. H. Heffner, M. Leon, S. A. Dodds, and T. L. Estle, Hyperfine Interactions 8, 663 (1981).

4. S. P. Vernon, P. Thayamballi, R. D. Hogg, D. Hone, and V. Jaccarino, Phys. Rev. B 24, 3756 (1981).

5. M. E. Schillaci, R. H. Heffner, R. L. Hutson, M. Leon, D. W. Cooke, S. A. Dodds, P. M. Richards, D. E. MacLaughlin, and C. Boekema, Proc. of the Third Int. Conf. on Muon Spin Rotation, Tokyo, Japan, April 1983 (to appear in Hyperfine Interactions).

6. K. W. Becker, P. W. Fulde, and J. Keller, Z. Phys. B 28, 9 (1977).

7. R. Kubo and T. Toyabe, in *Magnetic Resonance and Relaxation*, R. Blinc, Ed. (North-Holland, Amsterdam, 1966).

8. M. Celio and P. F. Meier, Phys. Rev. B 27, 1908 (1983).

9. M. Celio and P. F. Meier, "Exact Calculation of the Muon Polarization Function," Yamada Conference on Muon Spin Rotation and Associated Problems, Shimoda, Japan, April 1983 (to be published in Hyperfine Interactions).

10. E. Holzschuh and P. F. Meier, "Zero-Field Spin Relaxation of Positive Muons," University of Zürich preprint (1983).

Muon-Spin-Rotation Study on Muon Bonding and Motion in Select Magnetic Oxides (Exp. 639, SMC)

[Los Alamos; Texas Tech Univ.; Univ. of Wyoming; Atomic Energy Research Establishment (AERE), Harwell, United Kingdom; Technical Univ., Eindhoven (NL)]

Spokesmen: C. Boekema (Texas Tech Univ.), D. W. Cooke (Los Alamos), and A. B. Denison (Univ. of Wyoming)

Muon-spin-rotation (μSR) studies on select magnetic oxides are nearing completion. Detailed knowledge and better understanding of muon behavior, especially bonding and localization, have been obtained.[1,2] These results are based primarily on work done at LAMPF, with contributions from experiments at SIN to complete the overall picture.

Our most recent efforts were directed to the sesquioxides, with emphasis on Al_2O_3 and V_2O_3. In addition to these experiments, efforts have been made to integrate the μSR data, taken on a larger set of (magnetic) oxides, into a consistent model of the muon in oxides.

Al_2O_3 (corundum) is a structure model for a set of magnetic oxides studied or currently under study [α-Fe_2O_3, Cr_2O_3, $FeTiO_3$ (Ref. 3), and V_2O_3]. This diamagnetic material has been examined with μSR to see if the muon behaves in a similar manner in the nonmagnetic host as it does in magnetic crystals of the same corundum structure. This question carries two aspects: (1) do we see free muon-like behavior, or is muonium (also) formed, as has been reported earlier[4]; and (2) if a μ-oxygen complex exists, what can we say about its mobility in these materials, particularly at low temperatures?

In zero-field measurements recorded between 50 and 200 K, a weak μSR signal is seen with an asymmetry of 0.04 and a constant relaxation rate of 0.05 μs^{-1}. This weak signal could be identified as the "1/3 component" of muon polarization, indicating strongly that the muon is localized. Above 200 K the signal disappears because of increasing relaxation effects, probably muon diffusion; below 50 K the signal strength increases as a result of an increasing asymmetry. Because ^{27}Al nuclear moments will fluctuate slower at decreasing temperatures, the muon polarization at short times (0.2-1.0 μs) therefore will increase.

Of special interest is the transverse field dependence of the relaxation rate (λ) at 5 K, illustrated in Fig. 1; λ decreases very rapidly by a factor of 2 for the first 100 G of externally applied field, then at higher fields remains constant within experimental error. This figure may be compared with Fig. 2 of Ref. 4, where the longitudinal field dependence of the muon polarization is depicted. A striking similarity can be seen.

From these experimental data we estimate that the effective local fields at the muon site are of the order of 100 Oe and may be caused by the ^{27}Al nuclear moments through superhyperfine effects. Here we assume that the muon is localized at low temperatures, as indicated by zero-field measurements and observed for similarly structured magnetic oxides.

Vanadium oxide V_2O_3 also possesses the corundum structure and is therefore isostructural with α-Fe_2O_3, $FeTiO_3$, and Cr_2O_3, which have been recently reviewed.[3] Of main interest is that a metal insulator (MI) as well as a magnetic transition occurs at 150 K. Below this temperature, V_2O_3 is an insulator and is antiferromagnetic, whereas above the transition temperature it is conducting and paramagnetic.

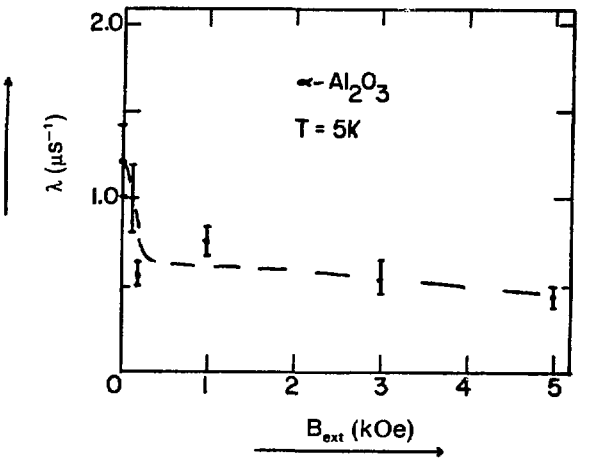

Fig. 1.
The muon-relaxation rate measured at 5 K for a single refined crystal of α-Al_2O_3 as a function of a transverse externally applied field.

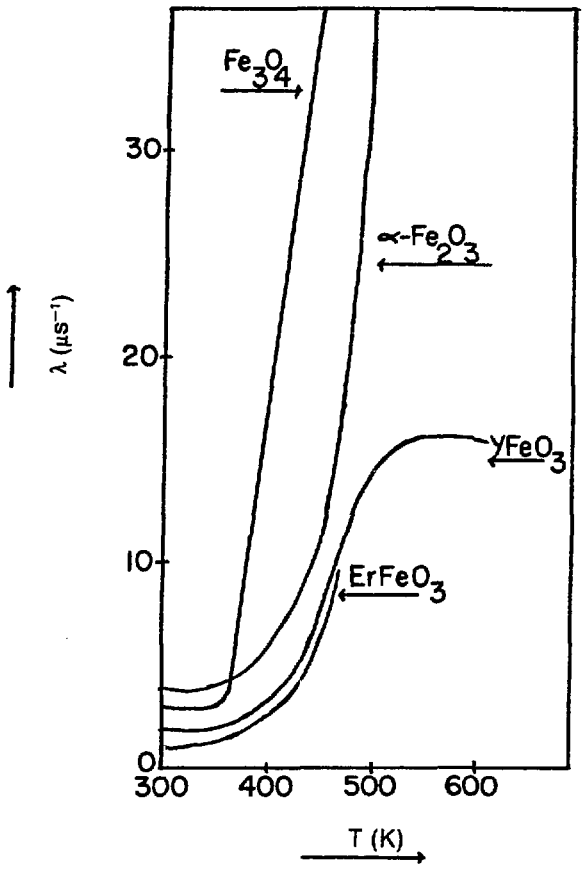

Fig. 2.
The temperature dependences of the relaxation rate (λ) in the temperature region (300-600 K) for the magnetic oxides. For comparison the data have been smoothed. Data are from Refs. 1, 2, and 8. The flattening of the $\lambda(T)$ curve above 500 K for the orthoferrites is due to decreasing magnetization (Ref. 8).

Of additional interest in light of other oxides investigated is the fact that the conduction in V_2O_3 is bandlike, whereas in Fe_3O_4 conduction is most likely due to phonon-assisted electron hopping above the (Verwey) MI transition[5] (the other oxides are insulating). Also, V_2O_3 is an end member of two most interesting mixed sesquioxide systems $(Ti_{1-x}V_x)_2O_3$ and $(V_{1-x}Cr_x)_2O_3$. The former is known because of remarkable spin-glass properties,[6] the latter, for interesting changes in conductive and magnetic properties.[7]

To date the temperature dependences of the μSR frequency and relaxation rate (λ) have been traced. Above the MI transition a strong μSR signal is seen at the free muon frequency with a low Gaussian λ of 0.06 μs^{-1}. Most likely this Gaussian behavior indicates local diffusive behavior. Below the transition temperature a strong signal was seen in zero field at 15 MHz, corresponding to a muon site with an internal field of 1.1 kOe. Presently we are pursuing a study of the phase transition in more detail and trying to determine the muon stop site from crystal-oriented transverse-field measurements.

A consistent picture of the muon behavior in (magnetic) oxides is developing, and a general model based on the collective knowledge of the different oxides appears to be emerging.[1,2] In this examination it is most helpful to consider μSR results from the rare-earth orthoferrites.[8]

Basically, it was found that in $RFeO_3$ the muon localizes near oxygen and engages in a muon-oxygen bond. These results are in agreement with those obtained earlier for α-Fe_2O_3, which showed for the first time that muon-oxygen bonding occurs in oxides and also that long-lived metastable muon states may be present in (magnetic) oxides well below room temperature.[9]

If one compares the muon-relaxation rates as a function of temperature for magnetically and structurally different oxides (α-Fe_2O_3, Fe_3O_4, $ErFeO_3$, and $YFeO_3$), it can be seen (Fig. 2) that the λ increase starts above 360 K. These combined-relaxation data also suggest that the muon is behaving similarly in various magnetic oxides.

Generally, at temperatures below 100 K the muon appears to find itself in several nonequivalent magnetic sites. As proposed by Stoneham,[9] the muon is trapped in a metastable state longer-lived than the muon decay time. Going up in temperature, local diffusion sets in; above 500 K, global diffusion through the whole lattice takes place.

With the chemical and physical muon behavior becoming understood the muon can now be used as a *bona fide* magnetic probe of the sample under investigation. The observation, for instance, of the anomalous behavior of the μSR frequency at 250 K in the Verwey transition temperature region is a good example.[1,2] Moreover, preliminary μSR measurements on V_2O_3 point in the same direction.

REFERENCES

1. C. Boekema, in the Proc. of the Yamada Conf. on Muon Spin Rotation and Associated Problems, Shimoda, Japan, April 1983 (to be published in Hyperfine Interactions).

2. A. B. Denison, Proc. of the 29th Annual Conf. on Magnetism and Magnetic Materials, Pittsburgh, Pennsylvania, November 1983.

3. C. Boekema, A. B. Denison, K. J. Rüegg, J. Magn. Magn. Mat. 36, 111 (1983).

4. E. V. Minaichev et al., Sov. Phys.-JETP 31, 849 (1970).

5. J. M. Honig, J. Solid State Chem. 45, 1 (1982).

6. J. Dumas and C. Schlenker, J. Phys. C 12, 2381 (1979).

7. H. Kuwamuto et al., Phys. Rev. B 22, 2626 (1980).

8. E. Holzschuh et al., Phys. Rev. B 27, 5294 (1983).

9. A. Browne and A. M. Stoneham, J. Phys. C 15, 2709 (1982).

Effects of Superconductivity on Rare-Earth Ion Dynamics in $(Ho_xLu_{1-x})Rh_4B_4$ (Exp. 640, SMC)

(Rice Univ., Los Alamos, and UC, Riverside)

Spokesmen: S. A. Dodds (Rice Univ.), R. H. Heffner (Los Alamos), and D. E. MacLaughlin (Univ. of California at Riverside)

Our previous μSR studies[1,2] in the rare-earth rhodium borides[3,4] $Ho_xLu_{1-x}Rh_4B_4$, for $x = 1.0$, 0.7, 0.35, and 0.0, have revealed a sharp shoulder in the temperature dependence of the muon-spin-lattice relaxation rate at the temperature T_s corresponding to the onset of superconductivity. Here we report zero-field measurements in $Ho_{0.02}Lu_{0.98}Rh_4B_4$, which becomes superconducting at $T_s = 11.3$ K.

Three distinct forms for the normalized muon-spin-relaxation function[1,5] $G_z(t)$ were observed in different temperature regimes (Fig. 1). At 50 K the $G_z(t)$ was found to be well described by the static zero-field relaxation function derived by Kubo and Toyabe,[6] which is appropriate for a time-independent Gaussian distribution of local magnetic fields at μ^+ sites.

The measured width of the field distribution, about 4 Oe, indicates that the μ^+ spin relaxation is caused primarily by μ^+ precession about the host nuclear dipolar fields. As the temperature is lowered, the form of $G_z(t)$ changes, until at 15 K the relaxation function can be approximated by a simple exponential $G_z(t) = \exp(-\lambda_1 t)$ (Fig. 1), where λ_1 is the μ^+ spin-lattice relaxation rate. At $T \leq 11$ K, the form of the relaxation function again changes, exhibiting the two-component form shown in Fig. 1 for $T = 6$ K. These data were fit with the function

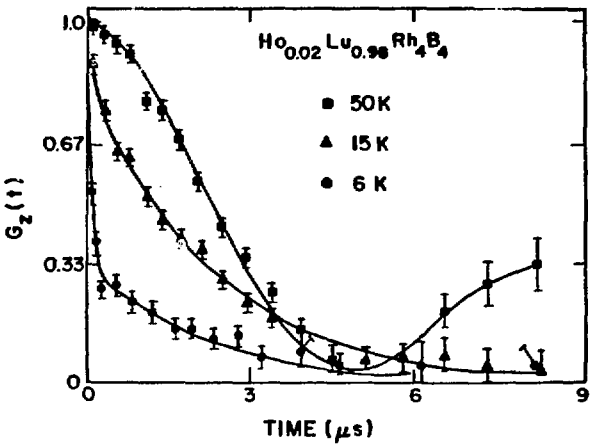

Fig. 1.
Zero-field muon-spin-relaxation function $G_z(t)$ at representative temperatures in $Ho_{0.02}Lu_{0.98}Rh_4B_4$. The curves are fits to the appropriate functions as discussed in the text.

$$G_z(t) = [1 - a]\exp(-\sigma t) + a\exp(-\lambda_2 t)\ , \qquad (1)$$

with $\sigma \gg \lambda_2$. One finds that

(1) σ is essentially independent of temperature, with an average value of $11.5 \pm 0.6\ \mu s^{-1}$;

(2) a is about 0.6 at $T = 11$ K, and falls to one-third for $T \leq 8$ K; and

(3) λ_2 falls exponentially with decreasing temperature below T_s, with an activation energy $\Delta = 9.8 \pm 1.3$ K (Fig. 2).

From these results we conclude that the stochastic motion of the Ho^{3+} moments becomes quasi-static below ~11 K. The value of one-third for a at low temperatures is itself indicative of a random, quasi-static field distribution.[1,5,6] Furthermore, the temperature independence of σ is evidence that the local field $h_L(t)$ reorients completely in a time τ_m such that $\sigma\tau_m \gg 1$, whence $\lambda_2 = 2/(3\tau_m)$ (Refs. 5 and 6).

A two-component form for $G_z(t)$ also can be due to limited-amplitude fluctuations of $h_L(t)$ around a static or quasi-static average value,[7] but in such a case σ increases markedly with decreasing temperature as the fluctuation amplitude decreases. This is not observed in $Ho_{0.02}Lu_{0.98}Rh_4B_4$, and we conclude that $h_L(t)$ reorients completely below 8-10 K.

The value of σ can be estimated using the formalism of Walstedt and Walker[8] for dipolar coupling and the holmium two-level Ising-like ground state discussed

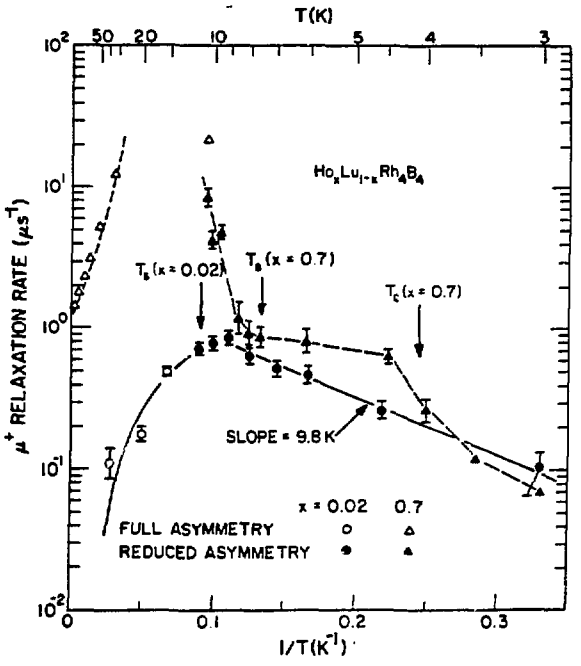

Fig. 2.

Temperature dependence of the zero-field μ^+ spin-lattice relaxation rate in $Ho_xLu_{1-x}Rh_4B_4$, $x = 0.02$ (circles and solid curves) and 0.7 (triangles and dashed curves).

Open symbols: **relaxation rate of the full μ^+ asymmetry (relaxation rate λ_1).**

Filled symbols: **relaxation rate of the reduced-asymmetry component of the μ^+ polarization below ~11 K (relaxation rate λ_2).**

Superconducting (T_s) and ferromagnetic (T_c) transition temperatures are indicated. The curves are guides to the eye.

below, with a magnetic dipole moment of ~10 μ_B (Ref. 9). For randomly oriented holmium moments this calculation yields $\sigma = 6.7\ \mu s^{-1}$, which indicates a significant dipole coupling to the μ^+ and is consistent with identification of the two-component structure of $G_z(t)$ with quasi-static inhomogeneous broadening.

Two basic processes, Korringa scattering of conduction electrons[10] and indirect exchange (RKKY) coupling between Ho^{3+} spins,[11] should be important in dilute magnetic alloys. For the Korringa mechanism the μ^+ spin-lattice relaxation rate λ should be proportional to x^2 at high temperatures, whereas $\lambda \propto x$ for the RKKY process. At 100 K our measured values of λ_1 for $x \geq 0.3$* are proportional to x^2, which indicates that the Korringa mechanism is dominant in this temperature regime. The concentration dependence of λ_1 for $x \geq 0.35$ cannot be determined in the temperature range 11 K < T < 50 K because λ_1 is too large.

We have calculated crystalline-electric-field (CEF) energies and wave functions for rare-earth (RE) 3+ ions in the RE Rh_4B_4 structure by diagonalizing the Hamiltonian for $\bar{4}2m$ point symmetry, using the crystal-field parameters of Dunlap and Niarchos.* For Ho^{3+} the ground and first excited states are each doubly degenerate, with nearly pure $|J_z = \pm 8\rangle$ and $|\pm 7\rangle$ wave functions, respectively. The first excited states occur at $\delta \simeq 55$ K. Allowed transitions from $|\pm 8\rangle$ to $|\mp 8\rangle$ therefore can occur only through small admixtures of different J_z eigenfunctions in the ground and excited states, which are separated by at least 55 K. The slow Ho^{3+}-moment fluctuations at low temperatures then can be accounted for by a combination of the large ground-state isolation and the weakness of $\Delta J_z = \pm 1$ transitions within the ground-state doublet.

Below ~9 K the values of λ_2 for $x = 0.02$ and $x = 0.7$, shown in Fig. 2, are remarkably similar considering the large difference in holmium concentrations. This observation can be understood if the dominant Ho^{3+}-moment relaxation mechanism is again Korringa scattering, as at 100 K. At least one source of difference in the temperature dependence of λ_2 between $x = 0.02$ and $x = 0.7$ is the onset of ferromagnetism below the Curie temperature $T_c = 4.1$ K at the latter concentration.

Below T_s the temperature dependence of λ_2 for $x = 0.02$ indicates an activation energy $\Delta \simeq 10$ K, which is much smaller than the CEF ground-state isolation δ. Since $\Delta \simeq 1.8\ T_s$, interpretation of Δ as a superconducting gap parameter yields a value considerably smaller than the BCS gap parameter $\Delta_{BCS} = 3.5\ T_s$. Such an interpretation is, however, speculative at this time, because it is not clear how the superconducting state could reduce the activation energy for Ho^{3+} fluctuations to a value much less than δ.

*See Ref. 12. The actual parameters used vary somewhat from this reference, and were obtained from B. D. Dunlap, private communication.

REFERENCES

1. C. Boekema, R. H. Heffner, R. L. Hutson, M. Leon, M. E. Schillaci, J. L. Smith, S. A. Dodds, and D. E. MacLaughlin, J. Appl. Phys. 53, 2625 (1982).

2. D. E. MacLaughlin, S. A. Dodds, C. Boekema, R. H. Heffner, R. L. Hutson, M. Leon, M. E. Schillaci, and J. L. Smith, J. Magn. Magn. Mat. 31-34, 497 (1983).

3. B. T. Matthias, E. Corenzwit, J. M. Vandenberg, and E. Barz, Proc. Natl. Acad. Sci. USA 74, 1334 (1977).

4. *Proceedings of the Int. Conf. on Ternary Superconductors*, G. K. Shenoy, B. D. Dunlap, and F. Y. Fradin, Eds. (North Holland, New York, 1981).

5. R. S. Hayano, Y. J. Uemura, J. Imazato, N. Nishida, T. Yamazaki, and R. Kubo, Phys. Rev. B 20, 850 (1979).

6. R. Kubo and T. Toyabe, in *Magnetic Resonance and Relaxation*, R. Blinc, Ed. (North Holland, Amsterdam, 1967), p. 810.

7. R. H. Heffner, M. Leon, M. E. Schillaci, D. E. MacLaughlin, and S. A. Dodds, J. Appl. Phys. 53, 2174 (1982).

8. R. E. Walstedt and L. R. Walker, Phys. Rev. B 9, 4857 (1974).

9. H. R. Ott, L. O. Woolf, M. B. Maples, and D. C. Johnson, J. Low Temp. Phys. 39, 383 (1980).

10. H. Hasegawa, Prog. Theor. Phys. 21, 483 (1959).

11. M. R. McHenry, B. G. Silbernagel, and J. H. Wernick, Phys. Rev. B 5, 2958 (1972).

12. B. D. Dunlap and D. Niarchos, Solid State Commun. 44, 1577 (1982).

Biomedical Research and Instrumentation

Instrumentation

J. D. Doss (Los Alamos)

Ophthalmology

This year has seen significant improvements in both instrumentation and treatment techniques in the thermokeratoplasty program. This work involves using shaped rf fields to thermally shrink the human cornea to alter shape and improve vision. Because the work done in the previous year to increase heat transfer at the corneal endothelium proved successful in animal experiments, human trials were resumed.

Introduction of a "triad" treatment, that is, three symmetric applications around the pupil—have proved very effective, both in shrinkage and, so far, in stability. Several patients have experienced dramatic clinical benefits, which will be observed for long-term stability.

A private corporation is seeking an exclusive license on the two USDOE patents that cover this technology. A version of the ray-trace program LENS has been supplied to the Doheny Eye Institute, University of Southern California, where it is expected to be used to evaluate animal experiments involving modification of the eye.

Hyperthermia

The hyperthermia unit loaned to China has been used to treat seven cases of human brain cancer, with some evidence of beneficial effect in two of the three cases where the highest dose was applied. This program will continue, with treatment of 30 patients planned. Additional instrumentation was supplied to China during 1983, following the initial treatments.

A protocol for treatment[1] of cervical intraepithelial neoplasia (CIN) has been approved and special electrodes have been designed for use at the University of Kansas. The field-calculating software FIELD has been supplied to the United States Environmental Protection Agency office in Las Vegas, Nevada. Work to develop less expensive, more efficient rf sources for hyperthermia continues.

Microwave Dosimetry

Several passive resonant microwave dosimeters[2] have been constructed and tested, in the frequency range from 50 to 1000 MHz. Maximum useful sensitivity is about 10 $\mu W\ cm^{-2}$. A patent[3] will be filed by the USDOE; two private companies are planning to develop the device for commercial production.

Microsurgery

An applicator for microclips used in blood vessel surgery has been developed, in collaboration with the University of New Mexico (UNM) School of Medicine. Initial tests indicate that the device will enable more effective and rapid anastomoses (joining) of small blood vessels. This work has implications for stroke victims, hand surgery, and a variety of related procedures. A joint UNM/USDOE patent is expected to be filed.

REFERENCES

1. C. J. Sternhagen and J. D. Doss, "Combined Radiation Therapy and Localized Current Field Hyperthermia with a 13-MHz Applicator in Head and Neck and Gynecological Cancer Therapy," in the Proc. of the meeting of the Radiation Research Society, San Antonio, Texas, February 28, 1983.

2. J. D. Doss, "Passive Dosimeters for rf and Microwave Fields," accepted for publication in Rev. Sci. Instrum.

3. J. D. Doss, "Multipolar Corneal-Shaping Electrode with Flexible Removable Skirt," U.S. Patent No. 4,381,007, issued April 26, 1983.

Time-of-Flight Isochronous (TOFI) Spectrometer for the Mass Measurements of Nuclei Far from Stability

D. J. Vieira, J. M. Wouter, G. W. Butler (Los Alamos), H. Wollnik (Univ. of Giessen), L. P. Remsberg (Brookhaven), and D. S. Brenner (Clark Univ.)

Introduction

In recent years there has been a rapid increase in our knowledge of the atomic-mass surface far from the valley of β stability.[1,2] However, even with these advances there remain more than 60 neutron-rich nuclei with $A < 70$ for which the only known information is that they are stable with respect to neutron emission. Clearly, more detailed information about these nuclei is essential.

Especially important are the measurements of ground-state atomic masses, because the ground-state mass is one of the most fundamental properties of a nucleus. A comparison of measured masses with those predicted by various mass models not only is a test of these models but is a serious test of our understanding of nuclear interactions in general.

Because the binding energy, and hence the mass, of a nucleus is dependent on the exact details of the nuclear force, its prediction requires an understanding of these details. In a strong sense, an atomic-mass model includes everything that we know about the nuclear force and nuclear interactions. A systematic study of accurately determined masses encompassing a wide variety of nuclei far from β stability would provide a most challenging test of current atomic-mass theories and should yield new insight into the nuclear structure of such exotic nuclei.

During discussions in 1979 with Hermann Wollnik of the University of Giessen concerning the limitations of performing direct mass measurements using a total kinetic-energy, time-of-flight measurement technique, the idea of building a recoil time-of-flight spectrometer was conceived and developed.[3]

Such a spectrometer, which we call the time-of-flight isochronous (TOFI) spectrometer, has vastly improved the ability to make direct mass measurements, overcoming to a large extent the limitations of the above approach. Moreover, this new type of recoil spectrometer has all the advantages of other direct mass measurement approaches, but with the added features of being both fast and universal (that is, all reaction products with half-lives greater than ~2 μs could be studied). Thus, with the development of the TOFI spectrometer, one expects for the first time to be able to systematically and globally investigate the entire nuclear-mass surface up to $A = 70$.

In this report we outline the basic features of the TOFI spectrometer and its associated transport line, discuss the mass measurement capabilities of the system, highlight progress during 1983, and review future plans.

TOFI Spectrometer

The basic principle of the TOFI spectrometer is that it is designed to be isochronous (the TOF is velocity independent). This means that the measured transit time of an ion through the system provides a precise measurement of the mass-to-charge ratio. Because charge is a quantized entity, only moderately accurate measurements (at the 1-2% level) of the energy and free-space time of flight, together with the known momentum acceptance of the spectrometer, are necessary to uniquely define the charge state. Having thus determined the charge, the mass can be deduced from the mass-to-charge ratio as obtained from the measured transit time of the ion through the spectrometer.

Another important feature of the spectrometer is that it can be focused in both energy and angle, thus allowing a long flight path (~13 m) with a relatively large solid angle (2.5 msr) and momentum acceptance (±2%). Because the spectrometer is nondispersive, there is no physical separation between different ions, allowing the simultaneous measurement of many nuclei (especially important are isobaric members with well-known masses that will be used as internal calibration points). Since approval of the funding proposal[4] to DOE, extensive work has gone into improving the design of the spectrometer, and during the last year significant engineering progress has been made (see section under Progress in 1983 in this report, p. 123). Figure 1 shows a sketch of the current system, which consists of a transport line and the TOFI spectrometer.

Through discussions with Karl Brown of SLAC, an improved version of the TOFI spectrometer has been developed that is optically superior to the original design. Applying Brown's ideas of an achromatic system consisting of identical unit cells,[5] the spectrometer is envisioned to consist of four integrated-function dipoles. Each dipole bends the beam by ~81° such that sufficient dispersion is produced to make the overall system isochronous (that is, ions of higher momentum are made to follow a longer flight path than those with lower momentum so that all ions take the same amount of time to traverse the

spectrometer). Edge angle focusing at the entrance and exit boundaries of the magnets is used to produce an intermediate image of the beam spot exactly at the midpoint of the system. Here the beam is dispersed and a momentum collimator defines the momentum acceptance of the spectrometer, after which the dispersion is removed by the last two dipoles.

The beauty of this system is its symmetry. Because of this symmetry, all first- and second-order geometric optical terms are identically zero, and because the system is made to be isochronous, all first- and second-order achromatic optical terms are essentially zero. Beyond second order, the symmetry of the system ensures that higher order terms should be small as well. This has been confirmed in RAYTRACE calculations performed by Harald Enge (MIT), who has consulted with us on the optics of both the spectrometer and the transport line and who has greatly assisted with the engineering and construction details. Thus, to the extent that the magnets follow design, no ray tracing of particle trajectories employing position-sensitive detectors will be necessary, and the mass resolution will be limited only by the timing between the start and stop signals.

In summary, the important features of the spectrometer are

(1) isochronicity;
(2) 1:1 imaging, nondispersive at focus;
(3) acceptance $\Delta\Omega = 2.5$ msr, $\Delta p = \pm 2.5\%$; and
(4) resolution $M/\Delta M = 2000$.

The first two features enable the time-of-flight technique to determine the mass of the ion, using small state-of-the-art timing counters to obtain the ultimate in mass resolution while simultaneously maintaining a large solid angle and momentum acceptance. Incorporating all these features, this unique spectrometer will make possible a series of direct atomic-mass measurements involving a large number of previously unmeasured nuclei that lie far from β stability.

Transport Line

Another important development is the idea of moving the spectrometer out of the LAMPF switchyard into a more accessible area with the reaction products being transported to the spectrometer via a secondary beam line. In the Thin Target Area there has always been provision for a 90° port and a pipe through the switchyard wall that leads to the basement area of the hot cells. This location has recently been vacated with the move of the machine shop to a new building. Working around the constraints of not disturbing the nuclear chemistry rabbit system and the hot water resin filters, we developed the layout shown in Fig. 1 for a secondar beam line connecting to the Thin Target Area scattering chamber. The advantages of incorporating such a transport line into the design include the ability to

(1) accept a larger phase space with better matching to the spectrometer acceptance,
(2) use a dedicated start-time counter to sharpen time-of-flight resolution (and thus mass resolution) independently of the primary beam timing,
(3) eliminate high-yield light ions before they enter the spectrometer, and
(4) work on the system during LAMPF beam operation.

Mass Measurement Capabilities

The TOFI spectrometer will greatly advance direct measurements of atomic masses of numerous light nuclei that lie far from stability. With a mass resolving power of $M/\Delta M = 2000$, an $A = 40$ reaction product would have a linewidth of ~19 MeV (FWHM) and a centroid uncertainty of

$$\sigma_A = \frac{A}{2.35\sqrt{N}} \frac{\Delta M}{M} ,$$

where N is the number of events in the mass line. This centroid uncertainty, which represents the mass measurement accuracy, can be minimized by good mass resolution and large sample size, both of which the TOFI spectrometer and high-intensity LAMPF beam can provide.

In the above case with an accumulation of 10^4 events, a mass accuracy of 80 keV can be achieved. Systematic errors, which also contribute to the overall uncertainty of the determination, are dramatically reduced ($\lesssim$30 keV), as our technique would take advantage of the fact that several members of an isobar (which are resolved in Z by a thin dE/dx detector) with accurately known masses would be measured simultaneously at each mass position. Thus, mass measurement accuracies ranging from 30 keV to 1 MeV are expected, depending on the production rates of these nuclei.

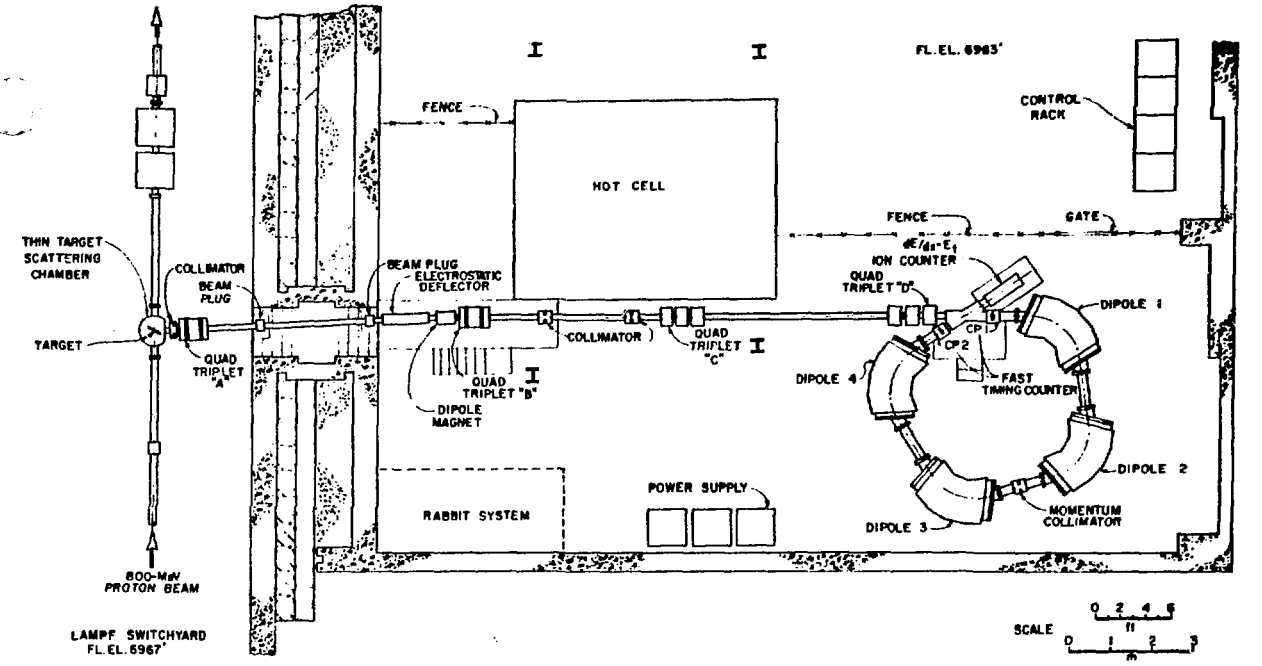

Fig. 1.
Layout of the TOFI spectrometer and transport line.

Scaling from the neutron-rich isotopic yields that we have observed in the nitrogen-through-chlorine region,[6] we estimate that the TOFI spectrometer can measure some 30 new or improved atomic masses with accuracies of 100 keV or better together with some 15 additional new measurements with accuracies ranging between 100 keV and 1 MeV. Outside this region, numerous mass measurements of other neutron-rich nuclei in the argon-to-zinc region appear feasible, where adequate Z resolution can still be obtained. Moreover, the masses of a limited number of neutron-deficient nuclei could also be measured.

In summary, the TOFI spectrometer will be able to measure the masses of from two to five new isotopes per element from $Z = 7$ to $Z = 30$. Development of such a spectrometer at LAMPF will provide a unique opportunity to systematically study the atomic-mass surface throughout the light mass region. Such measurements will permit a critical test for a variety of atomic-mass models, sufficiently constraining these theories to such a degree that significant advances in our understanding of the light nuclear-mass surface can be expected.

Progress in 1983

During the past year the TOFI spectrometer project has made significant progress in three major areas. First, detailed optical studies of the spectrometer and transport line have resulted in final designs. Second, the spectrometer dipoles have been designed, modeled (using the POISSON magnet code), and sent out for fabrication. And third, the first half of the transport line has been engineered and all four quadrupole triplets needed for the line have been refurbished.

In addition, conceptual layouts and engineering details of various other components of the spectrometer and transport line (magnet stands, vacuum tanks, collimators, control system, and beam boxes) have been developed. Finally, the room in which the spectrometer will reside has been prepared and fitted with water-cooling lines.

These undertakings have been carried out with the assistance of several MP-Division groups. In particular, we would like to acknowledge Jim Sims, Don Clark, and Joe Van Dyke (MP-8); Jim Little and Del Kercher (MP-1); Ed Schneider and Harold Ferguson (MP-11); and Dick Werbeck (MP-7). We greatly appreciate this essential LAMPF support.

Future Plans

During the 1984 winter/spring shutdown of LAMPF, the first of half of the transport line will be installed, which will enable the characterization and performance optimization of one of the key transport-line components: the mass-to-charge filter. Moreover, the first half of the transport line will be used to test and develop new detectors needed for the TOFI spectrometer. Finally, once this section of the transport line is operational, the remaining part of the transport line and the spectrometer can be assembled and tested independently of LAMPF beam operations.

The spectrometer dipole components are scheduled for delivery in early summer, at which time they will be assembled and the initial field mapping will take place. After one dipole has been thoroughly tested and optimized, the other dipoles will be trimmed in like fashion. Configuration of the four dipoles into final spectrometer form is planned for the fall when off-line testing using alpha and fission sources will begin. After optimization of the spectrometer performance and the completion of the secondary beam transport line in early 1985, the TOF spectrometer is scheduled to undertake its first on-line experiment.

REFERENCES

1. W. Benenson and J. Nolen, Eds., "Proceedings of the Sixth International Atomic Mass Conference," East Lansing, Michigan, September 1979 (Plenum Press, New York, 1980).

2. "Proceedings of the Fourth International Conference on Nuclei Far From Stability," Helsingor, Denmark, June 1981, CERN report 81-09 (1981).

3. H. Wollnik and T. Matsuo, Int. J. Mass Spectrom. Ion Phys. 37, 209 (1981); and J. M. Wouters, D. J. Vieira, H. Wollnik, H. A. Enge, S. B. Kowalski, and K. L. Brown, in preparation.

4. D. J. Vieira, G. W. Butler, L. P. Remsberg, A. M. Poskanzer, and H. Wollnik, "LAMPF Time-of-Flight Magnetic Spectrometer for Precision Mass Measurements of Very Neutron-Rich Light Nuclei," in the INC-Division proposal to DOE, WPAS-FY84 (1980), pp. 41-73.

5. K. L. Brown, IEEE Trans. Nucl. Sci. NS-26, 3490 (1979); and Stanford Linear Accelerator Center repor. SLAC-PUB-2257 (1979).

6. G. W. Butler, D. G. Perry, L. P. Remsberg, A. M. Poskanzer, J. B. Natowitz, and F. Plasil, Phys. Rev. Lett. 38, 1380 (1977).

Helium-Jet Transport of Fission and Spallation Reaction Products

Exp. 629, AB-Nucchem)

(Los Alamos, Idaho National Engineering Lab., Univ. of Oklahoma)

Spokesmen: M. E. Bunker and W. L. Talbert, Jr., (Los Alamos) and R. C. Greenwood (Idaho National Engineering Lab.)

Introduction

A unique opportunity exists at LAMPF for the production and study of nuclei far from stability. The properties of these highly unstable nuclei are of great interest to theorists, largely because they constitute an important extension of the systematic base of data that is used to test nuclear models and thus to improve our understanding of nuclear forces.

Approximately 3 years ago, advances in helium-jet technology, especially the coupling of helium-jet systems to isotope separators, suggested a relatively simple method of gaining access to the short-lived reaction products producible at LAMPF. The helium-jet technique, as a method for transporting radioisotopes to an isotope separator, has three main advantages:

(1) it provides access to many isotopes of a number of elements that cannot be efficiently extracted for study at any of the present or proposed on-line facilities;

(2) it allows transport of recoil reaction products over distances of many meters in fractions of a second, thus providing access to very short-lived activities; and

(3) it has a relatively low cost.

Except for gaseous products, all elemental species are transported efficiently with a helium-jet system, including the refractory metals such as zirconium, niobium, molybdenum, technetium, palladium, ruthenium, and rhodium. In contrast, the relatively massive targets that must be used (because of low beam currents) at other major on-line separator facilities almost completely retain the refractory-metal radionuclides, making these activities unavailable for study. Use of the thin targets required in the helium-jet method requires a very large incident beam current, of the order of that available at LAMPF, to get a sufficient yield of individual radioisotopes for detailed study.

The helium-jet technique involves stopping the atoms that recoil from the thin targets in aerosol-loaded helium, with subsequent attachment of the radioisotopes to the aerosol particles. The transport of the activity-laden gas from the target chamber to an evacuated collection chamber or mass-separator ion source then takes place through a long, small-diameter capillary, at velocities approaching sonic.

The separated ion beams extracted from the isotope separator would be directed to various experimental devices capable of determining basic nuclear properties such as half-life, spin, nuclear moments, mass, and nuclear structure. The data acquired would have broad application to theories of nuclear matter and such related topics as nucleosynthesis of the elements. Emphasis initially would be on the study of short-lived, neutron-rich fission products. Fission is the only way to reach very neutron-rich nuclei, and among the refractory metals alone it appears that we would have a good chance of identifying and making measurements on at least 150 previously unobserved isotopes, a prospect that would inevitably attract a sizable international user group.

Our studies of helium-jet systems at LAMPF were initiated in FY 1981. These initial experiments, which used a rather crude target chamber and activity collection arrangement, yielded very promising results on the activity transport efficiency for both fission and spallation products. The experiments were carried out with little flexibility; only one target chamber pressure was used, and the beam current and aerosol furnace temperature were not widely varied. Hence, additional experiments were outlined to better investigate the influences of beam-current variations, aerosol furnace temperatures, and target chamber pressures. Since the first experiments employed only NaCl as the aerosol, it was also considered important that another aerosol, namely $PbCl_2$, be studied in the next set of experiments.

For the second set of experiments at LAMPF, a new target chamber design was needed to determine pressure effects on transport efficiency and transport time. With assistance from Los Alamos Technical Associates, a new concept was developed that facilitated changes in chamber thickness for the pressures of interest (to keep the chamber thickness approximately equal to the fission-product range in helium when different pressures were used). Also, analytical calculations were made to predict the transit times through the capillary.

The above preparations were accompanied by a series of discussions with MP-Division staff, which resulted in including a helium-jet target in the plans to reconstruct the beam-stop area of LAMPF and in providing space in the LAMPF staging area for an on-line separator system.

Experimental Results

Much of our experimental effort has been directed toward (1) establishing whether a helium-jet system can be operated successfully when an 800-MeV, ~750-μA proton beam is incident on the target chamber, and (2) establishing whether transport times of <1 s for the reaction products can be achieved. Not until these questions were satisfactorily resolved could we consider that the planned facility is viable.

Because of the great difficulty of using the main beam (Line A) for our feasibility experiments, we chose instead to use the beam available in the Nuclear Chemistry cave on Line B, where the maximum beam current is only about 6 μA. However, since the beam-current densities on Lines A and B are comparable, many of the data obtained on Line B should be representative of what we can expect on Line A. In addition to the on-line LAMPF experiments, we have conducted on-line experiments at the Omega-West Reactor, as well as various bench-type experiments on helium-jet configurations, to study variations in performance caused by changes in critical design and operating parameters.

The second set of LAMPF experiments was performed in November 1982. The operations staff provided an intense, steady, tightly focused beam, which in effect made unnecessary the plans to continue these studies with a future Line A experiment. The major results of the experiments are summarized below.

The target chamber contained two 7.6-cm-diam depleted-uranium foils, of thickness ~10 mg/cm^2, situated facing each other across the chamber volume. At the collection chamber, we used a moving tape collector to rapidly transport collected samples of activity to a well-shielded Ge(Li) gamma-ray detector. The tape collector allowed us to observe short-lived activities, of half-life 1-5 s. The observed counting rates of $^{238}U(p,f)$ products were very high, and in the resulting spectra many of the gamma-ray peaks could not be identified from previously reported studies. The transport efficiencies for all non-gaseous-element activities averaged about 60%, measured absolutely. At higher target chamber pressures (up to 600 kPa), the short-lived activity levels were much higher than those observed at 200 kPa, in keeping with faster transport caused by higher flow rates.

Transit-time measurements were performed for various conditions, with the best result being 230 ms for a target chamber pressure of 500 kPa. The data are shown in Fig. 1. The calculated prediction of this transit time for a capillary length of 22 m is 320 ms. Since the calculation is based on an average flow velocity in the capillary, the experimental result illustrates that the aerosols are "herded" into the central part of the capillary during the flow, thus acquiring a larger-than-average flow velocity. The transit-time measurements provide convincing evidence that activities as short as 300 ms can be studied with the proposed helium-jet on-line mass-separator system.

The Line B current was varied over a range from 1.5 to 6.1 μA. The transport efficiency did not vary over this range. Postexperiment scans of the beam-induced activity in the ^{238}U target foils indicated that at the highest

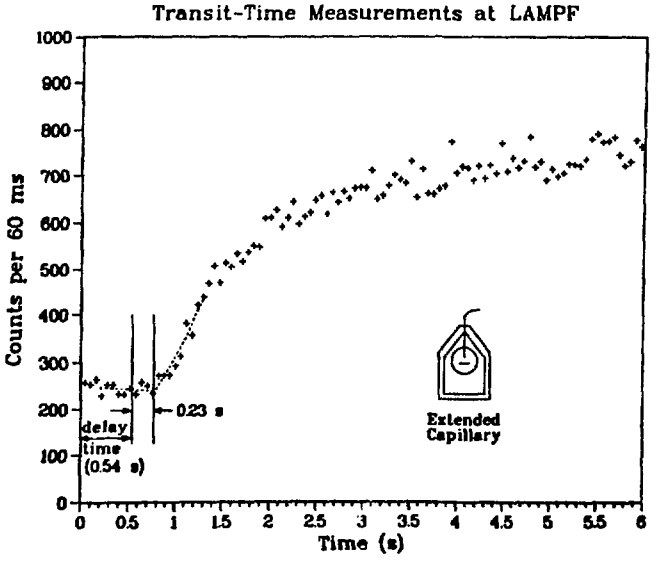

Fig. 1.
Activity transit-time measurements at LAMPF. Beam is turned on at 0 s, and the tape transport delay is 0.54 s. In the target chamber illustration, the beam spot is the horizontal line across the circular target foil.

current, a beam-current density of 45 $\mu A/cm^2$ had been achieved, about twice that expected for Line A. We conclude that the gas-transport system should function satisfactorily in the intense Line A beam.

The highest target chamber pressures used (500 and 600 kPa) resulted in capillary flow for which the Reynolds number exceeded conventional design limits (value of 2200). However, the activity rate continued to increase when these pressures were used. The conclusion was that any turbulence resulting from the flow did little to disturb the transport of the heavy aerosols.

The temperature dependence of the amount of activity transported verified that the activity attaches to the aerosols according to the total aerosol surface area, which had been indicated in unrelated studies at other laboratories for aerosols in the size range employed here (less than 0.1 μm). Samples were collected for electron microscopy, and aerosol size distribution measurements were made on activity-loaded aerosols. The $PbCl_2$ aerosols were seen to be chain-like aggregates with a large resulting surface area.

The availability of a several-micro-amp beam on Line B is too rare to make systematic studies of design parameters to optimize the configuration of a Line A target chamber. We therefore have installed a neutron beam shutter at the Omega-West Reactor to continue these studies and to arrive at an optimum configuration regarding these questions:

1. What will be the effect of using multiple capillaries rather than only one?
2. What design of capillary and helium supply-line placement will result in the highest target-volume sweep rate?
3. Which of the three candidate aerosol materials will provide the highest transport efficiency—NaCl, KCl, or $PbCl_2$?

The test target chamber has a number of possible configurations for gas inlet and exit ports. Preliminary results indicate that, for a circular target chamber (such as would be installed on Line A), a single capillary outlet line, opposite from two inlet lines 90° apart, would provide an optimum configuration. Multiple capillary outlets appear not to improve the flow characteristics, but two inlets provide improved performance over one or three inlets. $PbCl_2$ appears to be the most efficient aerosol for activity transport.

We have developed a series of figures showing the limits of known properties for nuclei and graphically depicting the large regions of nuclei that are unknown and yet have half-lives larger than 300 ms, consistent with the capabilities of the proposed helium-jet system. The illustrations for mass and ground-state spin are shown in Figs. 2 and 3, in which some of the regions that are available only with the use of a helium jet are highlighted. The neutron-rich regions are accessible by fission of ^{238}U, and the neutron-deficient regions are accessible by use of appropriate spallation targets.

The experimental results from the LAMPF experiments have been reported at APS meetings[1-3] and at a

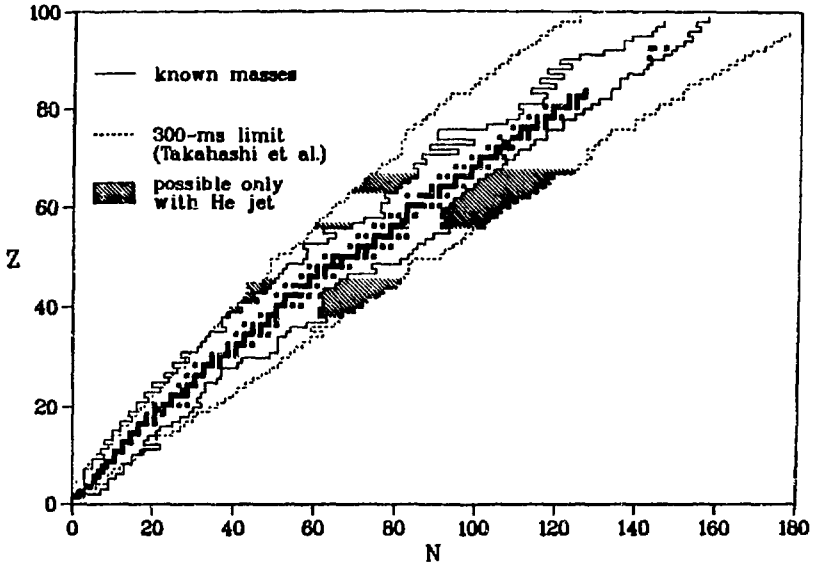

Fig. 2.
Chart of nuclides showing limit of known masses and predicted 300-ms half-life boundaries. The shaded areas are some of the regions where a helium-jet/isotope-separator system can uniquely provide separated isotopes for on-line study.

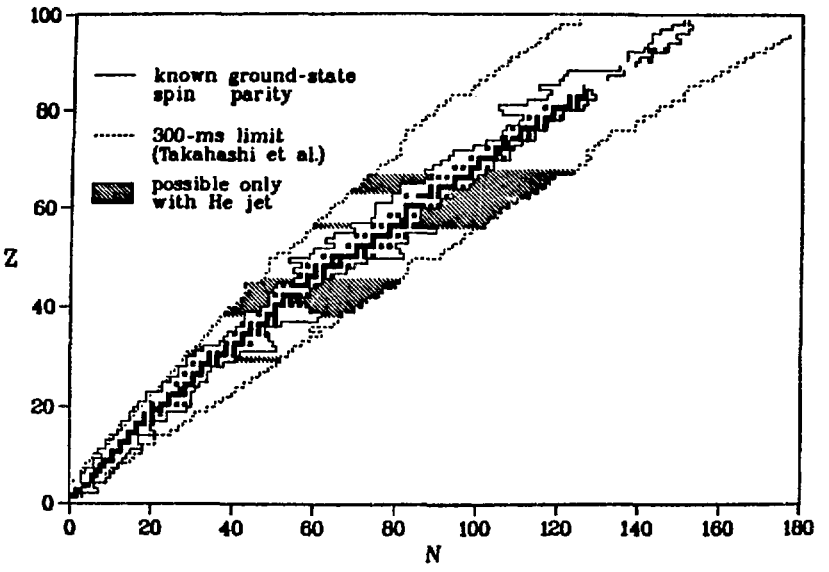

Fig. 3.

Chart of nuclides showing limit of known spin-parity assignments and predicted 300-ms half-life boundaries. The shaded areas are some of the regions where a helium-jet/isotope-separator system can uniquely provide separated isotopes for on-line study.

Nuclear Data Committee Specialists' Meeting on Yields and Decay Data for Fission Product Nuclides.[4] At the Third LAMPF II Workshop, a presentation was made of the results of Exp. 629, and the merits of a helium-jet system at a thin target area at LAMPF II were discussed.[5]

We are confident that the results obtained in Exp. 629 establish the feasibility of a helium-jet activity transport system at LAMPF, and no further beam requests are contemplated. A proposal for funding a helium-jet coupled mass separator at LAMPF is in preparation and will be submitted to the USDOE Division of High Energy and Nuclear Physics in early 1984.

REFERENCES

1. W. L. Talbert, Jr., M. E. Bunker, B. J. Dropesky, J. W. Starner, R. C. Greenwood, R. J. Gehrke, and V. J. Novick, Bull. Am. Phys. Soc. 26, 1156 (1981).

2. W. L. Talbert, Jr., M. E. Bunker, J. W. Starner, S. C. Soderholm, V. J. Novick, and R. F. Petry, Bull. Am. Phys. Soc. 28, 646 (1983).

3. W. L. Talbert, Jr., M. E. Bunker, J. W. Starner, and M. E. Schaffner, Bull. Am. Phys. Soc. 28, 990 (1983).

4. W. L. Talbert, Jr., M. E. Bunker, and J. W. Starner, in "Proceedings of the OECD/NEA Nuclear Data Committee Specialists' Meeting on Yields and Decay Data for Fission Product Nuclides" (October 1983).

5. D. J. Vieira and W. L. Talbert, Jr., in "Proceedings of the Third LAMPF II Workshop," Los Alamos National Laboratory report LA-9933-C (1983), Vol. II, p. 886.

Radioisotope Production

David C. Moody

During 1983 the Medical Radioisotopes Research Group (INC-3) substantially increased the quantity of radioisotopes made available to the nuclear medicine community (22 Ci in 1982 vs 35 Ci in 1983). This increase is tied directly to requests from the nuclear medicine community in general, but also can be linked to major new emphases in our own radiopharmaceuticals research program at Los Alamos, as well as new collaborative research directions.

Isotope Production and Separation

Table I shows radioisotope shipments made during FY 1983. Although this presents a reasonable summary of our production and separation activities, two areas of emphasis during 1983 warrant more detailed discussion (these are grouped under the principal isotopes involved, ^{123}I and ^{67}Cu, in the sections that follow).

Iodine-123

J. W. Barnes, M. A. Ott, K. E. Thomas, and P. M. Wanek

Current brain perfusion agents under development indicate a need for amounts of ^{123}I that far surpass the present supply. To evaluate LAMPF as a potential new source for this radioisotope, we have developed a batch process and are initiating the design and implementation of an on-line ^{123}Xe recovery system that is expected to substantially increase the ^{123}I yield and improve its radionuclidic purity.

At LAMPF, ^{123}I is produced through the decay of ^{123}Xe formed by spallation of cesium in CsCl. The batch process currently in use involves transferring of ^{123}Xe after irradiation to a generator where it is held for an appropriate decay period for the formation of ^{123}I. A proposed on-line process uses the same generator system, but differs from the currently used process in that the xenon is continuously transferred to the generator during irradiation.

The development of a reliable target container and a trouble-free vacuum system for ^{123}I production was reported in the INC-Division Annual Report in 1982. Additional experiments were performed to demonstrate the maximum production capability of the batch process at LAMPF. A target containing 175 g of CsCl was irradiated for 4 h and subjected to a 4-h growth period. The quantity of ^{123}I recovered, corrected to end-of-growth period, was 850 mCi with a 0.4% contamination by ^{125}I. The surface of the void above the salt was washed with dilute NaOH to extract the ^{123}I that resulted from the decay of ^{123}Xe during irradiation. The resultant solution contained 900 mCi of ^{123}I, corrected to the end-of-growth period, with a 0.5% contamination by ^{125}I. The ^{123}I in this last solution represents a proof of principle for the on-line process, but is not a usable product from the batch method because it contains undesirable spallogenic iodine species that were extracted from the surface of the solid CsCl block. However, the sum of the two solutions, 1750 mCi of ^{123}I, represents a conservative approximation of the 8-h production from the on-line operation.

Copper-67

G. Bentley and W. Taylor

A new separation method for ^{67}Cu has been developed, based on a novel electrochemical technique. The product from the separation is free from radioactive contaminants, with the exception of ^{64}Cu, and has minimal quantities of stable materials present as impurities.

The zinc oxide target is dissolved in 3*M* sulfuric acid. Following dissolution of the target material, the solution is transferred to an electrolytic cell that consists of a platinum working electrode, a platinum counter electrode that is isolated from the bulk of the solution by a glass frit, and a silver/silver chloride reference electrode. The electrodes are connected to a potentiostat that maintains a controlled potential at the working electrode. A potential of −0.35 V (all potentials are vs Ag/AgCl) is applied to the working electrode. This potential is sufficiently cathodic to result in the reduction of copper. Zinc, lead or cadmium (both of which are present in the zinc oxide as impurities), or nuclides other than copper formed during the irradiation are not reduced at this potential.

Following deposition of the copper onto the platinum electrode, the electrode is rinsed and the solution is replaced with a clean 0.1*M* sulfuric acid solution. A +0.1-V potential is applied to the working electrode and the copper is stripped off the electrode into the solution. The potential of the working electrode is again changed to −0.35 V and the copper replated onto it. This second plating operation affords additional decontamination of the copper from any zinc that is carried along with the copper product. The sulfuric acid solution is replaced

Table I. Medical Radioisotope Shipments—FY 1983.

Isotope	Institution	Number of Shipments	Amount (mCi)
^{26}Al	Oak Ridge National Laboratory, EPRI	1	0.004
	TOTAL	1	0.004
^{77}Br	George Washington University	4	624
	Johns Hopkins Medical Institute	4	955
	Los Alamos National Laboratory, Group INC-3	8	963
	Los Alamos National Laboratory, Group INC-7	1	1
	TRIUMF	1	50
	University of New Mexico	6	511
	Washington University	2	339
	TOTAL	26	3 443
^{77}Br Estradiol	University of Massachusetts	2	52.6
	Northeastern University	1	3
	University of New Mexico	1	1.36
	TOTAL	4	56.96
^{67}Cu	California State University, Fullerton	4	2 030
	Columbia University	1	5
	Hospital for Sick Children, Toronto, Canada	4	493
	Johns Hopkins Medical Institute	2	148.4
	Los Alamos National Laboratory, Group INC-3	1	2.4
	Los Alamos National Laboratory, Group LS-3	3	30
	Mayo Clinic	1	15
	University of California, Davis	5	1 083
	TOTAL	21	3 806.8
^{59}Fe	Los Alamos National Laboratory, Group INC-11	2	0.0042
	TOTAL	2	0.0042
^{148}Gd	Lawrence Livermore National Laboratory	2	10.8
	TOTAL	2	10.8
^{68}Ge	Brookhaven National Laboratory	1	10.12
	Medical Research Council, Hammersmith Hospital, London	2	11
	Mt. Sinai Medical Center, Florida	1	3
	Oak Ridge Associated Universities	2	11
	Office des Rayonnement Ionisant, France	1	20
	Oak Ridge National Laboratory/DOE	1	253
	University Hospital/The Netherlands	1	5
	University of Chicago	2	4
	University of Liege, Belgium	1	25.4
	Washington University	2	15.06
	TOTAL	14	357.58

Table I. Cont.

Isotope	Institution	Number of Shipments	Amount (mCi)
^{123}I	Benedict Nuclear	1	248
	Medi-Physics	1	31
	TOTAL	2	279
^{172}Lu	VA Hospital, San Diego	2	17.6
	TOTAL	2	17.6
^{173}Lu	Los Alamos National Laboratory, Group INC-11	1	0.8
	Los Alamos National Laboratory, Group INC-7	1	0.16
	TOTAL	2	0.96
^{86}Rb	New England Nuclear, University of South Carolina	1	0.04
	New England Nuclear	1	0.236
	University of South Carolina	1	0.04
	TOTAL	3	0.316
^{82}Sr	Medical Research Council, Hammersmith Hospital, London	4	550
	E. R. Squibb & Sons	5	3 392
	E. R. Squibb & Sons/Mt. Sinai and University of Texas	1	340
	E. R. Squibb & Sons/National Institutes of Health	1	125
	E. R. Squibb & Sons/Sloan Kettering Institute	2	310
	University of California, Donner Laboratory	4	1 031
	University of Liege, Belgium	4	432
	TOTAL	21	6 180
^{158}Tb	Los Alamos National Laboratory, Group INC-11	1	0.010
	TOTAL	1	0.010
^{44}Ti	Los Alamos National Laboratory, Group INC-DO	1	0.013
	TOTAL	1	0.013
^{48}V	California State University, Northridge	4	24.7
	Los Alamos National Laboratory, Group HSE-8	1	0.067
	Los Alamos National Laboratory, Group INC-11	1	0.15
	TOTAL	6	24.92
^{127}Xe	Brookhaven National Laboratory	5	20 820
	TOTAL	5	20 820
^{88}Y	Hybritech Inc., San Diego	1	10
	New England Nuclear	2	16
	VA Hospital, San Diego	1	10
	TOTAL	4	36

Total Shipments: 117
Total Curies Distributed: 35.03

with a 2*M* HCl solution and the copper is again removed from the electrode by applying an anodic potential. The solution is passed through an anion-exchange resin column to remove any remaining zinc contamination. Quantities of ^{67}Cu that have been recovered using this technique have been as large as 5-6 Ci.

Radiopharmaceutical Labeling Research

Our radiopharmaceutical labeling program is made possible by the availability of isotopes from LAMPF. These efforts continue to emphasize the use of silane intermediates to achieve regiospecific labeling with ^{77}Br and ^{123}I. This expertise in no-carrier-added radiochemistry is currently being applied to monoclonal-antibody labeling for radioimmunoimaging and therapy. We are evaluating direct halogenation-coupling reactions of small labeled precursors and complexing agents, such as metallochelates. These areas are briefly outlined below.

Radiohalogen Labeling: Brain and Heart Agents

D. S. Wilbur and Zitta V. Svitra

Brain. Amines play a major role in regulation of brain activities. Although many molecules circulating in the blood cannot cross the blood-brain barrier,[1] a variety of amines can pass readily into the cerebral cavity. The ability of some amines to pass through the blood-brain barrier makes these compounds attractive for radiolabeling. For example, an amine labeled with a gamma-emitting radionuclide might find wide use in single-photon-emission computed tomography (SPECT) for evaluation of the 400 000 hospitalized stroke patients in this country.[2] In addition to the benefits derived from the measurement of cerebral blood flow, radiolabeled amines might be used to measure brain amine metabolism and to quantify amine protein receptors in different regions of the brain. Metabolism of amines and amine receptor concentrations have been implicated in a number of mental disorders,[3] such as schizophrenia, manic-depressive psychoses, and parkinsonism.

Blau and Kung have studied several different amine-containing compounds that were able to cross the blood-brain barrier.[4-6] However, they found that only a few of the compounds stayed in the brain long enough to permit study of the regional blood flow. From their studies they have postulated that the difference in the intracelluiar brain pH (~7.0) and the blood pH (~7.4) is enough to retain some amines in the brain for extended periods of time. In one study[7] they were able to demonstrate that [^{125}I]-iodoxyldiamine, **1**, would stay in the brain for hours ($T_{1/2}$ = 18 h), whereas [^{125}I]-iodobenzylamine, **2**, came out of the brain within minutes ($T_{1/2}$ = 15 min). Despite the fact that **1** appeared to be a promising blood flow agent, the investigators chose to study other compounds[8] because the radiolabeling yields obtained for **1** were very poor.

Our model compound studies[9] using simple compounds similar to **1** and **2** had shown that aryltrimethylsilanes could be used to regiospecifically introduce radiobromine and radioiodine into such molecules. Therefore, a chemical study to investigate the use of arylsilanes in radiolabeling **1** and a benzylamine similar to **2** was carried out (for specific details, see the 1983 INC-Division Annual Report).

Another class of amines that is interesting with respect to brain studies is the phenethylamines. These compounds are congeners of the naturally occurring catecholamine, dopamine. Changes in substituents on the phenethylamine backbone yield a variety of compounds that produce physiological responses from a light euphoria (caused, for example, by amphetamines) to hallucinations (for example, from mescaline or the more potent DOM). The interest in radiolabeling these compounds comes from the fact that they most likely interact with dopaminergic or other catecholaminergic systems. Studies of the interactions may ultimately help delineate how these systems work and thus how malfunctions of the systems might be treated.

Preliminary radiobromination studies of benzylamines and phenethylamines demonstrate that the aryltrimethylsilane intermediates should work well for radiohalogenations of amines for brain studies. Collaborative studies with C.-Y. Shuie and A. Wolf (Brookhaven) are under way to determine if radiofluorinations might also be accomplished using arylsilanes. Applications of aryltrimethylsilanes and pentafluorosilicates[10] in radiohalogenations will continue to be studied since the results thus far have been very encouraging.

REFERENCES

1. H. Davson, "The Blood-Brain Barrier," J. Physiol. 225, 1-28 (1976).

2. T. C. Hill, "Single-Photon Emission Computed Tomography to Study Cerebral Function in Man," J. Nucl. Med. 21, 1197-1199 (1980).

3. P. L. McGeer, J. C. Eccles, and E. G. McGeer, *Molecular Neurobiology of the Mammalian Brain* (Plenum Press, New York, 1978), Chap. 8, pp. 493-500.

4. K. M. Tramposch, H. F. Kung, and M. Blau, "Radioiodine Labeled Amines as Brain Imaging Agents," *Applications of Nuclear and Radiochemistry*, R. Lambrecht and N. Morcos, Eds. (Pergamon Press, New York, 1982).

5. H. F. Kung and M. Blau, "Regional Intracellular pH Shift: A Proposed New Mechanism for Radiopharmaceutical Uptake in Brain and Other Tissues," J. Nucl. Med. 21, 147-152 (1980).

6. H. F. Kung and M. Blau, "Synthesis of Selenium-75 Labeled Tertiary Diamines: New Brain Imaging Agents," J. Med. Chem. 23, 1127-1130 (1980).

7. K. M. Tramposch, H. F. Kung, and M. Blau, "Synthesis and Tissue Distribution Study of Iodine-Labeled Benzyl- and Xylylamines," J. Med. Chem. 25, 870-873 (1982).

8. H. F. Kung, K. M. Tramposch, and M. Blau, "A New Brain Perfusion Agent: [I-123] HIPDM: N,N,N'Trimethyl-N'-[2-Hydroxy-3-Methyl-5-Iodobenzyl]-1,3-Propanediamine," J. Nucl. Med. 24, 66-72 (1983).

9. D. S. Wilbur, K. W. Anderson, W. E. Stone, and H. A. O'Brien, Jr., "Radiohalogenation of Non-Activated Aromatic Compounds Via Aryltrimethylsilyl Intermediates," J. Labelled Compd. Radiopharm. 19, 1171-1188 (1982).

10. D. S. Wilbur and Z. V. Svitra, "Organopentafluorosilicates: Reagents for Rapid and Efficient Incorporation of No-Carrier-Added Radiobromine and Radioiodine," J. Labelled Compd. Radiopharm. 20, 619-626 (1983).

Heart. An accurate assessment of the extent of the damage in myocardial infarcts or ischemia is critically important to heart patients. One method of evaluating damage to the myocardial tissue is to study the metabolic processes in that tissue. Because the major metabolic process in the heart is degradation of non-esterified fatty acids, it is not surprising that researchers from many different groups have been exploring radiolabeled fatty acids as a noninvasive method for evaluating regional myocardial metabolism.

The radionuclide of choice for metabolic studies using labeled fatty acids is carbon,[1] but as a positron emitter its application is limited to only a few institutions. Radiofluorinated fatty acids also have been studied,[2] but this label has the same shortcoming. Radioiodine- and radiobromine-labeled fatty acids have been studied as the best alternatives.[3,4]

Studies of radiolabeled fatty acids that encompassed modifying the fatty acids chain length,[4-6] degree of unsaturation,[7] and position of radiohalogen attachment[4,8] have been carried out. Researchers have found that long-chain fatty acids, 16-22 carbons in length, are most effectively extracted, and unsaturation appears to be unimportant. The most important factor appears to be the position of the label within the molecule. Addition of bulky halogens to unsaturations within the fatty acid chain or halogenation at the carbon adjacent to the carboxylic acid functionality has led to dramatic decreases in the extraction from the blood. Contrary to this, radiohalogen labeling at the carbon farthest from the carboxylic acid functionality (ω carbon) has shown little difference in extraction from that of the [^{11}C]-labeled analogs.[3,9]

Radiohalogen labeling at the ω carbon has been accomplished in high radiochemical yields by exchange reactions.[9-11] Despite this fact, problems still exist for the ω-radiohalogenated fatty acids. One of the problems arises because haloacetic acids are produced as metabolites of ω-radiohalogenated fatty acids and these compounds are extremely toxic substances. A solution to this problem can be obtained by making a very high specific-activity radiohalogen-labeled fatty acid. Unfortunately, this is not readily accomplished through exchange reactions.[12-13] A second problem arises because ω-radiohalogenated fatty acids are not very stable *in vitro* or *in vivo*, which seriously affects the blood activity for imaging studies. Stabilization of the radiohalogen label has been accomplished by attaching the radiohalogens to phenyl or vinyl substituents on the ω carbon. Although there are some questions about using these agents to measure metabolism,[14,15] a large effort has been devoted to the synthesis and evaluation of these compounds.[16-19]

The problems with obtaining high specific activities, long reaction times, and low radiochemical yields have led to an investigation of organosilanes as intermediates[20-22] to radiohalogen-labeled fatty acids. The investigation has been directed toward the synthesis of key precursor compounds that could be used to make

a series of ω-silylated fatty acids. Several intermediates necessary to the synthesis of these precursor compounds have been prepared. Synthesis procedures for converting these intermediates into the desired precursors and ultimately into the ω-silylated fatty acids are being developed.

REFERENCES

1. E. S. Weiss, E. F. Hoffman, M. E. Phelps, M. J. Welch, P. D. Henry, M. M. Ter-Pogossian, and B. E. Sobel, "External Detection and Visualization of Myocardial Ischemia with ^{11}C-Substrates In Vitro and In Vivo," Circ. Res. 39, 24-32 (1976).

2. E. J. Knust, M. Schüller, and G. Stöcklin, "Synthesis and Quality Control of Long-Chain ^{18}F-Fatty Acids," J. Labelled Compd. Radiopharm. 17, 353-363 (1979).

3. N. D. Poe, G. D. Robinson, and N. S. MacDonald, "Myocardial Extraction of Labeled Long-Chain Fatty Acid Analogs," Proc. Soc. Exp. Biol. Med. 148, 215-218 (1975).

4. H.-J. Machulla, G. Stöcklin, C. Kupfernagel, C. Freundlieb, A. Höck, K. Vyska, and L. E. Feinendegen, "Comparative Evaluation of Fatty Acids Labeled with C-11, Cl-34m, Br-77, and I-123 for Metabolic Studies of the Myocardium: Concise Communication," J. Nucl. Med. 19, 298-302 (1978).

5. C. A. Otto, L. E. Brown, D. M. Wieland, and W. H. Bierwaltes, "Radioiodinated Fatty Acids for Myocardial Imaging: Effects of Chain Length," J. Nucl. Med. 22, 613-618 (1981).

6. E. J. Knust, C. Kupfernagel, and G. Stöcklin, "Long-Chained ^{18}F-Labeled Fatty Acids for the Study of Myocardial Metabolism; Odd-Even Effects," J. Labelled Compd. Radiopharm. (Abstract) 16, 143-144 (1978).

7. W. H. Beierwaltes, R. D. Ice, M. J. Shaw, and U. Y. Ryo, "Myocardial Uptake of Labeled Oleic and Linoleic Acids," J. Nucl. Med. 16, 842-845 (1975).

8. G. D. Robinson and A. W. Lee, "Radioiodinated Fatty Acids for Heart Imaging: Iodine Monochloride Addition Compared with Iodine Replacement Labeling," J. Nucl. Med. 16, 17-21 (1975).

9. G. D. Robinson, "Synthesis of ^{123}I-16-Iodo-9-Hexadecanoic Acid and Derivatives for Use as Myocardial Perfusion Imaging Agents," Int. J. Appl. Radiat. Isotop. 28, 149-156 (1977).

10. P. Laufer, H.-J. Machulla, H. Michael, H. H. Coenen, A. S. El-Wetery, G. Kloster, and G. Stöcklin, "Preparation of ω-^{123}I-Labeled Fatty Acids by ^{123}I-For-Br Exchange: Comparison of Three Methods," J. Labelled Compd. Radiopharm. 18, 1205-1214 (1980).

11. H.-J. Machulla, K. Dutschka, and C. Astfalk, "Improved Synthesis of 17-^{123}I-Heptadecanoic Acid for Routine Preparation," Radiochem. Radioanal. Lett. 47, 189-192 (1981).

12. H.-J. Machulla and K. Dutschka, "Iodination Methods for Routine Preparation of 17-^{123}I-Heptadecanoic Acid and 15-(^{123}I-Phenyl)Pentadecanoic Acid," J. Radioanal. Chem. 65, 122-130 (1981).

13. M. Argentini, M. Zahner, and P. A. Schubiger, "Comparison of Several Methods for the Synthesis of ω-Iodine-123-Heptadecanoic Acid," J. Radioanal. Chem. 65, 131-138 (1981).

14. H.-J. Machulla, M. Marsmann, and K. Dutschka, "Biochemical Concept and Synthesis of a Radioiodinated Phenylfatty Acid for *In Vivo* Metabolic Studies of the Myocardium," Eur. J. Nucl. Med. 5, 171-173 (1980).

15. H. H. Coenen, M.-F. Harmand, G. Kloster, and G. Stöcklin, "15-(p-[^{75}Br]Bromophenyl)Pentadecanoic Acid: Pharmacokinetics and Potential as a Heart Agent," J. Nucl. Med. 22, 891-896 (1981).

16. H.-J. Machulla, M. Marsmann, K. Dutschka, and D. van Beuningen, "Radiopharmaceuticals. II. Radiobromination of Phenylpentadecanoic Acid and Biodistribution in Mice," Radiochem. Radioanal. Lett. 42, 243-250 (1980).

17. H.-J. Machulla, M. Marsmann, and K. Dutschka, "Synthesis of Radioiodinated Phenylfatty Acids for Studying Myocardial Metabolism," J. Radioanal. Chem. 56, 253-261 (1980).

18. H.-J. Machulla, K. Dutschka, D. van Beuningen, and T. Chen, "Development of 15-(p-^{123}I-Phenyl)Pentadecanoic Acid for *In Vivo* Diagnosis of the Myocardium," J. Radioanal. Chem. 65, 279-286 (1981).

19. G. W. Kabalka, S. A. R. Sastry, and K. Muralidhar, "Synthesis of Iodine-125 Labeled Aryl and Vinyl Iodides," J. Labelled Compd. Radiopharm. 19, 795-799 (1982).

20. D. S. Wilbur, K. W. Anderson, W. E. Stone, and H. A. O'Brien, "Radiohalogenation of Non-Activated Aromatic Compounds Via Aryltrimethylsilyl Intermediates," J. Labelled Compd. Radiopharm. 19, 1171-1188 (1982).

21. D. S. Wilbur, W. E. Stone, and K. W. Anderson, "Regiospecific Incorporation of Bromine and Iodine into Phenols Using (Trimethylsilyl)-Phenol Derivatives," J. Org. Chem. 48, 1542-1544 (1983).

22. D. S. Wilbur and Z. V. Svitra, "Organopentafluorosilicates: Reagents for Rapid and Efficient Incorporation of No-Carrier-Added Radiobromine and Radioiodine," J. Labelled Compd. Radiopharm. 20, 619-626 (1983).

Monoclonal-Antibody Labeling: ^{123}I, ^{77}Br, and ^{67}Cu

R. S. Rogers, J. A. Mercer-Smith, and W. A. Taylor

Monoclonal antibodies are produced using the hybridoma technique developed by Kohler and Milstein in which spleen cells from an immunized animal are fused with myeloma cells and the resulting hybrid cells are cloned.[1] The explosive growth in this field is due to the utility of the resulting homogeneous antibodies.[2] Labeled antibodies made to a specific tumor antigen may provide a highly specific way of delivering radionuclides to a tumor for diagnosis by radioimmunoassay or radioimmunoimaging and for radioimmunotherapy.[3,4] We are working to develop chemical methods of labeling antibodies in high radiochemical yield with high specific activity that result in biologically active antibodies for medical use. It is also important that the antibodies have good *in vivo* stability. We are collaborating with S. DeNardo's group at the University of California, Davis. We will examine the labeling chemistry and they will provide the monoclonal antibodies and do the biological testing. We are interested in three approaches to the radiolabeling of antibodies: radiohalogenation, chelate conjugation, and linking of tagged organic molecules to the proteins.

Methods for radioiodination have been used extensively for many years and are well characterized.[5-7] In general, electrophilic reagents are generated *in situ* through oxidation of iodide by chloramine-T, iodogen, enzymes, electrolysis, or iodine monochloride.[8-10] Iodination occurs primarily on tyrosyl residues.[6] Radiochemical yields vary from 75 to 100%. Unfortunately, iodinated proteins are not extremely stable *in vivo*, liberating free iodide on degradation. Though radioiodinated proteins have been used widely, free iodide increases background, thus limiting contrast in radioimmunoimaging and increasing whole-body dose in radioimmunotherapy.

The bromine carbon bond is stronger than the iodine carbon bond and should be more stable *in vivo*. Also important is the fact that bromine does not concentrate in the thyroid. Radiobromination offers high lethality for radiotherapy of tumors because the Auger electrons produced in the decay of ^{77}Br deposit their energy over a small distance.[11] For these reasons radiobromination of antibodies is of great interest.

The literature and our own preliminary work have shown that for the most part methods developed for iodination are not applicable to bromination. Some methods for bromination have been published, but in general they suffer from low yields, harsh conditions, or low availability of starting materials.[12-14] We have radioiodinated a model protein, ovalbumin, and an ascites mixture (the proteins isolated from the peritoneal cavity of a mouse in which a hybridoma is grown) in high yield using iodogen, enzymobeads (immobilized lactoperoxidase), and iodobeads (immobilized chloramine-T). However, radiobromination with ^{77}Br with these methods was unsuccessful. We have been successful in brominating ovalbumin in a buffered system (pH = 6.8) in 20% radiochemical yield with ^{77}Br and sodium hypochlorite, although an excessive amount of protein degradation was seen by high-performance liquid chromatography (HPLC). With ^{82}Br of low specific activity and iodobeads as oxidant, we found that some labeling had occurred with no observable protein degradation.

Neither of these methods is useful as they stand, but they suggest that two questions must be addressed: the first is the oxidation of radiobromide to an electrophilic form suitable for aromatic substitution, and the second is the stability of the proteins in the presence of the oxidizing agent. Our experience with the labeling of small molecules and model systems will allow us to optimize oxidation.[15-17] The denaturation of the antibodies may then be addressed by sequestering the oxidizing agent, thereby preventing direct oxidation of the protein. For example, we are examining different methods of forming the hypochlorite of a hydroxyl-containing resin with pores too small to allow the proteins to diffuse into the resin. We have found that t-butyl hypochlorite oxidizes radiobromide to bromine monochloride in solution, and we hope to be able to form BrCl in the pores of the resin from the reaction of the resin hypochlorite and bromide (which would freely diffuse into the resin). The BrCl so formed would then be able to diffuse out of the resin to react with the excluded protein. Our preliminary results using a Sephadex resin are promising.

Conjugation of chelating agents with proteins is another important method of labeling.[18-21] For this method a ligand that has a high binding affinity for the nuclide of choice is derivatized to allow covalent bonding to the protein. The activated ligand is then reacted with the protein, linking the ligand and protein. Radiolabeling is accomplished by adding the nuclide to the derivatized protein. This method is promising in that a number of different nuclides could be chelated by the same conjugated protein, allowing optimization of decay characteristics for different purposes. We are studying

the binding properties of porphyrins for nuclides that we produce, such as ^{67}Cu and ^{65}Zn, and we will then develop methods to conjugate the porphyrins and other chelating ligands to our antibodies.

In the area of ^{67}Cu-metalloporphyrin research, initial studies appear quite promising. Copper (II) mesotetra (4-carboxyphenyl) porphine (CuTCPP) was prepared from $CuCl_2$ and mesotetra (4-carboxyphenyl) porphine (H_2TCPP). A study of the effect of solvent on the metallation reaction indicates that dimethylformamide (DMF) is by far the best solvent tested for this reaction. ZnTCPP was prepared from $ZnCl_2$ and H_2TCPP, since Zn^{2+} is present in the ^{67}Cu hot cell preparation and can readily metallate H_2TCPP under the same conditions used for the copper metallation reaction. Conditions were developed to separate H_2TCPP, CuTCPP, and ZnTCPP by HPLC.

Once the methods of metallation and separation of H_2TCPP and CuTCPP were developed, carrier-added radiolabeling of H_2TCPP was performed. The $^{67}Cu^{2+}$ usually is supplied in 2*M* HCl. The HCl presents a problem because it protonates the pyrrole nitrogens of the porphyrin; this pyrrole protonation retards the metallation reaction. Therefore, a series of $^{67}Cu^{2+}$ solutions in different solvents was prepared. These solvents were used to optimize the carrier-added metallation reaction. Neutralizing the HCl solution increased the radiolabeling yield from 61 to 76%, but the phosphate buffer was only slightly soluble in DMF. The best radiolabeling yield, 93%, was obtained when the HCl solution was removed by evaporation and $^{67}Cu^{2+}$ was redissolved in DMF before initiation of the chelation reaction. This yield was obtained after 45 min of refluxing the porphyrin and $^{67}Cu^{2+}$. In the analogous no-carrier-added reaction, a radiolabeling yield of 76% was obtained. Two additional porphyrin bands could be seen by HPLC and radio-HPLC under no-carrier-added conditions; these are under study to determine their identity.

REFERENCES

1. G. Kohler and C. Milstein, "Continuous Culture of Fused Cells Secreting Antibody of Predefined Specificity," Nature 265, 495 (1975).

2. D. E. Yelton and M. D. Scharff, "Monoclonal Antibodies: Powerful New Tool in Biology and Medicine," Ann. Rev. Biochem. 50, 657-680 (1980).

3. V. R. McCready, "Tumour Localization," Br. Med. Bull. 36(3), 209 (1980).

4. T. Ghose, A. Guclu, J. Tai, A. S. MacDonald, S. T. Norvell, and J. A. Aquino, "Antibody as Carrier of ^{131}I in Cancer Diagnosis and Treatment," Cancer 36, 1648 (1975).

5. W. C. Eckelman, C. H. Paik, and R. C. Reba, "Radiolabeling Antibodies," Cancer Res. 40, 3036-3042 (1980).

6. K. A. Krohn, K. C. Knight, J. F. Harwig, and M. J. Welch, "Differences in the Sites of Iodonation of Proteins Following Four Methods of Radioiodination," Biochim. Biophys. Acta 490, 497 (1977).

7. L. R. Chervu and D. R. K. Murty, "Radiolabeling of Antigens: Procedures and Assessment of Properties," Semin. Nucl. Med. 5(2), 157 (1957).

8. K. A. Krohn, L. Sherman, and M. Welch, "Studies of Radioiodinated Fibrinogen. I. Physicochemical Properties of the ICl, Chloramine-T, and Electrolytic Reaction Products," Biochim. Biophys. Acta 285, 404 (1972).

9. P. R. P. Salacinski, C. McLean, J. E. C. Sykes, V. V. Clements-Jones, and P. J. Lowery, "Iodination of Proteins, Glycoproteins, and Peptides Using a Solid-Phase Oxidizing Agent, 1,3,4,6-Tetrachloro-3, 6-Diphenyl Glycoluril (Iodogen)," Anal. Biochem. 117, 136 (1981).

10. A. Sinda, B. Lucka, and K. Russin, "Enzymatic Labeling of Carcinoembryonic Antigen with Iodine-125," J. Labelled Compd. Radiopharm. 18(12), 1797 (1981).

11. A. I. Kassis, S. J. Adelstein, C. Haydock, K. S. R. Sastry, K. D. McElvany, and M. J. Welch, "Lethality of Auger Electrons from the Decay of Bromine-77 in the DNA of Mammalian Cells," Radiat. Res. 90, 362 (1982).

12. L. Knight, K. A. Krohn, M. J. Welch, and B. Spomer, "LPH, ^{77}Br: A New Protein Label," in *Radiopharmaceuticals*, G. Subramanian, B. A. Rhodes. J. F. Cooper, and V. J. Sodd, Eds. (Soc. Nucl. Med., New York, 1975), pp. 149-154.

13. K. D. McElvany, J. W. Barnes. and M. J. Welch, "Characterization of Bromine-77-Labeled Proteins Prepared Using Myeloperoxidase," Int. J. Appl. Radiat. Isotop. 31, 679 (1980).

14. G. Petzold and H. H. Coenen, "Chloramine-T for 'No-Carrier-Added' Labeling of Aromatic Biomolecules with Bromine-75,77," J. Labelled Compd. Radiopharm. 18, 1319 (1981).

15. D. S. Wilbur and K. W. Anderson, "Bromine Chloride from N-Chlorosuccinimide Oxidation of Bromide Ion. Electrophilic Addition Reactions in Protic and Aprotic Solvents, "J. Org. Chem. 47(2), 358 (1982).

16. D. S. Wilbur and H. A. O'Brien, "A-Ring Bromination of Estradiol and 17α-Ethynylestradiol with N-Chlorosuccinimide and Bromide Ion. Possible Evidence for Hybrointe Intermediates," J. Org. Chem. 47(2), 359 (1982).

17. D. S. Wilbur, K. W. Anderson, W. E. Stone, and H. A. O'Brien, "Radiohalogenation of Non-Activated Aromatic Compounds Via Aryltrimethylsilyl Intermediates," J. Labelled Compd. Radiopharm. 19, 1171 (1982).

18. G. E. Krejcarek and K. L. Tucker, "Covalent Attachment of Chelating Groups to Macromolecules," Biochem. Biophys. Res. Commun. 77(2), 581 (1977).

19. M. W. Sundberg, C. F. Meares, D. A. Goodwin, and C. I. Diamanti, "Chelating Agents for the Binding of Metal Ions to Macromolecules," Nature 250, 587 (1974).

20. M. W. Sundberg, C. F. Meares, D. A. Goodwin, and C. I. Diamanti, "Selective Binding of Metal Ion to Macromolecules Using Bifunctional Analogs of EDTA," J. Med. Chem. 17(12), 1304 (1974).

21. C. F. Meares, D. A. Goodwin, C. S.-H. Leung, A. G. Girgis, D. J. Silvester, A. D. Nunn, and P. J. Lavender, "Covalent Attachment of Metal Chelates to Proteins: The Stability In Vivo and In Vitro of the Conjugates of Albumin with a Chelate of Indium-111," Proc. Nat. Acad. Sci. USA 73(11), 3803 (1976).

Group INC-3 Publications

J. W. Barnes, M. A. Ott, P. M. Wanek, G. E. Bentley, K. E. Thomas, F. J. Steinkruger, and H. A. O'Brien, Jr., "Iodine-123 Yields from 800-MeV Proton Irradiation of CsCl Target," Proc. Thirtieth Annual Meeting of the Society of Nuclear Medicine, St. Louis, Missouri, June 7-10, 1983, J. Nucl. Med. (Abstract) 24, P24 (1983).

W. Cole, S. DeNardo, C. Meares, G. DeNardo, and H. O'Brien, "Development of Copper-67 Chelate Conjugated Monoclonal Antibodies for Radioimmunotherapy," Proc. Thirtieth Annual Meeting of the Society of Nuclear Medicine, St. Louis, Missouri, June 7-10, 1983, J. Nucl. Med. (Abstract) 24, P30 (1983).

R. E. Gibson, W. C. Eckelman, B. Francis, H. A. O'Brien, J. K. Mazaitis, D. S. Wilbur, and R. C. Reba, "[^{77}Br]-17-α-Bromoethynylestradiol: *In Vivo* and *In Vitro* Characterization of an Estrogen Receptor Radiotracer," Int. J. Nucl. Med. Biol. 9, 245-250 (1982).

R. A. Goldstein, N. A. Mullani, D. J. Fisher, S. K. Marani, H. A. O'Brien, and K. L. Gould, "Quantification of Regional Myocardial Flow with Rb-82 Despite Pharmacologic Intervention," Proc. Thirtieth Annual Meeting of the Society of Nuclear Medicine, St. Louis, Missouri, June 7-10, 1983, J. Nucl. Med. (Abstract) 24, P30 (1983).

D. A. Miller, P. M. Grant, J. W. Barnes, G. E. Bentley, and H. A. O'Brien, Jr., "Research-Scale Experimentation on the Production and Purification of Spallogenic Germanium-68 at Los Alamos for Nuclear Medicine Applications," in *Applications of Nuclear and Radiochemistry*, R. M. Lambrecht and N. Morcos, Eds. (Pergamon Press, New York, 1982), Chap. 4, pp. 37-44.

H. A. O'Brien, Jr., and P. M. Grant, "Biomedical Positron Generators," in *Applications of Nuclear and Radiochemistry*, R. M. Lambrecht and N. Morcos, Eds. (Pergamon Press, New York, 1982), Chap. 6, pp. 57-68.

A. P. Selwyn, R. M. Allan, A. L'Abbate, P. Horlock, P. Camici, J. Clark, H. A. O'Brien, Jr., and P. M. Grant, "Relation Between Regional Myocardial Uptake of Rubidium-82 and Perfusion: Absolute Reduction of Cation Uptake in Ischemia," Am. J. Cardiol. 50, 112-121 (1982).

D. S. Wilbur, K. W. Anderson, W. E. Stone, and H. A. O'Brien, Jr., "Radiohalogenation of Non-Activated Aromatic Compounds Via Aryltrimethylsilyl Intermediates," J. Labelled Compd. Radiopharm. 19, 1171-1186 (1982).

D. S. Wilbur, W. E. Stone, and K. W. Anderson, "Regiospecific Incorporation of Bromine and Iodine into Phenols Using Trimethylsilylphenol Derivatives," J. Org. Chem. 48, 1542-1544 (1983).

D. S. Wilbur and Z. V. Svitra, "Organopentafluorosilicates: Reagents for Rapid and Efficient Incorporation of No-Carrier-Added Radiobromine and Radioiodine," J. Labelled Compd. Radiopharm. 20, 619-626 (1983).

D. S. Wilbur, Z. V. Svitra, and H. A. O'Brien, Jr., "Applications of Aryltrimethylsilanes in Radiobrominations," J. Nucl. Med. (Abstract) 24, P43 (1983).

D. S. Wilbur, Z. V. Svitra, and H. A. O'Brien, Jr., "Applications of Aryltrimethylsilanes in Radiobrominations," Proc. Thirtieth Annual Meeting of the Society of Nuclear Medicine, St. Louis, Missouri, June 7-10, 1983, J. Nucl. Med. (Abstract) 24, P43 (1983).

Papers Accepted for Publication

G. E. Bentley, F. J. Steinkruger, and P. M. Wanek, "Electrochemistry as a Basis for Radiochemical Generator Systems," Proc. of the Symp. on New Radionuclide Generator Systems for Nuclear Medicine, 185th American Chemical Society National Meeting, Seattle, Washington, March 20-25, 1983 (in press); Los Alamos National Laboratory document LA-UR-83-898.

D. T. Cromer, R. R. Ryan, and D. S. Wilbur, "Structure of 1-H-Azepine- 2-1-5-Methoxime, $C_7H_8N_2O_2$," Acta *Crystallogr. Sect. C (in press)*; Los Alamos National Laboratory document LA-UR-83-2303.

H. A. O'Brien, Jr., "Overview of Radionuclides Useful for Radioimmunoimaging and Current Status of Preparing Radiolabeled Antibodies," in *Radioimmunoimaging* (Elsevier Biomedical Press, New York, in press); Los Alamos National Laboratory document LA-UR-83-154.

H. A. O'Brien, Jr., J. W. Barnes, G. E. Bentley, F. J. Steinkruger, K. E. Thomas, M. A. Ott, F. H. Seurer, and W. A. Taylor, "The Development of Short-Lived Radionuclides at Los Alamos," Proc. of the Int. Symp. on the Developing Role of Short-Lived Radionuclides in Nuclear Medical Practice, Washington, DC, May 3-5, 1982 (in press); Los Alamos National Laboratory document LA-UR-83-791.

F. J. Steinkruger, G. E. Bentley, H. A. O'Brien, Jr., M. A. Ott, F. H. Seurer, W. A. Taylor, and J. W. Barnes, "Production and Recovery of Large Quantities of Radionuclides for Nuclear Medicine Generator Systems," Proc. of the Symp. on New Radionuclide Generator Systems for Nuclear Medicine, 185th American Chemical Society National Meeting, Seattle, Washington, March 20-25, 1983 (in press); Los Alamos National Laboratory document LA-UR-83-835.

K. E. Thomas, "Recovery and Isolation of Curie Quantities of Hafnium and the Lanthanides from LAMPF-Irradiated Tantalum Targets," *Radiochim. Acta (in* press); Los Alamos National Laboratory document LA-UR-83-579.

K. E. Thomas, "Proposal for the Production of Carrier-Free Osmium-191," Proc. of the Int. Conf. on Single Photon Ultra-Short-Lived Radionuclides, Pan American Health Organization, Washington, DC, May 9-10, 1983; Los Alamos National Laboratory document LA-UR-83-1367 (in press).

K. E. Thomas and J. W. Barnes, "Large Scale Isolation of Strontium-82 for Generator Production," Proc. of the Symp. on New Radionuclide Generator Systems for Nuclear Medicine, 185th American Chemical Society National Meeting, Seattle, Washington, March 20-25, 1983 (in press); Los Alamos National Laboratory document LA-UR-83-939.

D. S. Wilbur, Z. V. Svitra, R. S. Rogers, and W. E. Stone, "Radiohalogen Labeling Studies at Los Alamos," Proc. of the Int. Symp. on the Developing Role of Short-Lived Radionuclides in Nuclear Medical Practice, Washington, DC, May 3-5, 1982 (in press).

Papers Submitted for Publication

K. W. Thomas and the Los Alamos Medical Radioisotopes Group, "Production of Microcurie Amounts of Carrier-Free Aluminum-26," Los Alamos National Laboratory document LA-UR-83-1413 (submitted to Radiochim. Acta).

D. S. Wilbur, "Structural Determinations of Some Chloroazepin-2,5-Diones Using a Lanthanide Shift Reagent," Los Alamos National Laboratory document LA-UR-83-2233 (submitted as a Note to J. Org. Chem.).

Theory

Spin Dependence of NN and $NN\pi$ Reactions and the Question of Dibaryon Resonances*

Richard R. Silbar (Los Alamos)

Abstract

Recent experiments on the spin dependence of the coupled NN and $NN\pi$ systems are reviewed and compared with theory. Conventional models involving the usual interactions of mesons and nucleons appear to explain the rich spin dependence observed.

Introduction

The experimental information on spin dependence in the coupled NN and $NN\pi$ systems for medium energies has mushroomed in the past few years. The energies involved run from pion-production threshold (around 300-MeV incident nucleon laboratory energy) to about 1500 MeV (where two-pion production becomes important).

At the same time theoretical models for the coupled NN and $NN\pi$ systems have undergone vigorous development. Both experiment and theory have been much stimulated by the observation of relatively sharp energy-dependent structures.[1] It was quickly recognized that these might be manifestations of new degrees of freedom, such as the dibaryon resonances suggested by the quark bag model.[2]

This report summarizes recent experimental progress in this field** and discusses to what extent the new data require an interpretation of new quark substructures.

What is a Dibaryon Resonance?

A resonance is more than just a bump in a cross section. The classic example of an elastic resonance is provided by a Breit-Wigner amplitude

$$T_J = \frac{1}{2}\,\frac{\Gamma}{E_R - E - i\Gamma/2}\ ,$$

where J denotes the partial-wave amplitude that is resonating. Such a structure has a pole in the complex energy plane at $E = E_R - i\Gamma/2$, that is, "on the second sheet." As the energy increases through E_R, the complex amplitude T_J traces a counterclockwise path along a circle of radius $\frac{1}{2}$ centered at $+\frac{1}{2}$, the so-called unitarity circle. In this example without any background, the partial-wave amplitude reaches the top of the circle ($+i$) at the resonance energy E_R and moves around into the left half plane for energies above E_R. This counterclockwise motion on an Argand diagram is typical of a resonance. However, a warning is definitely in order: such motions can arise from other kinds of analytical structures, as well as from resonance poles.

In the presence of inelasticity (that is, coupling to other open channels), the scattering amplitude becomes a matrix, and a resonance shows up as a pole in each matrix element. As the energy increases, the path traced by the elastic amplitude T_J is still counterclockwise, but the conservation of probability (unitarity) constrains it only to be somewhere within the unitarity circle.

At least two such counterclockwise looping behaviors deep inside the unitarity circle have been found in phase-shift analyses for NN elastic scattering.[4] These occur in the $^1D_2$ and $^3F_3$ partial waves, the two prime candidates for dibaryon resonances. One needs a model to extrapolate the physical amplitude into the complex energy plane and search for resonance poles. There is an extensive theoretical literature that deals with whether the looping behavior is due to resonance poles (that is, dibaryons).* The issue is not settled, but it is clear from simple models that coupled-channel resonance poles certainly can be present. On the other hand, the cut from the $NN \rightarrow N\Delta$ threshold also produces a resonance-like behavior, and it could be the combined effect of poles and the $N\Delta$ cut that causes the structures seen in the observables.

The existence of dibaryons was first suggested in 1977 by the energy-dependent structures found in spin-dependent total cross-section differences.[6] These and other structures go hand in hand with inelasticity, which in this energy region means single-pion production,

---

*To be published in Comments on Nuclear and Particle Physics 12(4), 177-189 (March 1984).

**Experiments involving electromagnetic probes are not discussed; references in this subfield may be traced, for example, from K. Baba et al., Ref. 3.

*Recent literature may be traced from W. M. Kloet and J. A. Tjon, Ref. 4.

$NN \rightarrow NN\pi$. If dibaryons are actually given by resonance poles, the next questions are: What is their origin? Can they be explained by conventional models of mesons interacting with nucleons? Or, does their existence imply a new underlying hadronic structure, such as that associated with quarks and color degrees of freedom?

Theoretical Framework

In the energy region under discussion, the standard description of the $NN \rightarrow NN\pi$ or $\pi d \rightarrow \pi d$ scattering amplitudes uses the isobar model,[7] as illustrated by the graphs in Figs. 1(a) and (b). Originally, the isobar amplitudes (the "blobs" in the figure) were simply fit to the available data or calculated in the Born approximation. Today, however, these amplitudes are calculated in a unified and unitary way. There are two approaches.

(1) The coupled two-body channel approach involves solving coupled scattering equations with transition potentials between the NN, $N\Delta$, and πd two-body channels. This method has been applied to calculate inelasticity parameters and phase shifts for NN scattering above the pion-production threshold[8-10] and spin observables for the $pp \rightarrow d\pi$ reaction.[11]

(2) The three-body-equation approach has been the most realistic path to the elastic scattering of pions by deuterons, with important work being done by Rinat and Thomas,[12] Garcilazo,[13] and the Lyon group.[14] Garcilazo has extended his calculations to the breakup process $\pi d \rightarrow \pi NN$ with good success.[15] The other two groups have emphasized the treatment of NN intermediate states, which is closely connected to an alternative approach and which involves the truncation of an underlying field theory to consider, at any given time, only two nucleons or two nucleons and a pion. The original work was by Afnan and Thomas.[16] Later developments[17-20] vary in their details and philosophical basis. The major emphasis of Refs. 18-20 so far has been on the $pp \rightarrow d\pi$ reaction, whereas the authors of Ref. 17 have concentrated on calculating spin observables for the three-body final state, $NN \rightarrow NN\pi$ (Ref. 21).

All these models, two-body as well as three-body, are conventional in that they involve only the known mesons and nucleons interacting in the usual way. If there are explicit dibaryon resonances—that is, resonances *not* generated by the conventional meson-nucleon dynamics—these models must be supplemented by contributions that look like Figs. 1(c) and (d). Incorporating such graphs without destroying the unitarity of the conventional models is slightly problematical. One way of doing this has been discussed by Locher and co-workers.[22]

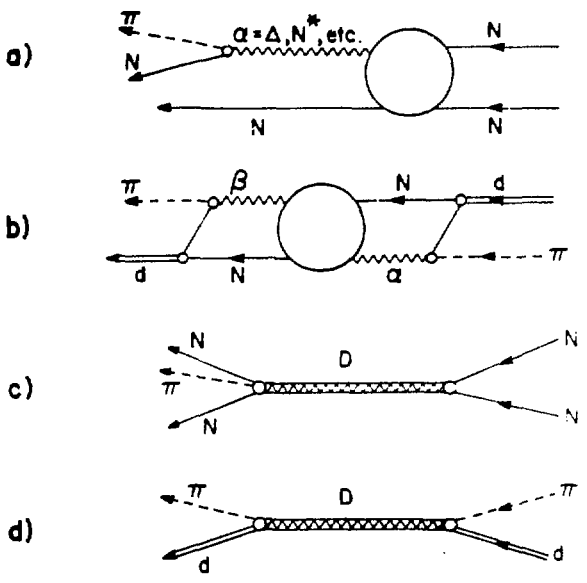

Fig. 1.
Four Feynman graphs: (a) and (b) show graphs for the isobar-model treatment of the $NN \rightarrow NN\pi$ and $\pi d \rightarrow \pi d$ reactions, respectively, and (c) and (d) indicate explicit dibaryon-resonance graphs.

Recent Experiments

It is convenient to discuss separately five kinds of spin-observable experiments: (1) πd elastic scattering, (2) $pp \rightarrow d\pi$ (and its inverse), (3) spin-dependent total cross sections, and (4) inclusive and (5) exclusive experiments on the $NN \rightarrow NN\pi$ reaction. Table I gives definitions for these different spin observables.

(1) Elastic pion-deuteron scattering. Two different spin observables are measured for this reaction. The sharp angular oscillations in the vector polarization (iT_{11}), found[23] at $T_{\pi,lab}$ = 256 MeV, have been particularly suggestive of a $^1G_4$ dibaryon resonance. The extant (conventional) three-body calculations (see, for example, Ref. 14) give rather smooth angular variations for iT_{11}. By incorporating explicit dibaryon-resonance

Table I. Definitions of Spin Observables.

$\pi d + \pi d$:

$$iT_{11}(\theta) = (\sqrt{3/2})\ \left[\sigma(M_d = +1) - \sigma(M_d = -1)\right] \Big/ \left[\sum_{M_d=-1,0,1} \sigma(M_d)\right] ,$$

$$T_{20}(\theta) = (1/\sqrt{2})\left[\sigma(+1) - 2\sigma(0) + \sigma(-1)\right] \Big/ \left[\sum_{M_d=-1,0,1} \sigma(M_d)\right] .$$

The deuteron spin is quantized normal to the scattering plane.

Total Cross-Section Differences:

$$\Delta\sigma_T = \sigma(\uparrow\downarrow) - \sigma(\uparrow\uparrow) .$$

Initial nucleon spins are quantized in a direction transverse to the beam direction; $\Delta\sigma_L$ is defined likewise, but with spins quantized along the beam direction (longitudinal).

$NN \rightarrow NN\pi$ (or $d\pi$):

$$A_N(\theta,...) = [\sigma(\uparrow) - \sigma(\downarrow)]/[\sigma(\uparrow) + \sigma(\downarrow)] ,$$

$$A_N^{(tgt)}(\theta,...) \neq A_N^{(beam)}(\theta,...) ,$$

$$A_{NN} = [\sigma(\uparrow\uparrow) - \sigma(\uparrow\downarrow) - \sigma(\downarrow\uparrow) + \sigma(\downarrow\downarrow)]/\text{ sum} .$$

Initial nucleon spins are quantized normal to the reaction plane. Similar formulae define A_{LL}, A_{SS}, A_{LS}, and $A_{SL} \neq A_{LS}$, but with longitudinal and sideways quantization axes; likewise for spin-transfer observables D_{NN}, K_{LL}, etc., except that one spin is for an initial nucleon, the other for a final nucleon.

graphs, as in Fig. 1(d), Locher et al.[22] could predict oscillatory behavior very much like that observed.

Recently, however, Gibbs* noticed that the three-body calculations are quite sensitive to the small πN interactions that enter as input. The vector polarization is basically an interference effect between the dominant P_{33} πN interaction and the smaller contributions. In particular, the earlier three-body calculations used input πN potentials, which were in fact unsupported by the πN experimental data. Gibbs and Gibson[24] have shown that a single-scattering-approximation calculation with πN input directly related to the πN phase shifts can do a reasonable job of reproducing the 256-MeV iT_{11} angular distribution, with the exception of a singularly negative datum at 135°. That datum, in the meantime, has been remeasured and was found to be positive.** Thus, on the whole, the experimental data set for iT_{11}, over the whole energy range measured, now seems not to require (explicit) dibaryon resonances.

The other spin observable of current interest in πd scattering is the tensor polarization T_{20} of the recoil deuteron. Two groups have obtained very different experimental results. The Argonne group[25] finds T_{20}'s in agreement with conventional expectations—that is, predictions of the three-body models. In contrast, the ETH group obtained data[26] sufficiently oscillatory that, if correct, may demand an interpretation involving explicit dibaryon resonances. In view of the present discrepancy in the T_{20} data, it is difficult at this time to draw any conclusions about the existence of dibaryon resonances.

*Reference 24. A similar observation was evidently made earlier by J. Arvieux and A. S. Rinat (unpublished).

**Private communication to W. R. Gibbs, spring 1983, from Dubach et al., authors of Ref. 21.

(2) The reaction $pp \rightarrow d\pi$ *and its inverse.* Because the two-body final state is easier to deal with experimentally than the three-body state, there is already an extensive data set for this reaction from threshold to above 1000 MeV. Three kinds of spin observables have been measured: polarization asymmetries, spin-spin correlations, and polarization transfers.[27]

The data, especially for the asymmetries A_N, are smoothly varying with energy and generally have very small error bars. At the moment, no conventional theoretical model[11,18,20] does a very good job. However, the models do reproduce the general trends of the data. To judge from the differences among the various models, which are big compared with the experimental errors, it is reasonable to presume that a conventional model can someday fit this data set.

Incidentally, the spin-spin correlations A_{NN} for $pp \rightarrow d\pi$ are large and negative, $A_{NN} \simeq -0.8$, a result that comes from conventional models quite easily since the reaction is dominated by $N\Delta$ intermediate states with orbital angular momenta $L' = 0$. These states are produced in the initial NN state from the $^1D_2$ partial wave. Thus, the basic negativeness of A_{NN} is largely determined by nearly model-independent considerations (see definition, Table I).

(3) Spin-dependent total cross sections. It was the Argonnne ZGS measurements of the cross-section differences $\Delta\sigma_L$ and $\Delta\sigma_T$ that created the great interest in dibaryons.[1] These quantities have since been remeasured at all the meson factories. The sharp energy-dependent structures in $\Delta\sigma_L$ and $\Delta\sigma_T$ have been confirmed, although there is not yet complete agreement as to what the magnitudes of the cross-section differences are.

The peak in $\Delta\sigma_T$ and $\Delta\sigma_L$ at 550 MeV is related to the resonance-like structure of the $^1D_2$ amplitude, whereas the dip in $\Delta\sigma_L$ near 750 MeV is related to the $^3F_3$ amplitude ($\Delta\sigma_L$ contains contributions from the $L = J$ triplet partial waves but $\Delta\sigma_T$ does not). From the point of view of conventional models, these structures to a large extent are due to the onset of the $NN \rightarrow N\Delta$ reaction as it opens up in the s and p waves of the $N\Delta$ state, respectively. However, none of the conventional models has as yet reproduced the details of the experimentally observed structures. As an example, Fig. 2 compares the predictions of Ref. 28 with the data.

Conventional models also might be running into trouble with the inelastic part of the longitudinal cross-section difference $\Delta\sigma_L^{inel}$, which is negative (-3.5 ± 1 mb) at 800 MeV.[29] Three different conventional

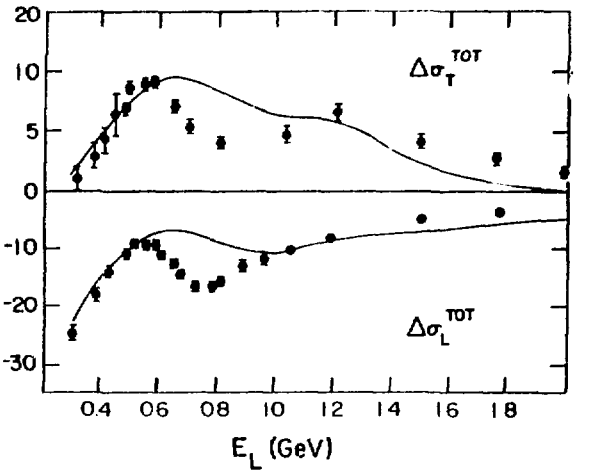

Fig. 2.
Experimental data for $\Delta\sigma_T$ and $\Delta\sigma_L$ (in millibarns), compared with the conventional model prediction of Ref. 28 (from which this figure was taken).

models[17,30,31] give positive ($\simeq$7-mb) predictions for this quantity at that energy. Even the shape of the energy dependence differs markedly between the models and data. It should be pointed out that extracting $\Delta\sigma_L^{inel}$ is difficult, involving the difference of two large numbers obtained from two different experiments. The results of Ref. 29 should be checked.

The above remarks all refer to $I = 1$ cross sections. Little is known about the $I = 0$ cross-section differences, although a flat $\Delta\sigma_L$ observed in pd interactions has been interpreted as requiring a $^1F_3$ "antidip" to compensate for the $^3F_3$ dip a t 750 MeV.[32] Such a structure, if it exists, would be very difficult to interpret in terms of conventional models.

(4) Inclusive $NN \rightarrow NN\pi$ *reactions.* In these reactions, typically, only one particle in the three-body final state is detected. Such experiments are more easily performed and more precise than exclusive experiments, which use detectors in coincidence to determine the momentum and direction of every final-state particle. The results of inclusive experiments measuring spin observables are just now appearing in the literature.

One such experiment measures the analyzing power A_N in the reaction $\vec{p}p \rightarrow pX$ ($X = n\pi^+$ or $p\pi^0$) at 800 MeV.[33] The prominent feature in the data is a sharp rise to a value of 0.3 at the upper end of the outgoing proton momentum spectrum (Fig. 3). This feature can be

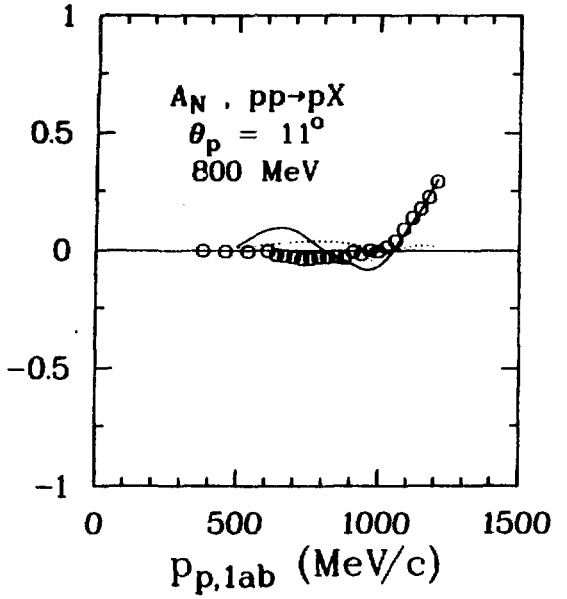

Fig. 3.
Asymmetry for the inclusive reaction $\vec{p}p \rightarrow pX$, $X = n\pi^+$ or $p\pi^0$. Data are from Ref. 33 and the curves are the unitary (solid) and Born approximation (dashed) predictions from Ref. 34.

reproduced in a unitary model[34] (the solid line in Fig. 3) but appears difficult to explain using a Born approximation approach[35] (dashed line). Spin observables such as A_N result from interference between different complex amplitudes and thus are sensitive to unitarization.

Another group has measured the polarization transfers K_{NN} and K_{LL} in the $\vec{p}p \rightarrow \vec{n}X$ reaction, $X = p\pi^+$, again at 800 MeV.[36] There are as yet no unitary model predictions for these quantities, but a Born approximation calculation[35] fails to reproduce the features of the data entirely. It will be interesting to see if unitarity alone can cure the disagreement.

(5) Exclusive NN → NNπ *reactions.* Until recently, kinematically complete information about this fundamental pion-production process came mostly from a small number of bubble chamber experiments performed in the 1960s. The data base was therefore embarrassingly small. With the advent of meson factories, however, there are now counter experiments that measure complete kinematics for the reaction (although usually only for in-plane geometry). Two particles (at least) must be measured in coincidence to determine five kinematical quantities: for example, p_p, θ_p, ϕ_p, θ_π, and ϕ_π.

The first such experiment[37] measured the polarization asymmetry in $\vec{p}p \rightarrow p\pi^+n$ at 800 MeV, and it established the crucial importance of dealing with unitarity properly. As the first data were being processed, Umland, Duck, and Mutchler[38] made Born approximation predictions of A_N as a function of the outgoing proton momentum for the various angle pairs measured. Not surprisingly, since A_N depends on the relative phases between complex amplitudes, the agreement with the data was quite poor. They then tried including explicit dibaryon-resonance graphs [Fig. 1(c)], fitting a free phase between those graphs and the usual isobar graphs [Fig. 1(a)]. The agreement with the experimental A_N was much improved, but still not remarkably good.

Soon after this, Dubach et al.[21] applied the unitary model of Ref. 17 to the problem, using the no-free-parameter version of the model based solely on one-pion exchange (OPE). These predictions, although still not agreeing very well with the data of Ref. 37, were qualitatively much more like the data than the Born approximation results. Considering the simple nature of the model (only OPE forces between the nucleons and isobars, only P_{33} and P_{11} πN input forces, etc.), one can be optimistic that a more complete model eventually might be able to explain these data.

The asymmetry experiment[37] also was able to record data at the same time for the reaction $\vec{p}p \rightarrow pp\pi^0$. It is curious that the predictions of the unitary model[21] seem to fit these data much better than the data* for $np\pi^+$. It is not clear why this happens.

Another set of exclusive experiments measures spin-spin correlations A_{NN}, A_{LL}, etc., for the reaction $\vec{p}\vec{p} \rightarrow np\pi^+$ at three energies near 500 MeV[39] and at 650 and 800 MeV.[40] The no-free-parameter OPE predictions of Ref. 21 are compared with preliminary data at 500 MeV in Fig. 4. The agreement is quite good—that is, these data provide no surprises in comparison with a conventional model. All the spin-spin correlation coefficients in Fig. 4 are large and negative, again reflecting the dominance of the $NN(^1D_2) \rightarrow N\Delta(^5S_2)$ partial-wave amplitude.

The experiment on A_{NN} and A_{LL} at 650 and 800 MeV[40] has fewer data points (but smaller errors). These data also are in agreement with the predictions of Ref. 21. At 800 MeV, A_{LL} has become slightly positive, indicating a cancellation between the $^1D_2$ and $^3F_3$ partial waves for this quantity (see definition in Table I).

*G. S. Mutchler, private communication.

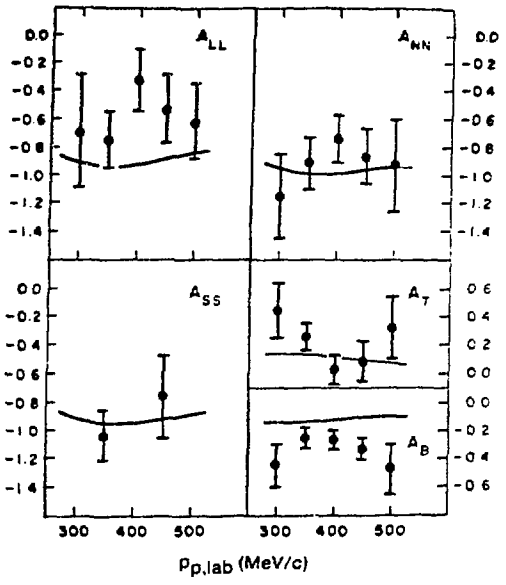

Fig. 4.
Spin-spin correlation coefficients for $\vec{p}\vec{p} \rightarrow np\pi^+$ at 500 MeV. Data are from Ref. 39 and the curves were calculated as in Ref. 21. This figure is a corrected version of one appearing in Ref. 39.

It is curious that in both experiments (and in the calculations) the beam and target particle asymmetries for a given angle pair are approximately equal and opposite in sign. There is no evident simple reason for this. (Identical-particle symmetry gives exact equalities between *different* angle pairs.)

A third kind of experiment involves the measurement of the polarization transfer coefficient D_{NN}, for the reaction $\vec{p}p \rightarrow n\vec{p}\pi^+$ at 800 MeV.[41] The one data point measured (right at the peak of the Δ^{++} resonance) is also in good agreement with the prediction of Ref. 21. The differential cross-section data elsewhere indicate the presence of a strong final-state interaction between the outgoing nucleons. One naturally wonders how well the unitary models (which generally do not contain such interactions in their input) will compare with a more extensive D_{NN} data set.

Conclusions

In general, we have seen that conventional models of mesons and nucleons, so far, are able to explain a substantial amount of new experimental data on the rich spin dependence of the coupled NN and $NN\pi$ interactions. Not all predictions agree perfectly, but that is to be expected at this stage. It seems a little peculiar that the gross quantities (total cross-section differences) are harder to understand in this picture than the detailed ones (exclusive cross sections). Nonetheless, the major point to be emphasized is that there is no obvious need at this time to invoke new quark substructures to explain the present data.

So where, then, are the effects of the quarks and gluons in the $A = 2$ interacting systems to be seen? It may simply be that the present round of experiments is not very sensitive to quark degrees of freedom.[42] To find out what experiments *are* sensitive, perhaps of this type or perhaps of some totally different kind, will probably require a lot more experimental and theoretical work.

Acknowledgments

I wish to thank the many experimentalists who have discussed with me their data, often while still preliminary. My colleagues J. Dubach and W. M. Kloet have contributed greatly to my understanding of the theory, and T. S. Bhatia urged me to write this summary of the rapidly changing experimental situation.

This work was supported by the USDOE.

REFERENCES

1. A. Yokosawa, Phys. Rep. 64, 47 (1980); and D. V. Bugg, Nucl. Phys. A 374, 95c (1982).

2. A. Aerts et al., Phys. Rev. Lett. 40, 1543 (1978).

3. K. Baba et al., Phys. Rev. C (July 1983).

4. R. A. Arndt, phase-shift analysis WI82 (winter 1982).

5. W. M. Kloet and J. A. Tjon, Nucl. Phys. A 392, 271 (1983).

6. K. Hidaka et al., Phys. Lett. 70B, 479 (1977).

7. S. J. Lindenbaum and R. M. Sternheimer, Phys. Rev. 105, 1874 (1957); and 123, 333 (1961).

8. A. M. Green, J. A. Niskanen, and M. E. Sainio, J. Phys. G (Nucl. Phys.) 4. 1055 (1978).

9. E. L. Lomon, Phys. Rev. D 26, 576 (1982).

10. E. E. van Faassen and J. A. Tjon, Phys. Lett. 120B, 39 (1983); and Phys. Rev. C (August 1983).

11. J. A. Niskanen, Santa Fe Polarization Conf., AIP Conf. Proc. 69, 62 (1981).

12. A. S. Rinat and A. W. Thomas, Nucl. Phys. A 282, 365, (1977); and A. S. Rinat, Y. Starkand, and E. Hammel, Nucl. Phys. A 364, 486 (1981).

13. H. Garcilazo, Phys. Rev. Lett. 45, 780 (1980).

14. C. Fayard, G. H. Lamot, and T. Mizutani, Phys. Rev. Lett. 45, 524 (1980).

15. H. Garcilazo, Phys. Rev. Lett. 48, 577 (1982).

16. I. R. Afnan and A. W. Thomas, Phys. Rev. C 10, 109 (1974).

17. W. M. Kloet and R. R. Silbar, Nucl. Phys. A 338, 281 and 317 (1980); and A 364, 346 (1981).

18. B. Blankleider and I. R. Afnan, Phys. Rev. C 24, 1572 (1981).

19. M. Betz and T.-S. H. Lee, Phys. Rev. C 23, 375 (1981).

20. A. S. Rinat, Nucl. Phys. A 397, 381 (1983).

21. J. Dubach et al., Phys. Lett. 106B, 29 (1981); and J. Phys. G (Nucl. Phys.) 8, 475 (1982).

22. K. Kubodera et al., J. Phys. G (Nucl. Phys.) 6, 171 (1980).

23. J. Bolger et al., Phys. Rev. Lett. 46, 167 (1981); and 484, 1667 (1982).

24. W. R. Gibbs, invited talk, Baltimore APS Meeting, April 1983, Los Alamos National Laboratory preprint LA-UR-83-245 (1983).

25. R. J. Holt et al., Phys. Rev. Lett. 47, 472 (1981).

26. W. Grüebler et al., Phys. Rev. Lett. 49, 444 (1982).

27. P. Walden et al., Phys. Lett. 81B, 156 (1979); E. Aprile et al., Nucl. Phys. A 335, 245 (1980); R. Bertini et al., "High Energy Spin Physics," AIP Conf. Proc. 95, 231 (1982); A. Saha et al., submitted to Phys. Lett. B; M. D. Corcoran et al., Phys. Lett. 120B, 309 (1983); and W. B. Tippens et al., to be published.

28. T.-S. H. Lee, Argonne preprint (June 1983).

29. I. P. Auer et al., Argonne preprint ANL-HEP-PR-83-27 (July 1983).

30. A. S. Rinat and R. S. Bhalerao, Weizmann preprint WIS-82 155 (1982).

31. A. König and P. Kroll, Nucl. Phys. A 356, 345 (1981).

32. I. P. Auer et al., Phys. Rev. Lett. 46, 1177 (1981).

33. J. A. McGill et al., submitted to Phys. Lett. B, July 1983.

34. R. R. Silbar et al., contribution to the Few-Body Conf., Karlsruhe, Germany, August 1983.

35. B. J. VerWest, Phys. Lett. 83B, 161 (1979).

36. G. Glass et al., Phys. Lett. B (to be published).

37. A. D. Hancock et al., Phys. Rev. C 27, 2742 (1983).

38. E. A. Umland, I. M. Duck, and G. S. Mutchler, Santa Fe Polarization Conf., AIP Proc. Conf. 69, 172 (1981).

39. R. Shypit et al., Phys. Lett. 124B, 314 (1983).

40. T. S. Bhatia et al., Phys. Rev. C (to be published).

41. B. E. Bonner et al., contribution to the Few-Body Conf., Karlsruhe, Germany, August 1983.

42. P. J. Mulders, Phys. Rev. D 25, 1269 (1982).

Medium-Energy Probes and the Interacting Boson Model

J. N. Ginocchio (Los Alamos)

Introduction

In medium and heavy nuclei far from closed shells, the number of shell-model degrees of freedom in the low-lying spectrum of nuclei becomes enormous. For example, the number of shell-model $J^\pi = 2^+$ states with only the valence nucleons active for ^{154}Sm is of the order of 10^{14}. Hence, spherical shell-model calculations of these nuclei are impossible. The collective model of Bohr and Mottelson can explain spectroscopic properties of the most interesting collective states for nuclei that have a very stable equilibrium deformation, but most nuclei do not have a stable equilibrium deformation. Such nuclei are called *transitional* nuclei. The series of samarium isotopes from ^{148}Sm to ^{154}Sm, for example, fall into this category.

Recently the interacting boson model (IBM) of the nucleus,[1] which is an approximation to the shell model, has been able to describe these transitional nuclei. This model has three basic assumptions. One is that the low-lying spectra of nuclei are composed primarily of collective pairs of valence nucleons coupled to angular momentum 0 and 2 moving about a spherical doubly magic core. The second is that these collective monopole and quadrupole nucleon pairs are approximated as bosons. And the third assumption is that the effect of the Pauli principle and other degrees of freedom, such as excitations of other pairs and excitations of the core, are assumed to be take into account through a renormalized effective boso. Hamiltonian and transition operators.

There are two versions of the IBM. The original version, called IBM-1, does not distinguish between neutrons and protons. This version has had phenomenological success in many regions of the periodic table, and can be related to the geometrical Bohr-Mottelson model.[2] In Fig. 1 we show a comparison of the spectrum of ^{168}Er produced by IBM-1 along with the spectrum seen in (n,γ) experiments.[3] These experiments measure not only the ground state band but the sidebands as well. The IBM-1 with three parameters gives a remarkable reproduction of this pattern of excited states, as well as reproducing transition rates.[3]

The second version, called IBM-2, distinguishes between neutrons and protons. This model has been used to study a number of different types of nuclei. A few examples are the samarium and thorium isotopes,[4] the palladium isotopes,[5] xenon, barium, and cesium isotopes,[6] platinum and osmium isotopes,[7] and the tungsten isotopes.[8]

Although IBM-1 is relatively simple, IBM-2 is necessary to develop a deep understanding of nuclei for several reasons. First, we have learned through phenomenological studies of the shell model that the effective interaction between like nucleons inside the nucleus is

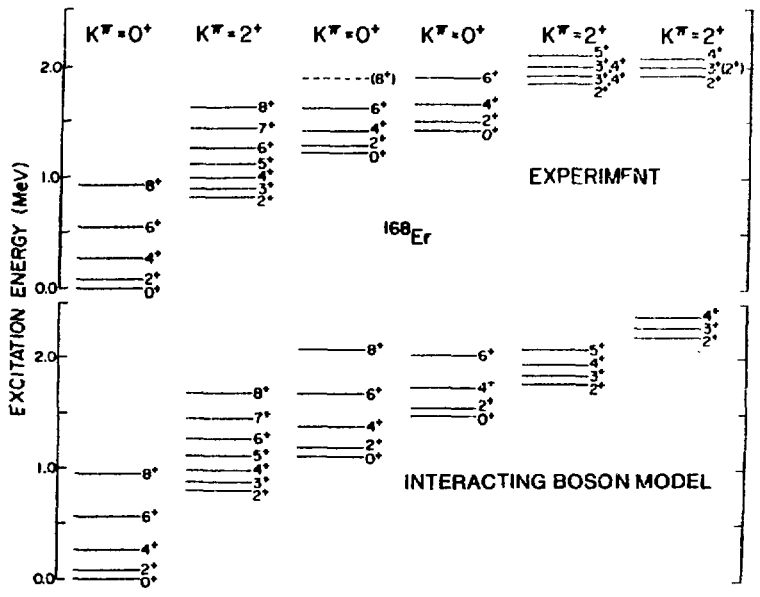

Fig. 1.
The experimental and IBM-1 spectrum for ^{168}Er from Ref. 3.

dominated by the pairing interaction and tends to make nuclei spherical. On the other hand, the effective neutron-proton interaction is dominated by a quadrupole interaction and produces nuclear deformation. Furthermore, IBM-2 has additional states that can be excited that are not in the IBM-1 space.

The states in IBM-2 that correspond to those in IBM-1 are the ones most symmetric in the neutron-proton degrees of freedom. However, the less symmetric states also may occur in the low-lying spectrum. The combined use of medium-energy electrons, pions, and protons can sort out the nature of the neutron and proton excitations in nuclei. Finally, the parameters of IBM-2 may be derived from an underlying fermion many-body system.

Here we review some of these aspects of the IBM, particularly as they apply to medium-energy scattering.

The Boson Hamiltonian

The boson Hamiltonian reflects the properties of the effective nucleon-nucleon interaction mentioned above:

$$H = \epsilon_\nu N_\nu + \epsilon_\pi N_\pi - \kappa Q_\nu \cdot Q_\pi \quad , \tag{1}$$

where ν refers to neutron bosons and π refers to proton bosons. The operators N_ν and N_π count the number of neutron and proton quadrupole bosons, respectively,

$$N_\sigma = \sum_m d^\dagger_{m\sigma} d_{m\sigma} \quad ; \quad \sigma = \nu,\pi \quad , \tag{2}$$

where $d^\dagger_{m\sigma}(d_{m\sigma})$ creates (destroys) a quadrupole boson; $m = 2, 1, 0, -1, -2$; and $\sigma = \pi$ or ν. The energies ϵ_σ are the excitation energies of the quadrupole boson with respect to the monopole boson. This part of the Hamiltonian reflects pairing between like nucleons. The second part reflects the quadrupole interaction between neutrons and protons. The operator $Q_{m\sigma}$ is the quadrupole operator and is given by

$$Q_{m\sigma} = d^\dagger_{m\sigma} s_\sigma + s^\dagger_\sigma \tilde{d}_{m\sigma} + \chi_\sigma (d^\dagger_\sigma \tilde{d}_\sigma)^{(2)}_m \quad ; \quad \sigma = \pi,\nu \quad , \tag{3}$$

where $\tilde{d}_m = (-1)^m d_{-m}$ and $s^\dagger(s)$ creates (destroys) a monopole pair. The quadrupole transition operator is

$$T_m = \sum_{\sigma=\pi,\nu} e^B_\sigma Q_{m\sigma} \quad , \tag{4}$$

where e^B_σ is the boson effective charge.

The quadrupole operator in Eq. (3) has two parts. The first changes a monopole boson into a quadrupole boson, and the second reorients the quadrupole boson. The attractive ($\kappa > 0$) quadrupole interaction reflects the neutron-proton quadrupole interaction, with the monopole-changing component producing deformed nuclei. Hence, the pairing interaction and the quadrupole interaction compete with each other. As neutrons are added to a given nucleus, the role of the proton-neutron interaction becomes more important and mixes more quadrupole bosons into the low-lying spectrum, inducing deformation.

The samarium isotopes illustrate this effect very well. The isotope ^{144}Sm is semimagic, having the neutron shells closed at magic number 82 and having no valence neutrons. The excitation energy of the first $J^\pi = 2^+$ is 1660 keV. As neutrons are added, the number of interactions between valence neutrons and protons increases, resulting in a decrease of the $J^\pi = 2^+$ excitation energy to 73 keV in ^{158}Sm.

Figure 2 shows this dramatic drop in excitation energy. Furthermore, since the pairing interaction favors pairs of protons coupled to angular momentum 0, or monopole pairs, the lowest $J^\pi = 4^+$ state in ^{144}Sm is primarily composed of monopole proton pairs, with one pair coupled to $J^\pi = 4^+$.

However, the IBM does not have such a state in its space. The only way to produce a $J^\pi = 4^+$ in the IBM space is to have two quadrupole pairs couple to angular momentum $J^\pi = 4^+$. Such a state has two broken monopole pairs; hence in a semimagic nucleus these will lie higher in energy than the one broken-pair state. However, the implicit assumption in the IBM is that the quadrupole interaction lowers the energy of the state with the quadrupole pairs more than that of the states with pairs with higher angular momentum.

In Fig. 2, calculated results are shown that illustrate this point. A schematic fermion model was used that has an SO_8 dynamical symmetry,[9] but otherwise has many features in common with the IBM-2. With only three

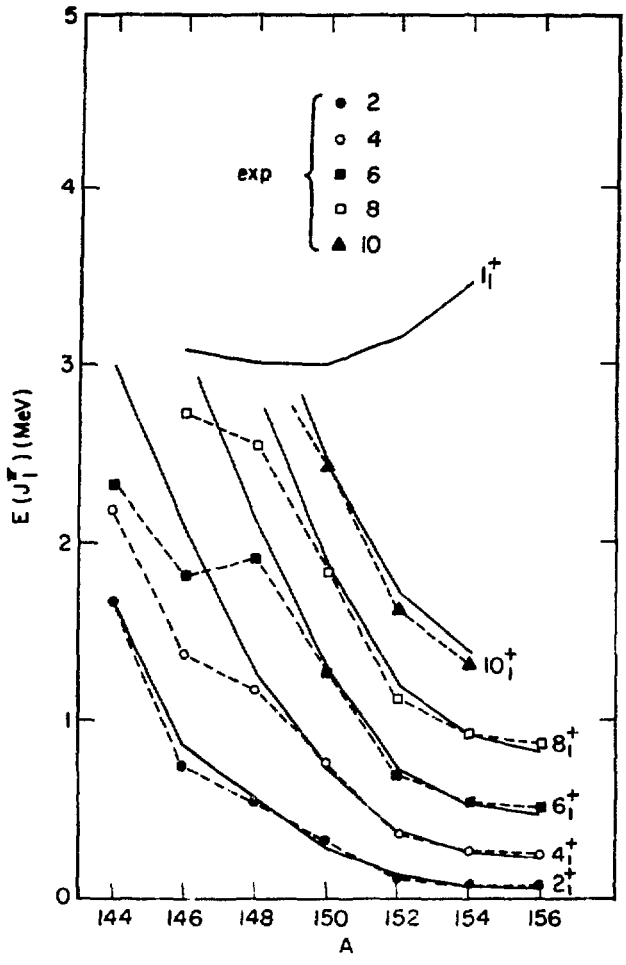

Fig. 2.
Excitation energy for some low-lying states in the samarium isotopes vs mass number. The solid lines are calculated (Ref. 9), the symbols are empirical.

parameters, the dramatic decrease in energy for the yrast levels is reproduced for the isotopes $^{148\text{-}156}$Sm. However, for the lighter isotopes the calculated levels with $J > 2$ rise much higher than the measured excitation energy.

As suggested in the previous paragraphs, the explanation for this is that for the isotopes with neutron number close to magic, the pairing interaction favors states with the fewest broken pairs. Hence the $J^\pi = 4^+$ state, for example, with one $J^\pi = 4^+$ pair, will lie lower in energy than the $J^\pi = 4^+$ state with two quadrupole pairs. Thus the $J^\pi = 4^+$ state in the IBM space, which must have at least two quadrupole pairs, will rise in energy as the nucleus becomes more nearly singly magic. Investigations are under way[10] to determine whether medium-energy scattering to high momentum transfer can help sort out these different parts of the nuclear wave function and thereby test this basic premise of the IBM.

The first $J^\pi = 1^+$ state that is predicted by this model is also plotted in Fig. 2, although experimentally no such state has yet been detected. This state is of special interest because within IBM-1 it cannot exist. This follows from the fact that identical quadrupole bosons cannot couple to angular momentum $J^\pi = 1^+$, which is obvious for two quadrupole bosons, but it turns out to be true no matter what the number of identical quadrupole bosons. However, for nuclei with neutron and proton quadrupole bosons that are active, such a state is possible. For ^{144}Sm, which has only valence protons, we see that this state does not exist, but as neutrons are added, this state appears at about 3 MeV in excitation energy. This energy prediction is a by-product of the model. Recently such a $J^\pi = 1^+$ state has been observed in electron scattering in the neighboring $^{156}_{64}$Gd nucleus at an excitation energy of about 3 MeV.[11] These types of neutron-proton excitations are of interest to probe further.

Microscopic Basis of IBM

As we stated in the Introduction, the IBM is an approximation to the nuclear shell model. How, then, do we produce a boson Hamiltonian and transition operators from a fermion Hamiltonian and transition operators?

This question is actually an old one in nuclear physics and was originally stimulated by the quadrupole vibrator model. However, there has not been a satisfactory resolution of this problem. The most difficult point is to determine the coordinate-space wave function of the monopole and quadrupole bosons. The reason for the difficulty is that this wave function varies with mass number because the renormalization effects due to the Pauli principle and the excluded pair and core excitations vary with mass number.

For nuclei near closed shells there has been some success. The procedure here is to diagonalize the shell-model Hamiltonian in the two-nucleon space and to take as the collective monopole and quadrupole pair the lowest $J^\pi = 0^+$ and 2^+ pairs. The boson Hamiltonian and transition operators are then determined by calculating matrix elements of the fermion Hamiltonian and transition operators in the subspace of fermion states with only monopole and quadrupole pairs. These matrix elements are then equated to the corresponding boson matrix elements. Since a transition operator is at most a one-boson operator, only the matrix elements with at most one quadrupole pair need be mapped, whereas for the Hamiltonian, only the matrix elements with at most two quadrupole pairs need to be mapped.[12-14] This method is called the OAI method, using the initials of the original authors[12] (the first initial belongs to Takaharu Otsuka, at present a postdoctoral fellow in T-5, who continues to pursue the microscopic understanding of the IBM).

For highly deformed nuclei there also has been some success.[15] In this case the collective pair is determined by a Hartree-Fock-Bolgolubov minimization of the fermion Hamiltonian. Because the nucleus is deformed, this pair will be an admixture of different angular momenta. About 90% of the pair is made up of a $J^\pi = 0^+$ and $J^\pi = 2^+$ pair, with the remaining 10% being a $J^\pi = 4^+$ pair.[16] The matrix elements between many collective fermion pairs are then set equal to the matrix elements between many collective bosons, with the collective boson having the same angular-momentum composition as the collective fermion pair. The effects of the $J^\pi = 4^+$ boson, or g boson, are removed by renormalizing the resulting boson Hamiltonian and transition operators.

Using this procedure, the parameters of the boson Hamiltonian [Eq. (1)] and transition operator [Eq. (4)] are determined for the nucleus ^{158}Gd (Ref. 15). The microscopic results are given in Table I. Phenomenological parameters determined by fitting spectra and transition rates of ^{158}Gd are listed in the fourth column. We see that agreement between the microscopic and phenomenologically determined parameters is very good. The last column gives the parameters determined by the OAI method, valid near spherical nuclei but invalid for a deformed nucleus like ^{158}Gd. In fact, the parameters derived by the OAI method do not produce a stable equilibrium deformation because the absolute magnitudes of χ_π and χ_ν are too small. The third column gives the

Table I. Parameters in the Boson Quadrupole Interaction and in the Boson $E2$ Operator for ^{158}Gd. The second column shows calculations obtained using the mapping method described in the text with renormalization resulting from the elimination of the g boson; the unrenormalized result is shown in the next column in parentheses. Parameters obtained by a phenomenological calculation and those by the OAI method are also shown (from Ref. 15).

Parameter	Microscopic Calculation	Unrenormalized Result	Phenomenological Parameters	OAI Method
κ (MeV)	0.094	(0.12)	0.08 ~ 0.09	0.19
χ_π	−0.86	(−0.80)	−0.8 ~ −0.9	0.04
χ_ν	−1.18	(−1.03)	−1.1 ~ −1.2	−0.55
e_π^B (e-fm^2)	12.0	(10.6)	12 ~ 14	14.3
e_ν^B (e-fm^2)	10.0	(6.7)	12 ~ 14	8.4

results before renormalization. In each case the renormalization improves agreement, but is not too large a correction—less than 35% for all parameters.

The difficult task is to handle the transitional nuclei, those between spherical and deformed. The search for a unified mapping procedure continues.

Transition Densities

The range of momentum transfer involved in medium-energy electron and proton scattering provides a tool for probing the nuclear transition density. Within the IBM, the quadrupole transition density operator is a generalization of the transition operator given in Eq. (4):

$$\hat{T}_m(r) = \sum_{\sigma=\pi,\nu} [\alpha_\sigma(r)\ (d^\dagger_{m\sigma} s_\sigma + s^\dagger_\sigma \tilde{d}_{m\sigma}) + \beta_\sigma(r)\ (d^\dagger_\sigma \tilde{d}_\sigma)^{(2)}_m] \qquad (5)$$

The boson wave transition densities $\alpha_\sigma(r)$ and $\beta_\sigma(r)$ can be determined phenomenologically or from a microscopic theory.

Recently the $0^+_g \rightarrow 2^+_1$ transition densities for $^{134}_{56}Ba_{78}$, $^{138}_{56}Ba_{82}$, and $^{124}_{50}Sn_{74}$ were measured in electron scattering.[17] The nucleus $^{138}_{56}Ba_{82}$ has a closed neutron shell, hence the density is due primarily to the valence protons. Furthermore, since it is singly magic, the ground state is primarily monopole bosons. Hence the matrix element of $(d^\dagger_\sigma \tilde{d}_\sigma)^{(2)}_m$ to the first $J^\pi = 2^+$ state will vanish. Therefore the transition density will depe predominantly on $\alpha_\pi(r)$. Consequently, this function can be determined phenomenologically. Likewise, $\alpha_\nu(r)$ can be determined from the transition density for $^{144}_{50}Sn_{74}$.

Because $^{133}_{56}Ba_{78}$ has both valence neutrons and protons, it is more complicated than either ^{138}Ba or ^{124}Sn, but the wave functions have been determined in IBM-2 (Ref. 6). To determine the transition density for ^{134}Ba, we need to know $\beta_\sigma(r)$. It turns out, however, that the matrix elements of $(d^\dagger_\sigma \tilde{d}_\sigma)^{(2)}_m$ between 0^+_g and 2^+_1 i. !% or less of the matrix element of $s^\dagger \tilde{d}_m + d^\dagger_m s$ between these two states.[17] Hence the transition density will not be sensitive to β_σ.

Ignoring β_σ, we can determine the transition density of ^{134}Ba from the phenomenologically determined α_σ and the IBM-2 wave functions. Of course we must assume that the structure of the monopole and quadrupole pair does not change appreciably between ^{138}Ba (^{124}Sn) and ^{134}Ba. In Fig. 3 the empirical transition density is given by the hatched line, where the hatches measure the uncertainty in experimental analysis. The solid line is the IBM-2 transition density, determined by combining the phenomenologically determined α_σ's and the IBM-2 wave functions. On the surface the measured and IBM-2 transition densities overlap and are undistinguishable.[17]

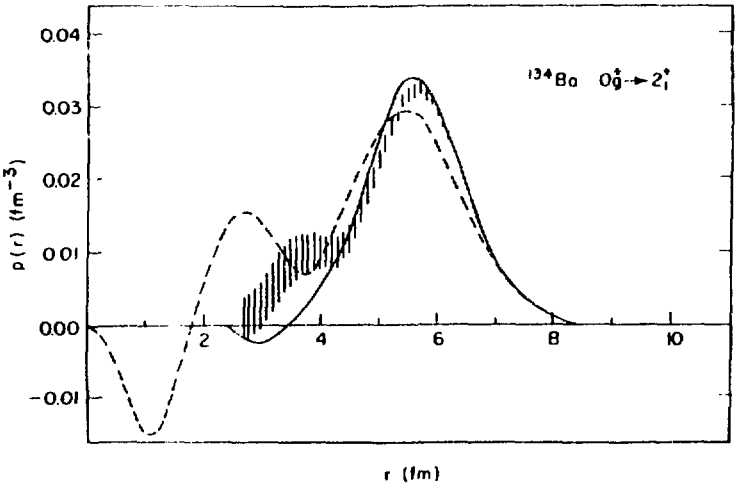

Fig. 3.
The transition density $p(r)$ for the $0^+_g \rightarrow 2^+_1$ transition in ^{134}Ba. The hatched line is the empirical transition density, the solid line is the phenomenological IBM-2 density, and the dashed line is the microscopic IBM-2 density, as explained in the text.

In the interior region there seems to be some disagreement. However, since the phenomenologically determined $\alpha_\sigma(r)$ is less certain in the interior, the extent of al disagreement is unclear. Further, since the IBM-2 transition density becomes small for $r \sim 3.5$ fm, the neglected effects such as β_σ and renormalization of α_σ may be important. Although not shown on the curve, the Tassie transition density extends further out on the surface, in disagreement with the empirical transition density.

The functions $\alpha_\sigma(r)$ can be determined microscopically as well. The structure of the monopole pair has been determined from a BCS calculation for both ^{124}Sn and ^{138}Ba within one major shell using harmonic oscillator wave functions. The quadrupole pair is determined by operating on the monopole pair with the (fermion) quadrupole operator.[17] The result is given by the dashed line in Fig. 3. The microscopic result is shifted to a lower radius than that of the empirical transition density (hatched line). However, core polarization was neglected in the microscopic transition density; this could reduce the wiggles. Improved calculations are under way in which core polarization and more realistic single-nucleon wave functions can be included in the microscopic transition density.*

Glauber Approximation and IBM

Because the interaction of electrons with nuclei is weak, medium-energy electron scattering can be analyzed using the distorted-wave Born approximation (DWBA). For hadronic probes this is not necessarily the case. For 800-MeV protons, multiple scattering is important at high momentum transfer.[18,19] One approach for taking multiple scattering into account is to solve a set of coupled-channel equations.[18] Another approach is to calculate the transition matrix to all orders in the Glauber approximation.[20] Although the physics content of these two approaches is similar, the Glauber approximation gives more insight and is numerically simpler.[19]

For a strongly deformed nucleus such as ^{154}Sm, the Bohr-Mottelson model can be used to evaluate the Glauber transition matrix to all orders.[19] In Fig. 4 the results of this calculation are shown for 800-MeV proton elastic and inelastic scattering from ^{154}Sm (solid line) and

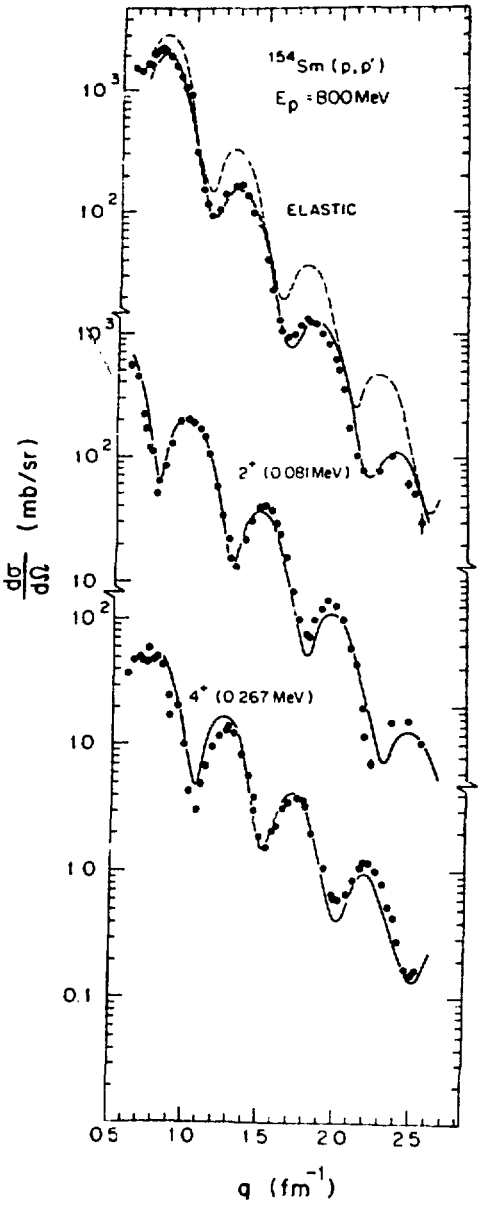

Fig. 4.
The differential cross section vs momentum transfer for 800-MeV proton elastic and inelastic scattering from ^{154}Sm. The dots are the data (Ref. 18), the solid line is the Glauber approximation using a deformed density (Ref. 19), and the dashed line is the distorted-wave approximation to the elastic scattering.

*T. Otsuka, private communication.

are compared to the experimental data.[18] The agreement is very good. The dashed line shows the DWBA prediction for elastic scattering. One sees the inadequacy of the DWBA in reproducing the phase and amplitudes of the differential cross section at high momentum transfer.

Recently we have realized that the Glauber approximation can be combined with the IBM such that the transition matrix can be evaluated to all orders in closed form.[10] This combination arises from the fact that the Glauber transition operator is a linear rotation in the IBM space. For example, if the incoming projectile has a quadrupole interaction with the target, the Glauber transition matrix for scattering a projectile with momentum $\vec{k}$ to $\vec{k'}$ with resulting momentum transfer,

$$\vec{q} = \vec{k'} - \vec{k} \quad , \tag{6a}$$

is

$$\langle f | T | i \rangle = \frac{k}{2\pi i} \int d^2b \quad e^{i\vec{q}\cdot\vec{b}} (U_{fi}^{(\pi)} U_{fi}^{(\nu)} - \delta_{fi}) \quad , \tag{6b}$$

where

$$U_{fi}^{(\sigma)} = e^{i\eta_\sigma} M_{fi}^{(\sigma)} \tag{6c}$$

and the reduced transition matrix is

$$M_{fi}^{(\sigma)} = \langle f_\sigma | e^{i\psi_\sigma C^{(2)}(\hat{b})\cdot Q_\sigma} | i_\sigma \rangle \quad . \tag{6d}$$

In the above, f and i label the final and initial states, respectively. Denoting the positon of the incoming projectile as $\vec{r}$, the two-dimensional impact radius $\vec{b}$ is

$$\vec{r} = \vec{b} + k\hat{z} \quad , \tag{7}$$

where $\hat{k}$ is the unit vector of the projectile momentum. Within an optical-model approximation, the Glauber phases are

$$\eta_\sigma = \frac{2\pi f_\sigma}{k} \int_{-\infty}^{\infty} \rho_\sigma[(b^2 + z^2)^{1/2}] \, dz \quad , \tag{8a}$$

$$\psi_\sigma = \frac{2\pi f_\sigma g_\sigma}{k} \int_{-\infty}^{\infty} \frac{r d\rho_\sigma}{dr} dz \quad , \tag{8b}$$

where f_σ is the forward-scattering amplitude of the projectile and proton ($\sigma = \pi$) or neutron ($\sigma = \nu$); g_σ is the quadrupole coupling strength between the projectile and target nucleon; $C_m^{(\ell)}(\hat{b})$ is the projectile unit spherical tensor of rank ℓ,

$$C_m^{(\ell)}(\hat{b}) = \left(\frac{4\pi}{2\ell + 1} \right)^{1/2} Y_m^{(\ell)}(\hat{b}) \quad , \tag{9}$$

and $\rho_\sigma(r)$ is the proton ($\sigma = \pi$) or neutron ($\sigma = \nu$) matter density.

Because the operator in the matrix element [Eq. (6d)] is an exponential function of the boson quadrupole operator [Eq. (3)], this operator has the effect of rotating the bosons in the initial nuclear wave function into those of the final nuclear wave function. For the example of a quadrupole vibrator, this transition matrix from the ground state can be simply derived.[10]

The ground state of the quadrupole vibrator is a boson condensate of N monopole bosons, where N is one-half the number of valence nucleons. Excited states are labeled by the number n of quadrupole bosons, or "phonons," with the energy of the states increasing approximately linearly with n. For a given n there is a multiplet of states, with the quantum number τ designating the number of quadrupole bosons not coupled, in pairs, to angular momentum 0, the quantum number n_Δ designating the number of quadrupole bosons coupled in triplets to angular momentum 0, and of course the angular momentum J and its projection M. The allowed values of these quantum numbers are

$$\tau = n \ , \quad n-2 \ , \quad \ldots \ , \text{ and finally 1 or 0} \quad , \tag{10a}$$

and for each τ the allowed angular momenta and n_Δ are determined by all possibilities of partitioning τ,

$$\tau = 3n_\Delta + \lambda \quad , \tag{10b}$$

where n_Δ and λ are integers. Then the allowed J are

$$J = 2\lambda \ , \quad 2\lambda - 2 \ , \quad 2\lambda - 3 \ , \quad \ldots \ , \quad \lambda \quad . \tag{10c}$$

The reduced transition matrix for scattering from the initial ground state ($n = \tau = n_\Delta = J = M = 0$) to an excited final state with quantum numbers n, τ, n_Δ, J, M is

$$M_{fi}^{(\sigma)} = \left[\frac{N!(2\tau+3)!!}{(N-n)!(n+\tau+3)!!(n-\tau)!!} \right]^{1/2} \times e^{iN\tilde{\chi}_\sigma} W_\sigma^{(N-n)} X_\sigma^{\ n} A_{\tau n_\Delta J} C_M^{(J)}(\hat{b})^* \quad , \tag{11}$$

where $A_{\tau n_\Delta J}$ is a constant that is independent of the Glauber phase ψ_σ. The functions W, X are

$$W_\sigma = \cos\psi_\sigma |1+\tilde{\chi}_\sigma^2|^{1/2} - \frac{i\tilde{\chi}_\sigma}{|1+\tilde{\chi}_\sigma^2|^{1/2}} \sin\psi_\sigma |1+\tilde{\chi}_\sigma^2|^{1/2} \quad , \tag{12a}$$

$$X_\sigma = i \frac{\sin\psi_\sigma |1+\tilde{\chi}_\sigma^2|^{1/2}}{|1+\tilde{\chi}_\sigma^2|^{1/2}} \quad , \tag{12b}$$

and

$$\tilde{\chi}_\sigma = -\left(\frac{1}{14}\right)^{1/2} \chi_\sigma \quad . \tag{12c}$$

The coefficients $A_{\tau n_\Delta J}$ are given in Table II for the lowest values of τ.

In Fig. 5 an example of the elastic differential cross section for the scattering of 800-MeV protons from a vibrational nucleus is shown as a function of the momentum transfer. The solid line is the differential cross section given by the transition matrix of Eq. (11), which includes all the multiple scattering. The dashed line does not include the multiple scattering but is the DWBA elastic differential cross section. We see that for high momentum transfer the higher order multiple scattering makes a substantial difference even in the elastic channel, particularly in the phase relationship between maxima and minima.

Table II. Coefficients $A_{\tau n_\Delta J}$ for the Lowest Values of τ.

τ	n_Δ	J	A
0	0	0	1
1	0	2	1
2	0	2	$-[1/7]^{1/2}$
2	0	4	$[9/35]^{1/2}$
3	0	6	$[3/77]^{1/2}$
3	0	4	$-(1/7)[6/5]^{1/2}$
3	0	3	0
3	1	0	$-[1/105]^{1/2}$

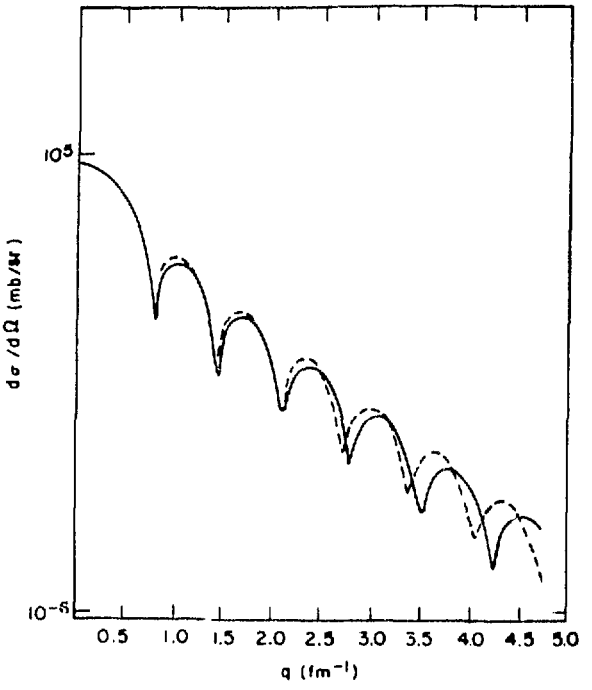

Fig. 5.
The differential cross section vs momentum transfer for 800-MeV proton scattering from a typical quadrupole vibrator in the Glauber approximation (Ref. 10). The dashed line is the distorted wave approximation to the elastic scattering.

Summary

Because medium-energy projectiles can probe the nucleus at high momentum transfer, detailed information about static and transition densities can be determined. The IBM gives a framework to study these derived densities both phenomenologically and microscopically. Of particular interest is the transition from spherical to deformed nuclei. Furthermore, because of the algebraic nature of the IBM, multiple scattering in the Glauber approximation, which becomes important at high momentum transfer, can be treated exactly to all orders.

Also, because medium-energy probes have varieties of electromagnetic and hadronic charge, the neutron and proton static and transition densities can be disentangled. These neutron and proton degrees of freedom can be analyzed in IBM-2.

Although in this review we have restricted ourselves to even-even nuclei, odd nuclei can be studied in a similar manner in the interacting boson-fermion model.[21]

REFERENCES

1. A. Arima and F. Iachello, Ann. Rev. Nucl. Part. Sci. 31, 75 (1981).
2. J. N. Ginocchio and M. W. Kirson, Nucl. Phys. A 350, 31 (1980).
3. D. D. Warner, R. F. Casten, and W. F. Davidson, Phys. Rev. C 24, 1713 (1981).
4. O. Scholten, "A Phenomenological Study of Even-Even Nuclei in the Neutron-Proton IBM," in *Interacting Bosons in Nuclei*, F. Iachello, Ed. (Plenum Press, New York, 1979), pp. 17-35.
5. P. van Isacker and G. Paddu, Nucl. Phys. A 348, 125 (1980).
6. G. Paddu, O. Scholten, and T. Otsuka, Nucl. Phys. A 348, 109 (1980).
7. R. Bijker, A. E. L. Dieperink, O. Scholten, and R. Spanhoff, Nucl. Phys. A 344, 207 (1980).
8. B. R. Barrett and P. D. Duval, "Recent IBM-2 Calculations," in *Interacting Bose-Fermi Systems in Nuclei*, F. Iachello, Ed. (Plenum Press, New York, 1981), pp. 47-52.
9. A. Arima, J. Ginocchio, and N. Yoshida, Nucl. Phys. A 384, 112 (1982).
10. J. N. Ginocchio, in the Proc. of the Workshop on Nuclear Collective States, Suzhow University, China, L. M. Yang, G. O. Zhou, S. S. Wu, Z. Q. Zhou, and D. H. Feng, Eds., (1983); Los Alamos National Laboratory document LA-UR-83-3638; and to be published in a special issue of Nucl. Phys. A (1984).
11. A. Richter, in the Proc. of the Int. Conf. on Nuclear Physics, Florence, Italy (1983), Vol. 2.
12. T. Otsuka, A. Arima, and F. Iachello, Nucl. Phys. A 309, 1 (1978).
13. T. Otsuka, Phys. Rev. Lett. 46, 710 (1981).
14. S. Pittel, P. D. Duval, and B. R. Barrett, Ann. Phys. 144, 168 (1982).
15. T. Otsuka, Los Alamos National Laboratory document LA-UR-83-1744, to be published in Phys. Lett. (1984).
16. T. Otsuka, A. Arima, and N. Yoshinaga, Phys. Rev. Lett. 48, 387 (1982).
17. T. Otsuka, K. Mori, Y. Mizuno, T. Terasawa, and Y. Torizuka, "Test of the Interacting Boson Model by Inelastic Electron Scattering for the 2^+ State of ^{134}Ba," to be published in Phys. Lett. (1984).
18. M. L. Barlett, J. A. McGill, L. Ray, M. M. Barlett, G. W. Hoffman, N. M. Hintz, G. S. Kyle, M. A. Franey, and G. Blanpied, Phys. Rev. C 22, 1168 (1980).
19. R. D. Amado, J. A. McNeil, and D. A. Sparrow, Phys. Rev. C 25, 13 (1982).
20. R. J. Glauber, "High-Energy Collision Theory," in *Lectures in Theoretical Physics*, Vol. 1, W. E. Brittin and L. G. Dunham, Eds. (Interscience Publishers, Inc., New York, 1959), pp. 315-414.
21. F. Iachello, "Present Status of the Interacting Boson-Fermion Model," in *Interacting Bose-Fermi Systems in Nuclei*, F. Iachello, Ed. (Plenum Press, New York, 1981), pp. 273-283.

Implications of Using Approximate Chiral-Dynamics $\pi N \rightarrow \pi\pi N$ Amplitude in the Calculation of $A(\pi,2\pi)$ Cross Sections

R. S. Bhalerao and L.-C. Liu (Los Alamos)

We have completed a study of the relative importance of the diagrams contributing to the $\pi N \rightarrow \pi\pi N$ reaction in the framework of the Weinberg effective Lagrangian theory. Various approximate schemes in the recent literature used to calculate the $\pi N \rightarrow \pi\pi N$ amplitude and thus the $A(\pi,2\pi)$ cross sections have been found to be inadequate. Besides the total cross sections, we have studied for the first time the angular correlations of the outgoing pions and the energy spectrum of the outgoing nucleon in the $\pi N \rightarrow \pi\pi N$ reaction. A brief description of this investigation, which we think is of vital importance for theoretical interpretation of the $A(\pi,2\pi)$ experiments planned at LAMPF, is given here. (Details can be found in a paper, with the same title as this experiment, to be submitted to Phys. Rev. C.)

For definiteness, we consider the reaction

$$\pi^-(Q) + p(p_i) \rightarrow \pi^+(q_1) + \pi^-(q_2) + n(p_f) \quad , \qquad (1)$$

with the four-momenta of the respective particles written in parentheses. The invariant amplitude T for this reaction, which can be calculated using Weinberg's effective Lagrangian[1,2] in the lowest order perturbation theory, and has the form[3]

$$T = T^{(1)} + T^{(2)} + T^{(3)} + T^{(K)} \quad . \qquad (2)$$

$T^{(1)}$ is composed of the pion-pole term and the contact term. $T^{(2)}$ and $T^{(3)}$ are the so-called two- and three-point diagrams with one- and two-nucleon propagators, respectively. $T^{(K)}$ is the anomalous magnetic-moment term. Various approximations to the above amplitude have been proposed in the literature. We describe them briefly in the following paragraphs.

Olsson and Turner[2] (OT) have neglected the contributions of $T^{(3)}$ and $T^{(K)}$ and have calculated $T^{(1)}$ and $T^{(2)}$ in the threshold approximation defined by $q_1 = q_2 = (m_\pi, \vec{0})$, $p_f = (m_N, \vec{0})$, $Q = Q_{thr}$, and $p_i = p_{i,thr}$. They have made this approximation also in the invariant phase space and have calculated $\pi N \rightarrow \pi\pi N$ cross sections up to $T_\pi = 300$ MeV.

Rockmore[4] (R1) has neglected $T^{(2)}$, $T^{(3)}$, and $T^{(K)}$ and has calculated $T^{(1)}$ and the invariant phase space in the threshold approximation defined above. He has used this procedure to calculate $A(\pi,2\pi)$ cross sections up to $T_\pi = 290$ MeV.

Recently, Rockmore[5] (R2) has neglected $T^{(2)}$, $T^{(3)}$, $T^{(K)}$, and the contact term in $T^{(1)}$, made the threshold approximation, and thus calculated $A(\pi,2\pi)$ cross sections up to $T_\pi = 280$ MeV.

Eisenberg and Cohen[6] (EC) retained the contributions of $T^{(1)}$ and $T^{(2)}$, made the threshold approximation, and used the center-of-mass amplitude in the laboratory frame to calculate the $A(\pi,2\pi)$ cross sections.

In spite of the diversity of these approximations, we note that as soon as the threshold approximation is invoked, the amplitude T becomes independent of the energy and momentum of the particles in the final state. As a consequence, these different approximate calculations differ from each other and from the phase space only by constant multiplicative factors. That is to say, they all have the same energy and angular dependence as that predicted by the phase space.

Figures 1 and 2 show the relative importance of the various terms in Eq. (2), with and without the threshold approximation. It is evident from Fig. 1 that even at $T_\pi = 190$ MeV the contact term and $T^{(2)}$ are far from negligible with respect to the pion-pole term. $T^{(3)}$, however, is relatively less important until $T_\pi \sim 240$ MeV; $T^{(K)}$ is negligible over the entire energy region considered.

It is clear from Fig. 2 that even in the near-threshold region there are sizable differences among the exact and the approximate curves. The relatively close agreement of the curve labeled R2 with the low-energy data is somewhat fortuitous in that this curve is based on the most extreme of the approximations—that which neglects all but the pion-pole term in Eq. (2).

The remaining curves tend to underestimate the exact theoretical cross sections significantly. Considering that the exact theoretical cross sections in turn are much smaller than the experimental data, the approximate amplitudes for $\pi N \rightarrow \pi\pi N$ (except R2), when used in the calculation of $(\pi,2\pi)$ cross sections on nuclei, tend to underestimate the $A(\pi,2\pi)$ data, in some cases by an order of magnitude. Results in Refs. 4-6 should be viewed in light of these remarks. (Incidentally, our remark above concerning the essential phase-space nature of the calculations in Refs. 2 and 4-6 is borne out by Fig. 2.)

It has been suggested in Ref. 6 that the existence of pion condensation precursor phenomena would enhance the $A(\pi,2\pi)$ cross sections considerably above what would be observed otherwise, and that such an enhancement could provide partial evidence in support of such

REFERENCES

1. S. Weinberg, Phys. Rev. Lett. 18, 188 (1967).

2. M. G. Olsson and L. Turner, Phys. Rev. Lett. 20, 1127 (1968).

3. R. A. Arndt et al., Phys. Rev. D 20, 651 (1979).

4. R. Rockmore, Phys. Rev. C 11, 1953 (1975).

5. R. Rockmore, Phys. Rev. C 27, 150 (1983).

6. J. M. Eisenberg, Phys. Lett. 93B, 12 (1980); J. Cohen and J. M. Eisenberg, Nucl. Phys. A 395, 389 (1983), and Nuovo Cimento 76A, 488 (1983); and J. Cohen, J. Phys. G 9, 621 (1983).

7. C. W. Bjork et al., Phys. Rev. Lett. 44, 62 (1980).

Report of the T-5 Theoretical Group

T. Goldman (Los Alamos)

This is a brief summary of some of the T-5 research activities relevant to LAMPF and LAMPF II. Because this report is included in a basically experimental document, items of a primarily technical nature have been omitted.

While continuing their research role, T-5 staff members have invested a substantial amount of time and effort to further the LAMPF II project, including preparing for and running conferences and workshops, reporting at plenary sessions, and contributing to and editing the resulting proceedings. Major efforts included the Theoretical Symposium on Intense Medium-Energy Sources of Strangeness at the University of California, Santa Cruz, and the Third LAMPF II Workshop at Los Alamos. Material in the Santa Cruz[1] and Los Alamos[2] Proceedings is not repeated here. In addition, T-5 staff members have argued the physics justification for LAMPF II in public forums and in the LAMPF II proposal.

Research Related to LAMPF

We have made several developments in the code PIPROD. Motivated by the imminence of a number of experiments at LAMPF and elsewhere, we have extended PIPROD to calculate spin-transfer coefficients (Wolfenstein parameters, D_{LL}, etc.) that measure the dependence of the $NN \rightarrow NN\pi$ reaction on the spin directions of one initial and one final nucleon. We have numerically integrated exclusive cross-section predictions from PIPROD to produce inclusive cross sections and spin observables. Our parameter-free prediction (using only one-pion-exchange forces) for the polarized beam asymmetry in the reaction $\vec{p}+p \rightarrow p'+X$ is in good agreement with a recent HRS experiment. Our preliminary results on the spin-transfer coefficients for $\vec{p}+p \rightarrow \vec{n}+X$, however, do not agree so well with another recent experiment. This is perhaps an indication that a dibaryon resonance can show up in this particular spin observable but not in others.

We have also employed PIPROD to calculate the relative absorption rates of pions on a pair of (free) nucleons, using a relativistic isobar model for the coupled NN and $NN\pi$ systems that respects two- and three-body unitarity. In contrast with an earlier calculation that only considered $N\Delta$ intermediate states, we found that much of the absorption takes place through an intermediate state involving a nucleon and a (nonresonant) interacting pion-nucleon pair with the same quantum numbers as the nucleon. Moreover, this effect was able, for the first time, to explain qualitatively the order-of-magnitude changes in the proton-proton to proton-neutron suppression as the incident pion energy increases from zero (capture at rest) to above the Δ resonance. In general, for the inverse reaction $NN \rightarrow NN\pi$, this mechanism is rather unimportant compared with the $N\Delta$ state. Thus, the experimental investigation of two-nucleon pion absorption in light nuclei may clarify details of the weaker πN interactions. Much of our $NN\pi$ work is summarized in the preceding report in this section by R. Silbar.

Configuration-space, local-potential Faddéev calculations were extended to the Coulomb problem of elastic scattering of protons by deuterons at zero incident energy. We found that the spin-doublet scattering length a_2^{pd} was approximately zero. This differs substantially from (1) the accepted experimental value, (2) theoretical estimates using approximation schemes to combine Coulomb effects with known neutron-deuteron amplitudes to obtain a_2^{pd}, and (3) intuitive estimates based on the established linear relationship between the triton binding energy and the neutron-deuteron doublet scattering length. (The fact that the binding energy of ^{3}He is smaller than that of ^{3}H led people to expect that a_2^{pd} would be larger than $a_2^{nd} \cong 0.7$ fm.) However, the qualitative features of the Coulomb correction to the doublet scattering length are analogous to Coulomb corrections in the two-body scattering problem when the scattering length is small (as for pion-nucleon scattering). Thus, although novel, the results of our Faddéev calculations are *a posteriori* quite understandable.

Eikonal expansions were developed for the amplitudes in the scattering of Dirac particles (protons) by central scalar and vector potentials, and for the corresponding Schrödinger case with central and spin-orbit potentials. The eikonal phases were calculated through second-order corrections. Our motivation was to correlate the Dirac and Schrödinger approaches to proton-nucleus scattering, to develop systematically a practical formalism for calculation, and to provide insight into the scattering process. Recently, the Dirac phenomenology approach to optical potentials has given a more economical description of spin-dependent observables in medium-energy proton-nucleus scattering than the usual Schrödinger approach. Our analysis elucidates the simple physical reasons for this.

The $\pi^0 \rightarrow \mu^{\pm} e$ decays were investigated and an experimental upper limit of

$$\frac{1}{2} \frac{\Gamma(\pi^0 \rightarrow \mu^+ e^-) + \Gamma(\pi^0 \rightarrow \mu^- e^+)}{\Gamma(\pi^0 \rightarrow all)}$$

$$< 7 \times 10^{-8} \text{(90\% confidence level)}$$

was deduced from available data. We also considered the existing constraints on the underlying muon-number-violating interaction. We found that the present experimental information on $\mu^- \rightarrow e^-$ conversion in sulfur implies an upper bound on the individual $\pi^0 \rightarrow \mu^{\pm} e$ branching ratios of about 10^{-15}.

Research Relevant to LAMPF II

Study of K^+-nucleus elastic scattering has been pursued. Comparison with the available data on ^{12}C and ^{40}Ca shows no conflicts with the scattering theory. We conclude that the goal of precision measurements of the nuclear density, as seen by a K^+, can be achieved as soon as accurate data on the fundamental K^+-nucleon system can be obtained.

A new investigation of the Λ lifetime in nuclear matter has been completed. The free decay $\Lambda \rightarrow \pi N$ is severely inhibited in nuclei because of Pauli blocking of the nucleon, and the weak nonleptonic transition $\Lambda N \rightarrow NN$ dominates the decay process. The long-standing discrepancy between the calculation of Adams ($\Gamma_{nm}/\Gamma_{free} = 0.06$) and the single experimental value for ^{16}O, which was determined by only 22 events ($\Gamma_{nm}/\Gamma_{free} = 3 \pm 1$), has been resolved; an incorrect coupling constant was used in the earlier theoretical investigation. Including model estimates of the effects of short-range correlations, tensor forces, and heavy-meson exchange in the weak interaction (in addition to one-pion exchange), and allowing for uncertainties in the various coupling constants and the vertex form factors, we estimate the ratio by $\log_{10}(\Gamma_{nm}/\Gamma_{free}) = 0 \pm 0.3$.

Detailed studies of the muon-number-violating decay modes of hyperons were carried out, both in a phenomenological framework and in considering some possible sources of muon-number violation. We find that branching ratios as large as 10^{-6} cannot be excluded by available data and that they are consistent with some extensions of the three-generation minimal (standard) electroweak model. However, such branching ratios require the muon-number-violating interaction to be of a very special structure.

The experimental limit of $d_n \lesssim 6 \times 10^{-25}$ e-cm for the electric-dipole moment of the neutron has ruled out some of the many theories proposed to explain the CP and T violation observed in kaon decays. We have demonstrated that many-body effects can lead to large enhancements of nuclear electric-dipole moments, which in certain cases fully compensate for the effects of atomic shielding; thus, the latter need no longer limit measurements of the proton electric-dipole moment d_p. The recent development of experimental techniques to measure atomic-dipole moments at levels well below the limit on d_n leads us to conclude that comparable stringent new limits on both d_n and d_p may be obtained with significant implications for predictions in the kaon system.

Anyone wishing further information on these subjects may contact Group T-5 members J. L. Friar, W. R. Gibbs, B. F. Gibson (Group Leader), J. N. Ginocchio, T. Goldman, W. C. Haxton, L. Heller, P. Herczeg, R. R. Silbar, or G. J. Stephenson, Jr. (Acting P-3 Group Leader).

REFERENCES

1. T. Goldman, H. E. Haber, and H. F.-W. Sadrozinski, Eds., *Intense Medium-Energy Sources of Strangeness*, University of California, Santa Cruz, 1983. AIP. Conf. Proc. No. 102, Particles and Fields Subseries No. 31 (American Institute of Physics, New York, 1983).

2. "Proceedings of the Third LAMPF II Workshop," Vols. I and II, Los Alamos National Laboratory report LA-9933-C (1983).

Group T-5 Publications

J. L. Friar, B. F. Gibson, and G. L. Payne, "Three-Nucleon Forces and Meson-Exchange Currents in the Trinucleon," Comments Nucl. Part. Phys. **11**, 51 (1983).

J. L. Friar, "Classification of Exchange Currents," Phys. Rev. C 27, 2078 (1983).

J. L. Friar and E. L. Tomusiak, "Threshold Pion Photoproduction from the Trinucleon," Phys. Lett. **122B**, 11 (1983).

J. L. Friar and B. H. J. McKellar, "Pion Exchange Contributions to the Lobashov Experiment," Phys. Lett. 123B, 284 (1983).

J. L. Friar, S. Fallieros, E. L. Tomusiak, D. Skopik, and E. G. Fuller, "Electric Polarizability of the Deuteron," Phys. Rev. C 27, 1364-1366 (1983).

J. L. Friar, "Three-Body Forces," Indiana University Cyclotron Facility (IUCF) Workshop on the Interaction Between Medium-Energy Nucleons in Nuclei—1982, H. O. Meyer, Ed., AIP Conf. Proc. 97, 378 (1983).

J. L. Friar, B. F. Gibson, and G. L. Payne, "The Proton-Deuteron Scattering Length," Phys. Lett. 124B, 287 (1983).

B. F. Gibson, C. B. Dover, G. Bhamati, and D. R. Lehman, "Binding Energy Estimates for Charmed Few-Body Systems," Phys. Rev. C 27, 2085 (1983).

B. F. Gibson, W. M. Kloet, G. J. Stephenson, Jr., and E. M. Henley, "Parity Nonconserving Asymmetry in Neutron-Deuteron and Proton-Deuteron Scattering," Phys. Rev. C 27, 2529 (1983).

J. L. Friar, B. F. Gibson, and G. L. Payne, "Configuration-Space Faddéev Calculations: VI. Triton Wave Function," Z. Phys. A 312, 169 (1983).

J. L. Friar, B. F. Gibson, and G. L. Payne, "Configuration-Space Faddéev Calculations: *pd s*-Wave Scattering Length," Phys. Rev. C 28, 983 (1983).

B. F. Gibson and D. R. Lehman, "Structure of the $^3H \rightarrow nd\ (d^*)$ Vertices," Los Alamos National Laboratory document LA-UR-83-2960 (to be published in Phys. Rev. C).

W. C. Haxton and E. M. Henley, "Enhanced T-Nonconserving Nuclear Moments," Phys. Rev. Lett. 51, 1937 (1983).

W. C. Haxton, "Double Beta Decay," Comments Nucl. Part. Phys. 11, 41 (1983).

W. C. Haxton, "Double Beta Decay," in the *McGraw-Hill 1984 Yearbook of Science and Technology.*

E. G. Adelberger, W. C. Haxton, M. M. Hindi, C. D. Hoyle, and R. D. Von Lintig, "The Beta Decays of ^{18}Ne and ^{19}Ne and their Relation to Parity Mixing in ^{18}F and ^{19}F," Phys. Rev. C 27, 2833 (1983).

G. A. Cowan, M. Goldhaber, and W. C. Haxton, "A Radiochemical Test of Double Beta Decay," Phys. Rev. C 28, 467 (1983).

W. C. Haxton and G. J. Stephenson, Jr., "A Comment on 'Nilsson-Pairing Model for Double Beta Decay,'" Phys. Rev. C 28, 458 (1983).

W. C. Haxton et al., "Neutron and Proton Transition Matrix Elements for ^{90}Zr from a Microscopic Analysis of 0.8-GeV Proton Inelastic Scattering," Phys. Rev. C 28, 294 (1983).

P. Herczeg and T. Oka, "Study of Muon-Number-Violating Hyperon Decays" (to be published in Phys. Rev. D, February 1984).

P. Herczeg and C. M. Hoffman, "Study of $\pi^0 \rightarrow \mu^{\pm}e$ Decays" (submitted to Phys. Rev. D).

Dean Preston and T. Goldman, "The Strangeness-Conserving Effective Weak Interaction in the Quark Basis," Nucl. Phys. B 217, 31 (1983).

T. Goldman and Dean Preston, "A Quark Model Calculation of the Weak Parity-Violating Asymmetry in High-Energy Proton-Nucleon Scattering," Nucl. Phys. B 217, 61 (1983).

R. R. Silbar and E. Piasetzky, "Isospin Dependence of Pion Absorption on Nucleon Pairs," Los Alamos National Laboratory document LA-UR-83-1883 (to be published in Phys. Rev. C).

R. R. Silbar and E. Piasetzky, "Ratio of Pion-Induced Nucleon Removal Cross Section Involving Charge Exchange," Phys. Rev. C 27, 894 (1983).

T. S. Bhatia, J. G. J. Boissevain, J. J. Jarmer, J. E. Simmons, G. Glass, J. C. Hiebert, R. A. Kenefick, L. C. Northcliffe, W. B. Tippens, R. R. Silbar, W. M. Kloet, and J. Dubach, "Analyzing Powers and Spin Correlations A_{NN} and A_{LL} for $pp \rightarrow np\pi^+$ at 650 and 800 MeV" (to be published in Phys. Rev. C).

J. N. Ginocchio, "A Class of Exactly Solvable Potentials: I. One-Dimensional Schrödinger Equation" (to be published in Ann. Phys. 152, 1984).

J. N. Ginocchio, "An SO_8 Model of Collectivity in Nuclei," in *Bosons in Nuclei*, D. H. Feng, M. Vallieres, and S. P. Hel, Eds. (World Scientific Publishers Press, Singapore, 1984).

W. R. Gibbs, J. Kogut, M. Stone, H. W. Wyld, J. Shigemitsu, S. H. Shanker, and D. K. Sinclair, "Deconfinement and Chiral Symmetry Restoration at Finite Temperatures in $SU(2)$ and $SU(3)$ Gauge Theories," Phys. Rev. Lett. 50, 393 (1983).

W. R. Gibbs, "Analytic Structure of the $\bar{p}$-Nucleus Optical Potential," Phys. Rev. C 27, 408 (1983).

W. R. Gibbs and W. B. Kaufmann, "Nuclear Medium Effects in Pion Elastic Scattering and Charge Exchange," Los Alamos National Laboratory document LA-UR-83-736 (Phys. Rev. C, in press).

B. F. Gibson, "Hyperon and Hypernuclear Physics with Intense Beams," in *Intense Medium Energy Sources of Strangeness*, T. Goldman, H. E. Haber, and H. F.-W. Sadrozinski, Eds., AIP Conf. Proc. 102, 43 (1983).

B. F. Gibson, "Electromagnetic and Weak Interactions in Few Nucleon Systems," in the Proc. of the 10th Int. Conf. on Few-Body Problems in Physics, Karlsruhe, Germany, August 21-27, 1983.

M. M. Nieto, W. C. Haxton, C. M. Hoffman, E. W. Kolb, V. D. Sandberg, and J. W. Toevs, Eds., *Science Underground*, AIP Conf. Proc. No. 96 (American Institute of Physics, New York, 1983).

T. Goldman, H. E. Haber, and H. F.-W. Sadrozinski, Eds., *Intense Medium Energy Sources of Strangeness*, University of California, Santa Cruz, 1983, *AIP Conf. Proc. No. 102*, Particles and Fields Subseries No. 31 (American Institute of Physics, New York, 1983).

MP-Division Publications; Papers Submitted for Publication and Papers Presented

S. Adachi and N. Auerbach, "Widths of Isovector Monopole Resonances," Phys. Lett. **131B**, 11 (1983), Los Alamos National Laboratory document LA-UR-83-1811

L. Agnew, D. Grisham, R. J. Macek, W. F. Sommer, and R. D. Werbeck, "Design Features and Performance of the LAMPF High-Intensity Beam Area," presented at ICANS VII meeting, Chalk River Nuclear Laboratories, Ontario, Canada, September 12-16, 1983, Los Alamos National Laboratory document LA-UR-83-2693.

J. F. Amann, R. J. Macek, T. W. L. Sanford, H. A. Thiessen, O. van Dyck, et al., "Measurement of Production Cross Sections for Negative Pions, Kaons, and Protons at 10, 18, and 24 GeV," Los Alamos National Laboratory report LA-9486-MS (1982).

G. Anderson, M. Oothoudt, J. Amann, and T. Kozlowski, "Dynamic Parameter Array System," IEEE Trans. Nucl. Sci. NS-30, 3975 (1983).

I. P. Auer, W. R. Ditzler, D. Hill, K. Imai, H. Spinka, R. Stanek, K. Toshioka, D. Underwood, R. Wagner, A. Yokosawa, E. W. Hoffman, J. J. Jarmer, G. R. Burleson, W. B. Cottingame, S. J. Greene, and S. Stuart, "Measure of $\Delta\sigma_L$ and D_{LL} = (L,L;O,O) in Proton-Proton Scattering Between 300 and 800 MeV," submitted to Phys. Rev., Los Alamos National Laboratory document LA-UR-83-3612.

N. Auerbach, "Coulomb Effects in Nuclear Structure," Phys. Rep. 98, 273 (1983), Los Alamos National Laboratory document LA-UR-83-535

N. Auerbach, J. D. Bowman, M. A. Franey, and W. G. Love, "(p,n) and (n,p) Reactions as Probes of Isovector Giant Monopole Resonances," Phys. Rev. C 28, 280 (1983).

N. Auerbach and A. Klein, "Excitation of Giant Electric Isovector Resonances in Pion Charge Exchange Reactions," Phys. Rev. C 28, 2075 (1983), Los Alamos National Laboratory document LA-UR-1810 (1983).

N. Auerbach and A. Klein, "Excitation of Giant Resonances in the Ca Isotopes in (π^+,π^0) Reactions," to be published in Nucl. Phys. A, Los Alamos National Laboratory document LA-UR-83-2978.

N. Auerbach and A. Klein, "The Structure of Isovector Spin Excitations in Nuclei," submitted to Phys. Rev. C, Los Alamos National Laboratory document LA-UR-83-2943.

H. W. Baer, J. A. Bistirlich, K. M. Crowe, W. Dahme, C. Joseph, J. P. Perroud, M. Lebrun, C. J. Martoff, U. Straumann, and P. Truöl, "Study of the $T = 2$ States in $A = 14$ Nuclei with the $^{14}C(\pi^-,\gamma)^{14}B$ Reaction," submitted to Phys. Rev. C, Los Alamos National Laboratory document LA-UR-83-170.

H. W. Baer, J. A. Bistirlich, K. M. Crowe, W. Dahme, C. Joseph, J. P. Perroud, M. Lebrun, "Isovector $M2$ State Observed in the $^{14}C(\pi^-,\gamma)$ Reaction," Phys. Rev. C 28, 761 (1983).

R. D. Bolton, R. D. Carlini, M. D. Cooper, J. S. Frank, V. E. Hart, H. S. Matis, R. E. Mischke, V. D. Sandberg, and U. Sennhauser, "A Stereo, Cylindrical Drift Chamber for Muon Decay Experiments at LAMPF," presented at the Wire Chamber Conf., Vienna, Austria, February 15-18, 1983; Nucl. Instrum. Methods 217, 173 (1983); Los Alamos National Laboratory document LA-UR-83-796.

R. L. Boudrie, "Spectrometers at LAMPF," invited talk at Magnetic Spectrometer Workshop, College of William and Mary, Williamsburg, Virginia, October 10-12, 1983, Los Alamos National Laboratory document LA-UR-83-3294

J. D. Bowman and M. D. Cooper, "Pion Charge Exchange and Nuclear Structure," submitted to Comments on Nucl. Part. Phys., Los Alamos National Laboratory document LA-UR-83-3097.

D. J. Brenner and M. Zaider, "The Applications of Track Calculations to Radiobiology. II. Calculations of Microdosimetric Quantities," Rad. Res. 98 (in press), Los Alamos National Laboratory document LA-UR-83-809

D. J. Brenner and M. Zaider, "Soft X Rays as a Tool to Investigate Radiation-Sensitive Sites in Mammalian Cells," presented at Conf. on Advances in Soft X-Ray Science and Technology, Brookhaven National Laboratory, Long Island, New York, October 17-19, 1983; Los Alamos National Laboratory document LA-UR-83-3156

R. D. Brown, J. R. Cost, and J. T. Stanley, "Effects of Neutron Irradiation on Magnetic Permeability of Amorphous and Crystalline Magnetic Alloys," presented at the 29th Ann. Conf. on Magnetism and Magnetic Materials, Pittsburgh, Pennsylvania, November 1983; to be published in J. Appl. Phys. Magnetism and Magnetic Materials Conf., 1983, Los Alamos National Laboratory document LA-UR-83-2718.

R. D. Brown and D. L. Grisham, "Graphite Targets at LAMPF," presented at the 1983 Particle Accelerator Conf., Santa Fe, New Mexico, March 21-23, 1983; IEEE Trans. Nucl. Sci. NS-30, 2801 (1983); Los Alamos National Laboratory document LA-UR-83-956.

S. K. Brown, "The Use of a Commercial Data Base Management System in the LAMPF Control System," presented at the 1983 Particle Accelerator Conf., Santa Fe, New Mexico, March 21-23, 1983, IEEE Trans. Nucl. Sci. NS-30, 2302 (1983).

R. D. Carlini, H. A. Thiessen, and J. M. Potter, "A High-Q Perpendicular Biased Ferrite-Tuned Cavity," presented at the 12th Int. Conf. on High-Energy Accelerators, Fermi National Accelerator Laboratory, Batavia, Illinois, August 1983; Los Alamos National Laboratory document LA-UR-83-2445 and LA-9946-MS (1983).

R. D. Carlini and G. J. Stephenson, "On the Feasibility of Performing Neutrino Experiments at an Intense Source of Strangeness," presented at the Conf. on Intense Medium Energy Sources of Strangeness, University of California, Santa Cruz, March 1983, AIP Conf. Proc. No. 102, Particle and Field Subseries No. 31, pp. 170-180; Los Alamos National Laboratory document LA-UR-83-1788.

E. P. Chamberlin, J. F. Benage, Jr., and H. E. Williams, "Developing a 500-eV Proton Beam," presented at the 1983 Polarized Ion Workshop, Vancouver, B.C., May 23-28, 1983 (American Institute of Physics) and to be published in its Proceedings; Los Alamos National Laboratory document LA-UR-83-1466

E. P. Colton, "Beam Transfer and Extraction at LAMPF II," presented at the 12th Int. Conf. on High-Energy Accelerators, Fermi National Accelerator Laboratory, August 1983, and to be published in its Proceedings; Los Alamos National Laboratory report LA-9878-MS (1983).

E. P. Colton, "4-GeV Preaccelerator for LAMPF II," Los Alamos National Laboratory report LA-9889-MS (1983).

I. P. Auer, E. Colton, W. R. Ditzler, D. Hill, R. Miller, H. Spinka, G. Theodosiou, J. J. Tavernier, N. Tamura, K. Toshioka, D. Underwood, R. Wagner, A. Yokosawa, P. Kroll, and W. Jauch, "Measurement of Spin Parameters for a Decisive Clarification of the Structure Observed in the p-p System,"
Phys. Rev. Lett. 51, 1411 (1983).

E. P. Colton, "Simulation of Betatron-Synchrotron Coupling," Los Alamos National Laboratory report LA-9901-MS (1983).

E. P. Colton, "SSC rf Design Example," presented at the SSC Workshop, University of Michigan, Ann Arbor, Michigan, December 12-17, 1983, to be published in the Proceedings; Los Alamos National Laboratory document LA-UR-84-327 (in press).

E. P. Colton, "A Staged Approach for LAMPF II," Los Alamos National Laboratory report LA-9946-MS (1983).

J. K. Corley and S. C. Schaller, "Particle Accelerator Control and Data Acquisition in the Context of VAX-VMS," presented at the Digital Equipment Computer Users Society Symp., Las Vegas, Nevada, October 23-28, 1983, to be published in the Proceedings; Los Alamos National Laboratory document LA-UR-83-3444.

J. F. Dicello, C. W. McCabe, J. D. Doss, and M. Paciotti, "The Relative Efficiency of Soft-Error Induction in 4*K* Static RAMs by Muons and Pions," IEEE Trans. Nucl. Sci. NS-30, 4613 (1983).

J. B. Donahue, "Power Deposition of LAMPF Proton Beam in Various Materials," Group MP-7 Technical Note 9MP-7-TN-14, October 1980, Los Alamos National Laboratory document LA-UR-83-2769.

J. D. Doss, "Passive Dosimeters for rf and Microwave Fields," Rev. Sci. Instrum. (in press); Los Alamos National Laboratory document LA-UR-83-2333

L. M. Earley, H. A. Thiessen, R. Carlini, and J. M. Potter, "A High-Q Ferrite-Tuned Cavity," presented at the 1983 Particle Accelerator Conf., Santa Fe, New Mexico, March 21-23, 1983, IEEE Trans. Nucl. Sci. NS-30, 3469 (1983), Los Alamos National Laboratory report LA-9823-MS (1983).

R. A. Fisher, M. M. Nieto, and V. D. Sandberg, "Nonexistence of the Naive Generalization of Many-Photon Coherent States," submitted to Phys. Rev.; Los Alamos National Laboratory document LA-UR-84-21.

D. L. Grisham and J. E. Lambert, "Applying Accelerator Remote Technology to Fusion Devices," presented at the American Nuclear Society annual meeting, Detroit, Michigan, June 12-15, 1983; Los Alamos National Laboratory document LA-UR-83-1558.

D. L. Grisham and J. E. Lambert, "Human Factors Considerations in the Monitor System," presented at the American Nuclear Society annual meeting, Detroit, Michigan, June 12-15, 1983; Los Alamos National Laboratory document LA-UR-83-1559.

D. L. Grisham and J. E. Lambert, "Monitor 1983," presented at the Particle Accelerator Conf., Santa Fe, New Mexico, March 21-23, 1983, IEEE Trans. Nucl. Sci. NS-30, 2267 (1983), Los Alamos National Laboratory document LA-UR-83-955.

D. L. Grisham and J. E. Lambert, "Remote Handling at LAMPF," presented at the ICANS VII meeting, Chalk River Nuclear Laboratories, Chalk River, Ontario, Canada, September 12-16, 1983; Los Alamos National Laboratory document LA-UR-83-2692.

D. L. Grisham and J. E. Lambert, "Remote Handling Experience at LAMPF," to be presented at the American Ceramic Society meeting May 1984; Los Alamos National Laboratory document LA-UR-83-3613.

D. Grisham and J. Lambert, "Water-Cooled Target Box Design at LAMPF," presented at the Particle Accelerator Conf., Santa Fe, New Mexico, March 21-23, 1983, IEEE Trans. Nucl. Sci. NS-30, 2270 (1983), Los Alamos National Laboratory document LA-UR-83-954.

P. Herczeg and C. M. Hoffman, "Study of $\pi^0 \rightarrow \mu^{\pm} e^{\mp}$ Decays," submitted to Phys. Rev. D, Los Alamos National Laboratory document LA-UR-83-3573.

C. M. Hoffman, "LAMPF II," invited talk at the Theoretical Symp. on Intense Medium-Energy Sources of Strangeness, Universityof California, Santa Cruz, California, March 1983, AIP Conf. Proc. No. 102, Particle and Field Subseries, No. 31; Los Alamos National Laboratory document LA-UR-83-795.

J. W. Hurd, "Solution to the Transverse Phase Space-Time Dependence Problem with LAMPF's High-Intensity H^+ Beam," presented at the 1983 Particle Accelerator Conf., Santa Fe, New Mexico, March 21-23, 1983, IEEE Trans. Nucl. Sci. NS-30 No. 4 (1983), p. 2487.

G. C. Idzorek and L. G. Atencio, "Fabrication of a Hermetically Sealed Connector," Los Alamos National Laboratory report LA-9849-MS (1983).

T. Kozlowski, J. Amann, G. Anderson, R. Floyd, J. Harrison, and M. Oothoudt, "Performance Results for the New RSX-11M Q System," IEEE Trans. Nucl. Sci. NS-30, 3998 (1983).

R. W. Lourie, W. Bertozzi, T. N. Buti, J. M. Finn, F. W. Hersman, C. Hyde, J. Kelly, M. A. Kovash, S. Kowalski, M. V. Hynes, B. E. Norum, and B. L. Berman, "Inelastic Electron Scattering from ^{9}Be," Phys. Rev. C 28, 489 (1983).

R. J. Macek, D. L. Grisham, J. E. Lambert, and R. Werbeck, "Radiation-ResistantBeam-Line Components at LAMPF," presented at the ICANS VII Conf., Chalk River Nuclear Laboratories, Chalk River, Ontario, Canada, September 13-16, 1983, to be published in the Proceedings; Los Alamos National Laboratory document LA-UR-83-2736.

Y. Mori, K. Ikegami, A. Takagi, Z. Igarashi, S. Fukumoto, W. Cornelius, and R. York, "Optically Pumped Polarized H^- Ion Source,"to be published in the Proc. of the 3rd Symp. on the Production and Neutralization of the Negative Hydrogen Ions and Beams, Brookhaven National Laboratory, Upton, New York, November 14-17, 1983.

M. Oothoudt and T. Kozlowski, "ALECS: Assembly Language Extensions and Control Structures," Proc. Digital Equipment Users Society (1982), p. 537; Los Alamos National Laboratory document LA UR-82-3334.

M. Oothoudt, J. Amann, R. Floyd, J. Harrison, and T. Kozlowski, "The Q Memory Resident Histogramming System," IEEE Trans. Nucl. Sci. NS-30, 3838 (1983).

G. C. Phillips, E. A. Umland, G. S. Mutchler, J. B. Roberts, M. Duong-Van, J. A. Buchanan, J. B. Donahue, J. C. Allred, B. W. Noel, T. A. Mulera, B. Aas, and B. W. Mayes, "A Novel Neutrino Detection System," to be published in Nucl. Instrum. Methods; Los Alamos National Laboratory document LA-UR-83-2519

W. Reuter, E. B. Shera, M. V. Hoehn, F. W. Hersman, T. Millman, J. M. Finn, C. Hyde-Wright, R. Lourie, B. Pugh, and W. Bertozzi, "Nuclear Charge Densities in the Transition Region ^{192}Os," to be published in Phys. Rev. Lett.; Los Alamos National Laboratory document LA-UR-83-3313.

L. Rosen, "The Pros and Cons of a Nuclear Freeze," invited talk at Trinity on the Hill Episcopal Church, Los Alamos, New Mexico, March 15, 1983.

V. D. Sandberg, "An Heuristic Introduction to Gravitational Waves," Proc. Workshop on Science Underground, Los Alamos National Laboratory, Los Alamos, New Mexico, September 27-October 1, 1982, Los Alamos National Laboratory document LA-UR-83-333.

G. H. Sanders, "The Imagery of Physics in Psychology: A Physicist's Reactions," presented at the Conf. on Nuclear Reactions: A Three-Day Dialogue Between Physicists and Psychologists, University of New Mexico, Albuquerque, New Mexico, November 1983, to be published in the Proceedings; Los Alamos National Laboratory document LA-UR-83-744.

S. C. Schaller and P. A. Rose, "Data-Acquisition Software for the LAMPF Control System," presented at the 1983 Particle Accelerator Conf., Santa Fe, New Mexico March 21-23, 1983; IEEE Trans. Nucl. Sci. NS-30, 2308 (1983); Los Alamos National Laboratory document LA-UR-83-744.

P. Schuler, K. Hardt, C. Gunther, K. Freitag, P. Herzog, H. Niederwestberg, H. Reif, E. B. Shera, and M. V. Hoehn, "Experimental Investigation of Low-Lying Excited States in ^{201}Hg," Z. Phys. A. 313, 305 (1983).

C. J. Sternhagen and J. D. Doss, "Combined Radiation Therapy and Localized Current Field Hyperthermia with a 13 MHz Applicator in Head and Neck and Gynecological Cancer Therapy," in the Proc. of the meeting of the Radiation Research Society, San Antonio, Texas, February 28, 1983.

R. R. Stevens, Jr., and R. L. York, "A Cusped Field *H* Ion Source for LAMPF," presented at the 1983 Particle Accelerator Conf., Santa Fe, New Mexico, March 21-23, 1983, Los Alamos National Laboratory document LA-UR-83-815.

G. W. Swift, A. Migliori, J. Wheatley, C. R. Waller, and G. Suazo, "Fabrication and Leak-Tight Furnace Brazing of Intricate Objects," submitted to Rev. Sci. Instrum.; Los Alamos National Laboratory document LA-UR-83-3455.

H. A. Thiessen and E. J. Scheidker, "Production of Pions, Kaons, and Muons by 16-GeV Protons," Los Alamos National Laboratory report LA-9587-MS (1983).

H. A. Thiessen, "A Reference Design for LAMPF II," Proc. of the 12th Int. Conf. on High Energy Accelerators, Fermi National Accelerator Laboratory, August 11-16, 1983; Los Alamos National Laboratory document LA-UR-83-2426.

J. L. Warren and H. A. Thiessen, "Simulation of Transition Crossing in LAMPF II," Proc. of the 12th Int. Conf. on High-Energy Accelerators, Fermi National Accelerator Laboratory, August 11-16, 1983; Los Alamos National Laboratory document LA-UR-83-2367.

R. R. Wilson, "Acceleration in a Synchrotron by Harmonic Hopping," Los Alamos National Laboratory report LA-9904-MS (1983).

A. Yaouanc, "Correlation Functions, Generalized Susceptibility, and μSR Spectroscopy," submitted to J. Phys. Lett., Los Alamos National Laboratory document LA-UR-83-664.

R. L. York and R. R. Stevens, Jr., "A Cusped Field H^- Ion Source for LAMPF," IEEE Trans. Nucl. Sci. NS-30, 2704 (1983).

R. L. York and R. R. Stevens, Jr., "Development of a Multicusp H^- Ion Source for Accelerator Applications," to be published in the Proc. of the 3rd Int. Symp. on the Production and Neutralization of Negative Ions and Beams, Brookhaven National Laboratory, Upton, New York, November 14-17, 1983; Los Alamos National Laboratory document LA-UR-83-3273.

R. L. York, R. R. Stevens, Jr., K. N. Leung, and K. W. Ehlers, "Extraction of H^- Beams from a Magnetically Filtered Multicusp Source," to be published in Rev. Sci. Instrum., Los Alamos National Laboratory document LA-UR-83-3098.

LAMPF Experimental Program Reports and Publications

(EXP. 2) R. H. Jeppesen, M. J. Jakobson, M. D. Cooper, D. C. Hagerman, M. B. Johnson, R. P. Redwine, G. R. Burleson, K. F. Johnson, R. E. Marrs, H. O. Meyer, I. Halpern, and L. D. Knutson, "Pion-Nucleus Forward Scattering Amplitudes from Total Cross Section Measurements," Phys. Rev. C 27, 697 (1983).

(EXP. 9) K. G. Boyer, W. J. Braithwaite, W. B. Cottingame, S. J. Greene, L. E. Smith, C. F. Moore, C. L. Morris, H. A. Thiessen, G. S. Blanpied, G. R. Burleson, J. F. Davis, J. S. McCarthy, R. C. Minehart, and C. A. Goulding, "Pion Elastic and Inelastic Scattering from ^{40,42,44,48}Ca and ^{54}Fe," Phys. Rev. C. 29, 182 (1984); Los Alamos National Laboratory document LA-UR-82-3171.

(EXPS. 9, 310, 401, 412, 448, 523, 680, 716) M. B. Johnson, "Recent Developments in the Understanding of Pion-Nucleus Scattering," lectures presented at the 1983 Int. Symp. on Nucleon-Nucleon Interaction and Nuclear Many-Body Problems, Beijing, China, September 1983; Los Alamos National Laboratory document LA-UR-83-2851

(EXP. 12) C. Gunther, E. B. Shera, M. V. Hoehn, H. D. Wohlfahrt, R. J. Powers, Y. Tanaka, and A. R. Kunselman, "Muonic X Ray Study of ^{199}Hg and ^{200}Hg," Phys. Rev. C 27, 816 (1983).

(EXP. 15) G. Pauletta, G. Adams, S. M. Haji-Saeid, G. J. Igo, J. B. McClelland, A. T. M. Wang, C. A. Whitten, Jr., A. Wriekat, M. M. Gazzaly, and N. Tanaka, "Differential Cross Section and Analyzing Powers for *pp* Elastic Scattering at 1.46 GeV/c in the Coulomb-Nuclear Interference Region," Phys. Rev. C 27, 282 (1983).

(EXP. 22) R. Kunselman, R. J. Powers, M. V. Hoehn, and E. B. Shera, "Pionic $3d \rightarrow 2p$ X-Ray Measurements in ^{50,52,54}Cr, ^{45}Sc, ^{51}V, ^{55}Mn, and Fe," Nucl. Phys. A 405, 627 (1983).

(EXP. 31) J. S. Frank, R. L. Burman, D. R. F. Cochran, P. Nemethy, S. E. Willis, V. W. Hughes, R. P. Redwine, J. Duclos, H. Kaspar, C. K. Hargrove, and U. Moser, "Reply to Direct Comparison Between the γ-Ray Fluxes from Proton Beam Dumps at LAMPF and SIN," submitted to Phys. Rev. D; Los Alamos National Laboratory document LA-UR-83-1345

(EXP. 32) W. K. McFarlane, L. B. Auerbach, F. C. Gaille, V. L. Highland, E. Jastrzembski, R. J. Macek, F. H. Cverna, C. M. Hoffman, G. E. Hogan, R. E. Morgado, J. C. Pratt, and R. D. Werbeck, "New Measurement of the Rate for Pion Beta Decay," Phys. Rev. Lett. 51, 249 (1983).

(EXP. 87) J. Källne, R. C. Minehart, R. R. Whitney, R. L. Boudrie, J. B. McClelland, and A. W. Stetz, "Pion Scattering and Absorption Contributions to Proton Emission from Pion-Nucleus Collisions at T_π = 50-295 MeV," Phys. Rev. C 28, 304 (1983).

(EXP. 96) J. S. Frank, A. A. Browman, P. A. M. Gram, K. A. Klare, R. E. Mischke, D. C. Moir, D. E. Nagle, R. H. Heffner, J. M. Potter, R. P. Redwine, and M. A. Yates, "Measurement of Low-Energy Elastic $\pi^+ p$ Differential Cross Sections," Phys. Rev. D 28, 1569 (1983); Los Alamos National Laboratory document LA-UR-83-1490.

(EXPS. 120, 363) D. H. Fitzgerald, "πN Scattering at LAMPF: Baryon Spectroscopy at 1200-1500 MeV/c," presented at the University of Colorado, April 25, 1983, Los Alamos National Laboratory document LA-UR-83-1179.

(EXPS. 120, 363) D. H. Fitzgerald, "πN Scattering at LAMPF: Natural Baryon Spectroscopy at 1200-1500 MeV/c^2," presented at George Washington University, Washington, D.C., March 11, 1983; Los Alamos National Laboratory document LA-UR-83-635.

(EXP. 249) B. Höistad, M. Gazzaly, B. Aas, G. Igo, A. Rahbar, C. Whitten, G. S. Adams, and R. Whitney, "^{3,4}He($\vec{p}$,π^+)^{4,5}He$_{g.s.}$ Reactions at 800 MeV," Phys. Rev. C 29, 553 (1984).

(EXP. 298) F. Irom, G. J. Igo, J. B. McClelland, C. A. Whitten, Jr., and M. Bleszynski, "Measurements of Small-Angle Elastic $\vec{p}$-d Scattering at 796 MeV Using a Recoil Method," Phys. Rev. C 28, 2380 (1983).

(EXP. 309) S. A. Wood, "An Experimental Study of Inclusive Pion Double Charge Exchange Reactions in the Delta Resonance Region," Ph.D. thesis, Massachusetts Institute of Technology, Cambridge, Massachusetts, 1983; Los Alamos National Laboratory report LA-9932-T (1983).

(EXP. 333) M. J. Leitch, R. L. Burman, R. Carlini, S. Dam, V. Sandberg, et al., "Pion-Nucleus Elastic Scattering at 80 MeV," Phys. Rev. C 29, 561 (1984); Los Alamos National Laboratory document LA-UR-83-2569.

(EXP. 335) D. B. Laubacher, Y. Tanaka, R. M. Steffen, E. B. Shera, and M. V. Hoehn, "Muonic X-Ray Measurement of the Monopole and Quadrupole Charge Parameters of ^{154,155,156,157,158,160}Gd," Phys. Rev. C 27, 1772 (1983).

(EXP. 336) A. D. Hancock, R. W. Hackenburg, E. V. Hungerford, B. W. Mayes, L. S. Pinsky, J. C. Allred, T. M. Williams, S. D. Baker, J. A. Buchanan, J. M. Clement, M. Copel, I. M. Duck, G. S. Mutchler, G. P. Pepin, E. A. Umland, G. C. Phillips, M. W. McNaughton, C. Hwang, and M. Furic, "Asymmetries and Cross Sections for the Reaction $\vec{p} + p \rightarrow p + \pi^+ + n$ at 800 MeV," Phys. Rev. C 27, 2742 (1983).

(EXP. 348) C. J. Martoff, J. A. Bistirlich, C. W. Clawson, K. M. Crowe, M. Kroike, J. P. Miller, S. S. Rosenblum, W. A. Zaje, H. W. Baer, A. H. Wapstra, G. Strassner, and P. Truöl, "Spin-Flip Transitions in ^{13}C^{19}F Probed with the (π^-,γ) Reaction," Phys. Rev. C 27, 1621 (1983).

(EXP. 357) J. D. Knight, C. J. Orth, M. E. Schillaci, R. A. Naumann, F. J. Hartmann, and H. Schneuwly, "Target Density Effects in Muonic-Atom Cascades," Phys. Rev. A 27, 2936 (1983).

(EXPS. 385, 563) M. L. Barlett, G. W. Hoffmann, J. A. McGill, B. Höistad, L. Ray, R. W. Fergerson, E. C. Milner, J. A. Marshall, J. F. Amann, B. E. Bonner, J. B. McClelland, G. S. Blanpied, and R. A. Arndt, "Forward-Angle Elastic and Quasi-elastic Proton-Nucleon Cross Sections and Analyzing Powers at 0.8 GeV," Phys. Rev. C 27, 682 (1983).

(EXP. 389) D. F. Geesaman, D. Kurath, G. C. Morrison, C. Olmer, B. Zeidman, R. E. Anderson, R. L. Boudrie, H. A. Thiessen, G. S. Blanpied, G. R. Burleson, R. E. Segel, and L. W. Swenson, "Inelastic Scattering of 162-MeV Pions by ^{14}N," Phys. Rev. C 27, 1134 (1983); Los Alamos National Laboratory document LA-UR-82-3258.

(EXP. 390) S. M. Levenson, D. F. Geesaman, E. P. Colton, R. J. Holt, H. E. Jackson, J. P. Schiffer, J. R. Specht, K. E. Stephenson, B. Zeidman, R. E. Segel, P. A. M. Gram, and C. A. Goulding, "Inclusive Pion Scattering in the Δ(1232) Region," Phys. Rev. C 28, 326 (1983).

(EXP. 400) R. Bolton, R. Carlini, J. D. Bowman, M. Cooper, A. Hallin, J. Frank, C. Hoffman, H. Matis, R. Mischke, D. Nagle, F. Mariam, V. Sandberg, U. Sennhauser, G. Sanders, R. Werbeck, R. Williams, R. Hofstadter, E. Hughes, S. Wilson, J. Rolfe, S. Wright, D. Grosnick, G. Hogan, V. Highland, and M. Van, "The Crystal Box: Rare Decays of the Muon," presented at the Blacksburg, Virginia, Workshop on Low-Energy Tests of Conservation Laws in Particle Physics, September 11-15, 1983; Los Alamos National Laboratory document LA-UR-83-2908.

(EXP. 400) J. P. Sandoval, L. Bayliss, T. Gordon, G. Hart, C. M. Hoffman, G. E. Hogan, V. D. Sandberg, G. H. Sanders, and S. L. Wilson, "Alternatives to Coaxial Cable for Delaying Analog and Digital Signals in a Particle Physics Experiment," Nucl. Instrum. Methods 216, 171 (1983); Los Alamos National Laboratory document LA-UR-83-967.

(EXP. 401) M. D. Cooper, H. W. Baer, R. D. Bolton, J. D. Bowman, F. H. Cverna, N. S. P. King, M. Leitch, J. Alster, A. Doron, A. Erell, M. A. Moinester, E. Blackmore, and E. Siciliano, "Angular Distribution for $^{15}N(\pi^+,\pi^0)^{15}O(g.s)$ at $T_\pi = 48$ MeV," submitted to Phys. Rev. Lett.; Los Alamos National Laboratory document LA-UR-83-1030.

(EXP. 407) D. J. Farnum, W. F. Sommer, and O. T. Inal, "A Study of Defects Produced in Tungsten by 800 MeV Protons Using Field Ion Microscopy," presented at the Third Topical Meeting on Fusion Reactor Materials, Albuquerque, New Mexico, September 19-22, 1983, to be published in J. Nucl. Mater.; Los Alamos National Laboratory document LA UR-83-2572.

(EXP. 407) W. F. Sommer, D. S. Phillips, W. V. Green, L. W. Hobbs, and C. A. Wert, "Proton Irradiation Damage in Cyclically Stressed Aluminum," J. Nucl. Mater. 114, 267 (1983).

(EXPS. 412, 523, 827) N. Auerbach, M. B. Johnson, A. Klein, and E. R. Siciliano, "Nuclear Structure Effects in Pion Single Charge Exchange," Phys. Rev. C 29 526 (1984); Los Alamos National Laboratory document LA-UR-83-2699.

(EXPS. 412, 607) A. E. Erell, J. Alster, J. Lichtenstadt, M. A. Moinester, J. D. Bowman, M. D. Cooper, F. Irom, H. S. Matis, E. Piasetzky, U. Sennhauser, and Q. Ingram, "Properties of the Isovector Monopole and Other Giant Resonances in Pion Charge Exchange," submitted to Phys. Rev. Lett.; Los Alamos National Laboratory document LA-UR-84-599.

(EXP. 412) U. Sennhauser, E. Piasetzky, H. Baer, J. D. Bowman, M. D. Cooper, H. S. Matis, H. J. Ziock, J. Alster, A. Erell, M. A. Moinester, and F. Irom, "Isobaric Analog States in Pion Single-Charge-Exchange Reactions On and Above the (3,3) Resonance Energy," Phys. Rev. Lett. 51, 1324 (1983).

(EXP. 452) S. Seestrom-Morris, C. L. Morris, R. L. Boudrie, H. A. Thiessen, D. Dehnhard, and M. A. Franey, "Analysis of Elastic and Inelastic Scattering of 162 MeV Pions from ^{13}C by an Optical Potential and a Collective Model," Phys. Rev. C 28, 1301 (1983); Los Alamos National Laboratory document LA-UR-83-452.

(EXP. 479) D. L. Adams and M. Bleszynski, "On the Relevance of the Dirac Equation to the Scattering of Medium-Energy Nucleons from Nuclei," submitted to Phys. Lett.; Los Alamos National Laboratory document LA-UR-83-2749.

(EXP. 484) C. L. Morris, S. J. Seestrom-Morris, P. A. Seidl, R. R. Kiziah, and S. J. Greene, "Pion Elastic and Inelastic Scattering from ^{152}Sm," Phys. Rev. C 28, 2165 (1983); Los Alamos National Laboratory document LA-UR-82-2542.

(EXP. 495) C. L. Morris, N. Tanaka, R. L. Boudrie, L. C. Bland, H. T. Fortune, R. Gilman, S. J. Seestrom-Morris, C. F. Moore, and D. Dehnhard, "Small Angle Pion Inelastic Scattering from ^{12}C at 162 MeV," submitted to Phys. Rev. C; Los Alamos National Laboratory document LA-UR-84-16.

(EXP. 498) I. P. Auer, W. R. Ditzler, D. Hill, K. Imai, H. Spinka, R. Stanek, K. Toshioka, D. Underwood, R. Wagner, A. Yokosawa, E. W. Hoffman, J. J. Jarmer, G. R. Burleson, W. B. Cottingame, S. J. Greene, and S. Stuart, "Measure of $\Delta\sigma_L$ and C_{LL} in Proton-Proton Scattering Between 300 and 800 MeV," submitted to Phys. Rev. D; Los Alamos National Laboratory document LA-UR-83-3612.

(EXP. 498) G. R. Burleson, W. B. Cottingame, S. J. Greene, S. Stuart, E. W. Hoffman, J. J. Jarmer, I. P. Auer, W. R. Ditzler, D. Hill, K. Imai, H. Spinka, R. Stanek, K. Toshioka, D. Underwood, R. Wagner, and A. Yokosawa, "$C_{LL} = (L,L;0,0)$ Measurements and a Structure Due to a P Partial Wave in the pp System," Nucl. Phys. B 213, 365 (1983).

(EXP. 517) W. B. Tippens, "Measurement of A_N and A_{NN} for the Reaction $pp \rightarrow d\pi^+$ at Six Energies from 500 to 800 MeV," Ph.D. thesis, Texas A&M University, College Station, Texas, 1983; Los Alamos National Laboratory report LA 9909-T (1983).

(EXPS. 517, 518) T. S. Bhatia, J. G. J. Boissevain, J. J. Jarmer, R. R. Silbar, J. E. Simmons, G. Glass, J. C. Hiebert, R. A. Kenefick, L. C. Northcliffe, W. B. Tippens, W. M. Kloet, and J. Duback, "Analyzing Powers and Spin Correlations A_{NN} and A_{LL} for $pp \rightarrow np\pi^+$ at 650 and 800 MeV," Phys. Rev. C 28, 2071 (1983).

(EXP. 523) F. Irom, J. R. Comfort, R. Jeppeson, J. J. Kraushaar, R. A. Ristinen, W. Tew, J. L. Ullmann, H. W. Baer, J. D. Bowman, M. D. Cooper, A. Erell, M. A. Moinester, E. Piasetsky, U. Sennhauser, and E. R. Siciliano, "Pion Single Charge Exchange on ^{14}C," Phys. Rev. C 28, 2568 (1983).

(EXP. 545) R. D. Brown, J. R. Cost, and J. T. Stanley, "Effects of Neutron Irradiation on Magnetic Permeability of Amorphous and Crystalline Magnetic Alloys," presented at the 29th Ann. Conf. Magnetism and Magnetic Materials, Pittsburgh, Pennsylvania, November 8-11, 1983, to be published in J. Appl. Phys.; Los Alamos National Laboratory document LA-UR-83-2718.

(EXP. 558) P. A. Seidl, R. R. Kiziah, M. K. Brown, C. F. Moore, C. L. Morris, H. Baer, S. J. Greene, G. R. Burleson, W. B. Cottingame, L. C. Bland, R. Gilman, and H. T. Fortune, "Observation of Analog and Nonanalog Transitions in the Reaction $^{56}Fe(\pi^+,\pi^-)^{56}Ni$," Phys. Rev. Lett. 50, 1106 (1983); Los Alamos National Laboratory document LA-UR-83-248.

(EXP. 558) P. A. Seidl, M. D. Brown, R. R. Kiziah, C. F. Moore, H. Baer, C. L. Morris, G. R. Burleson, W. B. Cottingame, S. J. Greene, L. C. Bland, R. Gilman, and H. T. Fortune, "Pion Double Charge Exchange on $T = 1$ Nuclei," submitted to Phys. Rev. C; Los Alamos National Laboratory document LA-UR-84-17.

(EXP. 561) M. Blecher, K. Gotow, R. L. Burman, M. V. Hynes, M. J. Leitch, N. S. Chant, L. Rees, P. G. Roos, F. E. Bertrand, E. E. Gross, F. E. Obenshain, T. P. Sjoreen, G. S. Blanpied, B. M. Preedom, and B. G. Ritchie, "Isospin Effects in π^+ Elastic Scattering from ^{12}C, ^{13}C, and ^{14}C at 65 and 80 MeV," Phys. Rev. C 28, 2033 (1983).

(EXP. 601, 659) C. L. Morris, S. J. Seestrom-Morris, and L. C. Bland, "Excitation of Giant Resonances in Pion Inelastic Scattering," invited talk at the HESANS '83 Int. Symp., Orsay, France, September 5-8, 1983; Los Alamos National Laboratory document LA UR-83-3237.

(EXP. 606) M. O. Kaletka, "Core Excitation Effects in Pion Double Charge Exchange," Ph.D. thesis, Northwestern University, Evanston, Illinois, 1983; Los Alamos National Laboratory report LA-9947-T.

(EXP. 607) J. D. Bowman, H. W. Baer, M. D. Cooper, H. S. Matis, F. Irom, E. Piasetzky, U. Sennhauser, N. S. P. King, J. Alster, A. Erell, M. A. Moinester, J. Lichtenstadt, and C. H. Q. Ingram, "A Dependence of the Excitation Energy, Width, and Cross Section of the Isovector Monopole Resonance," presented at the HESANS '83 Int. Symp., Orsay, France, September 5-8, 1983; Los Alamos National Laboratory document LA-UR-83-2924.

(EXP. 616) J. B. McClelland, J. M. Moss, B. Aas, A. Azizi, E. Bleszynski, M. Bleszynski, J. Geaga, G. Igo, A. Rahbar, J. B. Wagner, G. S. Weston, C. Whitten, Jr., K. Jones, S. Nanda, M. Gazzaly, and N. Hintz, "Complete Measurement of Polarization Transfer Observables for the $^{12}C(p,p')^{12}C^*$," Phys. Rev. Lett. 52, 98 (1984); Los Alamos National Laboratory document LA-UR-83-3292.

(EXP. 625) J. L. Ullmann, J. J. Kraushaar, T. G. Masterson, R. J. Peterson, R. S. Raymond, R. A. Ristinen, N. S. P. King, R. L. Boudrie, C. L. Morris, W. W. True, R. E. Anderson, and E. R. Siciliano, "Excitation of the Isoscalar Giant Quadrupole Resonance in ^{118}Sn $(\pi^+,\pi^{+\prime})$," Phys. Rev. Lett. 51, 1038 (1983); Los Alamos National Laboratory document LA-UR-83-2226.

(EXP. 627) R. A. Riskinen, A. M. Bernstein, B. Quinn, S. A. Wood, G. S. Blanpied, B. G. Ritchie, and V. R. Brown, "DWIA Predictions of (p,p') Data Using Electromagnetically Constrained Densities," Phys. Lett. 131B, 26 (1983).

(EXP. 634) J. D. Bowman, R. Carlini, R. Damjanovich, R. W. Harper, R. E. Mischke, D. E. Nagle, R. Talaga, and V. Yuan, "Low-Noise Ionization Chambers for Use in Transmission Measurements with Medium- and High-Energy Beams," Nucl. Instrum. Methods 216, 399 (1983).

(EXP. 635) S. Tsu-hsun, B. E. Bonner, M. W. McNaughton, O. B. van Dyck, G. S. Weston, B. Aas, E. Bleszynski, M. Bleszynski, G. J. Igo, H. Ohnuma, D. J. Cremans, C. L. Hollas, K. H. McNaughton, P. J. Riley, R. F. Rodebaugh, S. Zu, and S. E. Turpin, "Measurements of the Spin-Rotation Parameters for $\vec{p}d \rightarrow \vec{p}d$ Elastic Scattering at 496, 647, and 800 MeV," submitted to Phys. Rev. C; Los Alamos National Laboratory document LA-UR-83-3484.

(EXP. 659) L. C. Bland, "Forward-Angle Pion Inelastic Scattering," Ph.D. thesis, University of Pennsylvania, Philadelphia, 1983; Los Alamos National Laboratory report LA-9960-T (1983).

(EXP. 659, 659U) L. C. Bland, R. Gilman, G. S. Stephans, G. P. Gilgoyle, H. T. Fortune, C. L. Morris, S. J. Seestrom-Morris, S. J. Greene, P. A. Seidl, R. R. Kiziah, and C. F. Moore, "Forward-Peaked Angular Distributions Observed in (π,π') on Light Nuclei," submitted to Phys. Rev.; Los Alamos National Laboratory document LA-UR-83-3086.

(EXP. 660) J. B. McClelland, "Spin Excitation Studies via (p,p') at the HRS," invited talk at the Int. Symp. on Electromagnetic Properties of Atomic Nuclei, Tokyo, Japan, November 9-12, 1983; Los Alamos National Laboratory document LA-UR-83-3236.

(EXP. 698) Y. Tanaka, R. M. Steffen, E. B. Shera, W. Reuter, M. V. Hoehn, and J. D. Zumbro, "Muonic X-Ray Study of ^{151}Eu and ^{153}Eu," to be published in Phys. Rev. C; Los Alamos National Laboratory document LA-UR-84-22.

(EXP. 698) Y. Tanaka, R. M. Steffen, E. B. Shera, W. Reuter, M. V. Hoehn, and J. D. Zumbro, "Precision Muonic-Atom Measurements of Nuclear Quadrupole Moments and the Sternheimer Effect in Rare-Earth Atoms," Phys. Rev. Lett. 51, 1633 (1983).

(EXP. 701) L. C. Bland, R. Gilman, M. Carchidi, K. Dhuga, C. L. Morris, H. T. Fortune, S. J. Greene, P. A. Seidl, and C. F. Moore, "Systematics of Pion Double-Charge-Exchange Reactions on $T = 0$ Nuclei," Phys. Lett. 128B, 157 (1983); Los Alamos National Laboratory document LA-UR-83-1195.

(EXP. 705) R. R. Silbar and E. Piasetzky, "Isospin Dependence of Pion Absorption on Nucleon Pairs," to be published in Phys. Rev. C; Los Alamos National Laboratory document LA-UR-83-1883.

(EXP. 720) C. L. Morris, J. F. Amann, S. J. Seestrom-Morris, J. A. McGill, C. Glashausser, K. Jones, S. Nanda, M. Barlett, G. W. Hoffman, C. Milner, C. F. Moore, J. R. Comfort, L. C. Bland, and R. Gilman, "Low-Momentum Delta Production in the ^{13}C$(p,d)^{12}$C* Reaction," Phys. Lett. 123B, 37 (1983); Los Alamos National Laboratory document LA-UR-82-2877.

(EXP. 727) S. E. Jones, A. N. Anderson, A. J. Caffrey, J. B. Walter, K. D. Watts, J. N. Bradbury, P. A. M. Gram, M. Leon, H. R. Maltrud, and M. A. Paciotti, "Experimental Investigatioin of Muon-Catalyzed *d-t* Fusion," Phys. Rev. Lett. 51, 1757 (1983).

(EXPS. 727, 745) M. A. Paciotti, J. N. Bradbury, and O. M. Rivera, "Muon Beams at the LAMPF Biomedical Channel," presented at the Particle Accelerator Conf., Santa Fe, New Mexico, March 21-23, 1983, IEEE Trans. Nucl. Sci. NS-30, 2359 (1983).

(EXP. 780) R. Gilman, H. T. Fortune, L. C. Bland, R. R. Kiziah, C. F. Moore, P. A. Seidl, C. L. Morris, and W. B. Cottingame, "Nonanalog (π^+,π^-) Double Charge Exchange on ^{18}O," submitted to Phys. Rev. Lett.; Los Alamos National Laboratory document LA-UR-84-436.

(EXP. 783) E. Piasetzky, P. A. M. Gram, D. W. MacArthur, G. A. Rebka, Jr., C. A. Bordner, S. Hoibraten, E. R. Kinney, J. L. Matthews, S. A. Wood, D. Ashery, and J. Lichtenstadt, "Pion-Induced Pion Production on the Deuteron," submitted to Phys. Rev. Lett.; Los Alamos National Laboratory document LA-UR-84-231.

IV. PROTON STORAGE RING CONSTRUCTION AND RESEARCH PROGRAM DEVELOPMENT

Overview

C. D. Bowman

A world-class facility is under development on Line D for pulsed neutron and other research. The principal elements in this facility are the Proton Storage Ring (PSR) now under construction and the existing Weapons Neutron Research (WNR) facility target and experimental areas. The storage ring will convert the long LAMPF macropulses into short, intense proton bursts for a variety of experimental programs. Two pulse structures will be provided: the long-burst, low-frequency (LBLF) mode with 270-ns pulses at 12 Hz for an average current of 100 μA, and the short-burst, high-frequency (SBHF) mode with 1-ns pulses at 720 Hz for an average current of 12 μA.

The long-burst mode will be devoted primarily to condensed matter research using pulsed neutron scattering techniques and will be the major facility for this type of pulsed neutron research in the United States. A User program is being developed under the auspices of the Division of Materials Science of the USDOE, which should grow to more than 100 Users annually when the PSR becomes operational. This User program began in calendar year 1983 with the availability of pulsed neutrons produced by 5-μs bursts of LAMPF beam on the present WNR target-moderator system. More than 100 visitors from 30 institutions participated in the pulsed-neutron planning and research in 1983.

Plans also were completed for a major increase in experimental space around the WNR target area to accommodate as many as 15 spectrometers for this research. Funds were received in FY 1983 for a $2.7-million 3-year WNR program to upgrade the target area and beam-transport system to handle the required current and to improve the neutron-production target and shielding.

Research in the field of neutron-nuclear physics will receive a major boost from the short, intense bursts of neutrons produced from the PSR, the extension of useful neutron energies up to several hundred MeV, and the absence of an intense gamma flash associated with the neutron burst. Neutron physics experiments were performed this year at the WNR using sub-micro-amp currents of LAMPF micropulses. Although these experiments are unsurpassed in intensity and resolution, orders-of-magnitude improvements will be possible when the PSR short-pulse mode becomes operational.

The low duty cycle and high-current capacity of the PSR almost certainly will be major advantages for low-energy neutrino research. In anticipation of such a program, a new beam line (Line E) has been assembled parallel to Line D and in the Line D channel, with a pulsed magnet for multiplexing LAMPF beam between Lines D and E. Neutrino experiments requiring an unshared target will be conducted on this line using a target and detector area now under construction.

The rapid progress on the installation of Line E, carried out by a collaboration of Los Alamos Groups P-3, P-9, P-14, and MP Division, the University of New Mexico, University of California at Riverside, and Temple and Valparaiso Universities, should enable measurements on ν_μ-nucleus charged-current cross sections during the summer of 1984. These data are crucial for the design of future detectors for use with any Los Alamos neutrino source. This measurement also will provide data on possible $\nu_\mu \rightarrow \nu_e$ oscillations with a sensitivity of about 10^{-3}, although this is far from the limit ultimately achievable at LAMPF.

The construction of the PSR is supported by Laboratory Defense Program Funding. A substantial defense research program will be conducted using the PSR and associated facilities. On infrequent occasions, defense

---

The WNR/PSR facility, located south of the LAMPF switchyard, accepts 800-MeV proton beam pulses from the LAMPF accelerator. Its design was accomplished in large part by the Accelerator Technology (AT) Division of Los Alamos National Laboratory.

The research program at WNR/PSR is managed by the Physics (P) Division at Los Alamos and is supported jointly by Laboratory internal funding and the Office of Energy Research of the USDOE. Researchers from P Division collaborate with other Los Alamos staff and outside Users in their experiments.

Progress at LAMPF thanks the management of P Division, especially Charles Bowman, for this section of reports on developments and research at WNR/PSR.

programs will require the unshared use of the PSR, but the typical defense experiment will only require the use of one or more of the many neutron drift tubes that view a common pulsed source of neutrons.

Participation in the PSR research programs is encouraged. Interested individuals should contact Richard N. Silver for condensed matter physics, and Gerard J. Stephenson for neutron or neutrino physics.

PSR Construction

G. A. Sawyer

The PSR is a major addition to the WNR facility at LAMPF. It will be a bunch compressor for the relatively long linac macropulses from LAMPF, tailoring them into short, intense pulses ideally suited for neutron-scattering research.

The PSR is located in a tunnel adjacent to, and below the level of, the existing beam line (Line D) that serves the WNR facility. A plan view of the ring and tunnel, showing component locations, is given in Fig. 1. Beam enters the ring from Line D; after accumulation, it returns to Line D, through which it is transported to the WNR neutron-production target. Connections with Line D are made by short, sloped, beam-transport channels. Located above the ring tunnel and on top of a 4.9-m-thick earth shield are service and assembly buildings.

The ring operates in two accumulation modes, each independently optimized to provide the desired neutron-source pulse structure for nuclear physics and materials research programs.

Operational characteristics of the two PSR storage modes are summarized in Table I. In the short-bunch high-frequency (SBHF) mode, protons are accumulated in six equally spaced 1-ns bunches during each LAMPF macropulse. The bunches are individually extracted by a fast kicker during the 8.2-ms interval between injection pulses. Because the linac macropulse frequency is 120 Hz, this program produces an extraction rate of 720 pps. For PSR injection, the final 108 μs of each macropulse is modified by a chopper-buncher system in the linac low-energy transport to form a sequence of micropulses spaced at 60-ns intervals. The ring circulation period is chosen so that this injected pulse train is synchronized with the six bunches already stored. Each incoming micropulse, containing 3.3×10^8 protons, merges with a ring bunch; 300 micropulses are accumulated in each ring bunch. The narrow bunch width in this mode is maintained by a high-frequency buncher located in the ring.

In the long-bunch low-frequency (LBLF) mode, the ring accumulates complete linac macropulses (5.2×10^{13} protons) in a single 270-ns bunch. Each stored bunch is extracted after completion of the injection cycle, with a maximum delay of 4 ms. The cycle repetition rate is 12-Hz peak current, assuming a parabolic longitudinal charge distribution, is 46.3 A; average circulating current is 100 μA. For injection, a slow-wave chopper in the linac low-energy transport carves 90 ns out of each 360 ns throughout the macropulse, permitting entering pulses to be overlapped with those that are already stored in the 360-ns circulation period. A first-harmonic buncher keeps the 90-ns gap clear of protons to facilitate low-loss

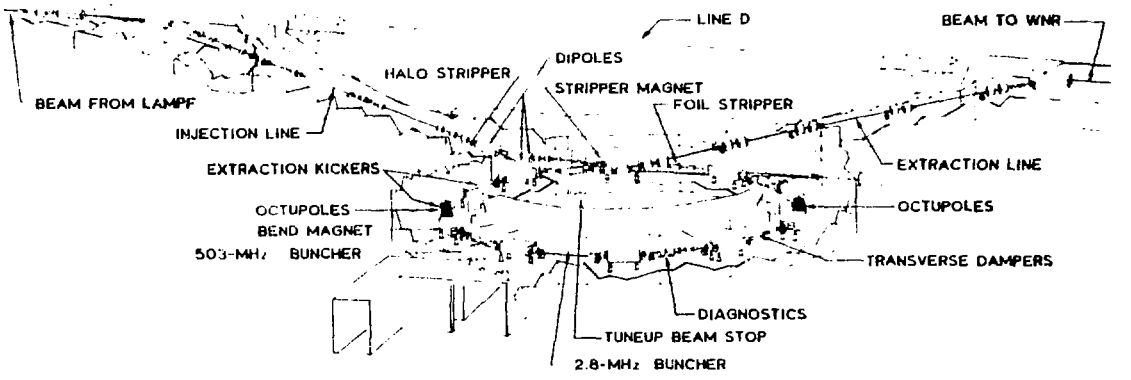

Fig. 1.
Plan view of the Proton Storage Ring.

Table I. PSR Operating-Mode Characteristics.

	Short Bunch, High Frequency	Long Bunch, Low Frequency
Parameter	Nuclear physics	Materials science
Number of bunches in ring	6	1
Bunch length in ring	1 ns	270 ns
Bunch interval in ring	59.63 ns	—
Buncher frequency	603.75 MHz	2.795 MHz
Protons/bunch accumulated	1×10^{13}	5.2×10^{13}
Accumulated turns	300	2100
Injection rate	120 bursts/s	12 pps
Filling time	108 μs	750 μs
Extraction rate	720 pps	12 pps
Peak circulating current	24.0 μA	100 μA

extraction. After accumulation is complete, the ring is emptied in a single turn by the fast-extraction kicker.

The PSR was authorized as a $21.8-million construction project in FY 1981, and a staging building for development and assembly of equipment was built by the end of that year. Construction of the main-ring tunnel and its associated equipment building started in May 1982 and is now complete.

It was necessary to develop specialized equipment systems for the PSR, including an intense negative-ion source, a beam chopper to provide the desired beam-bunch pattern, kicker magnets to deflect the beam into and out of the ring, and beam bunchers to compress the beam into well-defined short pulses. These developments have been under way for several years and satisfactory designs are proven for all systems. Final component assembly is in progress.

Procurement of standard equipment, such as magnets and vacuum components, is nearly complete and installation in the ring has started.

First operation of the PSR is expected on schedule in the spring of 1985. At first the beam current will be small, but as tuneup proceeds, the beam current will increase and we expect to reach the 100-μA level at the end of FY 1986.

WNR Upgrade

R. Woods

The WNR upgrade will raise beam-handling capability to the 100-μA level of the PSR design. The project requires improvements to the proton beam-transport line and the target-moderator-reflector (TMR) system.

To allow continuing hands-on maintenance of the proton beam-transport line under higher current conditions, beam losses must be kept low, requiring a larger aperture in the beam-transport system. The change from H^+ to H^- and the revamping of the switchyard also require reworking the beginning of Line D. There are time-sharing modes in which some beam will be going to the PSR and other beam pulses will be going either to the WNR or to the neutrino facility. A kicker magnet and stripper foil will be mounted in Line D to permit this time sharing.

The major thrust of the upgrade will be seen in the TMR. The increased current, from 10 to 100 μA, must be dissipated in the new design. We are also planning for a depleted uranium target and designing to permit the installation of a boosted target in the future.

The new concept for the TMR is shown in Fig. 2. The concept is a split target with a void between and moderators located around this void in an arrangement termed the flux trap geometry. The neutron flight paths that view these moderators thus will not "see" the neutron target itself. This arrangement significantly reduces the background of unwanted high-energy neutrons.

The existing WNR flight paths will view these moderators. The upper target will be provided with wing moderators that can be viewed by future flight paths. In this design the target and moderators are surrounded by a 1-mm-diam cylinder of material that reflects neutrons back into the moderators and also adds to the shielding.

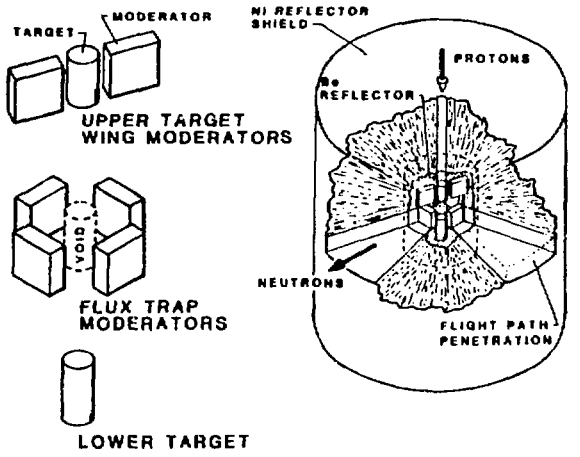

Fig. 2.
New concept for target-moderator-reflector (TMR) system.

The installation of a depleted uranium target in the spring of 1985 will give a factor of ~2 in useful neutron production. A liquid-hydrogen moderator also will be installed at that time to provide a source of cold and ultracold neutrons. A separate insertable target with little or no moderation will be provided for higher energy neutron experiments.

The increased neutron flux resulting from these improvements requires an additional 0.6 m of iron shielding above the WNR target for equipment protection; additional shielding and a water-cooled beam stop also will be provided below the WNR target.

Experimental Halls Expansion

H. Robinson

The original plan for the existing WNR experimental hall did not contemplate the 100-fold increase in neutron source capability made possible by the PSR. This greater intensity and optimized pulse structure from the PSR transforms the source into the most intense spallation neutron source in the nation, and perhaps in the world. These extraordinary capabilities have proved attractive not only to the Los Alamos National Laboratory staff, but to a large contingent of researchers from universities and industry. Soon after the PSR becomes operational, the facility expects to host approximately 100 visiting experimenters each year.

To provide an adequate experimental area to accommodate the User community and permit the full use of the neutron source, construction funding of $15.7 million is requested for FY 1985 to expand the present experimental hall and support facility.

This funding will provide a 929-m^2, pre-engineered, high-bay structure attached to the east side of the existing hall on the existing grade. The hall will be equipped with the full complement of services required for six major neutron-scattering spectrometers. A 186-m^2 pre-engineered wing attached to this structure, shown in Fig. 3, will house quiet rooms, set-up areas, and restroom facilities.

In addition, a 1115-m^2 reinforced concrete subterranean structure attached to the west side of the existing hall at the same floor elevation will be built. The complement of mechanical and electrical services provided in the east hall will be installed here for six more experiments.

A 745-m^2, two-story, reinforced concrete and pre-engineered laboratory and support complex will adjoin the present control room and the west experimental hall. This building, shown in Fig. 4, will be equipped for offices and used for data collection and technician work space.

Modifications will be made to the existing hall to allow better access and control of experiments and to provide penetrations for additional neutron-beam tubes from the target crypt. The proposed project includes funding for the construction of three new spectrometers especially designed to make optimum use of the intense pulsed-neutron beam, plus funding for six additional data-collection computers and a hub computer for data analysis.

In summary, the combined floor space of the experimental halls (2230 m^2) will more than quadruple the space available for the spectrometers and staging of experiments, thus assuring full use of the source for the national neutron-scattering program. The 743 m^2 of support area on the west side will provide adequate room for data collection and light technician service to experimenters using this world-class facility.

Line E for Neutrino Physics

T. Dombeck and G. J. Stephenson, Jr.

The neutrino beam line designated Line E lies to the south of the LAMPF switchyard in the WNR complex, as shown schematically in Fig. 5. A kicker magnet was

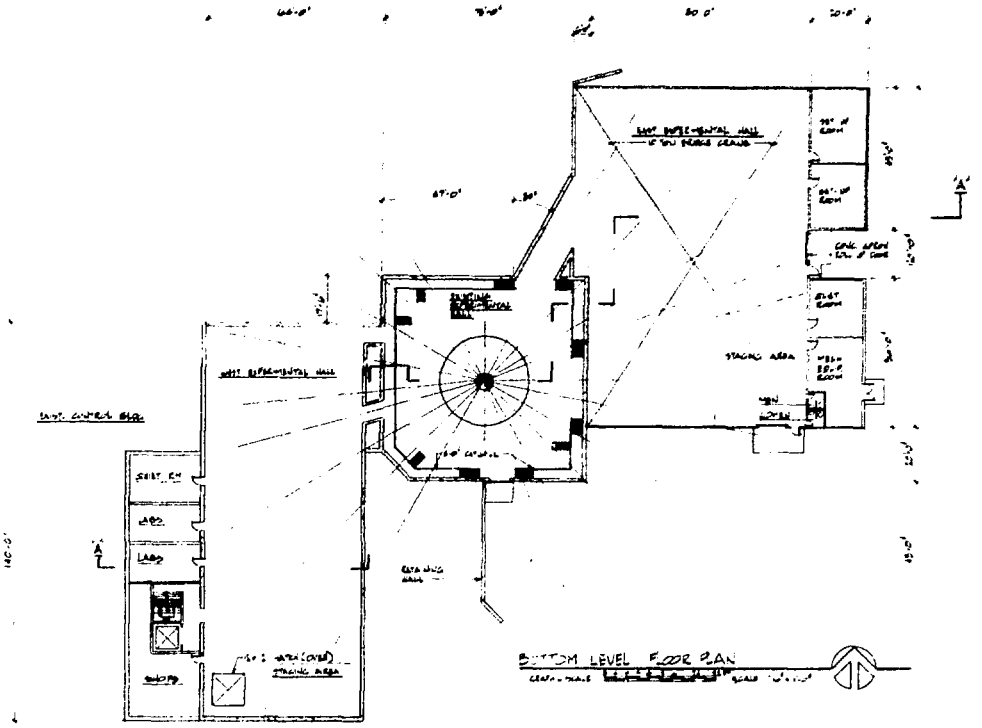

Fig. 3.
Lower level floor plan for experimental halls.

inserted into Line D to divert LAMPF 800-MeV macropulses into Line E with current initially at ~20 μA, upgradable to perhaps 200 μA. The beam line consists of four quadrupole doublets, two bending dipoles, a graphite target, and a tungsten beam stop. The target station is followed by a 12-m-long, 4-m-diam pion-decay tunnel and an iron-concrete shield approximately 9 m thick. The detector sits on a concrete pad beyond the iron shield in a concrete blockhouse used for cosmic-ray attenuation. Biological shielding is provided by concrete and earth overburden.

The target and beam-stop areas are water cooled and designed for remote handling. Iron shielding around the target allows manual maintenance to within a few feet of the target. The target is viewed by a beam pipe at 9° that allows one to monitor the pion flux continuously during the run.

Engineering for the construction and beam-line components was performed by Los Alamos Groups ENG-2 and P-12, construction was carried out by the Zia Corporation, and alignment was done by the Antares alignment crew (Group P-5). Beam-line magnets and power supplies were provided by LAMPF. Various beam components were fabricated or provided by university groups: vacuum pieces and electronics trailer (New Mexico State University); harp boxes (Temple University); target and computer (University of California, Riverside); and pion monitor (UCLA). Shielding material was provided by LAMPF and P Division.

A number of features incorporated into Line E will be used in future beam lines. The kicker magnet, its power supply, and the vacuum fan-out pipe will be duplicated for the PSR. The skew in Line E is a first at LAMPF and required a novel method of alignment, sighting along the bore tubes of the magnets. The harps for beam monitoring in Line E also are of a new design that will be duplicated for use in the PSR and other LAMPF beams.

The expected flux of muon neutrinos in the detector for a current of 20 μA is shown in Fig. 6. Provision has been made for a magnetic pion-focusing device that will be inserted just downstream of the target; it will enhance the neutrino flux by an order of magnitude. Flux calculations were performed using two Monte Carlo programs based on pion yields that were measured for carbon targets.

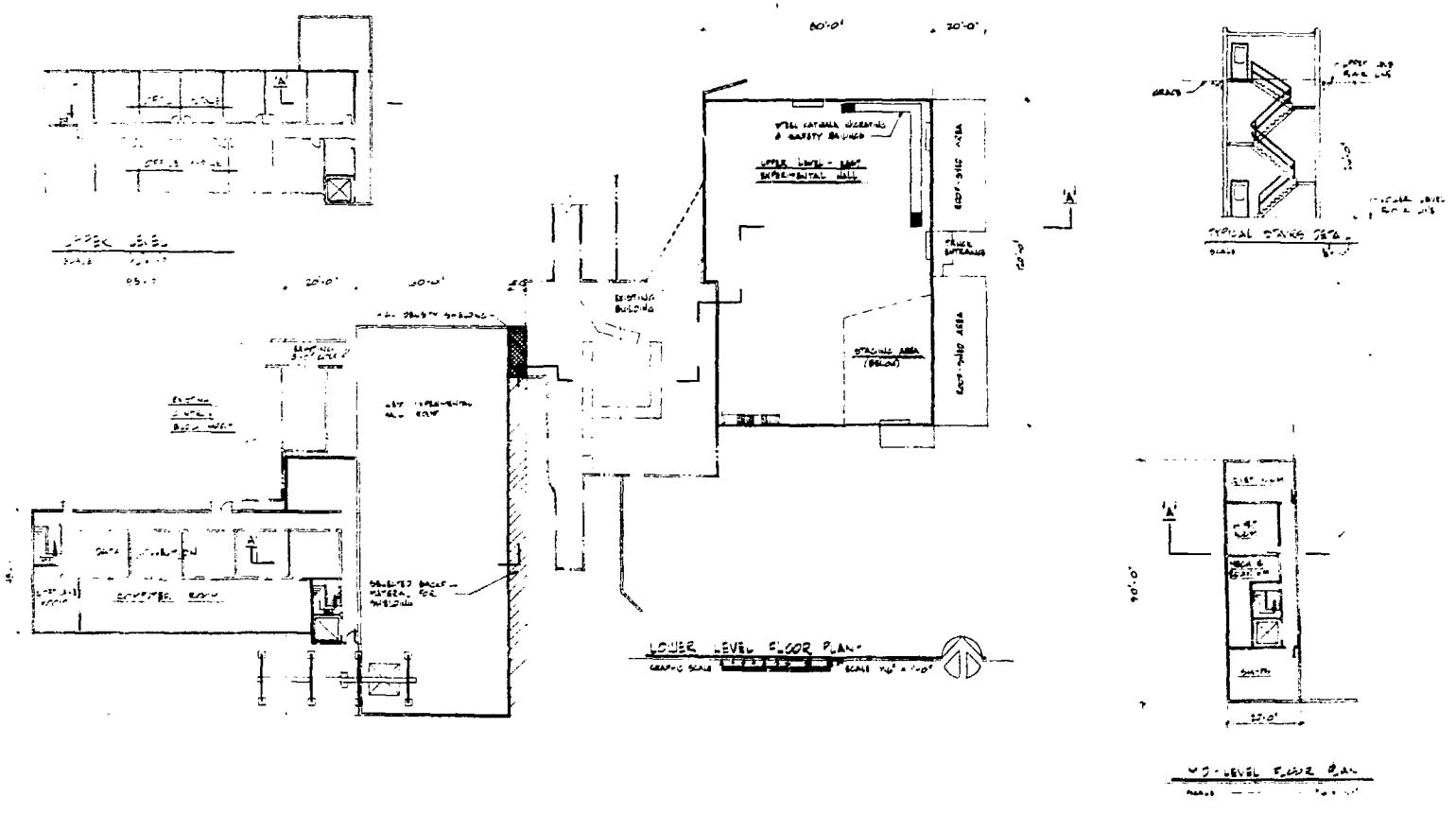

Fig. 4.
Upper level floor plan for experimental halls.

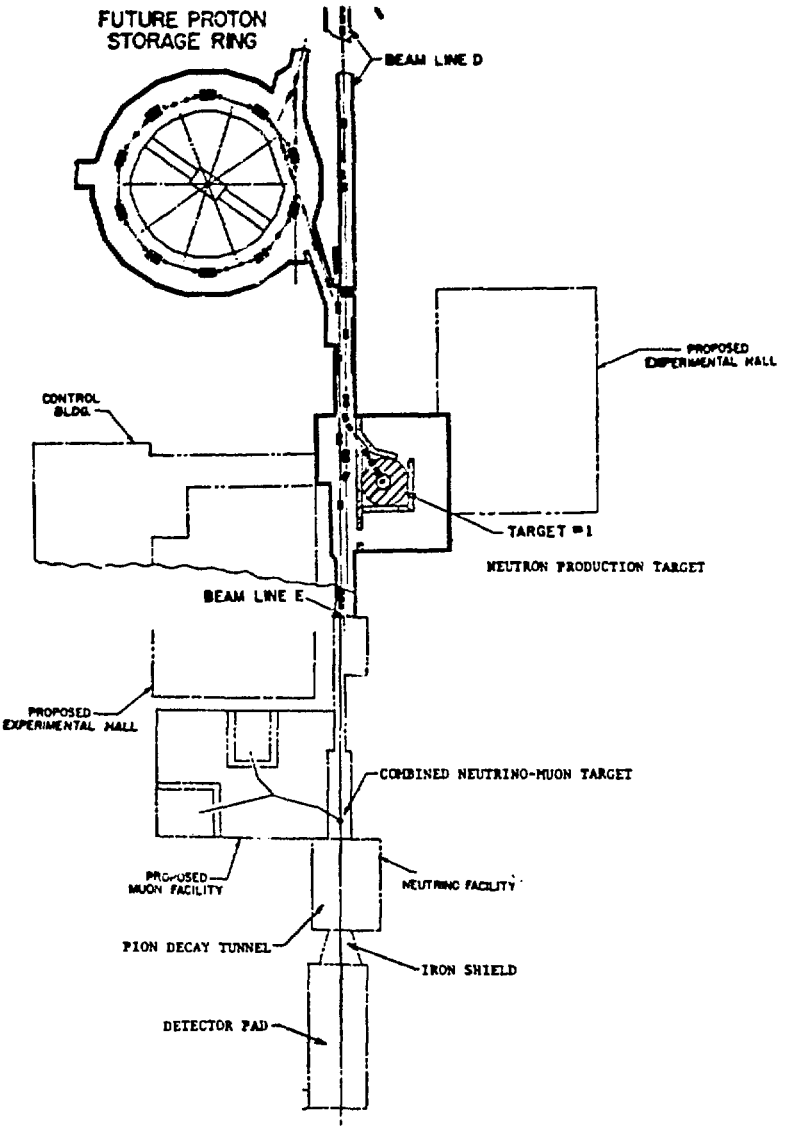

Fig. 5.

Layout of the WNR/PSR complex showing location of neutrino beam line (Line E), neutrino-production target, *pion decay channel, shielding, and neutrino detector.*

At the end of 1983, the construction is approximately two-thirds complete. Beam-line magnet elements and a vacuum system are installed and tested, and alignment is complete, as are the wire connections. A test to transport a small proton current was successfully performed in January 1984.

Publication

1. P. Denes et al., Phys. Rev. C 27, 1339 (1983).

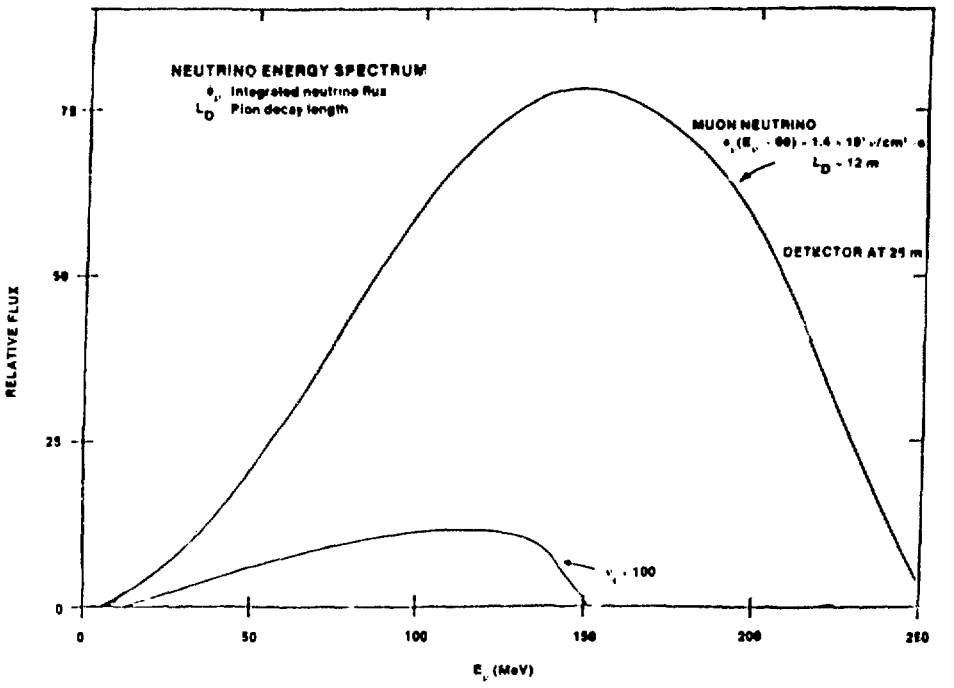

Fig. 6.
Calculated neutrino energy spectrum. Calculated flux is for a bare target with 20-μA beam of 800-MeV protons.

Research Programs

WNR/PSR Neutron Scattering Research

R. N. Silver, R. Alkire, G. Christoph, J. Eckert, J. Goldstone, A. Larson, R. Robinson, P. Seeger, P. Vergamini, and A. Williams

In 1983 the neutron-scattering group (P-8) announced a National User Program at the WNR/PSR facility. This announcement formally opened the facility to the national and international scientific communities in solid-state physics, chemistry, materials science, and biology. Proposals for the use of neutron-scattering instrumentation are reviewed by a nationally appointed Program Advisory Committee, which also reviews proposals for the Intense Pulsed Neutron Source (IPNS) at the Argonne National Laboratory. Proposals are reviewed on the basis of scientific excellence and optimal use of WNR/PSR characteristics.

The first two instruments in the formal User program are the Be-BeO Filter Difference Spectrometer (FDS) and the Single-Crystal Diffractometer (SCD). The FDS, shown in Fig. 7, is used for chemical spectroscopy, localized modes, and phonon density-of-state measurements. The FDS instrument is the responsibility of J. Eckert. The SCD, shown in Fig. 8, uses the Laue-TOF technique and is the responsibility of P. Vergamini. In 1983, 24 proposals for experiments were received and 15 were approved by the Program Advisory Committee.

In 1984 the Neutron Powder Diffractometer (NPD) will join the User program. The NPD is used for neutron powder diffraction by the Rietveld profile-refinement technique. The scientist responsible for the NPD is G. Christoph.

In 1983 major progress was made in the construction of neutron-scattering instrumentation. The present arrangement of instrumentation at the WNR is shown in Fig. 9.

(1) The prototype FDS and SCD instruments were completely rebuilt into well-engineered instruments suitable for the National User Program. These modifications greatly improved instrument performance and reliability.

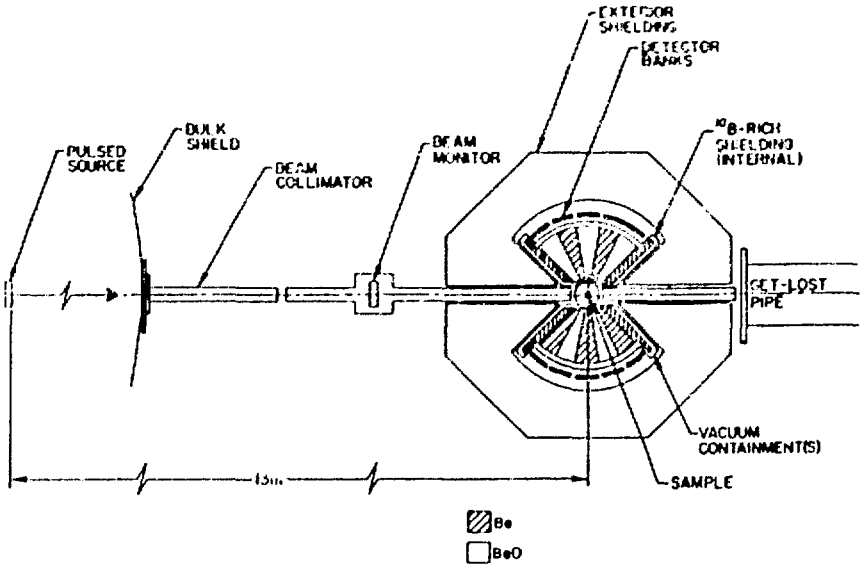

Fig. 7.
Filter Difference Spectrometer.

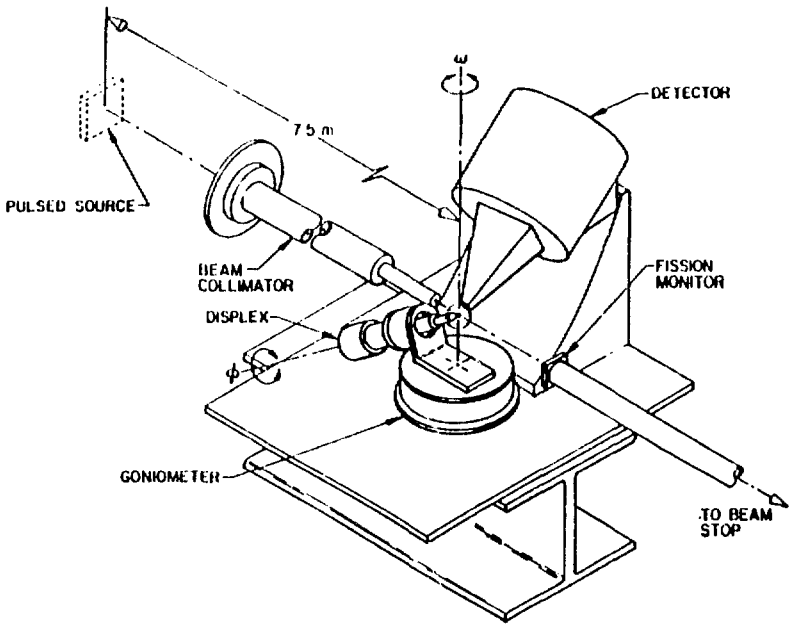

Fig. 8.
Single-Crystal Diffractometer.

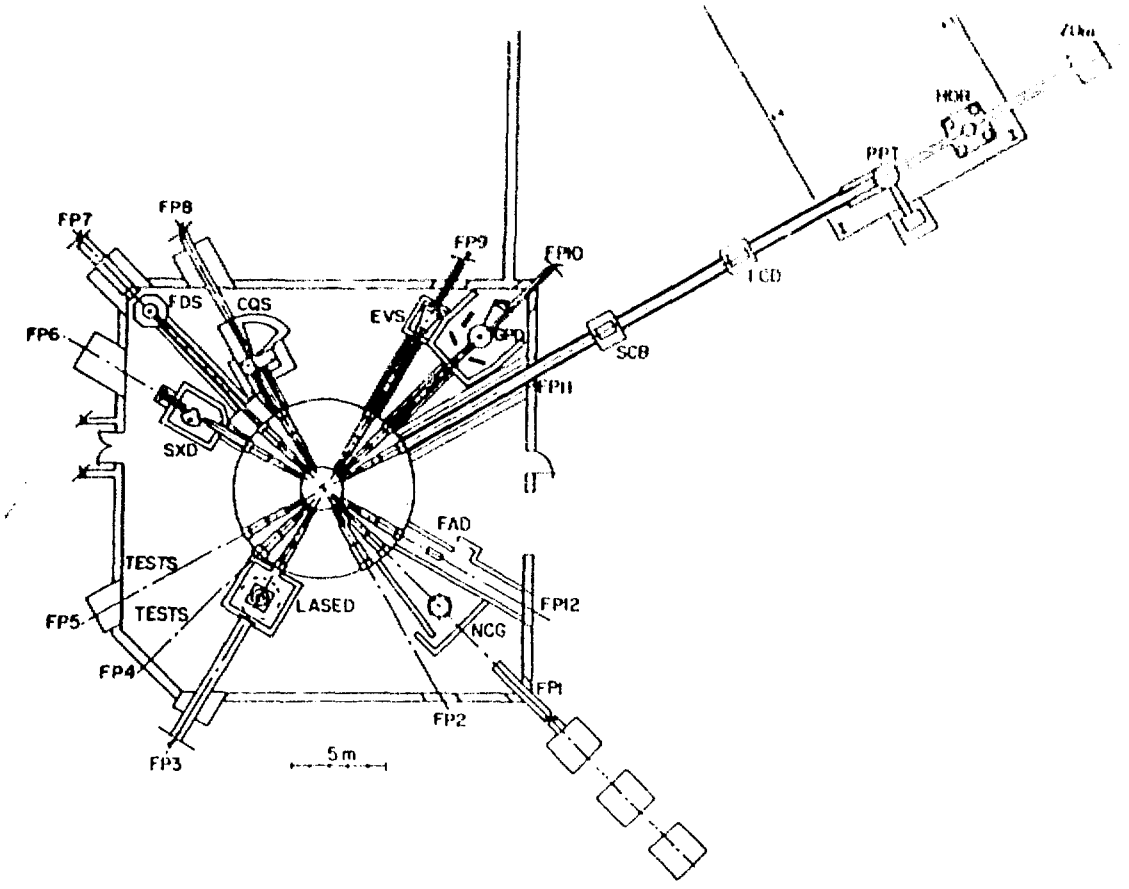

Fig. 9.
WNR layout of instrumentation.

(2) A prototype Constant-Q Spectrometer (CQS) began operation. The CQS, shown in Fig. 10, will be used to study elementary excitations, such as phonons and magnons in single-crystal samples.

(3) The nuclear-resonance-filter difference technique for electron-volt spectroscopy was extended to low-Q measurements appropriate for the study of magnetic and electronic excitations. In a collaboration with the Rutherford Appleton Laboratory, a prototype low-Q electron-volt spectrometer (EVS) was constructed and brought into initial operation at the WNR.

(4) An instrument optimized for low-angle diffractive scattering with epithermal neutrons at high intensities and low resolution is required for diffraction of liquids and amorphous materials. Such an instrument requires special attention to keep backgrounds low. A protoype diffractometer for liquid, amorphous, and special-environment materials (LASED) built with these goals in mind began operation at the WNR.

(5) A new sample environment container was constructed for the NPD, and additional detectors were installed.

Some highlights of neutron-scattering research in 1983 included the following.

- ***First Molecular Hydrogen Complex***
  P. Vergamini and A. Larson (P-8) and H. Wasserman and R. Ryan (INC-4)

  The structure of the first complex that reversibly binds molecular hydrogen was determined by single-crystal neutron diffraction at the WNR facility. This is an intermediate species in the catalysis of hydrogen, a long-sought missing link. The structure is shown in Fig. 11.

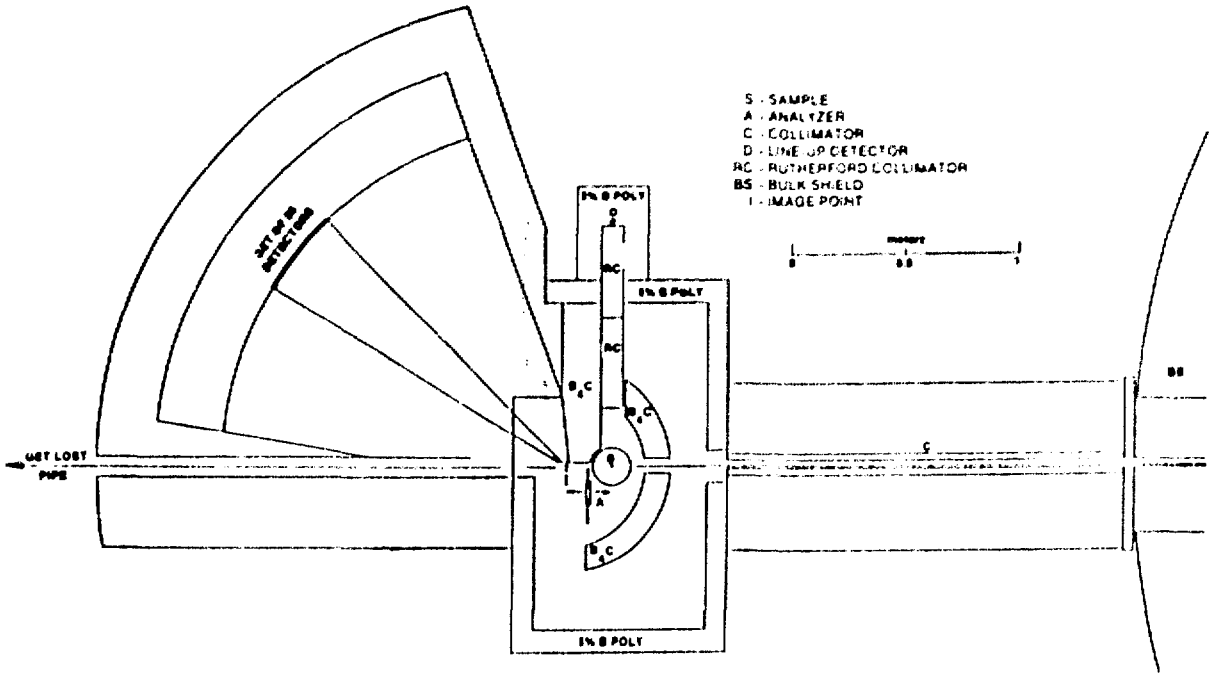

Fig. 10.
Schematic of the Los Alamos Constant-Q Spectrometer.

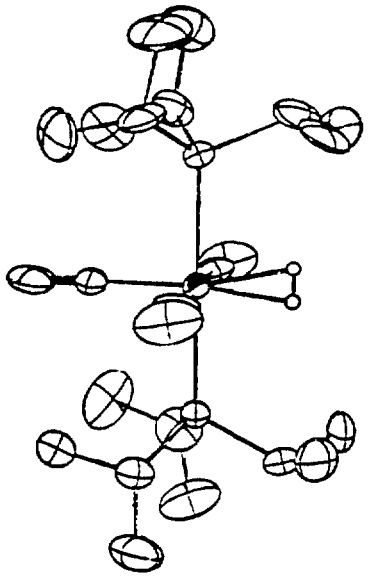

W H2(CO)3 (P ipr3)2

ORTEP PLOT OF THE STRUCTURE OF W $H_2(CO)_3$ (P $ipr_3)_2$

Fig. 11.
Molecular hydrogen complex.

- *High-Pressure Structure of ReO_3*
  R. Alkire, A. Larson, J. Schirber, and B. Morosin (Sandia National Labs.)

  ReO_3 is an unusual material because it undergoes a "compressibility collapse" at high pressures with a factor-of-10 decrease in compressibility above 10 kbar. The long-sought structure of the high-pressure phase has finally yielded to a time-of-flight neutron-scattering experiment in which one can take advantage of the strong penetrating power of the neutron and its ability to Bragg scatter at fixed angles with a white neutron beam in a high-pressure (15-kbar) cell using the SCD.

- *Hydrogen Sites in PbO_2 Battery-Plate Material*
  J. Eckert, J. Goldstone, J. Jorgensen, and R. Varma (Argonne National Lab.)

  The problem of hydrogen bonding in electrochemical cells is of immense practical interest. The strong penetrating power of the neutron, its sensitivity to hydrogen, and the high epithermal flux of the WNR facility make it a very suitable probe for addressing practical problems of this sort. Figure 12 shows inelastic neutron spectra taken with the Filter Difference Spectrometer of PbO_2 before and after

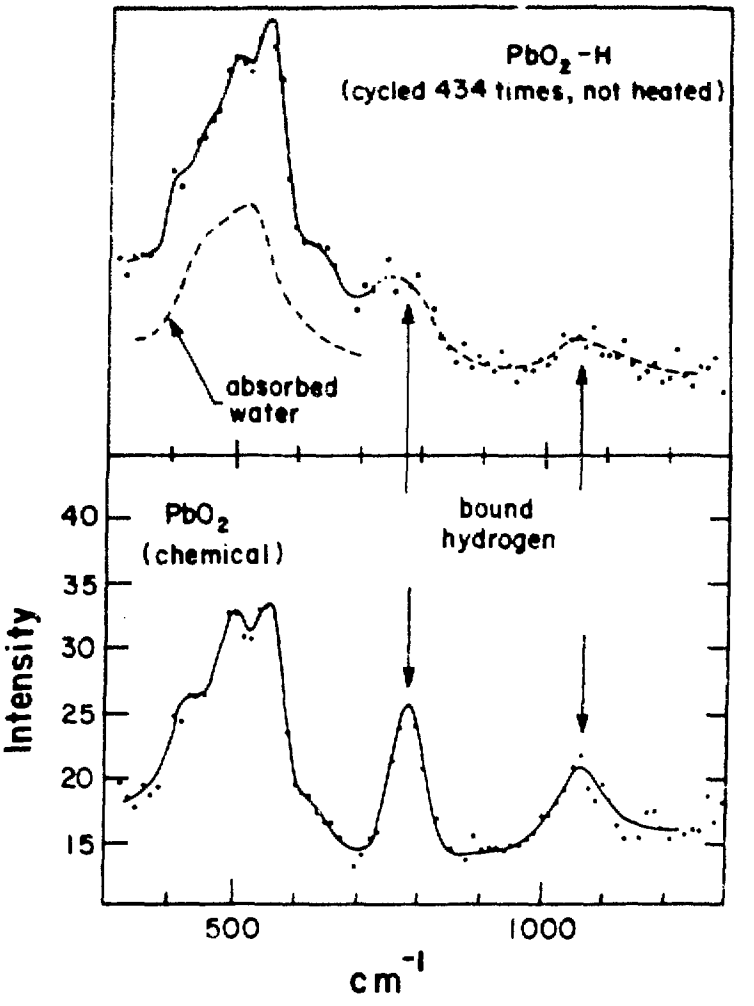

Fig. 12.
Inelastic neutron spectra of lead dioxide PbO_2 battery-plate material.

cycling. The spectra clearly show that the hydrogen introduced in the cells appears as vibrational modes of water H_2O and not as increased bound-hydrogen modes.

- *Octahedral-Site Occupancy in Rare-Earth Hydrides J. Goldstone, J. Eckert, G. Venturini, and P. Richards (Sandia National Labs.)*

In LaH_x, CeH_x, and other rare-earth hydrides, the hydrogen atoms primarily occupy tetrahedral sites until $x > 2$ is reached, at which point octahedral sites begin to be filled. The relative occupancy of these sites can be determined by the differing vibrational modes in inelastic neutron scattering and by powder diffraction. In YH_x, octahedral sites were found to be occupied before $x = 2$ composition was reached, and the occupation of these sites increased with decreasing temperature, in contradiction to expectations of increasing order at low temperatures. Experiments at the WNR using the FDS and NPD instruments showed that the "octahedral" sites were not quite octahedral as the temperature decreased, leading to an increased degeneracy that could explain the observed temperature dependence.

Other important activities in the neutron-scattering group in 1983 included the following.

- ***Development of a Proposal for the Expansion of the Experimental Halls at the WNR Facility.*** In accordance with the recommendations of the DOE review committees (Brinkman I and II, and Rowe), a proposal has been developed and submitted to the

DOE for expansion of the experimental halls, computer support, and instrumentation in order for the WNR/PSR to serve as a national User facility. This proposal was submitted for FY 1985 funding.

- ***Workshops and Conferences.*** A workshop was held in September 1983 on "Frontiers in Condensed Matter Physics with the WNR/PSR Pulsed Neutron Source," chaired by R. Birgeneau of MIT. A mini-workshop was held in November on "Biological Applications of the WNR/PSR Facility." Planning was carried out for a conference to be held in February 1984 on "High Energy Excitations in Condensed Matter," and commitments were made to sponsor an "International Conference on Neutron Scattering" in August 1985 in Santa Fe.

WNR/PSR Nuclear Science

Search for Resonance Structure in Few-Nucleon Systems

P. W. Lisowski and G. F. Auchampaugh (P-3); M. Moore and G. Morgan (P-15); and R. Shamu (Western Michigan Univ.)

During the past few years, both experimental claims and theoretical predictions for the existence of dibaryon resonances have been made. The conventional meson approach interprets observed structure in the nucleon-nucleon system as resulting from inelastic channels in various partial waves. A more exciting possibility is that the resonances may result from six-quark bound states. In this model the nucleons are pictured as two bags of quarks, with the resulting overlap producing a rich density of dibaryon states. Before experiments performed at Los Alamos in 1982 and 1983, there was no undisputed picture of the energy or width of the proposed resonances. In fact, searches at LAMPF and elsewhere had insufficient energy resolution to observe the narrow structure predicted by some models.

A search for resonance structure in the nucleon-nucleon system was completed by performing a high-resolution, high-precision *np* total cross-section measurement over the entire range of interest. These data showed no evidence for narrow structure. A broad anomaly previously seen in the *np* system, attributed to an $I = 1$, $^3F_3$ dibaryon resonance, was confirmed. An $I = 0$, $^1F_3$ state proposed by other authors was not observed. From 200 to 700 MeV, our data (Fig. 13) indicate that existing cross sections may be as much as 6% too low.

A second set of measurements searching for resonance effects in the nine-quark system *nD* was partially completed in 1983. These data will provide accurate cross sections to test both the theory of binding effects in the

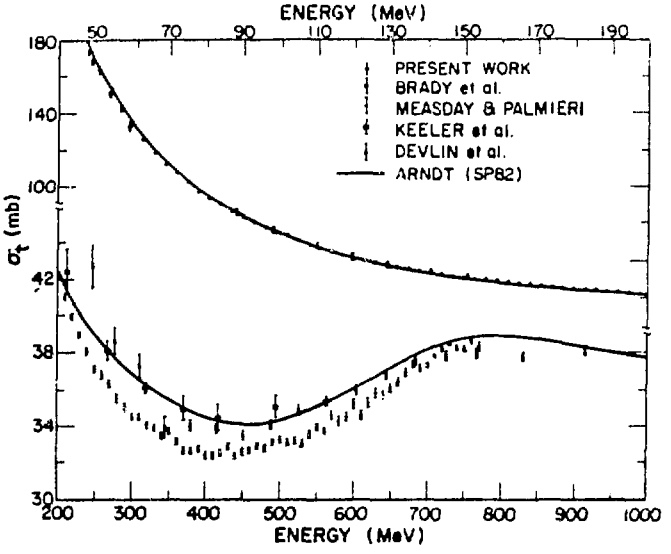

Fig. 13.

Comparison of present results with selected high-accuracy *np* total cross-section data and with phase-shift predictions. The upper (lower) data correspond to the upper (lower) energy scale. Note that the cross-section scale for the upper data is a factor of 10 smaller than that for the lower data.

deuteron and charge symmetry effects in the three-nucleon system.

REFERENCE

1. P. W. Lisowski, R. E. Shamu, G. F. Auchampaugh, N. S. P. King, M. S. Moore, and T. S. Singleton, "Search for Resonance Structure in the *np* Total Cross Section Below 800 MeV," Phys. Rev. Lett. **49**, 255 (1982).

High-Resolution Nucleon-Induced Charge-Exchange Reaction Studies at 800 MeV

P. Lisowski (P-3); G. Morgan and N. King (P-15); and P. Craig, D. Lind, R. Jeffesen, J. Shepard, J. Ullman, and C. Zafiratos (Univ. of Colorado)

Nucleon-induced charge-exchange reactions at bombarding energies of several hundred MeV have indicated that there are interesting but poorly understood processes involved. For example, in (p,n) reactions the strength of Gamow-Teller (GT) transitions may be computed from a simple sum rule. Recent data near 200 MeV indicate that approximately 30% of the expected GT strength is missing.

One exciting possibility is that the GT strength is "quenched" because of appreciable delta-isobar, nucleon-hole (Δ-hole) components in the low-lying GT levels. Such a theory, if correct, would imply that nucleon excitations such as the Δ, which have been considered to be too high in energy to be of importance in the low-energy domain, must be considered. Alternative conventional nuclear-structure effects also have been proposed to account for the GT quenching effect. Our studies of (p,n) reactions at the WNR will permit a search for the transfer of GT strength directly.

To study this and other aspects of nucleon-induced charge-exchange, we are using a 213-m-long 0° reaction angle flight path at the WNR, the only facility in the world capable of neutron energy resolution sufficient to permit the observation of nuclear-structure effects at 800 MeV. Preliminary results thus far obtained for (p,n) indicate that we can obtain information addressing four areas of interest: (1) the excitation of discrete levels leading to unique information on the isovector and isovector spin-flip parts of the effective *NN* interaction; (2) the nature of the Pauli-blocked quasi-elastic knock-on peak; (3) the nature of the broad resonances associated with the Δ and the possible implications for Δ-hole configurations in nuclear spectra; and (4) the excitation of charge-exchange analogs specifically using (n,p) reactions.

As an example of the above, we have compared our spectra for $^{13}C(p,n)$, shown in Fig. 14, with those available at lower energies and have conclusively identified GT and Fermi transitions, thus greatly extending the energy range over which these transitions have been studied.

To obtain angular distributions, we plan to install a beam swinger to change the angle of incidence of the proton beam and thereby obtain angular distributions using the existing equipment.

Neutron-Induced γ-Ray Processes

S. A. Wender and G. F. Auchampaugh (P-3); L. R. Nilsson (Tandem Accelerator Lab., Uppsala, Sweden); and N. R. Roberson (Triangle Universities Nuclear Lab., Duke Univ.)

Experiments that study γ rays in the energy range from 4 to 30 MeV produced by fast neutron-induced reactions have been hampered by low data acquisition rates, restricted neutron energy ranges, and high backgrounds. Typical systems for studying fast neutron-capture reactions, for example, have been located at Van de Graaff accelerators and have used large-volume NaI detectors with massive active and passive shielding. These detector systems have been limited to one or two detectors because of their large size and high costs. The neutron sources have been limited in their energy range and resolution because they usually relied on secondary production targets [for example, the $D(d,n)$ reaction with gas cells].

During FY 1983 we developed a unique system to study high-energy γ rays produced by neutron-induced reactions. This system consists of five bismuth germanate (BGO) scintillators used in conjunction with a pulsed spallation neutron source at the WNR. The simultaneous acquisition of γ-ray excitation functions and angular distributions for incident neutrons in the energy range from 1 to 200 MeV is possible with this system (a paper describing this method has been accepted for publication in Nuclear Instruments and Methods). Figure 15 shows a diagram of the apparatus.

The physics program based on this system is being formulated as the particular parameters and capabilities of the system are determined. The program presently

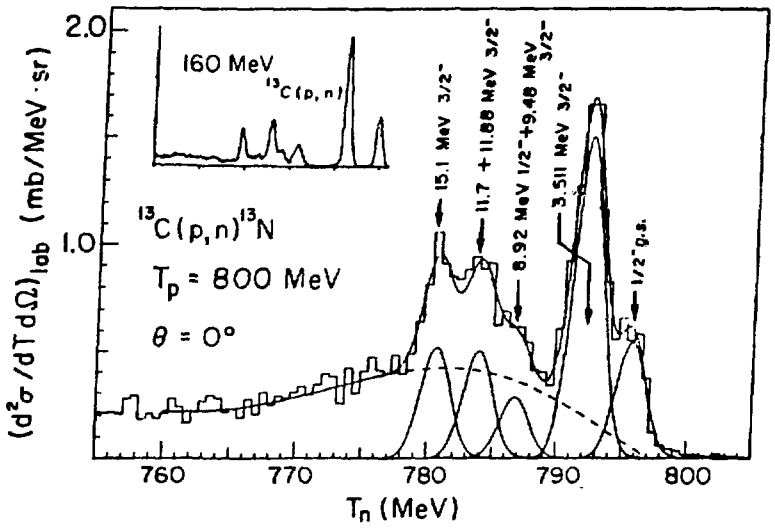

Fig. 14.
An 800-MeV $^{13}C(p,n)$ TOF spectrum at $\theta = 0°$. Overall resolution is approximately 2.5 MeV (FWHM). Arrows indicate expected locations of peaks observed in the 160-MeV spectrum shown in the inset. The smooth curves indicate best fits to the background and peaks.

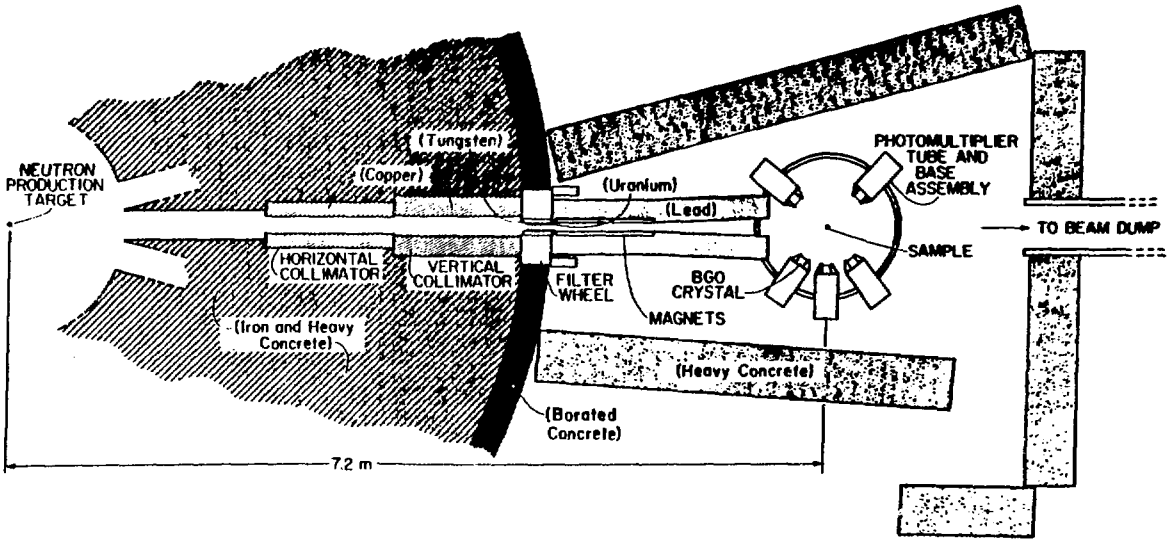

Fig. 15.
Experimental setup showing neutron collimators, shielding, and detector assembly.

consists of studying two broad areas: (1) inelastic neutron excitation of γ rays from bound states using the (n,n') reaction, and (2) fast-neutron-capture reactions into the giant-resonance region of nuclei.

In addition to these two programs we are also investigating the properties of the BGO detectors to optimize their characteristics.

Inelastic γ-Ray Production. As an initial test of the system, we measured the $^{12}C(nn'\gamma = 4.44\text{-MeV})$ reaction cross section for incident neutron energies from threshold (4.9 MeV) to 100 MeV. This reaction previously has been studied up to 20 MeV. Figure 16 shows the results of our measurements. These data represent approximately 13 h of beam time.

In this run we used only four BGO detectors at $\theta_{lab} = 55$, 90, 125, and 140°. The data from these detectors were fitted to an expansion in Legendre polynomials,

$$d\sigma(\theta)/d\Omega = A_0 \{ 1 + \Sigma a_k P_k[\cos(\theta)] \} \ .$$

The a_2 coefficient to the order of $k = 2$ as a function of neutron energy agrees well with previous results, and is shown in Fig. 17. However, the data show the need for terms to the order of $k = 4$, consistent with the results of the $^{12}C(p,p'\gamma = 4.44\text{-MeV})$ reaction. Because only four detectors were used and two of them were at symmetric angles, the errors in the Legendre coefficients are large when the expansion includes $k = 4$ terms; a remeasurement is planned.

Fast-Neutron Capture. For our first fast-neutron-capture experiment we studied the $^{40}Ca(n,\gamma)$ reaction. Because the cross section for this reaction in the giant-resonance region is only on the order of 10 μb, we used a relatively large sample of natural calcium (500 g, 7.6 cm long by 7.6 cm diameter). Data were acquired for approximately 50 h. Preliminary analysis of the ground-state γ-ray yield as a function of neutron energy, corrected for incident neutron flux and neutron energy bin size, is

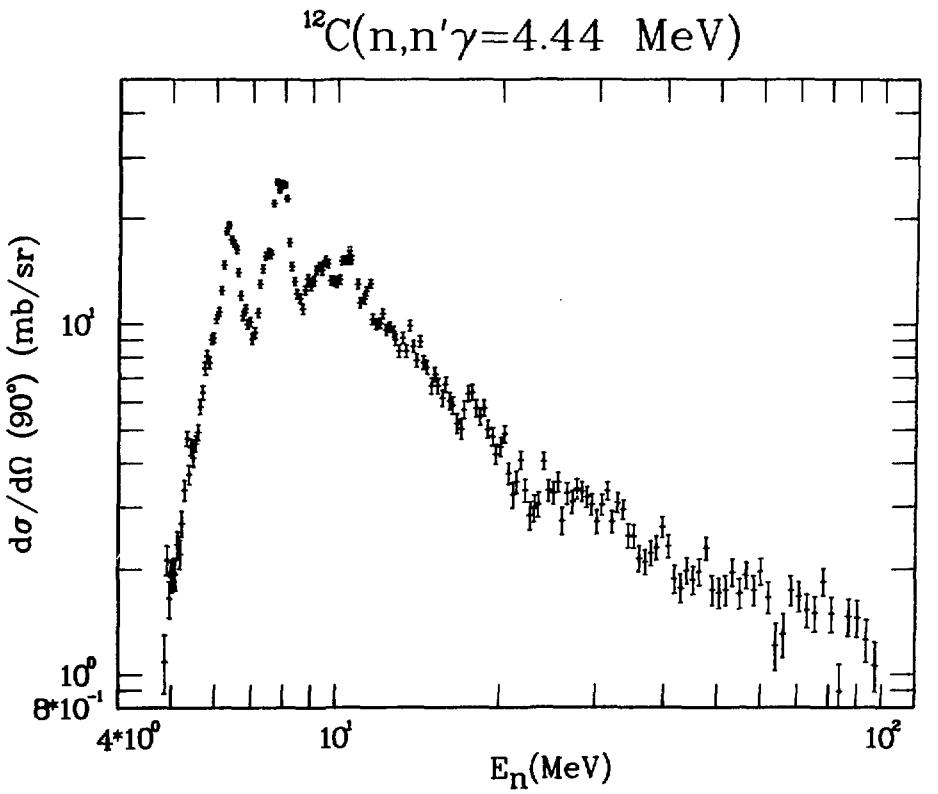

Fig. 16.
The 90° differential cross section for the $^{12}C(n,n'\gamma) = 4.44$-MeV reaction as a function of neutron energy.

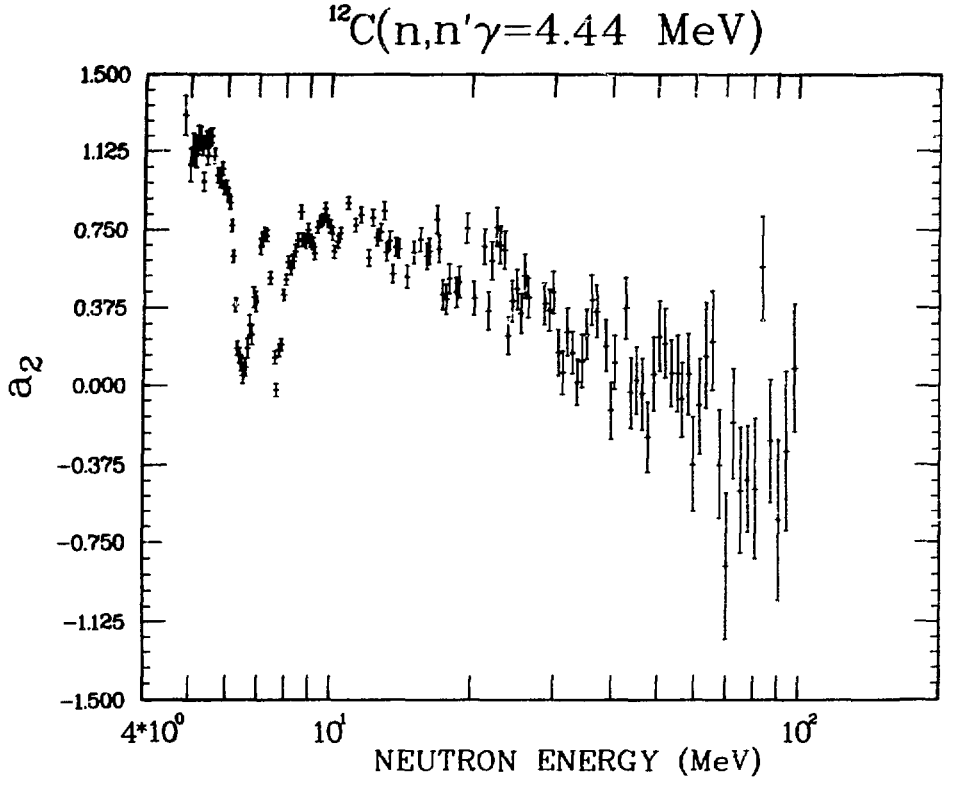

Fig. 17.
The A_2 Legendre polynomial coefficient for the 4.44-MeV γ ray from the $^{12}C(n,n'\gamma)$ reaction. The plot corresponds to fitting the data to A_0 and A_2 only.

shown in Fig. 18. The absolute cross section was obtained by normalizing to previous results. The maximum in the yield curve at $E_n = 11$ MeV corresponds to the peak of the giant dipole resonance in ^{41}Ca. The shape of this excitation function is in good agreement with previous results.

BGO Detector Development. The use of BGO scintillators to detect high-energy γ rays is a relatively recent development. We therefore have spent some time studying their characteristics and have considered methods to improve their performance.

In a paper submitted to Nuclear Instruments and Methods, we report the measurement of absolute efficiency of a 7.6- by 7.6-cm BGO detector at 15 MeV. We used the $^{12}C(p,\gamma_0)$ reaction at $E_p = 14.2$ MeV and determined the efficiency to be (51 ± 4)%. We expect to obtain response functions and efficiencies over the energy range 1-30 MeV.

Planned Work. We plan to continue our study of the $^{12}C(n,n'\gamma)$ reaction to improve the quality of the preliminary data, and to study ^{11}B, which shows several isolated resonances in the γ-ray yield for the 2.0- and 4.4-MeV states. In addition, we plan to measure the γ-ray production cross section of ^{14}N and ^{15}N.

The fast-neutron-capture program will continue the study of the giant-resonance region of nuclei — in particular, the search for the isovector $E2$ resonance in ^{208}Pb. In addition, we plan to search for giant resonances built on excited states in ^{14}C using the $^{13}C(n,\gamma)$ reactions. Such resonances previously have been seen in proton-capture studies. Visitors interested in participating in this research are welcome.

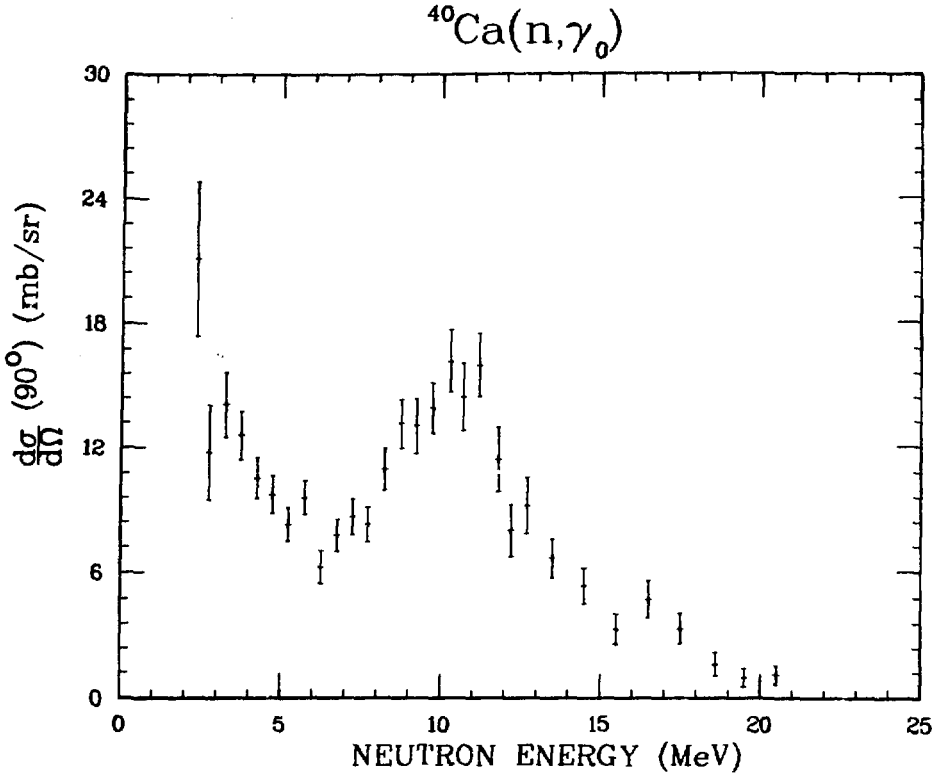

Fig. 18.
The 90° differential cross section for the $^{40}Ca(n,\gamma_0)$ reaction as a function of incident neutron energy.

Fission Fragment Angular and Kinetic Distributions for Actinide Nuclei

G. F. Auchampaugh (P-3); M. S. Moore (P-15); C. E. Olsen (MST-13); C. Goulding (Q-2); N. W. Hill (Oak Ridge National Lab.); and R. White (Lawrence Livermore National Lab.)

Angular, kinetic-energy, and mass distributions as functions of excitation energy play an important role in revealing the physics of the fission process. Answers to questions such as the importance of shell effects and angular momentum on the potential energy surface, the nature of vibration and complex structures associated with this surface, and the time scale and energy dissipation mechanism in fission are all addressed by such measurements. The paucity of high-quality data in this area opens a rich field of research in neutron physics.

During the past year we developed a double-volume Frisch-grid ionization chamber that permits simultaneous measurements of the angular, kinetic-energy, and mass distributions of each fragment as a function of neutron energy for low α-active targets. A detector with cathode foils of $^{235,238}U$ and ^{232}Th was used to obtain data from 0.8 to 20 MeV at the WNR facility. The ^{235}U data have been examined in detail and show systematic effects that are attributed to nonuniformity in the conductivity of the foils and base-line shifts because of pulse pileup from charged particles in the neutron beam. Further development and measurements are planned.

On the Nature of the Coupling in Subthreshold Fission of ^{238}Np

G. F. Auchampaugh and J. D. Moses (P-3); M. S. Moore (P-15); R. O. Nelson (P-9); R. C. Extermann (P-3 Visiting Staff Member); C. E. Olsen (MST-13); and N. W. Hill and J. A. Harvey (Oak Ridge National Lab.)

Although intermediate structure in subthreshold fission was first observed in the neutron-induced fission of ^{237}Np (Refs. 1 and 2), and the structure at 40 eV has been

extensively studied,[3,4] the nature of the coupling between the first and second wells of the ^{238}Np fission barrier remains unknown.

Inspection of high-resolution fission data[4] reveals that several levels are strongly enhanced in the fission channel, so that the mixing between the class II level underlying the intermediate structure and the class I background is neither extremely weak nor very strong. The mixing can, however, be attributed to two very different physical causes, as discussed by Bjørnholm and Lynn.[5] In the simplest case, the two classes of states may be weakly mixed because of a high intermediate barrier. Bjørnholm and Lynn refer to this kind of mixing as moderately weak mixing to a narrow class II state. Alternatively, the class II state may have a very large fission width that leads to weak mixing because of rapid decay of the class II state. This is known as very weak mixing to a broad class II state. The data for ^{237}Np have not clearly distinguished between these alternatives.

Our work was an attempt to resolve this question by measuring the fission and total cross sections with very good energy resolution (1) to expose any underlying broad resonance near 40 eV, if possible; and (2) to obtain good enough resonance parameters to permit detailed analysis of the fine structure of the class II fission resonances at 40 and 120 eV.

The total cross section was measured at the Oak Ridge Electron Linear Accelerator using a 78-m flight path and metallic samples cooled to liquid-nitrogen temperature (~77 K) to reduce Doppler broadening. The fission cross section was measured at the WNR using a 30-m flight path and a unique cryogenic ionization chamber that maintained the samples at a temperature of 84 K. Both experiments were designed to achieve the highest statistical accuracy and the smallest possible neutron resolution at the 40- and 120-eV class II states.

We attempted to determine the relative sizes of the coupling and fission widths of the subthreshold resonances in ^{238}Np by measuring and analyzing the fission and total cross sections with great care and by analyzing the resulting resonance parameters by a variety of techniques. We believe we succeeded to the extent that we carried these techniques as far as they can reasonably be taken with current technology. We did not succeed in providing a clear answer to the nature of the coupling in ^{238}Np.

The multilevel analysis neither requires nor precludes the presence of a broad resonance underlying the 40-eV structure. The statistical analysis of the resonance-spacing distribution gives some indication that an anomalous intruder level is present at 40 eV, but the data also permit the alternate hypothesis. We believe that this problem will not be resolved by precise measurements of the type described here, but by a more sensitive measurement of a different type that can be carried out at the WNR.

V. STATUS OF LAMPF II*

H. A. Thiessen
(Los Alamos)

I will give you a report on progress since the beginning of the summer, including the physics that we learned at the July workshop. One way of organizing the physics we would like to do at LAMPF II is to order it by the needed energy of the proton beam. This list is presented in Table I.

One of the stars of the LAMPF II program will be muon-neutrino physics, which would be quite interesting if we had a 5-GeV proton beam. We could make a better muon factory than LAMPF, even with the 5-GeV beam. We would get variable-energy polarized protons, higher energy pions, and most likely the nuclear chemists would see the bulk of the changes in the reaction mechanism that occur between 1 and 10 GeV in the first 5 GeV.

At 12 GeV we get kaon physics; charge-parity (CP) violation is one of the important things—the study of the rare decays, the hypernuclei. We get kaon-nucleon scattering; we get a way to study the spectrum of the hadrons, some of which are missing, and the low-energy K-N scattering has lots of holes in the data. We get kaon-nucleus scattering, and we get more flux of pions, muons, and neutrinos. If we get up to a 32-GeV class of machine, then we have a decent antiproton factory, we get much higher-energy kaons and pions, and we have a much higher flux of low-energy kaons than we would have with lower-energy protons. And if we get above Brookhaven, then we begin to get into new territory; we could have a machine with the capability of the highest-energy polarized protons available anywhere, as well as improved kaon and antiproton flux.

Table I. Physics at Various Proton Energies.

5 GeV	Neutrino physics
	Improved muon physics
	Polarized protons
	High-energy pions
	Nuclear chemistry
10 GeV	Kaon physics: charge-parity violation
	Rare decays
	Hypernuclei
	Kaon-nucleus scattering
	More flux of pions and muons
30 GeV	Antiproton physics
	Higher energy K's
	More kaon flux
50 GeV	Higher energy polarized P
	Better antiproton beams

What I saw in the July Workshop was the best workshop ever held here on any subject. We brought in some new physics topics, including the high-$p_\perp$ exclusive processes that Glynnis Farrar talked about. We had some fine talks on high-energy antiproton physics; high energy means well above LEAR but nowhere near the collider energies. We briefly discussed extending the energy range of polarized protons, and we talked about glueballs. We learned that the long lifetime of the B meson and the apparent large mass of the top quark may make some huge differences in the details of our write-up of the kaon decays, but they may in fact make it even more interesting.

You should receive the Proceedings of the Third LAMPF II Workshop about January 1. I would like to thank Tarlochan Bhatia (he managed to solicit from you every talk save one, which was held up in the French postal strike) and the Proceedings production staff. It is a beautiful job—this is the best workshop we have ever had, and the best documented one.

At the end of the workshop, we were talking about a 32-GeV machine, something like the biggest machine at 12 kG that will fit on the mesa. This machine is shown in Fig. 1. It would be injected by H^- beam; it would be tunneled under the existing machine and would have four major experimental areas: a neutrino pulsed-muon area and three slow-extractive beam areas with a thin target upstream.

Our cost estimate for the 32-GeV machine was started before the workshop, but the numbers came out later. We had a machine that cost about $130 million. We had a stretcher that might cost half that, thus the total was $200 million for the machine and stretcher. We had four experimental areas at about $50 million each, with beams and detectors. So that gave us $400 million, and adding 20% extra for contingencies raised the total to roughly

*This report is excerpted from a presentation to the Seventeenth LAMPF Users Group Inc., Meeting, November 7-8, 1983. The full text is available in Los Alamos National Laboratory report LA-10080-C (1984).

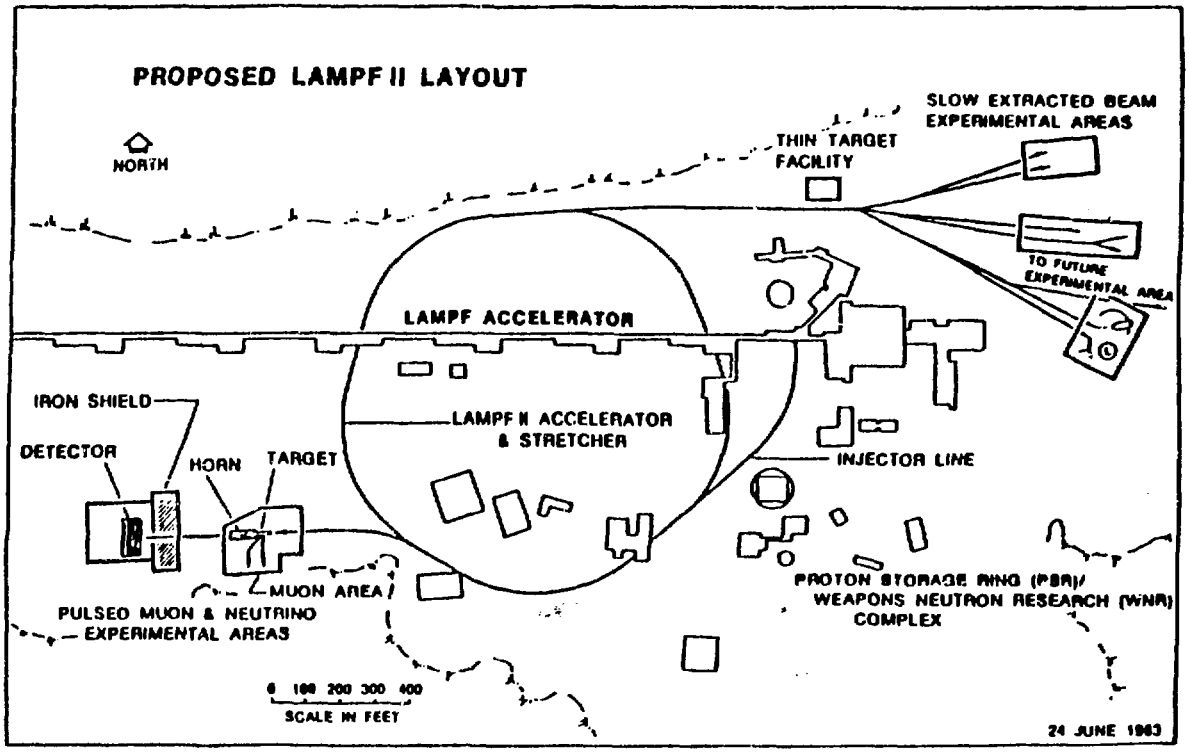

Fig. 1.
LAMPF II site layout

$500 million. We had a very expensive proposal as shown in Fig. 1, and that did not include cooled antiprotons, which may cost, as a wild guess, another $100 million.

At the end of the summer, the system consisted of the following: we had a 32-GeV accelerator and its stretcher, but we also had a booster. We did not know exactly what energy booster we wanted, and still do not, but the proposal included a booster, and because of a need for polarized beam, it had a stretcher on the booster so the unused pulses of the booster could be used for variable-energy polarized proton beam. We have not carefully priced this, but it costs about the same to build a 32-GeV machine with a booster or without. The big machine gets cheaper if we have a booster, but first we have to make up the additional cost of the booster.

The last day of the workshop I talked about a staged proposal; we would build the facility in several stages. The first stage, for example, might be just the injection line in the neutrino area. The second stage might be a booster that could feed that neutrino area, and maybe it would have one experimental area in addition, with the booster set up so that the next stage, which would be a higher energy machine, could use the same experimental area. And then we would add experimental areas and probably add the $\bar{p}$'s last. So, the features were: we had a booster, we had a higher energy machine, we had several experimental areas, and we build them one at a time.

Just before the workshop, the news hit that the Nuclear Science Advisory Committee group making a long-range plan decided that there should be a heavy-ion collider, and that such a collider represented a unique opportunity in the area of nuclear physics. And, given the constraints of that report, it is not possible to have two expensive facilities. And so LAMPF II was postponed for a very long time. I see no way, as the committee is now constituted and the ground rules are now set up, to build the full facility, even in stages, because it is recognized that the whole accelerator is going to be very expensive in the end, and what difference does it make if it is staged?

We must step back and ask, in some order, what does the country need? Let us say that it needs a next-generation e^+e^- or $\mu^+\mu^-$ collider somewhere. It needs a Desertron. I think we need some kind of a factory for fixed-target physics that includes the physics we have

been talking about. We appear to need a heavy-ion collider, and we are already committed to a 4-GeV lectron machine.

At present, we are trying to come up with the minimum factory that we could build here. It would be at least a 12-GeV, 100-μa kaon factory. We have several ideas for reducing the cost. We can reduce the energy, which means reducing the counting rate, and thus it may be possible to eliminate the stretcher. Eliminating the stretcher would dictate that the duty factor be one-third instead of 1, but that goes with the counting rate, and so it is probably acceptable. And as you saw, if we had no money in the accelerator, it would still cost $200 million for the experimental areas, so we are thinking about ways to run with about half the number of beams talked about at the workshop. (I think we had 15 or 16 beams at the end of the workshop.) And we may be able to save some money by reconfiguring the existing experimental areas.

I remind you about the flux arguments. Figure 2 shows a plot (linear scale) of the kaon yield at fixed 1.4-GeV

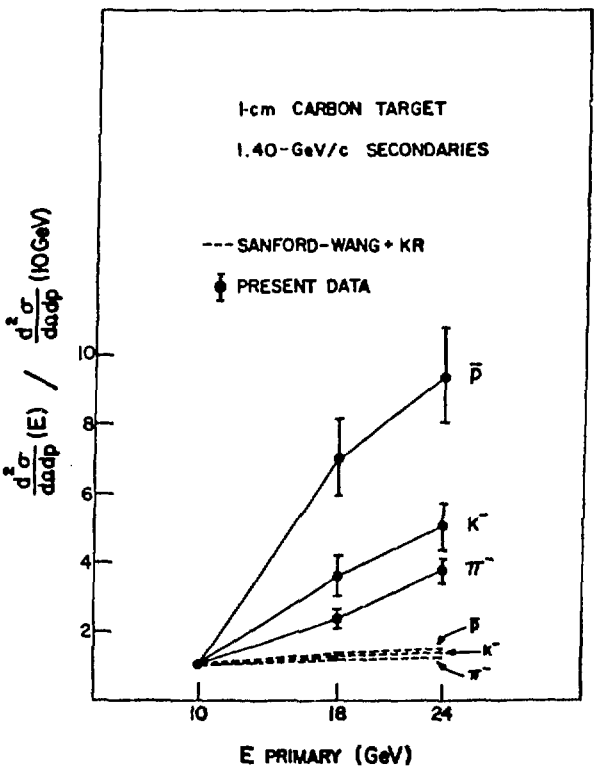

Fig. 2.
Energy dependence of production cross sections on 1-cm carbon target normalized to 10-GeV cross section.

secondary energy as a function of proton energy. You can see that there is no sharp structure in the region proposed. The kaon yield is about 5 times more at 24 GeV than at 10 GeV, so the first factor we have lost in lowering the energy is the beam power. And then maybe another factor of 2 at most. It is a penalty we have to pay if we lower the beam energy, but it is not a dramatic one, and there is no clear threshold in the region 10-24 GeV for kaons. For $\bar{p}$'s it is different. If we go down much below 32 GeV, we lose fast on the $\bar{p}$'s.

Suppose we propose a 12-GeV machine like the one shown in Fig. 3. It would have 10 times the flux of the existing Brookhaven AGS slow-extracted beam, 20 times the flux of kaons below 1 GeV, and of course at Brookhaven they have to divide the beam many ways. We have to divide the beam many ways; let us call that even. So as a kaon factory, it is 20 Brookhavens. A 12-GeV machine is smaller, there may be a cheaper site, and we have a way to do it with no interference with PSR. Figure 3 is a scheme in which we reconfigure Area A; that means at least a shutdown like the Great Shutdown for Area A. And in that picture, Areas B and C are not easily used after we go to LAMPF II.

To see this concept in its simplest form, let us put a ring as shown, where it does not cross through the forest of existing buildings. It could be built at the same elevation as the present linac, and it could be injected off the present Line B and reinjected into the switchyard with minimum trouble. We could then reconfigure Area A to have some very useful beams in it. Should we decide to have a booster for such a machine, there is a natural location for it in the present parking lot for Area B, and there could be an experimental area for the booster.

Figure 4 is a blown-up drawing of Area A reconfigured for 12 GeV. It is conceptual only. The idea is to extract from the accelerator at one point and to provide, down a single line, the capability of alternating pulses of a fast-extracted beam and a slow-extracted beam. On the slow-extracted pulses, which would have duty factor of about one-third, the beam would hit the first three targets.

The first target might be used for making a stopping K^+ and K^- beam off th- me target, with a first magnet being a bending magnet common to both. This system gives very clean beams, and it is clear that there is a need for stopping K^+ beams and stopping K^- beams, both. When there are stopping beams, the energy is rarely varied. So this scheme might work for kaons even though they are coupled and even though it is an awkward arrangement for muon beams at existing meson factories.

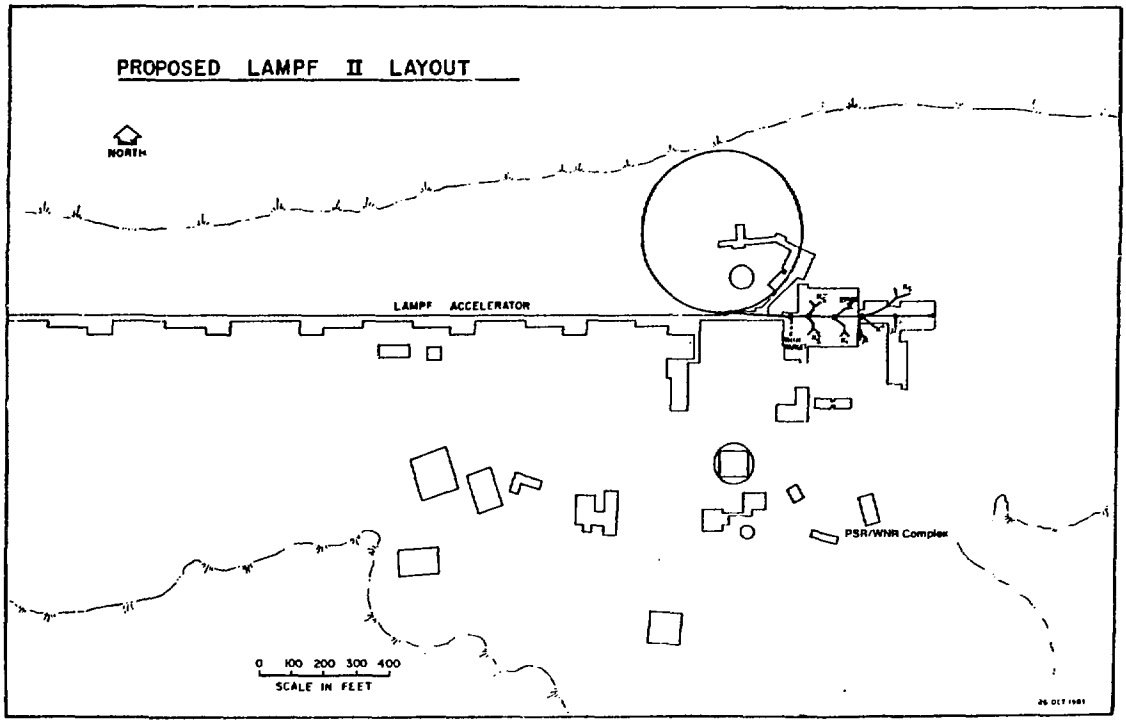

Fig. 3.
A scheme for a 12-GeV machine.

The next target cell might include two medium-energy beams, and two examples might be an EPICS II and the 1.8-GeV kaon beam. Anything could go there, but, looking at that target, they may have to be nonzero-degree beams independent of each other.

The third target cell would contain the high-energy beam. If the machine is only 12 GeV, then the beam would be about a 6-GeV $\pi,K,\bar{P}$ beam and it could share that target with a K^0 beam. Bob Macek has suggested putting a bending magnet right upstream of the target and aiming the proton beam toward the south side of the building so that 0° for K^0's points into a useful experimental area, and then bend it back to get onto the dump. There could be a muon beam produced at this thick target. We would have the best duty factor and the best muon rate. There could also be a test beam at this target. So for the slow-extracted beams, we would get a nice set containing most of the secondary-beam physics shown in the proposal.

Another idea for the fast-extracted beam is to let it go on down the same beam line, either with rotating targets with holes, or the beam kicked around the upstream targets, or slow and fast-extracted beam scheduled during different time periods. In any case, there is a fourth target, which is used as a neutrino target and a pulsed-muon target. For neutrinos, there is a horn with the existing Line A as the decay region, putting the neutrino area downstream of the present beam stop. We might even be able to use the Biomed beam as a pulsed-muon beam if we add a vacuum chamber. So we have beautiful neutrino physics, beautiful pulsed-muon physics, beautiful kaon physics up to 6 GeV, and somewhere else where we can get a not-too-expensive, low-energy, variable-energy polarized beam. If we choose to have no booster, we could put a jet target in Area B. Polarized proton experiments could be done at variable energy by just watching what happens as the circulating beam energy changes. The beam could be polarized; we will certainly design the accelerator for polarized protons.

What does this scenario cost? Table II shows the accelerator cost estimate. We scaled the cost estimate we had for the 32-GeV machine and came up with the following set of numbers, which says that for about $60 million, we could build such a machine. We made a guess,

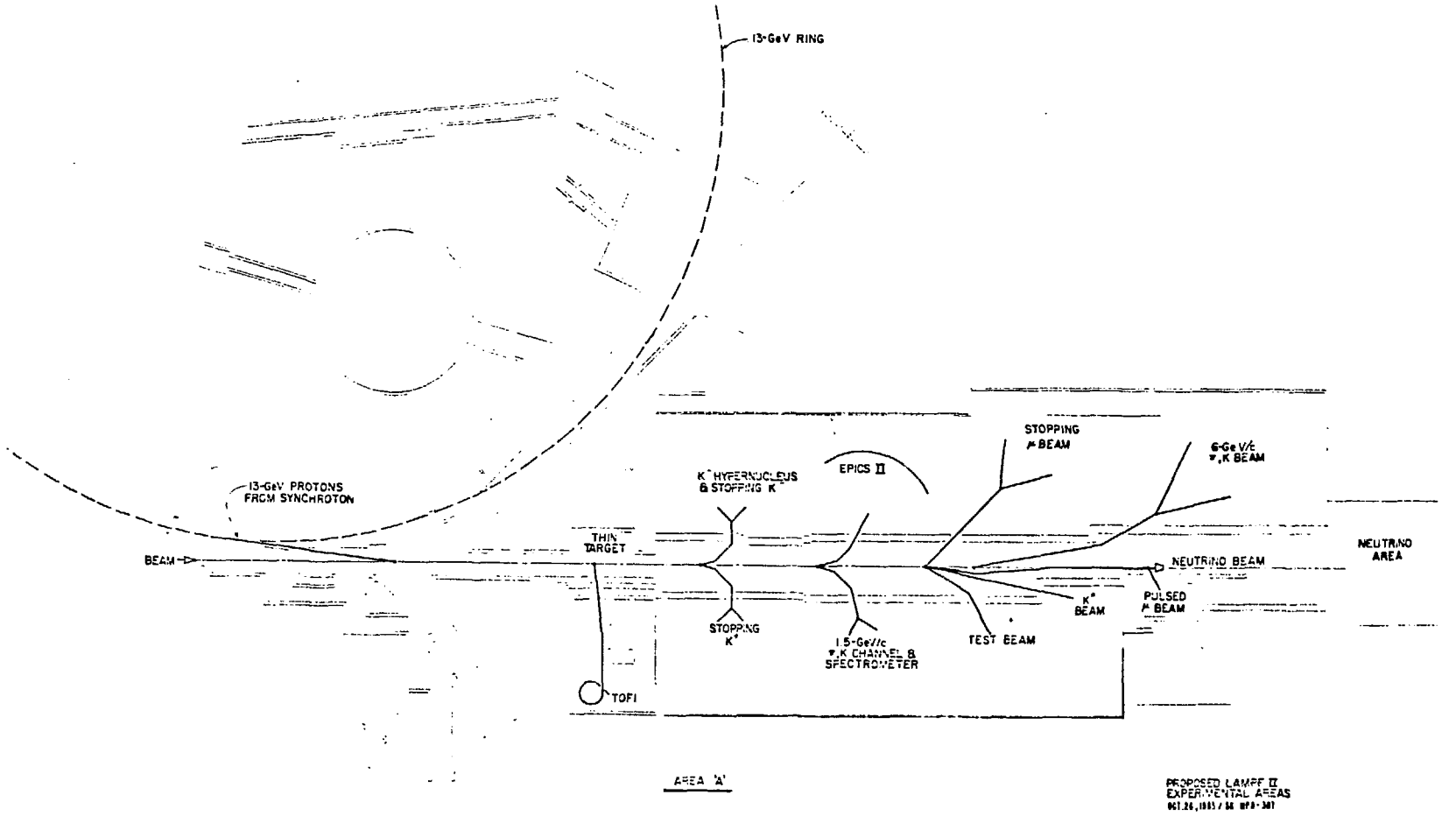

Fig. 4.
A conception of Area A reconfigured for 12 GeV.

Table II. Accelerator Cost Estimate, October 28, 1983.

		Dollars (in Millions)
Accelerator		
	Magnets and power supplies	$ 15.8
	rf system	13.6
	Diagnostic and controls	12.0
	Vacuum	6.0
	Extraction systems	2.0
	Fast dampers	1.5
	Injection	1.4
	Fast abort and dump	1.0
	Collimator system	1.0
	Bucket rotator	1.0
	LAMPF injector mods	0.3
	Installation	7.5
		$ 63.1
Buildings		
	3 electromechanical equipment	5.4
	1500-ft tunnel @ $2000/ft	3.0
	Support lab	2.0
	Office for 100 people	2.0
	Control building expansion	1.3
	Ring entrance building	0.2
		$ 13.9
Experimental-area modules		
	See Table III	68.0
	TOTAL	145.0
	Contingency +20%	29.0
	TOTAL (in 1984 dollars)	174×10^6

not yet verified, that we really can have efficient slow extraction from single ring that goes along with a lower intensity overall, a lower beam power overall. It may have a booster with a similar total cost. We have not proved that we can do it, but we are working on it.

The buildings are mostly mechanical equipment buildings for this new ring. We are making very good use of what we already have, so we need only a small number of additional buildings.

Table III shows the cost of the experimental area. Macek suggests reworking about two-thirds of the steel and concrete that we already have. We add 10 kilotons (kt) of new steel, some train—or canyon—fill (filling the trains containing the secondary beam lines out to a standardized cross section), and some new concrete. The costs for shielding, beam transport, etc., are shown. The biggest single item is the beams, seven beams guessed at $5 million apiece.

So we have a rather cost-effective experimental area where at least half of the funds go directly into things we want, namely, into the beams. By using Area A, we save shielding, beam transport, water, power, and buildings, and we can use the existing remote handling equipment; the final savings is over $30 million. The total cost, including a contingency in this year's dollars, is about $175 million, which is sufficiently close to Louis Rosen's guideline of $150 million to meet his request.

Table III. LAMPF II Experimental Area Cost Estimates, October 28, 1983.

			Dollars (in Millions)
Shielding installed			$18
		Cost	
	(Kilotons	Per ton	Total (in Millions)
Reworked steel	20	$ 200	$ 4
New steel	10	800	8
Train fill	4	1000	4
New concrete	10	200	2
			$18
Primary beam transport			6
Primary beam tunnel rework			1
Targets and target chambers (4 targets)			4
Rework beam-stop area and neutrino-area construction			5
Secondary beam lines (7)			35
Extend building			2
TOTAL			$71

VI. FACILITY AND EXPERIMENTAL DEVELOPMENT

The New Transition Region

A. A. Browman

Introduction

The first 100 MeV of energy gain at the LAMPF facility is provided by an Alvarez-type[1] accelerating structure operating at 201.25 MHz. The remaining acceleration is provided by the side-coupled linac,[2] which operates at 805 ($\equiv 4 \times 201.25$) MHz. The transition region (TR) connects these two types of accelerating structures and provides proper phase-space adjustments of the 100-MeV beams so they can be accelerated without loss in the side-coupled linac.

The original TR (Ref. 3) was unable to provide correct matching of H^+ and H^- (P^-) beams simultaneously without causing unacceptable beam losses. When only one high-current beam was being run at a time, the TR could be adjusted to handle it properly by allowing the other (low-current) beam to be not as well matched. The necessary "compromise tunes" were time consuming to achieve, and often did not result in very good beam quality for the low-current beams. In addition, the new Proton Storage Ring (PSR) was designed to use high-current H^- beams, so LAMPF will be required to operate with two high-current beams when the PSR comes on line in 1985. Thus, the decision was made to replace the TR.

Features of the TR

The most obvious requirement of the TR arises because the operating frequency of the side-coupled linac is an *even* multiple (4) of that in the Alvarez linac. Thus, for dual-beam operation the phase of one of the beams must be changed relative to the other one by 180° (805 MHz) (see Fig. 1). In the TR this is achieved by separating the beams and causing the paths followed by the two beams to differ in length by 8 cm (nominally) before they are recombined. Other functions that the TR must perform are the correct steering and matching of both beams. Detailed descriptions of these requirements may be found in Refs. 4 and 5.

Both the original and new TR are shown schematically in Fig. 2. In addition to the features described, the new TR includes larger apertures, additional diagnostics, a "straight-through" path, beam-path-length adjustment, quadrupole and steering magnets on all beam lines for independent control of each beam, and a much neater installation, as shown in Fig. 3. Considerable effort was

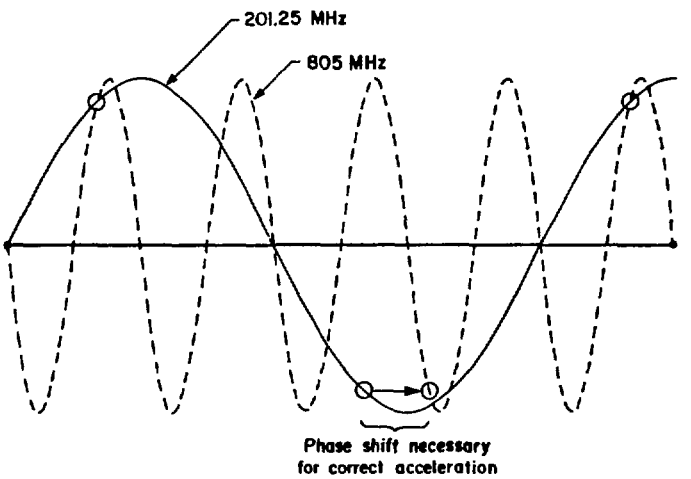

Fig. 1.

Representation of 201.25- and 805-MHz accelerating fields. The circles on the 201.25-MHz trace show the approximate location of the different sign beam bunches. Note that the 805-MHz wave would decelerate one bunch of particles if their phase were not shifted.

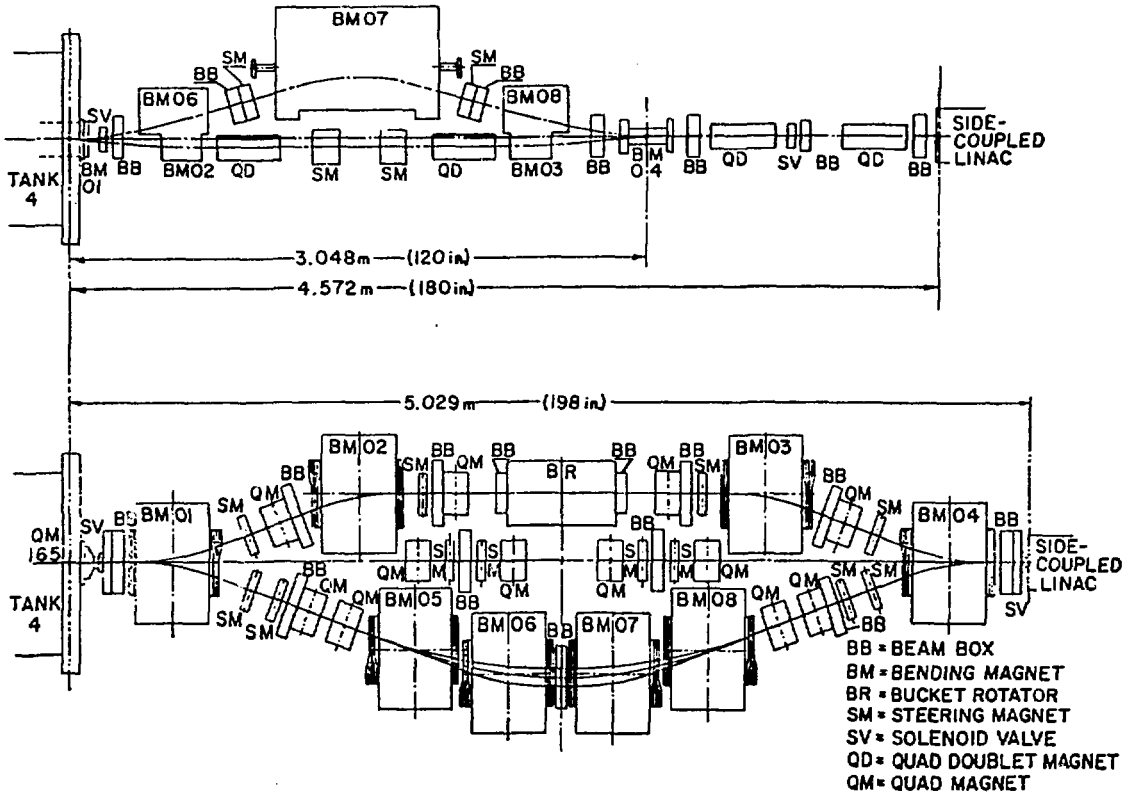

Fig. 2.

Original TR (top) and new TR (bottom). The first module in the side-coupled linac was moved to obtain more room. Each beam line in the new TR has its independent quadrupole and steering magnets. Space was allowed for longitudinal matching (bucket rotator) in the new TR.

expended to make the TR installation as uncluttered and serviceable as possible (see Ref. 6 for a detailed description of the mechanical fabrication of the TR, as well as a list of the drawings used in the TR construction).

To minimize beam loss in the side-coupled linac caused by "emittance growth" in the TR, field quality in the magnetic elements must be quite good. The magnets used in the TR were extensively mapped and trimmed (see Refs. 7 and 8 for a detailed report of the methods used and the results obtained). The final TR design enabled a single type of bending magnet, quadrupole magnet, and steering magnet to be used. This approach allowed spares for all elements to be built and mapped during construction of the TR.

Because the entire LAMPF facility would be rendered inoperable during the removal of the old TR and installation of the new one, extensive planning was necessary before the work began. Most major components were assembled and staged at the Equipment Test Laboratory (ETL) during production running and then moved to the beam channel during the shutdown period. As a result, we were able to resume operation with a new working TR by the end of the same shutdown period that was scheduled for experimental area maintenance and repairs.

Operation of the TR

Approximately 1 month was used to commission the new TR. During this time beams were run through all three beam lines, matched, steered, and checked for beam quality. A major effort was needed to get the diagnostic equipment checked out, but everything was working in time for production running.

By the end of 1983 we had run for several months with high-current H^+ beam (up to 900 μA) and low-current

Fig. 3.
Photograph of the new TR. Note success achieved in cleaning up the installation; maintenance is considerably easier.

polarized H^- beams. Beam quality is improved, tuning is easier and faster, and the beams are stable.

At this time no changes to the TR have been necessary and we believe the TR will satisfactorily handle the high-current H^- beam when it becomes available in early 1985.

REFERENCES

1. D. A. Swenson, E. A. Knapp, J. M. Potter, and E. J. Schneider, "Stabilization of the Drift-Tube Linac by Operation in the $\pi/2$ Cavity Mode," R. A. Mack, Ed., Sixth Int. Conf. on High-Energy Accelerators, Cambridge, Massachusetts, September 11-15, 1967, Cambridge Electron Accelerator report CEAL-2000 (1967), pp. 167-173.
2. E. A. Knapp, "High-Energy Structures," in *Linear Accelerators*, P. O. Lapostolle and A. L. Septier, Eds. (North-Holland, Amsterdam, 1970), pp. 601-616.
3. D. A. Swenson, "The Transition Region," Los Alamos National Laboratory Group MP-3 document MP-3-75, February 24, 1969.
4. O. R. Sander, "LAMPF Transition Region," Los Alamos National Laboratory report LA-9315-MS (June 1982).
5. O. R. Sander, A. A. Browman, and E. D. Bush, "Redesign of the LAMPF Transition Region," in Proc. of the 1981 Particle Accelerator Conference, Washington, DC, IEEE Trans. Nucl. Sci. NS-28, 2914-2915 (1981).

6. E. D. Bush, Jr., J. D. F. Gallegos, R. Harrison, V. E. Hart, W. T. Hunter, S. E. Rislove, J. R. Sims, and W. J. Van Dyke, "LAMPF Transition Region Mechanical Fabrication," to be available in a Los Alamos National Laboratory LA-UR document.

7. A. A. Browman, "TR Bending Magnet Description," Los Alamos National Laboratory Group MP-DO memo, August 18, 1983.

8. A. A. Browman, "TR II Quadrupole Magnets," Los Alamos National Laboratory Group MP-DO memo, April 7, 1983.

New Experimental Staging Area

The Experimental Staging Area was completed and in use in September 1983. The primary purpose of this 9000-sq-ft facility is to provide an area for experimental teams to assemble and test their experiments before installation in the experimental caves.

The facility is equipped with a 30-ton bridge crane and ample utilities for User requirements. In addition, an office is available, as well as power pedestals adjacent to the Staging Area to accommodate trailers.

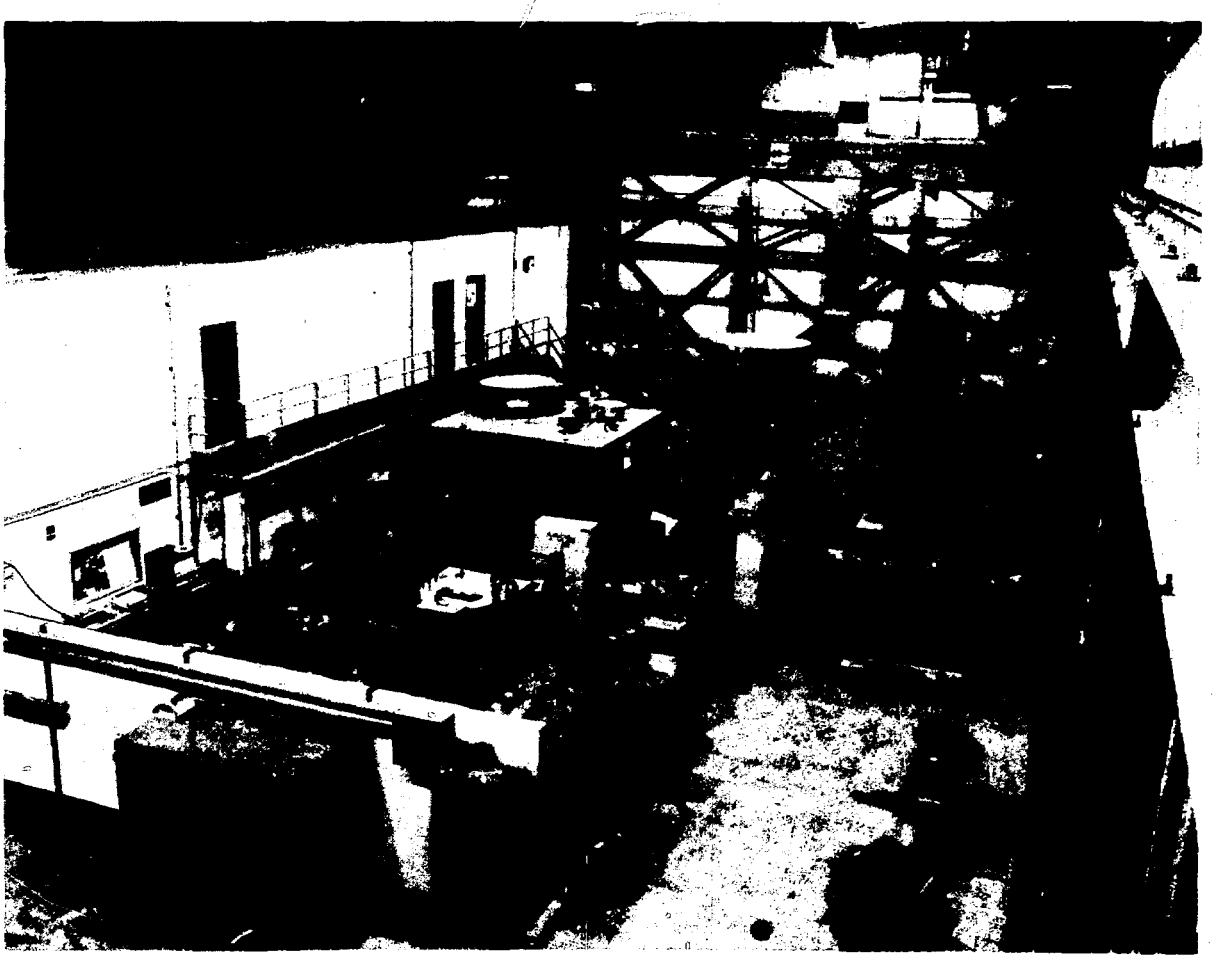

Fig. I.
New Experimental Staging Area.

EPICS and HRS Data Systems

Group MP-10 spectrometer software has been rewritten in the conversion from RSX-11D to -11M operating systems. In addition, some special features from the old spectrometer software are now available in the new standard Q program from MP-1. Improvements include core histogram storage, easier implementation of data cuts, data reduction before taping, and batch replay on VAXes with spooled tapes.

An array processor (a used AP-120B) has been acquired for EPICS and upgraded to be compatible with the two in place at the HRS, but software conversion to RSX-11M is still in progress. The HRS array processors have developed problems that have been difficult to resolve during production.

Other planned upgrades include the addition of a VAX-11/730 to replace the on-line PDP-11/45 at either HRS or EPICS, and higher density tape drives to reduce the number of tapes used by a factor of 3 or 4.

Instrumentation Technology Developments in MP-4

Vernon Sandberg

The instrumentation developments in MP-4 during 1983 have been to

- design a magnetic horn and pulser for a high flux neutrino facility;
- develop a high-speed, high-voltage, variable-width pulser for beam chopping;
- construct a CAMAC-controlled pulser monitor for the flash chamber system used in Exp. 225;
- construct a computer-controlled test and repair station for the multiwire proportional chamber (MWPC) input electronics used in Exp. 225;
- design and fabricate the signal-processing electronics for the drift chamber and the sodium iodide detectors used in Exp. 400;
- develop and build a variety of control systems for Exp. 634;
- upgrade the chamber wire-winding shop with new controllers; and
- provide miscellaneous support to LAMPF facilities and experiments.

A brief description and a few highlights of some of these instruments follows.

Portions of a design have been done for a neutrino horn system. The system consists of a capacitor bank, horn, and silicon control rectifier (SCR) switches. The capacitor bank energy is switched into the horn, which acts as a resonating inductor. The current flow recharges the capacitors through a bridge rectifier circuit, thus completing one-half of a sinusoidal cycle. The horn size is 2 m in diameter and 4 m in length; its capacitance is 0.1 F. The peak voltage is 500-800 V, and the peak current is 300 kA.

A high-voltage pulser for the injector beam-chopper system has been built. It produces a positive pulse of adjustable amplitude from 1 to 15 kV, adjustable pulse width from 40 ns to ∞, and rise and fall times of 20 ns across a 1-MΩ load shunted by 150 pF. The pulse is "flat" to within 5% of its peak voltage and recovers to within $\pm$10 V of ground potential. The pulser is a hybrid system composed of hard triode vacuum tubes, MOSFET power transistors, bipolar microwave transistors, integrated circuits, and fiber optics systems. The pulser, which is mounted in a cylinder 1 m in diameter and 1.5 m in length, will be installed in the injector area in 1984.

In support of Exp. 225 a system to monitor the high-voltage pulsers that drive the detector flash chambers has been built. The monitor watches several key parameters in the flash chamber system (for example, the charging voltage and current, the trigger pulser waveform, and the main pulser waveform) and reports their status to the experiment computer. When a major fault is detected (such as a capacitor failure), the monitor compares the pulser-system status with its past history and then takes appropriate action (such as disconnecting the high-voltage charging power supply from the shorted capacitor bank). The monitor is fabricated with TTL logic and communicates with the experiment's computer through CAMAC.

To facilitate testing and repair of the electronics used in the cosmic-ray anticoincidence system for Exp. 225, we have built a computer-controlled test station that tests the memory, logic, and shift registers of the input cards, the PAL layer logic, and the control-test cards. It is based on a Hewlett-Packard HP-85 portable computer and standard CAMAC-control modules. Its software is very flexible and can be easily adapted to changing requirements encountered in diagnosing problems in the anticoincidence system.

In support of Exp. 400, a system of amplifiers, analog delay lines, and pulse-shaping circuits has been developed and fabricated. To run the Crystal Box detector at an instantaneous muon stopping rate of 5-million muon stops per second, the sodium iodide signals must be clipped to reduce pileup and improve energy resolution.

The photomultiplier-tube base and amplifier system used on the Crystal Box sodium iodide detectors clips the signal (to a 100-ns-wide pulse) and then amplifies and further shapes the pulse leading edge with a pole-zero filter. The processed signal is then split three ways and sent to a constant fraction discriminator, an analog summing circuit, and into a 450-ns-wide bandwidth delay line, after which the analog signal is further split and sent to two parallel integrating analog-to-digital (ADC) channels. Before clipping, the sodium iodide pulses have 250-ns decay time; after processing, the pulses are approximately square and 100 ns wide. This system has 432 such amplifier cards and each card is independently accessible.

Group MP-1 Electronic Instrumentation and Computer Systems

Computer Maintenance Section

Since its inception 3 years ago, the MP-1 Computer Maintenance (COMAINT) section has grown from six to its current staff of eight technicians. Meanwhile, the maintenance value of the equipment maintained by the section has increased 60%. The increase in maintenance efficiency is largely due to three factors: (1) replacement and/or redesign of older more troublesome hardware; (2) increased experience and training within the section; and

Martha Hoehn and Elvira Martinez working at a VAX-11/780 console.

Sharon Lisowski and Mark Kaletka shelving magnetic tapes in the Data Analysis Center tape library.

(3) more efficient utilization of manpower by using split shifts, with reduced on-call and overtime hours.

The COMAINT section is responsible for the maintenance of more than 50 computer systems and 200 computer terminals at LAMPF. During operating cycles, the section is staffed from 7 a.m. to 12 p.m. midnight, Monday through Friday, with weekends and early mornings covered by assigned on-call duty. The section handles more than 100 trouble calls per month and counts most of the personnel at LAMPF among its clientele.

Data Analysis Center (DAC)

The year 1983 brought several changes to the LAMPF Data Analysis Center (DAC). In cooperation with the Medium-Energy Physics Theory Group (T-5), MP-1 purchased and installed a new VAX-11/780 system (MPBG1), bringing the total number of VAX computers in the DAC to four. Delivered as part of this new system were two 125-in./s, 6250-bits/in. TU-78 tape drives, an

Tony Gonzales making adjustments to MPSERF in the Data Analysis Center.

Andy Steck, Gerry Maestas, and Jim Santana performing routine maintenance on the Data Analysis Center computer MPSERF.

Leon Guerin and Kelly Blount at the Computer Maintenance section repair facility.

Bob Critchfield inspecting a removable disk system in the computer maintenance shop.

Bryan O'Malley and Boyd Cummings testing the operation of a line printer.

HSC-50 disk and tape controller, four RA-81 Winchester-type disk drives, and an RP-07 Winchester-type disk drive.

The VAX systems are now connected to each other via a CI-780 computer interconnect, a high-speed (70-megabit/s) bus link that replaces the slower DMR-32 hardware for network links. The CI-780 hardware also forms the basis for a future VAX-cluster architecture, a closely cooperating network of VAX computers that shares common resources, such as disk storage, batch queues, and print queues. Because full software support for the VAX-cluster features is not available with the current (version 3.4) release of the VMS operating system, MP-1 is acting as a test site for a pre-release of VMS version 4.0. The pre-release was installed on MPBG1 in December 1983 and will be extended to the other three VAX systems during the early months of 1984. The test phase will run until the official release of VMS version 4.0 in mid-1984.

The year also saw the completion of the LAMPF terminal network, with the Micom Micro-600 port selector system becoming fully operational. All terminals connected to the DAC are now routed through this sytem, which allows flexible terminal switching between computers. The system is undergoing its first expansion, with equipment on order to service the new VAX MPBG1, provide additional terminals in the Laboratory Office Building, and possibly expand access to terminals at the experimental areas.

A committee convened for 3 days during October 1983 to consider long-range (5- to 10-year) computing needs at LAMPF. This committee consisted of representatives from MP Division and LAMPF Users, and was chaired by Martha Hoehn of MP-1. The committee heard presentations on topics including parallel and front-end processing, computer networks, word processing, and new central processing unit (CPU) standards, while considering future directions for both data acquisition and analysis at LAMPF. Presentations were made by speakers from SLAC, Fermilab, and TRIUMF on the computer facilities and philosophies of those institutions. The final report of the committee should be available in early 1984.

Design for a Muon Channel Based on the Proton Storage Ring

A muon channel using the proton beam from the LAMPF Proton Storage Ring (PSR) would provide pulsed muon beams uniquely applicable to a wide class of experiments. Beam-optics studies led to a design for such a PSR-based channel capable of providing either decay muon beams, with momenta as high as 80 MeV/c, or surface muon beams at 30 MeV/c.

The design incorporates a superconducting solenoid as a pion decay section for producing decay muons, and includes an electrostatic chopper for short-pulse surface muon beams. The PSR is designed to run at 100 μA average in the long-bunch mode at 12 Hz with 270-ns proton bunches or at 10 μA average in the short-bunch mode at 720 Hz with 1-ns pulses.

In the long-bunch mode, the chopper selects a small interval of the surface beam to produce intense 5- to 10-ns pulses of surface muons at 12 Hz. In the short-bunch mode of PSR operation, the surface beam will not be chopped; then the muon pulses are approximately 30 ns wide at 720 Hz. In neither mode of PSR operation will the higher momentum decay beams be chopped. Calculated positive muon fluxes range from $\simeq 1 \times 10^6$/s for chopped long-bunch-mode surface beams to $\simeq 8 \times 10^7$/s for long-bunch-mode decay beams.

VII. ACCELERATOR OPERATIONS

This report covers operating cycles 37 through 39. The accelerator was in operation from December 30, 1982 through February 8, 1983, and again from August 1 through December 1, 1983. Beams were provided for research for 136 days, and for facility development for 11 days. A summary of information on beams provided for research is given in Table I.

Machine operation continued to be reliable and stable. The H^+ beam intensity was increased to the 800- to 900-μA range for routine production, and the beam duty factor was increased to 10.5%.

As noted in LAMPF News in this report, the H^+ average beam intensity reached and exceeded the design level of 1 mA for the first time on February 1. In a 3-h demonstration run, 1.2 mA of 800-MeV beam was delivered to Area A at 10.5% duty factor.

Installation of the new transition region between the drift-tube and side-coupled linacs during the February-to-July shutdown has made the machine-tuning task much easier. Dual-beam operation with no steering magnets energized in the 805-MHz linac has become routine.

A summary of unscheduled facility downtime during research shifts is given in Table II. Because some of the outages are concurrent, the total is greater than the beam downtime.

Accelerator development efforts concentrated on making the new transition region operational and on improving the H^+ beam deflector in the low-energy transport.

Table I. Beam Statistics for Cycles 37 Through 39.

		Cycle 37	Cycle 38	Cycle 39
Number of experiments served		33	33	23
H^+	scheduled beam (h)	860	884	792
H^-	scheduled beam (h)	276	200	----
P^-	scheduled beam (h)	588	1356	784
H^+	beam availability (%)	89	80	87
H^-	beam availability (%)	80	86	-
P^-	beam availability (%)	90	80	82
H^+	average current (μA)	625	770	825
H^-	average current (μA)	1	2	----
P^-	average current (nA)	~10	~10	~10
H^+	beam duty factor (%)	6-9	6-9	7-10.5
H^-, P^-	beam duty factor (%)	3-9	3-9	3.5-10.5

Table II. Unscheduled Machine Downtime from December 30, 1982 to December 1, 1983.

Category	Downtime (h)	Per Cent of Total
201-MHz amplifiers and transmission lines	86	14
805-MHz amplifier systems	96	16
Vacuum systems	69	12
Magnets	36	6
Magnet power supplies	48	8
Interlocks	16	3
Ion sources and Cockcroft-Walton hv supplies	170	29
Cooling water systems	18	3
Computer control and data acquisition	23	4
Production targets	26	4
Miscellaneous (utilities, ligtning)	7	1
TOTAL	595	

MILESTONES

Official Ground Breaking	February 15, 1968
Spinoff: Adoption of LAMPF Accelerating Structure for X-Ray Therapy and Radiography Machines	*ca* 1968
5-MeV Beam Achieved	June 10, 1970
Adoption of a LAMPF-Standard Data-Acquisition System	August 1970
100-MeV Beam Achieved	June 21, 1971
211-MeV Beam Achieved	August 27, 1971
800-MeV Beam Achieved	June 9, 1972
Spinoff: First Use of Electrosurgical Forceps in Open-Heart Surgery (University of New Mexico)	September 13, 1972
Discovery of ^{236}Th (Experiment Zero)	September 25, 1972
Dedication to Senator Clinton P. Anderson	September 29, 1972
Spinoff: First Hyperthermic Treatment of Animal Tumors	October 1972
First H^- Injector Beam	March 28, 1973
First Simultaneous H^+ and H^- Beams	May 4, 1973
Beam to Area B	July 15, 1973
First Experiment (#56) Received Beam	August 24, 1973
First Meson Production, Beam to Area A	August 26, 1973
Beam to Area A-East	February 6, 1974
First Medical Radioisotope Shipment	July 30, 1974
Usable 100-μA Beam to Switchyard	September 5, 1974
Pi-Mesic Atoms with "Ticklish" Nuclei	October 13, 1974
First Experimental Pion Radiotherapy	October 21, 1974
First Tritium Experiment (*80 000 Ci*)	November 1974
Start of Great Shutdown	December 24, 1974
New Precise Measurements of Muonium Hyperfine-Structure Interval and μ^+ Magnetic Moment	1975-77-80
Q Data-Acquisition Software Operational	June 1975
Spinoff: First Use of ^{82}Rb for Myocardial Imaging in Humans (Donner Laboratory, Lawrence Berkeley Laboratory)	June 1975
Spinoff: First Hyperthermic Treatment of Human Cancer (University of New Mexico)	July 11, 1975
Accelerator Turn On	August 1, 1975
Acceptable Simultaneous 100-μA H^+ and 3-μA H^- Beams to Switchyard	September 14, 1975
Production Beam to Area B	October 7, 1975
First Pions Through EPICS Channel	March 18, 1976
Production Beam in Areas A and A-East: End of Great Shutdown	April 5, 1976
Muon-Spin-Rotation Program	June 1976
Spinoff: First Hyperthermic Treatment of "Cancer Eye" in Cattle (*Jicarilla Reservation*)	June 3, 1976
100-μA Production Beam in Area A	August 1976

MILESTONES

(Continued)

Experiment in Atomic Physics (H^- + laser beam): Observation of Feshbach and Shape Resonances in H^-	October 1976
Double Charge Exchange in ^{16}O: LEP Channel	October 5, 1976
Start Up of Isotope Production Facility	October 15, 1976
HRS Operation Begins	November 1976
Maintenance by "Monitor" System of Remote Handling	Fall 1976
Proton Beam to WNR	March 12, 1977
Polarized Proton Beam Available	April 1977
Spinoff: First Practical Applications Patent Licensed to Private Industry	April 12, 1977
Pion Radiotherapy with Curative Intent	May 1977
Proton-Computed Tomography Program	June 1977
Experimental Results at Neutrino Facility	July 1977
Cloud and Surface Muon Beams: SMC Channel	July 1977
EPICS Operation Begins	August 1977
300-μA Production Beam in Area A	Fall 1977
AT Division Established	January 1, 1978
π^0 Spectrometer Begins Operation	February 1978
Operation of Polarized-Proton Target	Spring 1978
Successful Water-Cooled Graphite Production Target	November 1978
Spinoff: First Thermal Modification of Human Cornea (University of Oklahoma)	July 11, 1979
600-μA Production Beam in Area A	November 1979
New Limit on $\mu \rightarrow e\gamma$	December 1979
Experimental Measurement of the Strong-Interaction Shift in the $2p$-$1s$ Transition for Pionic Hydrogen	1980-81-82
Commercial Production of Radioisotopes	January 1980
Spin Precessor Begins Operation	February 1980
Data-Analysis Center Operational	April 1980
Variable-Energy Operation	June 1980
Single-Isobaric-Analog States in Heavy Nuclei	June 1980
Spinoff: First Use of ^{82}Rb for Brain Tumor Imaging in Humans (Donner Laboratory, Lawrence Berkeley Laboratory)	September 1980
Production of Fast Muonium in Vacuum	Fall 1980
Double-Isobaric-Analog States in Heavy Nuclei	October 1980
Focal-Plane Polarimeter Operational at HRS	October 1980
Safety Award to LAMPF Users Group, Inc., for Working One Million Man-Hours Since 1975 Without a Disabling Injury	October 27, 1980
New Measurement of Pion Beta Decay — Improved Test of Conserved Vector Current	November 1980
First Excitation of Giant Dipole Resonance by Pion Single-Charge Exchange	March 1981
First Excitation of Isovector Monopole Resonance in ^{120}Sn and ^{90}Zr by Pion Single-Charge Exchange	March 1981

MILESTONES

(Continued)

Search for Critical Opalescence in ^{40}Ca	September 1981
Average Beam Current of LAMPF Accelerator Established at 750 μA	1982
Staging Area Constructed	1982
Particle Separator Installed at Stopped Muon Channel	1982
"Dial-A-Spin" Capability on Line B Permits Different Spin Orientations for HRS, Line B, and EPB Simultaneously	1982
Time-Projection Chamber in Operation	1982
Improved Test of Time-Reversal Invariance in Strong Interactions	January 1982
Search for Parity Nonconservation in *p-p* Scattering	November 1982
d-t Fusion Catalyzed by Muons	November 1982
LAMPF Accelerator Produces Proton Beam of 1.2 mA	February 7, 1983
First Observation of ν_e-e^- Scattering	October 1983

APPENDIX A

EXPERIMENTS RUN IN 1983

Exp. No.	Experiment Title	Channel	Beam Hours
106	Proton-Induced Spallation Reactions Related to the Isotope Production Program at LAMPF	AB-Nucchem	7.0
190	A Precision Measurement of the $\pi^-\pi^0$ Mass Difference	LEP	133.0
225	A Study of Neutrino-Electron Elastic Scattering	Neutrino Area	692.0 709.0
267	Preparation of Radioisotopes for Medicine and the Physical Services Using the LAMPF Isotope Production Facility	ISORAD	709.0 692.0
294	High-Energy Nuclear Reactions	AB-Nucchem	16.0
308	An Attempt to Make Direct Atomic Mass Measurements in the Thin Target Area	Thin Target Area	70.0 692.0
392	A Measurement of the Triple-Scattering Parameters D, R, A, R′, and A′ for Proton-Proton and Proton-Neutron Scattering at 800 MeV	HRS	104.0
400	Search for the Rare Decay $\mu^+ \rightarrow e^+e^+e^-$	SMC	402.0 329.0
449	Survey of the Single and Double Photodetachment Cross Section of the H^- Ion from 14 to 21.8 eV	SMC	112.0
455	High-Precision Study of the μ^+ Decay Spectrum	P^3	95.0
465	Radiochemical Study of Pion Single Charge Exchange	LEP	8.0
470	Reactive Content of the Optical Potential	HRS	70.0
474	A Measurement of Spin-Dependent Effects in P + D Elastic and Inelastic Scattering	HRS	60.0
523	Study of the $^{14}C(\pi^+,\pi^0)^{14}N$ Reaction	LEP	64.0
545	Fusion Materials Neutron Irradiation — A Parasite Experiment	RADAMAGE-1	260.0
553	Study of Target Thickness Effects in the Cross-Section Measurement of the Pion Single-Charge-Exchange Reaction $^{13}C(\pi^+,\pi^0)^{13}N$ (g.s.) from 50 to 350 MeV	LEP	15.0
571	Muon Spin Rotation Studies of Dilute Magnetic Alloys	SMC	17.0
587	Fundamental Experiments with Relativistic Hydrogen Atoms: Exploratory Work	EPB	400.0

Exp. No.	Experiment Title	Channel	Beam Hours
601	Determination of Isoscalar and Isovector Transition Rates for Low-Lying Collective States in ^{90}Zr and ^{208}Pb by π^+ and π^- Inelastic Scattering	LEP	414.0
626	Measurement of the Depolarization Parameters $D_{NN'}$, $D_{LS'}$, and $D_{SS'}$ in Proton-Nucleus Scattering at Very High Excitation Energies	HRS	154.0
635	Spin Measurements in pd Elastic Scattering	EPB	166.0
639	Muon-Spin-Rotation Study of Muon Bonding and Motion in Selected Magnetic Oxides	SMC	44.0
640	Transverse and Longitudinal Field μSR Measurements in Selected Ternary Metallic Compounds	SMC	102.0
654	Measurement of the Spin-Rotation Parameter Q for 800-MeV p + ^{16}O, ^{40}Ca, and ^{208}Pb Elastic Scattering	HRS	153.0
665	The Measurement of the Initial-State Spin-Correlation Parameters C_{LL} and C_{SL} in n-p Elastic Scattering at 500, 650, and 800 MeV	AB-Nucchem	727.0 175.0
675	Nuclear Distributions from the Study of the 2p States of Pionic Atoms	Biomed	126.0
681	Measurements of Large-Angle Pion-Nucleus Scattering with EPICS	EPICS	266.0
685	Spin Correlations in the Reaction $\vec{p}(\vec{d},d)\vec{p}$ at 500 MeV	HRS	447.0
698	Ground-State Quadrupole Moments of Deformed Nuclei	Biomed	157.0
705	Study of Pion Absorption in ^3He On and Above the (3,3) Resonance	P3	283.0
708	A Measurement of the Depolarization, the Polarization, and the Polarization Rotation Parameters and the Analyzing Power for the Reaction $p\vec{p} \rightarrow \vec{p}\pi^+n$	EPB	608.0 43.0 43.0
709	Measurements of A_{NN}, A_{SS}, and A_{SL} in the Coulomb-Interference Region at 650 and 800 MeV	HRS	522.0
724	Measurement of the Lamb Shift in Muonium	SMC	380.0
727	Measurement of the Efficiency of Muon Catalysis in Deuterium-Tritium Mixtures at High Densities	Biomed	341.0
728	Study of Pion Charge-Exchange Mechanisms by Means of Activation Techniques	P3	88.0 51.0
730	Pion Production in Pion-Nucleon and Pion-Nucleus Interactions	P3	16.0
735	Pion-Induced Emission of Light Nuclear Fragments	LEP	173.0
741	Investigation of the Longitudinal-Spin Response of ^{208}Pb and Implications of Spin-Transfer Form Factors for Non-Nucleon Degrees of Freedom in Nuclei	HRS	189.0

Exp. No.	Experiment Title	Channel	Beam Hours
745	Hexadecapole Moments in Uranium: ^{233}U and ^{234}U	Biomed	284.0
749	$^{16}O(\pi+,\pi-)^{16}Ne$ (g.s.) Angular-Distribution Measurements at T_π = 120 MeV and T_π = 200 MeV	EPICS	357.0
750	Inclusive $\pi+$ and $\pi-$ Double Charge Exchange on ^4He	P3	641.0
765	800-MeV Proton Irradiation of Materials for the SIN Beam Stop	ISORAD	570.0 692.0
780	A Study of the Double-Charge-Exchange Reactions $^{14}C(\pi-,\pi+)^{14}Be$ and $^{18}O(\pi-,\pi+)^{18}C$	EPICS	220.0
783	Pion-Induced Pion Production on Deuterons	P3	242.0
789	Two-Nucleon-Out Products Following the Absorption of of 10-MeV $\pi+$ in ^{26}Mg and ^{74}Ge	LEP	7.9
792	*Measurement of Parity Violation in the* $\vec{p}$-p *and* $\vec{p}$-Nucleon Total Cross Sections at 800 MeV	EPB	176.0 351.0
796	Core Excitation Effects in Pion Double Charge Exchange	EPICS	328.0
798	Fission Induced by Energetic $\pi^{\pm}$ Particles	LEP	61.0
808	0° Excitation Functions for $\pi-p \rightarrow \pi^0 n$	LEP	71.0

APPENDIX B

NEW PROPOSALS

Proposal No.	Title	Spokesmen	Institutions
808	0° Excitation Function for $\pi^- p \rightarrow \pi^0 n$	M. Cooper D. Fitzgerald	Los Alamos Los Alamos
809	Study of π^-, p and π^+, p Reactions with EPICS	G. S. Blanpied J.-P. Egger	Univ. of South Carolina Univ. of Neuchatel, Switzerland
810	Test Channel		
811	Study of Unnatural-Parity States in Nuclei Using Low-Energy Pions	B. G. Ritchie	Univ. of Maryland
812	Back-Angle Charge Asymmetries for Elastic π-Deuteron Scattering	R. J. Peterson	Univ. of Colorado
813	Pion Charge Asymmetries for ^{13}C at Low Beam Energies on the LEP Spectrometer	J. J. Kraushaar R. J. Peterson	Univ. of Colorado Univ. of Colorado
814	$\pi^{\pm}$-Nuclear Elastic Scattering from Nickel and Tin Isotopes at Energies Between 30 and 80 MeV	M. Blecher M. Hynes	VPI and State Univ. Los Alamos
815	Measurement of A_{NO}, A_{SL}, and A_{LL} in $\vec{p}\vec{p} \rightarrow pn\pi^+$ at 500, 580, 650, 720, and 800 MeV	D. V. Bugg	Queen Mary College, London
816	Radiation Effects on the Field Strength of Samarium-Cobalt Permanent Magnets	R. D. Brown	Los Alamos
817	I. Elastic Scattering of Polarized Protons from ^3H at Intermediate Energy	A. Azizi M. Bleszynski G. Igo	UCLA UCLA UCLA
818	Proton-Deuteron Elastic Scattering at 800-MeV Two- and Three-Spin Observables	G. Igo	UCLA
819	II. Elastic Scattering of Polarized Protons from ^3H at Intermediate Energy	A. Azizi M. Bleszynski G. Igo	UCLA UCLA UCLA
820	Pion-Induced Pion Production on ^3He	E. Piasetzky P. A. M. Gram G. A. Rebka, Jr. J. Lichtenstadt	Los Alamos Los Alamos Univ. of Wyoming Tel Aviv Univ.
821	Pion Charge Exchange to Delta-Hole States of Complex Nuclei	R. J. Peterson	Univ. of Colorado
822	Inelastic π^+ and π^- Scattering on ^{48}Ca at 50 and 75 MeV	J. J. Kraushaar J. L. Ullmann	Univ. of Colorado Univ. of Colorado
823	Development of an (n,p) Reaction Capability at Area B or Beam Line D	N. S. P. King P. Lisowski J. D. Bowman J. Shepard	Los Alamos Los Alamos Los Alamos Univ. of Colorado

Proposal No.	Title	Spokesmen	Institutions
824	A Study of Low-Energy Pion Scattering as a Probe of Nuclear Magnetic Dipole Excitation	H. E. Jackson	Argonne
825	Investigation of the $N\Delta$ Interaction Via $\pi^+d \rightarrow pn^+n$	G. S. Mutchler	Rice Univ.
826	Isospin Dependence of Nonanalog Pion Double Charge Exchange	C. L. Morris C. Fred Moore R. Gilman	Los Alamos Univ. of Texas Univ. of Pennsylvania
827	Study of Isobaric-Analog States in Pion Single-Charge-Exchange Reactions in the 300- to 500-MeV Region	J. Alster H. W. Baer E. Piasetzky U. Sennhauser	Tel Aviv Univ. Los Alamos Los Alamos Los Alamos Natl. Lab.
828	Total and Differential Cross Sections for $\pi^+d \rightarrow pp$ Below 20 MeV	K. Gotow R. C. Minehart	VPI and State Univ. Univ. of Virginia
829	A Measurement of the Width and Position of the Δ^{++} Resonance in ^{6}Li and ^{12}C	K. Ziock	Univ. of Virginia
830	The Reaction $(\pi,\pi p)$ on ^{3}He and ^{4}He at Energies Above the (3,3) Resonance	R. Minehart	Univ. of Virginia
831	The $[\pi^+,p(pp)]$ Reaction on Light Nuclei	C. F. Perdrisat R. Minehart	College of William & Mary Univ. of Virginia
832	Gamma-Ray Angular Correlation from $^{12}C(\vec{p},p')^{12}C^*(15.11$ MeV)	B. J. Lieb C. F. Perdrisat H. O. Funsten	George Mason Univ. College of William & Mary College of William & Mary
833	Continuation of the Investigation of Large-Angle Pion-Nucleus Scattering	G. R. Burleson	New Mexico State Univ.
834	The Pion-Nucleus Interaction Studied with the $4f \rightarrow 3d$ Transition of Rare-Earth Pionic Atoms	Y. Tanaka R. M. Steffen E. B. Shera	Purdue Univ. Purdue Univ. Los Alamos
835	Target Mass Dependence of the Isovector Contribution to the Giant Quadrupole Resonance	S. J. Seestrom-Morris	Univ. of Minnesota
836	Energy Dependence of Pion Scattering to the Giant Resonance Region of ^{208}Pb	S. J. Seestrom-Morris	Univ. of Minnesota
837	Measurement of Spin-Flip Cross Sections up to 40-MeV Excitation in ^{58}Ni and ^{90}Zr	C. Glashausser S. Nanda	Rutgers Univ. Rutgers Univ.
838	Pion-Induced Pion Production on Nuclei at 400 MeV	M. J. Leitch E. Piasetzky	Los Alamos Los Alamos
839	Pion Inelastic Scattering from the 1^+ Doublet in ^{12}C	C. F. Moore C. L. Morris	Univ. of Texas Los Alamos
840	Inelastic Pion Scattering from ^{16}O at $T_\pi = 120$ and 200 MeV	L. C. Bland H. T. Fortune	Univ. of Texas, Austin Univ. of Pennsylvania
841	Forward-Angle Pion Inelastic Scattering on Light Nuclei	L. C. Bland C. F. Moore H. T. Fortune	Univ. of Texas, Austin Univ. of Texas, Austin Univ. of Pennsylvania
842	μSR Shift and Relaxation Measurements in Itinerant Magnets	L. C. Gupta R. H. Heffner D. E. MacLaughlin	Tata Inst., India Los Alamos Univ. of Calif., Riverside

Proposal No.	Title	Spokesmen	Institutions
843	A Search for $\Delta_{3,3}$ Components of Ground-State Nuclear Wave Functions	C. L. Morris C. F. Moore	Los Alamos Univ. of Texas
844	Measurement of A_{NN}, A_{ss}, and A_{Ls} for the Reaction $\vec{p}\vec{p} \rightarrow p + n + \pi^+$ at 800 MeV	G. Pauletta M. Gazzaly N. Tanaka	UCLA Univ. of Minnesota Los Alamos
845	Pion Inelastic Scattering from ^{9}Be	J. J. Kelly	Los Alamos
846	$NN \rightarrow NN\pi$: Cross Sections and Analyzing Powers for the 800-MeV $\vec{p}p \rightarrow \pi^+(np)$ and $\vec{p}n \rightarrow \pi^-(pp)$ Inclusive Reactions	T. S. Bhatia G. Glass	Texas A&M Univ. Texas A&M Univ.
847	A Precision Test of Nuclear Charge Symmetry	T. S. Bhatia J. C. Hiebert	Texas A&M Univ. Texas A&M Univ.
848	In-Flight Absorption of Low-Energy Negative Pions	Y. Ohkubo	Los Alamos
849	A. Measurement of the Differential Cross Section for $\pi^-p \rightarrow \pi^0 n$ at 0 and 180° in the Momentum Region 471-687 MeV/c B. Test of Isospin Invariance in πN Scattering at 180° in the Momentum Region 471-687 MeV/c	D. H. Fitzgerald W. J. Briscoe M. E. Sadler	Los Alamos George Washington Univ. Abilene Christian Univ.
850	Study of the Mass and Energy Dependence of Low-Energy Pion Single Charge Exchange at 0°	F. Irom M. J. Leitch	Los Alamos Los Alamos
851	Search for Recoil-Free Δ Production and High-Spin States in the ^{208}Pb$(p,t)^{206}$Pb Reaction at $E_p \simeq 400$ MeV	N. M. Hintz	Univ. of Minnesota
852	Measurements of $(\pi^{\pm},\eta)$ Reactions on Nuclear Targets to Study the Production and Interaction of η Mesons with Nuclei	J. C. Peng	Los Alamos
853	Measurement of Wolfenstein Parameters at 650 MeV and $d\sigma/d\Omega$ at 500, 650, and 800 MeV for $\vec{p}d \rightarrow \vec{p}d$ Elastic Scattering	G. S. Weston G. J. Igo	UCLA UCLA
854	Muon Spin Research in Oxide Spin Glasses	C. Boekema D. W. Cooke	Texas Tech Univ. Los Alamos
855	Measurement of ^{204}Pb-^{206}Pb Ground-State Neutron Density Difference	N. Hintz	Univ. of Minnesota
856	Comparison of Double Charge Exchange and Inclusive Scattering in ^{3}He	P. A. M. Gram J. L. Matthews G. A. Rebka, Jr.	Los Alamos MIT Univ. of Wyoming
857	Inelastic Pion Scattering from ^{16}O at $T_\pi = 50$ MeV	L. C. Bland C. F. Moore	Univ. of Texas, Austin Univ. of Texas, Austin
858	Additional Measurements of ^{18}O$(\pi^+,\pi^-)^{18}$Ne(g.s.)	H. T. Fortune R. Gilman	Univ. of Pennsylvania Univ. of Pennsylvania
859	Study of the A Dependence of Inclusive Pion Double Charge Exchange in Nuclei	P. A. M. Gram J. L. Matthews G. A. Rebka, Jr.	Los Alamos MIT Univ. of Wyoming
860	Inelastic $\pi^{\pm}$ Scattering to Excited 0^+ States at Energies Between 30 and 80 MeV	B. M. Preedom C. S. Whisnant	Univ. of South Carolina Univ. of South Carolina

Proposal No.	Title	Spokesmen	Institutions
861	Measurements of the Spin-Correlation Parameter $A_{NN}(\theta)$ for n-p Elastic Scattering at 800 MeV	L. C. Northcliffe	Texas A&M Univ.
862	Study of the $M1$ Transition in ^{88}Sr by the Inelastic Scattering of π^+ and π^-	S. K. Nanda D. K. Dehnhard	Univ. of Minnesota Univ. of Minnesota
863	Study of Giant Resonances in the Palladium Isotopes Via Pion Scattering	A. Saha K. K. Seth	Northwestern Univ. Northwestern Univ.
864	Study of Deeply Bound Hole States in the Tin Isotopes Via the $(\vec{p}, d)$ Reaction	A. Saha K. K. Seth	Northwestern Univ. Northwestern Univ.
865	Spin-Rotation Measurement of ^{4}He at 320, 500, and 800 MeV	B. Aas M. Bleszynski G. Igo	UCLA UCLA UCLA
866	Neutrino Source Calibration	R. Hausammann J. Donahue	Univ. of Calif., Irvine Los Alamos
867	Measurement of Isovector Quadrupole Transition Densities in the Palladium Isotopes	A. Saha K. K. Seth	Northwestern Univ. Northwestern Univ.
868	An Experimental Test of the Δ-Hole Model of Nonanalog Double Charge Exchange	K. K. Seth	Northwestern Univ.
869	Higher Precision Measurement of the Lamb Shift in Muonium	V. W. Hughes A. Badertscher M. W. Gladisch	Yale Univ. Yale Univ. Heidelberg Univ.
870	Search for New Magic Numbers: Direct Mass Measurements of the Neutron-Rich Isotopes with $Z = 4$ to 9	J. M. Wouters	Los Alamos
871	Coincident Nuclear γ-Ray and Pionic X-Ray Study of π Absorption at Rest on ^{12}C	B. J. Lieb H. O. Funsten	George Mason Univ. College of William & Mary
872	Direct Atomic Mass Measurements of Neutron-Rich Isotopes in the Region Z = 13-17 Using the Time-of-Flight Isochronous Spectrometer	D. S. Brenner	Clark Univ.
873	Pionic X-Ray Study of the Carbon Isotopes	E. B. Shera A. R. Kunselman	Los Alamos Univ. of Wyoming
874	Elastic Scattering of π^+ from Deuterium in the Region of the $^3F_3$ Dibaryon Resonance	C. L. Blilie D. Dehnhard	Univ. of Minnesota Univ. of Minnesota

APPENDIX C

ACTIVE AND COMPLETE EXPERIMENTS BY CHANNEL

BR NEUTRONS AND PROTONS

Exp. No.	Title	Spokesman	Phase No. * = Complete	Beam Hours
56	STUDY OF NEUTRON SPECTRUM FROM PROTON BOMBARDMENT OF DEUTERIUM IN THE 300-600-MeV REGION	NORTHCLIFFE SIMMONS	1 * 2 *	0.0 0.0
65	NEUTRON-PROTON POLARIZATION MEASUREMENTS USING A POLARIZED TARGET — PHASE I: THE n-p POLARIZATION OBSERVABLE P(θ)	SIMMONS	1 *	996.8
66	NEUTRON-PROTON POLARIZATION MEASUREMENTS WITH A POLARIZED TARGET — PHASE II: THE n-p SPIN-CORRELATION OBSERVABLE $C_{NN}(\theta)$	SIMMONS	1 * 2 *	343.4 472.0
125	ELASTIC NEUTRON-PROTON BACK-ANGLE DIFFERENTIAL CROSS-SECTION MEASUREMENTS 300-800 MeV	DIETERLE	1 *	0.0
129	PION PRODUCTION IN NEUTRON-PROTON COLLISIONS	WOLFE	1 *	319.0
189	SEARCH FOR CONDENSED NUCLEAR STATES AND STUDY OF HIGH-q^2 LOW-ν NUCLEAR INTERACTIONS	VAN DYCK	1 *	0.0
193	MEASUREMENT OF SMALL-ANGLE NEUTRON ELASTIC SCATTERING FROM PROTONS	DIETERLE McFARLANE	1 * 2 *	1091.1 0.0
205	(n,p) CHARGE-EXCHANGE AND NEUTRON-INDUCED QUASI-FREE SCATTERING ON LIGHT NUCLEI	KENEFICK RILEY	1 *	38.5
255	MEASUREMENT OF σ(θ) FOR n-p ELASTIC SCATTERING AT 460 MeV	NORTHCLIFFE	1 *	5.0
262	TEST OF ISOSPIN INVARIANCE IN THE REACTION $np \rightarrow d\pi^0$	BONNER	1 *	304.8
263	MEASUREMENT OF THE ENERGY AND ANGULAR VARIATION OF THE np CHARGE-EXCHANGE CROSS SECTION	BONNER	1 *	237.1
264	MEASUREMENT OF THE ENERGY VARIATION OF THE nd ELASTIC DIFFERENTIAL CROSS SECTION NEAR 180°	BONNER	1 *	473.1
279	TEST OF CHARGE SYMMETRY IN nd AND pd SCATTERING	DIETERLE McFARLANE	F S*[a]	101.0
360	THE MEASUREMENT OF THE POLARIZATION TRANSFER COEFFICIENTS D_t AND A_t AT 800 MeV FOR THE REACTIONS $d(\vec{p},\vec{n}2p)$, $^6Li(p,n)^6Be$, AND $^9Be(p,n)^9B$	RILEY SIMMONS	1 *	493.5
366	NONRESONANT PION PRODUCTION IN THE REACTION $np \rightarrow \pi^- pp$	MAYES MUTCHLER	1 *	427.7

[a]FEASIBILITY STUDY.

Exp. No.	Title	Spokesman	Phase No. * = Complete	Beam Hours
402	A MEASUREMENT OF THE POLARIZATION TRANSFER COEFFICIENTS $D_t(0°)$ AND $A_t'(0°)$ IN THE REACTION $\vec{p}\,p \rightarrow \vec{n}X$ AT 800 MeV	GLASS SIMMONS	1 * 2 *	166.1 83.8
403	A MEASUREMENT OF THE TRIPLE-SCATTERING PARAMETER D_t FOR THE CHARGE-EXCHANGE REGION IN np SCATTERING	BONNER	1 * 2 *	0.0 223.8
457	MEASUREMENT OF THE QUASI-FREE pn AND pp AND FREE pp ANALYZING POWERS, 500-800 MeV	BHATIA SIMMONS	1 *	785.0
492	POLARIMETER CALIBRATIONS AND SEARCH FOR ENERGY-DEPENDENT STRUCTURE IN pp ELASTIC SCATTERING VIA CROSS SECTION, ANALYZING POWER, AND WOLFENSTEIN PARAMETER MEASUREMENTS	McNAUGHTON WILLARD	1 *	860.2
504	MEASUREMENT OF THE TOTAL CROSS-SECTION DIFFERENCE FOR PROTON-PROTON AND PROTON-NEUTRON SCATTERING IN PURE TRANSVERSE INITIAL SPIN STATES IN THE 400-800-MeV REGION	PHILLIPS	1 *	1568.0
505	MEASUREMENT OF THE TRANSVERSE SPIN-SPIN ASYMMETRY IN THE REACTION $pp \rightarrow d\pi^+$ IN THE 500-800-MeV REGION	PHILLIPS	1 * 2	860.2 0.0
517	POLARIZED BEAM AND TARGET EXPERIMENTS IN THE p-p SYSTEM: PHASE 1. A_Y AND A_{YY} FOR THE $d\pi^+$ CHANNEL AND A_{YY} FOR THE ELASTIC CHANNEL FROM 500 TO 800 MeV	SIMMONS JARMER NORTHCLIFFE	1	1294.9
518	POLARIZED BEAM AND TARGET EXPERIMENTS IN THE p-p SYSTEM: PHASE 2. MEASUREMENTS OF A_{ZZ} AND A_{XZ} FOR THE $d\pi^+$ CHANNEL AND FOR THE ELASTIC CHANNEL FROM 500 TO 800 MeV	SIMMONS JARMER NORTHCLIFFE	1	1409.0
589	FREE-FORWARD np ELASTIC-SCATTERING ANALYZING-POWER MEASUREMENTS AT 800 MeV	GLASS NORTHCLIFFE	1	0.0
590	MEASUREMENT OF $D(\theta)$ IN p-n AND n-p SCATTERING AT 800 AND 650 MeV AND OTHER ENERGIES WITH ASSOCIATED p-p MEASUREMENTS	SIMMONS NORTHCLIFFE	1 2	330.0 0.0
664	THE MEASUREMENT OF THE POLARIZATION TRANSFER COEFFICIENTS A_t' AND D_t AT 500, 650, AND 800 MeV FOR THE REACTION $d(\vec{p},\vec{n})2p$	GLASS STANEK	1	426.0
665	THE MEASUREMENT OF THE INITIAL-STATE SPIN-CORRELATION PARAMETERS C_{LL} AND C_{SL} IN n-p ELASTIC SCATTERING AT 500, 650, AND 800 MeV	BURLESON WAGNER	1	1258.0
683	MEASUREMENT OF $\Delta\sigma_L$ IN FREE NEUTRON-PROTON SCATTERING AT 500, 650, AND 800 MeV	DITZLER SIMMONS	F S	0.0
739	P-A FOR 800-MeV np SCATTERING: TEST OF TIME-REVERSAL INVARIANCE IN STRONG INTERACTIONS	BHATIA KENEFICK	1 2	0.0 0.0
770	THE MEASUREMENT OF np ELASTIC-SCATTERING SPIN-CORRELATION PARAMETERS WITH L- AND S-TYPE POLARIZED BEAM AND TARGET BETWEEN 500 AND 800 MeV	SPINKA BURLESON	1	0.0

Exp. No.	Title	Spokesman	Phase No. * = Complete	Beam Hours
847	A PRECISION TEST OF NUCLEAR CHARGE SYMMETRY	BHATIA HIEBERT	1	0.0
861	MEASUREMENTS OF THE SPIN-CORRELATION PARAMETER $A_{NN}(\theta)$ FOR np ELASTIC SCATTERING AT 800 MeV	NORTHCLIFFE	1	0.0

AREA B NUCLEAR CHEMISTRY (AB-Nucchem)

Exp. No.	Title	Spokesman	Phase No. * = Complete	Beam Hours
103	SPALLATION YIELD DISTRIBUTIONS FROM PION INTERACTIONS WITH COMPLEX NUCLEI	HUDIS	2 *	0.4
104	PROPOSAL FOR LAMPF EXPERIMENT: STUDIES OF THE PROTON- AND PION-INDUCED FISSION OF MEDIUM-MASS NUCLIDES	PATE	1 * 2 *	0.0 5.0
105	NUCLEAR SPECTROSCOPY STUDIES OF PROTON-INDUCED SPALLATION PRODUCTS	BUNKER	1 * 2 *	10.0 58.6
106	PROTON-INDUCED SPALLATION REACTIONS RELATED TO THE ISOTOPE-PRODUCTION PROGRAM AT LAMPF	O'BRIEN	1 * 2	0.7 46.1
118	FRAGMENT EMISSION FROM PION INTERACTIONS WITH COMPLEX NUCLEI	PORILE	1 * 2	0.0 0.0
119	CROSS SECTIONS OF SIMPLE NUCLEAR REACTIONS INDUCED BY π MESONS	KAUFMAN	2 *	15.2
123	NUCLEAR STRUCTURE EFFECTS IN PION-INDUCED NUCLEAR REACTIONS	KAROL	1 * 2 *	0.0 1.0
150	SEARCH FOR POLYNEUTRON SYSTEMS	TURKEVICH	1 * 2 *	0.0 14.2
169	PROTON IRRADIATIONS FOR PROJECT JUMper	ORTH SATTIZAHN	1 *	0.0
243	RECOIL STUDIES OF DEEP SPALLATION AND FRAGMENTATION PRODUCTS FROM THE INTERACTION OF 800-MeV PROTONS WITH HEAVY ELEMENTS	PORILE	1 *	55.8
282	MEASUREMENT OF CROSS SECTIONS FOR PROTON-INDUCED FORMATION OF SPALLATION PRODUCTS IN COPPER BY ACTIVATION ANALYSIS	DONNERT	1 * 2 * 3 *	0.6 1.5 0.1
294	HIGH-ENERGY NUCLEAR REACTIONS	KAROL	1	134.2
301	IMPAIRMENT OF SUPERCONDUCTING CHARACTERISTICS BY PROTON IRRADIATION	WILSON	1 *	185.0
349	NUCLEAR REACTIONS OF ^{127}I WITH PIONS	PORILE	3 *	3.6
407	THE EFFECT OF DISLOCATION VIBRATION ON VOID GROWTH IN METALS DURING IRRADIATION	SOMMER PHILLIPS	1 * 2	516.2 0.0

Exp. No.	Title	Spokesman	Phase No. * = Complete	Beam Hours
410	RADIATION EFFECTS IN AMORPHOUS METALS DUE TO 800-MeV PROTONS	COST	1 *	563.0
424	PRELIMINARY EXPERIMENTS FOR DOUBLE CHARGE EXCHANGE AND (μ^-,e^+) SEARCHES	TURKEVICH WARREN	1 *	8.0
465	RADIOCHEMICAL STUDY OF PION SINGLE CHARGE EXCHANGE	RUNDBERG	1 *	0.5
579	A RADIOCHEMICAL STUDY OF NEUTRON-DEFICIENT PRODUCTS OF ^{238}U FROM 500 MeV	FAUBEL	1	0.8
603	SEARCH FOR DELTAS IN A COMPLEX NUCLEUS BY A RADIOCHEMICAL TECHNIQUE	TURKEVICH	1 * 2	38.5 234.0
610	USE OF LAMPF BEAM STOP TO OBTAIN ^{60}Fe	HENNING KUTSCHERA	1	0.0
629	FEASIBILITY OF HELIUM-JET TECHNIQUES FOR STUDYING SHORT-LIVED NUCLEI PRODUCED AT LAMPF	GREENWOOD BUNKER TALBERT, J.	1 * 2	47.5 135.0
679	A RADIOCHEMICAL STUDY OF THE ^{209}Bi(p,π^0)^{210}Po, ^{209}Bi(p,π^- xn)$^{210-x}$At, AND ^{209}Bi(p,p2π^- xn)$^{209-x}$At PION PRODUCTION REACTIONS AT 500-800 MeV	DAURIA WARD	1	9.4
690	SIMULATIONS OF COSMIC-RAY-PRODUCED GAMMA RAYS FROM THICK TARGETS	REEDY	1	0.0
728	STUDY OF PION CHARGE-EXCHANGE MECHANISMS BY MEANS OF ACTIVATION TECHNIQUES	GIESLER	1 1 2	52.0 58.0 0.0
762	COMPONENT IRRADIATION	HOLTKAMP JOSEPH	1	0.0
789	TWO-NUCLEON-OUT PRODUCTS FOLLOWING THE ABSORPTION OF 10-MeV π^+ in ^{26}Mg AND ^{74}Ge	OHKUBO	1	0.0

BIOMEDICAL PION AND MUON CHANNEL (BIOMED)

Exp. No.	Title	Spokesman	Phase No. * = Complete	Beam Hours
44	RADIOBIOLOGY OF π^- MESONS, A PRELIMINARY STUDY	CARLSON	1 *	75.0
84	QUALITY OF MESON RADIATION FIELDS	PHILLIPS	1 *	0.0
143	STUDY OF THE RADIOBIOLOGICAL PROPERTIES OF NEGATIVE PIONS	KLIGERMAN KNAPP	1 * 2 * 3 *	0.0 0.0 0.0
151	AN INVESTIGATION OF PION DOSIMETRY BY PASSIVE PARTICLE DETECTORS	KNOWLES	1 *	8.0
167	HEAVY FRAGMENT FORMATION FOLLOWING THE ABSORPTION OF π^- IN ^{12}C	ZIOCK	1 *	0.0

Exp. No.	Title	Spokesman	Phase No. *=Complete	Beam Hours
171	STUDY OF NEGATIVE-PION BEAMS BY MEANS OF PLASTIC NUCLEAR TRACK DETECTORS	BENTON	1	0.0
187	NUCLEAR GAMMA RAYS PRODUCED BY NEGATIVE PIONS STOPPING IN CARBON, NITROGEN, OXYGEN, AND TISSUE	REIDY	1	21.6
195	NUCLEAR RESONANCE EFFECT IN PIONIC ATOMS	LEON REIDY	1 * 2 *	0.0 155.2
196	A VISUALIZATION EXPERIMENT WITH CHARGED PARTICLES	DANIEL REIDY	1 *	0.0
198	EFFECTS OF PIONS ON DNA OF NONDIVIDING CELL SYSTEMS	POWERS	1 *	0.0
207	MEASUREMENT OF NEUTRON SPECTRUM AND INTENSITY RESULTING FROM π^- CAPTURE IN WATER PHANTOM AND HUMAN TISSUE	BRADBURY ALLRED	1 *	0.0
209	PION INTERACTIONS IN NUCLEAR EMULSIONS	BRADBURY ALLRED	1 *	0.0
212	COMPARATIVE EFFECTIVENESS OF NEGATIVE PIONS vs ^{252}Cf IN A TUMOR-ANIMAL SYSTEM	MEWISSEN	1 *	0.0
215	VISUALIZATION OF STOPPING PION DISTRIBUTION	PEREZ-MENDEZ BRADBURY	1	172.1
217	π^- PRODUCTION CROSS SECTIONS	PACIOTTI	1	5.9
218	PION DOSIMETRY WITH NUCLEAR EMULSIONS AND ALANINE	KATZ	1	0.0
235	RADIATION REPAIR OF NORMAL MAMMALIAN TISSUES	GILLETTE	1 *	68.4
236	BIOLOGICAL EFFECTS OF NEGATIVE PIONS	RAJU	1	556.0
239	STUDY OF ^{11}C AND ^{13}N PRODUCTION BY π^- IRRADIATION OF CARBON, NITROGEN, OXYGEN, AND TISSUE FOR RADIOTHERAPY MONITORING	FRIEDLAND MAUSNER	1 * 2 *	55.0 8.0
242	SURVIVAL OF SYNCHRONIZED CULTURED HUMAN KIDNEY T-1 CELLS EXPOSED TO STOPPING PIONS AND X RAYS AT VARIOUS TIMES AFTER MITOSIS	TODD	1 *	105.5
244	SYSTEMS DEVELOPMENT FOR EFFICIENT UTILIZATION OF HIGH-PURITY GERMANIUM MOSAIC DETECTORS FOR TUMOR UTILIZATION	BRILL	1 *	0.0
270	THERAPY BEAM DEVELOPMENT — BIOMEDICAL CHANNEL TUNING	PACIOTTI	1	992.8
271	THERAPY BEAM DEVELOPMENT — DOSIMETRY	SMITH	1	3225.1
272	THERAPY BEAM DEVELOPMENT — MICRODOSIMETRY	DICELLO	1 *	566.2
273	THERAPY BEAM DEVELOPMENT — LET MEASUREMENTS		1 *	783.7
274	PION RADIOBIOLOGY	BUSH	1 *	2910.0

Exp. No.	Title	Spokesman	Phase No. *=Complete	Beam Hours
275	PION CLINICAL TRIALS	BUSH	1 *	7297.4
285	MIGRATION OF ^{11}C AND ^{13}N RADIOACTIVITY PRODUCED *IN VIVO* BY π^-	MAUSNER	1 *	13.0
300	π^- COULOMB CAPTURE AND π^- TRANSFER IN TISSUE, TISSUE-EQUIVALENT LIQUID, AND SIMPLE COMPOUNDS	DANIEL LEON	1 *	37.0
304	STUDY OF THE AUGER PROCESS IN PIONIC ATOMS	LEON MAUSNER	1 *	9.2
380	RBE AND OER FOR NORMAL AND TUMOR TISSUES	PHILLIPS GOLDSTEIN	1 *	52.1
384	BIOLOGICAL INTERCOMPARISON OF π^- THERAPY BEAMS AT TRIUMF AND LAMPF USING MOUSE TESTES AS A BIOLOGICAL TEST SYSTEM	GERACI	1 *	23.7
675	NUCLEAR DISTRIBUTIONS FROM THE STUDY OF THE 2P STATES OF PIONIC ATOMS	KUNSELMAN	1	126.0
698	GROUND-STATE QUADRUPOLE MOMENTS OF DEFORMED NUCLEI	STEFFEN SHERA	1 * 3	305.0 0.0
727	MEASUREMENT OF THE EFFICIENCY OF MUON CATALYSIS IN DEUTERIUM-TRITIUM MIXTURES AT HIGH DENSITIES	JONES	1 2	919.0 341.0
732	HEAVY ELEMENT FISSION INDUCED BY ENERGETIC PIONS	PETERSON RISTINEN	1 * 2	271.0 0.0
745	HEXADECAPOLE MOMENTS IN URANIUM: ^{233}U AND ^{234}U	ZUMBRO SHERA	1 4	565.0 0.0
763	NATURE OF OXYGEN CONTAMINATION IN TITANIUM WITH STOPPED MUONS	TAYLOR	1	259.0
787	MUON CHANNELING FOR SOLID-STATE PHYSICS INFORMATION	MAIER PACIOTTI FLIK	1	0.0
834	THE PION-NUCLEUS INTERACTION STUDIED WITH THE 4f → 3d TRANSITION OF RARE-EARTH PIONIC ATOMS	TANAKA STEFFEN SHERA	1	0.0

BEAM STOP A RADIATION (BSA-RAD)

Exp. No.	Title	Spokesman	Phase No. *=Complete	Beam Hours
45	RADIATION-DAMAGE STUDIES — HIGH-TEMPERATURE REACTOR MATERIALS AND TYPE II SUPERCONDUCTORS	DUDZIAK GREEN GIORGI	1 * 2 *	0.0 1833.0
111	SEARCH FOR NEW NEUTRON-RICH NUCLIDES PRODUCED BY FAST NEUTRONS	HILL	1 * 2 *	0.0 10.8

Exp. No.	Title	Spokesman	Phase No. * = Complete	Beam Hours
113	RADIATION DAMAGE AND HELIUM EMBRITTLEMENT IN ELEVATED-TEMPERATURE REACTOR STRUCTURAL ALLOYS	MICHEL	1	0.0
161	THE MICRODISTRIBUTION OF THORIUM IN METEORITES	BURNETT	1	11.7
174	INVESTIGATION OF THE CHEMICAL REACTIONS OF ATOMIC ^{18}F AS A MEANS FOR DIRECT SYNTHESIS OF ^{18}F-LABELED COMPOUNDS	ROWLAND MILLER	1 * 2 *	0.0 7.0
326	ELECTRICAL COMPONENT RADIATION-EFFECTS STUDY	HARVEY	1 1	179.9 294.5
406	NEUTRON FLUX CHARACTERIZATION AT A-6 RADIATION-EFFECTS FACILITY	HARVEY	1	1306.3
415	TWO-NUCLEON-OUT PRODUCTS FROM STOPPED π^- INTERACTIONS	ORTH	1 *	0.0
467	IRRADIATIONS IN SUPPORT OF FERFICON STUDIES	GILMORE	1	0.4
542	FEASIBILITY STUDY: USING AN EXISTING NEUTRON BEAM PIPE AT LAMPF BEAM STOP FOR CRYSTAL DIFFRACTION SPECTROMETER EXPERIMENTS	LU	1 * 2	699.7 0.0
545	FUSION MATERIALS NEUTRON IRRADIATIONS — A PARASITE EXPERIMENT	BROWN	1 2	0.0 0.0
554	IRRADIATION OF TECHNOLOGICALLY IMPORTANT METALS WITH 800-MeV PROTONS USING THE ISOTOPE PRODUCTION FACILITY AT LAMPF	BROWN COST	1 2	75.2 0.0
560	STUDY OF NEUTRON-IRRADIATION-INDUCED GROWTH OF METALS AT RADIATION-EFFECTS FACILITY	HARVEY	1	63.4
691	SIMULATION OF COSMIC-RAY PRODUCTION OF NUCLIDES BY SPALLATION-PRODUCED NEUTRONS	REEDY	1	0.0
769	PROTON IRRADIATION EFFECTS ON CANDIDATE MATERIALS FOR THE GERMAN SPALLATION NEUTRON SOURCE (SNQ)	LOHMANN SOMMER	1	0.0
816	RADIATION EFFECTS ON THE FIELD STRENGTH OF SAMARIUM-COBALT PERMANENT MAGNETS	BROWN	1	0.0

EXTERNAL PROTON BEAM (EPB)

Exp. No.	Title	Spokesman	Phase No. * = Complete	Beam Hours
26	NEUTRON TIME-OF-FLIGHT EXPERIMENT AT BEAM STOP	VEESER	1 *	0.0
27	p-p SPIN-CORRELATION EXPERIMENTS	WILLARD	1 * 2 *	0.0 1141.8
42	BREAKUP OF FEW-NUCLEON SYSTEMS AND NUCLEI	COLE	1 *	530.8
81	STUDY OF NEUTRON-PROTON AND PROTON-PROTON COINCIDENCE SPECTRA FROM $p + d \rightarrow n + p + p$ REACTION	PHILLIPS	1 * 2 *	0.0 600.5

Exp. No.	Title	Spokesman	Phase No. * = Complete	Beam Hours
128	WNR STORAGE RING STRIPPER EXPERIMENT	HAYWARD	1 *	0.0
137	SEARCH FOR PARITY-VIOLATING CONTRIBUTION TO SCATTERING OF HADRONS	NAGLE MISCHKE FRAUENFELDER	1 * 2 * 3 *	316.6 363.4 346.5
153	INVESTIGATION OF NUCLEAR GAMMA RAYS RESULTING FROM IN-FLIGHT PION AND PROTON REACTIONS	EISENSTEIN	1 *	0.0
159	CHARGED-PARTICLE EMISSION IN PROTON-INDUCED REACTIONS AS A FEASIBILITY STUDY IN THE USE OF INTRINISIC GERMANIUM DETECTORS WITH THE PRIMARY LAMPF BEAM	EISENSTEIN	1 *	0.0
176	p-NUCLEUS TOTAL AND TOTAL REACTION CROSS-SECTION MEASUREMENTS	ANDERSON	1 * 2 *	0.0 296.6
192	MEASUREMENT OF THE EMITTANCE GROWTH IN H^- STRIPPING	HAYWARD	1 *	70.0
194	p-p, D, R, AND A MEASUREMENTS	McNAUGHTON	1 * 2 *	185.2 498.5
197	INVESTIGATION REACTION $p + d \rightarrow {}^3He + \pi^0$ AT LAMPF ENERGIES	HUNGERFORD	1 *	363.0
200	STUDY OF THE PHOTODETACHMENT SPECTRUM OF H^- IN THE VICINITY OF 11 eV	BRYANT	1 *	128.8
219	DOUBLE PION PRODUCTION IN PROTON-PROTON SCATTERING	BEVINGTON	1 *	422.0
223	STUDIES OF THE (p,np) CHARGE-EXCHANGE REACTION	HOFFMANN	F S*	66.3
241	DIRECT LEPTON PRODUCTION AT LAMPF ENERGIES	HOFFMAN MISCHKE	1 *	531.2
278	STUDY OF REACTION MECHANISMS USING INTERNAL CONVERSION TECHNIQUES	HOFFMANN MOORE	1 *	53.0
279	TEST OF CHARGE SYMMETRY IN nd AND pd SCATTERING	DIETERLE McFARLANE	F S* 1 *	67.0 0.0
289	MEASUREMENT OF THE PHASE OF THE FORWARD NUCLEON-NUCLEON SPIN-INDEPENDENT ELASTIC-SCATTERING AMPLITUDE AT 800 MeV	WHITTEN	1 *	354.6
323	STARK-EFFECT QUENCHING OF RESONANCES IN THE PHOTODISINTEGRATION OF THE H^- ION	BRYANT GRAM	1 *	350.6
336	STUDY OF THE SPIN DEPENDENCE OF PROTON-PROTON PION-PRODUCTION REACTIONS	MUTCHLER PINSKY	1 * 2 *	419.4 747.0
339	SURVEY OF PHOTODETACHMENT CROSS SECTION OF H^- FROM THRESHOLD TO 15 eV AND ITS DEPENDENCE UPON ELECTRIC FIELD	BRYANT GRAM	1 *	1363.1
341	STUDY OF $pd \rightarrow d\pi^+ n$ REACTION MECHANISMS	PHILLIPS	1 *	229.0

Exp. No.	Title	Spokesman	Phase No. *=Complete	Beam Hours
392	A MEASUREMENT OF THE TRIPLE-SCATTERING PARAMETERS D, R, A, R′, AND A′ FOR PROTON-PROTON AND PROTON-NEUTRON SCATTERING AT 800 MeV	HOFFMANN BONNER	5 *	87.0
449	SURVEY OF SINGLE AND DOUBLE PHOTODETACHMENT CROSS SECTION OF THE H^- ION FROM 14 TO 21.8 eV	BRYANT DONAHUE	1 * 2 *	570.7 229.9
468	MECHANISMS OF LUMINESCENCE INDUCED BY PROTONS INCIDENT ON ULTRAVIOLET GRADE OPTICAL MATERIALS	BECHER	1 *	70.8
492	POLARIMETER CALIBRATIONS AND SEARCH FOR ENERGY-DEPENDENT STRUCTURE IN pp ELASTIC SCATTERING VIA CROSS SECTION, ANALYZING POWER, AND WOLFENSTEIN PARAMETER MEASUREMENTS	McNAUGHTON WILLARD	1 *	0.0
498	MEASUREMENTS OF LONGITUDINAL CROSS-SECTION DIFFERENCE FOR LONGITUDINAL POLARIZED BEAM AND TARGETS (pp, pd, np)	WAGNER BURLESON	1 * 2 3	1664.5 0.0 0.0
512	PROTON-PROTON ELASTIC-SCATTERING MEASUREMENTS OF THE $A_{SS}(\theta)$, $A_{LL}(\theta)$, AND $A_{SL}(\theta)$ SPIN-CORRELATION PARAMETERS AT 500, 650, and 800 MeV	GREENE IMAI	—NU —NU 1 *	0.0 0.0 835.0
530	H− MAGNETIC STRIPPING RATES	JASON	1 *	237.2
586	A STUDY OF THE EFFECTS OF VERY STRONG ELECTRIC FIELDS ON THE STRUCTURE OF THE H^- ION	BRYANT GRAM	1 2	517.0 0.0
587	FUNDAMENTAL EXPERIMENTS WITH RELATIVISTIC HYDROGEN ATOMS: EXPLORATORY WORK	SMITH DONAHUE	1 * 2 * 4	400.0 0.0 0.0
588	A SEARCH FOR LONG-LIVED STATES OF THE H^- ION	CLARK BRYANT	1	0.0
591	AN INVESTIGATION OF INCLUSIVE ONE-PION PRODUCTION IN PROTON-NUCLEUS COLLISIONS	DEVRIES DiGIACOMO	1 * 2	651.1 243.0
592	AN INVESTIGATION OF TWO-PION PRODUCTION AND CORRELATIONS IN PROTON-NUCLEUS COLLISIONS AT 800 MeV	DEVRIES DiGIACOMO	1	0.0
633	MEASUREMENT OF p-p ELASTIC SCATTERING IN THE COULOMB INTERFERENCE REGION BETWEEN 300 AND 800 MeV	PAULETTA IROM	1	0.0
634	MEASUREMENT OF PARITY VIOLATION IN THE p-NUCLEON TOTAL CROSS SECTIONS AT 800 MeV	CARLINI TALAGA YUAN	1 * 2	299.2 471.0
635	SPIN MEASUREMENTS IN pd ELASTIC SCATTERING	BONNER IGO BLESZYNSKI	1 2	507.7 622.0
636	A MEASUREMENT OF THE WOLFENSTEIN POLARIZATION PARAMETERS D_{LL}, D_{SL}, K_{LL}, AND K_{SL} FOR p-p ELASTIC SCATTERING	HOLLAS	1	683.0
637	A MEASUREMENT OF THE VECTOR POLARIZATION OF THE DEUTERON IN THE REACTION $pp \rightarrow d\pi^+$	BONNER	1	430.0

Exp. No.	Title	Spokesman	Phase No. *=Complete	Beam Hours
708	A MEASUREMENT OF THE DEPOLARIZATION, THE POLARIZATION, AND THE POLARIZATION ROTATION PARAMETERS AND THE ANALYZING POWER FOR THE REACTION $pp \rightarrow p\pi^+n$	HOLLAS	1 2	651. 0.0
792	MEASUREMENT OF PARITY VIOLATION IN THE $\vec{p}$-p AND $\vec{p}$-NUCLEON TOTAL CROSS SECTIONS AT 800 MeV	YUAN	1	527.0
815	MEASUREMENT OF A_{NO}, A_{SL}, AND A_{LL} IN $\vec{p}\vec{p} \rightarrow pn\pi^+$ AT 500, 580, 650, 720, AND 800 MeV	BUGG	1	0.0
817	ELASTIC SCATTERING OF POLARIZED PROTONS FROM ^3H AT INTERMEDIATE ENERGY	BLESZYNSKI AZIZI IGO	1	0.0
818	PROTON-DEUTERON ELASTIC SCATTERING AT 800-MeV TWO- AND THREE-SPIN OBSERVABLES	IGO	1	0.0
832	GAMMA-RAY ANGULAR CORRELATION FROM $^{12}C(\vec{p},p')^{12}C^*$ (15.11 MeV)	LIEB PERDRISAT FUNSTEN	1	0.0
866	NEUTRINO SOURCE CALIBRATION	HAUSAMMANN DONAHUE	1	0.0

ENERGETIC PION CHANNEL SPECTROMETER (EPICS)

Exp. No.	Title	Spokesman	Phase No. *=Complete	Beam Hours
9	ELASTIC AND INELASTIC PION SCATTERING FROM CALCIUM ISOTOPES	McCARTHY MORRIS	1 *	646.7
13	STUDY OF π^+-INDUCED DOUBLE-CHARGE-EXCHANGE REACTIONS	SETH	1 *	334.5
14	π^+ AND π^- ELASTIC AND INELASTIC SCATTERING FROM ^{16}O	THIESSEN	1 * 2 *	798.8 218.0
18	SURVEY OF π SCATTERING BY COMPLEX NUCLEI	ZEIDMAN	1 * 2 * 3 *	289.8 198.4 64.3
23	A SURVEY OF PION-NUCLEUS ELASTIC AND INELASTIC SCATTERING AT 180 MeV	WHARTON	1 *	300.5
39	SEARCH FOR (π,p) REACTIONS WITH EPICS	MACEK THIESSEN	1 *	295.5
74	STUDY OF PION-INDUCED DOUBLE-CHARGE-EXCHANGE REACTIONS ON LOW-Z ELEMENTS	PEREZ-MENDEZ STETZ	1 *	346.0
87	π^+ AND π^- SCATTERING FROM ^3He AND ^4He	McCARTHY	1 *	358.1
130	EPICS TUNEUP PROPOSAL: PION CARBON SCATTERING	THIESSEN	1 * 2 *	221.0 674.4
133	PRELIMINARY PION-CHANNELING EXPERIMENTS	GEMMELL	1 *	200.9

Exp. No.	Title	Spokesman	Phase No. *=Complete	Beam Hours
156	SURVEY OF QUASI-ELASTIC PION SCATTERING	SWENSON	1 *	190.0
229	π^+ vs π^- INELASTIC EXCITATION OF LOW-LYING COLLECTIVE STATES IN N = 28 NUCLEI	BRAITHWAITE MOORE	1 *	281.8
245	STUDY OF THE (π^-,n) AND (π,πp) REACTIONS IN ^{3,4}He AND HEAVIER NUCLEI BY DETECTING RECOILING TRITONS OR DEUTERONS	KALLNE THIESSEN	1 *	943.9
246	STUDIES OF π^+ SCATTERING AT 50 MeV FROM LIGHT NUCLEI	EISENSTEIN	1 *	564.0
265	STUDY OF PROMPT NUCLEAR DEEXCITATION GAMMA RAYS FROM PION INTERACTIONS WITH ^{6,7}Li AND ^{12}C	MORRIS BRAITHWAITE	1 *	319.0
310	(π^+,π^-) DOUBLE-CHARGE-EXCHANGE REACTIONS USING CORE 2n TARGETS	BRAITHWAITE MORRIS	1 *	265.2
317	INELASTIC PION SCATTERING TO THE 1^+ STATES OF ^{12}C	PETERSON	1 *	246.5
325	PION AND MUON MULTIPLE COULOMB-SCATTERING EXPERIMENT ON THE EPICS BEAM LINE	HANSON	1 *	69.7
342	STUDY OF THE (π^+,p) REACTION IN ^{12}C	McCARTHY KALLNE	1 *	151.2
368	INELASTIC PION SCATTERING TO THE 19.2 $\pm$ 0.3-MeV STATE IN ^{12}C	MOORE	1 *	246.5
369	INELASTIC PION SCATTERING BY ^{17}O, ^{18}O, AND ^{19}F	DEHNHARD	1 *	318.1
389	INELASTIC PION SCATTERING FROM LIGHT NUCLEI ^{10}B, ^{11}B, ^{14}N, AND ^{15}N	MORRISON ZEIDMAN	1 * 2 * 3 *	685.0 0.0 132.0
391	INELASTIC $\pi^\pm$ SCATTERING ON ^{7}Li	PETERSON	1 *	201.7
413	MASS MEASUREMENT OF ^{26}Ne AND ^{48}Ar BY THE (π^-,π^+) REACTION	SETH NANN	1 *	0.0
419	π^+ vs π^- INELASTIC EXCITATION OF SINGLE-PARTICLE AND CORE-COUPLED STATES IN ^{207}Pb AND ^{209}Bi	BRAITHWAITE MORRIS MOORE	1 *	25.3
442	STUDY OF THE INCLUSIVE PION DOUBLE-CHARGE-EXCHANGE REACTION	KALLNE	1 *	124.7
446	STUDY OF E0 GIANT RESONANCES	HALPERN EISENSTEIN THIESSEN	1 *	0.0
448	STUDY OF π^+ DOUBLE-CHARGE-EXCHANGE SCATTERING AT SMALL ANGLES ON VARIOUS NUCLEI	BURLESON	1 *	399.7
452	ELASTIC AND INELASTIC SCATTERING OF $\pi^\pm$ BY ^{13}C	DEHNHARD	1 *	219.5
456	THE (π,d) REACTION ON ^{12}C AT 60 MeV	HOISTAD	1	0.0
460	AN INVESTIGATION OF THE STABILITY OF ^{6}H, ^{7}H, AND ^{9}He BY (π^-,π^+) REACTIONS	SETH	1 *	444.7

Exp. No.	Title	Spokesman	Phase No. *=Complete	Beam Hours
463	COMPARATIVE STUDY OF THE (π^+,π^-) AND (π^-,π^+) REACTIONS ON ^{12}C	NANN SETH	1 *	444.7
478	$\pi^\pm$ ELASTIC SCATTERING FROM DEUTERIUM	MASTERSON	1 *	148.3
481	EXCITATION OF HIGH-SPIN STATES IN $T_z = 0$ s-d SHELL NUCLEI BY PION INELASTIC SCATTERING	GEESAMAN	1 *	134.7
484	INELASTIC PION SCATTERING FROM ^{148}Sm AND ^{152}Sm	MORRIS	1 *	70.7
495	ISOSPIN MIXING IN ^{12}C	MORRIS BRAITHWAITE	1 *	424.1
506	INELASTIC PION SCATTERING TO THE UNNATURAL PARITY LEVELS IN ^{12}C AND ^{6}Li	COTTINGAME BRAITHWAITE	1 *	0.0
510	ENERGY DEPENDENCE OF ELASTIC AND INELASTIC SCATTERING OF $\pi^\pm$ BY ^{13}C BETWEEN 116 AND 280 MeV	DEHNHARD	1 * 2 *	61.1 239.0
516	THE (π^+,p) REACTION ON $^{16,18}O$	ANDERSON HOISTAD	1 *	36.0
522	EXCITATION OF GIANT RESONANCE STATES IN ^{90}Zr AND ^{208}Pb WITH 150-MeV PIONS	KING ANDERSON PETERSON	1 *	198.6
539	SEARCH FOR PURE NEUTRON/PROTON TRANSITIONS IN ^{14}C	BAER HOLTKAMP	1 *	345.7
546	INVESTIGATION OF THE SPIN FORM FACTOR OF TRITIUM AND ^{3}He	BRISCOE NEFKENS	F S* 1 *	60.9 240.0
549	A STUDY OF THE DCX REACTION MECHANISM — THE $^{42}Ca(\pi^+,\pi^-)^{42}Ti$ REACTION	SETH	1 *	349.3
550	EXCITED-STATE SPECTRA OF THE EXOTIC NUCLEI ^{18}C AND ^{26}Ne BY (π^-,π^+) DCX REACTIONS	SETH	1	0.0
558	MEASUREMENT OF (π^+,π^-) REACTIONS ON $^{13,14}C$ AND ^{26}Mg	BAER BURLESON	1 *	432.0
565	EXCITATION OF HIGH-SPIN PARTICLE-HOLE STATES IN ^{54}Fe AND ^{58}Ni	ZEIDMAN GEESAMAN	1 *	209.0
570	INVESTIGATION OF THE STRUCTURE OF ^{16}O WITH PION INELASTIC SCATTERING	HOLTKAMP FORTUNE	1 *	325.0
572	A-DEPENDENCE OF THE (π^+,π^-) REACTION AND THE WIDTH OF A DOUBLE ISOBARIC ANALOG STATE IN HEAVY NUCLEI	GREENE MOORE MORRIS	1 2	0.0 0.0
573	PION SCATTERING FROM ^{24}Mg AND ^{26}Mg	BLANPIED	1	159.0
577	MEASUREMENT OF ANGULAR DISTRIBUTIONS FOR $^{16}O(\pi^+,\pi^-)^{16}Ne$	GREENE FORTUNE	1 *	237.0
581	$\pi^\pm$ ELASTIC SCATTERING FROM DEUTERIUM AT 237 MeV	MASTERSON BOUDRIE	1 * 2 *	193.0 236.0

Exp. No.	Title	Spokesman	Phase No. *=Complete	Beam Hours
597	THE STUDY OF BROAD-RANGE PION INELASTIC SCATTERING SPECTRA (WITH EMPHASIS ON THE EXCITATION OF THE GIANT MONOPOLE RESONANCE)	HALPERN EISENSTEIN	1 *	190.0
598	INELASTIC PION SCATTERING TO THE UNNATURAL PARITY LEVELS IN ^{6}Li	COTTINGAME KIZIAH	1	332.0
601	DETERMINATION OF ISOSCALAR AND ISOVECTOR TRANSITION RATES FOR LOW-LYING COLLECTIVE STATES IN ^{90}Zr AND ^{208}Pb BY π^+ AND π^- INELASTIC SCATTERING	HINTZ	1	0.0
602	NEUTRON-PROTON COMPONENTS OF INELASTIC TRANSITIONS IN PION SCATTERING ON ^{23}Na AND ^{25}Mg	HARVEY DEHNHARD	1	0.0
604	AN INVESTIGATION OF THE NEAR STABILITY OF ^{5}H	SETH	1 *	254.8
605	A DIBARYON SEARCH AT EPICS	SETH	1 *	107.0
606	TESTS OF THE (N − Z) DEPENDENCE OF PION DOUBLE CHARGE EXCHANGE	SETH	1 *	431.0
617	A STUDY OF THE (3/2,3/2) RESONANCE IN LIGHT NUCLEI	ZIOCK	1 * 2 *	321.0 0.0
619	INELASTIC PION SCATTERING TO 0^+ AND 2^+ STATES IN ^{40}Ca AND ^{42}Ca	MOORE FORTUNE MORRIS	*	136.6
622	INVESTIGATION OF THE STRONG CANCELLATIONS OF NEUTRON-PROTON TRANSITION AMPLITUDES IN ^{14}C	HOLTKAMP BAER	1 *	138.1
625	INELASTIC SCATTERING OF PIONS TO GIANT RESONANCES	KING ANDERSON PETERSON	1 *	162.0
651	MEASUREMENT OF A LOWER LIMIT FOR THE SUBTHRESHOLD PRODUCTION OF KAONS WITH 800-MeV PROTONS	MORRIS	1	0.0
657	INELASTIC $\pi^{\pm}$ SCATTERING FROM THE N = 28 ISOTONES	SEIDL MOORE	1	0.0
659	SPIN-FLIP GIANT RESONANCE EXCITATION	BLAND MOORE	1 * 2 *	174.0 108.0
661	GOOD-RESOLUTION STUDY OF ^{18}O(π,π')	MORRIS BLAND	1	0.0
662	ELASTIC AND INELASTIC π^- AND π^+ SCATTERING FROM ^{32}S, ^{31}P AND ^{90}Zr, ^{89}Y	KRAUSHAAR PETERSON	1	0.0
671	EXPERIMENTAL INVESTIGATIONS OF ISOVECTOR PROPERTIES OF COLLECTIVE TRANSITIONS	SAHA SETH	1	271.0
672	STUDY OF GIANT RESONANCES IN ^{90}Zr, ^{116}Sn, AND ^{208}Pb WITH π^+ AND π^- INELASTIC SCATTERING	CAREY MOSS	1 *	233.0
677	A DETERMINATION OF $\Delta S = 1$ CONTRIBUTIONS IN INELASTIC PION SCATTERING FROM ODD-A NUCLEI	HOLTKAMP FUNSTEN	1	0.0

Exp. No.	Title	Spokesman	Phase No. *=Complete	Beam Hours
678	STUDY OF THE M1 TRANSITION IN ^{48}Ca BY INELASTIC SCATTERING OF π^+ AND π^-	DEHNHARD MORRIS	1 *	281.0
681	MEASUREMENTS OF LARGE-ANGLE PION-NUCLEUS SCATTERING WITH EPICS	BURLESON	1	266.0
701	PION DOUBLE CHARGE EXCHANGE ON SELF-CONJUGATE NUCLEI	MORRIS FORTUNE	1 *	314.0
702	NUCLEAR STRUCTURE EFFECTS IN PION SCATTERING FROM $^{92\text{-}100}Mo$	COMFORT	1	0.0
703	STUDY OF M4 STRENGTH IN ^{15}N BY π^+ AND π^- INELASTIC SCATTERING	HOLTKAMP SEESTROM-MORRIS	1 *	245.0
716	PION DOUBLE CHARGE EXCHANGE ON HEAVY NUCLEI	SETH	1 * 2	120.0 0.0
717	PION SCATTERING TO COLLECTIVE STATES IN SELENIUM ISOTOPES	BLAND MORRIS GREENE	1	0.0
723	MEASUREMENT OF THE NEUTRON AND PROTON CONTRIBUTIONS TO EXCITED STATES IN ^{39}K BY π^+ AND π^- INELASTIC SCATTERING	HARVEY FORTUNE	1	0.0
744	PION INELASTIC SCATTERING FROM ^{20}Ne	MOORE FORTUNE	1	0.0
746	PION INELASTIC SCATTERING FROM ^{6}Li	KIZIAH COTTINGAME	1 * 2	114.0 0.0
748	MEASUREMENT OF $(M_n/M_p)^2$ FOR 2^+ TRANSITIONS IN T = 1 NUCLEI	SEESTROM-MORRIS	1	0.0
749	$^{16}O(\pi^+,\pi^-)^{16}Ne$ (g.s.) ANGULAR DISTRIBUTION MEASUREMENTS AT T_π = 120 MeV AND T_π = 200 MeV	BLAND FORTUNE	1 *	357.0
755	MEASUREMENT OF M1 GIANT RESONANCES IN PION INELASTIC SCATTERING	SEESTROM-MORRIS BLAND	1 *	169.0
756	$\pi^\pm$ INELASTIC SCATTERING FROM ^{4}He: AN EXAMINATION OF ISOSPIN-SYMMETRY BREAKING	HOLTKAMP COTTINGAME	1	0.0
772	NEUTRON-PROTON COMPOSITION OF TRANSITIONS IN ^{23}Na AND ^{25}Mg FROM INELASTIC SCATTERING OF π^+ AND π^-	HARVEY DEHNHARD	1	0.0
773	MEASUREMENTS OF (π^+,π^-) ANGULAR DISTRIBUTIONS ON ^{56}Fe AT 164 AND 292 MeV	SEIDL BURLESON	1	0.0
777	ANGULAR DISTRIBUTIONS FOR DCX ON ^{14}C AND ^{18}O	SEIDL FORTUNE BAER	1	0.0

Exp. No.	Title	Spokesman	Phase No. *=Complete	Beam Hours
778	CONTINUATION OF THE STUDY OF THE M1 TRANSITION IN ^{48}Ca BY THE INELASTIC SCATTERING OF π^+ AND π^-	DEHNHARD MORRIS	1	0.0
780	A STUDY OF THE DOUBLE-CHARGE-EXCHANGE REACTIONS $^{14}C(\pi^-,\pi^+)^{14}Be$ AND $^{18}O(\pi^-,\pi^+)^{18}C$	BAER SEIDL GILMAN	1	220.0
782	ELASTIC SCATTERING OF π^+ AND π^- FROM ^3He AND ^4He BETWEEN 88.5 AND 194.3 MeV	DEHNHARD SEESTROM-MORRIS	1	0.0
791	ISOSCALAR QUENCHING IN THE EXCITATION OF 8^- STATES IN ^{52}Cr	ZEIDMAN MORRISON	1	0.0
793	PION DOUBLE CHARGE EXCHANGE ON SELF-CONJUGATE NUCLEI (CONTINUED)	BLAND MOORE MORRIS	1	0.0
796	CORE EXCITATION EFFECTS IN PION DOUBLE CHARGE EXCHANGE	SETH	1 *	328.0
797	THE STUDY OF GIANT RESONANCES AND LOW-LYING COLLECTIVE STATES IN ^{90}Zr BY INELASTIC π^- AND π^+ SCATTERING	ULLMANN KING	1	0.0
800	INELASTIC PION SCATTERING FROM ^{22}Ne	FORTUNE MOORE	1	0.0
809	STUDY OF π^-,p AND π^+,p REACTIONS WITH EPICS	EGGER BLANPIED	1	0.0
812	BACK-ANGLE CHARGE ASYMMETRIES FOR ELASTIC π-DEUTERON SCATTERING	PETERSON	1	0.0
826	ISOSPIN DEPENDENCE OF NONANALOG PION DOUBLE CHARGE EXCHANGE	MORRIS MOORE GILMAN	1	0.0
833	CONTINUATION OF THE INVESTIGATION OF LARGE-ANGLE PION-NUCLEUS SCATTERING	BURLESON	1	0.0
835	TARGET MASS DEPENDENCE OF THE ISOVECTOR CONTRIBUTION TO THE GIANT QUADRUPOLE RESONANCE	SEESTROM-MORRIS	1	0.0
836	ENERGY DEPENDENCE OF PION SCATTERING TO THE GIANT RESONANCE REGION OF ^{208}Pb	SEESTROM-MORRIS	1	0.0
839	PION INELASTIC SCATTERING FROM THE 1^+ DOUBLET IN ^{12}C	MOORE MORRIS	1	0.0
840	INELASTIC PION SCATTERING FROM ^{16}O AT T_π = 120 AND 200 MeV	BLAND FORTUNE	1	0.0
841	FORWARD-ANGLE PION INELASTIC SCATTERING ON LIGHT NUCLEI	BLAND MOORE FORTUNE	1	0.0
843	A SEARCH FOR Δ_{3-3} COMPONENTS OF GROUND-STATE NUCLEAR WAVE FUNCTIONS	MORRIS MOORE	1	0.0
845	PION INELASTIC SCATTERING FROM ^9Be	KELLY	1	0.0

Exp. No.	Title	Spokesman	Phase No. *=Complete	Beam Hours
858	ADDITIONAL MEASUREMENTS OF $^{16}O(\pi^+,\pi^-)^{16}Ne$ (g.s.)	FORTUNE GILMAN	1	0.0
862	STUDY OF THE M1 TRANSITION IN ^{88}Sr BY THE INELASTIC SCATTERING OF π^+ AND π^-	NANDA DEHNHARD	1	0.0
863	STUDY OF GIANT RESONANCES IN THE PALLADIUM ISOTOPES VIA PION SCATTERING	SAHA SETH	1	0.0
868	AN EXPERIMENTAL TEST OF THE Δ-HOLE MODEL OF NONANALOG DOUBLE CHARGE EXCHANGE	SETH	1	0.0
874	ELASTIC SCATTERING OF π^+ FROM DEUTERIUM IN THE REGION OF THE $^3F_3$ DIBARYON RESONANCE	BLILIE DEHNHARD	1	0.0

HIGH-RESOLUTION SPECTROMETER (HRS)

Exp. No.	Title	Spokesman	Phase No. *=Complete	Beam Hours
4	LARGE ANGLE ELASTIC SCATTERING OF PROTONS FROM HELIUM AND QUASI-ELASTIC KNOCKOUT OF ALPHA PARTICLES BY 800-MeV PROTONS	IGO	1 *	458.0
5	INELASTIC SCATTERING OF 800-MeV PROTONS FROM NUCLEI TO STUDY QUASI-FREE MODES	CHRIEN PALEVSKY	1 *	532.7
10	SEARCH FOR (p,π) REACTIONS WITH HRS	SPENCER	1 *	167.9
15	ELASTIC SCATTERING AND TOTAL CROSS-SECTION MEASUREMENTS OF PROTON ON HYDROGEN, DEUTERIUM, AND HELIUM	IGO TANAKA	1 * 2 * 3 *	0.0 75.0 249.0
49	ELASTIC AND INELASTIC PROTON SCATTERING FROM THE NICKEL ISOTOPES AND FROM ^{89}Y	PETERSON	1 *	68.3
117	HIGH-RESOLUTION STUDY OF THE NEUTRON PICK-UP REACTION	IGO	1 *	273.2
138	INELASTIC PROTON SCATTERING AND EXCITATION OF STATES OF INTERMEDIATE COLLECTIVITY IN OPEN-SHELL NUCLEI	McDANIELS SWENSON	1 *	184.2
139	PRELIMINARY PROTON SCATTERING SURVEY WITH HRS	SPENCER TANAKA	1 *	695.1
178	PROTON SCATTERING SURVEY ON s-d SHELL NUCLEI	SPENCER HINTZ	1 *	209.3
183	PROTON SCATTERING SURVEY ON HEAVY DEFORMED NUCLEI	HINTZ SPENCER	1 *	382.1
204	EXCITATION AND ASYMMETRY MEASUREMENT OF T = 1, HIGH-SPIN, NONNORMAL-PARITY PARTICLE-HOLE STATE BY (p,p') SCATTERING IN THE INTERMEDIATE-ENERGY RANGE	IGO	1 *	127.0
223	STUDIES OF THE (p,np) CHARGE-EXCHANGE REACTION	HOFFMANN	F S*	0.0

Exp. No.	Title	Spokesman	Phase No. *=Complete	Beam Hours
233	SEARCH FOR DELTA CONFIGURATIONS IN NUCLEI	SETH SPENCER	1 *	167.9
249	THE (p,π^+) REACTION ON ^{4}He WITH 800-MeV PROTONS	WHITTEN	1 *	296.7
256	p-NUCLEUS ELASTIC SCATTERING AT $q^2 = 8$ GeV^2 IN Be, C, AND THE STUDY OF p-NUCLEUS INTERACTIONS IN COBALT AND GOLD UP TO $m^* = q^2/2\nu \cong 20$	FRANKEL	1 *	107.6
258	STUDY OF MECHANISMS FOR THE EJECTION OF HIGH-MOMENTUM PARTICLES FROM NUCLEI BY STUDY OF THE COINCIDENCE SPECTRUM IN $p + a \rightarrow (p,d,t) + (p,d,t) + X$	FRANKEL FRATI	1 * 2	178.7 0.0
261	INTERMEDIATE-ENERGY (p,d) REACTION MECHANISM STUDIES	RICKEY SHEPARD PETERSON	1 *	0.0
311	ELASTIC-SCATTERING SURVEY USING POLARIZED PROTONS	HOFFMANN	1 * 2 *	715.3 245.6
346	STUDY OF HIGH-MOMENTUM COMPONENTS IN NUCLEI USING A POLARIZED PROTON BEAM	FRANKEL	1 *	209.8
347	SEARCH FOR ORBIT-FLIP STATES BY INELASTIC PROTON SCATTERING	HINTZ	1 *	209.3
352	DETERMINATION OF NEUTRON-MASS DISTRIBUTION FROM ELASTIC PROTON MEASUREMENTS [P(t) AND $d\sigma/dt$] ON ISOTOPES IN THE CALCIUM REGION	WHITTEN	1 *	204.8
354	SCATTERING OF 800-MeV PROTONS FROM ^{12}C AND ^{13}C AT MOMENTUM TRANSFER >4 fm^{-1}	BLANPIED	1 *	324.1
355	FURTHER ELASTIC SCATTERING CROSS SECTION AND ANALYZING POWER MEASUREMENTS ON ^{208}Pb AND ^{116,124}Sn	HOFFMANN	1 * 2 *	130.0 55.0
356	ANALYZING POWER AND CROSS-SECTION MEASUREMENTS FOR INELASTIC PROTON EXCITATION OF SIMPLE STATES	GLASHAUSSER BAKER SCOTT	1 * 2 *	199.9 88.1
385	MEASUREMENT OF THE POLARIZED PROTONS + NEUTRONS ANALYZING POWER $A_Y(\theta)$ FROM $\theta_{c.m.}$ 10-70°	HOFFMANN	1 * 2 *	140.6 108.8
386	TOTAL REACTION CROSS SECTIONS FOR p^+ NUCLEI AT 800 MeV	HOFFMANN BURLESON YOKOSAWA	1 * 2 * 3 * 4 *	404.0 113.5 113.5 0.0
392	A MEASUREMENT OF THE TRIPLE-SCATTERING PARAMETERS D, R, A, R′, AND A′ FOR PROTON-PROTON AND PROTON-NEUTRON SCATTERING AT 800 MeV	HOFFMANN BONNER	1 * 2 * 3 * 4 5 *	208.6 491.0 146.0 0.0 104.0
395	THE (p,π^+) REACTION ON ^{16}O AND ^{40}Ca	BAUER HOISTAD NANN	1 *	195.8

Exp. No.	Title	Spokesman	Phase No. *=Complete	Beam Hours
399	EXCITATION OF GIANT MULTIPOLE RESONANCES BY 200-400-MeV PROTONS	BERTRAND	1 * 2 *	40.0 144.0
405	THE (p,π^-) REACTION ON ^{12}C AND ^{13}C	HOISTAD BAUER SETH	1 *	271.7
411	MEASUREMENT OF SPIN-FLIP PROBABILITIES IN PROTON INELASTIC SCATTERING AT 800 MeV AND SEARCH FOR COLLECTIVE SPIN-FLIP MODES, PRELIMINARY SURVEY	HINTZ MOSS	1 *	247.0
425	PROTON ELASTIC SCATTERING AT ~600 MeV BY $^{40,48}Ca$, ^{90}Zr, AND ^{208}Pb	SETH HOFFMANN	1 *	283.2
431	CROSS SECTION AND ANALYZING POWER FOR INELASTIC PROTON EXCITATION OF UNNATURAL PARITY STATES IN ^{6}Li, ^{12}C, ^{14}N, AND ^{16}O	GLASHAUSSER MOSS	1 *	181.0
432	CROSS SECTION FOR EXCITATION OF UNNATURAL PARITY STATES IN ^{12}C AT $E_p < 800$ MeV	GLASHAUSSER MOSS	1 *	148.9
433	ELASTIC SCATTERING DIFFERENTIAL CROSS SECTIONS AND ANALYZING POWERS FOR POLARIZED p + $^{40,48}Ca$, ^{90}Zr, AND ^{208}Pb AT ~400 MeV	HOFFMANN SETH	1 *	0.0
438	THE (p,d) REACTIONS ON $^{12,13}C$, ^{7}Li, ^{16}O, ^{25}Mg, ^{28}Si, AND ^{40}Cu BETWEEN 650 AND 800 MeV	IGO	1 *	249.5
451	INELASTIC PROTON SCATTERING IN THE RANGE 300 TO 500 MeV	HINTZ	1 2	221.3 0.0
462	ANALYZING POWER AND DIFFERENTIAL CROSS SECTIONS FOR THE REACTIONS $p + p \rightarrow d + \pi^+$ AND $p + d \rightarrow t + \pi^+$ AT ~600 AND 400 MeV	SETH NANN	1 *	118.0
470	REACTIVE CONTENT OF THE OPTICAL POTENTIAL	BARLETT HOFFMANN	1 * 2 *	247.5 83.0
472	STUDY OF THE (p,d) REACTION ON ^{90}Zr, ^{140}Ce, AND ^{208}Pb AT 800 MeV	WHITTEN	1 *	79.5
473	STUDY OF GIANT MULTIPOLE RESONANCES WITH 800-MeV PROTONS	MOSS ADAMS CAREY	1 * 2 *	110.8 197.7
474	A MEASUREMENT OF SPIN-DEPENDENT EFFECTS IN p + d ELASTIC AND INELASTIC SCATTERING	CORNELIUS	1 * 2 *	71.0 60.0
475	SCATTERING OF 0.8-GeV PROTONS FROM ^{20}Ne AND ^{22}Ne	BLANPIED	1 * 2 *	154.9 133.0
476	THE ANALYZING POWER FOR POLARIZED PROTONS + $^{24,26}Mg$ AT 500 AND 800 MeV	BLANPIED	1 *	147.6
485	THE ENERGY DEPENDENCE IN THE $(p,\pi^{\pm})$ REACTION	HOISTAD SHEPARD	1	0.0
486	INELASTIC SCATTERING OF PROTONS POPULATING THE 4^- (3.44-MeV) LEVEL OF ^{208}Pb — A SEARCH FOR CRITICAL OPALESCENCE	IGO GLASHAUSSER MOSS	1 *	65.6

Exp. No.	Title	Spokesman	Phase No. *=Complete	Beam Hours
489	SEARCH FOR M1 GIANT RESONANCES IN THE (p,p') REACTION AT E_p = 800 MeV	MOSS	1 *	63.9
508	DIBARYON RESONANCES IN PION PRODUCTION	SETH	1 * 2 * 3 4	178.0 171.0 0.0 0.0
519	STUDY OF THE REACTION p(pol) + d → (p,π) + X TO MEASURE THE ANALYZING POWER AND STRUCTURE FUNCTION FOR BACKWARD PARTICLES	FRANKEL	1 *	130.3
520	STUDY OF THE REACTION p(POLARIZED) + ^{3,4}He → (p,d,π..) + X TO MEASURE THE ANALYZING POWER STRUCTURE FUNCTIONS FOR BACKWARDS PARTICLES	VAN DYCK	1 *	127.0
531	EXCITATION OF UNNATURAL PARITY STATES IN ^{12}C AT 500 MeV	GLASHAUSSER MOSS	1	101.3
532	MEASUREMENTS OF CROSS SECTIONS AND ANALYZING POWER IN THE (p,2p) REACTION ON DEUTERIUM	VAN DYCK	1	0.0
533	THE ASYMMETRY IN THE (p,π) REACTION ON ^{6}Li AT 800 MeV	HOISTAD SETH	1	0.0
535	A STUDY OF THE RELATION BETWEEN THE (p,d) AND (π,p) REACTION IN A PION EXCHANGE MODEL	ANDERSON HOISTAD	1	0.0
538	ANALYZING POWER AND CROSS-SECTION MEASUREMENTS OF THE ^{4}He(p,d)^{3}He REACTION	SHEPARD KING	1 * 2	43.0 0.0
540	ELASTIC SCATTERING FROM LIGHT NUCLEI	IGO BLESZYNSKI	1 *	0.0
556	A PROPOSAL TO STUDY THE (p,p') PROCESS LEADING TO π-ATOMIC STATES	BERTOZZI	1 *	52.6
563	p + p ELASTIC SCATTERING AT 800 AND 500 MeV	HOFFMANN	1 *	143.3
580	CROSS SECTIONS AND ANALYZING POWERS FOR ELASTIC AND INELASTIC SCATTERING OF 515-MeV PROTONS FROM ^{13}C	SEESTROM-MORRIS DEHNHARD	1	43.6
583	MEASUREMENT OF C_{LL} IN THE COULOMB INTERFERENCE REGION	PAULETTA GAZZALY	1 2	0.0 0.0
585	MEASUREMENT OF p-p AND p-d ELASTIC SCATTERING IN THE COULOMB INTERFERENCE REGION BETWEEN 500 AND 800 MeV	PAULETTA	1 *	106.0
616	MEASUREMENT OF THE WOLFENSTEIN PARAMETERS FOR THE 1^{+} STATES OF ^{12}C	BLESZYNSKI McCLELLAND HINTZ MOSS	1 * 2 *	324.4 0.0
623	MEASUREMENT OF CROSS SECTION, ANALYZING POWER, AND DEPOLARIZATION PARAMETERS IN THE ^{28}Si(p,p')^{28}Si (6^{-}, T = 0 AND T = 1) REACTION AT 400 MeV	GLASHAUSSER	1	0.0

Exp. No.	Title	Spokesman	Phase No. *=Complete	Beam Hours
626	MEASUREMENT OF THE DEPOLARIZATION PARAMETERS $D_{NN'}$, $D_{LS'}$, AND $D_{SS'}$ IN PROTON-NUCLEUS SCATTERING AT VERY HIGH EXCITATION ENERGIES	GLASHAUSSER McGILL	1 *	208.0
627	MEASUREMENT OF THE RELATIVE SIGN OF NEUTRON AND PROTON TRANSITION MATRIX ELEMENTS IN (p,p') REACTIONS	HYNES BERNSTEIN	1 *	64.0
630	A STUDY OF PROTON INELASTIC SCATTERING AT 0° AND A SEARCH FOR GIANT MONOPOLE AND GIANT MAGNETIC DIPOLE EXCITATIONS	CAREY HINTZ McCLELLAND MOSS	1 * 2 3	133.0 76.0 0.0
632	CAN PROTON DENSITY DIFFERENCES BE EXTRACTED FROM MEDIUM-ENERGY p-NUCLEUS ELASTIC-SCATTERING DATA	BARLETT HOFFMANN	1	0.0
642	REACTIVE CONTENT OF THE OPTICAL POTENTIAL — PHASE 2	McGILL HOFFMANN	1 *	151.3
643	STRUCTURE OF STATES IN THE OXYGEN ISOTOPES VIA MEASUREMENTS OF THE SPIN DEPOLARIZATION AND SPIN-ROTATION OBSERVABLES	AAS HYNES	1 * 2 *	20.0 325.0
644	TESTS OF THE POLARIZATION-ANALYZING POWER EQUALITY IN ELASTIC SCATTERING OF INTERMEDIATE-ENERGY PROTONS FROM NUCLEI	IGO	1	0.0
649	$^{9}Be(p,\pi^{\pm})$ REACTION AT 650 MeV	HOISTAD	1 * 2	85.9 0.0
654	MEASUREMENT OF THE SPIN-ROTATION PARAMETER Q FOR 800-MeV p + ^{16}O, ^{40}Ca, AND ^{208}Pb ELASTIC SCATTERING	HOFFMANN	1 *	400.0
658	STUDY OF THE SPIN-FLIP PROBABILITY FOR ELASTIC AND INELASTIC SCATTERING FROM ODD-MASS NUCLEI	SEESTROM-MORRIS CAREY MOSS DEHNHARD	1	0.0
660	MEASUREMENT OF POLARIZATION PARAMETERS FOR M1 TRANSITIONS IN THE $^{90}Zr(p,p')^{90}Zr^*$ AND $^{116}Sn(p,p')^{116}Sn^*$ REACTIONS AT 500 MeV	GLASHAUSSER	1	156.0
663	ELASTIC SCATTERING OF POLARIZED PROTONS FROM ^{3}H AND ^{3}He AT INTERMEDIATE ENERGIES	IGO BLESZYNSKI	1 *	205.0
666	THE $^{12}C(p,p'\pi)^{12}C$ REACTION AND THE SEARCH FOR COHERENT ISOBAR-HOLE RESONANCES	GLASHAUSSER WHITTEN	1	0.0
669	INVESTIGATION OF THE N = 28 NEUTRON SHELL CLOSURE BY ELASTIC SCATTERING OF 800-MeV POLARIZED PROTONS	SHERA	1	0.0
670	CONTINUATION OF GIANT RESONANCE STUDIES AT THE HRS	MOSS CAREY ADAMS	1 *	116.0
685	SPIN CORRELATIONS IN THE REACTION $\vec{p}(\vec{d},d)\vec{p}$ AT 500 MeV	BLESZYNSKI IGO	1 2	447.0 0.0

Exp. No.	Title	Spokesman	Phase No. *=Complete	Beam Hours
686	DETERMINATION OF NEUTRON TRANSITION DENSITIES IN ^{16}O AND ^{208}Pb BY INELASTIC SCATTERING OF ~400-MeV PROTONS	HINTZ	1 *	105.0
687	MEASUREMENT OF THE SPIN-ROTATION PARAMETERS IN ^{208}Pb AND IN ^{40}Ca AT 400 MeV	AAS IGO	1 *	134.0
709	MEASUREMENTS OF A_{NN}, A_{SS}, AND A_{SL} IN THE COULOMB INTERFERENCE REGION AT 650 AND 800 MeV	GAZZALY PAULETTA TANAKA	1 2	0.0 522.0
712	INELASTIC PROTON SCATTERING ON ^{48}Ca AND ^{50}Ti — AN ATTEMPT TO IDENTIFY MESONIC EFFECTS AS THE CAUSE OF M1 QUENCHING	SEGEL COMFORT	1	0.0
718	ENERGY DEPENDENCE OF THE TWO-NUCLEON EFFECTIVE INTERACTION	KELLY HYNES	1 *	143.0
720	RECOILLESS DELTA PRODUCTION IN THE REACTION $^{13}C(p,d)^{12}C\Delta$	MORRIS McGILL	1 * 2 *	218.0 140.0
722	MEASUREMENT OF CROSS SECTIONS AND ANALYZING POWERS FOR ELASTIC AND INELASTIC SCATTERING OF 400-500-MeV PROTONS FROM ^{14}C	HARVEY SEESTROM-MORRIS	1	0.0
736	STUDIES OF MULTIPLE-SCATTERING THEORY, THE EFFECTIVE INTERACTION AND Δ-HOLE INTERMEDIATE STATES IN 300-MeV p-NUCLEUS ELASTIC SCATTERING	HOFFMANN	1 2	0.0 0.0
740	LARGE-ANGLE ELASTIC SCATTERING OF PROTONS FROM ^{90}Zr AND ^{208}Pb	AAS BLESZYNSKI IGO	1	0.0
741	INVESTIGATION OF THE LONGITUDINAL-SPIN RESPONSE OF ^{208}Pb AND IMPLICATIONS OF SPIN-TRANSFER FORM FACTORS FOR NONNUCLEON DEGREES OF FREEDOM IN NUCLEI	CAREY McCLELLAND	1 *	189.0
758	TO CATCH A DEMON. . .	SETH	1	0.0
760	PROTON ELASTIC SCATTERING ON ^{40}Ca AND ^{208}Pb	HOFFMANN	1 *	44.0
761	Q MEASUREMENTS AT 650 MeV ON ^{40}Ca	IGO	1 * 2	65.0 0.0
766	ASYMMETRY MEASUREMENT OF THE $p\text{-}^{9}Be \rightarrow d\pi X$ REACTION AT 800 MeV	HOISTAD	1 *	89.0
768	DEVELOPMENT OF 0° CAPABILITIES AT THE HRS FACILITY	McCLELLAND CAREY SEESTROM-MORRIS	1	0.0
774	EXCITATION OF GIANT MULTIPOLE RESONANCES IN sd-SHELL NUCLEI VIA MEDIUM-ENERGY PROTON INELASTIC SCATTERING	BERTRAND	1	0.0
775	SEARCH FOR M1 RESONANCES IN HEAVY NUCLEI USING SMALL-ANGLE PROTON SCATTERING	MOSS HINTZ	1	0.0

Exp. No.	Title	Spokesman	Phase No. *=Complete	Beam Hours
784	CROSS SECTION AND ANALYZING POWER MEASUREMENTS FOR THE (p,d) REACTIONS ON ^{16}O, ^{56}Fe, AND ^{90}Zr	OHNUMA WHITTEN	1	0.0
785	ELASTIC SCATTERING OF POLARIZED PROTONS FROM ^{3}H AT INTERMEDIATE ENERGY	AZIZI BLESZYNSKI	1	0.0
786	STUDY OF ISOSCALAR M(1) EXCITATIONS IN LIGHT NUCLEI BY PROTON INELASTIC SCATTERING	HINTZ	1	0.0
790	I = 1 NN INELASTIC CROSS SECTIONS AND AND FIRST MEASUREMENTS OF T_{20} FOR THE $pp \rightarrow d\pi^{+}$ REACTION AT 800 AND 650 MeV	PAULETTA GAZZALY TANAKA	1	0.0
795	A PRECISION TEST OF CHARGE INDEPENDENCE	SETH	1	0.0
799	LARGE-MOMENTUM TRANSFER MEASUREMENTS OF A_Y FOR 800-MeV p + ^{208}Pb ELASTIC SCATTERING	BLESZYNSKI WHITTEN	1	0.0
801	A MEASUREMENT OF THE WOLFENSTEIN PARAMETERS FOR $^{48}Ca(p,p')^{48}Ca(1^{+}, 10.2\ MeV)$	JONES McCLELLAND IGO BLESZYNSKI	1	0.0
803	CROSS-SECTION AND ANALYZING-POWER MEASUREMENTS IN THE M1,M2 REGION IN ^{90}Zr AND ^{88}Sr AT 318 MeV	GLASHAUSSER McCLELLAND NANDA	1	0.0
819	II. ELASTIC SCATTERING OF POLARIZED PROTONS FROM ^{3}H AT INTERMEDIATE ENERGY	AZIZI BLESZYNSKI IGO	1	0.0
837	MEASUREMENT OF SPIN-FLIP CROSS SECTIONS UP TO 40-MeV EXCITATION IN ^{58}Ni AND ^{90}Zr	GLASHAUSSER NANDA	1	0.0
844	MEASUREMENT OF A_{NN}, A_{SS}, AND A_{LS} FOR THE REACTION $\vec{p}\,\vec{p} \rightarrow p + n + \pi^{+}$ AT 800 MeV	PAULETTA GAZZALY TANAKA	1	0.0
846	NN → NNπ: CROSS SECTIONS AND ANALYZING POWERS FOR THE 800-MeV $\vec{p}p \rightarrow \pi^{+}(np)$ AND $\vec{p}n \rightarrow \pi^{-}(pp)$ INCLUSIVE REACTIONS	BHATIA GLASS	1	0.0
851	SEARCH FOR RECOIL-FREE Δ PRODUCTION AND HIGH-SPIN STATES IN THE $^{208}Pb(p,t)^{206}Pb$ REACTION AT $E_p \simeq 400$ MeV	HINTZ	1	0.0
855	MEASUREMENT OF ^{206}Pb-^{208}Pb GROUND-STATE NEUTRON DENSITY DIFFERENCE	HINTZ	1	0.0
864	STUDY OF DEEPLY BOUND HOLE STATES IN THE TIN ISOTOPES VIA THE $(\vec{p},d)$ REACTION	SAHA SETH	1	0.0
865	SPIN-ROTATION MEASUREMENT ON ^{4}He AT 320, 500, AND 800 MeV	AAS BLESZYNSKI IGO	1	0.0
867	MEASUREMENT OF ISOVECTOR QUADRUPOLE TRANSITION DENSITIES IN THE PALLADIUM ISOTOPES	SAHA SETH	1	0.0

ISOTOPE PRODUCTION AND RADIATION-EFFECTS FACILITY (ISORAD)

Exp. No.	Title	Spokesman	Phase No. *=Complete	Beam Hours
184	PRODUCTION OF ^{82}Sr	O'BRIEN	1 *	0.0
210	ISOTOPE PRODUCTION FACILITY IRRADIATION VANADIUM, MOLYBDENUM, AND LANTHANUM TARGETS	O'BRIEN	1 *	0.0
211	NEUTRON IRRADIATION OF COPPER SINGLE CRYSTALS	GREEN	1 *	0.0
267	PREPARATION OF RADIOISOTOPES FOR MEDICINE AND THE PHYSICAL SCIENCES USING THE LAMPF ISOTOPE PRODUCTION FACILITY	O'BRIEN	1 1 1	643.0 19889.3 709.0
407	THE EFFECT OF DISLOCATION VIBRATION ON VOID GROWTH IN METALS DURING IRRADIATION	SOMMER PHILLIPS	3	0.0
725	THE EFFECT OF RARE-EARTH ADDITIONS ON RADIATION DAMAGE IN ALLOY HT-9 (FERRITIC/MARTENSITIC) ALLOY STEEL	DAVIDSON WECHSLER SOMMER	1	0.0
765	800-MeV PROTON IRRADIATION OF MATERIALS FOR THE SIN BEAM STOP	BROWN	1 1 1	692.0 0.0 570.0

LOW-ENERGY PION (LEP)

Exp. No.	Title	Spokesman	Phase No. *=Complete	Beam Hours
2	TOTAL PION CROSS SECTIONS	JAKOBSON	2 *	663.4
25	PION DOUBLE-CHARGE-EXCHANGE REACTION	BURMAN	1 * 2 * 3 *	0.0 681.2 268.2
28	STUDIES OF THE π^+,π^0 REACTION	YAVIN	1 *	195.0
29	ELASTIC SCATTERING OF π^+ AND π^- AT 10-30 MeV	PREEDOM	1 * 2 *	0.0 0.0
35	CLUSTER EFFECTS IN NUCLEAR PION CAPTURE	ZIOCK	1 *	297.5
50	RADIATIVE PION CAPTURE IN LIGHT NUCLEI	CROWE ROWE	1 * 2 *	0.0 460.3
54	ELASTIC SCATTERING OF MESONS IN THE ENERGY RANGE 20-60 MeV	PREEDOM	1 * 2 *	264.6 707.4
67	DEVELOPMENT OF PION BEAM-MONITORING TECHNIQUES	DROPESKY	1 * 2 *	0.0 87.5
79	CALIBRATION OF THE PION BEAM TRANSPORT SYSTEMS AND A PION BEAM MONITOR	PHILLIPS	1 *	0.0
96	SCATTERING OF 20-50-MeV $\pi^{\pm}$ BY HYDROGEN AND DEUTERIUM	NAGLE	1 * 2 *	0.0 728.0
102	EXCITATION FUNCTIONS AND ANGULAR DISTRIBUTION RECOIL STUDIES OF SIMPLE PION-INDUCED NUCLEAR REACTIONS	MARKOWITZ	1 *	0.0

Exp. No.	Title	Spokesman	Phase No. *=Complete	Beam Hours
121	PION-INDUCED NUCLEAR REACTIONS	SEGEL	1 *	0.0
			2 *	150.0
122	PIONIC ATOM X RAYS AND NUCLEAR DISTRIBUTIONS	KUNSELMAN	1 *	0.0
123	NUCLEAR- STRUCTURE EFFECTS IN PION-INDUCED NUCLEAR REACTIONS	KAROL	5 *	25.0
131	A STUDY OF THE $\pi^+ + d \rightarrow p + p$ REACTION AT PION ENERGIES 10-60 MeV	PREEDOM	1 *	0.0
			2 *	260.0
140	STUDY OF THE ($\pi^{\pm}$,d) REACTION WITH AN INTRINSIC GERMANIUM DETECTOR	BARNES	1 *	0.0
			2 *	385.0
			3 *	0.0
144	SEARCH FOR THE C-VIOLATING DECAY $\pi^0 + 3\gamma$	HIGHLAND MACEK	1 *	333.0
162	STUDIES OF THE (π^+,π^0) REACTION ON LIGHT ELEMENTS	YAVIN ALSTER	1 *	0.0
164	PION TOTAL CROSS-SECTION MEASUREMENTS WITH AN ORIENTED ^{165}Ho TARGET	FISHER MARSHAK	1 *	88.0
170	STUDY OF REACTION $^{13}C(\pi^+,\pi^0)^{13}N$ (GROUND STATE)	ALSTER	1 *	0.0
180	ELASTIC AND INELASTIC π^+ NUCLEUS SCATTERING AT 25, 50, AND 75 MeV	EISENSTEIN	1 *	0.0
			2 *	191.3
181	MEASUREMENTS OF THE $\pi^- p \rightarrow \pi^0 n$ ANGULAR DISTRIBUTION AT LOW ENERGIES AND CALIBRATION OF THE π^0 SPECTROMETER	ALSTER BOWMAN	1 *	346.0
			2 *	859.2
190	A PRECISION MEASUREMENT OF THE $\pi^- - \pi^0$ MASS DIFFERENCE	ZIOCK	1	133.0
191	π^+ NUCLEUS INELASTIC SCATTERING TO GIANT RESONANCES	HALPERN	1 *	0.0
			2 *	292.7
			3 *	484.4
			4 *	284.4
209	PION INTERACTIONS IN NUCLEAR EMULSIONS	BRADBURY ALLRED	1 *	0.0
234	A STUDY OF THE INELASTIC PION SCATTERING REACTION AT PION ENERGIES 10-100 MeV	GOTOW	1 *	436.3
247	DISTRIBUTION OF PRODUCTS FROM INTERACTIONS OF STOPPED π^- WITH SEVERAL MEDIUM- AND HEAVY-MASS NUCLEI	ORTH	1 *	35.6
			2 *	59.5
284	MEASUREMENT OF THE $^3He(\pi^-,\pi^0)^3He$ ANGULAR DISTRIBUTION	COOPER WHITNEY	1	209.0
			2 *	0.0
293	STUDY OF THE DOMINANT REACTION MODES FOR PIONS INTERFACING WITH COMPLEX NUCLEI	SEGEL	1 *	151.0
295	STUDY OF THE PION-DEUTERON SINGLE-CHARGE-EXCHANGE REACTION $d(\pi^-,\pi^0)2n$	BOWMAN MOINESTER	1	75.8

Exp. No.	Title	Spokesman	Phase No. *=Complete	Beam Hours
299	AN INVESTIGATION OF THE REACTION ($\pi^+,\pi^+ + p$)	ZIOCK	1 *	0.0
			2 *	960.1
			3 *	0.0
303	A SURVEY OF PION SINGLE-CHARGE-EXCHANGE SCATTERING USING BACK-ANGLE GAMMA SPECTROSCOPY	JACKSON	1 *	152.8
			2 *	290.9
			3 *	304.0
315	HIGH-RESOLUTION STUDY OF THE (π^+,2p) REACTION	WHARTON	1 *	0.0
			2 *	338.1
			3 *	862.4
316	π^- NUCLEUS ELASTIC SCATTERING BETWEEN 20 AND 50 MeV	SETH BURLESON	1 *	699.6
			2 *	0.0
320	A COMPARISON OF (π^+,xn) AND (π^-,xn) REACTIONS	CHURCH	3 *	33.0
			4	0.0
322	SYSTEMATIC STUDY OF PION-INELASTIC SCATTERING AT ENERGIES BELOW 100 MeV	BERTRAND GOTOW	1 *	877.1
324	PRECISION MEASUREMENT OF RATIOS OF CERTAIN LIGHT ELEMENT PION EXCITATION FUNCTIONS	HALPERN	1 *	118.6
333	$\pi^\pm$ NUCLEAR ELASTIC SCATTERING AT ENERGIES BETWEEN 50 AND 100 MeV	GOTOW	1 *	512.2
348	STUDY OF GIANT RESONANCES WITH RADIATIVE PION CAPTURE ON MEDIUM-Z NUCLEI AT LEP	CROWE	1 *	761.7
349	NUCLEAR REACTIONS OF ^{127}I WITH PIONS	PORILE	2 *	25.0
			3 *	28.0
350	STUDY OF PION-ABSORPTION MECHANISMS IN NUCLEI	SEGEL SCHIFFER	1 *	225.8
388	LOW-ENERGY PION ELASTIC SCATTERING FROM THE PROTON AND DEUTERON AT 180°	HOLT	1 *	392.2
393	ANGULAR DISTRIBUTION MEASUREMENTS OF THE PION SINGLE-CHARGE-EXCHANGE REACTION ON ^{13}C	ALSTER MOINESTER	1	279.8
401	STUDY OF THE ISOBARIC ANALOG CHARGE-EXCHANGE REACTION ^{15}N(π^+,π^0)^{15}O	BOWMAN COOPER	1 *	357.1
			2	0.0
412	SEARCH FOR ANALOG STATE TRANSITIONS IN (π^+,π^0) REACTIONS ON ^{7}Li, ^{27}Al, ^{93}Zr, ^{120}Sn, AND ^{208}Pb AND FOR COLLECTIVE ISOVECTOR STATES IN THE (π^-,π^0) REACTION ON ^{93}Zr	BAER BOWMAN CVERNA	1 *	270.6
			2 *	224.0
415	TWO-NUCLEON-OUT PRODUCTS FROM STOPPED π^- INTERACTIONS	ORTH	1 *	121.6
416	STUDY OF FAST PION-INDUCED FISSION OF URANIUM	DROPESKY	3 *	15.0
			4 *	11.0
465	RADIOCHEMICAL STUDY OF PION SINGLE CHARGE EXCHANGE	RUNDBERG	1 *	46.0
			2	61.4
483	MEASUREMENT OF THE ANGULAR DEPENDENCE OF TENSOR POLARIZATION IN THE ^{2}H(π^+,π^+)^{2}H REACTION	HOLT	1 *	478.3

Exp. No.	Title	Spokesman	Phase No. * = Complete	Beam Hours
487	MEASUREMENT OF THE NUCLEAR RESONANCE EFFECT IN SOME PIONIC ATOMS	REIDY LEON	1 *	202.8
523	STUDY OF $^{14}C(\pi^+,\pi^0)^{14}N$ REACTION	GOODMAN BAER	1 * 3 3	103.4 154.0 0.0
524	STUDY OF THE ISOVECTOR TERMS IN π-NUCLEUS INTERACTIONS WITH (π^+,π^0) REACTIONS ON $^{40,42,44,48}Ca$ AND $^{112,118,124}Sn$	BAER BOWMAN CVERNA	1 *	243.9
525	EXCITATION OF ISOVECTOR TRANSITIONS WITH PION SINGLE CHARGE EXCHANGE ON ^{12}C	KING MOINESTER	1	24.2
527	STUDY OF THE $^{10}B(\pi^-,\pi^0)^{10}B$ REACTION	BAER BOWMAN	1	0.0
536	EFFICIENCY MEASUREMENTS FOR π^+ IDENTIFICATION IN THE PLASTIC BALL DETECTOR	GUTBROD	1 *	106.7
541	A SEARCH FOR NUCLEAR CRITICAL OPALESCENCE USING THE REACTION $^{40}Ca(\pi^+,2\gamma)$	COOPER	1 *	773.7
543	A PRODUCT RECOIL STUDY OF THE $(\pi^\pm,\pi^\pm n)$ REACTION	CARETTO	1 2	7.8 51.5
544	SEARCH FOR A FAST FISSION PROCESS	WILHELMY	1 * 2 *	48.0 76.0
553	STUDY OF TARGET THICKNESS EFFECTS IN THE CROSS-SECTION MEASUREMENT OF THE PION SINGLE-CHARGE-EXCHANGE REACTION $^{13}C(\pi^+,\pi^0)^{13}N$ (g.s.) FROM 50 TO 350 MeV	RUNDBERG	1 * 2 * 3	69.0 14.0 100.0
557	EXPOSURE, IN A PARASITIC MODE, OF A 3-cm BY 3-cm BY 1-cm STACK OF SOLID-TRACK DETECTORS TO A π^- BEAM	COWSIK	1 *	0.0
561	$\pi^\pm$-NUCLEAR ELASTIC SCATTERING AT ENERGIES BETWEEN 30 AND 80 MeV	BLECHER OBENSHAIN HYNES	1 * 2 *	241.0 294.0
567	A STUDY OF THE $\pi^+ + d \rightarrow p + p$ REACTION AT PION ENERGIES 5-200 MeV	GOTOW MINEHART RITCHIE	1 *	503.0
576	STUDY OF THE $(\pi^+,2p)$ AND $(\pi^\pm,2p)$ REACTIONS ON THE ISOTOPIC PAIRS ^{16}O-^{18}O AND ^{40}Ca-^{48}Ca	ROOS PREEDOM CHANT	1	246.0
595	AN ON-LINE GAMMA-RAY STUDY OF PION-INDUCED SINGLE-NUCLEON-REMOVAL REACTIONS ON ^{13}C AND ^{48}Ca	ORTH VIEIRA	1	34.0
601	DETERMINATION OF ISOSCALAR AND ISOVECTOR TRANSITION RATES FOR LOW-LYING COLLECTIVE STATES IN ^{90}Zr and ^{208}Pb BY π^+ AND π^- INELASTIC SCATTERING	HINTZ	1	414.0
607	STUDY OF ISOVECTOR GIANT RESONANCES WITH PION CHARGE EXCHANGE	ALSTER BAER BOWMAN	1 * 2 * 3	259.5 774.0 0.0

Exp. No.	Title	Spokesman	Phase No. * = Complete	Beam Hours
511	EXCITATION FUNCTIONS OF THE FOUR $^{130}Te(\pi^{\pm},\pi^{\pm}n)$ REACTIONS	HOGAN	1	0.0
650	A SEARCH FOR NEUTRINO MIXING VIA NONEXPONENTIAL $\pi \rightarrow \mu\nu$ DECAY	BOWMAN MOINESTER	1 *	249.0
675	NUCLEAR DISTRIBUTIONS FROM THE STUDY OF THE 2p STATES OF PIONIC ATOMS	KUNSELMAN	1	0.0
676	STUDY OF PION ABSORPTION ON ^{58}Ni AT $T_\pi = 160$ MeV	CHANT REDWINE ROOS	1	557.0
688	STUDY OF THE MASS AND ENERGY DEPENDENCE OF LOW-ENERGY PION SINGLE CHARGE EXCHANGE	LEITCH COOPER	1	157.0
732	HEAVY ELEMENT FISSION INDUCED BY ENERGETIC PIONS	PETERSON RISTINEN	1 *	0.0
735	PION-INDUCED EMISSION OF LIGHT NUCLEAR FRAGMENTS	KAUFMAN	1	173.0
738	ANALOG STATE CROSS SECTIONS OF THE $^{92,96,100}Mo(\pi^+,\pi^0)$ REACTION	COMFORT	1	0.0
767	$\pi^{\pm}$ DEUTERON ELASTIC SCATTERING AT THREE ENERGIES BETWEEN 30 AND 80 MeV	GOTOW	1	0.0
776	STUDY OF THE $^{16}O(\pi^+,\pi^0p)$ REACTION	GILAD PIASETZKY ALSTER	1	0.0
789	TWO-NUCLEON-OUT PRODUCTS FOLLOWING THE ABSORPTION OF 10-MeV π^+ IN ^{26}Mg AND ^{74}Ge	OHKUBO	1	100.0
794	$\pi^{\pm}$-NUCLEAR ELASTIC SCATTERING AT ENERGIES BETWEEN 30 AND 65 MeV	BLECHER HYNES OBENSHAIN	1	452.0
798	FISSION INDUCED BY ENERGETIC $\pi^{\pm}$ PARTICLES	HICKS PETERSON RISTINEN	1	61.0
808	0° EXCITATION FUNCTION FOR $\pi^- p \rightarrow \pi^0 n$	COOPER FITZGERALD	1	71.0
811	STUDY OF UNNATURAL-PARITY STATES IN NUCLEI USING LOW-ENERGY PIONS	RITCHIE	1	0.0
813	PION CHARGE ASYMMETRIES FOR ^{13}C AT LOW BEAM ENERGIES ON THE LEP SPECTROMETER	KRAUSHAAR PETERSON	1	0.0
814	$\pi^{\pm}$-NUCLEAR ELASTIC SCATTERING FROM NICKEL AND TIN ISOTOPES AT ENERGIES BETWEEN 30 AND 80 MeV	BLECHER HYNES	1	0.0
822	INELASTIC π^+ AND π^- SCATTERING ON ^{48}Ca AT 50 AND 75 MeV	KRAUSHAAR	1	0.0
824	A STUDY OF LOW-ENERGY PION SCATTERING AS A PROBE OF NUCLEAR MAGNETIC DIPOLE EXCITATION	JACKSON	1	0.0

Exp. No.	Title	Spokesman	Phase No. *=Complete	Beam Hours
828	TOTAL AND DIFFERENTIAL CROSS SECTIONS FOR $\pi^+ \rightarrow$ pp BELOW 20 MeV	GOTOW MINEHART RITCHIE	1	0.
829	A MEASUREMENT OF THE WIDTH AND POSITION OF THE Δ^{++} RESONANCE IN ^{6}Li AND ^{12}C	ZIOCK	1	0.0
848	IN-FLIGHT ABSORPTION OF LOW-ENERGY NEGATIVE PIONS	OHKUBO	1	0.0
850	STUDY OF THE MASS AND ENERGY DEPENDENCE OF LOW-ENERGY PION SINGLE CHARGE EXCHANGE AT 0°	IROM LEITCH	1	0.0
857	INELASTIC PION SCATTERING FROM ^{16}O AT T_π = 50 MeV	BLAND MOORE	1	0.0
860	INELASTIC $\pi^\pm$ SCATTERING TO EXCITED 0° STATES AT ENERGIES BETWEEN 30 AND 80 MeV	PREEDOM WHISNANT	1	0.0
871	COINCIDENT NUCLEAR γ-RAY AND PIONIC X-RAY STUDY OF π ABSORPTION AT REST ON ^{12}C	LIEB FUNSTEN	1	0.0

LINE B (LB)

Exp. No.	Title	Spokesman	Phase No. *=Complete	Beam Hours
179	DIFFERENTIAL PRODUCTION CROSS SECTIONS OF MULTIPLY CHARGED FRAGMENTS IN PROTON- AND PION-INDUCED SPALLATION OF LIGHT NUCLEI	BOWMAN	1 *	1341.4

LINE X BEAM STOP (LX-BS)

Exp. No.	Title	Spokesman	Phase No. *=Complete	Beam Hours
184	PRODUCTION OF ^{82}Sr	O'BRIEN	1 *	0.0

NEUTRINO AREA (Neutrino-A)

Exp. No.	Title	Spokesman	Phase No. *=Complete	Beam Hours
31	A NEUTRINO EXPERIMENT TO TEST MUON CONSERVATION	NEMETHY	1 * 2 *	6713.2 1097.4
148	NEUTRINO-ELECTRON ELASTIC SCATTERING AT LAMPF (A FEASIBILITY STUDY)	CHEN REINES	1 * 2 *	0.0 1132.0
225	A STUDY OF NEUTRINO-ELECTRON ELASTIC SCATTERING	CHEN	1 1	709.0 3213.0
254	FEASIBILITY STUDY FOR THE MEASUREMENT OF THE INELASTIC NEUTRINO-SCATTERING CROSS SECTIONS IN ^{39}K	FIREMAN	1 *	1026.0

Exp. No.	Title	Spokesman	Phase No. *=Complete	Beam Hours
638	A SEARCH FOR OSCILLATIONS USING MUON-NEUTRINOS	DOMBECK	1	0.0
645	A SEARCH FOR NEUTRINO OSCILLATIONS AT LAMPF	LING	1	0.0
		ROMANOWSKI	2	0.0
647	A NEUTRON OSCILLATION EXPERIMENT AT LAMPF	ELLIS	1	0.0
708	A MEASUREMENT OF THE DEPOLARIZATION, THE POLARIZATION, AND THE POLARIZATION ROTATION PARAMETERS AND THE ANALYZING POWER FOR THE REACTION $\vec{p}p \rightarrow \vec{p}\pi^+ n$	HOLLAS	3	0.0
764	SEARCH OF NEUTRINO OSCILLATIONS AND MEASUREMENT OF CROSS SECTIONS USING A LIQUID SCINTILLATOR DETECTOR IN A MUON-NEUTRINO BEAM AT THE LINE D STUB	DOMBECK KRUSE	1	0.0
823	DEVELOPMENT OF AN (n,p) REACTION CAPABILITY AT AREA B OR BEAM LINE D	KING LISOWSKI BOWMAN SHEPARD	1	0.0

PROTON IRRADIATION PORT (PIP)

Exp. No.	Title	Spokesman	Phase No. *=Complete	Beam Hours
298	MEASUREMENT OF LIGHT OUTPUT vs ENERGY FOR VARIOUS SCINTILLATORS	SELOVE	1 *	0.0
302	800-MeV PROTON IRRADIATION OF AN ALUMINUM SAMPLE	GREEN	1 *	326.6
327	PIP, PROTON IRRADIATION PORT	WILSON	1 *	16.9

PION PARTICLE PHYSICS (P^3)

Exp. No.	Title	Spokesman	Phase No. *=Complete	Beam Hours
32	PRECISION MEASUREMENT OF THE PROCESSES $\pi^\pm \rightarrow \pi^0 + e^\pm + \nu$	McFARLANE	1 *	0.0
		MACEK	2 *	1092.2
34	ELASTIC SCATTERING OF $\pi^\pm$ ON DEUTERONS	MINEHART	1 *	0.0
58	MEASUREMENT OF $\pi^- + p \rightarrow \gamma + n$	NEFKENS	1 *	0.0
		FITZGERALD		
67	DEVELOPMENT OF PION BEAM-MONITORING TECHNIQUES	DROPESKY	1 *	0.0
			2 *	220.2
			3	6.3
79	CALIBRATION OF THE PION BEAM TRANSPORT SYSTEMS AND A PION BEAM MONITOR	PHILLIPS	1 *	0.0

Exp. No.	Title	Spokesman	Phase No. *—Complete	Beam Hours
80	FORWARD ELASTIC SCATTERING OF π^+ AND π^- FROM ^{12}C, ^{13}C, ^{16}O, ^{40}Ca, AND ^{208}Pb	PHILLIPS	1 * 2 *	0.0 528.8
82	INVESTIGATION OF PION-INDUCED REACTIONS ON LIGHT ELEMENTS WITH THREE PARTICLES IN THE FINAL STATE	PHILLIPS	1 *	425.3
90	A TEST OF THE REVERSAL INVARIANCE IN SINGLE-PION PHOTOPRODUCTION THROUGH A STUDY OF RECIPROCITY IN THE REACTIONS $\pi^- {}^3He \leftrightarrows \gamma T$ AND $\pi^+ T \leftrightarrows {}^3He\gamma$	SHERMAN SHIVELY GLODIS SPENCER WADLINGER NEFKENS	1 * 2 *	0.0 806.9
99	MEASUREMENT OF THE CROSS SECTION FOR $\pi^- + p \rightarrow \pi^- + \pi^+ + n$ WITH A MAGNETIC SPECTROMETER	REBKA GRAM	1 * 2 *	0.0 646.0
102	EXCITATION FUNCTIONS AND ANGULAR DISTRIBUTION RECOIL STUDIES OF SIMPLE PION-INDUCED NUCLEAR REACTIONS	MARKOWITZ	1 *	0.0
103	SPALLATION YIELD DISTRIBUTIONS FOR PION INTERACTIONS WITH COMPLEX NUCLEI	HUDIS	1 * 2 *	0.0 295.7
104	PROPOSAL FOR LAMPF EXPERIMENT: STUDIES OF THE PROTON- AND PION-INDUCED FISSION OF MEDIUM-MASS NUCLIDES	PATE	1 * 2 *	0.0 118.7
118	FRAGMENT EMISSION FROM PION INTERACTIONS WITH COMPLEX NUCLEI	PORILE	1 * 2 *	0.0 97.0
119	CROSS SECTIONS OF SIMPLE NUCLEAR REACTIONS INDUCED BY π MESONS	KAUFMAN	1 * 2 *	27.8 186.8
120	MEASUREMENT OF THE POLARIZATION ASYMMETRY AND THE DIFFERENTIAL CROSS SECTION OF PION-NUCLEON CHARGE EXCHANGE FROM 160 TO 500 MeV	NEFKENS FITZGERALD	1 * 2 * 3 *	870.2 90.3 1543.0
121	PION-INDUCED NUCLEAR REACTIONS	SEGEL	1 * 2 *	0.0 0.0
123	NUCLEAR STRUCTURE EFFECTS IN PION-INDUCED NUCLEAR REACTIONS	KAROL	1 * 2 * 3 * 4 * 5	0.0 75.0 135.1 0.0 21.0
144	SEARCH FOR THE C-VIOLATING DECAY $\pi^0 + 3\gamma$	HIGHLAND MACEK	2 *	602.1
153	INVESTIGATION OF NUCLEAR GAMMA RAYS RESULTING FROM IN-FLIGHT PION AND PROTON REACTIONS	EISENSTEIN	1 *	0.0
154	ELASTIC SCATTERING OF π^+ AND π^- FROM THE HELIUM ISOTOPE	MINEHART McCARTHY	1 * 2 *	7.2 316.0
181	MEASUREMENTS OF THE $\pi^- p \rightarrow \pi^0 n$ ANGULAR DISTRIBUTION AT LOW ENERGIES AND CALIBRATION OF THE π^0 SPECTROMETER	ALSTER BOWMAN	2 *	204.3

Exp. No.	Title	Spokesman	Phase No. * = Complete	Beam Hours
195	NUCLEAR RESONANCE EFFECT IN PIONIC ATOMS	LEON REIDY	2 * 3 *	0.0 163.1
201	THE $\pi^+ d \rightarrow 2d$ REACTION AT 100-500 MeV	MINEHART	1 *	338.0
214	PIONIC X-RAY ABSOLUTE YIELDS AS A FUNCTION OF Z	HARGROVE LEON	1 *	199.1
221	PRECISION MEASUREMENT OF THE DECAY RATE FOR THE DALITZ DECAY MODE OF THE π^0 MESON	HOFFMAN	1 *	351.5
222	MEASUREMENT OF THE DECAY RATE FOR $\pi^0 \rightarrow e^+ e^-$	MISCHKE	1 *	945.8
247	DISTRIBUTION OF PRODUCTS FROM INTERACTIONS OF STOPPED π^- WITH SEVERAL MEDIUM- AND HEAVY-MASS NUCLEI	ORTH	2 *	28.0
248	STUDY OF THE (π,π), (π,Δ), (π,B_Δ), AND (π,n) REACTIONS IN ^{3,4}He AND ^{6}Li BY MEASURING RECOIL SPECTRA	KALLNE McCARTHY GUGELOT	1 *	674.4
283	CHARGED-PARTICLE EMISSION FOLLOWING μ^- CAPTURE	KRANE SHARMA	1 *	31.0
286	PROTON AXIAL TOMOGRAPHY	HANSON	1 *	345.5
304	STUDY OF THE AUGER PROCESS IN PIONIC ATOMS	LEON MAUSNER	1 *	78.6
309	INCLUSIVE π^+ AND π^- DOUBLE CHARGE EXCHANGE ON ^{16}O AND ^{40}Ca	REBKA	1 *	594.0
319	DETERMINING THE MECHANISM FOR MULTINUCLEON AND CLUSTER REMOVAL IN 200-MeV π-NUCLEAR INTERACTIONS	LIND	1 *	283.0
320	A COMPARISON OF (π^+,xn) AND (π^-,xn) REACTIONS	CHURCH	1 * 2 *	57.8 170.1
337	MEASUREMENT OF THE CROSS SECTION FOR $\pi^- p \rightarrow \pi^- \pi^+ n$ AT 200 AND 229 MeV	REBKA GRAM	1 *	999.8
349	NUCLEAR REACTIONS OF ^{127}I WITH PIONS	PORILE	1 * 2 * 3 *	74.5 55.2 9.0
358	ELASTIC SCATTERING OF PIONS FROM DEUTERIUM	MINEHART	1 *	514.0
363	MEASUREMENT OF $\pi^\pm + p$ ELASTIC SCATTERING	SADLER NEFKENS	1 * 2 *	700.5 844.5
373	A COMPARISON OF RESIDUAL NUCLEI YIELDS FROM π^- ABSORPTION IN ^{112}Cd (GROUND STATE) AND ^{112}Cd (FIRST EXCITED STATE)	REIDY LEON	1 *	94.1
390	A STUDY OF INCLUSIVE INELASTIC PION SCATTERING NEAR THE $\Delta(3/2,3/2)$ RESONANCE	JACKSON	1 *	453.0
394	APPLICATION OF PROTON-COMPUTED TOMOGRAPHY	HANSON	1 *	195.3

Exp. No.	Title	Spokesman	Phase No. * = Complete	Beam Hours
396	COMPARISON OF MEASURED PIONIC-ATOM CASCADE INTENSITIES WITH THEORETICAL INTENSITIES OBTAINED USING PARAMETERS FROM MUONIC-ATOM STUDIES	REIDY	1 *	110.5
400	SEARCH FOR THE RARE DECAY $\mu^+ \rightarrow e^+e^+e^-$	HOFFMAN	1 *	156.8
404	A KINEMATICALLY COMPLETE STUDY OF THE (π,π'p) REACTION ON ^{16}O ABOVE THE RESONANCE BY DETECTING PIONS AND PROTONS IN COINCIDENCE	HAMM SWENSON	1 *	401.5
416	STUDY OF FAST PION-INDUCED FISSION OF URANIUM	DROPESKY	1 * 2 * 3 * 4 *	141.0 17.0 26.2 0.0
455	HIGH-PRECISION STUDY OF THE μ^+ DECAY SPECTRUM	ANDERSON KINNISON	1 2	1739.3 95.0
458	THE EXCITATION FUNCTION FOR THE SINGLE-CHARGE-EXCHANGE REACTION $^{65}Cu(\pi^-,\pi^0)^{65}Ni$	KAUFMAN	1 *	80.4
459	CROSS-SECTION MEASUREMENTS OF THE $^{14}N(\pi^+,\pi^0)^{14}O$ (g.s.) REACTION	VIEIRA	1 *	96.0
465	RADIOCHEMICAL STUDY OF PION SINGLE CHARGE EXCHANGE	RUNDBERG	1 * 2	99.1 104.4
466	NUCLEAR CONFIGURATION OF INDIVIDUAL CORE-COUPLED STATES IN ^{209}Bi FROM INELASTIC $\pi^\pm$ SCATTERING	FUNSTEN PLENDL	1 *	219.6
500	FISSION FRAGMENT DISTRIBUTIONS IN FAST PION-INDUCED FISSION OF ^{238}U	RUNDBERG	1 * 2	72.2 0.0
513	π^+ QUASI-FREE SCATTERING FROM THE HELIUM ISOTOPES	McCARTHY MINEHART	1 * 2 *	0.0 557.7
543	A PRODUCT RECOIL STUDY OF THE $(\pi^\pm,\pi^\pm n)$ REACTION	CARETTO	1	96.5
553	STUDY OF TARGET THICKNESS EFFECTS IN THE CROSS-SECTION MEASUREMENT OF THE PION SINGLE-CHARGE-EXCHANGE REACTION $^{13}C(\pi^+,\pi^0)^{13}N$ (g.s.) FROM 50 TO 350 MeV	RUNDBERG	1 * 2 *	61.3 37.5
555	TOTAL CROSS-SECTION MEASUREMENTS OF THE SINGLE-CHARGE-EXCHANGE REACTION $^{12}C(\pi^+,\pi^0)^{12}N$ (g.s.)	IMANISHI VIEIRA	1 *	139.0
562	STUDY OF THE PION ABSORPTION MECHANISM THROUGH THE A(π,p)X REACTION AT T_π = 500 MeV	JACKSON SCHIFFER	1 *	428.0
564	STUDY OF SMALL-ANGLE $^4He(\pi^-,\pi^+)$ REACTION	McKEOWN	1 *	435.5
595	AN ON-LINE γ-RAY STUDY OF PION-INDUCED SINGLE-NUCLEON-REMOVAL REACTIONS ON ^{13}C AND ^{48}Ca	ORTH VIEIRA	1	89.0
603	SEARCH FOR DELTAS IN A COMPLEX NUCLEUS BY A RADIOCHEMICAL TECHNIQUE	TURKEVICH	2	13.0
611	EXCITATION FUNCTIONS OF THE FOUR $^{130}Te(\pi^\pm,\pi^\pm n)$ REACTIONS	HOGAN	1	8.5

Exp. No.	Title	Spokesman	Phase No. * = Complete	Beam Hours
617	A STUDY OF THE (3/2,3/2) RESONANCE IN LIGHT NUCLEI	ZIOCK	1	0.0
628	STUDY OF THE (π,πp) REACTION AND QUASI-FREE SCATTERING IN ^4He	JACKSON	1	0.0
673	MEASUREMENTS OF THE ANGULAR DEPENDENCE OF TENSOR POLARIZATION IN THE $^2H(\pi^+,\pi^+)^2H$ REACTION AT T_π = 180 AND 256 MeV	HOLT	1	634.0
674	MEASUREMENTS OF PION-NUCLEUS ELASTIC AND DOUBLE-CHARGE-EXCHANGE SCATTERING AT ENERGIES ABOVE 300 MeV	BURLESON MORRIS	1	0.0
682	SEARCH FOR DIBARYON RESONANCES IN THE REACTION $\pi D \rightarrow pnn$ AT P_π^- = 200 TO 600 MeV/c	IMAI GREENE	1	0.0
689	A. NEUTRON COUNTER CALIBRATION USING TAGGED NEUTRONS FROM THE REACTION $-\ ^-d \rightarrow nn$. B. FEASIBILITY STUDY: MEASUREMENTS OF THE DIFFERENTIAL CROSS SECTION FOR $-\ ^-d \rightarrow nn$ TO TEST CHARGE SYMMETRY AND ISOSPIN INVARIANCE	NEFKENS FITZGERALD	1 *	332.0
705	STUDY OF PION ABSORPTION IN ^3He ON AND ABOVE THE (3,3) RESONANCE	ASHERY	1	283.0
728	STUDY OF PION CHARGE-EXCHANGE MECHANISMS BY MEANS OF ACTIVATION TECHNIQUES	GIESLER	1	160.0
730	PION PRODUCTION IN PION-NUCLEON AND PION-NUCLEUS INTERACTIONS	SAGHAI PREEDOM DROPESKY	1 2	166.5 0.0
734	PION PRODUCTION IN PION-NUCLEUS COLLISIONS	PIASETZKY DiGIACOMO LICHTENSTADT	1	0.0
750	INCLUSIVE π^+ AND π^- DOUBLE CHARGE EXCHANGE ON ^4He	GRAM MATTHEWS REBKA	1	641.0
753	RECOILLESS Δ PRODUCTION IN THE REACTION $^{13}C(\pi^+,p)^{12}C\Delta$	AMANN MORRIS McGILL	1	0.0
783	PION-INDUCED PION PRODUCTION ON DEUTERONS	GRAM PIASETZKY REBKA LICHTENSTADT	1	622.0
804	MEASUREMENT OF THE ASYMMETRY PARAMETER IN $\pi^- + p \rightarrow \gamma + n$ USING A TRANSVERSE POLARIZED TARGET	NEFKENS	1	0.0
806	MEASUREMENT OF SPIN ROTATION PARAMETERS "A AND R" IN $\pi^+p \rightarrow \pi^+p$ AND $\pi^-p \rightarrow \pi^-p$	NEFKENS BRISCOE SADLER	1	0.0
807	AN ABSOLUTE CALIBRATION OF A PROTON POLARIMETER BETWEEN 90 AND 250 MeV	BRISCOE	1	0.0

Exp. No.	Title	Spokesman	Phase No. *=Complete	Beam Hours
820	PION-INDUCED PION PRODUCTION ON ^{3}He	PIASETZKY REBKA GRAM LICHTENSTADT	1	0.0
821	PION CHARGE EXCHANGE TO DELTA-HOLE STATES OF COMPLEX NUCLEI	PETERSON	1	0.0
825	INVESTIGATION OF THE NΔ INTERACTION VIA $\pi+d \rightarrow p\pi+n$	MUTCHLER	1	0.0
827	STUDY OF ISOBARIC-ANALOG STATES IN PION SINGLE-CHARGE-EXCHANGE REACTIONS IN THE 300- TO 500-MeV REGION	ALSTER BAER PIASETZKY SENNHAUSER	1	0.0
830	THE REACTION $(\pi,\pi p)$ ON ^{3}He AND ^{4}He AT ENERGIES ABOVE THE (3,3) RESONANCE	MINEHART	1	0.0
831	THE $[\pi^+,p(pp)]$ REACTION ON LIGHT NUCLEI	PERDRISAT MINEHART	1	0.0
838	PION-INDUCED PION PRODUCTION ON NUCLEI AT 400 MeV	LEITCH PIASETZKY	1	0.0
849	A. MEASUREMENT OF THE DIFFERENTIAL CROSS SECTION ON $\pi^-p \rightarrow \pi^0n$ AT 0° AND 180° IN THE MOMENTUM REGION 471-687 MeV/c B. TEST OF ISOSPIN INVARIANCE IN πN SCATTERING AT 180° IN THE MOMENTUM REGION 471-687 MeV/c	FITZGERALD BRISCOE SADLER	1	0.0
852	MEASUREMENTS OF $(\pi^{\pm},\eta)$ REACTIONS ON NUCLEAR TARGETS TO STUDY THE PRODUCTION AND INTERACTION OF η MESONS WITH NUCLEI	PENG	1	0.0
856	COMPARISON OF DOUBLE CHARGE EXCHANGE AND INCLUSIVE SCATTERING IN ^{3}He	GRAM MATTHEWS REBKA	1	0.0
859	STUDY OF THE A DEPENDENCE OF INCLUSIVE PION DOUBLE CHARGE EXCHANGE IN NUCLEI	GRAM MATTHEWS REBKA	1	0.0

RADIATION DAMAGE A-1 (RADAMAGE-1)

Exp. No.	Title	Spokesman	Phase No. *=Complete	Beam Hours
302	800-MeV PROTON IRRADIATION OF AN ALUMINUM SAMPLE	GREEN	1 *	0.0
545	FUSION MATERIALS NEUTRON IRRADIATIONS — A PARASITE EXPERIMENT	BROWN	1	3821.8

STOPPED MUON CHANNEL (SMC)

Exp. No.	Title	Spokesman	Phase No. *=Complete	Beam Hours
7	NUCLEAR-STRUCTURE PHYSICS USING STOPPED MUONS	SHERA	1 * 2 *	0.0 617.3
12	MUONIC X RAYS AND NUCLEAR CHARGE DISTRIBUTIONS	POWERS KUNSELMAN	1 * 2 *	173.0 141.9
37	ULTRA-HIGH-PRECISION MEASUREMENTS OF MUONIUM GROUND-STATE ENERGY LEVELS: HYPERFINE STRUCTURE INTERVAL AND MUON MAGNETIC MOMENT	HUGHES CRANE	1 *	0.0
51	TECHNIQUES FOR MATERIALS IDENTIFICATION AND ANALYSIS	MALANIFY	1 *	119.3
60	CHEMICAL EFFECTS IN THE CAPTURE OF NEGATIVE MESONS IN MATTER	KNIGHT SCHILLACI	1 * 2 *	0.0 451.5
76	SEARCH FOR MUONIUM-ANTIMUONIUM TRANSITION	CHANG KANE	1 *	0.0
85	GAMMA-NEUTRINO CORRELATION AFTER NEGATIVE-MUON CAPTURE	WELSH	1 *	193.6
100	TISSUE CHEMICAL ANALYSIS WITH MU-MESIC X RAYS	HUTSON	1 * 2 *	0.0 167.0
101	FEASIBILITY STUDIES: MEASUREMENT OF MUONIC X RAYS AND NUCLEAR GAMMA RAYS WITH CRYSTAL DIFFRACTION SPECTROMETERS AT LAMPF	BOEHM LU	F S*	103.0
122	PIONIC-ATOM X RAYS AND NUCLEAR DISTRIBUTIONS	KUNSELMAN	2 *	64.8
142	NEGATIVE-MUON-INDUCED FISSION IN THE ACTINIDE ELEMENTS	HUIZENGA	1 * 2 *	0.0 520.3
163	INVESTIGATION OF CHANGES IN CHARGE DISTRIBUTIONS FOR NUCLEI NEAR Z = 28 BY ELECTRON SCATTERING AND MUONIC X RAYS	PERKINS SHERA	1 *	0.0
165	MUONIUM FORMATION IN HELIUM AND OTHER RARE GASES	HUGHES	1 *	0.0
166	MUONIC X RAYS AND NUCLEAR CHARGE DISTRIBUTIONS ELECTRIC QUADRUPOLE MOMENTS OF $_{67}Ho^{165}$ AND $_{73}Ta^{181}$	POWERS	1 *	0.0
173	PHYSICS OF THE PION AND THE PIONIC ATOM	BOEHM VOGEL	1 * 2 *	600.9 309.6
175	SEARCH FOR THE FORMATION OF MUONIC HELIUM $(a\mu - e)$	HUGHES	1 *	0.0
206	SEARCH FOR THE 2S METASTABLE STATE OF MUONIC HYDROGEN	HUGHES EGAN	1 *	497.0
213	MUON-TRANSFER STUDY	SHERA STEFFEN	1 *	50.9
240	ISOTOPE AND ISOTONE SHIFTS IN THE $1f_{7/2}$ SHELL	SHERA	1 *	294.1

Exp. No.	Title	Spokesman	Phase No. *=Complete	Beam Hours
266	TRAPPING OF POSITIVE MUONS AT DEFECTS IN METALS	GAUSTER HEFFNER	1 * 2 * 3 *	223.0 106.1 9.0
268	MEASUREMENT OF THE GROUND-STATE HYPERFINE STRUCTURE INTERVAL OF THE MUONIC HELIUM ATOM ($\alpha\mu-e-$)	SOUDER HUGHES	1 *	518.6
276	PERTURBED CIRCULAR POLARIZATION OF MUONIC X RAYS	YAMAZAKI	1 * 2 * 3 *	0.0 183.0 235.1
277	MUONIC X-RAY ANALYSIS OF CORE SAMPLES FROM OIL-BEARING FORMATIONS	ALLRED	1 *	33.0
283	CHARGED-PARTICLE EMISSION FOLLOWING $\mu-$ CAPTURE	KRANE SHARMA	1 * 2 *	138.3 88.6
288	STUDIES OF $\mu-$ CAPTURE PROBABILITIES FOR SOLID-STATE SOLUTIONS	NAUMANN	1 *	180.1
292	NEUTRON EMISSION FROM MUON-INDUCED REACTIONS ON ACTINIDE ELEMENTS	HUIZENGA	1 * 2 *	196.2 138.3
297	A BICENTENNIAL PROPOSAL TO STUDY THE BEHAVIOR OF POSITIVE MUONS IN SOLIDS	BROWN	1 * 2 * 3 *	144.1 137.1 47.1
328	MEASUREMENT OF THE DECAY RATE AND PARITY-VIOLATING ASYMMETRY FOR $\mu^+ \rightarrow e^+\gamma$	BOWMAN COOPER	1 *	1666.3
330	FUNDAMENTAL MUONIC X-RAY MEASUREMENTS OF INTEREST TO MATERIALS ANALYSIS	HUTSON YATES-WILLIAMS	1 * 2 *	90.4 67.8
331	FAST MUON REACTIONS WITH ^{12}C, ^{48}Ti, AND ^{58}Ni	ORTH	1 * 2 *	97.2 78.0
334	NUCLEAR CHARGE PARAMETERS OF ^{41}Ca AND STABLE CADMIUM AND TELLURIUM ISOTOPES	SHERA	1 * 2 *	162.4 170.3
335	MONOPOLE AND QUADRUPOLE CHARGE DISTRIBUTIONS IN THE SAMARIUM AND GADOLINIUM ISOTOPES	SHERA YAMAZAKI	1 * 2 * 3 *	298.7 65.0 0.0
344	HIGHER PRECISION MEASUREMENT OF MUON MAGNETIC MOMENT AND OF MUONIUM hfs INTERVAL	HUGHES	1 *	425.6
357	MUONIC X-RAY SPECTRA OF GASES: 1. DENSITY AND ADMIXTURE EFFECTS	KNIGHT	1 *	145.1
364	SEARCH FOR THE EXCITED 2S STATE OF MUONIUM	EGAN DENISON HUGHES	1 * 2 *	535.8 167.7
371	MUONIC X-RAY SPECTRA OF GASES: 2. CAPTURE PROBABILITIES IN MIXTURES	HUTSON	1 *	122.7
374	$\mu-$ CAPTURE PROBABILITIES FOR SELECTED SOLID BINARY COMPOUNDS	SCHILLACI	1 *	161.7

Exp. No.	Title	Spokesman	Phase No. * = Complete	Beam Hours
375	μSR STUDY OF DIFFUSION IN METALS IN THE PRESENCE OF PARAMAGNETIC IONS	SCHILLACI	1 * 2 * 3 *	194.5 287.0 45.0
377	INVESTIGATION ON THE EFFECT OF GRAIN SIZE IN MUON CAPTURE IN INHOMOGENEOUS SYSTEMS	REIDY	1 *	28.0
382	A μSR INVESTIGATION OF THE EFFECTS OF IMPURITIES ON THE TRAPPING AND DIFFUSION OF μ^+ PARTICLES IN bcc METALS	KOSSLER	1 *	111.4
400	SEARCH FOR THE RARE-DECAY $\mu^+ \rightarrow e^+e^+e^-$	HOFFMAN	1 2	651.4 1297.9
408	MACROSCOPIC DIFFUSION STUDIES IN METALS	HEFFNER LEON	1 *	81.0
414	BONE CALCIUM ASSAY WITH MUONIC X RAYS — SIGNAL/NOISE AND REPRODUCIBILITY STUDIES	HUTSON REIDY	1 *	113.6
421	SENSITIVE SEARCH FOR $\mu^- \rightarrow e$ CONVERSION	SOUDER FRANKEL HUGHES	1	42.0
427	MAGNET RESONANCE STUDIES OF μ^+-ELECTRON DEFECT COMPLEXES IN NONMETALS	ESTLE	1 * 2 3	253.3 161.4 24.0
436	NEGATIVE MUON SPIN ROTATION AND RELAXATION IN MAGNETIC MATERIALS	YAMAZAKI HAYANO	1 *	196.2
444	SEARCH FOR THE DECAY $\mu \rightarrow e\gamma$	BOWMAN HOFSTADTER	1	0.0
445	SEARCH FOR THE LEPTON-FLAVOR-VIOLATING DECAY $\mu^+ \rightarrow e^+\gamma\gamma$	MATIS BOWMAN	1	54.4
449	SURVEY OF SINGLE AND DOUBLE PHOTODETACHMENT CROSS SECTION OF THE H^- ION FROM 14 TO 21.8 eV	BRYANT DONAHUE	3	112.0
464	RADIATIVE MUON CAPTURE IN GASEOUS ^{3}He	ROBERTS MILLER	1	0.0
491	EXPERIMENTAL DETERMINATION OF THE STRONG INTERACTION SHIFT IN THE 2p-1s TRANSITION OF PIONIC DEUTERIUM AND HYDROGEN ATOMS	LEE FORSTER	1 * 2 * 3 * 4 *	646.6 376.1 306.0 0.0
494	NUCLEAR CHARGE PARAMETERS OF THE STABLE RUTHENIUM AND PALLADIUM ISOTOPES	HOEHN	1	169.0
499	MUON LONGITUDINAL AND TRANSVERSE RELAXATION STUDIES IN SPIN-GLASS SYSTEMS	DODDS MacLAUGHLIN HEFFNER	1 * 2 3 4	329.6 456.0 0.0 0.0
517	POLARIZED BEAM AND TARGET EXPERIMENTS IN THE p-p SYSTEM: PHASE I. A_γ AND $A_{\gamma\gamma}$ FOR THE $d\pi^+$ CHANNEL AND $A_{\gamma\gamma}$ FOR THE ELASTIC CHANNEL FROM 500 TO 800 MeV	SIMMONS JARMER NORTHCLIFFE	2	0.0

Exp. No.	Title	Spokesman	Phase No. *=Complete	Beam Hours
529	PART 1: MEASUREMENT OF THE RESIDUAL MUON POLARIZATION IN ^{3}He MUONIC ATOM (A FEASIBILITY TEST FOR PART 2), AND PART 2: ANGULAR CORRELATIONS IN THE CAPTURE OF POLARIZED MUONS IN GASEOUS ^{3}He	WU DUGAN HUGHES	1 * 2	136.0 765.0
547	SEARCH FOR FAST MUONIUM IN VACUUM	EGAN HUGHES KANE	1 * 2 * 3 *	231.4 144.0 100.1
552	ULTRA-HIGH-PRECISION MEASUREMENTS ON MUONIUM	HUGHES EGAN	1	0.0
571	MUON-SPIN-ROTATION STUDIES OF DILUTE MAGNETIC ALLOYS	DODDS HEFFNER SCHILLACI	1 2	359.4 110.0
594	PRECISION DETERMINATIONS OF SOME RELATIVE MUONIC COULOMB-CAPTURE RATIOS IN OXIDES OF DIFFERENT VALENCES	REIDY	1 *	93.0
639	MUON-SPIN-ROTATION STUDY OF MUON BONDING AND MOTION IN SELECT MAGNETIC OXIDES	BOEKEMA DENISON COOKE	1 2	144.0 44.0
640	TRANSVERSE AND LONGITUDINAL FIELD μSR MEASUREMENTS IN SELECTED TERNARY METALLIC COMPOUNDS	DODDS HEFFNER MacLAUGHLIN	1 * 2	246.0 177.0
646	HYPERFINE STRUCTURE OF MUONIC ^{3}He AND MUONIC ^{4}He ATOMS	HUGHES EGAN	1 * 2	414.0 0.0
653	THE ^{241}Am AND ^{243}Am MUONIC ATOM STUDIES	SHERA JOHNSON NAUMANN	1 *	151.1
693	INVESTIGATION OF THE TWO-PHOTON DECAY RATE FROM THE $(\mu^4\text{He})^+_{2S}$ STATE AS A FUNCTION OF PRESSURE	REIDY	1	0.0
698	GROUND-STATE QUADRUPOLE MOMENTS OF DEFORMED NUCLEI	STEFFEN SHERA	1 * 2	0.0 0.0
724	MEASUREMENT OF THE LAMB SHIFT IN MUONIUM	EGAN GLADISCH HUGHES	1 * 2 *	786.0 380.0
726	SEARCH FOR THE C-NONINVARIANT DECAY $\pi^0 \rightarrow 3\gamma$	HIGHLAND SANDERS	1	0.0
727	MEASUREMENT OF THE EFFICIENCY OF MUON CATALYSIS IN DEUTERIUM-TRITIUM MIXTURES AT HIGH DENSITIES	JONES	1 2	0.0 0.0
742	SEARCH FOR THE NEGATIVE MUONIUM ION	EGAN SOUDER	1	0.0
745	HEXADECAPOLE MOMENTS IN URANIUM: ^{233}U AND ^{234}U	ZUMBRO SHERA	1 3	0.0 0.0
763	NATURE OF OXYGEN CONTAMINATION IN TITANIUM WITH STOPPED MUONS	TAYLOR	1	0.0

Exp. No.	Title	Spokesman	Phase No. *=Complete	Beam Hours
771	MUON DIFFUSION IN fcc METALS	COOKE HEFFNER	1	0.0
842	μSR SHIFT AND RELAXATION MEASUREMENTS IN ITINERANT MAGNETS	GUPTA HEFFNER MacLAUGHLIN	1	0.0
854	MUON-SPIN RESEARCH IN OXIDE SPIN GLASSES	BOEKEMA COOKE	1	0.0
869	HIGHER PRECISION MEASUREMENT OF THE LAMB SHIFT IN MUONIUM	BADERTSCHER GLADISCH HUGHES	1	0.0
873	PIONIC X-RAY STUDY OF THE CARBON ISOTOPES	SHERA KUNSELMAN	1	0.0

SWITCHYARD LINE A BEAM STOP (LA-BS)

Exp. No.	Title	Spokesman	Phase No. *=Complete	Beam Hours
105	NUCLEAR SPECTROSCOPY STUDIES OF PROTON-INDUCED SPALLATION PRODUCTS	BUNKER	1 *	0.0
118	FRAGMENT EMISSION FROM PION INTERACTIONS WITH COMPLEX NUCLEI	PORILE	1 *	0.0
269	800-MEV PROTON IRRADIATION OF METAL SAMPLES	GREEN	1 *	4.5
381	ALUMINA CERAMIC RADIATION EFFECTS STUDY	HARVEY	1 *	0.0
648	TEST OF EQUIPMENT FOR THE MEASUREMENT OF THE Σ^- FOR THE MAGNETIC MOMENT AT BNL	MILLER	1	0.0
652	TESTS OF PROTOTYPE SEMICONDUCTOR DETECTORS	SKUBIC	1	0.0

THIN TARGET AREA (TTA)

Exp. No.	Title	Spokesman	Phase No. *=Complete	Beam Hours
86	COUNTER EXPERIMENTS IN THE THIN TARGET AREA	POSKANZER	1 * 2 * 3 *	0.0 743.0 1128.0
308	AN ATTEMPT TO MAKE DIRECT ATOMIC MASS MEASUREMENTS IN THE THIN TARGET AREA	BUTLER POSKANZER	1 * 2	7692.4 762.0
692	GERMANIUM-DETECTOR LOW-LEVEL RADIATION-DAMAGE EQUILIBRATION EXPERIMENT	REEDY	1	0.0
752	TUNEUP OF THE TIME-OF-FLIGHT SPECTROMETER DIRECT ATOMIC MASS MEASUREMENTS	VIEIRA	1	0.0

Exp. No.	Title	Spokesman	Phase No. * = Complete	Beam Hours
870	SEARCH FOR NEW MAGIC NUMBERS: DIRECT MASS MEASUREMENTS OF THE NEUTRON-RICH ISOTOPES WITH Z = 4-9	WOUTERS	1	0.0
872	DIRECT ATOMIC MASS MEASUREMENTS OF NEUTRON-RICH ISOTOPES IN THE REGION Z = 13-17 USING THE TIME-OF-FLIGHT ISOCHRONOUS SPECTROMETER	BRENNER	1	0.0

APPENDIX D

ACTIVE SPOKESMEN, INSTITUTIONS, AND EXPERIMENTS

SPOKESMEN	INSTITUTIONS	EXPERIMENTS
ANDERSON, H. L.	LOS ALAMOS	455
ANDERSON, R. E.	UNIV. OF NORTH CAROLINA	535
BAER, H. W.	LOS ALAMOS	523 527
BARLETT, M. L.	UNIV. OF TEXAS, AUSTIN	632
BENTON, E. V.	UNIV. OF SAN FRANCISCO	171
BLANPIED, G. S.	UNIV. OF SOUTH CAROLINA	475 573
BLESZYNSKI, M.	UCLA	635
BOEKEMA, C.	TEXAS TECH UNIV.	639
BONNER, B. E.	LOS ALAMOS	635 637
BOWMAN, J. D.	LOS ALAMOS	295 401 444 445 527
BRADBURY, J. N.	LOS ALAMOS	215
BROWN, R. D.	LOS ALAMOS	545 554
BRYANT, H. C.	UNIV. OF NEW MEXICO	586 588
BUNKER, M. E.	LOS ALAMOS	629
BURLESON, G. R.	NEW MEXICO STATE UNIV.	498
BURNETT, D. S.	CALTECH	161
BUTLER, G. W.	LOS ALAMOS	308
CARETTO, A. A.	CARNEGIE-MELLON UNIV.	543
CAREY, T. A.	LOS ALAMOS	630
CARLINI, R. D.	LOS ALAMOS	634
CHANT, N. S.	UNIV. OF MARYLAND	576
CHEN, H. H.	UNIV. OF CALIFORNIA, IRVINE	225
CLARK, D. A.	LOS ALAMOS	588
COOKE, D. W.	MEMPHIS STATE UNIV.	639
COOPER, M. D.	LOS ALAMOS	401
COST, J. R.	LOS ALAMOS	554
COTTINGAME, W. B.	NEW MEXICO STATE UNIV.	598
DEHNHARD, D. K.	UNIV. OF MINNESOTA	580 602
DENISON, A. B.	UNIV. OF WYOMING	639
DEVRIES, R. M.	LOS ALAMOS	591 592
DIGIACOMO, N.	LOS ALAMOS	591 592
DODDS, S. A.	RICE UNIV.	499 571 640
DOMBECK, T. W.	UNIV. OF MARYLAND	638
DONAHUE, J. B.	LOS ALAMOS	587
DUGAN, G.	COLUMBIA UNIV.	529
EGAN, P. O.	YALE UNIV.	552 646
ELLIS, R. J.	LOS ALAMOS	647
ESTLE, T. L.	RICE UNIV.	427
FAUBEL, W.	KARLSRUHE	579
FRANKEL, S.	UNIV. OF PENNSYLVANIA	421
GAZZALY, M. M.	UNIV. OF MINNESOTA	583
GILMORE, J. S.	LOS ALAMOS	467
GLASHAUSSER, C.	RUTGERS UNIV.	531 623
GLASS, G.	TEXAS A&M UNIV.	589
GOODMAN, C. D.	INDIANA UNIV.	523
GRAM, P. A. M.	LOS ALAMOS	586

SPOKESMEN	INSTITUTIONS	EXPERIMENTS
GREENE, S. J.	LOS ALAMOS	572
GREENWOOD, R. C.	IDAHO NATIONAL ENGINEERING LAB.	629
HARVEY, A.	LOS ALAMOS	326 406 560
HARVEY, C. J.	UNIV. OF TEXAS, AUSTIN	602
HEFFNER, R. H.	LOS ALAMOS	499 571 640
HENNING, W.	ARGONNE	610
HINTZ, N. M.	UNIV. OF MINNESOTA	601 630
HOEHN, M. V.	LOS ALAMOS	494
HOFFMAN, C. M.	LOS ALAMOS	400
HOFFMANN, G. W.	UNIV. OF TEXAS, AUSTIN	632
HOFSTADTER, R.	STANFORD UNIV.	444
HOGAN, J. J.	McGILL UNIV.	611
HOISTAD, B.	UNIV. OF TEXAS, AUSTIN	456 485 533 535 649
HOLLAS, C. L.	UNIV. OF TEXAS, AUSTIN	636
HUGHES, V. W.	YALE UNIV.	421 529 552 646
IGO, G. J.	UCLA	635 644
IROM, F.	ARIZONA STATE UNIV.	633
JACKSON, H. E.	ARGONNE	628
JARMER, J. J.	LOS ALAMOS	518
KAROL, P. J.	CARNEGIE-MELLON UNIV.	294
KATZ, R.	UNIV. OF NEBRASKA	218
KING, N. S. P.	LOS ALAMOS	525 538
KINNISON, W. W.	LOS ALAMOS	455
KIZIAH, R. R.	UNIV. OF TEXAS, AUSTIN	598
KUTSCHERA, W.	ARGONNE	610
LING, T. Y.	OHIO STATE UNIV.	645
LU, D. C.	YALE UNIV.	542
MacLAUGHLIN, D. E.	UNIV. OF CALIFORNIA, RIVERSIDE	499 640
MATIS, H. S.	LAWRENCE BERKELEY	445
McCLELLAND, J. B.	LOS ALAMOS	630
MICHEL, D. J.	NAVAL RESEARCH LAB.	113
MILLER, J.	BOSTON UNIV.	648
MILLER, J. P.	BOSTON UNIV.	464
MOINESTER, M. A.	LOS ALAMOS/TEL AVIV UNIV.	295 525
MOORE, C. F.	UNIV. OF TEXAS, AUSTIN	572
MORRIS, C. L.	LOS ALAMOS	572 651
MOSS, J. M.	LOS ALAMOS	531 630
NORTHCLIFFE, L. C.	TEXAS A&M UNIV.	518 589 590
O'BRIEN, H. A.	LOS ALAMOS	106 267
ORTH, C. J.	LOS ALAMOS	595
PACIOTTI, M. A.	LOS ALAMOS	217 270
PAULETTA, G.	UCLA	583 633
PEREZ-MENDEZ, V.	LAWRENCE BERKELEY	215
PHILLIPS, D. S.	UNIV. OF ILLINOIS	407
POSKANZER, A. M.	LAWRENCE BERKELEY	308
PREEDOM, B. M.	UNIV. OF SOUTH CAROLINA	576
RAJU, M. R.	LOS ALAMOS	236
REIDY, J. J.	UNIV. OF MISSISSIPPI	187
ROBERTS, B. L.	BOSTON UNIV.	464
ROMANOWSKI, T.	OHIO STATE UNIV.	645
ROOS, P. G.	INDIANA UNIV. CYCLOTRON FACILITY	576

SPOKESMEN	INSTITUTIONS	EXPERIMENTS
RUNDBERG, R. S.	LOS ALAMOS	465 553
SCHILLACI, M. E.	LOS ALAMOS	571
SEESTROM-MORRIS, S. J.	UNIV. OF MINNESOTA	580
SETH, K. K	NORTHWESTERN UNIV.	508 533 550
SHEPARD, J. R.	UNIV. OF COLORADO	485 538
SIMMONS, J. E.	LOS ALAMOS	518 590
SKUBIC, P.	UNIV. OF OKLAHOMA	652
SMITH, A. R.	UNIV. OF NEW MEXICO	271
SMITH, W. W.	UNIV. OF CONNECTICUT	587
SOMMER, W. F.	LOS ALAMOS	407
SOUDER, P. A.	YALE UNIV.	421
TALAGA, R. L.	UNIV. OF MARYLAND	634
TALBERT, JR., W. L.	LOS ALAMOS	629
TURKEVICH, A. L.	UNIV. OF CHICAGO	603
VAN DYCK, O. B.	LOS ALAMOS	532
VIEIRA, D. J.	LOS ALAMOS	595
WAGNER, R.	ARGONNE	498
WU, C. S.	COLUMBIA UNIV.	529
YUAN, V.	UNIV. OF ILLINOIS	634
ZIOCK, K. O. H.	UNIV. OF VIRGINIA	190

APPENDIX E

VISITORS TO LAMPF DURING THE PERIOD
JANUARY 1 — DECEMBER 31, 1983

Bjarne Aas . . . . . UCLA
Daniel S. Acton . . . . . Abilene Christian Univ.
David L. Adams . . . . . UCLA
Gary S. Adams . . . . . Univ. of South Carolina
Steven D. Adrian . . . . . Abilene Christian Univ.
Douglas M. Aldo . . . . . Columbia Univ.
Richard C. Allen . . . . . UC, Irvine
John C. Allred . . . . . Consultant, New Mexico
Peter W. F. Alons . . . . . Univ. of Colorado
Jonas Alster . . . . . Tel Aviv Univ.
Aharon Amittay . . . . . Yale Univ.
Adam W. Anderson . . . . . Yale Univ.
Alan N. Anderson . . . . . EG&G, Idaho
Bryon D. Anderson . . . . . Kent State Univ.
Daniel H. Anderson . . . . . UCLA
Konrad A. Aniol . . . . . TRIUMF
Hans-Jurgen Arends . . . . . Catholic Univ.
Richard A. Arndt . . . . . Virginia Poly. Inst./State Univ.
Daniel Ashery . . . . . Tel Aviv Univ.
Leonard B. Auerbach . . . . . Temple Univ.
Naftali Auerbach . . . . . Tel Aviv Univ.
David A. Axon . . . . . TRIUMF
Alirozn Azizi . . . . . UCLA
Andrew D. Bacher . . . . . Indiana Univ.
Mark G. Bachman . . . . . Univ. of Texas
Andreas Badertscher . . . . . Univ. of Berne
Leonard J. Balka . . . . . Argonne
Martin L. Barlott . . . . . Univ. of Texas
David B. Barlow . . . . . Northwestern Univ.
Charles A. Barnes . . . . . Caltech
Bernd Bassalleck . . . . . Univ. of New Mexico
Thomas S. Bauer . . . . . SIN
Stephen C. Bayliss . . . . . Univ. of New Mexico
Frederick D. Becchetti . . . . . Univ. of Michigan
T. H. Bergeman . . . . . State Univ. of New York, Stony Brook
Michael G. Berlein . . . . . Univ. of Pennsylvania
Barry L. Berman . . . . . Lawrence Livermore Lab.
Raimondo P. M. Bertini . . . . . CEN, Saclay
William Bertozzi . . . . . MIT
Vinod K. Bhargadwaj . . . . . UC, Irvine
Tarlochan S. Bhatia . . . . . Texas A&M Univ.
Hans Bichsel . . . . . Univ. of Washington
Leslie C. Bland . . . . . Univ. of Texas
Gary S. Blanpied . . . . . Univ. of South Carolina
Marvin Blocher . . . . . Virginia Poly. Inst./State Univ.
Marek Blenzynski . . . . . UCLA
Charles L. Blilie . . . . . Univ. of Minnesota
Carolus Boekema . . . . . Texas Tech Univ.
Joseph E. Bolger . . . . . Univ. of Texas
Joe H. Booth . . . . . Abilene Christian Univ.
Michael J. Borden . . . . . New Mexico Inst. of Mining Tech.
Charles A. Bordner . . . . . Colorado College
William J. Briscoe . . . . . George Washington Univ.
Mark D. Brown . . . . . Univ. of Texas
Paul A. Bruhwiler . . . . . Univ. of Virginia
Howard C. Bryant . . . . . Univ. of New Mexico
William J. Burger . . . . . MIT
George R. Burleson . . . . . New Mexico State Univ.
Marshall Burns . . . . . Univ. of Texas
Mary J. Burns . . . . . Univ. of New Mexico
Kenneth B. Butterfield . . . . . Univ. of New Mexico
Karen L. Byrum . . . . . Argonne
Augustine J. Caffrey . . . . . EG&G, Idaho
Nicholas S. Chant . . . . . Univ. of Maryland
Herbert H. Chen . . . . . UC, Irvine
Huan-Ching Chiang . . . . . Inst. of High Energy Phys.
Katherine W. C. Chol . . . . . Louisiana State Univ.
Gheorghe Ciangaru . . . . . Boston Univ./Univ. of Maryland
David A. Clark . . . . . Univ. of New Mexico
Nance L. Colbert . . . . . UC, Irvine
Joseph B. Comfort . . . . . Arizona State Univ.
Genevieve B. Comfort . . . . . Centre Nat. de la Recherche Sci.
Dominic C. Constantino . . . . . Yale Univ.
David C. Cook . . . . . Univ. of Minnesota
D. Wayne Cooke . . . . . Memphis State Univ.
William Cottingame . . . . . New Mexico State Univ.
John B. Cozo . . . . . Temple Univ.
David J. Crabtree . . . . . Abilene Christian Univ.
Donna J. Cremans . . . . . Univ. of Texas
Gerald G. Crough . . . . . UCLA
David J. Cunningham . . . . . Abilene Christian Univ.
James A. Dalton . . . . . Abilene Christian Univ.
Gourisankar Das . . . . . Univ. of Virginia
Sunayana Datta . . . . . Temple Univ.
Dorothy R. Davidson . . . . . Iowa State Univ.
John K. Dayton . . . . . Univ. of Connecticut
Dietrich Debinhard . . . . . Univ. of Minnesota
Peter P. Denes . . . . . Univ. of New Mexico
Arthur B. Denison . . . . . Univ. of Wyoming
Burton A. Devolk . . . . . Univ. of New Mexico
Satish Dhawan . . . . . Yale Univ.
Kalvh Singh Dhugn . . . . . Univ. of Pennsylvania

Byron D. Dieterle . . . . . Univ. of New Mexico
W. Rodney Ditzler . . . . . Argonne
Stanley A. Dodds . . . . . Rice Univ.
George W. Dodson . . . . . MIT
Peter J. Doe . . . . . UC, Irvine
Argyrios Doumas . . . . . Texas A&M Univ.
Minh V. Duong-Van . . . . . Rice Univ.
Morton Eckhause . . . . . Coll. of William & Mary
Patrick O. Egan . . . . . Lawrence Livermore Lab.
Andrew D. Elchon . . . . . UCLA
Judah M. Eisenberg . . . . . Tel Aviv Univ.
Mohammed Emadi-Babaki . George Washington Univ.
Jon M. Engelage . . . . . UCLA
Peter A. J. Englert . . . . . Univ. of Koln
Adoram Erell . . . . . Tel Aviv Univ.
David J. Ernst . . . . . Texas A&M Univ.
Jorge A. Escalante . . . . . Univ. of South Carolina
Monouchehr Farkhondeh . . . . . MIT
David J. Farnum . . . . Now Mexico Inst. of Mining Tech.
John A. Faucett . . . . . Univ. of Oregon
Ali Fazely . . . . . Louisiana State Univ.
Raymond W. Forgerson . . . . . Univ. of Texas
Brian E. Fick . . . . . Virginia Poly. Inst./State Univ.
John M. Finn . . . . . MIT
David B. Fisher . . . . . Ohio State Univ.
Steven B. Fisher . . . . . Ohio State Univ.
Donald G. Fleming . . . . . TRIUMF
Gottfried Flik . . . . . Max-Planck Inst.
Carlos A. Fontenla . . . . . New Mexico State Univ.
Irene Forster . . . . . Univ. of Koln
H. Terry Fortune . . . . . Univ. of Pennsylvania
Bernhard J. Franczak . . . . . Gesellsch. für Schwerionf.
Michael Franey . . . . . Univ. of Minnesota
Dan M. Fraser . . . . . Utah State Univ.
Hans Frauenfelder . . . . . Univ. of Illinois
Stuart J. Freedman . . . . . Argonne
William S. Freeman . . . . . Argonne
Hiroshi Fujisawa . . . . . Univ. of Minnesota
Avraham Gal . . . . . Hebrew Univ.
Mehryar K. Garrahani . . . . . Univ. of Minnesota
Robert W. Garnett . . . . . New Mexico State Univ.
Albert G. Gay . . . . . Abilene Christian Univ.
M. Maggy Gazzaly . . . . . Univ. of Minnesota
Donald F. Geesaman . . . . . Argonne
David R. Gleblink . . . Texas A&M Univ./Univ. of Maryland
Shalev Gilad . . . . . MIT
Gerard P. Gilfoyle . . . . . Univ. of Pennsylvania
Ronald A. Gilman . . . . . Univ. of Pennsylvania
Grant A. Glat . . . . . Rice Univ.
Michael Gladisch . . . . . Univ. of Heidelberg
Charles Glashausser . . . . . Rutgers Univ.
George Glass . . . . . Texas A&M Univ.
Roy J. Glauber . . . . . Harvard Univ.
A. S. Goldhaber . State Univ. of New York, Stony Brook
Peggy A. Goldman . . . . . Univ. of New Mexico
Dudley T. Goodhead . . . Medical Res. Council, Harwell
Kazuo Gotow . . . . . Virginia Poly. Inst./State Univ.
Charles A. Goulding . . . . . EG&G, Los Alamos
Scott C. Graessle . . . . . Abilene Christian Univ.
Michael C. Green . . . . . Argonne
Ray E. L. Green . . . . . Simon Fraser Univ.
Steven J. Greene . . . . . New Mexico State Univ.
Chilton B. Gregory . . . . . Univ. of New Mexico
David P. Grosnick . . . . . Univ. of Chicago
Franz L. Gross . . . . . Coll. of William & Mary
Willi Grübler . . . . . Lab. Fur Kernphysik
Laxmi Chand Gupta . Tata Inst. of Fund. Research, India
William Haberichter . . . . . Argonne
Jeffrey A. Hall . . . . . Abilene Christian Univ.
Hisashi Harada . . . . . Columbia Univ.
Serge Haroche . . . . . Univ. of Paris
Ronnie W. Harper . . . . . Univ. of Illinois
Margye P. Harrington . . . . . Univ. of New Mexico
Benjamin L. Harris . . . . . Northwestern Univ.
Carol J. Harvey . . . Univ. of New Mexico/Univ. of Texas
Hiromi Hasai . . . . . Hiroshima Univ.
Rene Hausammann . . . . . Univ. of Geneva/UC, Irvine
John Walker Helmaster . . . . . Ohio State Univ.
Dale J. Henderson . . . . . Argonne
Jose Luis Hernandez . . . . . Univ. of South Carolina
Kenneth H. Hicks . . . . . Univ. of Colorado
John C. Hiebert . . . . . Texas A&M Univ.
Virgil L. Highland . . . . . Temple Univ.
Daniel A. Hill . . . . . Argonne
Roger E. Hill . . . . . Univ. of New Mexico
Norton M. Hintz . . . . . Univ. of Minnesota
Gerhard W. J. Hoehler . . . . . Univ. of Karlsruhe
Gerald W. Hoffmann . . . . . Univ. of Texas
John H. Hoffiezer . . . . . Argonne
Gary L. Hogan . . . . . Temple Univ.
Steinar Holbraten . . . . . MIT
Bo Holstad . . . . . Univ. of Texas
Karl F. Hollinde . . . . . Univ. of Bonn
Charles L. Hollas . . . . . Univ. of Texas
Barry R. Holstein . . . . . Univ. of Massachusetts
James A. Holt . . . . . UCLA
Roy J. Holt . . . . . Argonne
Masaharu Hoshi . . . . . Hiroshima Univ.
David Huang . . . . . Temple Univ.
E. Barrie Hughes . . . . . Stanford Univ.
Vernon W. Hughes . . . . . Yale Univ.
Jon R. Hurd . . . . . Univ. of Virginia
George J. Igo . . . . . UCLA
C. H. Quentin Ingram . . . . . SIN
Farokh Irom . . . Arizona State Univ./Arizona State Univ.
Shigeru Isagawa . . . . . KEK
Shigaru Ishimoto . . . . . KEK
Vincent Jaccarino . . . . . UC, Santa Barbara

Harold E. Jackson . . . . . Argonne
Mark J. Jakobson . . . . . Univ. of Montana
Randolph H. Jeppesen . . . . . Univ. of Montana
Robert S. Johnson . . . . . Argonne
Wayne A. Johnson . . . . . UC, Irvine
Garth Jones . . . . . TRIUMF
Kevin W. Jones . . . . . UCLA
Steven E. Jones . . . . . EG&G, Idaho
William P. Jones . . . . . Indiana Univ.
Richard J. Joseph . . . . . U.S. Air Force Academy
Donald Joyce . . . . . Coll. of William & Mary
Jan Kaline . . . . . JET/Harvard Smithsonian
John R. Kane . . . . . Coll. of William & Mary
Ju Hwan Kang . . . . . Univ. of New Mexico
Paul J. Karol . . . . . Carnegie-Mellon Univ.
Thomas E. Kasprzyk . . . . . Argonne
Sheldon Kaufman . . . . . Argonne
Robert A. Kenefick . . . . . Texas A&M Univ.
George J. Kim . . . . . UCLA
Edward R. Kinney . . . . . MIT
Leonard S. Kisslinger . . . . . Carnegie-Mellon Univ.
Rex R. Kiziah . . . . . Univ. of Texas
Todd E. Kiziah . . . . . Univ. of Texas
Harrold B. Knowles . . . . . Univ. of New Mexico
James N. Knudson . . . . . Arizona State Univ.
Lawrence J. Kocenko . . . . . Argonne
Dale S. Koetke . . . . . Valparaiso Univ.
Donald D. Koetke . . . . . Valparaiso Univ.
Donald K. Kohl . . . . . Consultant, New Mexico
Norman R. Kolb . . . . . Valparaiso Univ.
Kathryn L. Kolsky . . . . . Carnegie-Mellon Univ.
Ralph G. Korteling . . . . . Simon Fraser Univ.
Robert S. Kowalczyk . . . . . Argonne
Daniel A. Krakauer . . . . . Univ. of Maryland
Jack J. Kraushaar . . . . . Univ. of Colorado
Raymond Kunselman . . . . . Univ. of Wyoming
Dieter Kurath . . . . . Argonne
Peter H. Kutt . . . . . Univ. of Pennsylvania
Gary Kyle . . . . . SIN
Chris P. Leavitt . . . . . Univ. of New Mexico
Samuel M. Levenson . . . . . Northwestern Univ.
Jechiel Lichtenstadt . . . . . Tel Aviv Univ.
Roger L. Lichti . . . . . Texas Tech Univ.
Chung-Yi Lin . . . . . Ohio State Univ.
David A. Lind . . . . . Univ. of Colorado
Richard A. Lindgren . . . . . Univ. of Massachusetts
Ta-Yung Ling . . . . . Ohio State Univ.
Jerry E. Lisantti . . . . . Univ. of Oregon
Stanley Livingston . . . . . Consultant, New Mexico
Earle L. Lomon . . . . . MIT
David Lopiano . . . . . UCLA
Daniel C. J. Lu . . . . . Yale Univ.
Henry J. Lubatti . . . . . Univ. of Washington
Donald R. Machen . . . . . Sci. Systems Int.
Douglas Maclaughlin . . . . . UC, Riverside
Richard Madey . . . . . Kent State Univ.
Kazushige Maeda . . . . . Tohoku Univ
Hansjuerg Mahler . . . . . UC, Irvine
Jill Ann Marshall . . . . . Univ. of Texas
Richard M. Marshall . . . . . Univ. of Virginia
Akira Masaike . . . . . KEK
Terrence S. Mathis . . . . . UNM Cancer Center
June L. Matthews . . . . . MIT
Arthur B. Mcdonald . . . . . Princeton Univ.
James E. Mcdonough . . . . . Temple Univ.
John A. Mcgill . . . . . Rutgers Univ.
Carl Mchargue . . . . . Oak Ridge
Robert D. Mckeown . . . . . Caltech
Kok-Heong Mcnaughton . . . . . Univ. of Texas
Daniel W. Miller . . . . . Indiana Univ.
Cas Milner . . . . . Univ. of Texas
Richard G. Milner . . . . . Caltech
Ralph C. Minehart . . . . . Univ. of Virginia
Ricardo T. Miranda . . . . . Ohio State Univ.
Rachel E. Mischke . . . . . Univ. of Illinois
Chandrashekhar Mishra . . . . . Univ. of South Carolina
Joseph H. Mitchell . . . . . Univ. of Colorado
Joseph W. Mitchell . . . . . Ohio State Univ.
Murray Moinester . . . . . Tel Aviv Univ.
Alireza Mokhtari . . . . . UCLA
C. Fred Moore . . . . . Univ. of Texas
C. Fred Moore Sr . . . . . Univ. of Texas
Shaul Mordechai . . . . . Univ. of Pennsylvania
William G. Morterer . . . . . Louisiana State Univ.
Sanjoy Mukhopadhyay . . . . . Northwestern Univ.
Takemi Nakagawa . . . . . Tohoku Univ.
Sirish K. Nanda . . . . . Rutgers Univ.
James J. Napolitano . . . . . Argonne
Subrata Nath . . . . . Texas A&M Univ.
Robert A. Naumann . . . . . Princeton Univ.
B. M. K. Nefkens . . . . . UCLA
Ted E. Neil . . . . . Abilene Christian Univ.
Ronota A. Newberry . . . . . Abilene Christian Univ.
Charles Newsom . . . . . UCLA
Fumitaka Nishiyama . . . . . Hiroshima Univ.
Lee C. Northcliffe . . . . . Texas A&M Univ.
David S. Oakley . . . . . Univ. of Texas
Yuji Ohashi . . . . . UCLA
Hajime Ohnuma . . . . . Tokyo Inst. of Tech.
Pedro Oillataguerre . . . . . UCLA
Akira Okihana . . . . . Kyoto Univ. of Educ.
Glenn A. Olah . . . . . Abilene Christian Univ.
Hikonojo Orihara . . . . . Tohoku Univ.
Herbert Orth . . . . . Univ. of Heidelberg
Gianni Pauletta . . . . . UCLA
Judith D. Pelzer . . . . . Univ. of New Mexico
Benjie M. Peterson . . . . . Ohio State Univ.
Roy J. Peterson . . . . . Univ. of Colorado

Fred L. Petrovich . . . . . Florida State Univ.
Alan Picklesimer . . . . . Case Western Reserve Univ.
Sandra Pillai . . . . . Oregon State Univ.
Michael E. Potter . . . . . UC, Irvine
David H. Potterveld . . . . . Caltech
Barry M. Preedom . . . . . Univ. of South Carolina
Arthur M. Rask . . . . . Argonne
Mohini W. Rawool . . . . . New Mexico State Univ.
Glen A. Rebka . . . . . Univ. of Wyoming
Robert P. Redwine . . . . . MIT
James J. Reidy . . . . . Univ. of Mississippi
Louis P. Remsberg . . . . . Brookhaven
James H. Richardson . . . . . Consultant, New Mexico
Kenneth P. Riley . . . . . Univ. of Texas
Peter J. Riley
Robert A. Ristinen . . . . . Univ. of Colorado
Barry G. Ritchie . . . . . Univ. of Maryland
Michael W. Ritter . . . . . Yale Univ.
Warren M. Roane . . . . . Abilene Christian Univ.
Donald A. Roberts . . . . . Univ. of Wyoming
John P. Roberts . . . . . Abilene Christian Univ.
Raymond F. Rodebaugh . . . . . Univ. of Texas
Urs C. Rohrer . . . . . SIN
Sayed H. Rokni . . . . . Utah State Univ.
Joseph Rolfe . . . . . Stanford Univ.
Thomas A. Romanowski . . . . . Ohio State Univ.
Philip G. Roos . . . . . Univ. of Maryland
S. Peter Rosen . . . . . Purdue Univ.
Serge L. Rudaz . . . . . Rice Univ.
Michael E. Sadler . . . . . Abilene Christian Univ.
Arunava Saha . . . . . Northwestern Univ.
David P. Saunders . . . . . Univ. of Texas
John P. Schiffer . . . . . Argonne
S. Seestrom-Morris . . . . . Univ. of Minnesota
Colin J. Seftor . . . . . George Washington Univ.
Ralph E. Segel . . . . . Northwestern Univ.
Peter A. Seidl . . . . . Univ. of Texas
Roger V. Servrancks . . . . . Univ. of Saskatchewan
Kamal K. Seth . . . . . Northwestern Univ.
Stephen L. Shaffer . . . . . Abilene Christian Univ.
Tomikazu Shima . . . . . Argonne
Hajime Shimizu
Frank T. Shively . . . . . Lawrence Berkeley Laboratory
Edward R. Siciliano . Univ. of Georgia/Univ. of Colorado
Robert T. Siegel . . . . . Coll. of William & Mary
Terrence P. Sjoreen . . . . . Oak Ridge
Daniel M. Slate . . . . . Univ. of New Mexico
Elton S. Smith . . . . . Ohio State Univ.
Kaleen J. Smith . . . . . Abilene Christian Univ.
L. Cole Smith . . . . . Univ. of Virginia
Robert W. Smith . . . . . Abilene Christian Univ.
Winthrop W. Smith . . . . . Univ. of Connecticut
W. Rodman Smythe . . . . . Univ. of Colorado
Daniel I. Sober . . . . . Catholic Univ.

James R. Specht . . . . . Argonne
Franz Sperisen . . . . . UCLA
Brian M. Spicer . . . . . Univ. of Melbourne
Harold M. Spinka . . . . . Argonne
Robert W. Stanek
Rolf M. Steffen . . . . . Purdue Univ.
George S. F. Stephans . . . . . Argonne
Edward J. Stephenson . . . . . Indiana Univ.
Morton M. Sternheim . . . . . Univ. of Massachusetts
Tsu-Hsun Sun . . . . . Institute of Atomic Energy, PRC
Frank Tabakin . . . . . Univ. of Pittsburgh
Terry N. Taddeucci . . . . . Ohio Univ.
Richard L. Talaga . . . . . Univ. of Maryland
Yasutoshi Tanaka . . . . . Purdue Univ.
Peter C. Tandy . . . . . Kent State Univ.
Robert L. Tanner . . . . . Consultant, New Mexico
Morton F. Taragin . . . . . George Washington Univ.
Scott Taylor . . . . . Abilene Christian Univ.
Raphael M. Thaler . . . . . Case Western Reserve Univ.
Terry L. Thode . . . . . UCLA
T. Neil Thompson . . . . . UC, Irvine
Mark Timko . . . . . Ohio State Univ.
W. Bradford Tippens . . . . . Texas A&M Univ.
Benjamin Titov . . . . . UC, Irvine
Michael J. Tobin . . . . . Carnegie-Mellon Univ.
Gerald E. Tripard . . . . . Washington State Univ.
Stephen E. Turpin . . . . . Rice Univ.
John L. Ullmann . . . . . Univ. of Colorado
Ernst Ungricht . . . . . Argonne
Albert Van Der Kogel . . . . . UNM Cancer Center
Kamran Vaziri . . . . . Utah State Univ.
Bruce J. Ver West . . . . . Arco Oil/gas Company
Roberta J. Wade . . . . . Univ. of New Mexico
Robert G. Wagner . . . . . Argonne
John D. Walecka . . . . . Stanford Univ.
Robert L. Walker . . . . . Consultant, New Mexico
Thad G. Walker . . . . . Abilene Christian Univ.
Stephen J. Wallace . . . . . Univ. of Maryland
Russell E. Walstedt . . . . Bell Laboratories/murray Hill
John B. Walter . . . . . EG&G, Idaho
Angel T. M. Wang . . . . . UCLA
Jiunn-Ming Wang . . . . . Brookhaven
Keh-Chung Wang . . . . . UC, Irvine
Zhao-Min Wang . . . . . Univ. of Maryland
Cary M. Warren . . . . . UC, Riverside
John W. Watson . . . . . Kent State Univ.
Monroe S. Wechsler . . . . . Iowa State Univ.
Charles A. Wert . . . . . Univ. of Illinois
Christopher Wesselborg . . . . . Univ. of Koln
Gary S. Weston . . . . . UCLA
C. Steven Whisnant . . . . . Univ. of South Carolina
D. Hywel White . . . . . Brookhaven
R. Roy Whitney . . . . . Univ. of Virginia
Charles A. Whitten . . . . . UCLA

Robert J. Whyley . . . . . Coll. of William & Mary
Jay A. Wightman . . . . . .UCLA
Bruce D. Wilkins . . . . . Argonne
Kentner B. Wilson . . . . . .Remotion Co.
Robert R. Wilson . . . . . .Columbia Univ.
Steven L. Wilson . . . . . Stanford Univ.
Andreas Wirzba . State Univ. of New York, Stony Brook
Stephen A. Wood . . . . . Tel Aviv Univ./MIT
Kim A. Woodle . . . . . Yale Univ.
H. G. Worstell . . . . . Consultant, New Mexico
Bryan K. Wright . . . . . Jniv. of Virginia
Dennis H. Wright . . . . . .Virginia Poly. Inst./State Univ.
S. Courtenay Wright . . . . . Univ. of Chicago
Shen-Wu Xu . . . . . .Univ. of Texas
Shuheng Yan . . . . . Inst. of Atomic Energy, PRC
Ming-Jen Yang . . . . . Univ. of Chicago
Wilox Yang . . . . . .Fermila
Alain J. Yaouanc . . . . . .CEN, Grenob
Akihiko Yokosawa . . . . . Argonne
Vincent Yuan . . . . . Univ. of Illinois
Larry Zamick . . . . . .Rutgers Univ.
Benjamin Zeidman . . . . . Argonne
John J. Zimerle . . . . . Ohio State Univ.
Sandra R. Zink . . . . . .UNM Cancer Center
Hans J. Ziock . . . . . .UCLA
Klaus O. H. Ziock . . . . . .Univ. of Virginia
Gisbert zu Putlitz . . . . . Univ. of Heidelberg
John D. Zumbro . . . . . .Princeton Univ.

INFORMATION FOR CONTRIBUTORS

Progress at LAMPF is the progress report of MP Division of Los Alamos National Laboratory. In addition it includes brief reports on research done at LAMPF by researchers from other institutions and Los Alamos National Laboratory divisions.

Progress at LAMPF is published annually on April 1. This schedule requires that manuscripts be received by January 1.

Published material is edited to the standards of the *Style Manual* of the American Institute of Physics. Papers are not refereed, hence presentation in this report does not constitute professional publication of the material nor does it preempt publication in other journals. Readers should recognize that results reported in *Progress at LAMPF* are sometimes preliminary or tentative and that authors should therefore be consulted in the event that these results are cited.

Contributors can expedite the publication process by giving special care to the following specifics:

1. When possible, furnish computer files together with hardcopy of paper. *Progress at LAMPF* can accept files from DEC computers and word processors, Wang, and IBM System 6.

2. Drawings and figures submitted should be of quality suitable for direct reproduction after reduction to single-column width, 83 mm (3-1/4 in.).

3. Figure captions and table headings should be furnished.

4. References should be complete and accurate.

5. Abbreviations and acronyms should be avoided if possible (in figures and tables as well as text), and when used must be defined.

6. All numerical data should be given in SI units.

7. Authors are reminded that it helps the reader to have an introduction, which states the purpose(s) of the experiment, before presentation of the data.

Research reports should be brief but complete. A list of recent publications relating to the experiment, for separate tabulation in this report, is much appreciated.

Contributors are encouraged to include as authors all participants in experiments so that they may receive credit for authorship and participation.

Questions and suggestions should be directed to John C. Allred, Los Alamos National Laboratory, MS H850, Los Alamos, NM 87545.

☆U.S. GOVERNMENT PRINTING OFFICE:1984—776-688 / 4041